Identifying novel molecular mechanisms of medium-chain fatty acids using the model *Dictyostelium discoideum*

Eleanor Claire Warren

Research thesis submitted for the degree of Doctor of Philosophy at the Royal Holloway University of London in August 2020

Declaration of Authorship

I, Eleanor Claire Warren, hereby declare that the work presented in this thesis is my own unless otherwise stated, and that all published work has been acknowledged. Furthermore, I affirm that I have neither fabricated nor falsified the results reported herein.

Signed: 

Date: 20/08/20

Acknowledgments

Firstly, I would like to thank my supervisor Professor Robin Williams for his dedication and support throughout my PhD, as well as Philip Chen and Shobana Dissanayeke for their help and advice. I am grateful to the BBSRC and to Vitaflo for funding this project and would like to thank Tricia Rutherford, Maura O'Donnell and the Vitaflo clinical trials team for making my industrial placement so enjoyable.

I wish to express my gratitude to all my collaborators who have supported this project. Thank you to Adrian Harwood, Chris Thompson, Amy Baldwin and Balint Stewart for providing the mutant library. Thank you to Stephanie Dooves, Eleonora Lugarà, Vivi Heine and Mathew Walker for their input into our paper. I am also grateful to Simon Heales, Simon Eaton and Michael Orford for sharing their expertise.

I would like to thank Catherine Pears, Fusheng Chang and Peggy Paschke, who first introduced me to *Dictyostelium* and encouraged me to pursue a PhD. I could not have completed this project without the friendship of the members of the Williams lab and Biological Sciences department. I am grateful to Chris Perry, Dev Sharma and Marco Cocorocchio for their guidance in the lab, and to Judith Schaf, Erwann Pain, George Heslop-Harrison, Ant Godard, Sonia Shinmar, Maryam Nagib, Fraser Morgan, Katie Lloyd-Jones and Simona Ursu for their support and friendship. I would like to say an especially big thank you to Joe Damstra-Oddy, who has been there for me from day one with valuable scientific advice, friendship and tree climbing distractions.

To all my friends from Aberystwyth and Oxford, thank you so much for always being there for me and never questioning my love of slime moulds (social amoeba!). Thanks, as well to all my friends at Staines boat club for all our evenings on the river. An extra special thank you goes to Alex, my friend, housemate, fellow scientist and rowing partner, for putting up with me throughout!

I would especially like to thank my family for all their encouragement. To my brother Joe, thanks for being there whenever I needed to moan! I owe thanks to my Granny Marjorie and to my Grandparents Michael and Sheila for always believing in me, and to my parents for always encouraging me and supporting me even from the other side of the world. Finally, I would like to thank Jak for his unfaltering belief in me and for making every day special.

Abstract

The medium-chain triglyceride (MCT) ketogenic diet is a high fat diet used to prevent seizures in patients with drug resistant epilepsy. In addition, there is emerging evidence that the MCT diet could be useful in other areas of health and medicine, however, the molecular mechanisms behind these effects are poorly understood. In this study, the tractable model organism, *Dictyostelium discoideum,* was employed to investigate novel mechanisms of action of the two medium-chain fatty acids, decanoic acid and octanoic acid, provided by the diet. A non-biased genetic screen was utilised to identify a mechanism of decanoic acid dependent upon the activity of a ubiquitin regulatory X (UBX) domain containing protein (UBXD18). Investigating this mechanism identified that UBXD18-GFP interacts with the ubiquitous protein p97(-RFP), where decanoic acid inhibited p97(-RFP) activity in a UBXD18 dependent manner. Due to the role of p97 in regulating homeostasis through autophagy, the effects of both decanoic acid and octanoic acid on this pathway were investigated, with both fatty acids demonstrated to activate autophagy independently of UBXD18. To investigate this further, decanoic acid was found to inhibit the major regulator of autophagy, mTORC1, a process linked to a range of positive medical and health-related effects. This effect on mTORC1 was shown to be specific for decanoic acid, and thus supports a model where decanoic acid acts through UBXD18 dependent inhibition of p97 to reduce mTORC1 signalling. Finally, the inhibitory effect of decanoic acid on mTORC1 was shown to be conserved in a rat hippocampal slice model and in tuberous sclerosis complex (TSC) patient-derived astrocytes. Thus, this study provides a novel therapeutic approach to down-regulate mTORC1 signalling and activate autophagy through dietary decanoic acid intake, with potential relevance for a wide range of medical treatments.

Contents

List of tables and figures

Chapter 1

Chapter 2

Chapter 3

Chapter 4

Chapter 5

Chapter 6

Chapter 7

List of abbreviations and nomenclature

4-BCCA	4-butylcyclohexane carboxylic acid
4E-BP1	Eukaryotic initiation factor 4E-binding protein
AAA ATPase	ATPase Associated with diverse cellular activities
aCSF	Artificial cerebrospinal fluid
ADP	Adenosine diphosphate
AED	Antiepileptic drug
AKT	Protein kinase B (also known as PKB)
ALS	Amyotrophic lateral sclerosis
AMPK	Adenosine monophosphate-activated protein kinase
APOE	Apolipoprotein E
Atg	Autophagy-related
ATP	Adenosine triphosphate
Ax2	Axenic strain 2
Ax4	Axenic strain 4
BLAST	Basic Local Alignment Search Tool
bp	Base pair
BSA	Bovine serum albumin
BSR	Blasticidin S deaminase
cDNA	Complementary deoxyribonucleic acid
ChAc	Chorea-acanthocytosis
CNS	Central nervous system
CRAC	Cytosolic regulator of adenylyl cyclase
DA	Decanoic acid
DB	Development buffer
DBeQ	N2,N4-dibenzylquinazoline-2,4-diamine
DEPDC5	Dishevelled, Egl-10, and Pleckstrin domain-containing protein 5
DMSO	Dimethyl sulfoxide
DNA	Deoxyribonucleic acid
DNA-PKcs	DNA-dependent protein kinase, catalytic subunit
dNTP	Deoxynucleoside triphosphate
EDTA	Ethylenediaminetetraacetic acid
eIF4E	Eukaryotic translation initiation factor 4E
ER	Endoplasmic reticulum
ERAD	Endoplasmic reticulum associated degradation

FCD	Focal cortical dysplasia
FcsA	Fatty acyl-CoA synthetase
FFEVF	Familial focal epilepsy with variable foci
G418	Geneticin
GABA	Gamma aminobutyric acid
gDNA	Genomic deoxyribonucleic acid
GFP	Green fluorescent protein
gof	Gain of function
GTP	Guanosine triphosphate
HDAC	Histone deacetylase
IBMPFD	Inclusion body myopathy with early-onset Paget disease and frontotemporal dementia
IC50	Half maximal inhibitory concentration
iPSC	Induced pluripotent stem cells
IRE1	Inositol-requiring kinase 1
IRS	Insulin receptor substrate
KATP	ATP-sensitive potassium channels
KRAS	Kirsten rat sarcoma viral oncogene homolog
LC3	Microtubule-associated protein 1A/1B-light chain 3
LKB1	Liver kinase B
lof	Loss of function
MCCC1	Mitochondrial 3-methylcrotonyl-CoA carboxylase α
MCT	Medium-chain triglyceride
mTOR	Mechanistic target of rapamycin
mTORC1	Mechanistic target of rapamycin complex 1
mTORC2	Mechanistic target of rapamycin complex 2
MW	Molecular weight
NADPH	Nicotinamide adenine dinucleotide phosphate
NHEJ	Non-homologous end joining
NMR	Nuclear magnetic resonance
OA	Octanoic acid
PBS	Phosphate-buffered saline
PDB	Protein data bank
PDK1	Phosphoinositide-dependent kinase 1
PERK	Protein kinase-like ER kinase
PH domain	Pleckstrin homology domain

PI	Protease inhibitor
PI3K	Phosphoinositide 3-kinase
PIP	Phosphatidylinositol phosphate
PIP2	Phosphatidylinositol bisphosphate
PIP_3	Phosphatidylinositol trisphosphate
PKA	Protein kinase A
PMSE	Polyhydramnios megalencephaly symptomatic epilepsy syndrome
PPARγ	Peroxisome proliferator activator receptor γ
PTEN	Phosphatase and tensin homolog
PTZ	Pentylenetetrazol
qRT-PCR	Quantitative reverse transcription polymerase chain
REMI	Restriction enzyme mediated integration
RFP	Red fluorescent protein
Rheb	Rhas-homolog expressed in brain
RIPA	Radioimmunoprecipitation assay buffer
RNA	Ribonucleic acid
RS	Restriction site
RT-PCR	Reverse transcription polymerase chain
S6	Ribosomal protein S6
S6K	p70 ribosomal protein S6 Kinase
SAR	Structure-activity relationship
SDS	Sodium dodecyl sulfate
SDS-PAGE	Sodium dodecyl sulfate poly acrylamide gel electrophoresis
STRADα	STE20-related kinase adapter α
TBS	Tris-buffered saline
TEMED	Tetramethylethylenediamine
TFEB	Transcription factor EB
TKT	Transketolase
TRIS	Tris(hydroxymethyl)aminomethane
TSC	Tuberous sclerosis complex
TZD	Thiazolidinedione
UBX	Ubiquitin regulatory X
UBXD18	Ubiquitin regulatory X domain-containing protein 18
ULK1	Unc-51 like autophagy activating kinase
VCP	Vasolin- containing protein (p97)
VPA	Valproic acid

Genetic nomenclature in *Dictyostelium*

Gene names

Represented in italics e.g. *ubxd18, fcsA, tkt, dna-pkcs.*

Protein names

Referred to by the relevant gene symbol, non-italic with capitalisation e.g. UBXD18, FcsA, TKT, DNA-PKcs.

Expression vectors

Represented by tag (presented with regards to N or C terminal position) and protein names e.g. GFP-UBXD18, GFP-FcsA, p97-RFP, GFP-Atg8.

Strain names

Referred to as protein names in italics with superscript ($^{-}$ knockout, $^{-/+}$ reintroduced gene expression, $^{-/-}$ double knockout) e.g. *UBXD18*$^{-}$, *UBXD18*$^{-/+}$, *FcsA*$^{-}$, *FcsA*$^{-/+}$, *TKT*$^{-}$, *DNA-PKcs*$^{-}$, *PKB*$^{-/-}$.

Genetic nomenclature in Humans

Gene names

Represented in italics with all letters in uppercase e.g. *TSC1, TSC2, PTEN, MTOR, PI3K*, *AKT*, *RHEB, APOE.*

Protein names

Referred to by the relevant gene symbol, non-italic with capitalisation e.g. TSC1, TSC2, PTEN, MTOR, PI3K, AKT, RHEB, APOE.

Patient genotype

Referred to as protein names in italics with superscript e.g. *TSC1*$^{-}$, *TSC2*$^{-}$.

Chapter 1

Introduction

1.1 The ketogenic diet

Fasting has long been known to reduce seizures in patients with epilepsy, with records of this effect appearing in multiple ancient texts, including the Hippocratic collection (Bailey, Pfeifer and Thiele, 2005; Hippocrates and Adams, 1985), and the bible (Matthew 17:21, Mark 9:29). The anti-seizure effects of fasting are thought to result from a build-up of ketone bodies, produced from fatty acids when carbohydrate levels are low, providing an alternative energy supply to the brain (Simeone, Simeone and Rho, 2017). Developed to mimic the effects of fasting, the ketogenic diet was introduced in the 1920s as a treatment for refractory epilepsy (Wilder, 1921; Wheless, 2008). This diet involves restricting carbohydrates and supplementing long-chain triglycerides (making up 60 % to 80 % of dietary energy), which are converted to ketone bodies by the liver (Krebs, 1966). This process involves the breakdown of triglycerides into free fatty acids, which are activated though the addition of Coenzyme A to form fatty acyl-CoA esters, allowing transportation to the mitochondria. In the mitochondria, β-oxidation takes place forming acetyl-CoA, which is subsequently converted into the ketone bodies, 3-β-hydroxybutyrate, acetoacetate, and acetone, in a process called ketogenesis. Levels of these ketone bodies are naturally present in the blood at concentrations less than 0.5 mM, and are raised to around 5 mM to 8 mM in patients on the ketogenic diet (Laffel, 1999; Veech, 2004). While this diet has been demonstrated to lead to a reduction of seizures (Neal *et al.*, 2008), the severe dietary restrictions and adverse gastrointestinal effects associated with this diet (Cai *et al.*, 2017) lead to limited patient compliance. In order to overcome these limitations, modified forms of the ketogenic diet have been developed.

1.2 The medium-chain triglyceride (MCT) diet

Developed to provide increased flexibility over the classical ketogenic diet, a modified ketogenic diet called the medium-chain triglyceride (MCT) diet has been used as a treatment for drug resistant epilepsy since 1971 (Huttenlocher, Wilbourn and Signore, 1971). In contrast to the long-chain triglycerides provided by the classical ketogenic diet, this form of the diet involves the supplementary intake of medium-chain triglycerides. As in the classical ketogenic diet these triglycerides are

metabolised to form ketone bodies, however, due to the improved efficiency of absorption and transport of medium-chain triglycerides only 45 % of dietary energy is required as fatty acids to maintain raised levels of ketone bodies in the blood (compared with 60 % to 80 % on the classical ketogenic diet) (Neal, 2016). Although most fatty acids are metabolised in this process, some medium-chain fatty acids are distributed by the blood to the brain, with raised plasma levels of decanoic acid (raised to an average levels of 157 µM (87-552 µM)) and octanoic acid (raised to an average of 310 µM (194-859 µM) detected in patients on the diet (Fig. 1.1) (Sills, Forsythe and Haidukewych, 1986; Haidukewych, Forsythe and Sills, 1982; Dean, Bonser and Gent, 1989). This reduction in the proportion of total fat required allows a greater quantity of carbohydrate and protein to be included in the diet and thus, improves palatability and patient health, whilst maintaining equivalent seizure control (Neal *et al.*, 2008; Neal and Cross, 2010).

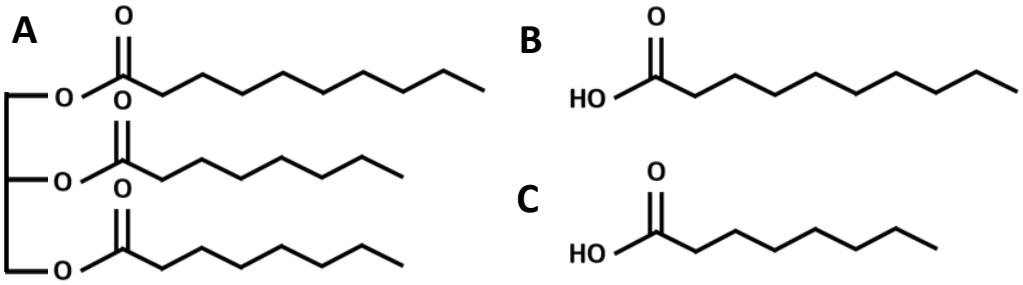

Figure 1. 1 Medium-chain triglycerides provided by the MCT diet are broken down into the free fatty acids decanoic acid and octanoic acid. The MCT ketogenic diet involves the oral intake of A) medium-chain triglycerides (such as Glycerol-1-decanoate-2,3-dioctanoate displayed here), which are converted into the fatty acids B) decanoic acid (capric acid) and C) octanoic acid (caprylic acid) in the intestine.

1.3 Epilepsy

Epilepsy is a chronic neurological disorder, which results in seizures caused by excessive, and hypersynchronous electrical discharge of neurons in the brain (Bazil, 2005). Occurring in 0.5 % to 1 % of the population, epilepsy is one of the most common serious neurological diseases (Bell and Sander, 2002). Epilepsy is a broad term representing a group of heterogenous disorders, often caused by interactions between genes and environmental factors (Steinlein, 2008). A range of epilepsy

disorders are linked to genetic factors such as mutations in ion channels (for example *SCN1A*), however, factors such as a head trauma, fever, brain tumours or stroke can also initiate epilepsy (Lukasiuk and Pitkanen, 2012; Maschio, 2012). Dysfunctions in mitochondria have also been suggested to play a critical role in seizure generation, with epilepsy commonly manifesting from mitochondrial disease (Kunz *et al.*, 2000). Genetic epilepsies arising from a single gene mutation, such as mutations leading to the epilepsy condition, Tuberous Sclerosis Complex (TSC), are rare, however, the identification of these genes has led to important discoveries into epilepsy aetiologies. Mutations in TSC patients have been identified as leading to dysregulation in mechanistic target of rapamycin complex 1 (mTORC1) signalling (Nabbout *et al.*, 2018) and autophagy (Parkhitko *et al.*, 2011), processes increasingly associated with epilepsy (Griffith and Wong, 2018; Wong, 2013). However, despite the prevalence of epilepsy research, in the majority of cases the cause of epilepsy remains unknown (Lukasiuk and Pitkanen, 2012).

1.4 Anti-epileptic drugs

The underlying physiology of epilepsy is an imbalance of excitatory and inhibitory neuronal activity (Scharfman, 2007), and altering this balance is the target of many antiepileptic drugs (AEDs). These AEDs provide the most commonly used approach for managing epilepsy, and they work by achieving a balance in neuronal activity, either through reducing excitatory activity by blocking ion channels (e.g. carbamazepine, and perampanel) (Lang, Wang and Cooper, 1993; Hibi *et al.*, 2012) or by increasing the inhibitory effect of GABA (e.g. Benzodiazepines, tiagabine and vigabatrin) (Isojarvi and Tokola, 1998; Hanada, 2014). Although AEDs provide complete seizure control for more than half of epilepsy patients, side effects including mental slowing, sedation, migraine, gastrointestinal disturbances, and behavioural changes limit the success of these drugs (Nevitt *et al.*, 2017). Furthermore, teratogenicity associated with AEDs (which is thought to be caused by an inhibitory effect on the activity of histone deacetylases) (Güveli *et al.*, 2017), can prevent these drugs being used in pregnant women, and with over 220,000 women of childbearing age with epilepsy in the UK alone (Epilepsy action), this highlights the need for improved AEDs lacking teratogenicity. Aside from problems associated with

side effects, roughly 30% of epilepsy sufferers are unresponsive to AEDs (Bialer and White, 2010), emphasising the need for the development of novel epilepsy treatments.

1.5 Classical ketogenic diet in seizure control

Unmanaged epilepsy is severely damaging, with repeated seizures enhancing excitatory brain circuits, perpetuating further seizures and leading to neuronal damage (Dingledine, Varvel and Dudek, 2014). Thus, despite there being over 20 available AEDs, in addition to surgical and other therapies to manage epilepsy, many patients remain without seizure control, substantially increasing their chances of neuronal damage and limiting their quality of life. Ketogenic diets provide an excellent alternative treatment for these patients.

The effects of the classical ketogenic diet on seizure control have been widely studied with multiple publications supporting a role of ketone bodies in this activity. Ketone bodies have been suggested to influence a range of cellular factors to provide seizure control, with no single mechanism able to explain the full effect of the diet. The antiseizure effect of ketone bodies has been suggested to be mediated through mitochondrial regulation, where ketone bodies are thought to enhance mitochondrial respiration and ATP production, and limit the production of reactive oxygen species (Kim *et al.*, 2015b; Kim, Vallejo and Rho, 2010; Maalouf and Rho, 2008). Further studies suggest that the ketogenic diet functions to provide seizure control through a mechanism involving increased activation of adenosine A1 receptors and regulation of adenosine metabolism (Masino *et al.*, 2011; Kovács *et al.*, 2017). Ketone bodies have also been suggested to function through epigenetic changes, such as restoring aberrant DNA methylation (Kobow *et al.*, 2013; Lusardi *et al.*, 2015). Finally, ketone bodies have also been shown to induce synaptic protection through regulating ATP-sensitive potassium (KATP) channels (Kim *et al.*, 2015a), thus providing further evidence in support of the efficacy of ketone bodies in seizure control.

Despite considerable evidence supporting the importance of ketone bodies in seizure control, this role remains controversial due to studies reporting poor correlation between levels of ketone bodies in the blood and anticonvulsant efficacy

(Likhodii *et al.*, 2000; Thavendiranathan *et al.*, 2000). Furthermore, mechanisms behind the anti-seizure effects of ketone bodies are unclear with one study demonstrating that the anticonvulsant properties of the ketogenic diet are not consistent with a direct effect of ketone bodies on the ion channels mediating hippocampal neurotransmission, since neither acetoacetate or β-hydroxybutyrate affect synaptic transmission in cultured neurones or brain slice models (Thio, Wong and Yamada, 2000). In addition, β-hydroxybutyrate and acetone have been shown not to block seizure activity in a rat hippocampal slice model (Chang *et al.*, 2016), where the established epilepsy drug valproic acid (VPA) shows efficacy (Chang, Walker and Williams, 2014; Chang *et al.*, 2012). As a diet-based therapy the ketogenic diet is expected to cause a wide range of cellular and biochemical changes thus, ketone bodies may only partly explain the anticonvulsant efficacy of the diet, with other mechanisms yet to be determined.

1.6 The medium-chain triglyceride ketogenic diet in seizure control

The MCT ketogenic diet has been developed as a less stringent version of the classical ketogenic diet, designed to maintain ketosis while delivering a reduced quantity of fat. Despite being developed to induce ketosis, the identification of raised levels of decanoic acid and octanoic acid in the plasma of patients on the MCT diet has led to research implicating these fatty acids in the seizure control effects of the diet independently of ketone bodies.

Decanoic acid has been demonstrated to provide seizure control in multiple in vitro and in vivo models. A rat hippocampal slice model, induced to display seizure like activity, using the gamma aminobutyric acid (GABA) receptor antagonist pentylenetetrazol (PTZ), has been used to demonstrate that decanoic acid but not octanoic acid reduces epileptiform activity (Chang *et al.*, 2013). Additionally, in mouse seizure models, chronic feeding with the triglyceride of decanoic acid (tridecanoin) has been shown to be anticonvulsant, while the triglyceride of octanoic acid (trioctanoin) has no effect (Tan *et al.*, 2017). Despite both fatty acids being capable of crossing the blood brain barrier (Wlaz *et al.*, 2015; Ebert, Haller and Walton, 2003), the majority of studies are consistent in suggesting that decanoic acid but not octanoic is the therapeutically effective component of the diet. Findings from

a neuronal cell line support this, suggesting that decanoic acid but not octanoic acid causes an increase in mitochondrial biogenesis, a mechanism credited with mediating the long-term anti-seizure effects of the diet (Hughes *et al.*, 2014). Additionally, a study suggesting a mechanism for the antiseizure effects of the MCT diet shows that decanoic acid, but not octanoic acid, acts as an antagonist of AMPA receptors thus inhibiting excitatory neurotransmission (Chang *et al.*, 2016). These findings support a role for decanoic acid in providing the anti-seizure effects of the MCT diet.

While octanoic acid has been widely reported to lack anticonvulsant activities it has been suggested that octanoic acid and decanoic acid have an additive interaction, with delivery of the two fatty acids together increasing the seizure threshold in the 6Hz seizure test on mice (Wlaz *et al.*, 2015). Furthermore, it has been demonstrated that the presence of octanoic acid in the MCT diet leads to the preferential metabolism of this fatty acid in neurones, allowing decanoic acid to escape breakdown, and thus accumulate to mediate therapeutic effects (Khabbush *et al.*, 2017).

Evidence supporting a direct role for decanoic acid in the anti-seizure effects of the MCT ketogenic diet and a supporting role for octanoic acid have informed the development of a dietary supplement called “Betashot”, made up of a high ratio of decanoic acid to octanoic acid supplied as triglycerides. This product developed by Vitaflo (International) Ltd, has recently progressed through a feasibility study to evaluate palatability, gastrointestinal tolerance and compliance in children and adults with epilepsy (ClinicalTrials.gov Identifier: NCT02825745).

1.7 Cellular targets of decanoic acid and octanoic acid provided by the MCT diet

Following the identification of a role for decanoic acid in seizure control in both in vitro (Chang *et al.*, 2013) and in vivo models (Tan *et al.*, 2017), mechanisms to explain this anti-seizure effect have been investigated. Several mechanisms of action of decanoic acid have been well established, such as the inhibition of excitatory neurotransmission through the direct inhibition of AMPA receptors, and the increase in mitochondrial biogenesis, while other potential mechanisms such as the regulation of mTORC1 signalling and cellular autophagy are not yet fully understood.

1.7.1 AMPA receptors

AMPA receptors are responsible for most of the fast-synaptic excitatory neurotransmission within the brain, and thus play an important role in initiating and propagating epileptiform discharges. Decanoic acid has been shown to possess strong inhibitory effects on excitatory neurotransmission in two ex vivo rat hippocampal slice models of epileptiform activity (Chang *et al.*, 2016). To establish a mechanism for this effect, electrophysiological characterisation has been carried out on AMPA receptor subunits expressed in a *Xenopus* oocyte model, finding that decanoic acid but not octanoic acid acts to reduce glutamate generated currents (Chang *et al.*, 2016). It has been further demonstrated that AMPA receptor inhibition using a pharmacological non-competitive inhibitor is sufficient to completely block epileptiform activity in vitro, indicating that this mechanism could explain the pharmacological effect of decanoic acid (Chang *et al.*, 2016). Furthermore, AMPA receptors have also been identified as targets for the AED perampanel (Rogawski and Hanada, 2013) and it has been revealed that decanoic acid and perampanel work synergistically in reducing AMPA receptor currents. These findings suggest that the MCT diet could be used in combination with perampanel to provide an improved strategy for the treatment for epilepsy (Augustin *et al.*, 2018b).

1.7.2 Mitochondrial biogenesis

Aside from evidence demonstrating that decanoic acid acutely controls seizure activity through the inhibition of AMPA receptors, it has been suggested that the anti-seizure effects of decanoic acid may also arise from beneficial effects of this fatty acid on brain energy metabolism. The classical ketogenic diet has been reported to increase mitochondrial biogenesis in the brains of rats, and since loss of respiratory chain enzyme activity is associated with seizure activity (Kunz *et al.*, 2000), this has led to the suggestion that an increase in mitochondrial proliferation could explain the antiseizure effects of this diet (Bough *et al.*, 2006). Investigations into the effects of decanoic acid on mitochondria have demonstrated that this fatty acid leads to an increase in mitochondrial biogenesis (citrate synthase levels) in the neuronal cell line SH-SY5Y and in cultured fibroblasts (Hughes *et al.*, 2014). This mitochondrial

enrichment was observed without a corresponding increase in oxidative stress, which was suggested to be minimised by elevated catalase activity (Hughes *et al.*, 2014). Decanoic acid has also been found to result in a significant increase in the activity of complex I, supporting evidence suggesting that this fatty acid leads to an increase in ATP production (Davey, Peuchen and Clark, 1998; Tan *et al.*, 2017; Hughes *et al.*, 2014). Furthermore, this study also demonstrated an increase in mitochondrial number in neuronal cells following treatment with decanoic acid (Hughes *et al.*, 2014). These findings suggest that the MCT diet as well as the classical ketogenic diet may lead to an increase in mitochondrial biogenesis.

To explain the effect of decanoic acid on mitochondrial biogenesis, this fatty acid has been characterised as an agonist for the transcription factor peroxisome proliferator activator receptor γ (PPARγ) (Malapaka *et al.*, 2012), with PPARγ stimulation sufficient to promote mitochondrial biogenesis. This mechanism appears to be specific for decanoic acid, with studies demonstrating that octanoic acid has no effect on PPARγ or mitochondrial function (Malapaka *et al.*, 2012; Hughes *et al.*, 2014; Tan *et al.*, 2017). The increase in mitochondrial biogenesis resulting from decanoic acid treatment is thought to lead to an increase in ATP availability and improved brain energy metabolism leading to reduced seizure activity, thus suggesting that a targeted more tolerable version of the MCT diet, with a higher decanoic acid content, could be developed for use in patients with epilepsy syndromes and mitochondrial disorders.

1.7.3 Autophagy regulation

Autophagy is a degradative process, by which cellular components are delivered to the lysosomes for recycling. This catabolic process plays an important role in maintaining cellular energy as well as removing misfolded proteins, and damaged organelles to maintain cellular homeostasis. Dysfunction of this process has been associated with a range of diseases including epilepsy and neurodegenerative disorders (Wong, 2013), and while the classical ketogenic diet has been linked to therapeutically activating this process (Wang *et al.*, 2018), the effects of medium-chain fatty acids on autophagy have not yet been well studied.

Macroautophagy, the most prevalent form of autophagy is well conserved throughout eukaryotes, enabling research into this pathway to be carried out in model organisms such as *Dictyostelium* as well as in higher eukaryotes. This pathway begins with the capture of intracellular cargo using a specialised membrane, called a phagophore, which engulfs material targeted for degradation to form a double membraned vesicle called an autophagosome (Fig. 1.2A). Fusion of this autophagosome with a lysosome, forming an autolysosome, allows the degradation of the sequestered material by lysosomal acid hydrolases (Fig. 1.2A). Following degradation, the resulting material is released back to the cytosol where it can be metabolised or re-used for building macromolecules (Glick, Barth and Macleod, 2010). Impairments in this pathway have been linked to epileptogenesis (Fig. 1.2B), and thus, strategies to activate autophagy are under investigation as novel therapeutics for epilepsy.

Fasting, a process known to reduce seizures in epileptic patients, is well established to activate autophagy, with this pathway widely linked to the associated therapeutic benefits (Yuen and Sander, 2014). In addition to providing nutrients during starvation, autophagy plays a role in degrading damaged organelles and misfolded proteins and this function has emerged as central in promoting health and longevity (Bareja, Lee and White, 2019). Impairments in autophagy have been suggested to play an important role in the development of epilepsy, with artificial inhibition of this pathway shown to result in spontaneous seizures in mice (McMahon *et al.*, 2012). Further links between autophagy and epilepsy have been established, with blockages in autophagy identified in patients with the genetic epilepsy conditions tuberous sclerosis complex (TSC) (Wong, 2013; McMahon *et al.*, 2012) and Lafora disease (Knecht et al., 2010). Furthermore, an accumulation of autophagy structures has been reported in the hippocampi of mice following repeated seizures (Shacka *et al.*, 2007), signifying a blockage in autophagic flux. Additional findings suggest that neuronal damage induced by seizures can be prevented by autophagy inducers (Fornai *et al.*, 2008; Caldero *et al.*, 2010), and thus, therapies known to activate autophagy are being investigated as potential epilepsy treatments (Kim et al., 2019; Giorgi et al., 2015).

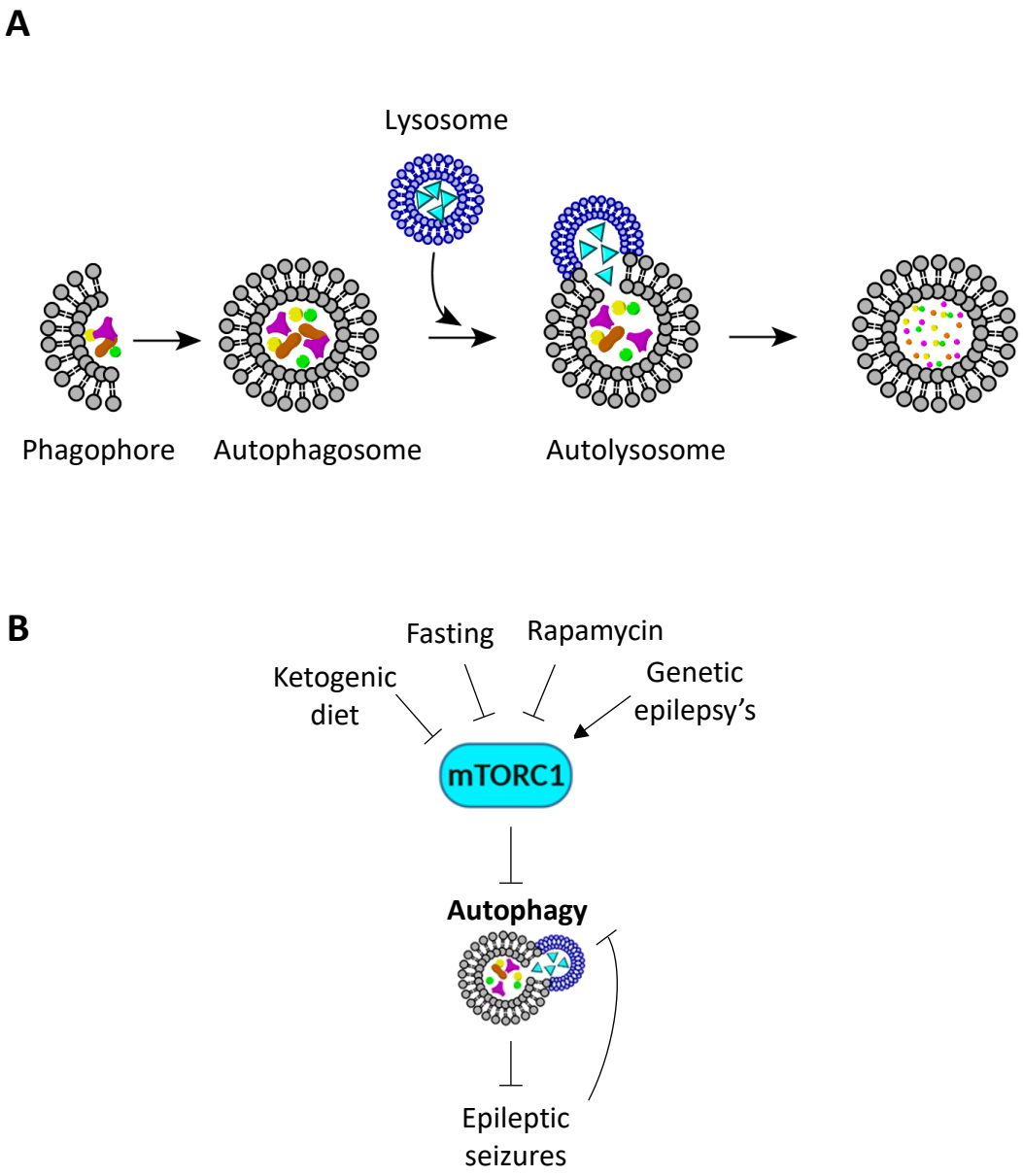

Figure 1. 2 The role of autophagy in epilepsy. A) Autophagy is initiated by the formation of the phagophore membrane that engulfs cytoplasmic material. This membrane matures into a double membraned vesicle called an autophagosome, which then fuses with a lysosome, causing degradation of the sequestered material. B) Schematic summarising links between autophagy and epilepsy. Artificial inhibition of autophagy leads to spontaneous seizures, with factors such as the ketogenic diet, fasting and rapamycin that are known to activate autophagy, via mTORC1 inhibition, demonstrating seizure suppression. Genetic epilepsies such as TSC and Lefora disease are known show dysfunctional autophagy, via overactivation of mTORC1. Furthermore, artificially triggered seizures have been demonstrated to lead to a blockage in autophagic flux, with autophagy activation under investigation as a potential therapy.

The classical ketogenic diet has been demonstrated to activate autophagy, with this mechanism suggested to provide a neuroprotective effect (Wang *et al.*, 2018; Camberos-Luna *et al.*, 2016). As with many autophagy inducing processes the classical ketogenic diet is thought to modulate autophagy through the major regulator of this pathway, mTORC1 (McDaniel *et al.*, 2011) (Fig. 1.2B), a complex with multiple links to epilepsy (Griffith and Wong, 2018). Further research into autophagy inducing therapies could lead to the development of improved epilepsy treatments. Additionally, investigations into the effects of medium-chain fatty acids on this process could shed light on the mechanisms of action of the MCT diet and may lead to the development of more effective therapies.

1.7.4 mTORC1 signalling

The mTORC1 pathway is a highly conserved pathway that functions as a central regulator of cellular nutrient and energy state. This pathway regulates downstream catabolic processes such as autophagy, as well as anabolic processes such as protein synthesis (Tatebe *et al.*, 2017). While mTOR is essential (Gangloff et al., 2004), uncontrolled activation of mTORC1 signalling and the corresponding reduction in autophagy has been linked to an increasing number of human diseases including certain epilepsies (Griffith and Wong, 2018).

mTORC1 is a protein complex that acts as a growth regulator sensing and integrating nutritional and environmental cues. Following exposure to nutrient rich conditions mTORC1 is activated by signals from growth factors via the phosphoinositide 3-kinase/protein kinase B (PI3K/AKT) signalling pathway (Fig. 1.3) (Bond, 2016). High energy levels (high ATP:ADP ratio) and glucose activate mTORC1 via inhibition of 5' AMP-activated protein kinase (AMPK), and amino acids activate mTORC1 by recruiting the protein complex to the lysosome allowing activation by Ras homolog enriched in brain bound to guanosine triphosphate (Rheb-GTP) (Fig. 1.3) (Bond, 2016). Activation of mTORC1 leads to the phosphorylation of the downstream effectors p70 ribosomal protein S6 kinase (S6K) and eukaryotic translation initiation factor 4E-binding protein (4E-BP1), which promotes the synthesis of proteins resulting in increased cell growth and proliferation (Fig. 1.3) (Tatebe *et al.*, 2017). Conversely, following nutrient starvation and the inhibition of mTORC1, the initiation

of autophagy is activated via dephosphorylation of a pro-autophagic complex (Atg1/ULK1) triggering degradation of cytoplasmic constituents allowing cells to reutilize their own constituents for energy and maintain homeostasis (Fig. 1.3) (Ganley *et al.*, 2009). In addition to regulating autophagy initiation, mTORC1 has also been demonstrated to directly regulate the subsequent steps of autophagy such as autophagosome elongation and maturation through modulating the phosphorylation state, and thus activation of the autophagy machinery, as well as altering gene expression through the phosphorylation of transcription factors (Dossou and Basu, 2019).

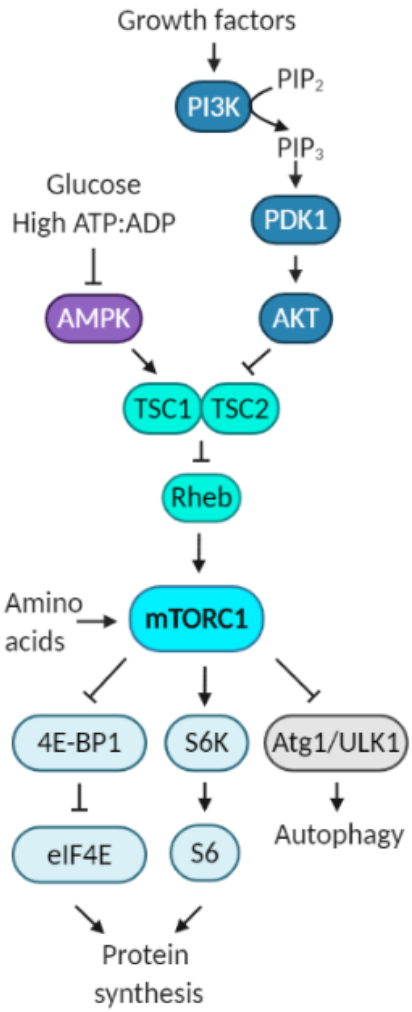

Figure 1. 3 Nutrient regulation of mTORC1 signalling The mechanistic target of rapamycin complex 1 (mTORC1) is a protein complex that senses cellular nutrient and energy state and regulates protein synthesis and degradation. Growth factors activate the PI3K/AKT pathway to inhibit the tuberous sclerosis complex (TSC), allowing GTP-bound RHEB to activate mTORC1. Glucose and high cellular energy (high ATP:ADP ratio) inhibit AMPK thus preventing the activation of the TSC complex and maintaining mTORC1 activation. Presence of amino acids leads to recruitment of mTORC1 to the lysosome allowing activation by RHEB. Activation of mTORC1 leads to the phosphorylation of 4E-BP1 inducing its dissociation from the eukaryotic translation initiation factor 4E (eIF4E) enabling translation. Activation of mTORC1 also leads to the phosphorylation of p70 ribosomal protein S6 kinase (S6K), which phosphorylates the S6 ribosomal protein, inducing protein synthesis at the ribosome. mTORC1 activation also leads to phosphorylation of the pro-autophagic complex Atg1/ULK1 inhibiting the degradation of cytoplasmic constituents by autophagy.

Hyperactivation of mTORC1 has been associated with a range of human diseases including epilepsy (McMahon *et al.*, 2012), as well as neurodegenerative disorders such as Alzheimer's disease (Tang *et al.*, 2013; Morita and Sobue, 2009) and certain cancers (Xie, Wang and Proud, 2016). Inhibition of this pathway has been suggested to provide clinical benefits in many of these conditions (Hillmann and Fabbro, 2019). Inhibition of mTORC1, caused by a reduction in glucose and insulin signalling, has been attributed to the therapeutic effects of ketogenic diets (McDaniel et al, 2011; Newman et al, 2017; Ostendorf & Wong, 2015; Roberts et al, 2017; Sweeney et al, 2017; Thio et al, 2006). While dietary intervention using the classical ketogenic diet is well established to reduce mTORC1 activity, this diet is highly restrictive for patients resulting in low compliance (Ye *et al.*, 2015a). The ability of the more palatable MCT diet to regulate this pathway has not yet been investigated. Investigating the effects of medium-chain fatty acids on mTORC1 signalling could help to establish whether this diet could prove useful for restoring balanced mTORC1 signalling in a range of human diseases.

1.7.5 Phosphoinositide signalling

Phosphoinositides, the phosphorylated derivatives of phosphatidylinositol are key regulators of plasma membrane signalling and membrane transport, and are thought to play an important role in neural function (Raghu *et al.*, 2019). A link between phosphoinositides and epilepsy has been suggested since increased phosphoinositide production has been shown during seizures (Van Rooijen *et al.*, 1986) and the loss of enzymes responsible for dephosphorylation of PIP_3 have been associated with seizures in mouse models (Backman *et al.*, 2001) and linked to seizure disorders (Hardies *et al.*, 2016; Raghu *et al.*, 2019).

The anti-epileptic drug VPA has been shown to reduce phosphoinositide production in *Dictyostelium* in relation to seizure control (Chang *et al.*, 2012) and the ability of fatty acids to reduce phosphoinositide turnover has been investigated in order to find compounds with enhanced potency (Chang *et al.*, 2012). Both decanoic acid and octanoic acid have been shown to attenuate phosphoinositide production more potently than VPA, leading to the direct demonstration that these fatty acids block PTZ-induced epileptiform activity in an in vitro rat hippocampal slice model

(Chang *et al.*, 2013). Not only do these findings provide an important insight into decanoic acid induced seizure control, they also emphasise the value of using *Dictyostelium* as a model in epilepsy research.

Phosphoinositides are well established to regulate both autophagy, and mTORC1 signalling, with these processes representing potential therapeutic roles for reduced phosphoinositide production in epilepsy treatment. Phosphatidylinositol 3-phosphate (PI3P), phosphatidylinositol 3,5-bisphosphate (PI-3,5-P_2) and phosphatidylinositol 3,4,5-trisphosphate (PIP_3) have all been demonstrated to activate mTORC1 either directly (Jin *et al.*, 2014) or through the recruitment of AKT and phosphoinositide-dependent kinase-1 (PDK1) to the plasma membrane enabling the phosphorylation of AKT, the activation of mTORC1 and the corresponding inhibition of autophagy (Fig. 1.3) (Palamiuc, Ravi and Emerling, 2020; Jang and Lee, 2016). Despite the well-established link between mTORC1 activation and autophagy inhibition, phosphoinositides have been suggested to play contrasting roles in this process, with PI3P and phosphatidylinositol 4,5-bisphosphate (PI-4,5-P_2) required for autophagy activation (Nascimbeni, Codogno and Morel, 2017; Burman and Ktistakis, 2010; Tan *et al.*, 2016; Rong *et al.*, 2012).

While both decanoic acid and octanoic acid have been demonstrated to reduce phosphoinositide production, with synthesis of phosphatidylinositol monophosphates (PIP) and phosphatidylinositol bisphosphates (PIP_2) shown to be reduced in *Dictyostelium* (Chang *et al.*, 2012), neither production of, nor total levels of PIP_3 have been assessed in the presence of medium-chain fatty acids, with changes in levels of this signalling molecule predicted to modulate mTORC1 and autophagy activity. Thus, alterations in PIP_3 levels caused by medium-chain fatty acids represent a potential, unexplored therapeutic mechanism for the MCT diet.

Multiple mechanisms of action for decanoic acid in the therapeutic effects of the MCT diet have been suggested. The effects of decanoic acid on AMPA receptors and mitochondrial biogenesis are well explained, while potential effects on signalling pathways such as mTORC1 and autophagy are yet to be fully explored. Understanding these mechanisms of action could help to develop a better understanding of the potential health benefits and could lead to the development of this diet for use in treating other medical conditions.

1.8 Ketogenic diets in disease treatment and health

In addition to treating epilepsy, the MCT diet has gained interest as a potential treatment for a range of conditions, such as cognitive impairment, mitochondrial disorders, diabetes, cancer and neurodegenerative disorders. It was initially assumed that the therapeutic mechanisms of the MCT diet in these areas would be through the provision of ketone bodies as an alternative energy source, however, recent findings suggest a potential role for medium-chain fatty acids in treating these conditions.

1.8.1 Cognitive impairment

Subjective assessment of patient experience has suggested that the ketogenic diet may improve cognitive function in children and adults on the MCT diet (IJff *et al.*, 2016; van Berkel, DM and Verkuyl, 2018). These reports have led to investigations into the use of medium-chain triglycerides to improve cognition in patients with diverse conditions associated with cognitive decline. Medium-chain triglycerides have been shown to prevent the decline in cognitive function associated with hypoglycaemia in patients with diabetes (Page *et al.*, 2009). Further studies have reported improved cognition in elderly patients and patients with Alzheimer's disease fed a MCT diet (Ota *et al.*, 2016; Ota *et al.*, 2019), however, whether these effects are derived from medium-chain triglycerides or ketone bodies is unclear. Recent data suggests that decanoic acid and octanoic acid may provide cognition enhancing properties independently of ketone bodies (Wang and Mitchell, 2016). Interestingly, a medium-chain triglyceride containing product is provided commercially to people over the age of fifty in China (Nestlé YIYANG Fuel for brain^{TM} senior milk powder) and is promoted to delay brain aging and to improve brain response and memory, based on findings from aged beagle dogs (Pan *et al.*, 2010). Further investigation into the cognitive benefits of medium-chain fatty acids could lead to more widespread use of MCT supplements to prevent cognitive decline associated with epilepsy, age, traumatic brain injury, hypoglycaemia and Alzheimer’s disease.

1.8.2 Mitochondrial diseases

Mitochondrial diseases are a group of disorders caused by defects in the respiratory chain, thus affecting tissues and organs with high energy demands such as the central nervous system, as well as skeletal and cardiac muscles. Decanoic acid has been implicated in regulating mitochondrial function following the finding that it activates the nuclear receptor, peroxisome proliferator-activated receptor gamma (PPAR-γ), involved in mitochondrial biogenesis (Malapaka *et al.*, 2012). Data from a neuronal cell line demonstrates that decanoic acid leads to an increase in mitochondrial number, along with an increase in the activities of citrate synthase (a biomarker for mitochondrial enrichment) and complex I (Hughes *et al.*, 2014). These findings have raised the possibility that the MCT ketogenic diet could provide potential therapeutic benefits for patients with mitochondrial disorders. Leigh syndrome is a severe mitochondrial disease resulting in progressive neurological abnormalities, such as loss of motor skills (Fassone and Rahman, 2012). Decanoic acid has been shown to increase mitochondrial content in fibroblasts from patients with nuclear-encoded complex I deficient Leigh syndrome, as well as increasing cellular resistance to oxidative stress (Kanabus *et al.*, 2016). These findings suggest that the MCT ketogenic could be used to provide therapeutic benefits in some patients with Leigh syndrome, and that further investigations into the use of decanoic acid to treat mitochondrial disorders should be carried out in in vivo mammalian models.

1.8.3 Diabetes mellitus

Diabetes mellitus represents a group of metabolic disorders characterised by raised blood sugar levels, caused by suppressed insulin production (type 1 diabetes) or insulin resistance caused by lifestyle factors, such as obesity and lack of exercise (type 2 diabetes). Dietary interventions, including the MCT diet, have been investigated as novel therapeutic approaches for treating type 2 diabetes. In multiple studies MCT diets have been shown to reduce serum lipid concentrations and improve lipid profiles, decrease body fat, and reduce total bodyweight in animals and humans (Geng *et al.*, 2016; Mumme and Stonehouse, 2015; Malapaka *et al.*, 2012).

Medium-chain triglycerides have also been shown to reduce insulin resistance and improve glucose tolerance (Geng *et al.*, 2016; Takeuchi *et al.*, 2006). Furthermore, findings linking mitochondrial dysfunction with insulin resistance and type 2 diabetes (Petersen *et al.*, 2004; Koves *et al.*, 2008), suggest that the beneficial effects associated with decanoic acid on mitochondrial function and biogenesis could prove therapeutic in patients with this disorder. Drugs in the thiazolidinedione (TZD) family are used to activate PPAR-γ in the treatment of type 2 diabetes, however, this family of drugs is associated with several adverse effects, such as weight gain and cardiovascular disease (Graham *et al.*, 2010; Larsen, Toubro and Astrup, 2003). Decanoic acid activates PPAR-γ without the associated side effects of TZDs (Malapaka *et al.*, 2012), suggesting that designing therapies based around decanoic acid activation of PPAR-γ could lead to safer treatments for type 2 diabetes.

1.8.4 Cancer

Since the discovery by Otto Warburg in the 1920s that cancer cells rely on glycolysis regardless of oxygen availability, dietary therapies that reduce glucose availability have gained substantial interest as cancer treatments (Warburg, Wind and Negelein, 1927). Reducing the glucose availability for cancer cells by administering the ketogenic diet while providing normal cells with ketone bodies as an alternative fuel, is thought to result in reduced tumour growth (Brooks, Woolf and Scheck, 2016; Branco *et al.*, 2016). This has been demonstrated in studies using mouse astrocytoma allograft models (Seyfried *et al.*, 2012), and in mouse models of glioma (Stafford *et al.*, 2010; Klement *et al.*, 2016). Observational studies in patients suggest that the ketogenic diet is effective alone and as an adjunctive therapy in patients with multiple cancer types (Scheck *et al.*, 2012; Poff *et al.*, 2013; Tan-Shalaby, 2017; Zuccoli *et al.*, 2010; Allen *et al.*, 2014), however, more evidence for clinical efficacy in randomised controlled trials is required. While reduced glucose availability remains the most accepted explanation for the efficacy of ketogenic diets in treating cancers, medium-chain fatty acids have been suggested to have direct anticancer effects (Narayanan *et al.*, 2015; Fauser *et al.*, 2013; Jóźwiak *et al.*, 2020). Further investigation into the effects of medium-chain fatty acids on cancer progression could lead to improved therapies.

1.8.5 Neurodegenerative diseases

Neurodegenerative diseases are incurable conditions resulting in the progressive degeneration of nerve cells. Ketogenic diets have been suggested to provide therapeutic benefits in a range of neurological disorders, such as amyotrophic lateral sclerosis (ALS), Alzheimer's disease and Parkinson's disease, with evidence suggesting potential benefits of medium-chain triglycerides in these conditions.

ALS is a neurodegenerative condition characterised by the degradation of motor neurons, leading to progressive motor weakness and death (Rowland and Shneider, 2001). Ketogenic diets have been suggested to improve degeneration in these patients (Siva, 2006; Zhao *et al.*, 2006; Paganoni and Wills, 2013), due to their beneficial effects on mitochondrial function (Carrì, D'Ambrosi and Cozzolino, 2017; Hughes *et al.*, 2014; Kim, Vallejo and Rho, 2010). Improved motor neuron survival has been reported in mice following administration of octanoic acid triglyceride, thought to be caused by an increase in mitochondrial energy production resulting from the use of an alternative energy source for neuronal metabolism (Zhao *et al.*, 2012). These findings suggest that using octanoic acid to restore energy metabolism could provide a therapeutic approach to treat patients with ALS. In addition, dysregulation of autophagy (Nguyen, Thombre and Wang, 2019; Hartman, 2012) and mTORC1 signalling has been reported in patients with ALS (Saxena *et al.*, 2013; Perera and Turner, 2016), suggesting that regulation of these pathways by the ketogenic diet (McDaniel *et al.*, 2011) could lead to therapeutic benefits in these patients.

Medium-chain triglycerides have also been suggested to have positive effects in patients with Alzheimer's disease. Alzheimer's is a neurodegenerative disease, characterised by deposits of β-amyloid peptide, resulting in neurotoxicity and loss of mental function (Murphy and LeVine, 2010). β-amyloid peptide is known to cause neurotoxicity via the formation of neurofibrillary tangles, inflammation and oxidative stress (Hardy and Allsop, 1991), with studies in cultured neurones and mouse models suggesting that ketogenic diets provide protection against the toxicity of this peptide (Kashiwaya *et al.*, 2000; Van der Auwera *et al.*, 2005). Furthermore, studies with Alzheimer's patients have demonstrated that treatment with medium-chain

triglycerides improves memory (Reger *et al.*, 2004; Henderson *et al.*, 2009; Ota *et al.*, 2019; Taylor *et al.*, 2018). Glucose hypometabolism is thought to be an underlying feature of the Alzheimer's brain, with the ketogenic diet widely believed to improve Alzheimer's symptoms by providing the brain with an alternative energy supply (Heiss *et al.*, 1991). The medical food, Axona®, which is primarily octanoic acid triglyceride, was developed to bypass glucose metabolism in the brain, and has been demonstrated to enhance memory and cognition in some patients in clinical trials (Henderson *et al.*, 2009; Roman, 2010; Ohnuma *et al.*, 2016). In addition to bypassing glucose metabolism, ketogenic diets are thought to provide benefits to patients through correcting mitochondrial disfunction (Johri and Beal, 2012) and restoring disrupted autophagy (Takahashi, Nagao and Gouras, 2017; Uddin *et al.*, 2018) processes which could be directly modulated by medium-chain fatty acids (Hughes *et al.*, 2014; Sauvat *et al.*, 2018). Interestingly, evidence from post-mortem brains has indicated that mTORC1 signalling is hyperactivated in patients with Alzheimer's disease (An *et al.*, 2003; Chang *et al.*, 2002), suggesting that regulation of this pathway by the ketogenic diet (McDaniel *et al.*, 2011), could provide corresponding therapeutic benefits. Further investigation into the mechanisms of medium-chain fatty acids is required to better understand their capacity to benefit patients with Alzheimer's disease.

Parkinson's disease is another disorder of the central nervous system that has potential to be treated by the ketogenic diet. This disease is characterised by the accumulation of a neuronal protein called α-Synuclein, which leads to the degeneration of dopaminergic neurons, and presents with defects in movement and cognition (Sveinbjornsdottir, 2016). The ketogenic diet and β-hydroxybutyrate have been suggested to provide neuronal protection in rodent models of Parkinson's disease (Tieu *et al.*, 2003; Yang and Cheng, 2010; Cheng *et al.*, 2009; Shaafi *et al.*, 2016). Additionally, clinical trials suggest that the ketogenic diet could lead to an improvement of symptoms in Parkinson's patients (Vanitallie *et al.*, 2005; Phillips *et al.*, 2018). Dysfunctional autophagy has been linked to the accumulation of α-synuclein in the brains of Parkinson's patients contributing to the pathogenesis of this disease (Lynch-Day *et al.*, 2012). Further evidence is required to establish whether medium-chain fatty acids provided by the MCT ketogenic diet could promote

autophagic activation to reduce neuronal loss and slow disease progression in these patients. Furthermore, as in other neurodegenerative diseases, mitochondrial dysfunction has been suggested be involved in the pathogenesis of this disease (Winklhofer and Haass, 2010), suggesting that the beneficial effects of decanoic acid on mitochondrial function (Hughes *et al.*, 2014) could provide therapeutic benefits in this condition.

A broad range of evidence supports the potential benefits of medium-chain triglycerides for use in neurodegenerative diseases. These conditions share common dysfunctionality in mitochondrial function, as well as in mTORC1 signalling and autophagic degradation, suggesting that modulation of these cellular processes could provide therapeutic benefits in multiple conditions. Further research into the mechanisms of actions behind the MCT diet could help to develop better targeted and more effective treatments.

1.9 Limitations of the MCT diet

Despite being effective for the treatment of drug resistant epilepsy, with multiple potential benefits in treating other conditions, the MCT diet is associated with adverse gastro-intestinal related side effects such as diarrhoea, vomiting, bloating and cramps (Raper, 1935; Liu, 2008). These side effects have limited the implementation of this diet in epilepsy treatment, especially in adults, due to difficultly with compliance (Ye *et al.*, 2015a). Developing a better understanding of the mechanisms of action of the fatty acids provided by the diet could lead to refined formulations that lack these adverse effects. Moreover, understanding the mechanisms of action behind the therapeutic effects of the diet will help to develop a better appreciation of the potential health benefits and could lead to the development of this diet for use in treating other medical conditions.

In this project we employ *Dictyostelium discoideum* as a model system to elucidate and verify mechanisms of action of medium-chain fatty acids. In addition to investigating decanoic acid and octanoic acid we also consider the cyclic derivative of octanoic acid, 4-butylcyclohexane carboxylic acid (4-BCCA), which has been identified as a potential anti-seizure agent (Fig. 1.4). Identified as displaying potent antiseizure activity (Chang *et al.*, 2015), while lacking the teratogenically associated inhibitory

effects on histone deacetylase (HDAC) activity that is often observed with AEDs, this compound represents an exciting potential therapeutic with an enhanced safety profile over traditional AEDs (Chang *et al.*, 2015; Koren *et al.*, 2006; Jentink *et al.*, 2010).

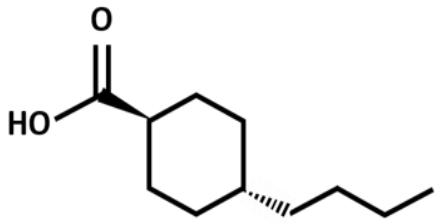

Figure 1. 4 Skeletal structure of 4-butylcyclohexane carboxylic acid. The compound 4-butylcyclohexane carboxylic acid (4-BCCA) has been identified as showing enhanced epileptiform activity over VPA, and decanoic acid in rat hippocampal slice models.

1.10 *Dictyostelium discoideum* as a model organism

The eukaryotic social amoeba*, Dictyostelium discoideum* (referred to as *Dictyostelium*) was first found by Raper in 1935, living in forest detritus in North America (Raper, 1935), and has since been established as a popular model organism. *Dictyostelium* belongs to the Phylum Amoebozoa (Schilde and Schaap, 2013) and possesses a unique developmental lifestyle that make it a valuable model for studying processes such as cell motility, chemotaxis, signal transduction, and cell differentiation. Under ideal growth conditions *Dictyostelium* amoeba grow as individual independent cells, using phagocytosis to feed on bacteria and dividing by binary fission (Raper, 1935). When faced with adverse conditions such as starvation the amoebae enter the developmental stage of their life cycle (Fig. 1.5). Development is initiated by the release of the extracellular chemoattractant cAMP, which signals the mass movement of cells towards a central region (Meima and Schaap, 1999). Upon aggregation the interacting cells form multicellular motile slugs allowing movement towards attractants such as heat and light (Bonner *et al.*, 1950). These slugs consist of prespore and prestalk cells which, during culmination, differentiate forming fruiting bodies consisting of viable spores held above the substratum by dead

vacuolated stalk cells (Thomason *et al.*, 1998). The whole process of fruiting body formation takes around 24 hours at which point mature spores can be released to germinate and re-enable unicellular growth when conditions are favourable. These spores can survive for months in the absence of food, thus, allowing *Dictyostelium* to endure starvation and desiccating conditions (Dubravcic, van Baalen and Nizak, 2014). This unique social behaviour has made *Dictyostelium* a popular system for studying altruism and cooperation.

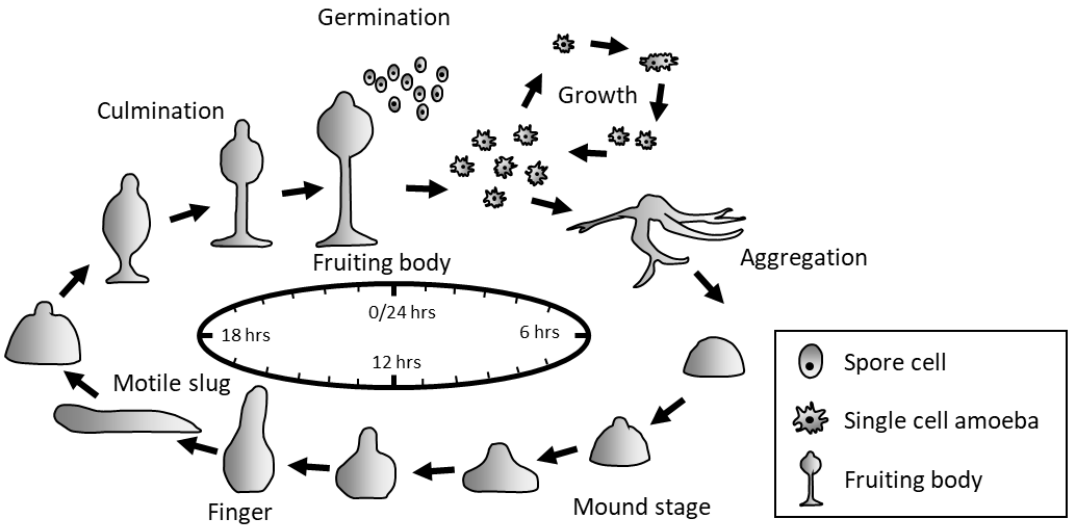

Figure 1. 5 The developmental cycle of *Dictyostelium discoideum*. During favourable conditions cells grow as individual free-living amoebae, dividing by binary fission. Following nutrient deprivation cells aggregate to form multicellular structures termed, mounds, fingers and motile slugs which are capable of movement towards chemoattractants. Culmination results in the formation of differentiated fruiting bodies, where spore cells are held aloft by dead vacuolated stalk cells. These viable spores can survive long periods of time, thus allowing dispersal and germination when conditions become favourable.

In addition to possessing a remarkable developmental cycle, the genetics of *Dictyostelium* make it an ideal model system. Despite having diverged from the animal lineage before the divergence of yeasts (Eichinger *et al.*, 2005), the evolutionary distance between *Dictyostelium* and humans is less than the distance between human and yeasts, due to the higher rate of evolutionary change in the yeast lineage (Insall, 2005). *Dictyostelium* is valuable as a simple system with many of

the genes in its 34 Mb genome homologous to those of higher eukaryotes (Eichinger *et al.*, 2005). The complete genome sequence of *Dictyostelium* is available (Eichinger *et al.*, 2005) and the molecular genetics of this haploid organism facilitate gene disruption experiments through insertional mutagenesis (Faix *et al.*, 2013). The generation of libraries of *Dictyostelium* mutants has enabled pharmacogenetic studies leading to the identification of targets for compounds such as naringenin, curcumin and cannabidiol (Cocorocchio *et al.*, 2018; Waheed *et al.*, 2014; Perry *et al.*, 2020). This approach allows rapid identification of genes encoding proteins that control the sensitivity to a compound, thus implicating the identified protein or the wider pathway in the action of the compound.

Dictyostelium is a well-established model for use in epilepsy research, with findings being translated into mammalian systems and directing clinical progress. Studies using *Dictyostelium* have shown that the anti-epileptic drug VPA acts to inhibit phosphoinositide signalling, implicating phosphoinositides as a target for epilepsy treatments (Xu *et al.*, 2007; Chang *et al.*, 2012). A structure-activity relationship (SAR) study in *Dictyostelium* has led to the discovery that decanoic acid is more potent than VPA in reducing phosphoinositide production (Chang *et al.*, 2012). Subsequently, these findings have been translated into mammalian models, identifying that decanoic acid has improved efficacy in seizure models over VPA (Chang *et al.*, 2013; Chang, Walker and Williams, 2014; Augustin *et al.*, 2018a). These findings have contributed to the development of a MCT diet with a high decanoic acid content (Betashot, ClinicalTrials.gov: NCT02825745) and have validated the use of *Dictyostelium* in ketogenic diet research.

Autophagy, a cellular process central to health, longevity and epilepsy has been widely studied in *Dictyostelium*. As in other eukaryotes, autophagy is required for *Dictyostelium* to survive starvation, and to degrade dysfunctional proteins and organelles. Autophagy has been recognised in this organism since 1969 (Cotter, Miura-Santo and Hohl, 1969), and since then many of the proteins and complexes involved in autophagy have been identified as being conserved in *Dictyostelium* (Mesquita *et al.*, 2016). This organism has been widely employed in studying this process, with findings in this organism providing important advances in the study of autophagy-related pathologies, such as in neurodegenerative diseases (Munoz-

Braceras, Calvo and Escalante, 2015), cancer (Calvo-Garrido and Escalante, 2010), and neuronal malfunction (Kim *et al.*, 2009; Schmauch *et al.*, 2009). The major regulator of autophagy, mTORC1 signalling, has also been well characterised in *Dictyostelium.* Components of the mTORC1 complex, including, TOR, Raptor and Lst8 are conserved throughout eukaryotes, as is the eukaryotic initiation factor 4E-binding protein (4E-BP1) (Morio *et al.*, 2001; Liao *et al.*, 2008). *Dictyostelium* has been used in a range of mTORC1-related studies, from studies on autophagy (Mesquita *et al.*, 2016) to studies on cell migration (Liu *et al.*, 2010) and phagocytosis (Rosel *et al.*, 2012). The prevalence of *Dictyostelium* research in the areas of autophagy and mTORC1 highlights the suitability of this model for studying these conserved processes.

1.10.1 Mutant library principles

Insertional mutant libraries of *Dictyostelium* have proved valuable in multiple pharmacogenetic studies identifying targets for a diverse range of compounds. These libraries are prepared though the use of restriction enzyme mediated integration (REMI) mutagenesis (Kuspa, 2006), a technique that has been available in *Dictyostelium* since 1992 (Kuspa and Loomis, 1992). This method involves the random insertion of linearized DNA (BamH1) from a plasmid carrying a selectable resistance gene (blasticidin resistance (BSR)) via electroporation with a restriction enzyme (Fig. 1.6A and B). Digestion of the genomic DNA with the supplied restriction enzyme (DpnII or NlaIII) generates complementary sticky ends to those of the linearized plasmid (GATC), thus allowing the plasmid to become integrated into the genome at the site of digestion. DpnII and NlaIII are the restriction enzymes used to digest the gDNA, chosen since more than 95 % of the protein coding genes in *Dictyostelium* contain one of these sites (Guerin and Larochelle, 2002) (Fig. 1.6B). This technique generates random insertions within the genome of *Dictyostelium* thereby disrupting gene expression at the sites of integration. This REMI process has been optimised to produce a maximum of one gene disruption per *Dictyostelium* cell. Mutants are then selected for in the presence of blasticidin, generating a pool of mutants termed a "library" with a wide coverage of mutated genes (Guerin and Larochelle, 2002) (Fig. 1.6C).

Mutant libraries generated using REMI mutagenesis can be used to identify *Dictyostelium* mutants with reduced sensitivity to compounds, either in growth (Fig. 1.6D), development or cell behaviour, thus suggesting that the encoded proteins are potential targets for these compounds. The genes disrupted by the REMI insert can be determined by isolating the flanking DNA sequence on either side of the integrated plasmid. In this process a restriction enzyme (Rsa1) that cuts within the integrated plasmid and within the flanking DNA is used to digest the genomic DNA (Fig. 1.6E) before self-ligation to generate a circular piece of DNA (Fig. 1.6F). Primers from within the REMI integration plasmid can then be used to amplify the flanking DNA using PCR (Fig. 1.6F). The DNA sequence of this PCR product can then be determined through sequencing (Fig. 1.6G), either directly or following amplification in bacteria, and the resulting DNA sequence can be used to identify where in the genome the integration took place. In order to confirm that an identified gene disruption is responsible for the resistant phenotype, this gene must be independently disrupted to recreate the genotype and confirm the phenotype. This recapitulation can be carried out using either homologous integration of knockout cassettes (Faix *et al.*, 2004) or by using the more recently established CRISPR/Cas9 techniques (Sekine, Kawata and Muramoto, 2018). Through identifying and analysing *Dictyostelium* mutants lacking potential target proteins, the cellular mechanisms of target compounds can be rapidly explored.

Dictyostelium provides a powerful model system, which has been well established in the fields of epilepsy, ketogenic diet, autophagy and mTORC1 research. Furthermore, *Dictyostelium* mutant libraries provide a valuable resource allowing the rapid identification of molecular targets for compounds. The position of *Dictyostelium* at the forefront of epilepsy research, and the availability of verified molecular genetic approaches, make this organism an appropriate model for investigating mechanisms of action of medium-chain fatty acids.

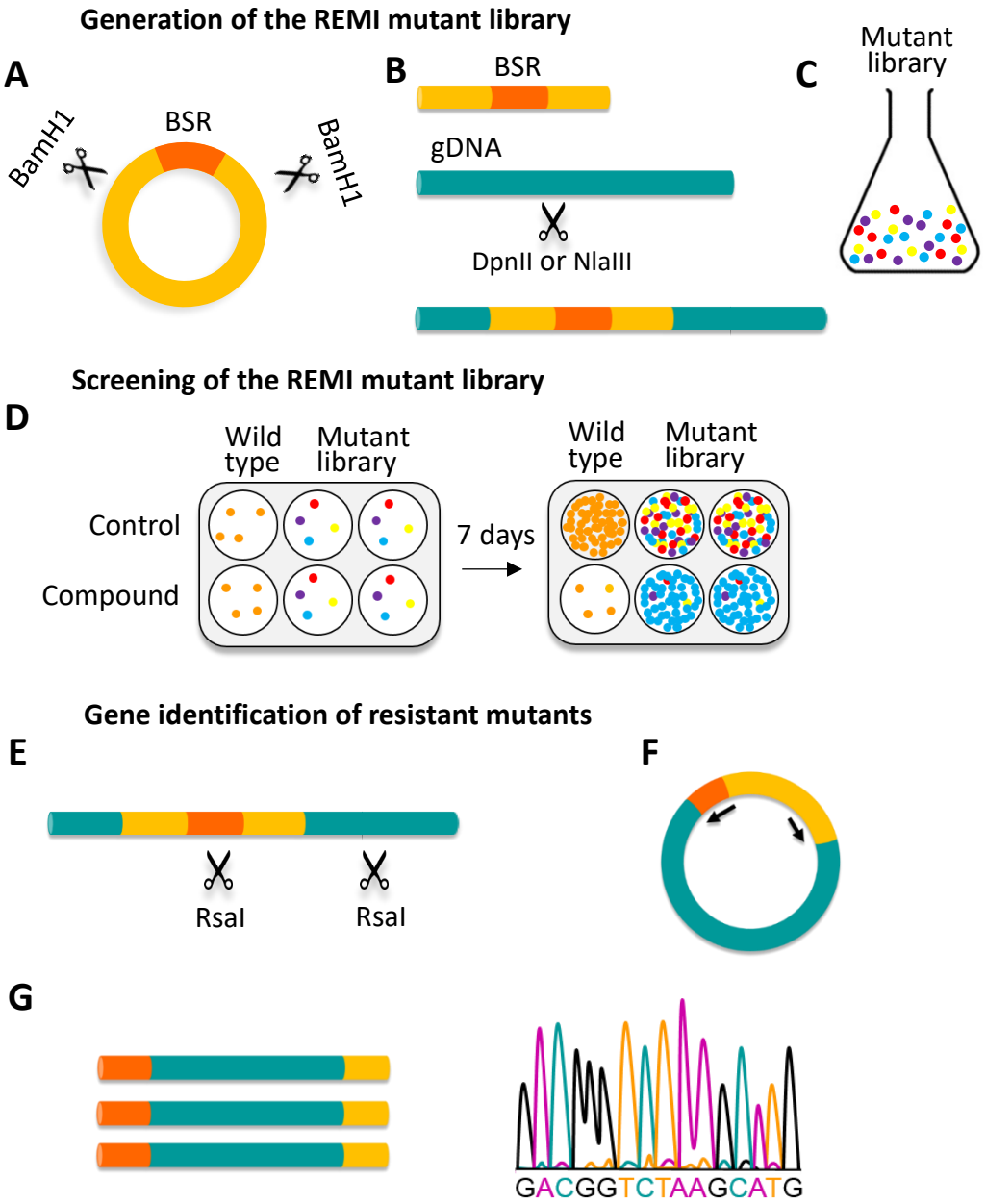

Figure 1. 6 Restriction enzyme-mediated integration (REMI) library generation, screening and gene identification. The REMI library is generated though A) the BamH1 digestion of a plasmid containing a blasticidin resistance (BSR) sequence. B) The resulting linearized plasmid DNA is electroporated into cells along with DpnII or NlaIII facilitating the integration of the plasmid sequence into the *Dictyostelium* genome. C) This technique allows the generation of libraries of *Dictyostelium* cells with thousands of different genes disrupted. D) These libraries can be screened for mutants resistant to the growth inhibitory effects of compounds. The disrupted genes leading to resistance can then be identified. E) To identify the disrupted genes first, genomic DNA is extracted from the mutants and digested using RsaI. F) This digested region is then subjected to self-ligation, and from this circularised DNA, primers from inside the known disruption cassette are used to PCR amplify the disrupted gene surrounding the insert. G) Sequencing of this amplified section allows the identification of the site of genomic integration.

1.11 Aims and objectives

The aim of this project was to investigate novel molecular targets for the medium-chain fatty acid, decanoic acid, provided by the MCT ketogenic diet. In order to achieve this, a molecular genetics approach was employed to screen a *Dictyostelium* mutant library for mutants resistant to the effects of decanoic acid. A role for the identified genes in the cellular response to decanoic acid were confirmed using independent gene knockouts, and the wider molecular pathways implicated by these genes were investigated for potential therapeutic benefits. Finally, novel findings from *Dictyostelium* were confirmed in a rat hippocampal slice model and in patient derived astrocytes.

Chapter 2

Materials and methods

2.1 **Cell culture**

Dictyostelium cell lines were stored at -80°C in freezing medium (Horse serum, 7% DMSO (VWR, VWRV0231)). Every month cells were taken from storage and grown on SM agar plates (ForMedium, SMA0102) in association with *Raoultella planticola* or axenically in HL5 media (ForMedium, HLB0103) with 10% glucose (Sigma, G8270). HL5 media was supplemented with 100 units/ml penicillin and 100 µg/ml streptomycin (Thermo Fisher Scientific, 15140122), and cells were maintained at 22°C in shaking suspension at 220 rpm in flasks, or without shaking in tissue culture dishes.

2.2 Growth assays

Cells were washed from a confluent 9 cm dish and diluted to 2 x 10^4 cells/ml in HL5. Stocks of decanoic acid (Alfa Aesar, A14788), octanoic acid (Alfa Aesar, A11149) and 4-BCCA (Tokyo Chemical Industry, B1136) were made in DMSO to a final concentration of 1 M. Compound stocks (1 M) or DMSO as a solvent control, were added to 500 µl of cells (in triplicate) in a 24 well plate, to achieve final concentrations of 0 - 125 µM (0.2 % final DMSO concentration). Cells were incubated at 22°C and counted at 24-hour intervals after the first 74 hours.

2.3 Development assay on nitrocellulose filters

Exponentially growing *Dictyostelium* cells were harvested by centrifugation at 500 g for 3 min, washed twice in KK2 and resuspended in KK2 at a density of 1 x 10^7 cells/ml. Cells (1 ml) were pipetted evenly onto a whole nitrocellulose filter (Millipore, HABP04700) on top of Whatman® cellulose chromatography paper (Sigma, WHA3030917) allowing the absorption of excess KK2. Millipore absorbent pads (Merck, AP1004700), were cut into quarters and placed in to 2 ml culture dishes and soaked with 500 µl of compound or control. The nitrocellulose membranes supporting cells were cut into quarters and transferred onto the compound soaked absorbent pads. Cells were then left in a humid environment at 22°C for 22 hours, before developmental morphology was observed using a dissection microscope (Leica) and a QICAM FAST 1394 camera (QImaging).

2.4 Electroporation procedure

Exponentially growing *Dictyostelium* cells were harvested, washed three times with ice-cold electroporation buffer (H50) and resuspended to a density of 5 x 10^7 cells/ml. Cells (100 µl) were mixed with 4 µg to 8 µg of plasmid and left to rest on ice for 5 minutes, followed by exposure to two consecutive pulses of 650 V (capacitance- 25 µF) with a 5 second recovery between pulses in a chilled 1 mm gap electroporation cuvette (Sigma, Z706078-50EA). Cells were left on ice for 5 min before plating in HL5. Transfected knockout cells were selected for with 10 µg/ml blasticidin (BS) (Apollo Scientific, BIB4432) in 96 well plates, and overexpressor cells were selected for with 10 µg/ml G418 (Geneticin) (Sigma, A1720) or 10 µg/ml hygromycin (InvivoGen, ant-hg-5) in 10 cm dishes.

2.5 Molecular biology methods

2.5.1 Restriction digests

Restriction digests were carried out according to manufacturer's protocol (all restriction enzymes were obtained from Thermo Fisher Scientific). In cases where multiple enzymes were required, appropriate buffer conditions were found using the DoubleDigest Calculator—Thermo Fisher Scientific.

2.5.2 Polymerase chain reaction

Amplification of DNA was carried out using GoTaq® G2 Flexi DNA Polymerase (Promega, M7801), or Q5 high fidelity DNA polymerase (New England Biolabs, M0491). For routine PCR with GoTaq® G2 Flexi DNA Polymerase, a standard 20 µl reaction was carried out containing 0.5 µg DNA template, 4 µl 5x GoTaq® Flexi Buffer, 2 mM $MgCl_2$, 0.5 mM dNTP mix, 0.5 µM primers, 0.1 µl GoTaq® G2 Flexi DNA Polymerase (5 U/µl), made up to 20 µl with nuclease-free water (Sigma, W4502). For PCR reactions requiring proofreading activity Q5® high fidelity DNA polymerase was used in a 20 µl reaction containing 0.5 µg DNA template, 0.5 µM primers, 4 µl 5x Q5 buffer, 0.5 mM dNTP mix, 0.2 µl Q5® DNA polymerase (2 U/µl), made up to 20 µl nuclease-free water. DNA amplifications were carried out using PCR with an initial denaturing step for step for 1 minute at 95°C, followed by 32 cycles of 95°C for 30

seconds (denaturation), 50-65°C (depending on primers) for 30 seconds (annealing) and 68°C for 1 minute per 1000 bps (extension) before a final extension step at 68°C for 10 minutes.

2.5.3 Agarose gel electrophoresis

Gel electrophoresis was used to separate and visualise DNA. Gels were made containing 1% agarose (Bioline, B10-41026) with TAE buffer (Severn Biotech Limited, 20-6001-50) and ethidium bromide (Bio-Rad, 1610433). 5x loading buffer (Bioline, BIO-37045) was added to DNA samples before running, and 1 kb plus hyperladder (Bioline, BIO-33026) was used as a marker for DNA size. Gels were run at 100 V for 30 minutes in TAE buffer. DNA was visualised using UV.

2.6 Mutant library screen

A *Dictyostelium* REMI mutant library containing 28000 insertional mutants was provided by Professor Harwood (Cardiff University) and Professor Thompson (Manchester University). This library was created using Ax4 cells transfected with the restriction enzymes DpnII and NlaIII and linearized DNA (REMI plasmid digested with BamH1) containing the blasticidin resistance (BSR) sequence. This process facilitated the incorporation of the BSR DNA into the genome at compatible sites, thus disrupting the genes at the sites of integration (Fig. 1.6A and B). Mutants were selected for in the presence of blasticidin.

To select for resistant mutants, the library was screened alongside Ax4 as a control. Mutant library cells or control Ax4 cells at 1.25 x 10^4 cells/ml were prepared in either compound or 0.5% DMSO control. Cells (2 ml) were added to each well of a 6 well plate resulting in 2.5 x 10^4 cells/well. Plates were left to grow until resistant colonies appeared, with the media being replaced every 3 days (Fig. 1.6D).

Once colonies appeared in the mutant library wells, these colonies were isolated and grown up on *Raoultella planticola* SM agar plates to allow selection of isogenic colonies. Isogenic colonies were selected from the bacterial plates and the rate of growth of these colonies in compound was compared to that of the REMI library and wild type (Ax4) to confirm resistance.

2.6.1 Identifying disrupted genes

Genomic DNA (gDNA) extraction of the resistant *Dictyostelium* mutants was carried out using Qiagen DNeasy kit (Qiagen, 69504) according to manufacturer's protocol. gDNA (10 µl) was digested with 5 units of Rsa1 (Thermo Fisher Scientific, ER1122) at 37 ºC for 2 hours in Tango buffer (Thermo Fisher Scientific, BY5). The digest was purified by ethanol precipitation using 0.1 x 3 M sodium acetate (Sigma, S2889) and 2x 100 % Ethanol (VWR, 20821.330DP) to precipitate the DNA at -20° which was then collected by centrifugation at 16,000g for 15 minutes. The DNA was then resuspended in nuclease-free water and circularised by ligation with T4 DNA ligase (Fermentas, 15224041) at room temperature for 1 hour (0.5 µl ligase per 10 µl reaction). The genomic sequence flanking the BsR insertion site was amplified by PCR with primers p09 and p10 (or p11 and p13) (Fig. 2.2) with an annealing temperature of 50°C.

PCR products were either spin column purified (Qiagen, 28104), according to manufacturer's protocol, and sent directly for sequencing or were ligated into the TOPO pCR® 2.1 vector and cloned into competent *E. coli* (TOP10) using TOPO TA Cloning® kit (Invitrogen, K450002) according to manufacturer's protocol. Plasmid DNA was isolated from the bacteria using the Qiagen miniprep kit (Qiagen, 27104) according to manufacturer's protocol. This DNA was then sequenced using the sequencing primers T7 and M13 (Fig. 2.2).

2.7 Bioinformatics

2.7.1 Protein sequence analysis

Sequences of proteins were taken from dictybase (http://dictybase.org) or uniprot (http://www.uniprot.org). Regions of similarity between proteins were found using the Basic Local Alignment Search Tool (BLAST) (https://blast.ncbi.nlm.nih.gov). Sequences were aligned using Clustal (http://www.ebi.ac.uk/Tools/msa/clustalo/) which annotates sequence homology results across the whole protein. The program MEGA 7 was used to generate neighbour joining phylogenetic trees from these alignments (http://www.megasoftware.net). Domains were identified based on

annotations from InterPro (https://www.ebi.ac.uk/interp ro/) and Oma Browser (http://omabrowser.org/oma/home/).

2.7.2 Predicted protein-ligand docking analysis

The tertiary structure of the *Dictyostelium* UBXD18 protein was predicted using Phyre2 (protein Homology and Analogy Recognition Engine V2.0) in the intensive modelling mode (Kelley *et al.*, 2015). SwissDock was used to provide protein docking predictions for decanoic acid and octanoic acid (Grosdidier, Zoete and Michielin, 2011a; Grosdidier, Zoete and Michielin, 2011b). Predicted docking files were visualised using UCSF chimera.

2.8 Knockout generation

2.8.1 Generation of knockout construct

Two techniques were employed for knockout generation. To knockout the gene *ubxd18* (official gene name *DDB_G0276057*) a knockout cassette was generated by PCR amplification over the REMI insert site of the REMI mutant DNA. This generated a construct with approximately 500 bp of gene homology on either side of the REMI insert sequence conveying blasticidin resistance. The PCR product was purified by spin column according to the manufacturer's protocol (Qiagen, 28104), then 6 µg was electroporated into *Dictyostelium* cells. This resulted in disruption of the *ubxd18* gene through homologous recombination.

To knockout the transketolase gene (*tkt*) a knockout construct was generated by PCR amplifying two sequences (arms) of approximately 500 bp from the 5' and 3' regions of the *tkt* gene sequence. A BamH1 site was inserted at the 5' end of the 5' arm and a pstI site at the 3' end of this arm. A Nco1 site was inserted at the 5' end of the 3' arm and a HindIII site at the 3' end of this arm. These arms were cloned sequentially into the pLPBLP vector at sites flanking the gene for blasticidin resistance (BSR). This process generated a disruption fragment with arms homologous to *tkt* flanking the BSR gene. Transfection of 6 µg of this knockout construct into wild type *Dictyostelium* resulted in disruption of the *tkt* gene via homologous recombination.

2.8.2 Screening for knockout cell lines

Cells transfected with the knockout constructs were grown in HL5 supplemented with 10 µg/ml of blasticidin in several 96 well plates. Cells resistant to blasticidin were collected and centrifuged in PCR tubes before lysis in 24 µl lyse B buffer and 1 µl proteinase K (Fermentas, EO0491). Cells were incubated at room temperature for 5 minutes before heat inactivation at 95°C for 5 minutes. The resulting cell lysate was used in PCR analysis to identify successful homologous recombinants. To screen for a *ubxd18* knockout, primers were designed that would generate 7 diagnostic fragments unique to the knockout (Fig. 2.2). To screen for a *tkt* gene knockout, primers were designed that would generate 6 diagnostic fragments (Fig. 2.2)

2.8.3 RT-PCR to confirm knockout

RNA was extracted from the wild type and the knockout cell lines using RNeasy mini kit (Qiagen, 74104) according to the manufacturer's protocol. DNA was removed from the RNA using the DNA-free kit (Invitrogen, AM1906) according to the manufacturer's protocol. cDNA was synthesised using the RevertAid First Strand cDNA Synthesis Kit using oligo(dT)18 primers (Thermo Fisher Scientific, K1621) according to the manufacturer's protocol. PCR amplification of the knockout gene and *Ig7* (positive control, DDB_G0294034) was carried out (Fig. 2.2).

2.8.4 qPCR to confirm knockdown

RNA was extracted from the wild type and the knockout cell lines using RNeasy mini kit (Qiagen, 74104) according to the manufacturer's protocol. DNA was removed from the RNA using the DNA-free kit (Invitrogen, AM1906) according to the manufacturer's protocol. cDNA was synthesised using the RevertAid First Strand cDNA Synthesis Kit using oligo(dT)18 primers (Thermo Fisher Scientific, K1621) according to the manufacturer's protocol. qPCR was carried out using primers within the region of *tkt* disrupted in the *tkt* null cell line (*TKT*$^{-}$) and the *Ig7* gene was used as an internal control (Fig. 2.2). qPCR was carried out using SYBR® Green JumpStart™ Taq ReadyMix™ (Sigma, S4438), and relative quantification was carried out using the $2^{-\Delta\Delta Ct}$ method.

2.9 Generation of overexpressor cell lines

2.9.1 Creation of GFP-UBXD18, GFP-FcsA and p97-RFP constructs

RNA was extracted from wild type cells using the RNeasy mini kit (Qiagen, 74104) according to the manufacturer's protocol. DNA was removed from the RNA using the DNA-free kit (Invitrogen, AM1906) according to the manufacturer's protocol. cDNA was synthesised using the RevertAid First Strand cDNA Synthesis Kit using oligo(dT)18 primers (Thermo Fisher Scientific, K1621) according to the manufacturer's protocol. *ubxd18*, *fcsA* or *p97* cDNA was amplified using primers designed to amplify the whole length of the coding sequence (Fig. 2.2). *ubxd18, fcsA* or *p97* cDNA was cloned into extrachromosomal vectors (ptx-GFP, ptx-GFP and pdm451-RFP respectively) and the resulting plasmids were sequenced by sanger sequencing to confirm that no mutations were introduced, before electroporation into *Dictyostelium* cells. Transfected overexpressor cells were selected for with 10 µg/ml G418 (ptx-GFP) or 10 µg/ml hygromycin (InvivoGen, ant-hg-1) (pdm451-RFP).

2.9.2 Western blotting for GFP-tagged and RFP-tagged proteins

Western blotting for GFP-tagged and RFP-tagged proteins was used to confirm functionality of expression constructs. Whole cell lysates were prepared harvesting cells by centrifugation at 500 g for 3 min followed by lysis in RIPA buffer (10×10^7 cells/ml) containing protease inhibitor (Roche, 04693159001), before mixing 1:1 in 2x laemmli buffer resulting in 5×10^7 cells/ml. Lysates were boiled in laemmli at 95°C for 5 minutes before vortexing, and centrifuging at max speed for 5 minutes. Samples (8 µl) were fractioned using a 12.5 % gel, and transferred to a PVDF membrane (Millipore, IPFL00010) by wet transfer using transfer apparatus according to the manufacturer's protocols (Bio-Rad, UK). After incubation with 5% BSA (Thermo Fisher Scientific, AM2616) in PBS (Thermo Fisher Scientific, 10010023) for 60 min, the membrane was incubated in 5% BSA in PBS with antibodies against GFP (Chromotek, 3H9, 1:1000) or RFP (Chromotek, 5F8, 1:1000) at 4°C overnight. Membranes were washed in PBST and incubated with a 1:10000 dilution of odyssey goat anti-rat IR DYE 800 (Li-Cor Biosciences, UK), and 1 in 10000 streptavidin (Thermo Fisher Scientific,

UK) in 5 % BSA in PBS for 1h. Blots were washed in PBST and visualised using the Odyssey CLx imager (LI-COR).

2.10 Fluorescent microscopy

Cells expressing the fluorescently tagged proteins GFP-UBXD18, GFP-FcsA and p97-RFP were assessed using fluorescent microscopy. Cells were washed and resuspended in KK2 before being photographed under 1 % KK2 agar (Sigma, A5306) using an Olympus IX71 wide-field fluorescence microscope at 96 x magnification. Images were captured using a QICAM FAST 1394 camera.

2.11 Methanol fixation and immunofluorescence

Glass coverslips were prepared by submersion in 50 % nitric acid (VWR, 20425.242) for two hours, before the nitric acid was decanted and the coverslips were washed 10 times in 100 % ethanol. Coverslips were placed into the base of a 12 well plate and cells in liquid media added and allowed to adhere overnight. The next day coverslips supporting adhered cells were briefly dabbed on tissue to remove excess media then plunged into -80°C methanol (Sigma, 179337). Fixed coverslips were then placed into a rack at the base of the ultra-cold methanol beaker for 30 minutes. Coverslips were removed and plunged 4 times into a beaker of room temperature PBS (Thermo Fisher Scientific, 10010023). Cells were then blocked for 30 minutes by inverting each coverslip onto a 50 µl drop of 5 % BSA (Thermo Fisher Scientific, AM2616) in PBS on a piece of para-film (Sigma, P7793). Excess blocking agent was removed, and the coverslip was inverted onto a second 50 µl drop of PBS containing 5 % BSA and primary antibodies (GFP tag monoclonal mouse (Proteintech, 66002-1), and RFP antibody rat (chromotek, 5F8)). After incubation with primary antibodies for 1 hour, the coverslips were washed twice by placing coverslips in the well of a 12 well plate containing 3 ml of PBS and soaked for 5 minutes each time. Coverslips were then inverted onto a 50 µl drop of PBS containing 5 % BSA and secondary antibodies (goat anti mouse alexafluor 568 IgG (Thermo Fisher Scientific, A-11004), rabbit anti rat alexafluor 488 IgG (Thermo Fisher Scientific, A-21210). After incubation for 1 hour, the coverslips were washed twice in PBS as before, plus a final wash in ddH2O to remove excess salt. All coverslips were mounted onto glass slides

using Fluoromount-GTM, with DAPI (Thermo Fisher Scientific, 00-4959-52). Fluorescent images were obtained using an Olympus IX71 wide-field fluorescence microscope. Images were captured using a QICAM FAST 1394 camera.

2.12 Immunoprecipitation

GFP-Trap®A beads were used for Immunoprecipitation of GFP-fusion proteins according to the manufacturer's protocol (Chromotek, gta). Briefly, *Dictyostelium* cells (1×10^7) co-expressing the indicated GFP-tagged and the RFP-tagged proteins were pelleted and washed in nutrient free phosphate buffer (KK2) before being suspended in GFP-trap Lysis buffer. The extract was centrifuged, and the pellet was discarded. The lysate was diluted with dilution buffer and incubated for 1 hour at 4°C with GFP-trap beads (Chromotek, gta). The beads were washed with dilution buffer, suspended in laemmli and boiled at 100°C for 5 min before running on an SDS-PAGE gel for analysis (as described 2.9.2).

2.13 ATPase assay

Dictyostelium cells (wild type or *UBXD18*$^-$ expressing p97-RFP) in the exponential phase of growth were treated for 24 hours with compound (60 µM decanoic acid, 120 µM octanoic acid or 7.5 µM p97 inhibitor DBeQ (Tocris Bioscience, 4417). RFP-Trap®A beads were used for the immunoprecipitation of RFP-tagged proteins (p97-RFP) (Chromotek, rta). Following immunoprecipitation the RFP-Trap®A beads were washed with dilution buffer, and suspended in 10 µl HNG buffer, and used for ATPase activity analysis using the malachite green phosphate assay kit (Sigma, MAK307) according to published methodology (Rule et al., 2016) and manufacturer's procedure. Briefly, ATP hydrolysis reactions were set up using 5 µl of RFP-Trap®A beads, 6 µl of 5x HNG buffer, 1.5 µl of $MgCl_2$ (100 µM) (Sigma, M8266) and 1.5 µl of ATP (100 µM) (Sigma, A2383), and 16 µl H_2O. The reaction was incubated at 37°C for one hour with 5 µl aliquots removed at 15-minute intervals and diluted 1:50 in HNG buffer before freezing on dry ice. Free phosphate concentrations were assessed using the malachite green phosphate assay kit according to manufacturer's instructions (Sigma, MAK307). Phosphate concentrations were standardised to protein concentration measured directly on the beads using a Bradford assay.

2.14 Autophagy quantification

Cells transfected with a vector designed to express *atg8a* with an N-terminal GFP tag, GFP-Atg8, were set up at a density of 1.33 x 10^6 cells/ml in 6 well plates. Cells were pre-treated with decanoic acid (60 μM), octanoic acid (120 μM) or DMSO control for 22 hours or 2 hours to provide final treatment durations of 24 and 4 hours. Autophagy inducer AR-12 (Selleckchem, OSU-03012), or DMSO control, was added and shaking was continued for 1 hour before addition of protease inhibitors (Roche, 11873580001) at a final concentration of 2.5-fold, or HL5 control. Shaking was continued for 1 hour before cells were removed (without additional pipetting) to tubes on ice. Cells were put aside for microscopy or were centrifuged for 3 min at 500 g at 4°C and prepared for western blot analysis of GFP levels (as described 2.9.2). Western blots were normalised to loading control (MCCC1) and free gfp/MCCC1 and GFP-Atg8/MCCC1 values were adjusted to the average readout for each blot.

2.14.1 Microscopy analysis of autophagosomes

For live-cell imaging, cells were washed and resuspended in KK2 and were imaged under a layer of 1 % KK2 agar. Time in KK2 and time under agar was kept constant between each condition (20 minutes in KK2, and 5 minutes under agar). Cells were imaged on an Olympus IX71 wide-field fluorescence microscope. Images were captured using a QICAM FAST 1394 camera. For size and number measurement of GFP-Atg8-positive structures (autophagosomes), images were analysed using ImageJ and GFP-Atg8-positive structures were measured across the largest diameter. Thirty cells or autophagsomes were analysed per experiment.

2.14.2 qPCR analysis of autophagy genes

Exponentially growing cells were treated for 1, 4 or 24 hours with either decanoic acid (60 μM), octanoic acid (120 μM) or solvent (DMSO) control). RNA was extracted from these samples using the RNeasy mini kit (Qiagen, 74104) according to the manufacturer's protocol. DNA was removed from the RNA using the DNA-free kit (Invitrogen, AM1906) according to the manufacturer's protocol. cDNA was synthesised using the RevertAid First Strand cDNA Synthesis Kit using oligo(dT)18 primers (Thermo Fisher Scientific, K1621) according to the manufacturer's protocol.

qPCR was carried out using primers within the genes for *atg8a* and *atg1*, and the *gapdh* gene was used as an internal control (Fig. 2.2). qPCR was carried out using SYBR® Green JumpStart™ Taq ReadyMix™ (Sigma, S4438), and relative quantification was carried out using the $2^{-\Delta\Delta Ct}$method.

2.15 Detection of PIP_3 production

Cells expressing green fluorescent protein (GFP) fused to the pleckstrin homology domain of cytosolic regulator of adenylyl cyclase (PHCRAC-GFP) (Nichols *et al.*, 2019) were made chemotactically competent as described (Kamimura, Tang and Devreotes, 2009). Briefly, cells were washed twice in development buffer (DB) before being resuspended in DB to 2 x 10^7 cells/ml and rotated for 1 hour at 110 rpm. Cells were pulsed with 60 nM of cAMP (Sigma, A6885) every 6 mins for 4 hours, in the presence or absence of compound (60 µM decanoic acid or octanoic acid). Cells were basalated by the addition of caffeine (Sigma, C0750) to a final concentration of 5 mM, with rotation at 200 rpm for 30 mins, before being washed twice in cold DB buffer and resuspended to 2 x 10^7 cells/ml. For time-lapse imaging of PIP_3 production, 360 µl chemotactically competent cells expressing PHCRAC-GFP at 5 x 10^5 cells/ml were placed into a well of a 8-well chambered cover glass (Thermo Fisher Scientific, 10384221) (PI3K inhibitor, LY294002 (Selleckchem, S1105) was added to one sample at a final concentration of 100 µM), and left to adhere for 10 minutes. Cells were stimulated by adding cAMP, to a final concentration of 1 µM, and images were captured every 2 seconds for 1 minute, using an Olympus IX71 wide-field fluorescence microscope and QICAM FAST 1394 camera. Images were analyzed using ImageJ where mean gray value of the cell membrane was quantified over time and adjusted relative to mean gray value of the whole cell.

2.16 Analysis of mTORC1 signalling

2.16.1 Preparation of *Dictyostelium* samples for western blot

Dictyostelium cells were treated as specified before centrifugation at 500 g for 3 min followed by direct cell lysis in 2x laemmli (7.5 x 10^7 cells/ml). Samples were

boiled at 98°C for 6.5 minutes, centrifuged at max speed and 6 µl (equivalent to 30 µg) was loaded onto an SDS-PAGE gel.

2.16.2 Preparation of rat hippocampal slices for western blot

Rat hippocampal slices were prepared by Dr Eleonora Lugarà in the lab of Professor Mathew C Walker at the Department of Clinical and Experimental Epilepsy, Institute of Neurology, University College London, as described. Sprague Dawley rats (approximately 270 g, males and females) were deeply anesthetised with 2% to 3% isoflurane in oxygen (2 L/min) and once unresponsive to toe and tail pinch, the animal was decapitated. The brain was quickly removed and placed in a glass Petri dish filled with bubbled ice cold artificial cerebral spinal fluid (125 mM NaCl, 26 mM $NHCO_3$, 15 mM Glucose, 1.25 mM NaH_2PO_4, 2.5 mM KCl, 1.3 mM $MgSO_4$ 7 H_2O, 2 mM $CaCl_2$, pH 7.4 and osmolality 305-310 mOsm). Coronal slices (350 µm) were sliced with a Leica VT1200 vibrating blade microtome. Hippocampal slices were quickly transferred to submerged chambers (95 % O_2, 5 % CO_2) containing either artificial cerebral spinal fluid only or artificial cerebral spinal fluid with solvent control (DMSO), 100 µM or 300 µM Decanoic acid (Sigma Aldrich #C1875) in DMSO. The chambers were placed into a warm bath (34°C) for 20 minutes and then moved at room temperature for 40 min in carbonated standard recording cerebral spinal fluid. Samples were snap frozen in liquid nitrogen and lysed in a mixture of RIPA buffer (150 mM sodium chloride, 1.0 % Triton X-100, 0.5% sodium deoxycholate, 0.1% sodium dodecyl sulfate, 50 mM Tris, pH 8.0. Sigma Aldrich, R0278) and protease inhibitors (Thermo Fisher Scientific, #A32963). The tissue was mechanically disrupted by a mechanical rotor type homogenizer (FastPrep-24, MP Biomedicals LLC) with the use of homogenizer beads (SLS Scientific Laboratory Supplies, D1031-01). The samples were then centrifuged at max speed for 10 minutes, the pellet discarded and stored at -80°C. All further analysis was carried out by Eleanor Warren. Protein concentrations were determined by Bradford assay. Samples were mixed 1:1 with 2x laemmli and centrifuged at max speed for 10 minutes at 4ºC before 15 µg of protein was analysed by western blot (without boiling).

2.16.3 Patient derived astrocyte differentiation and preparation for western blot

Patient derived astrocytes were prepared by Dr Stephanie Dooves, in the lab of Professor Vivi M Heine, at Vrije Universiteit Amsterdam, as described. iPSCs from 3 individual control patients (hVS-228, hVS-420, and hVS-421), 2 patients with *TSC1* mutations (*TSC1*$^{-}$) (hVS233, and hVS-401), and 2 patients with *TSC2* mutations (*TSC2*$^{-}$) (hVS-417, hVS-424), were differentiated into astrocytes as described in Nadadhur et al. (2018) (Nadadhur *et al.*, 2018). At day 45 of the differentiation protocol cells were switched to Sanbio medium to form a pure astrocyte culture and maintained until day 76. At day 76 astrocytes were plated on geltrex coated 12 well plates in Sanbio astrocyte medium and allowed to recover from plating. At day 80, half of the medium was refreshed with Sanbio astrocyte medium containing either decanoic acid (final concentration in well: 300 µM) or DMSO. After 24 hours, cells were harvested by removing medium, adding 50 µl lysis buffer (50 mM HEPES, 150mM NaCl, 1mM EDTA, 2.5 mM EGTA, 0.1 % Triton X-100, 10 % glycerol, 1mM DTT, 1x protease inhibitor, 1x phosphatase inhibitor) per well on ice and scraping cells off the plate. Cells from each well were collected in a tube and frozen at -80°C (n = 12 per patient). All further analysis was carried out by Eleanor Warren. Protein concentrations were determined by Bradford assay. Samples were mixed 1:1 with 2x laemmli and centrifuged at max speed for 10 minutes at 4°C before 7.5 µg of protein was analysed by western blot (without boiling).

2.16.4 Western blotting for p-4E-BP1, total-4E-BP1, p-ATK-substrate, p-AMPK, p-S6K and total-S6K

Samples were fractioned using a 15 % gel for p-4E-BP1, total-4E-BP1 and p-AKT-substrate and a 10 % gel for p-AMPK, total-AKT, p-AKT(Ser473), p-AKT (Thr308), p-S6K and total-S6K. Proteins were transferred to a 0.2 µm polyvinylidene difluoride membrane (Thermo Fisher Scientific, 88520) (p-4E-BP1 and total-4E-BP1), a 0.45 µm polyvinylidene difluoride (Millipore, IPFL00010) (p-AKT-substrate), or a 0.2 µm nitrocellulose membrane (Thermo Fisher Scientific, 15249794) (p-AMPK, total-AKT, p-AKT(Ser473), p-AKT (Thr308), p-S6K and total-S6K) by wet transfer at 15 Volts overnight (p-4E-BP1 and total-4E-BP1) or 90 Volts for 90 minutes (p-AKT substrate, p-AMPK, total-AKT, p-AKT (Ser473), p-AKT (Thr308), p-S6K and total-S6K) using transfer

apparatus according to the manufacturer's protocols (Bio-Rad, UK). After incubation with 5% milk in TBS for 1 to 4 hours, the membranes were incubated in 5% milk in TBST with antibodies against p-4E-BP1 (1:1000 p-4E-BP1(Thr37/46) rabbit antibody, cell signalling technology, 9459S), total-4E-BP1 (1:1000 non-phospho-4E-BP1 (Thr46) rabbit antibody, cell signalling technology, 4923), p-AKT substrate (1:1000 Phospho-Akt Substrate rabbit antibody, cell signalling technology 10001), p-AMPK (1:2000 Phospho-AMPKα (Thr172) (40H9) rabbit antibody, cell signalling technology 2535), or p-S6K (1:1000, Phospho-p70 ribosomal protein S6 kinase (Thr421/Ser424) rabbit antibody, 9204) or total-S6K (1:1000, p70 ribosomal protein S6 Kinase rabbit antibody, 9202), and streptavidin (1:5000 Streptavidin, Alexa Fluor™ 680 conjugate, Thermo Fisher Scientific, S21378) as a loading control for *Dictyostelium* samples, or β-Actin (Sigma, A1978) as a loading control for rat hippocampal samples and astrocytes at 4°C overnight. Alternatively, membranes were incubated with 5% BSA in TBS for 1 hour before incubation with antibodies against p-AKT (Ser473) (1:2000 Phospho-AKT (Ser473) rabbit antibody, cell signalling technology, 4060), p-AKT (Thr308) (1:1000 Phospho-AKT (Thr308) rabbit antibody, cell signalling technology, 9275), or total-AKT (1:5000 AKT rabbit antibody, cell signalling technology 9272) at 4°C overnight. The next day membranes were washed in TBST and incubated with a 1:2000 dilution of polyclonal goat anti-rabbit immunoglobulins/HRP (Agilent Technologies, DAKO P0448) (for p-4E-BP1, total 4E-BP1, and p-S6K) or a 1:10000 dilution of IRDye® 800CW goat anti-rabbit IgG secondary antibody (LI-COR, 925-3221) (for p-AKT-substrate, total-AKT, p-AKT (Ser473), p-AKT (Thr308), p-AMPK and total-S6K), and a 1:10000 goat anti-mouse antibody (Cell signalling technology, 5470) (for β-Actin) in 5% milk or BSA (as described) in TBST for 1 hour (Fig. 2.1). Blots were washed in TBST and visualised using the Odyssey CLx imager (LI-COR). For p-4E-BP1, total-4E-BP1 and p-S6K Odyssey chemifluorescent substrate kit (Li-Cor Biosciences, Odyssey®Chemifluorescent Substrate Kit 928-30005) was used according to the manufacturer's protocols.

2.17 Statistical analysis

The distribution of all experimental data was tested using the D'Agostino and Pearson omnibus normality test. Independent data showing a Gaussian distribution

were analysed using parametric tests. Normally distributed data from two groups were statistically analysed using two-tailed unpaired t-tests. The one-way ANOVA statistical test was used to test for significance between the means of three or more independent groups of normally distributed data, in conjunction with Dunnett's post hoc test. Two-tailed non-parametric Mann-Whitney tests were used to assess significance between independent samples from two groups not showing a Gaussian distribution. The Kruskal-Wallis test with Dunn's post hoc test was used to test significance between three or more independent groups of data not showing a Gaussian distribution. Western blot data from patient derived astrocytes showed a Gaussian distribution and were analysed using nested t-tests to account for a lack of independence between astrocytes from individual patients cultured in separate wells. Throughout this thesis where no significance is indicated, $p > 0.05$. Statistical analysis was carried out using GraphPad Prism Software.

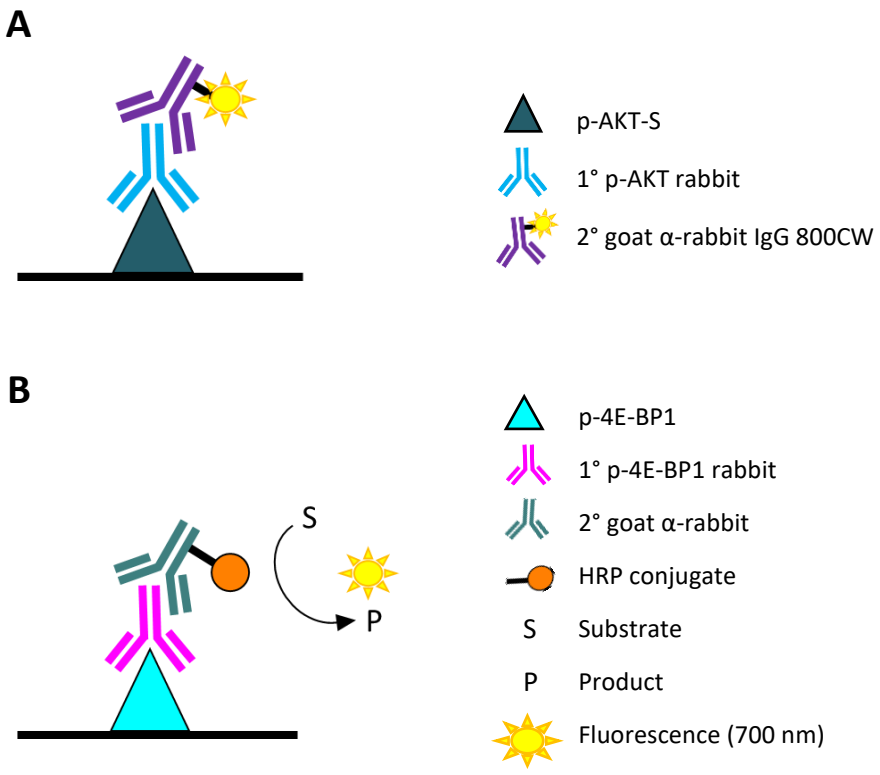

Figure 2. 1 Western blotting antibody types used. A) For western blotting (e.g. p-AKT-S) we used secondary antibodies conjugated to fluorescent dyes (e.g. goat α-rabbit IgG 800CW) for direct detection at 700 nm or 800 nm. B) When monitoring difficult to detect small phospho-proteins (e.g. p-4E-BP1) we employed a secondary antibody conjugated to horseradish peroxidase (HRP) (e.g. goat α-rabbit-HRP), in combination with a chemifluorescent substrate (S). HRP catalyses the conversion of the substrate (S) into a stable fluorescent compound (P) that can be detected at 700 nm allowing improved sensitivity over near infrared antibody detection.

2.18 Buffers, gels and reagents

Bradford reagent

50 mg Coomassie Brilliant Blue G-250 (Sigma, 1154440025), 50 ml Methanol (Sigma, 179337), 100 ml 85% (w/v) phosphoric acid (Sigma, W290017), 850 ml H_2O.

Development buffer (DB)

100 ml 10 × phosphate buffer, 1 ml 2 M $MgSO_4$ (Sigma, M7506), 0.2 ml 1 M $CaCl_2$ (Sigma, 449709), 989.8 ml H_2O.

GFP trap dilution buffer

10 mM Tris/HCl pH 7.5 (Trizma-Sigma, T1503) (HCl-VWR, 20252), 150 mM NaCl, 0.5 mM EDTA (Sigma, E9884).

GFP trap lysis buffer

10 mM Tris/HCl pH 7.5 (Trizma-Sigma, T1503) (HCl-VWR, 20252), 150 mM NaCl (Sigma, S9888), 0.5 mM EDTA (Sigma, E9884), 0.5% NP-40 substitute (Sigma, 74385).

H50 buffer

20 mM HEPES (Sigma, H3375), 50 mM KCl (Sigma, P9333), 10 mM NaCl (Sigma, S9888), 1 mM $MgSO_4$ (Sigma, M7506), 5 mM $NaHCO_3$ (Sigma, S5761), 1 mM NaH_2PO_4 (Sigma, S8282), pH 7.0.

HNG Buffer

20 mM HEPES pH 8.5 (Sigma, H3375), 13 mM NaCl (Sigma, S9888), 1 % glycerol (Sigma, G2025).

Laemmli (2x)

0.001 g Bromophenol blue (Sigma, B0126), 3 ml 2-mercaptoethanol (Sigma, M6250), 6 ml 100% glycerol (Sigma, G2025), 12 ml 10% SDS (Sigma, L5750), 7.5 ml Tris-HCl (0.5 M pH 6.8) (Trizma-Sigma, T1503)(HCl-VWR, 20252), 1.5 ml H_2O.

Lyse B

10 mM TRIS-HCl pH 8.3 (Trizma-Sigma, T1503) (HCl-VWR, 20252), 50 mM KCl (Sigma, P9333), 2.5 mM $MgCl_2$ (Sigma, M8266), 0.45% TWEEN (Sigma, P1379), 0.45% NP40 substitute (Sigma, 74385).

Nutrient free phosphate buffer (KK2)

6.2 mM KH_2PO_4 (Sigma, NIST200B), 4 mM K_2HPO_4 (Sigma, 1551128).

PBST

0.1 % Tween20 (Sigma, P1379) in 1 Litre phosphate-buffered saline (PBS) (Thermo Fisher Scientific, 10010023).

Phosphate buffer (10X)

6.8 g KH_2PO_4 (Sigma, NIST200B), 13.4 g $Na_2HPO_4 \cdot 7H_2O$ (Sigma, 431478), H_2O to 1 litre.

Radioimmunoprecipitation assay buffer (RIPA)

10 mM Tris/Cl pH 7.5, (Trizma-Sigma, T1503) (HCl-VWR, 20252), 150 mM NaCl (Sigma, S9888), 0.5 mM EDTA (Sigma, E9884), 0.1 % SDS, (Sigma, L5750), 1 % Triton X-100 (Sigma, X100), 1 % Deoxycholate (Sigma, D6750).

Resolving gel (10 %)

3.3 ml acrylamide (Sigma, 1006391000), 2.5 ml Tris-HCl (1.5 M pH 8.8) (Trizma-Sigma, T1503) (HCl-VWR, 20252), 4 ml dH_20, 100 µl 10 % SDS (Sigma, L5750), 100 µl Ammonium persulphate (Sigma, A3678), 4 µl TEMED (Sigma, T9281).

Resolving gel (12.5 %)

4.15 ml acrylamide, 2.5 ml Tris-HCl (1.5 M pH 8.8), 3.15 ml H_20, 100 µl 10 % SDS, 100 µl Ammonium persulphate, 4 µl TEMED.

Resolving gel (15 %)

5 ml acrylamide, 2.5 ml Tris-HCl (1.5 M pH 8.8), 2.3 ml H_20, 100 µl 10 % SDS, 100 µl Ammonium persulphate, 4 µl TEMED.

Stacking gel

212.5 µl acrylamide, 78.75 µl Tris-HCl (0.5 M pH 6.8), 0.938 µl dH_20, 12.5 µl 10 % SDS, 12.5 µl 10 % APS, 3.75 µl TEMED.

TBST

0.1 % Tween20 in 1 Litre Tris-buffered saline (TBS) (Thermo Fisher Scientific, 10776834).

2.19 Primers

All primers were obtained from Sigma.

Figure 2. 2 Table of primers.

No.	Primer name	Use	Sequence (Restriction sites, underlined)	Cut site
1	p9	Inverse PCR of mutant library and screening knockouts	5'-TGTATGCTATACGAAGTTATCC-3'	
2	p10	Inverse PCR of mutant library	5'-GTAGAAGTAGCGACAGAGAAG-3'	
3	p11	Inverse PCR of mutant library	5'-CCATTCGAAACTGCACTACC-3'	
4	p13	Inverse PCR of mutant library and screening knockouts	5'-TGAATGGTGAAGATAAATATATGC-3'	
5	M13	Sequencing TOPO cloned PCR products	5'-CAGGAAACAGCTATGACC-3'	
6	T7	Sequencing TOPO cloned PCR products	5'-TAATACGACTCACTATAGGG-3'	
7	UbxF	*ubxd18* KO generation screening and RT-PCR	5'-ATAGTCAAGGTGTTAGAGCAATGCC-3'	
8	UbxR	*ubxd18* KO generation screening and RT-PCR	5'-ATGCCATTTGGTGAGAGCTTG-3'	
9	5'ubxSF	Screening *ubxd18* KO (5' genomic control, 5' knockout with p9)	5'-ATAATGTCAAGAGTAAAAGGTGAGT-3'	
10	5'ubxSR	Screening *ubxd18* KO (5' genomic control)	5'-ATAATGCAAATGAAAGTTGTGGTTG-3'	
11	3'ubxSF	Screening *ubxd18* KO (3' genomic control)	5'-ATAGATATAAATGTAAGGTTTGCCC-3'	
12	3'ubxSR	Screening *ubxd18* KO (3' genomic control, 3' knockout with p13)	5'-ATAGACCAGCATCTTGAACTGAA-3'	

13	**Ig7F**	**RT-PCR for *Ig7* control**	**5'-GTACTGTGAAGGAAAGATGAAAAG-3'**	
14	**Ig7R**	**RT-PCR for *Ig7* control**	**5'-CTATGGACCTTAGCGCTC-3'**	
15	**5'ARM TKTF**	***tkt* knockout generation (5' arm) and knockout screening (5' vector control)**	**5'-ATAGGATCCGACAAGATGGTTAAATAGAG-3'**	**BamH1**
16	**5'ARM TKTR**	***tkt* knockout generation (5' arm) and knockout screening (5' genomic control)**	**5'-ATACTGCAGCTAATACTAATTGTACTTCG-3'**	**PstI**
17	**3' ARM TKT F**	***tkt* knockout generation (3' arm) and knockout screening (3' genomic control)**	**5'-ATACCATGGCACTCATGACTCTGTTGGTGTTG-3'**	**NcoI**
18	**3' ARM TKTR**	***tkt* knockout generation (3' arm) knockout screening (3' vector control)**	**5'-ATAAAGCTTCGGCATTACCTGGTGCAGAC-3'**	**HindIII**
19	**PLPBLP F**	**Screening *tkt* knockout (3' vector control, 3' knockout)**	**5'-ATGCTATACGAAGTTATCCGTGG-3'**	
20	**PLPBLP R**	**Screening *tkt* knockout (5' vector control, 5' knockout)**	**5'-GGTTAATTCCTGCAGCCC-3'**	
21	**3'KO (GC)S**	**Screening *tkt* knockout (3' genomic control)**	**5'-CAGAAGTCATACCTAATTGTTTC-3'**	
22	**5'KO (GC)S**	**Screening *tkt* knockout (5' knockout)**	**5'-ATAGGCAAAGTTGCAGAATACGCT-3'**	
23	**tktqF**	***tkt* qPCR**	**5'-GGCTCATTAATCAACGCCTATC-3'**	
24	**tktqR**	***tkt* qPCR**	**5'-GCTTCACCATGACCTTTATTGG-3'**	
25	**cdcD OEF**	***p97* overexpressor**	**5'-ATAGGATCCATGGCAACAATTGAAG-3'**	**BamH1**
26	**cdcD OER**	***p97* overexpressor**	**5'-ATAACTAGTAT26TACTGAAAAGATCATC-3'**	**SpeI**
27	**cdcD seqF1**	**Sequencing *p97* overexpressor**	**5'-GCAGAGATCCTCGAATC-3'**	
28	**cdcD seqF2**	**Sequencing *p97* overexpressor**	**5'-GGATGGTATGAACGCC-3'**	

29	**cdcD seqR1**	**Sequencing *p97* overexpressor**	**5'-GGTTGTTGGAACTTCGACG-3'**	
30	**cdcD seqR2**	**Sequencing *p97* overexpressor**	**5'-GCTTTCTTACACCACC-3'**	
31	**UBXOE N-F BamH1**	***ubxd18* overexpressor and rtPCR**	**5'-ATA GGATCC ATGTCAAGAGTAAAAG-3'**	**BamH1**
32	**UBXOE N-R Xba1**	***ubxd18* overexpressor and rtPCR**	**5'-ATATCTAGATTATAATTTTTGAACTTGAAGGG-3'**	**XbaI**
33	**UBX seqF**	**Sequencing *ubxd18* overexpressor**	**5'-ATAGTTCTCAATCTGCAATGGATTGG-3'**	
34	**UBX seqR**	**Sequencing *ubxd18* overexpressor**	**5'-ATAGGGCAAACCTTACATTTATATC-3'**	
35	**FcsAOE N-F**	***fcsA* overexpressor**	**5'-ATAGAGCTCATGTCAAGCCTTTCAACA-3'**	**Sac1**
36	**FcsAOE N-R**	***fcsA* overexpressor**	**5'-ATATCTAGATTATACGTCTGGATGATCACG-3'**	**Xba1**
37	**FseqF**	**Sequencing *fcsA* overexpressor**	**5'-ATAGTGGTGCCCCAAGAGTATGG-3'**	
38	**FseqR**	**Sequencing *fcsA* overexpressor**	**5'-ATAAATGGAGCGGAACCGGAAAG-3'**	
39	**Start screen R FcsA**	**Sequencing *fcsA* overexpressor**	**5'-ATAGTAATCACCTCTTTTGCCATCTGC-3'**	
40	**End screen F FcsA**	**Sequencing *fcsA* overexpressor**	**5'-ATAGAACATGAACCATTCACTGAGG-3'**	
41	**Atg8aF**	**Autophagy qPCR (*atg8a*)**	**5'-CTCCAAGATCAGATGCACCA-3'**	
42	**Atg8aR**	**Autophagy qPCR (*atg8a*)**	**5'-GCAGCAGTTGGTGGGATAGT-3'**	
43	**Atg1F**	**Autophagy qPCR (*atg1*)**	**5'-TCACGCCTCTTCACTTCCTT-3'**	
44	**Atg1R**	**Autophagy qPCR (*atg1*)**	**5'-CGGTTGTTGGATTGTAGTTGAT-3'**	
45	**gapdhF**	**Autophagy qPCR (housekeeping)**	**5'-GGTTGTCCCAATTGGTATTAATGG-3'**	
46	**gapdhR**	**Autophagy qPCR (housekeeping)**	**5'-CCGTGGGTTGAATCATATTTGAAC-3'**	

Chapter 3

Identifying potential molecular targets for medium-chain fatty acids using *Dictyostelium discoideum*

3.1 Introduction

Many widely prescribed pharmaceutical drugs have unknown or poorly defined mechanisms of action. While a detailed knowledge of a drug's molecular pharmacology is not required for its use, understanding the therapeutic targets of pharmaceutical drugs and novel compounds is beneficial for the development of new and improved treatments (Chang *et al.*, 2012). To identify a mechanism of action for a compound, the ability to knock out potential targets is invaluable in order to demonstrate a resulting resistance to the compound (Schenone *et al.*, 2013). The identification of such targets can be difficult, especially using mammalian models where ablation of potential target genes can be challenging. The simple tractable model *Dictyostelium discoideum* provides an excellent system for elucidating the therapeutic mechanisms of compounds since ablation of genes in *Dictyostelium* is rapid and straightforward due to the haploid nature of the organism (Faix *et al.*, 2004; Schaf, Damstra-Oddy and Williams, 2019). To enable the identification of molecular targets of compounds, large libraries of *Dictyostelium* restriction enzyme mediated integration (REMI) mutants have been generated (Kuspa, 2006). These mutant libraries provide a valuable resource allowing the screening of compounds to identify resistant mutants. Using this approach therapeutic mechanisms of compounds can be elucidated, facilitating the development of new and improved treatments.

Dictyostelium mutant libraries have been used to determine the mechanisms of action of a range of compounds, from natural products curcumin (Cocorocchio *et al.*, 2018), and naringenin (Waheed *et al.*, 2014), to the cancer treatment cisplatin (Li *et al.*, 2000). This approach has allowed the rapid identification of proteins that control the sensitivity to a compound, thus implicating the identified protein or the wider pathway in the action of the compound. In addition to identifying genes conferring resistance to specific compounds, REMI libraries in *Dictyostelium* have also been used to identify regulators of cellular processes such as cell adhesion and migration (Lampert *et al.*, 2017; Nagasaki and Uyeda, 2008). Discoveries made using *Dictyostelium* genetic screens are often validated by translation into mammalian models (Waheed *et al.*, 2014; Chang *et al.*, 2012). The availability and ease of genetic screens in *Dictyostelium* provides a powerful tool for the elucidation of molecular targets for compounds with poorly understood mechanisms of action.

In this chapter we demonstrate that the key component of the MCT ketogenic diet, decanoic acid, along with the accompanying fatty acid, octanoic acid, and related compound, 4-BCCA, inhibit *Dictyostelium* proliferation in a dose dependent manner while having no inhibitory effect on development. We utilise these inhibitory effects on cell proliferation to identify potential molecular targets for decanoic acid and 4-BCCA by isolating resistant mutants using an unbiased genetic screen. Further analysis of these mutants provide insight into the molecular mechanisms of medium-chain fatty acids.

3.2 Results

3.2.1 The effects of decanoic acid, octanoic acid and 4-BCCA on *Dictyostelium* proliferation

To identify potential molecular mechanisms for the medium-chain triglyceride (MCT) diet we initially investigated the effects of the key dietary component, decanoic acid, on *Dictyostelium* unicellular proliferation. *Dictyostelium* cell proliferation was quantified in the presence of a range of concentrations of decanoic acid, with cell counts being recorded once every 24 hours, from 72 hours to 168 hours (Fig. 3.1A). Treatment with decanoic acid caused a dose dependent inhibition of growth. The rate of the exponential growth phase was then used to plot a non-linear regression curve, and a half maximal inhibitory concentration (IC_{50}) was calculated (Fig. 3.1D). Decanoic acid provided an IC_{50} of 18 µM (95% CI: 17 µM to 20 µM). The effect of octanoic acid, an accompanying medium-chain fatty acid in the MCT diet, on *Dictyostelium* unicellular proliferation, was also investigated (Fig. 3.1B). Octanoic acid was less potent than decanoic acid with an IC_{50} of 86 µM (95% CI: 73 µM to 100 µM) (Fig. 3.1D). Finally, we investigated the effect of 4-BCCA, a related compound with improved epileptiform activity control, on *Dictyostelium* proliferation (Chang *et al.*, 2015) (Fig. 3.1C). The purified product 4-BCCA provided an IC_{50} of 1.5 µM (95% Cl: 1.1 µM to 1.8 µM) (Fig. 3.1D). We have therefore shown that decanoic acid, octanoic acid and 4-BCCA each inhibited *Dictyostelium* proliferation, thus demonstrating suitability for use in genetic screens where mutants resistant to these growth inhibitory effects can be isolated and characterised.

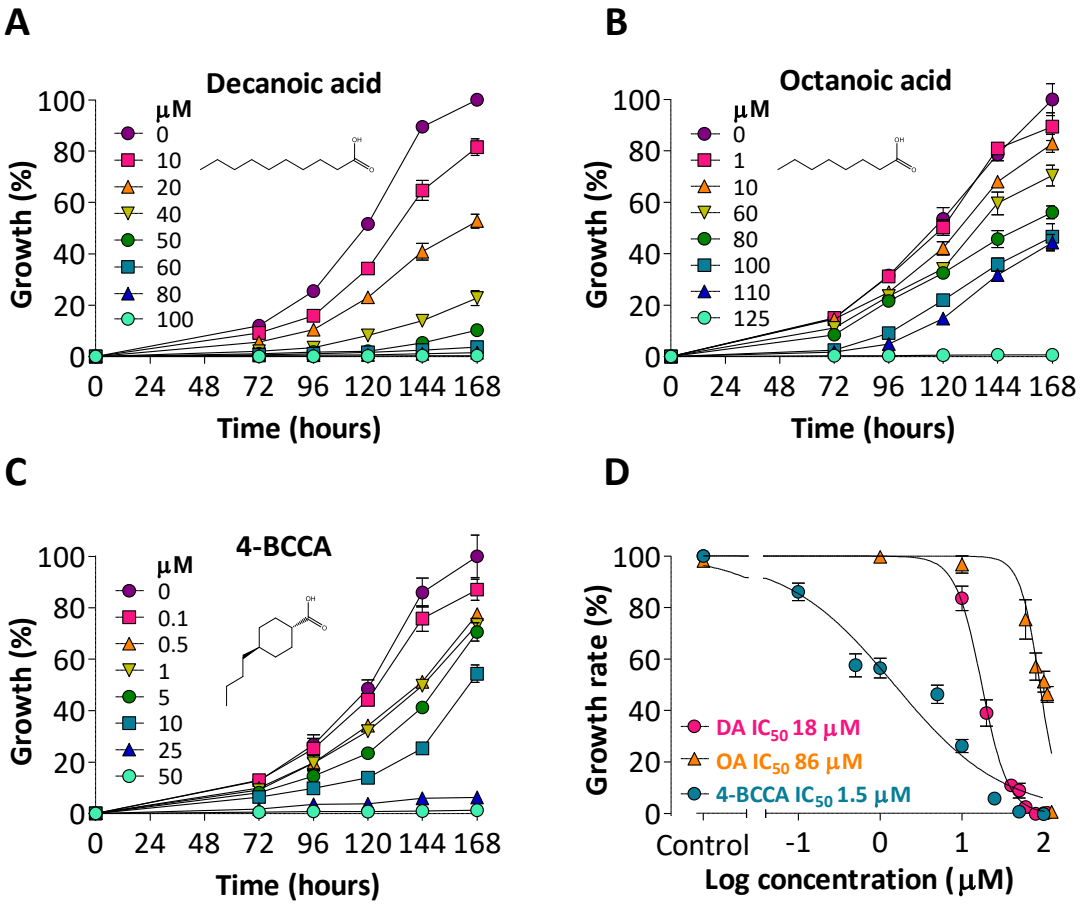

Figure 3. 1 Effects of decanoic acid octanoic acid and 4-BCCA on *Dictyostelium* growth. *Dictyostelium* (Ax2) cells were treated with A) decanoic acid (n = 6), B) octanoic acid (n = 6) or C) 4-BCCA (n = 6) for 168 hours (7 days) at a range of concentrations (µM). Percentage growth was plotted normalised to the solvent control (0 µM, 0.2 % DMSO) at 168 hours. C) Dose response curves of normalised growth rate plotted against Log concentration of compound were used to calculate IC_{50} values (n = 6). Data represent the mean ± SEM.

3.2.2 The effects of decanoic acid, octanoic acid and 4-BCCA on *Dictyostelium* development

Dictyostelium alternates between growing as single cells and developing as a multicellular organism, with different genes associated with these two stages (Loomis, 2015; Iranfar, Fuller and Loomis, 2003; Kuspa and Loomis, 1992). Where treatment with compound causes a visible alteration in *Dictyostelium* developmental morphology, mutant libraries can be screened for mutants resistant to these effects, thus identifying proteins controlling the sensitivity to the compound (Williams *et al.*,

2006). Furthermore, the effects of compounds on *Dictyostelium* multicellular development can be used as a readout for developmental toxicity, with teratogens such as valproic acid, tretinoin and thalidomide disrupting *Dictyostelium* development (Dannat *et al.*, 2003). We investigated the effects of decanoic acid on *Dictyostelium* development by starving cells for 22 hours on nitrocellulose filters in the absence or presence of 200 µM decanoic acid (Fig. 3.2). Under control conditions, cells formed fruiting bodies comprising dead vacuolated stalks holding viable spore heads aloft. This process of development was unaffected by decanoic acid at a far greater concentration than that which inhibited cell growth (200 µM). The effects of octanoic acid, and 4-BCCA on *Dictyostelium* development were also investigated (Fig. 3.2). The process of multicellular development was not affected by octanoic acid or by 4-BCCA at concentrations higher than completely inhibited cell growth (200 µM and 50 µM respectively). We have shown that *Dictyostelium* development was unaffected by decanoic acid, octanoic acid, and 4-BCCA, suggesting that these compounds regulate molecular targets involved in cell proliferation and not in development. These data also suggest that the medium-chain fatty acids have specific molecular effects on *Dictyostelium* rather than a general toxic effect.

3.2.3 Identifying potential molecular targets for decanoic acid

In order to identify potential molecular targets for decanoic acid we utilised the growth inhibitory effect of decanoic acid to isolate resistant mutants using an unbiased genetic screen of a library of *Dictyostelium* mutants. A REMI mutant library was screened in a concentration of decanoic acid that inhibits wild type growth (120 µM) (Fig. 3.3). Following a week-long incubation, mutants resistant to decanoic acid were isolated, made isogenic and decanoic acid resistance was confirmed by visual comparison of mutant and wild type growth in decanoic acid. Following confirmation of resistance, the location of the insertion site within the genome of these resistant mutants was determined to identify the genes controlling decanoic acid sensitivity. Through this approach, individual mutants with reduced sensitivity to the growth inhibitory effects of decanoic acid were identified.

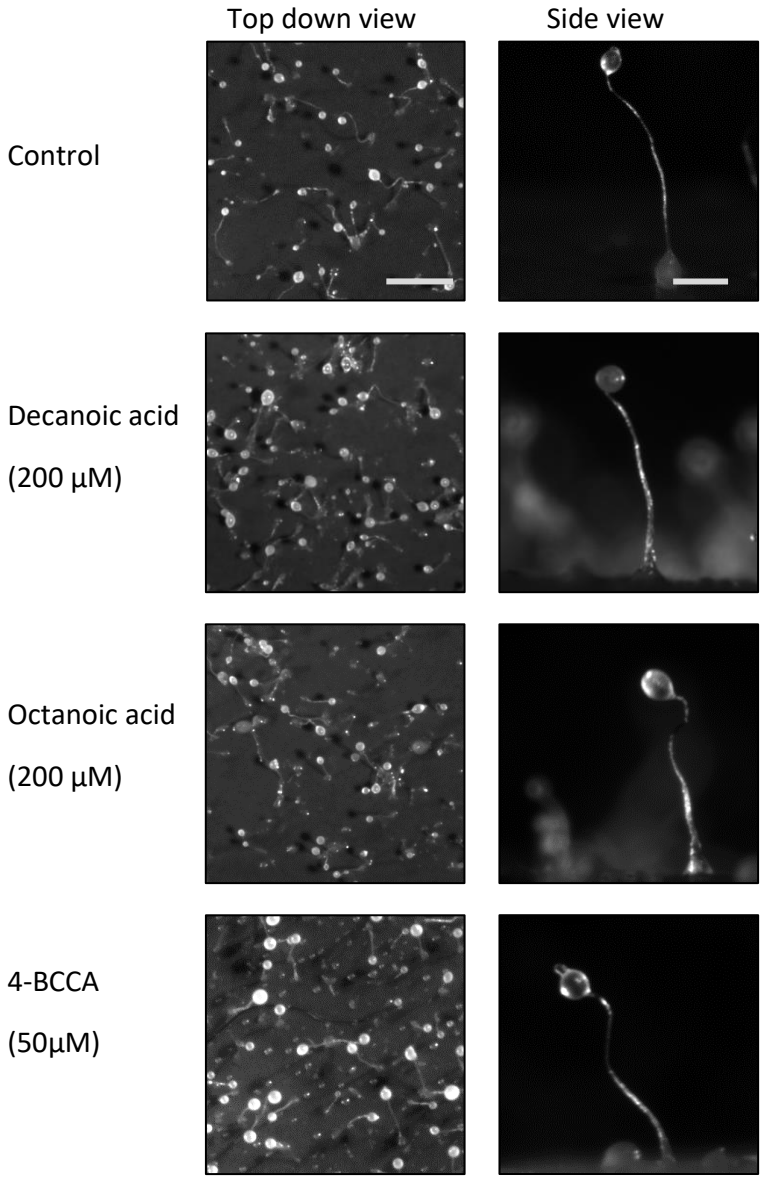

Figure 3. 2 Effects of decanoic acid, octanoic acid and 4-BCCA on *Dictyostelium* development. Qualitative evaluation of developmental effects of decanoic acid, octanoic acid and 4-BCCA on *Dictyostelium*. Phenotypes were monitored following starvation of *Dictyostelium* cells for 22 hours on nitrocellulose filters in the presence of compound or solvent control (DMSO). Top down view (scale bar 1 mm) and side on (scale bar 0.2 mm) images are displayed as representative results from triplicate experiments.

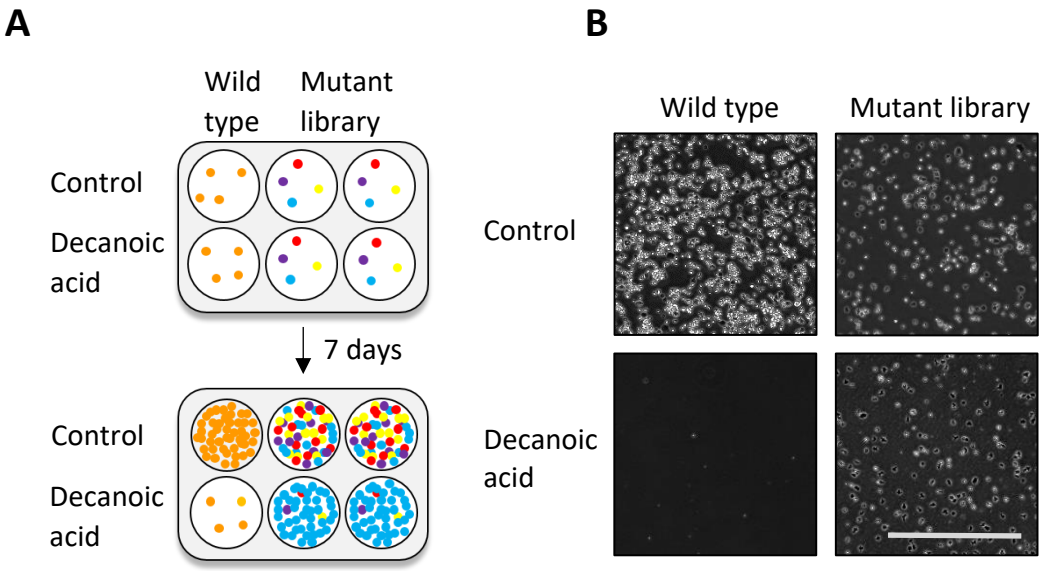

Figure 3. 3 *Dictyostelium* mutant library screen for mutants resistant to decanoic acid. A genetic screen of an insertional mutant library was carried out to identify mutants partially resistant to the growth inhibitory effects of decanoic acid. A) Schematic of mutant library screen. B) A representative image of the mutant library screen after 7 days incubation with 120 µM decanoic acid (Scale bar represents 0.5 mm).

In order to determine the location of the insertion within the decanoic acid resistant mutants an inverse PCR approach was used (Keim, Williams and Harwood, 2004). This technique involved extraction of genomic DNA from the mutants followed by restriction enzyme digestion, and self-ligation (Fig. 1.5). Genomic DNA flanking the insertion site was amplified using primers designed to bind within the insertion fragment and the precise sequence of this flanking DNA was determined by sequencing. The location of the insertion within the *Dictyostelium* genome was identified by using the blast local alignment search tool (BLAST) to locate the flanking DNA sequence (Fig. 3.4) (Altschul *et al.*, 1990).

From screening the *Dictyostelium* mutant library in decanoic acid, three distinct mutants partially resistant to the growth inhibitory effects of this fatty acids were identified. These mutants had gene disruptions within the genes encoding the proteins DNA-dependent Protein Kinase Catalytic Subunit (DNA-PKcs) (Fig. 3.4A), Transketolase (TKT) (Fig. 3.4B), or UBX domain-containing protein 18 (UBXD18) (Fig. 3.4C). The blast local alignment search tool was used to identify potential human

homologues and protein domain organisation was compared (Fig. 3.4). A human homologue of DNA-PKcs (uniprot P78527) was found to share 28.3 % sequence identity, and a human homologue of transketolase (uniprot P29401) was identified sharing 28.5 % identity. Human UBXN1 (uniprot Q04323), and UBXD2 (uniprot Q92575) proteins were identified as potential homologues of UBXD18. These proteins all contain UBX domains, the *Dictyostelium* UBX domain shares 28 % identical, and 51% similar amino acids with the UBXN1 UBX domain, and 27% identity and 51 % similarity with the UBXD2 UBX domain. Thus, this mutant library screen identified three genes in *Dictyostelium* with human homologues, that represent potential targets for decanoic acid.

3.2.4 Identifying potential molecular targets for 4-BCCA

A second mutant library screen was carried out using 4-BCCA, a cyclic fatty acid derivative with superior epileptiform activity control over decanoic acid (Chang *et al.*, 2015). The REMI mutant library was screened in a concentration of 4-BCCA capable of inhibiting wild type cell growth (80 μM) (Fig. 3.5). Following a week-long incubation, mutants resistant to 4-BCCA were isolated, made isogenic and the resistance to 4-BCCA was visually confirmed. The location of the insertion site within the genome of these resistant mutants was determined. One mutant partially resistant to 4-BCCA was identified with an insertion within the gene encoding the protein fatty acyl coenzyme A-synthetase (FcsA). The blast local alignment search tool was used to identify the existence of a human homologue of FcsA and protein domain organisation was compared (Fig. 3.6). The human homologue of FcsA is the long-chain fatty acid coA ligase (uniprot Q9ULC5) which shares 42 % identical amino acids with the *Dictyostelium* protein. The identification of a 4-BCCA resistant mutant with a disruption in the gene encoding FcsA implicates this protein in the cellular response to 4-BCCA, and the presence of a human FcsA homologue raises the possibility that this mechanism could be conserved between *Dictyostelium* and humans.

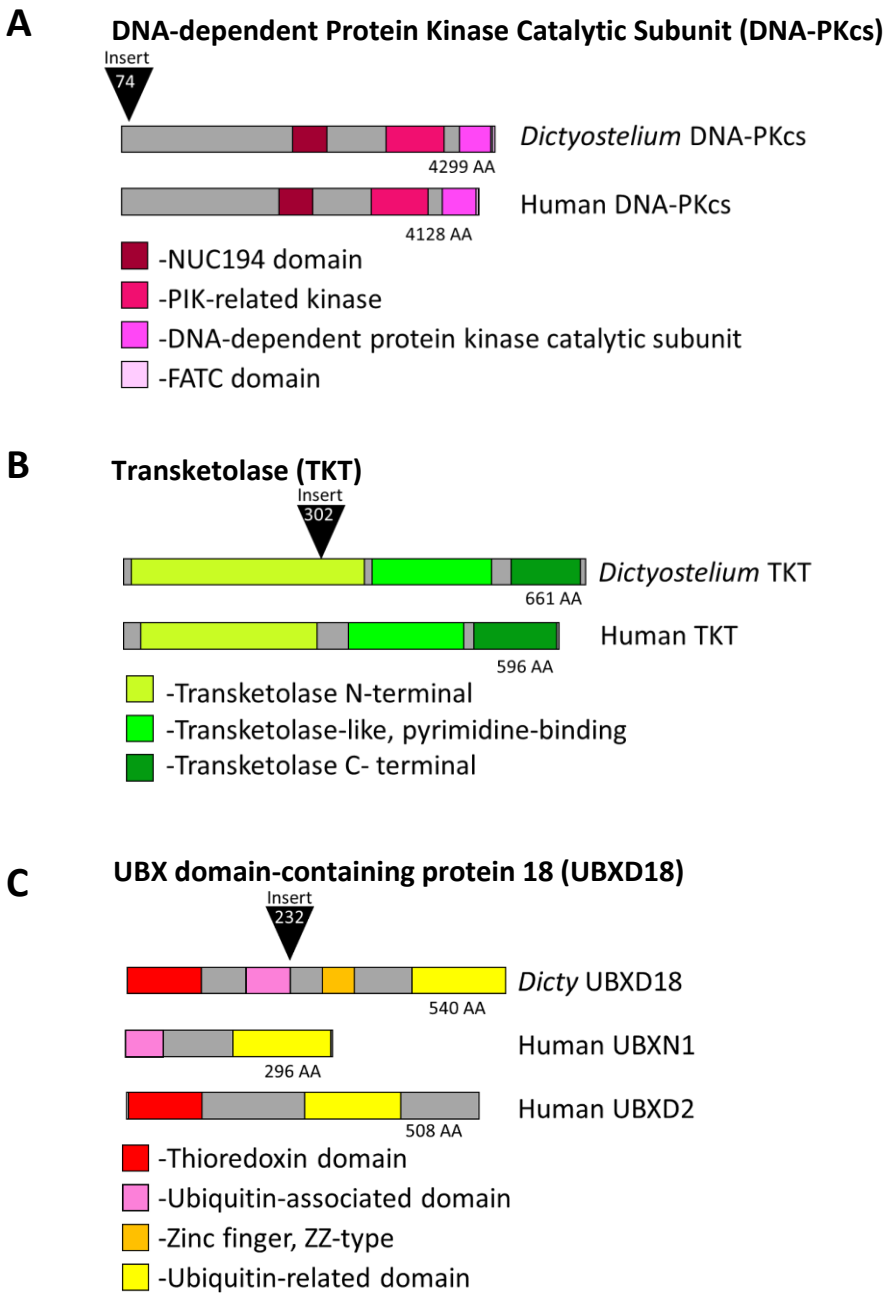

Figure 3. 4 ***Dictyostelium*** **decanoic resistant mutants identified from a genetic screen.** A genetic screen carried out to identify mutants resistant to decanoic acid identified genes encoding A) DNA protein kinase catalytic subunit (DNA-PKcs) (Dictybase ID. DDB_G0281167), B) Transketolase (TKT) (Dictybase ID. DDB_G0274019) and C) UBX domain containing protein 18 (UBXD18) (Dictybase ID. DDB_G0276057) which when disrupted confer partial resistance to 120 µM decanoic acid. *Dictyostelium* protein domain organisation is displayed, compared to that of the closest human homologue(s). The exact location at which the REMI insertion was located is labelled on the corresponding protein domain with a black triangle, and amino acid sequence number.

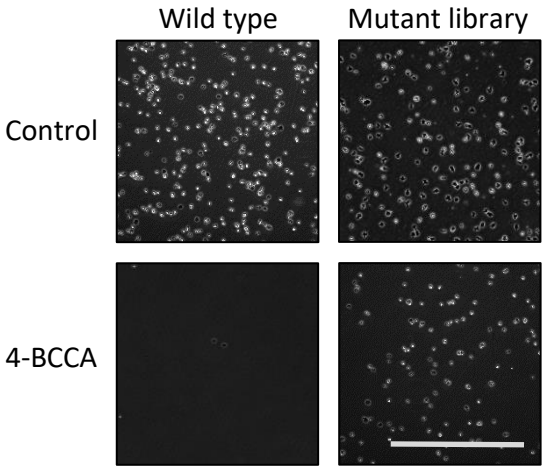

Figure 3. 5 *Dictyostelium* mutant library screen for mutants resistant to 4-BCCA. A genetic screen of an insertional mutant library was carried out to identify mutants partially resistant to the growth inhibitory effects of 4-BCCA. A representative image of the mutant library screen after 7 days incubation with 80 µM 4-BCCA is shown (Scale bar represents 0.5 mm).

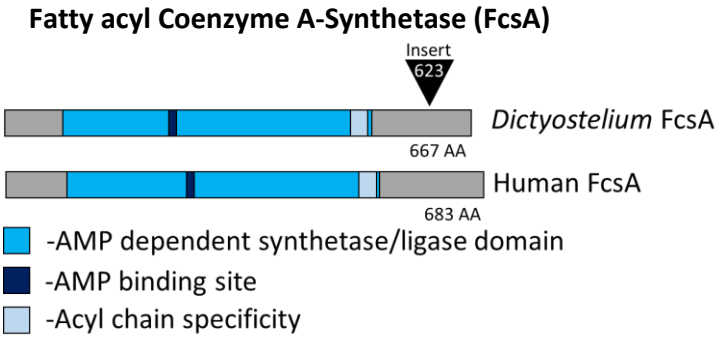

Figure 3. 6 A *Dictyostelium* 4-BCCA resistant mutant, with a disruption in *fcsA,* identified from a genetic screen. An independent mutant library screen using 80 µM 4-BCCA identified a mutant with a disruption in the gene encoding Fatty acyl Coenzyme A-Synthetase (FcsA) (Dictybase ID DDB_G0269242). *Dictyostelium* protein domain organisation is displayed, compared to that of the closest human homologue. The exact location at which the REMI insertion was located is labelled on the corresponding protein domain with a black triangle, and amino acid sequence number.

3.2.5 Analysis of potential molecular targets for decanoic acid and 4-BCCA

Following the identification of potential molecular targets for decanoic acid and 4-BCCA from mutant library screens it was necessary to confirm the fatty acid resistant phenotypes of these mutants. Since, mutants generated via restriction enzyme mediated integration (REMI) potentially have multiple sites of mutation, this could result in multiple gene disruptions within the REMI mutants. To confirm that the fatty acid resistant phenotypes were conferred by disruptions in the genes we have identified, we required independent knockouts for further investigation. Independent *dna-pkcs* and *fcsA* knockouts were available (Hudson *et al.*, 2005; von Lohneysen *et al.*, 2003). Thus, mutants lacking DNA-PKcs and FcsA proteins could be directly assessed for fatty acid resistance, whereas, generation of independent gene knockouts for *ubxd18* (official gene name *DDB_G0276057*) and *tkt* was required.

3.2.5.1 DNA-PKcs

To confirm that the decanoic acid resistant phenotype observed in the *dna-pkcs* disrupted REMI mutant was conferred by the insertion in this gene, we used an independent knockout to verify the effect of decanoic acid on *DNA-PKcs*$^-$ growth. *DNA-PKcs*$^-$ was partially resistant to the effect of decanoic acid, with an IC_{50} value 2-fold higher than that of the wild type cell line (*DNA-PKcs*$^-$ IC_{50} 36 µM, 95 % CI: 32 µM to 40 µM, compared to wild type (Ax2) IC_{50} 18 µM, 95 % CI: 17 µM to 20 µM, $p = 0.0357$, $n \geq 3$) (Fig. 3.7). These findings suggest a potential involvement for DNA-PKcs in the cellular response to decanoic acid.

3.2.5.2 FcsA

A mutant with a disruption in the gene *fcsA* was identified from a mutant library screen in 4-BCCA. In order to establish whether the resistance to 4-BCCA was a direct result of the disruption of *fcsA,* we investigated the sensitivity of an independent *FcsA*$^-$ knockout to 4-BCCA (Fig. 3.8A). *FcsA*$^-$ was partially resistant to effects of 4-BCCA (Fig. 3.8B). In *FcsA*$^-$, 4-BCCA had an IC_{50} value 28-fold higher than that of the wild type cell line (*FcsA*$^-$ IC_{50} 42 µM, 95 % CI: 29 µM to 61 µM, compared to wild type (Ax2) IC_{50} 1.5 µM, 95 % CI: 1.1 µM to 2 µM, $p = 0.0043$, $n \geq 5$) (Fig. 3.8C). In order to investigate if knocking out *fcsA* also conferred resistance to decanoic acid

we investigated the effects of decanoic acid on the growth of this knockout cell line (Fig. 3.8D). *FcsA*$^-$ was found to also be partially resistant to effects of decanoic acid, where *FcsA*$^-$ had an IC_{50} value roughly 2-fold higher than that of the wild type cell line (*FcsA*$^-$ IC_{50} 42 µM, 95 % CI: 37 µM to 49 µM, compared to wild type (Ax2) IC_{50} 18 µM, 95 % CI: 17 µM to 20 µM, p = 0.0159, n ≥ 4) (Fig. 3.8E and F).

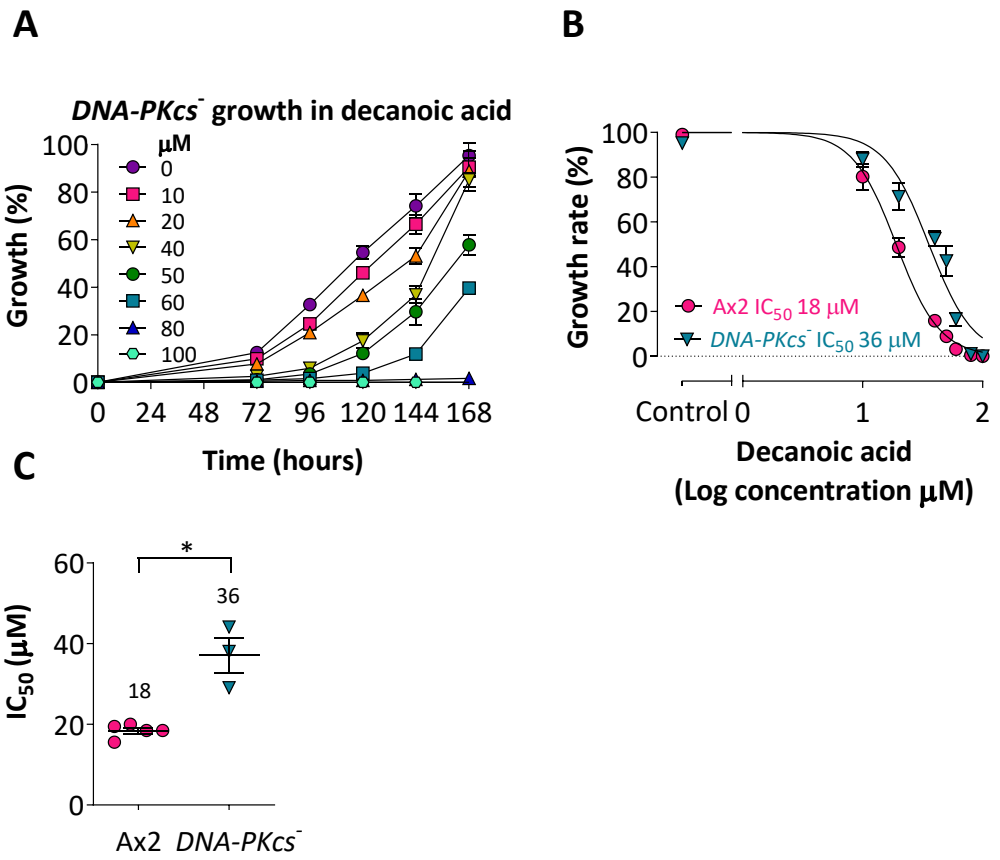

Figure 3. 7 Effects of decanoic acid on *DNA-PKcs*$^-$ growth. A) An independent knockout of *dna-pkcs* (*DNA-PKcs*$^-$) was treated with a range of concentrations of decanoic acid (µM), for 168 hours (n = 3). Percentage growth was plotted normalised to the solvent control (0 µM, 0.2 % DMSO) at 168 hours. B) Dose response curves of normalised growth rate plotted against Log concentration of decanoic acid were used to compare the decanoic acid sensitivity of wild type (Ax2) (n = 5) and *DNA-PKcs*$^-$ (n = 3). C) IC_{50} values for Ax2 (n = 5) and *DNA-PKcs*$^-$ (n = 3) in decanoic acid were compared. Data represent the mean ± SEM. Significance is indicated by * p ≤ 0.05 (Mann Whitney test).

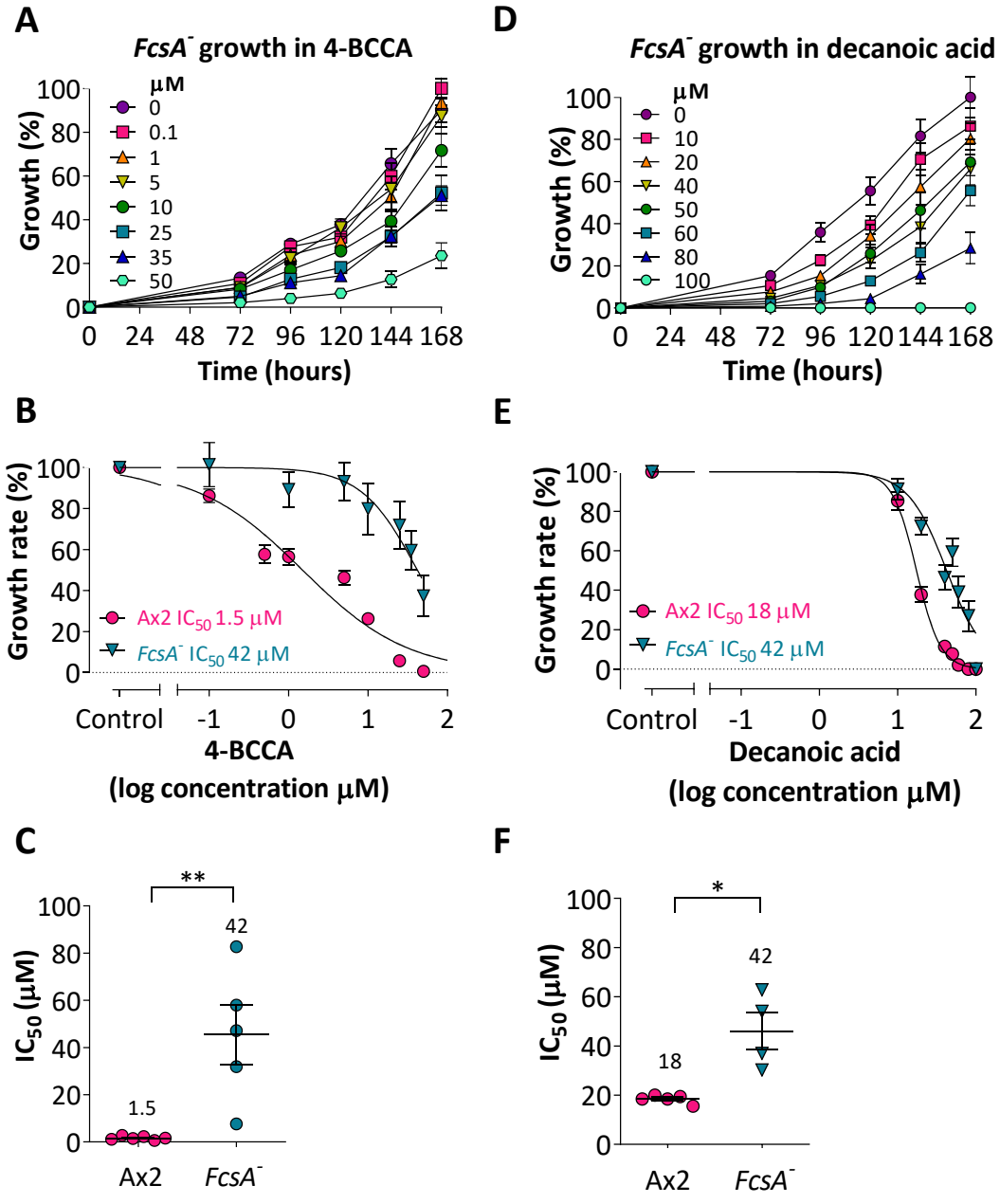

Figure 3. 8 Effects of 4-BCCA and decanoic acid on *FcsA*⁻ growth. A) An independent knockout of *fcsA* (*FcsA*⁻) was treated with a range of concentrations (µM) of 4-BCCA for 168 hours (n = 5). Percentage growth was plotted normalised to the solvent control (0 µM, 0.2 % DMSO) at 168 hours. B) Dose response curves of normalised growth rate plotted against Log concentration of 4-BCCA were used to compare the 4-BCCA sensitivity of wild type (Ax2) (n = 6) and *FcsA*⁻ (n = 5). C) IC_{50} values for Ax2 (n = 6) and *FcsA*⁻ (n = 5) in 4-BCCA were compared. D) *FcsA*⁻ was treated with a range of concentrations (µM) of decanoic acid for 168 hours (n = 4). E) Dose response curves were used to compare the decanoic acid sensitivity of (Ax2) (n = 5) and *FcsA*⁻ (n = 4). F) IC_{50} values for Ax2 (n = 5) and *FcsA*⁻ (n = 4) in decanoic acid were compared. Data represent the mean ± SEM. Significance is indicated by * $p \leq 0.05$, ** $p \leq 0.01$ (Mann-Whitney test).

In order to confirm that loss of a specific gene is responsible for the observed phenotype, reintroduction of gene expression can be analysed for restoration of the wild type phenotype (Levi, Polyakov and Egelhoff, 2000). Since *FcsA*$^{-}$ demonstrated a significant increase in resistance to both 4-BCCA and decanoic acid compared to wild type (28-fold and 2.3-fold respectively), we reintroduced *fcsA* gene expression to confirm the involvement of this target in the fatty acid resistant phenotype. In order to reintroduce *fcsA* gene expression, we generated an extrachromosomal vector designed to express *fcsA* with an amino-terminal GFP domain attached (Fig. 3.9A). The open reading frame of *fcsA* was amplified from wild type (Ax2) cDNA with the incorporation of restriction enzyme sites enabling cloning into the pTX-GFP vector. The expression vector was verified by sequencing before being transfected into *FcsA*$^{-}$. Reintroduction of gene expression was confirmed using rt-PCR (Fig. 3.9B), and western blotting using an antibody against GFP confirmed the presence of the correct size (approximately 100 kDa) GFP-tagged protein (Fig. 3.9C). Reintroducing *fcsA* gene expression restored a 4-BCCA sensitive phenotype (FcsA$^{-/+}$ IC_{50} 1 µM, 95 % Cl: 0.94 µM to 1.1 µM, $p = 0.0357$, $n \geq 3$) (Fig. 3.10A, B and C). Reintroducing *fcsA* gene expression also restored a decanoic acid sensitive phenotype (*FcsA*$^{-/+}$ IC_{50} 6.4 µM, 95 % Cl: 5.4 µM to 7.5 µM, $p = 0.0286$, $n \geq 3$) (Fig. 3.10D, E and F). We have shown that loss of *fcsA* leads to partial resistance to the effects of 4-BCCA and decanoic acid on cell proliferation, and that reintroduction of *fcsA* gene expression restores wild type levels of sensitivity. These findings suggest that *fcsA* is responsible for the observed fatty acid resistance, thus implicating the protein FcsA as a potential molecular target for 4-BCCA and decanoic acid.

3.2.5.3 TKT

Transketolase (TKT) was identified as a potential molecular target for decanoic acid in a *Dictyostelium* mutant library screen. To confirm that the decanoic acid resistance displayed by the *tkt* disrupted REMI mutant is conferred by the insertion in this gene rather than an off-target mutation, we generated an independent knockdown of this gene (Fig. 3.11). We employed a traditional knockout approach using the gene disruption vector pLPBLP (Faix *et al.*, 2004). This approach was chosen due to the presence of a genome duplication in the region of

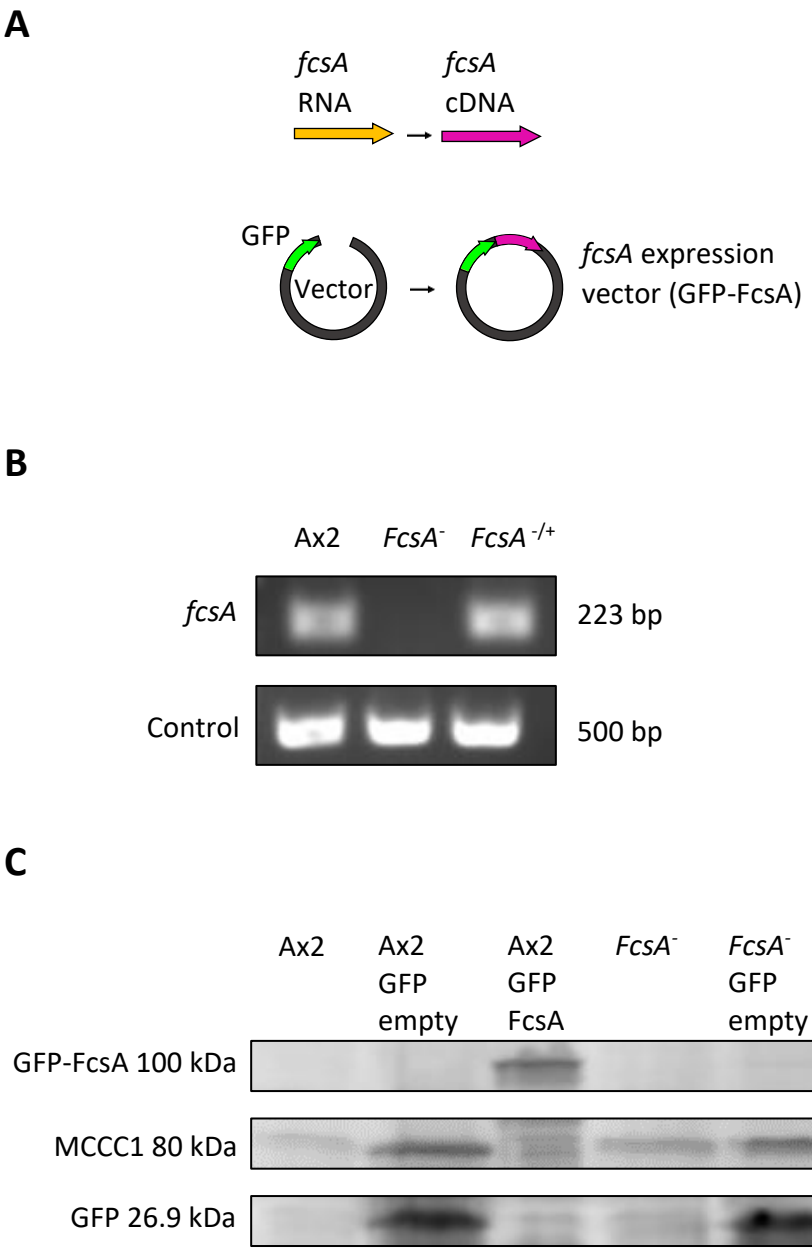

Figure 3. 9 Reintroduction of *fcsA* gene expression. A) The open reading frame of *fcsA* was amplified from cDNA with the incorporation of restriction sites for cloning into the vector pTX-GFP. B) The *fcsA* expression vector (GFP-FcsA) was transfected into *FcsA*$^-$ and expression was confirmed using rt-PCR (with *Ig7* as a positive control). C) Western blotting was used to confirm presence of the correct size protein using an antibody against GFP. MCCC1 was used as a loading control.

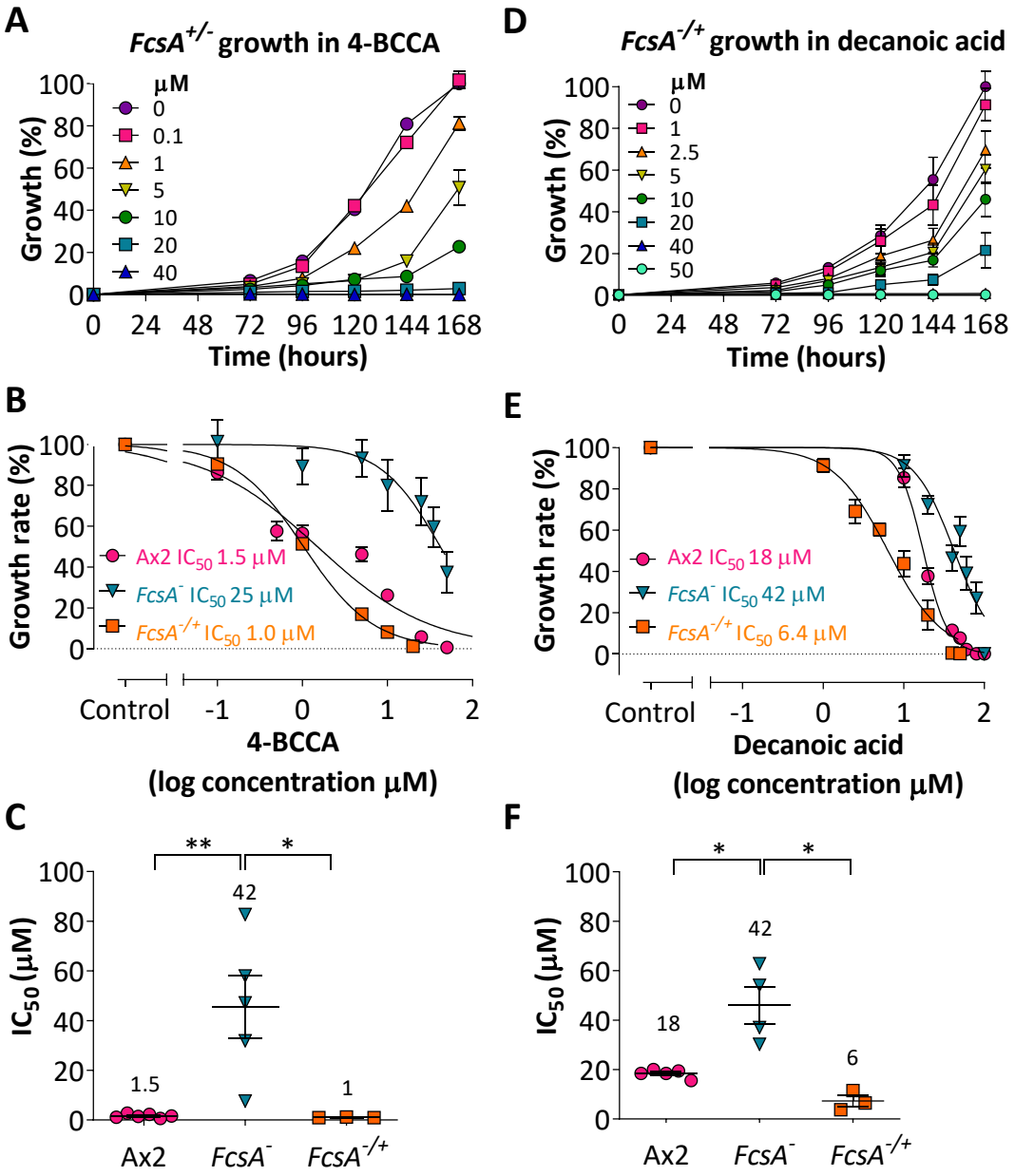

Figure 3. 10 Analysis of the effects of 4-BCCA and decanoic acid on *FcsA*$^{-/+}$ growth. A) *FcsA*$^{-/+}$ was treated with a range of concentrations (µM) of 4-BCCA for 168 hours (n = 3). Percentage growth was plotted normalised to the solvent control (0 µM, 0.2 % DMSO) at 168 hours. B) Dose response curves of normalised growth rate plotted against Log concentration of 4-BCCA were used to compare the sensitivity of wild type (Ax2) (n = 6), *FcsA*$^{-}$ (n = 5) and *FcsA*$^{-/+}$ (n = 3). C) 4-BCCA IC_{50} values for Ax2 (n = 6), *FcsA*$^{-/+}$ (n = 5) and *FcsA*$^{-/+}$ (n = 3) were compared. D) *FcsA*$^{-/+}$ was treated with a range of concentrations (µM) of decanoic acid for 168 hours (n = 3). E) Dose response curves were used to compare the decanoic acid sensitivity of Ax2 (n=5), *FcsA*$^{-}$ (n = 4) and *FcsA*$^{-/+}$ (n = 3). F) IC_{50} values for Ax2 (n = 5), *FcsA*$^{-/+}$ (n = 4) and *FcsA*$^{-/+}$ (n = 3) in decanoic acid were compared. Data represent the mean ± SEM. Significance is indicated by * $p \leq 0.05$, ** $p \leq 0.01$ (Mann-Whitney test).

chromosome 2 from bases 2249563 to 3002134 in Ax4 resulting in two copies of the *tkt* gene (Bloomfield *et al.*, 2008). A knockout construct was generated by PCR amplifying two sequences (arms) of approximately 500 bp from the 5' and 3' regions of the *tkt* gene sequence (Fig. 3.11A) and cloning these fragments into the pLPBLP vector at sites flanking the gene for blasticidin resistance (BSR) (Fig. 3.11B). This process generated a disruption fragment with sequences homologous to *tkt* flanking the BSR gene, designed to enable homologous recombination. Wild type, Ax4, *Dictyostelium* cells were transfected once with the disruption fragment for gene disruption by homologous recombination and were selected for resistance to blasticidin. Ax2 *Dictyostelium* cells were transfected three independent times. Blasticidin resistant cells (56 wells of Ax4 and 293 wells of Ax2) were screened using primers designed to produce six diagnostic fragments (Fig. 3.11D and E). This procedure generated three independent Ax4 mutants with a disruption in one copy of the *tkt* gene, recapitulating the genotype of the *tkt* REMI mutant identified from the mutant library. No successful homologous recombinants were identified in Ax2. Since the homologous recombination events into Ax4 are likely to disrupt just one copy of the gene, we used qPCR to monitor *tkt* gene expression normalised to the wild type (Ax4). Expression of *tkt* was reduced by 60 % in the *tkt* knockdown (*TKT*$^{-}$) (95% CI: 39 % to 98 %, p = 0.0286, n = 4) (Fig. 3.11F).

The creation of a *Dictyostelium tkt* knockdown (*TKT*$^{-}$) provided us with an independent mutant cell line recapitulating the genotype of the *tkt* REMI mutant identified from the genetic screen in decanoic acid. In order to establish whether disruption of one copy of the *tkt* gene is responsible for the observed decanoic acid resistance, we compared the decanoic acid sensitivity of the wild type cell line (Ax4) (Fig. 3.12A) to this *tkt* knockdown (*TKT*$^{-}$) (Fig. 3.12B). *TKT*$^{-}$ was partially resistant to the effect of decanoic acid, with an IC_{50} value 3-fold higher than that of the wild type cell line (*TKT*$^{-}$ IC_{50} 56 µM, 95% CI: 51 µM to 61 µM, compared to wild type (Ax4) IC_{50} 17 µM, 95% CI: 16 µM to 19 µM, p = 0.0286, n ≥ 3) (Fig. 3.12C and D). These findings demonstrate that knocking out one copy of *tkt* and reducing *tkt* gene expression is sufficient to recapitulate the decanoic acid resistant phenotype observed in the REMI mutant, suggesting that the protein TKT could play a role in regulating the cellular response to decanoic acid.

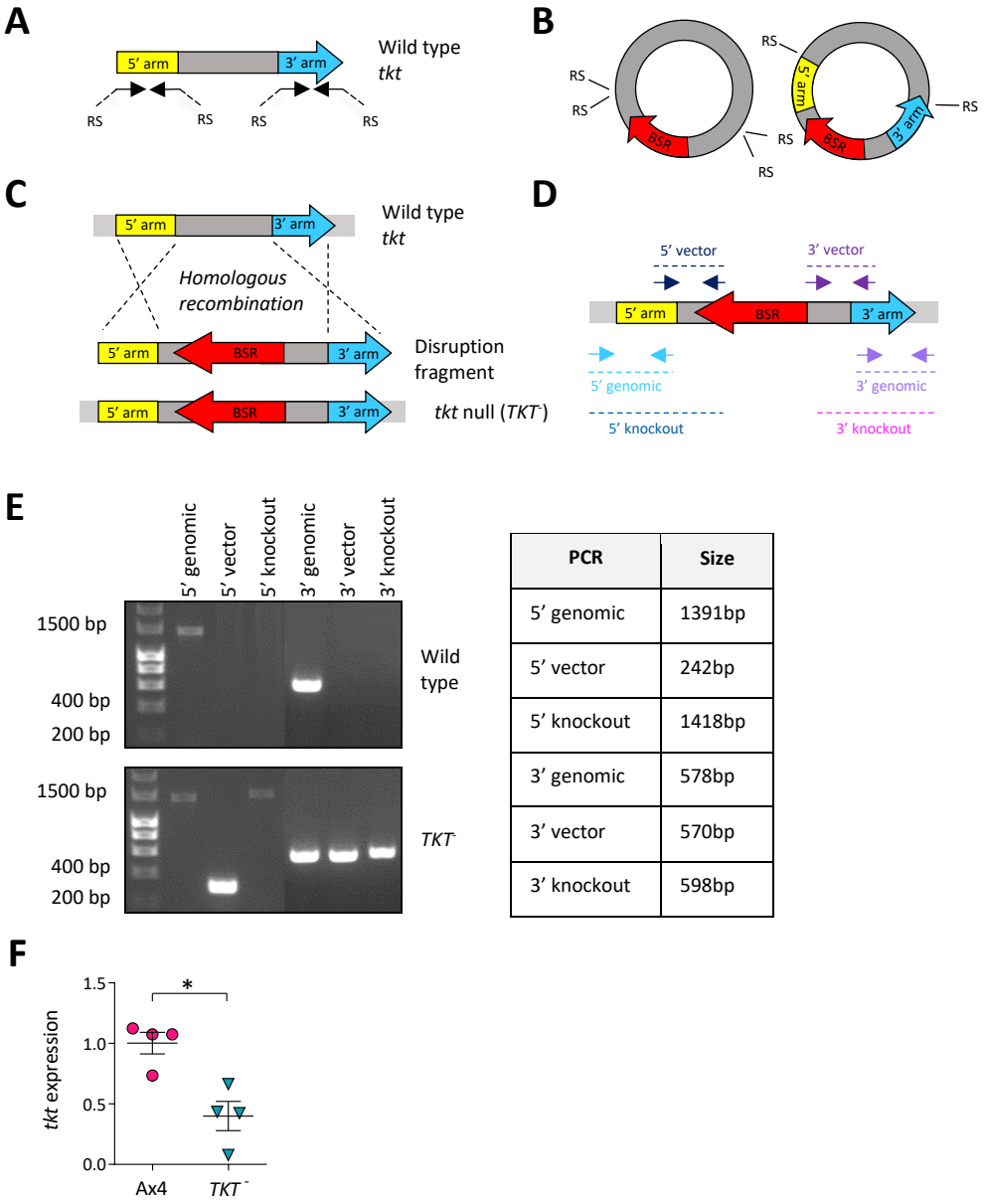

PCR	Size
5′ genomic	1391bp
5′ vector	242bp
5′ knockout	1418bp
3′ genomic	578bp
3′ vector	570bp
3′ knockout	598bp

Figure 3. 11 Generation of *tkt* gene knockdowns A) Two fragments (arms) of DNA of approximately 500 bp from the 5′ and 3′ regions of *tkt* were amplified by PCR introducing restriction sites (RS). B) These arms were cloned into the pLPBLP vector at multiple cloning sites flanking the gene for blasticidin resistance (BSR). The disruption fragment (homologous arms flanking the BSR gene) was isolated via restriction digest. C) Transfections of this disruption fragment into wild type (Ax4) *Dictyostelium* resulted in disruption of the *tkt* gene via homologous recombination. D) Blasticidin resistant cells were screened for the presence of homologous recombinants using primers designed to produce six diagnostic fragments. E) Representative screening confirming disruption of the *tkt* gene. F) qPCR was used to monitor *tkt* gene expression in the knockdown compared to Ax4 (n = 4). Data represent the mean ± SEM. Significance is indicated by * $p \leq 0.05$ (Mann-Whitney test).

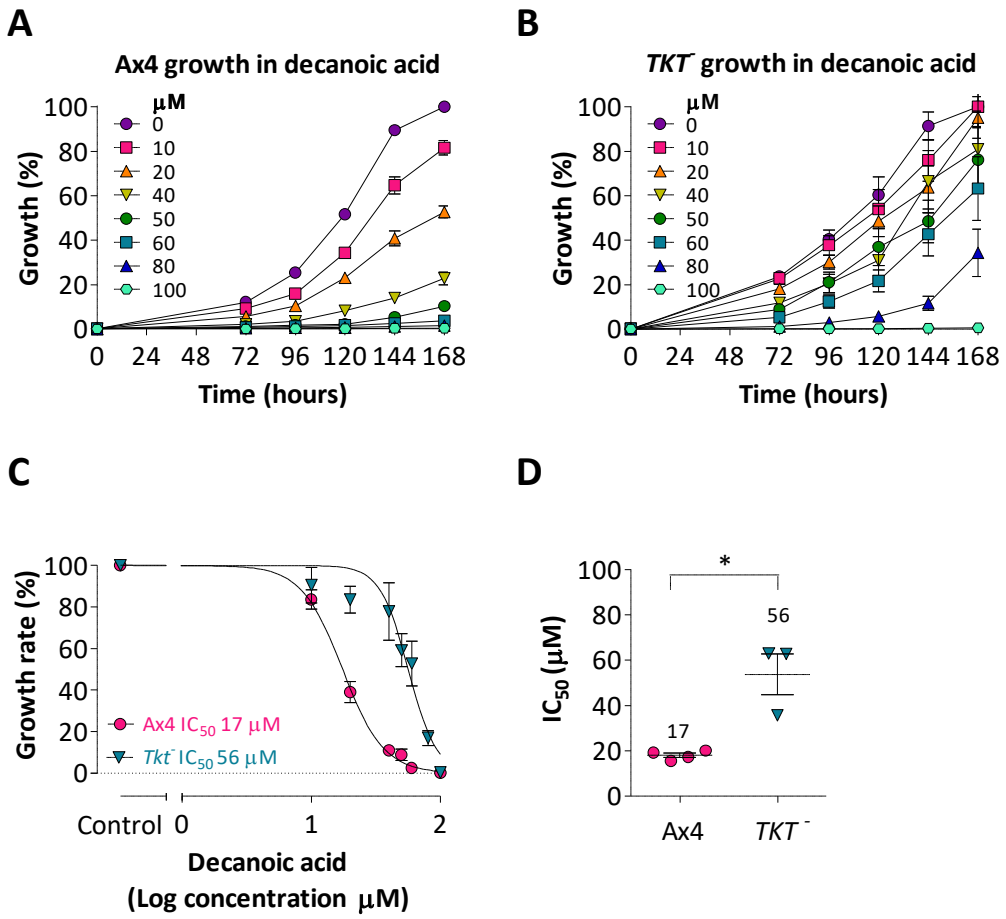

Figure 3. 12 Effects of decanoic acid on *TKT*⁻ growth. A) Wild type (Ax4) cells (n = 4) or B) an independent knockdown of *tkt* (*TKT*⁻) (n = 3) were treated with a range of concentrations of decanoic acid (µM), for 168 hours. Percentage growth was plotted normalised to the solvent control (0 µM, 0.2 % DMSO) at 168 hours. C) Dose response curves of normalised growth rate plotted against Log concentration of decanoic acid were used to compare the decanoic sensitivity of Ax4 (n = 4) and *TKT*⁻ (n = 3). D) IC_{50} values for Ax4 (n = 4) and *TKT*⁻ (n = 3) were compared. Data represent the mean ± SEM. Significance is indicated by * $p \leq 0.05$ (Mann-Whitney test).

3.2.5.4 UBXD18

A mutant with a gene disruption in *ubxd18* was identified from a mutant library screen in decanoic acid. To confirm that the decanoic acid resistance seen in the *ubxd18* REMI mutant is conferred by the disruption in the *ubxd18* gene, we generated an independent gene knockout of *ubxd18* (*UBXD18*⁻) (Fig. 3.13). In contrast to the traditional approach used to knockdown *tkt*, we employed a direct PCR method to generate a knockout construct for *ubxd18* due to the presence of only one

copy of the *ubxd18* gene in *Dictyostelium*. This knockout construct was generated by PCR amplification over the insertion site within the *ubxd18* REMI mutant (Fig. 3.13A). This amplified a construct comprising two sequences (arms) with homology to the *ubxd18* gene flanking the BSR insert, facilitating the insertion of the BSR sequence into the *ubxd18* gene through homologous recombination, effectively recapitulating the REMI mutant genotype (Fig. 3.13C). Wild type (Ax2) cells were transfected once with this purified knockout construct and transfectants were selected for in the presence of blasticidin. Resistant colonies (35 colonies) were screened for the presence of homologous recombinants using primers designed to produce seven diagnostic fragments unique to the homologous transfectants (Fig. 3.13C). This procedure generated four homologous recombinants, verified for correct insertion of the knockout construct disrupting *ubxd18* (Fig. 3.13D). Isogenic colonies were then selected and confirmed by PCR, before reverse transcriptase-PCR (RT-PCR) was used to verify the loss of *ubxd18* expression with *Ig7* as a positive control (Fig. 3.13E). The creation of a *Dictyostelium ubxd18* knockout (*UBXD18*$^-$) has provided us with an independent mutant cell line for the recapitulation of the decanoic acid resistant phenotype identified from our genetic screens in decanoic acid.

To confirm that the decanoic acid resistance observed in the *ubxd18* REMI mutant is conferred by a disruption in the *ubxd18* gene, we used an independent knockout to verify the decanoic acid resistant phenotype. *UBXD18*$^-$ was partially resistant to the effect of decanoic acid, with an IC_{50} value 2-fold higher than that of the wild type cell line (*UBXD18*$^-$ IC_{50} 37 µM, 95 % CI: 31 µM to 43 µM, compared to wild type (Ax2) IC_{50} 18 µM, 95 % CI: 17 µM to 20 µM, $p \leq 0.0001$) (Fig. 3.14).

In order to confirm that loss of *ubxd18* gene expression is responsible for the observed decanoic acid resistant phenotype, we reintroduced *ubxd18* gene expression to investigate restoration of the wild type phenotype. We generated an extrachromosomal vector designed to express *ubxd18* with an amino-terminal GFP domain attached (Fig. 3.15A). The open reading frame of *ubxd18* was amplified from wild type (Ax2) cDNA with the addition of restriction enzyme sites allowing the coding region to be cloned into the pTX-GFP vector. The expression vector was verified by sequencing before being transfected into *UBXD18*$^-$. Reintroduction of gene expression was confirmed using rt-PCR (Fig. 3.15B) and western blotting using an

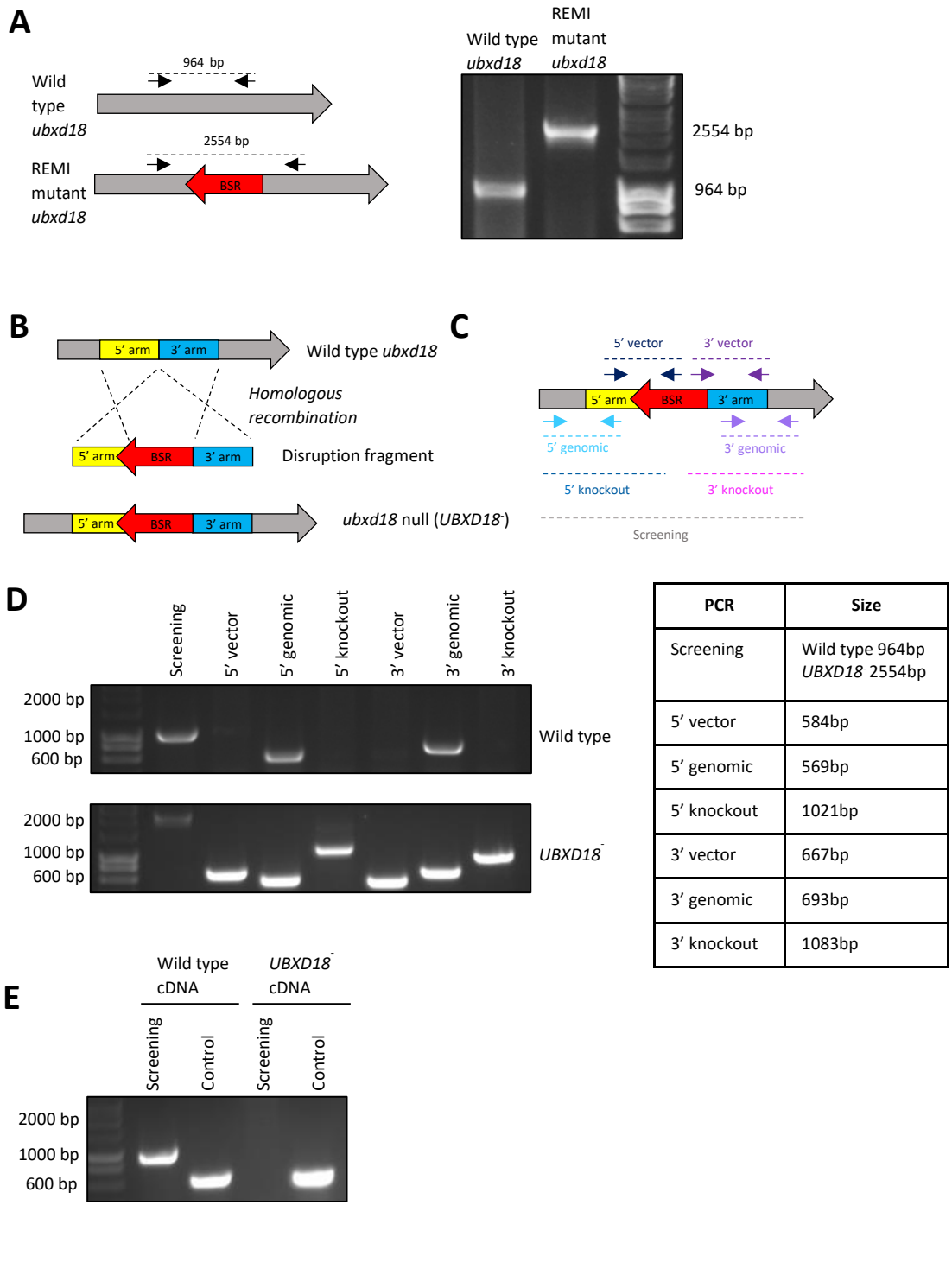

PCR	Size
Screening	Wild type 964bp *UBXD18*- 2554bp
5' vector	584bp
5' genomic	569bp
5' knockout	1021bp
3' vector	667bp
3' genomic	693bp
3' knockout	1083bp

Figure 3. 13 Generation of *ubxd18* gene knockouts. A) PCR amplification over the REMI insertion site was used to generate a knockout construct of 2554bp. B) Transfection of this knockout construct into wild type *Dictyostelium* results in disruption of the *ubxd18* gene via homologous recombination. C) Blasticidin resistant cells were screened for the presence of homologous recombinants using primers designed to produce seven diagnostic fragments. D) Representative screening of one out of four *ubxd18* knockouts. E) RT-PCR was used to confirm the loss of *ubxd18* expression in the knockout, with *Ig7* as a positive control.

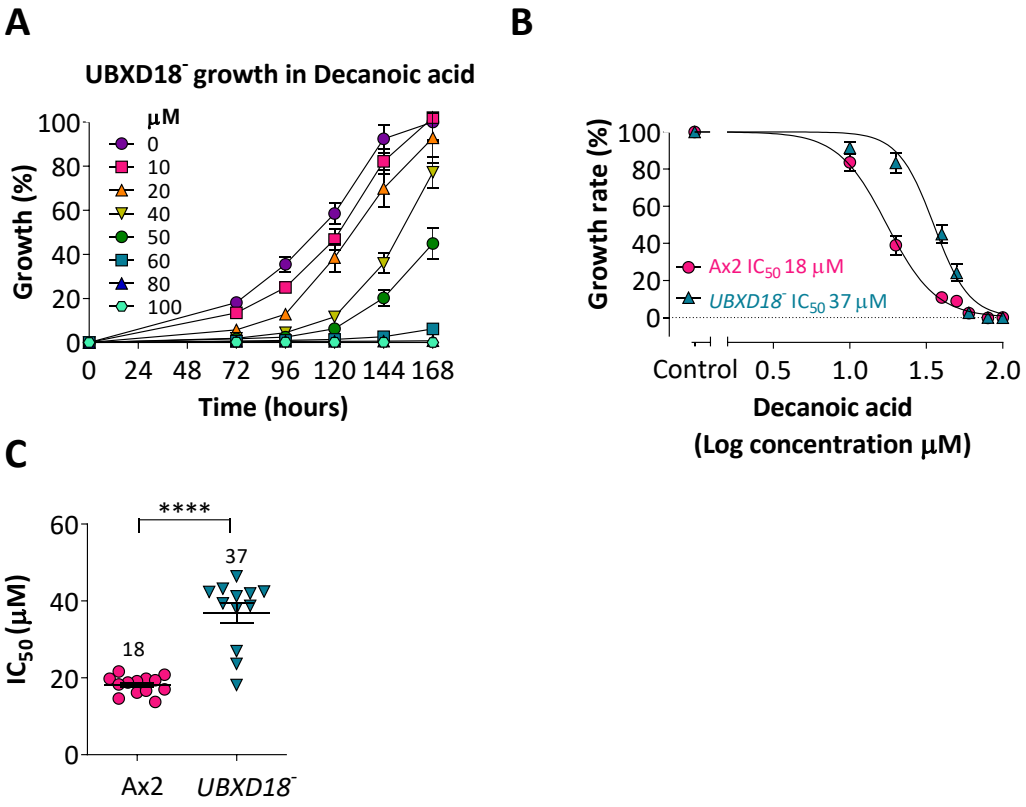

Figure 3. 14 Effects of decanoic acid on *UBXD18*- growth. A) An independent knockdown of *ubxd18* (*UBXD18*-) (n = 12) was treated with a range of concentrations of decanoic acid (µM) for 168 hours. Percentage growth was plotted normalised to the solvent control (0 µM, 0.2 % DMSO) at 168 hours. B) Dose response curves of growth rate plotted against Log concentration of decanoic acid were used to compare the decanoic sensitivity of wild type (Ax2) (n = 13) and *UBXD18*- (n = 12). C) IC_{50} values for Ax2 (n = 13) and *UBXD18*- (n = 12) in decanoic acid were compared. Data represent the mean ± SEM. Significance is indicated by **** $p \leq 0.0001$ (Mann-Whitney test).

antibody against GFP confirmed the presence of the correct size (86.9 kDa) GFP-tagged protein (Fig. 3.15C). Reintroducing *ubxd18* gene expression restored a decanoic acid sensitive phenotype (*UBXD18*$^{-/+}$ IC_{50} 13 µM, 95% CI: 8.3 µM to 18 µM, $p \leq 0.0001$) (Fig. 3.16A, B and C). We have demonstrated that loss of *ubxd18* leads to partial resistance to the effects of decanoic acid on growth, and that reintroduction of the *ubxd18* gene restores wild type sensitivity to decanoic acid. These findings suggest that *ubxd18* is responsible for the observed decanoic acid resistance, thus implicating UBXD18 as a potential molecular target for decanoic acid.

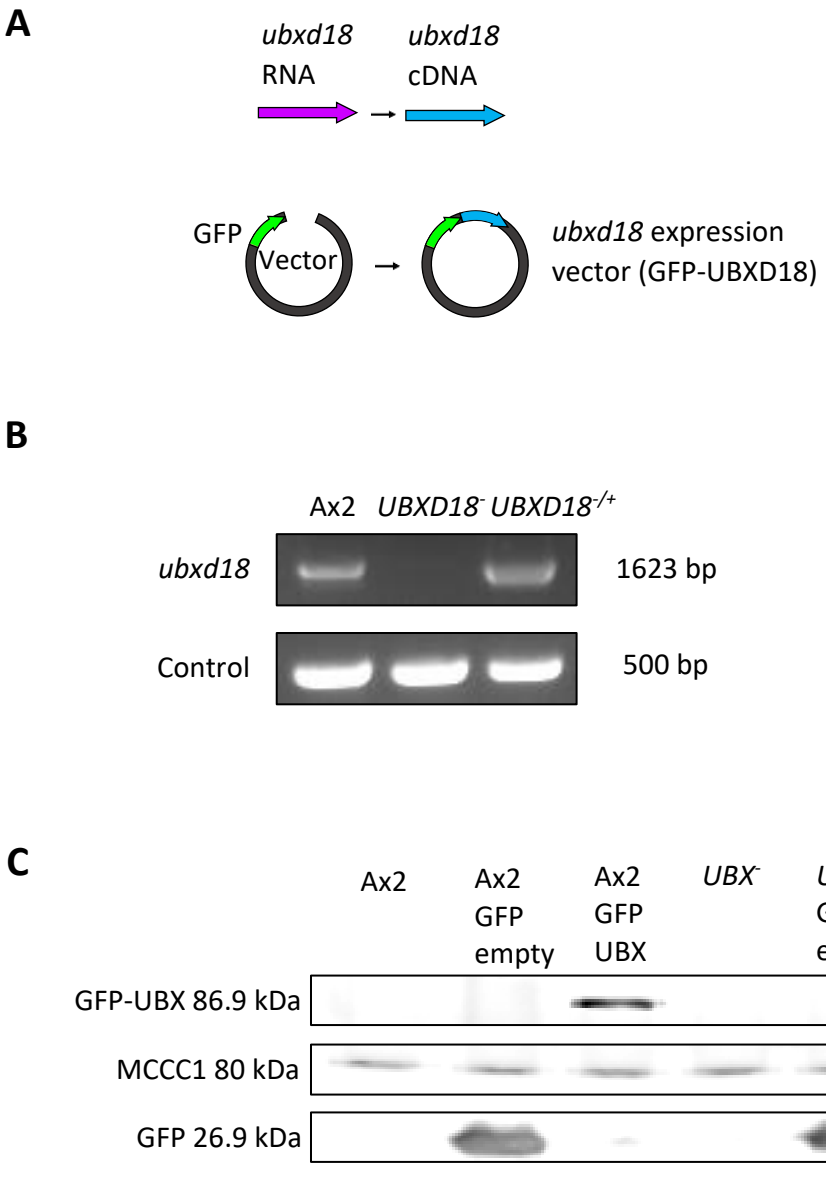

Figure 3. 15 Reintroduction of *ubxd18* gene expression. A) The open reading frame of *ubxd18* was amplified from cDNA with the incorporation of restriction sites for cloning into the pTX-GFP over-expression plasmid. B) The *ubxd18* expression vector (GFP-UBXD18) was transfected into *UBXD18*- and expression was confirmed using rt-PCR (with *Ig7* as a positive control). C) Western blotting was used to confirm presence of the correct size protein using an antibody against GFP. MCCC1 was used as a loading control.

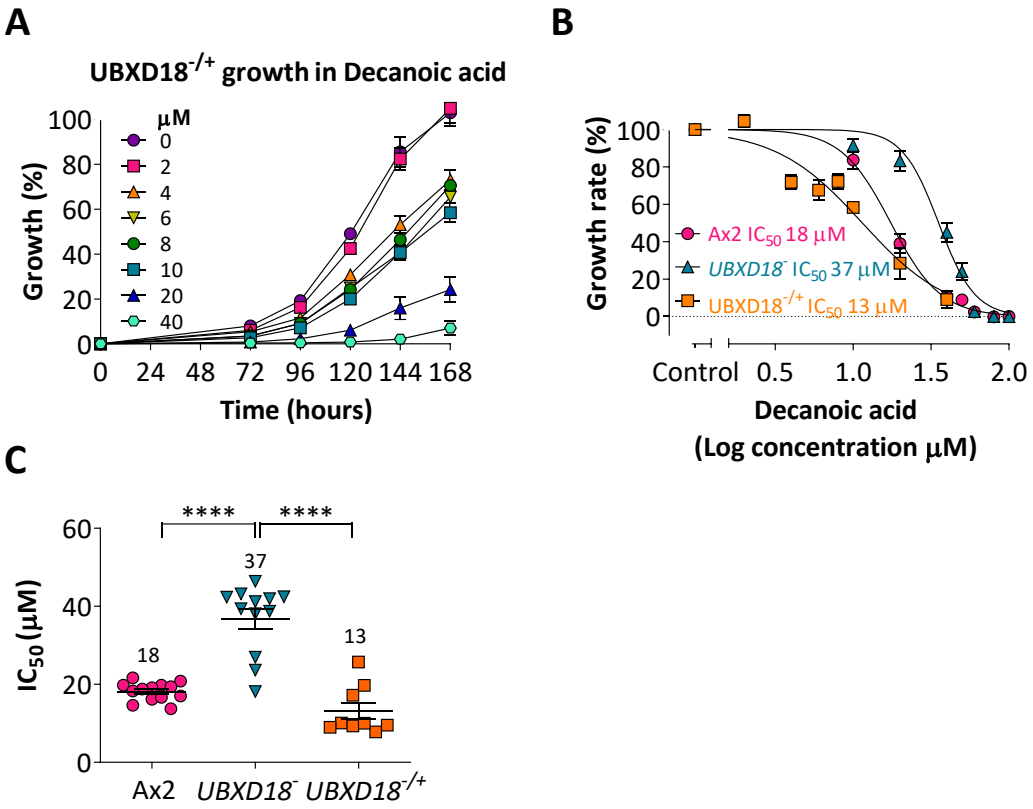

Figure 3. 16 Analysis of the effects of decanoic acid on UBXD18$^{-/+}$ growth.
A) *UBXD18*$^{-/+}$ (n = 9) was treated with a range of concentrations (µM) of decanoic acid, for 168 hours. Percentage growth was plotted normalised to the solvent control (0 µM, 0.2 % DMSO) at 168 hours. B) A dose response curve of growth rate plotted against Log concentration of decanoic acid was used to compare the decanoic sensitivity of wild type (Ax2) (n = 13), *UBXD18*$^{-+}$ (n = 12) and *UBXD18*$^{-/+}$ (n = 9). C) IC_{50} values for Ax2) (n = 13), *UBXD18*$^{-+}$ (n = 12) and *UBXD18*$^{-/+}$ (n = 9) in decanoic acid were compared. Data represent the mean ± SEM. Significance is indicated by **** $p \leq 0.0001$ (Mann-Whitney test).

3.3 Discussion

Ketogenic diets are well established treatments for epilepsy with exciting potential for use in other areas of health, however, the therapeutic mechanisms and secondary targets are not fully understood (Augustin *et al.*, 2018a). In this chapter, we have used *Dictyostelium* as a tractable model to establish that decanoic acid the key component of the MCT ketogenic diet, along with octanoic acid an accompanying dietary fatty acid, and 4-BCCA a related compound, all act on *Dictyostelium* to reduce cellular proliferation without disrupting *Dictyostelium* multicellular development. In

order to identify the cellular mechanisms behind the antiseizure effects of decanoic acid and 4-BCCA we utilised the growth inhibitory effects of these compounds to screen a mutant library. Mutants with disruptions in the genes *dna-pkcs*, *tkt* and *ubxd18* were found to confer resistance to decanoic acid, and a mutant with a gene disruption in *fcsA* was identified as conferring resistance to 4-BCCA, suggesting a potential role for the corresponding proteins in regulating the effects of these compounds.

Patients on the medium-chain triglyceride (MCT) ketogenic diet acquire around 45 % of their dietary energy from medium-chain triglycerides, which are metabolised in the intestine to generate free fatty acids (Neal *et al.*, 2008). Concentrations of medium-chain fatty acids in the plasma of patients on the MCT diet are raised to an average level of 157 µM for decanoic acid and 310 µM for octanoic acid (Sills, Forsythe and Haidukewych, 1986; Haidukewych, Forsythe and Sills, 1982; Dean, Bonser and Gent, 1989) compared to undetectable levels in individuals not on the diet. We have found that in *Dictyostelium,* decanoic acid and octanoic acid both inhibited cell proliferation at concentrations physiologically relevant to those seen in patients. In *Dictyostelium,* octanoic acid had a less potent effect on growth than decanoic acid (IC_{50} 86 µM compared to 18 µM), this is consistent with findings suggesting that octanoic acid is less potent than decanoic acid in regards to in vitro seizure control (Chang *et al.*, 2013). We found that 4-BCCA had a stronger growth inhibitory effect than decanoic acid or octanoic acid in *Dictyostelium* (IC_{50} 1.5 µM), this is also consistent with research showing that 4-BCCA has increased potency over these medium-chain fatty acids in in vitro seizure control (Chang *et al.*, 2015).

Demonstrating that *Dictyostelium* is sensitive to medium-chain fatty acids in cellular proliferation but not in development, suggests that these compounds are not having a general toxic effect, where a disruption in both proliferation and development would be expected, but are acting through specific molecular mechanisms (Perry *et al.*, 2020). In order to elucidate these molecular mechanisms, the growth inhibitory effects caused by decanoic acid and 4-BCCA were utilized to screen for resistant mutants representing potential molecular targets. Three genes, *dna-pkcs, tkt* and *ubxd18* were identified from a mutant library screen in decanoic acid. Growth assays with independent knockouts of *dna-pkcs* (*DNA-PKCs*$^{-}$) and

ubxd18 (*UBXD18*$^{-}$), and an independent knockdown of *tkt* (*TKT*$^{-}$) confirmed that a disruption in each of these genes results in partial resistance to decanoic acid. Growth assays with an independent gene knockout of *fcsA,* identified from a mutant library screen in 4-BCCA, demonstrated that a disruption in this gene confers partial resistance to both decanoic acid and 4-BCCA. These findings from independently generated mutants suggest that the observed fatty acid resistant phenotypes have arisen as a direct result of the disruptions in the identified genes, rather than any potential off target mutations, thus, implicating the corresponding proteins as potential molecular targets for decanoic acid or 4-BCCA.

The fundamental theory behind the *Dictyostelium* mutant library screen discussed in the chapter is that resistance to a compound arises due to a disruption in a gene encoding a protein that controls the sensitivity to that compound during growth, thus implicating that protein, or wider pathway in the action of the compound. However, if certain gene disruptions cause *Dictyostelium* cells to proliferate more rapidly, to expel the compound from the cell, or to prevent uptake of the compound, this could confer growth resistance to the cells without providing any useful insight into the mechanism of action of that compound. Therefore, consideration of potential targets is necessary to avoid false leads.

DNA-PKcs^{-} has been identified as partially resistant to the inhibitory effect of decanoic acid on *Dictyostelium* growth implicating DNA-PKcs as a potential target involved in regulating decanoic acid sensitivity. DNA-PKcs is the catalytic subunit of a protein kinase required for non-homologous end joining (NHEJ) in the repair of DNA double strand breaks (Ma *et al.*, 2002). DNA-PKcs has been shown to interact with a highly conserved AAA (ATPase Associated with diverse cellular activities) ATPase, p97, as part of the machinery for NHEJ (Jiang *et al.*, 2013; Livingstone *et al.*, 2005). Interestingly p97 is also known to interact with UBX domain containing proteins such as UBXD18*,* also identified as a potential molecular target for decanoic acid (Schuberth and Buchberger, 2008). This finding initially suggested a strong indication for p97 as a common target for decanoic acid. However, through communication with other members of the *Dictyostelium* community we became aware that the REMI mutant with a disruption within DNA-PKcs has been identified from multiple mutant library screens for unrelated compounds. It is unlikely that this protein is a target for

multiple unrelated compounds, suggesting that this mutant confers general resistance. Therefore, investigations into DNA-PKcs as a potential target for decanoic acid were halted. Since *DNA-PKcs*$^{-}$ is defective in repairing DNA double strand breaks (Hudson *et al.*, 2005), there is an increased chance of DNA damage resulting in additional gene disruptions in this cell line. Off-site mutations generated in this cell line may be responsible for the resistance to multiple compounds in growth.

The *Dictyostelium* mutant with an insertion within the gene *fcsA* has demonstrated growth resistance to both 4-BCCA and decanoic acid. This gene encodes a long-chain fatty acyl co A-synthetase (FcsA), an enzyme which catalyses the reaction between long-chain fatty acids and ATP to form fatty acyl-CoA. Fatty acyl-coA is the activated form of a fatty acid, available for metabolism (von Lohneysen *et al.*, 2003). As well as catabolic metabolism through beta oxidation or anabolism into triacylglycerol in fat droplets, acyl-coAs are involved in multiple processes such as membrane trafficking, cell signalling, enzyme activation, protein acylation, and the control of transcription, making the protein FcsA a potentially interesting molecular target for 4-BCCA and decanoic acid (von Lohneysen et al., 2003). However, in *Dictyostelium* the FcsA protein has been demonstrated to localise to the membranes of endocytic vesicles and mediate the fatty acid retrieval from endosomes into the cytoplasm (von Lohneysen *et al.*, 2003). This has been demonstrated by using a fluorescently labelled fatty acid analogue (C1-BODIPY-C12) to show that in *FcsA*$^{-}$ fatty acid uptake and fatty acid retrieval from phagosomes is reduced. Therefore, the fatty acyl coA-synthetase has been implicated in the retrieval of fatty acids from the phagosome thus making the activated fatty acyl-coA available to the cell. These findings are supported by results from mammalian cells that show that overexpression of long-chain fatty acyl co A-synthetase enhances fatty acid accumulation (Chiu et al., 2001). A defect in fatty acid uptake in *Dictyostelium FcsA*$^{-}$ cells could be responsible for conferring the partial resistance to decanoic acid and 4-BCCA that we have demonstrated. For this reason, we stopped investigations into FcsA as a potential target for medium-chain fatty acids. However, questions remain, as it unclear as to whether decanoic acid and 4-BCCA would be taken up into the cell through the same mechanisms as long-chain fatty acids.

The protein transketolase (TKT) has been implicated in regulating the sensitivity of *Dictyostelium* to decanoic acid, since knocking out the *tkt* gene confers partial growth resistance to this medium-chain fatty acid. Transketolase is a ubiquitous enzyme catalysing the reversible transfer of two carbon ketol units between ketose and aldose phosphates, connecting the pentose phosphate pathway to glycolysis, and thus is required for the production of reducing agent nicotinamide adenine dinucleotide phosphate (NADPH) (Boyle *et al.*, 2016). Following identification of the *tkt* REMI mutant, generation of an independent *tkt* knockdown (*TKT*$^{-}$) and recapitulation of the decanoic resistant phenotype, communication with other members of the *Dictyostelium* community has established that this mutant has also been identified as resistant in multiple mutant library screens. *TKT*$^{-}$ has been identified as resistant to compounds such as tanshinones, myrigalone A, and a range of mammalian teratogens. Furthermore, analysis of mutant pools by REMI-seq has identified *TKT*$^{-}$ as having a growth advantage (Gruenheit *et al.*, 2019). It is unclear how a disruption in the gene *tkt* could result in a general resistance to the growth inhibitory effects of multiple compounds or lead to a growth advantage, since a disruption in transketolase would reduce NADPH levels resulting in increased oxidative stress which would be expected to reduce proliferation rather than activate it (Xu *et al.*, 2016). The identification of a *tkt* REMI mutant from mutant library screens with multiple unrelated compounds and the discovery of an inherent growth advantage of this mutant suggest that TKT is not a specific molecular target for decanoic acid, but that when disrupted, confers general resistance. For this reason, investigations into TKT as a potential target for decanoic acid were concluded at this point.

The mutant library screen has implicated the protein UBXD18 as a regulator of sensitivity to decanoic acid. This target belongs to the UBX domain containing family of proteins, the largest group of cofactors for the ubiquitous p97 protein (Schuberth and Buchberger, 2008). p97 is a AAA ATPase known to function in multiple cellular processes such as autophagy, endoplasmic reticulum-associated degradation (ERAD), NF-κB signaling, and DNA damage response, making the UBXD18 protein an exciting potential target for decanoic acid (Yamanaka, Sasagawa and Ogura, 2012). This target is investigated in more detail in the following chapters.

Dictyostelium mutant libraries provide an excellent genetic system for understanding the molecular mechanisms of compounds and identifying regulators of cellular processes. In this chapter we have proposed UBXD18 as a potential target for decanoic acid and will address this target in the following chapters. However, the mutant library screens described in this chapter have led to the identification of potential false targets known to be resistant to other unrelated compounds, thus highlighting a limitation of this system. Further limitations of REMI mutant library screens exist, for example not all relevant genes can be discovered since some genes are vital for growth, precluding their appearance in a mutant library. Furthermore, using a traditional mutant library screen only genes conferring increased resistance to a compound can be identified, while mutants conferring increased sensitivity to a compound of interest are selected against. Recent innovations have been developed to overcome these deficits. An important new development is the REMI-seq approach which allows the frequency of each mutant to be quantified at the start and end of selection (Gruenheit *et al.*, 2019). This technique has employed a novel insertion vector containing sequences allowing identification of the insertion point via ligation of sequencing adapters. This technique allows illumina sequencing to accurately quantify the frequency of the different mutants before and after selection, increasing the throughput. Another recent development is an approach using chemical mutagenesis combined with whole genome sequencing (Li *et al.*, 2016). This technique utilises random mutagenesis via a chemical mutagen, followed by screening for a chosen trait. Whole genome sequencing can then be used to identify which genes carry frequent base changes, implicating that gene in the response to the trait. The benefit of this technique is the generation of partial loss of function or gain of function mutations in addition to null mutations primarily generated by REMI mutagenesis (Li *et al.*, 2016; Loomis, 2016).

In this chapter we have demonstrated that the key component of the MCT ketogenic diet, decanoic acid, along with the accompanying fatty acid, octanoic acid, and related compound, 4-BCCA, inhibit *Dictyostelium* cell proliferation in a dose dependent manner while having no effect on multicellular development. These findings indicate the presence of specific molecular targets for medium-chain fatty acids in *Dictyostelium.* In order to identify these targets, we utilised the growth

inhibitory effect of decanoic acid and 4-BCCA to screen a mutant library for mutants resistant to these effects. Using this process, we identified three genes from a screen in decanoic acid*, dna-pkcs, tkt* and *ubxd18* and one gene from a screen using 4-BCCA, *fcsA.* Investigation into these genes has implicated UBXD18 as an exciting potential target for decanoic acid, which is investigated in more detail in the following chapters.

Chapter 4

Investigating the UBX domain-containing protein 18 as a potential target for decanoic acid

4.1 Introduction

In order to identify mechanisms of action behind the antiseizure effects of decanoic acid we have shown that decanoic acid inhibits *Dictyostelium* cell proliferation, enabling the use of a genetic screen to identify that cells lacking a UBX domain containing protein (UBXD18) are partially resistant to these growth inhibitory effects. Using an independent *UBXD18*$^{-}$ mutant we have confirmed this resistant phenotype and have established that re-introducing *ubxd18* gene expression is capable of restoring sensitivity to decanoic acid. These findings implicate the UBX domain containing protein 18 as a potential target for decanoic acid.

UBXD18 belongs to the UBX domain containing family of proteins, of which there are eleven in *Dictyostelium*, and thirteen in humans (Rijal *et al.*, 2016). This family of proteins make up the largest subgroup of cofactors for the evolutionarily conserved protein p97 (Kloppsteck *et al.*, 2012; Schuberth and Buchberger, 2008). p97 is a AAA ATPase (Halawani and Latterich, 2006), also called VCP in Humans and CdcD in *Dictyostelium.* This ATPase uses the energy from ATP hydrolysis to extract substrate proteins from cellular structures such as protein complexes, membranes of cellular structures and chromatin (Meyer and Weihl, 2014; Patel and Latterich, 1998; Meyer *et al.*, 2000), allowing the released polypeptides to be degraded and protein homeostasis to be maintained. This function is required in processes such as endoplasmic reticulum-associated degradation (ERAD) (Ye, Meyer and Rapoport, 2001), autophagy (Ju *et al.*, 2009), golgi reassembly (Meyer, 2005), NFκB signalling (Li *et al.*, 2014), chromatin associated degradation (Vaz, Halder and Ramadan, 2013), DNA damage response (Indig *et al.*, 2004) as well as ribosomal and mitochondrial associated degradation (Fujii *et al.*, 2012; Meyer and Weihl, 2014) (Fig. 4.1). Mutations in p97 can lead to amyotrophic lateral sclerosis (ALS) (Tang and Xia, 2016) as well as to the rare multisystem degenerative disorder, inclusion body myopathy associated with Paget disease of bone and frontotemporal dementia (IBMPFD), that affects the central nervous system, muscle, and bone (Watts *et al.*, 2004). The importance of p97 in maintaining cellular homeostasis, and the association between p97 mutations and neurological disorders, highlights the disease relevance of this

protein, and establishes the cofactor UBXD18 as a potentially relevant target of decanoic acid.

In this chapter we demonstrate that the growth resistance of *UBXD18*$^{-}$ to decanoic acid is not shared with the related ketogenic diet associated fatty acid octanoic acid, suggesting a structurally specific response to decanoic acid. We establish the phenotypic characteristics of *UBXD18*$^{-}$, and through phylogenetic analysis identify potential human homologues. We further demonstrate that these conserved UBX domain containing proteins share a common UBX domain, containing a shared p97 binding site and establish that UBXD18 binds to p97 in *Dictyostelium,* implicating p97 as potential target for decanoic acid. Finally, we demonstrate that decanoic acid inhibits p97 activity in a UBXD18 dependent manner confirming an involvement of this ATPase as in the cellular response to decanoic acid.

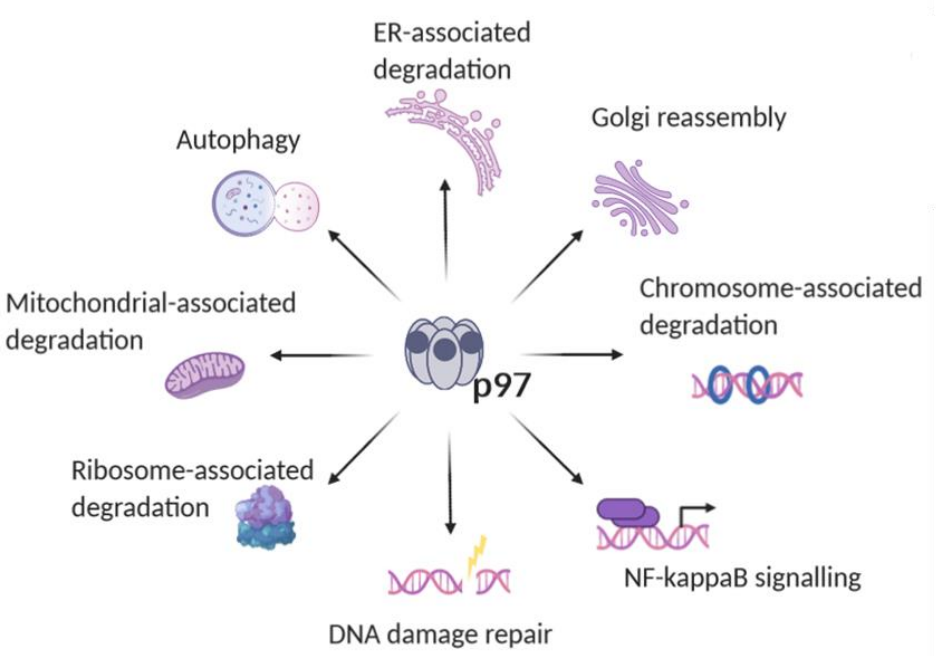

Figure 4. 1 Cellular functions of p97. Schematic showing the multiple roles of p97 dependent on the ATPase activity to extract substrate proteins from cellular structures.

4.2 Results

4.2.1 The effects of octanoic acid and 4-BCCA on *UBXD18*$^-$ proliferation

To establish whether UBXD18 regulates sensitivity to other medium-chain fatty acids in addition to decanoic acid, the effects of octanoic acid, and 4-BCCA on *UBXD18*$^-$ growth were investigated (Fig. 4.2A). *UBXD18*$^-$ showed no change in sensitivity to octanoic acid compared to wild type (Ax2) (wild type IC_{50} 79 µM, 95 % CI: 73 µM to 100 µM and *UBXD18*$^-$ IC_{50} 87 µM, 95 % CI: 82 µM to 113 µM, $p = 0.49$, $n \geq 4$), suggesting structural specificity in the targeting of UBXD18 by decanoic acid (Fig. 4.2B and C). The growth effect of the related compound 4-BCCA on *UBXD18*$^-$ was also investigated (Fig. 4.2D). *UBXD18*$^-$ showed partial resistance to 4-BCCA when compared to wild type (wild type IC_{50} 1.5 µM, 95 % CI: 0.83 µM to 2.46 µM and *UBXD18*$^-$ IC_{50} 7.4 µM, 95 % CI: 5.11 µM to 9.37 µM, $p = 0.0022$, $n = 6$) (Fig. 4.2E and F). Thus, growth sensitivity analysis implicates UBXD18 in the cellular response to 4-BCCA but not octanoic acid.

4.2.2 Phenotypic and phylogenetic analysis of *UBXD18*$^-$

In order to investigate the cellular function of UBXD18 we initially investigated the role of this protein in *Dictyostelium* growth and development (Fig. 4.3). *Dictyostelium* cell proliferation was quantified after 7 days, with no significant difference observed in cell number between wild type and *UBXD18*$^-$, indicating a comparable rate of proliferation between the two cell lines (Fig. 4.3A). To investigate whether UBXD18 is required for *Dictyostelium* development, we assessed the ability of *UBXD18*$^-$ to form fruiting bodies by starving cells on nitrocellulose filters for 22 hours (Fig. 4.3B). *UBXD18*$^-$ formed fruiting bodies in the same time frame and of the same morphology as those formed by wild type. These data suggest that knocking out *ubxd18* has no effect on *Dictyostelium* growth or development.

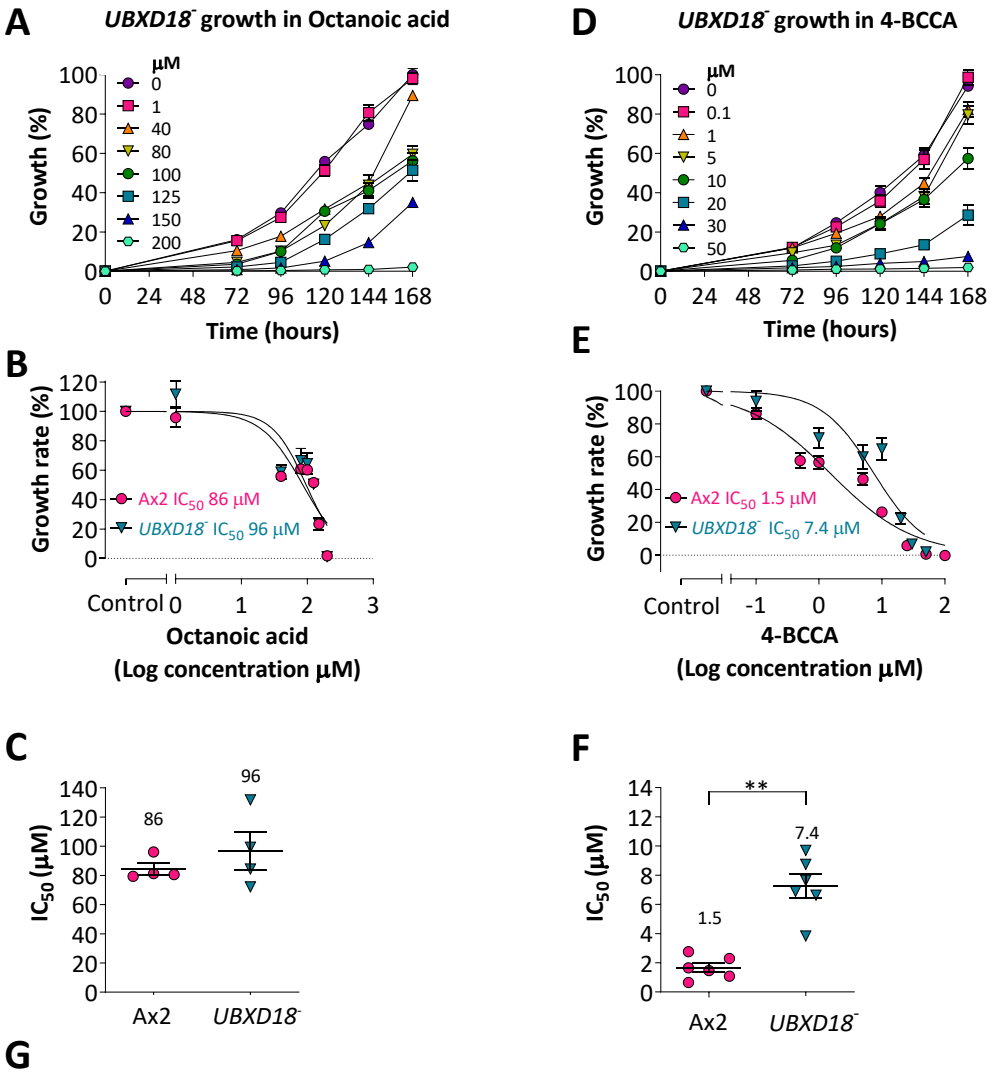

G

	Ax2 IC_{50} (µM)	*UBXD18*⁻ IC_{50} (µM)	Significance difference
Decanoic acid	18 (95% CI:17 to 20)	37 (95% CI:31 to 43)	$p \leq 0.0001$
Octanoic acid	86 (95% CI:73 to 100)	96 (95% CI:82 to 113)	$p = 0.49$
4-BCCA	1.5 (95% CI:0.83 to 2.46)	7.4 (95% CI:5.11 to 9.37)	$p = 0.0022$

Figure 4. 2 Effects of octanoic acid and 4-BCCA of on *UBXD18*⁻ growth.

A) An independent knockout of *UBXD18*⁻ was treated with a range of concentrations of octanoic acid (µM) for 168 hours. Percentage growth was plotted normalised to the solvent control (0 µM, 0.2 % DMSO) at 168 hours (n = 4). B) Dose response curves of normalised growth rate plotted against Log concentration of octanoic acid were used to compare the octanoic acid sensitivity of wild type (Ax2) (n = 4) to *UBXD18*⁻ (n = 4). C) IC_{50} values for wild type (n = 4) and *UBXD18*⁻ (n = 4) in octanoic acid were compared. D) *UBXD18*⁻ was treated with a range of concentrations of 4-BCCA (µM) for 168 hours (n = 6). E) Dose response curves were used to compare the 4-BCCA sensitivity of wild type (n = 6) and *UBXD18*⁻ (n = 6). F) IC_{50} values for wild type (n = 4) and *UBXD18*⁻ (n = 4) in 4-BCCA were compared. G) Sensitivity of wild type and *UBXD18*⁻ was compared. Data represent the mean ± SEM. Significance is indicated by ** $p \leq 0.01$ (Mann Whitney test).

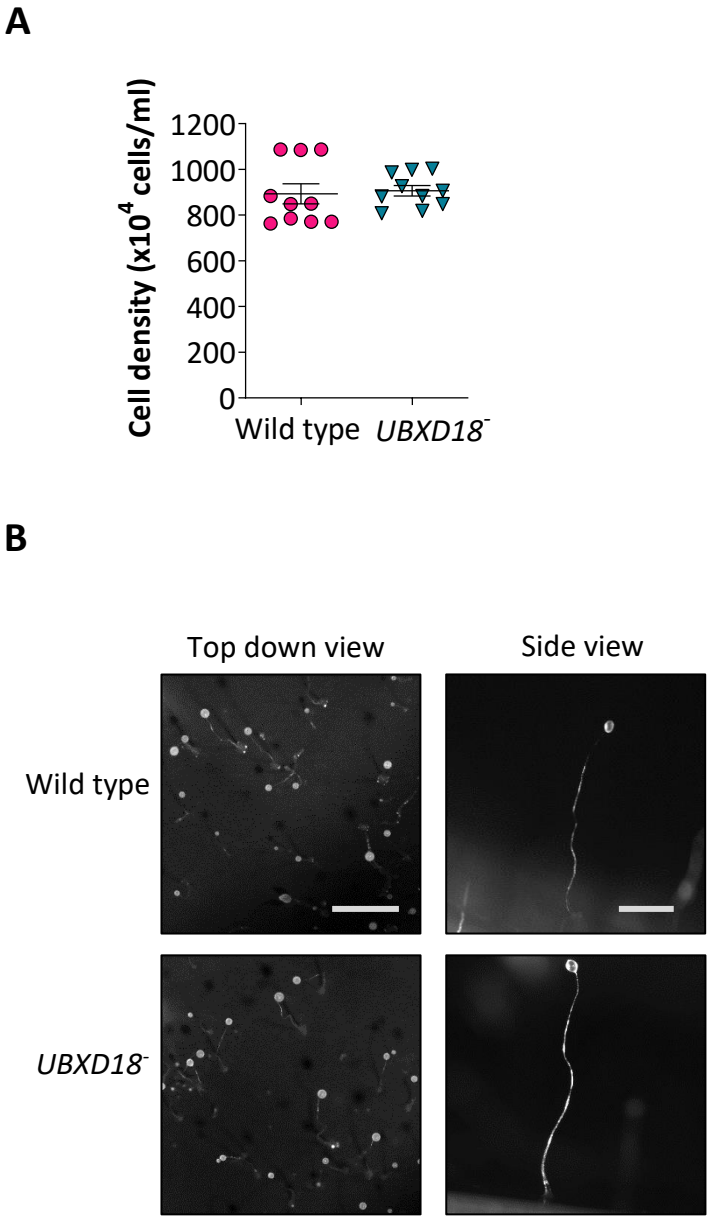

Figure 4. 3 *UBXD18*- behaves like wild type *Dictyostelium* in cellular proliferation and development. A) *Dictyostelium* wild type (Ax2) and *UBXD18*- cells were set up at 2 x 10^4 cells/ml. Cell density was quantified after 7 days (n = 10). Data represent the mean ± SEM (unpaired t-test). B) Qualitative evaluation of the developmental phenotype of *UBXD18*- compared to wild type following 22 hours starvation on nitrocellulose filters. Top down view (scale bar 1 mm) and side on (scale bar 0.2 mm) images represent results from triplicate experiments.

Cladistic analysis of all *Dictyostelium* and human UBX proteins was carried out with the aim of investigating their relatedness (Fig. 4.4A). This analysis suggested that the human UBXN1 (uniprot Q04323) and UBXD2 (uniprot Q92575) proteins are the most evolutionarily related to the *Dictyostelium* UBXD18 protein. These three proteins share a conserved UBX domain that was further analysed to assess amino acid conservation (Fig. 4.4B and C). The *Dictyostelium* UBX domain shared 28 % identical, and 51 % similar amino acids with the UBX domain of UBXN1, and 27 % identical and 51% similar amino acids with the UBX domain of UBXD2 (Fig. 4.4B). The AAA ATPase p97 binding loop (s3/s4 loop) was partially conserved between these proteins (Fig. 4.4B and C) (Dreveny *et al.*, 2004), suggesting that these proteins are potential p97 binding partners.

4.2.3 Phylogenetic analysis of p97

Since UBXD18 contains a general p97 interaction motif (Dreveny *et al.*, 2004; Schuberth and Buchberger, 2008) (Fig. 4.4B and C) we verified the presence of a conserved p97 protein in *Dictyostelium.* The *Dictyostelium* p97 protein shows conservation of domain organisation (Fig. 4.5A) and a high sequence identity (78 %) with the human protein (Fig. 4.5B). Amino acids (Asp35, Ser37, Val38 Phe52, Ile70, Leu72, Tyr110, and Tyr143) involved in creating a hydrophobic binding pocket for the p97 binding loop of UBX domain containing proteins (Hanzelmann, Buchberger and Schindelin, 2011; Dreveny *et al.*, 2004) are conserved between the *Dictyostelium* and human p97 proteins (Fig. 4.5B), indicating a potential cellular interaction between UBXD18 and p97 in *Dictyostelium*.

A

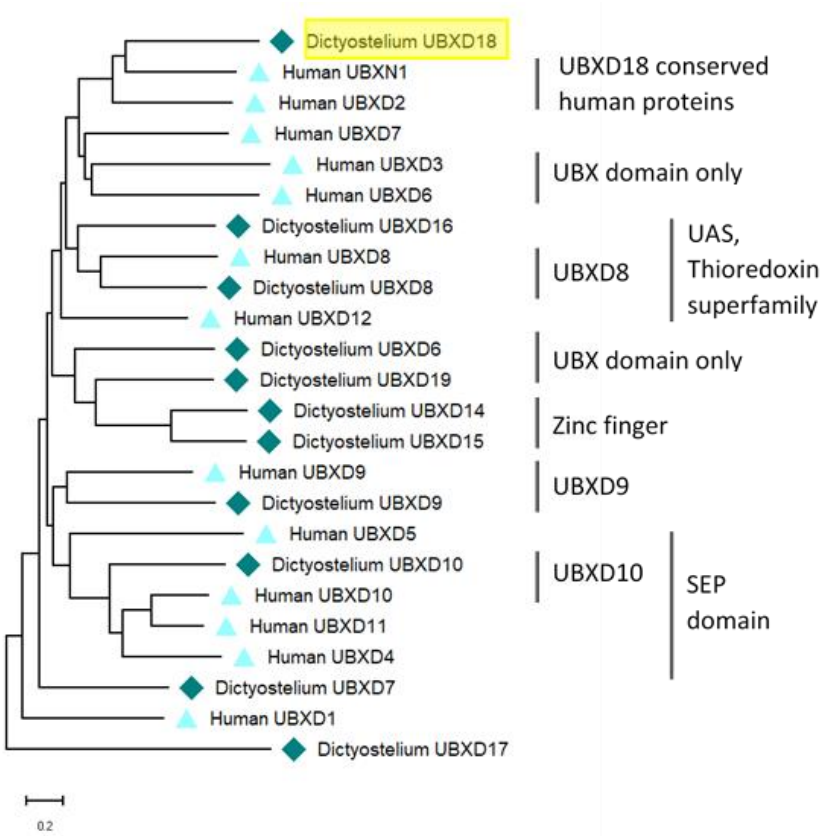
Dictyostelium UBXD18
Human UBXN1
Human UBXD2
Human UBXD7
Human UBXD3
Human UBXD6
Dictyostelium UBXD16
Human UBXD8
Dictyostelium UBXD8
Human UBXD12
Dictyostelium UBXD6
Dictyostelium UBXD19
Dictyostelium UBXD14
Dictyostelium UBXD15
Human UBXD9
Dictyostelium UBXD9
Human UBXD5
Dictyostelium UBXD10
Human UBXD10
Human UBXD11
Human UBXD4
Dictyostelium UBXD7
Human UBXD1
Dictyostelium UBXD17
0.2
UBXD18 conserved human proteins
UBX domain only
UBXD8
UAS, Thioredoxin superfamily
UBX domain only
Zinc finger
UBXD9
UBXD10
SEP domain

B

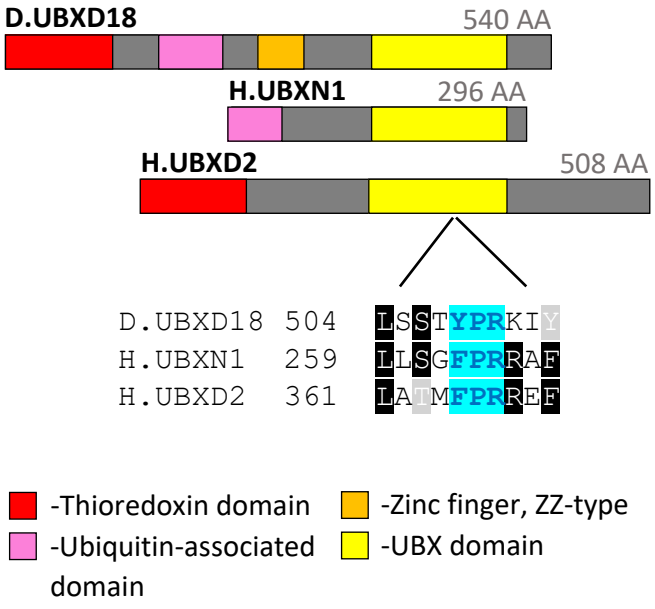
D.UBXD18
540 AA
H.UBXN1
296 AA
H.UBXD2
508 AA
D.UBXD18 504 LSSTYPRKIY
H.UBXN1 259 LLSGFPRRAF
H.UBXD2 361 LAIMFPRREF
-Thioredoxin domain
-Ubiquitin-associated domain
-Zinc finger, ZZ-type
-UBX domain

C

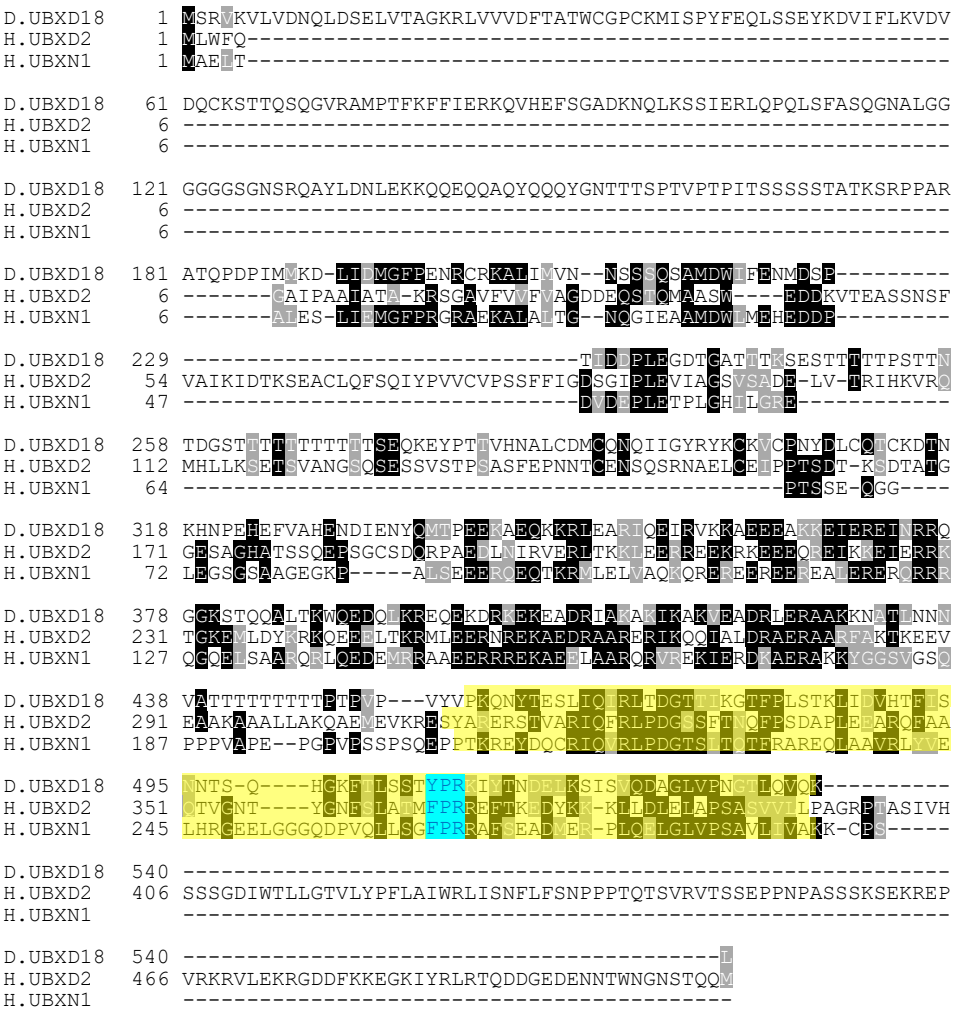

Figure 4. 4 The *Dictyostelium* UBXD18 protein, identified from a mutant library screen, contains the evolutionarily conserved UBX domain. A) Cladistic analysis of *Dictyostelium* and human UBX domain contacting proteins. Protein sequences were aligned using Clustal and the phylogenetic tree was generated using the neighbour joining method based on the alignment (MEGA7). The tree is drawn to scale, with branch lengths in the same units as those of the evolutionary distances used to infer the phylogenetic tree. The evolutionary distances were computed using the Poisson correction method and are in the units of the number of amino acid substitutions per site. B) The two most highly conserved human proteins UBXN1 and UBXD2 (H. UBXD2 and H. UBXN1) are shown alongside a schematic of the *Dictyostelium* UBXD18 protein (D. UBXD18). These proteins share a common UBX domain (highlighted in yellow) with a highly conserved s3/s4 loop involved in binding p97 (highlighted in blue). The s3/s4 loop consists of an aromatic amino acid tyrosine or phenylalanine, followed by proline and arginine. C) Full protein sequence alignment of the *Dictyostelium* UBXD18 protein with the two most highly conserved human proteins UBXN1 and UBXD2. Identical amino acids are coloured black, and similar amino acids are coloured grey. The UBX domains are highlighted in yellow and the s3/s4 loop is highlighted in blue.

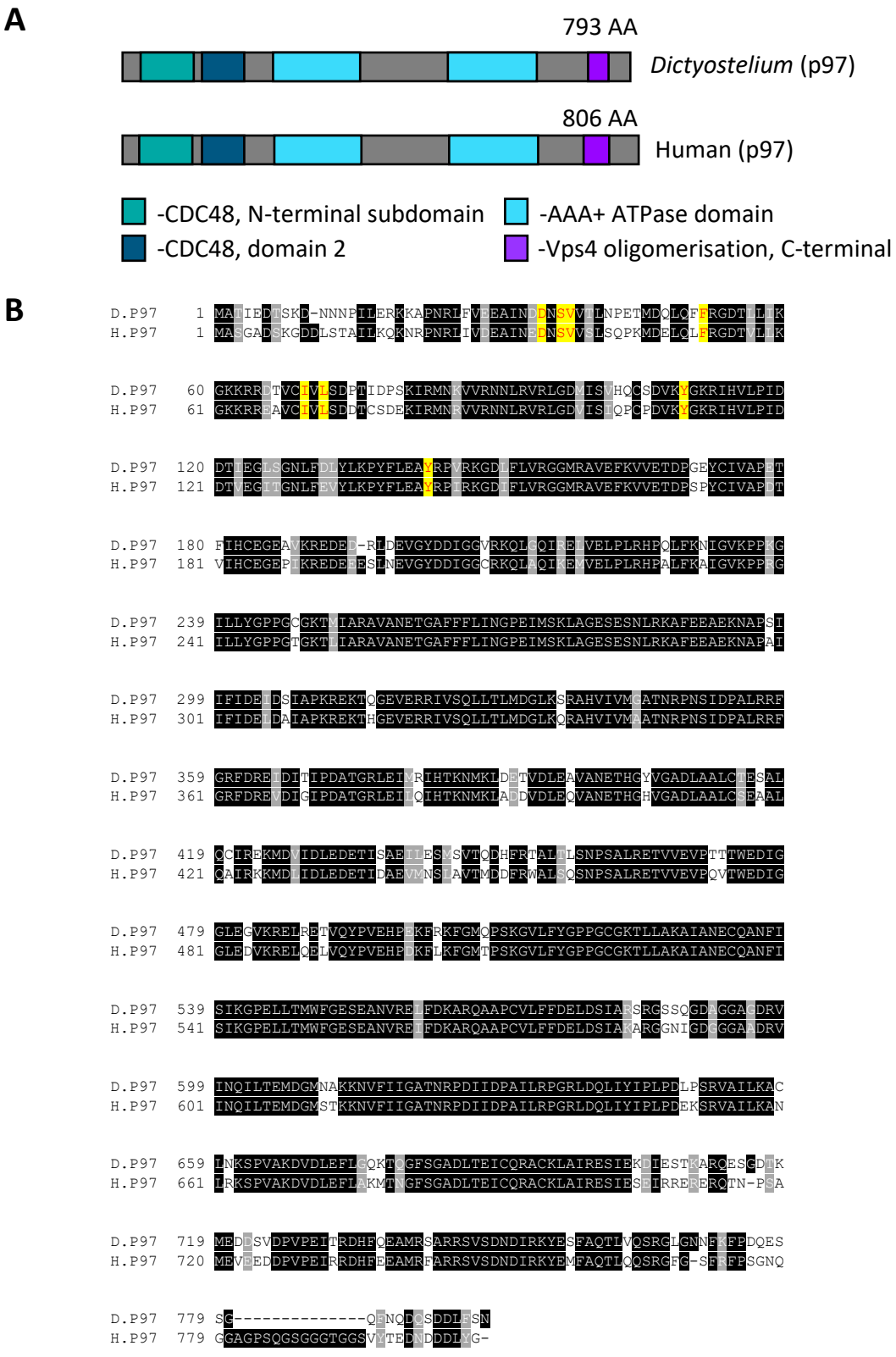

Figure 4. 5 *Dictyostelium* and human p97 proteins are highly conserved. A) Schematic of the *Dictyostelium* and human p97 proteins, showing 78% sequence identity. B) Full protein sequence alignment of the *Dictyostelium* p97 (D. p97) and human p97 (H. p97) proteins. Amino acids creating a hydrophobic binding pocket for the s3/s4 loop of UBX domain containing proteins are highlighted (Asp35, Ser37, Val38 Phe52, Ile70, Leu72, Tyr110, and Tyr143) (Hanzelmann, Buchberger and Schindelin, 2011; Dreveny *et al.*, 2004).

4.2.4 Analysis of an interaction between UBXD18 and p97

Following the identification of a general p97 interaction motif in UBXD18 (Dreveny *et al.*, 2004; Schuberth and Buchberger, 2008) (Fig. 4.4), and establishing that the *Dictyostelium* and human p97 proteins share high sequence identity (Fig. 4.5), we designed an immunoprecipitation experiment to investigate an interaction between UBXD18 and p97. For immunoprecipitation, cells co-expressing fluorescently tagged UBXD18 and p97 were required. We employed the GFP-UBXD18 expression vector (Fig. 3.15) and generated an extrachromosomal vector designed to express *p97* with a carboxy-terminal RFP domain attached (p97-RFP) (Fig. 4.6A). To make this vector the open reading frame of *p97* was amplified from wild type (Ax2) cDNA with the incorporation of restriction enzyme sites to enable cloning into the pTX-GFP vector. This expression vector was verified by sequencing before being transfected into wild type cells and cell lysates were analysed by western blotting to confirm the presence of the correct size (116 kDa) RFP-tagged protein (Fig. 4.6B). This p97-RFP vector was then transfected into *Dictyostelium* cells along with the GFP-UBXD18 vector to create a cell line co-expressing GFP-UBXD18 and p97-RFP. A cell line expressing the GFP vector (pTX-GFP) without the *ubxd18* coding sequence was also transfected into cells along with the p97-RFP vector as a control. To monitor binding of p97-RFP and GFP-UBXD18, cell lysates from both cell lines were mixed with agarose beads coated with GFP antibody, and the interacting proteins were isolated and analysed using western blot with anti-GFP and anti-RFP antibodies (Fig. 4.6C). p97-RFP was found to bind to GFP-UBXD18 but not to free-GFP (Fig. 4.6C), suggesting that UBXD18 interacts with p97 in *Dictyostelium.*

To confirm an interaction between GFP-UBXD18 and p97-RFP we investigated the cellular localisation of these fluorescently tagged proteins. Using live cell imaging, GFP-UBXD18 and p97-RFP were found to co-localise throughout the cytoplasm and the nucleus (Fig. 4.6D), consistent with that suggested for the human UBXD2 and UBXN1 proteins (Wang *et al.*, 2013; Liang *et al.*, 2006). Colocalization was also observed using immunofluorescence with antibodies against GFP and RFP and DAPI to confirm nuclear localisation (Fig. 4.6E).

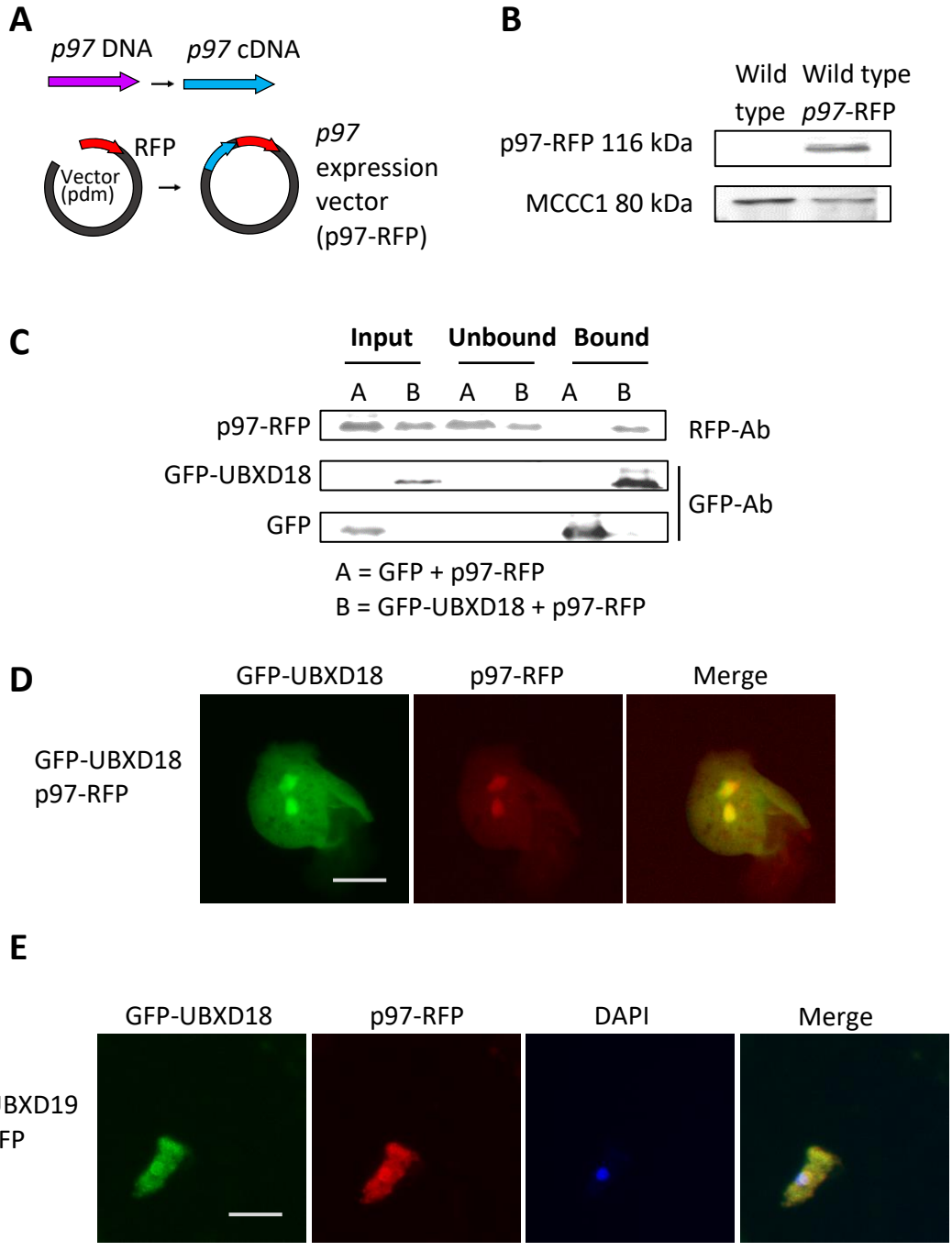

Figure 4. 6 *Dictyostelium* UBXD18 interacts with p97. A) Schematic for the generation of a *p97* expression vector (p97-RFP). B) The presence of p97-RFP within the Ax2 p97-RFP cell line was confirmed by western blot analysis using an antibody against RFP (with MCCC1 as a loading control). C) Cell lysates of *Dictyostelium* cells co-expressing GFP-UBXD18 (87 kDa) (or free-GFP (27 kDa) as a control) and p97-RFP (116 kDa) were subjected to pull down with GFP trap beads and the interaction analysed by western blot using anti-GFP and anti-RFP antibodies. Co-localisation of GFP-UBXD18 and p97-RFP observed by D) visualising fluorescence in live cells co-expressing GFP-UBXD18 and p97-RFP or by E) immunofluorescence using antibodies against GFP and RFP. Scale bars represent 10 µm.

4.2.5 Investigating the effect of decanoic acid on p97 activity

An interaction between UBXD18 and p97 suggests a role for UBXD18 in regulating p97 function, and thus implicates p97 in the cellular changes caused by decanoic acid in *Dictyostelium*. To analyse this, we assessed the effect of decanoic acid on p97 activity by treating wild type (Ax2) *Dictyostelium* p97-RFP expressing cells with decanoic acid, octanoic acid or the established selective p97 inhibitor DBeQ (N2,N4-dibenzylquinazoline-2,4-diamine) (Parzych *et al.*, 2015; Ching *et al.*, 2013) for 24 hours before immunoprecipitation of p97-RFP and the direct assessment of specific p97 activity (Rule, Patrick and Sandkvist, 2016) (Fig. 4.7A and D). Treatment with decanoic acid (60 µM) caused a 33 % decrease in p97-RFP ATPase activity (95 % Cl: 31 % to 36 %, $p = 0.038$, $n = 6$). Treatment with octanoic acid (120 µM) had no significant effect on p97-RFP ATPase activity (7 % decrease, $p > 0.99$, $n = 6$), while the p97 inhibitor DBeQ (7.5 µM) significantly reduced p97-RFP ATPase activity (51 % decrease, 95 % Cl: 47 % to 56 %, $p = 0.00040$, $n = 6$). Having demonstrated that decanoic acid but not octanoic acts to reduce p97-RFP activity, we assessed the effect of decanoic acid on p97-RFP activity in cells lacking UBXD18 (*UBXD18*$^{-}$) (Fig. 4.7B and E). p97-RFP activity in *UBXD18*$^{-}$ was unresponsive to treatment with decanoic acid (10 % decrease, $p = 0.31$, $n = 6$). *UBXD18*$^{-/+}$ showed restored decanoic acid sensitivity following 24-hour treatment (49 % decrease in p-4E-BP1 levels, 95 % Cl: 46 % to 57 %, $p = 0.026$, $n = 6$) (Fig. 4.7C and F). These findings suggest that decanoic acid is acting through a mechanism involving UBXD18 to reduce p97 activity in *Dictyostelium*.

4.2.6 Predicted binding of decanoic and octanoic acid to UBXD18

Following the identification that decanoic acid but not octanoic acid inhibits p97 activity in a UBXD18 dependent manner, we used computational docking software to predict how these fatty acids may interact with the UBXD18 protein, with the aim of highlighting differences capable of explaining differential effects on p97 activity. We first predicted the tertiary structure of UBXD18 using the protein prediction software Phyre2 (Kelley *et al.*, 2015), then used the swiss-dock ligand interaction programme to predict potential decanoic and octanoic acid docking sites (Grosdidier, Zoete and Michielin, 2011a; Grosdidier, Zoete and Michielin, 2011b).

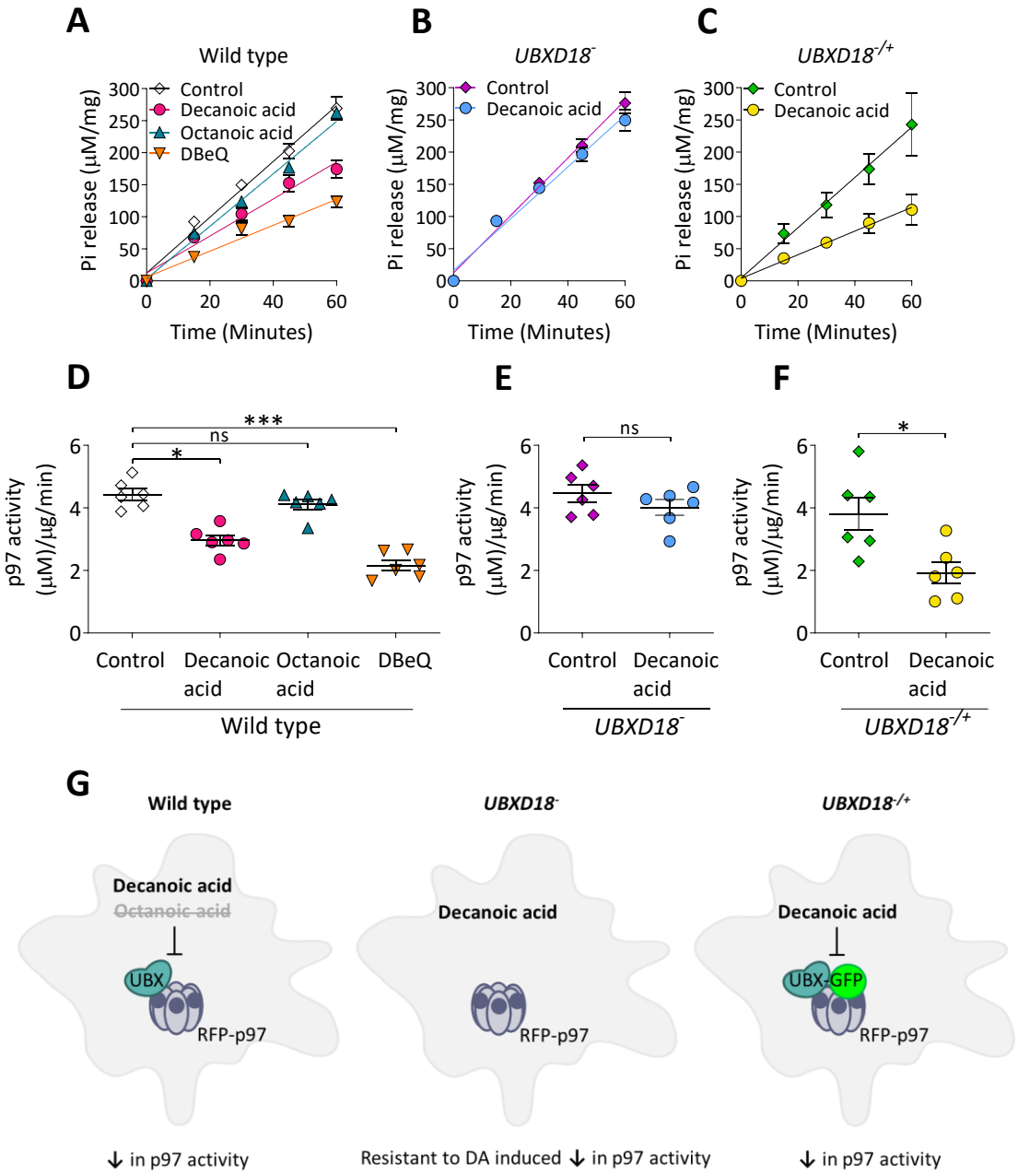

Figure 4. 7 Decanoic acid inhibits p97 activity in a UBXD18 dependent manner. A) Analysis of phosphate release from an ATP hydrolysis reaction with p97-RFP isolated from wild type *Dictyostelium* cells treated with decanoic acid (60 µM), octanoic acid (120 µM) or DBeQ (7.7 µM) for 24 hours (n = 6). Phosphate release was also analysed from ATP hydrolysis reactions with p97-RFP isolated from B) *UBXD18*$^{-}$ (n = 6) and C) *UBXD18*$^{-/+}$ (n = 6) treated with decanoic acid (60 µM) for 24 hours. The amount of released phosphate (µM) relative to protein concentration (µg) was plotted versus time (minutes) and subjected to linear regression analysis. The gradient was plotted, representing the rate of ATP hydrolysis (p97 activity µM phosphate/µg protein/min) for D) wild type (n = 6, Kruskal-Wallis test with Dunn's post hoc test), E) *UBXD18*$^{-}$ (n = 6, Mann-Whitney test) and F) *UBXD18*$^{-/+}$ (n = 6, Mann-Whitney test). G) Schematic of UBXD18 (UBX) dependent decanoic acid (DA) induced p97 inhibition. Significance is indicated by ns $p > 0.05$, * $p \leq 0.05$, *** $p \leq 0.001$.

Protein templates from 14 proteins with structures deposited in the protein data bank (PDB) were selected to model UBXD18. This approach provided good coverage of the thioredoxin domain and the UBX domain of the UBXD18 protein. Docking analysis of both decanoic acid and octanoic acid to the modelled structure for UBXD18 suggests that the location of the most energetically favourable location for binding is conserved between these fatty acids (Fig. 4.8A). The location of this predicted docking site is in the vicinity (within 5 angstroms) of the s3/s4 loop involved in binding p97 (Fig. 4.8A). Binding of decanoic acid to this site is predicted to be slightly more energetically favourable than the binding of octanoic acid (decanoic acid ΔG -9.1 and octanoic acid ΔG -8.7). Docking analysis of all viable interaction sites for decanoic and octanoic acid suggests that there are multiple binding sites predicted to exclusively bind decanoic acid (Fig. 4.8B), which could explain the specificity to this fatty acid.

While this protein model provides good coverage of the thioredoxin and UBX domains, the modelling of the mid-section of this protein is unreliable, due to a lack of homologous protein structures. To overcome these problems, and to investigate predicted binding to a human protein, we also investigated the predicted docking of decanoic acid and octanoic acid to the UBX domain of the human UBXD2 protein. The structure of this domain was available (solution NMR) on the protein data bank, avoiding complications resulting from *ab initio* modelling. Docking analysis on this domain predicted that the most energetically favourable location for the binding of decanoic acid (ΔG -7.53) is at a different location to that of octanoic acid (ΔG -7.51) (Fig. 4.9A). However, when all viable binding sites are considered clusters of octanoic acid are observed at the same locations as decanoic acid (Fig. 4.9B). Observing predicted docking of these fatty acids in the vicinity (within 5 angstroms) of the p97 binding site, reveals that both fatty acids bind in the same conformation, with decanoic acid binding slightly more favourably than octanoic acid (decanoic acid ΔG -6.69, octanoic acid ΔG -6.54) (Fig. 4.9C). While these data, gathered from computational docking programmes, highlight some differences in binding site and affinity of decanoic acid and octanoic acid, lack of an exact structure limits the reliability of these predictions.

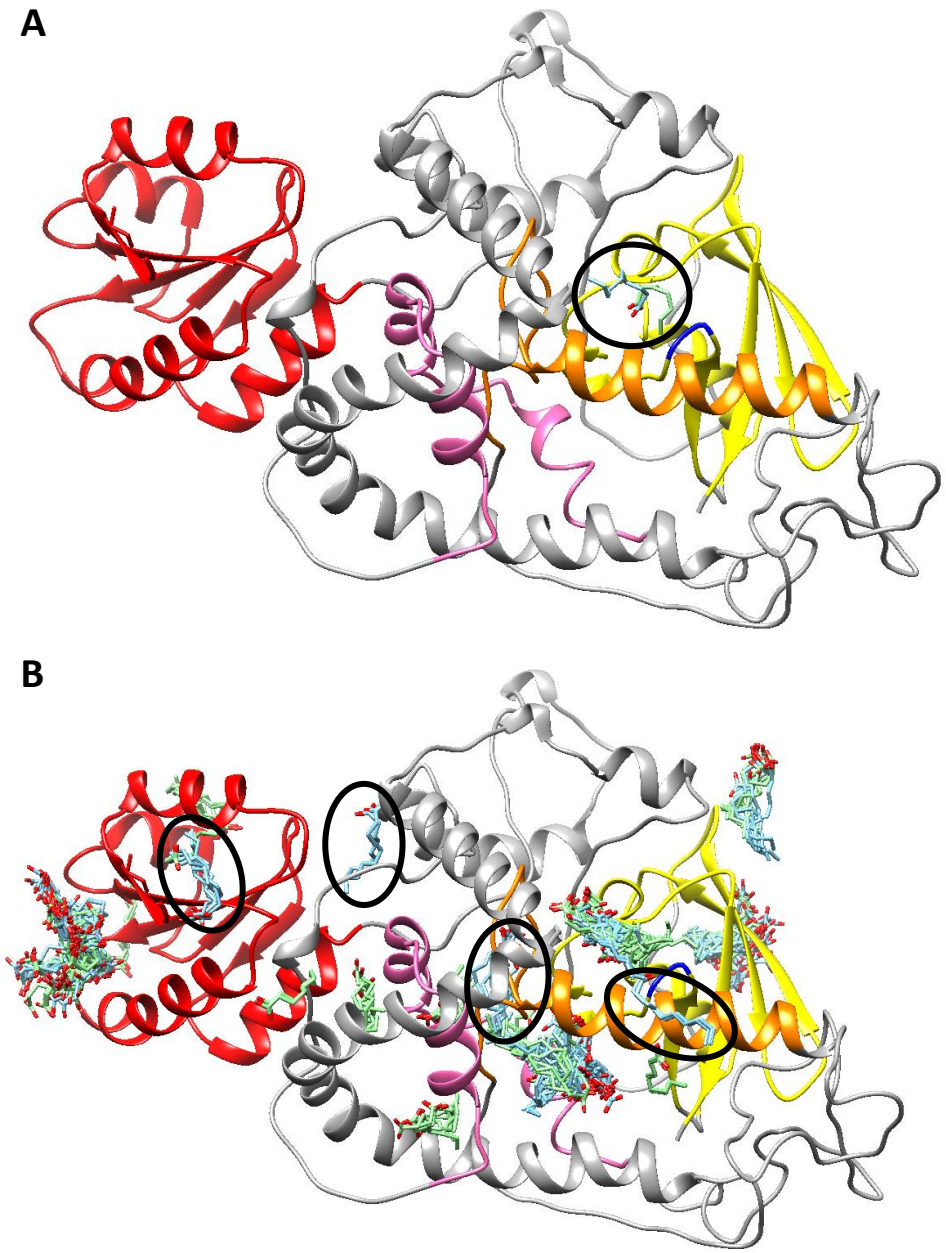

Figure 4. 8 Predicted docking analysis of decanoic acid (blue) and octanoic acid (green) to the *Dictyostelium* UBXD18 protein. The tertiary structure of the *Dictyostelium* UBXD18 protein was predicted using phyre2 protein prediction software. The thioredoxin domain is labelled in red, the ubiquitin-associated domain is labelled in pink, the zinc finger domain is labelled in orange, and the UBX domain is labelled in yellow, with the s3/s4 loop (within the UBX domain), involved in binding p97, highlighted in blue. Potential decanoic acid and octanoic acid sites have been identified using swiss-dock ligand interaction software. A) The most energetically favorable locations for decanoic acid (ΔG -9.1) and octanoic acid (ΔG -8.7) are displayed. B) All viable binding sites are displayed, with decanoic acid only binding clusters highlighted.

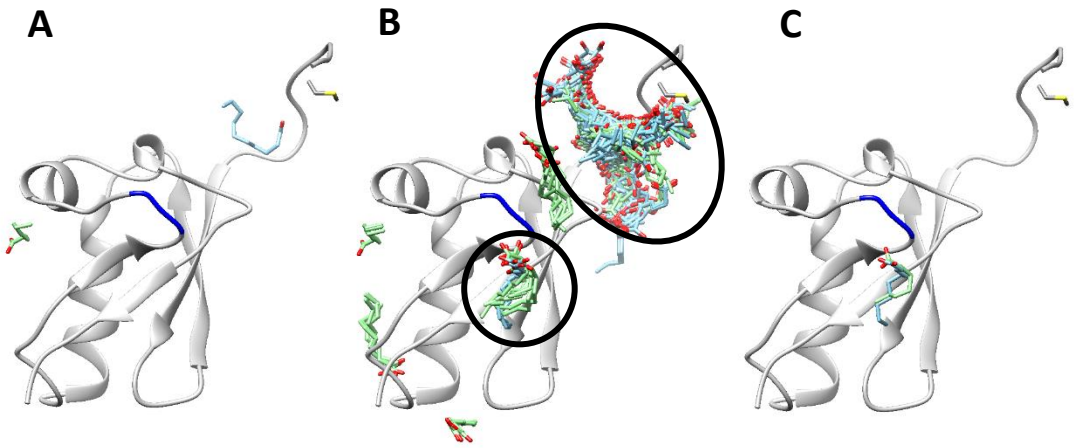

Figure 4. 9 Predicted docking analysis of decanoic acid (blue) and octanoic acid (green) to the UBX domain of human UBXD2. The structure of the UBX domain of human UBXD2 has been determined by solution NMR, with the s3/s4 loop, involved in binding p97, highlighted in blue. Potential decanoic acid and octanoic acid sites have been identified using swiss-dock ligand interaction software. A) The most energetically favorable locations for decanoic acid (ΔG -7.53) and octanoic acid (ΔG -7.51) are displayed. B) All viable binding sites are displayed, with decanoic acid binding clusters highlighted. C) Predicted docking of decanoic acid and octanoic acid in the vicinity (within 5 angstroms) of the p97 binding site is displayed (decanoic acid ΔG -6.69, octanoic acid ΔG -6.54).

4.3 Discussion

In order to understand the therapeutic mechanisms of decanoic acid provided by the ketogenic diet, we have screened a *Dictyostelium* mutant library to identify UBXD18 as a potential target for this fatty acid. We have confirmed that a mutant with a disruption in the gene *ubxd18* is partially resistant to the effects of decanoic acid implicating the protein UBXD18 in regulating the cellular effects of decanoic acid. In this chapter we demonstrate that *UBXD18*$^{-}$ is not resistant to octanoic acid, the other fatty acid provided at high concentrations by the MCT diet, suggesting that UBXD18 is regulating the response to decanoic acid in a structurally specific manner. In order to understand the potential role of the relatively uncharacterised UBXD18 protein in *Dictyostelium* we demonstrate that the basic cellular characteristics of growth and development are unaffected in the mutant *UBXD18*$^{-}$. Furthermore, we use phylogenetic analysis to identify the human proteins, UBXN1 and UBXD2 as the

closest related human UBX domain containing proteins to *Dictyostelium* UBXD18. Following the identification of a conserved p97 binding site in this protein, we demonstrate an interaction between *Dictyostelium* GFP-UBXD18 and p97-RFP. Finally, we show that decanoic acid but not octanoic acid inhibits p97 in a UBXD18 dependent manner, indicating an involvement of p97 in the cellular changes caused by decanoic acid.

Having implicated UBXD18 as a potential target for decanoic acid, we demonstrated that *UBXD18*$^{-}$ does not confer resistance to the growth inhibitory effects of octanoic acid, suggesting that the UBXD18 is not a generic target for all medium-chain fatty acids (Fig. 4.2A, B and C). We established that *UBXD18*$^{-}$ is partially resistant to 4-BCCA (Fig. 4.2B, C and D), suggesting that 4-BCCA and decanoic acid both act on *Dictyostelium* in a UBXD18 dependent manner. This is of interest since decanoic acid and 4-BCCA have similar effects in reducing epileptiform activity in an ex vivo hippocampal slice model (Chang *et al.*, 2015; Chang *et al.*, 2016), suggesting a potential conserved mechanism between these related fatty acids.

Confirming the role of UBXD18 in the cellular response to decanoic acid requires an understanding of the cellular function of this protein. While this protein is uncharacterised in *Dictyostelium*, we analysed sequence similarity to identify UBXN1 and UBXD2 as the most highly conserved human proteins (Fig. 4.4) and investigated the known roles of these proteins to help us to better understand the function of UBXD18. Both human proteins are involved in endoplasmic reticulum-associated protein degradation (ERAD) (Liang *et al.*, 2006; Lim *et al.*, 2009; LaLonde and Bretscher, 2011), via binding to p97, with UBXD2 promoting ERAD, and UBXN1 negatively regulating ERAD. These findings suggest that *Dictyostelium* UBXD18 might also play a role in ERAD, however, while these proteins all share a UBX domain, they also possess diverse domains allowing these proteins to have potentially different functional properties and bind to select partners (Rezvani, 2016). The presence of a zinc finger domain in UBXD18, not present in any human UBX domain containing protein indicates that UBXD18 may have a different function to UBXN1 and UBXD2. This type of ZZ zinc finger domain is thought to be involved in protein-protein interactions, but can also bind DNA, RNA, and lipids (Ponting *et al.*, 1996; Klug, 2010; Brown, 2005; Matthews and Sunde, 2002). Thus, due to the disparity between the

sequences and domains of UBX domain containing proteins the cellular function of UBXD18 is unclear, with potential for a conserved role in maintaining protein homeostasis.

The functional activities of proteins correspond with their subcellular expression, and therefore, establishing the localization of a protein can help to elucidate its function. With this aim, we ascertained that UBXD18 is localised throughout the cytoplasm and nucleus of *Dictyostelium* (Fig. 4.6D and E), suggesting that this protein is more closely related to the human UBXN1 which also localises throughout the cytoplasm (Wang et al., 2013), than to UBXD2 which localises to the endoplasmic reticulum (ER) and the nuclear envelope (Liang et al., 2006). This conclusion is supported by the lack of transmembrane domains in both the *Dictyostelium* UBXD18 protein and the human UBXN1 protein (TMHMM, TMPRED, HMMTOP), and the presence of one transmembrane domain in the human UBXD2 protein. Our data suggesting that UBXD18 also localises to the nucleus in *Dictyostelium*, could indicate a role for UBXD18 in nuclear protein degradation. Taken together these findings implicate UBXN1 as the closest related human protein to UBXD18, while differences in subcellular localisation suggest potentially diverse functions of these proteins.

The conserved s3/s4 loop present in the UBX domain of UBX domain containing proteins has been demonstrated to be involved in binding to p97, via insertion into a hydrophobic pocket (Dreveny *et al.*, 2004) conserved in *Dictyostelium* (Fig. 4.5). Furthermore, deletion of, or point mutations within this loop reduce p97 binding, suggesting that UBX domains act as general p97 binding modules (Dreveny *et al.*, 2004). We have demonstrated that GFP-UBXD18 binds to *Dictyostelium* p97-RFP (Fig. 4.6), implicating p97 in the cellular changes caused by decanoic acid. Thus, we demonstrated that decanoic acid but not octanoic acid inhibits the ATPase activity of p97 in a UBXD18 dependent manner (Fig. 4.7). The identification of decanoic acid as an inhibitor of p97 is of interest since p97 inhibitors have been proposed as treatments for cancer and epilepsy (Tang and Xia, 2016; Han *et al.*, 2015; Tang *et al.*, 2019).

Since we have demonstrated efficacy of decanoic acid but not octanoic acid in UBXD18 dependent inhibition of p97 we utilised computational docking software

to highlight differences in binding locations and affinities of these fatty acids to a model of the UBXD18 protein (Fig 4.8). Due to the lack of defined protein structure for UBXD18 we utilised a model generated by Phyre2. Predictions from this model suggested that the most energetically favourable binding site is conserved for both decanoic acid and octanoic acid (Fig 4.8A). While analysis of all viable interaction sites, predicted multiple sites exclusively binding decanoic acid (Fig. 4.8B). Investigations into these exclusive sites could explain the difference in activity of these fatty acids. However, due to *ab initio* modelling, only 50% of the protein was modelled at >90% confidence, suggesting that ligand docking from this model may be unreliable (Kelley *et al.*, 2015). To overcome this, we investigated the predicted docking of decanoic acid and octanoic acid to a solution NMR derived structure of the UBX domain of the human UBXD2 protein. Predictions from this model suggest that octanoic acid binds to the same sites as decanoic acid with comparable affinity (Fig. 4.9). However, ligand binding is likely to be affected by interactions with other domains, thus limiting the reliability of these predictions. Accurate modelling of ligand binding can shed light on the biological activity of ligands and can be used to aid the development of improved drugs by determining how drug modifications can alter binding affinity and activity (Grosdidier, Zoete and Michielin, 2011b; Boehm *et al.*, 2000). Therefore, reanalysis of decanoic acid and octanoic acid docking following validation of a reliable protein structure could clarify the molecular interactions of these fatty acids.

Our discovery that decanoic acid acts with structural specificity to inhibit p97 activity in a UBXD18 dependent manner, suggests that decanoic acid could impact a variety of cellular processes regulated by p97 (Fig. 4.1). Autophagy is a key homeostatic process regulated by p97 that is essential for cell survival. Loss of p97 results in an impairment in this pathway and an accumulation of autophagosomes (Ju *et al.*, 2009) and inhibitors of p97 have been demonstrated to block autophagosome maturation (Chou *et al.*, 2011). Autophagy dysfunction has been linked to neurodegenerative disorders including epilepsy (Giorgi *et al.*, 2015; Wong, 2013), with ketogenic diets credited with activating this pathway via mTORC1 inhibition (McDaniel *et al.*, 2011). Our findings implicating decanoic acid in p97 inhibition, suggest a potential effect of decanoic acid on autophagy. Autophagy has

been widely studied in *Dictyostelium* with multiple established methods available (Dominguez-Martin *et al.*, 2017; Mesquita *et al.*, 2013), thus, this pathway provides a rational avenue of investigation.

In this chapter we have identified UBXD18 as a p97 binding partner and demonstrate that decanoic acid inhibits p97 activity in a UBXD18 dependent manner. Inhibiting p97 has been proposed to have therapeutic benefits in cancers and epilepsy, suggesting potential efficacy for decanoic acid in these areas. Since p97 has a well-established role in autophagy, a process closely associated with cancer and epilepsy, we investigate the effect of decanoic acid on autophagy in *Dictyostelium* in the following chapter.

Chapter 5

Investigating the effects of medium-chain fatty acids on autophagy in *Dictyostelium*

5.1 Introduction

In previous chapters we have identified that in *Dictyostelium,* decanoic acid acts via a UBXD18 dependent mechanism to inhibit p97 activity, thus implicating this protein in the therapeutic effects of this fatty acid. Since p97 is known to play a significant role in protein homeostasis, in this chapter we investigate the effects of decanoic acid on autophagy, a key homeostatic process associated with neurodegenerative disorders, cancer and epilepsy (Wong, 2013; Saha *et al.*, 2018).

Macroautophagy, the most prevalent form of autophagy, is conserved between *Dictyostelium* and humans. In *Dictyostelium,* macroautophagy (hereafter referred to as autophagy) is required to liberate nutrients during starvation, as well as in the degradation of proteins, and in response to pathogen infection (Otto *et al.*, 2003; Cardenal-Munoz *et al.*, 2017; Mesquita *et al.*, 2016). *Dictyostelium* has been widely used as a model to study autophagy with findings from this organism providing important advances in the study of autophagy-related pathologies. Research in *Dictyostelium* has demonstrated a link between the neurodegenerative disease, Chorea-acanthocytosis (ChAc), and autophagy (Munoz-Braceras, Calvo and Escalante, 2015), with further research implicating Vmp1, an ER protein involved in cancer, in the clearance of ubiquitinated protein aggregates through autophagy (Calvo-Garrido and Escalante, 2010). In addition to this, several studies in *Dictyostelium* have suggested a role for protein sequestration in neuronal malfunction (Kim *et al.*, 2009; Schmauch *et al.*, 2009). The prevalence of autophagy related studies using this model highlights the value of using *Dictyostelium* to research this conserved cellular process.

Due to the widespread use of *Dictyostelium* in autophagy research there are several well-established methods for assessing autophagy in this model. Fluorescence microscopy is widely employed to visualise autophagy structures within the cell, with Atg8a (Atg8) (microtubule-associated protein 1A/1B-light chain 3 (LC3) in mammals) tagged to GFP (GFP-Atg8) used extensively in *Dictyostelium* as a fluorescent marker (Mesquita *et al.*, 2016). GFP-Atg8 is employed as an autophagy marker since this protein is incorporated into the membrane of the phagophore following the induction of autophagy, and remains in the membrane until the

autophagosome is degraded (King, Veltman and Insall, 2011; Mesquita *et al.*, 2013). An increase in the number of GFP-Atg8 positive structures in the cell indicates an induction in autophagy, whereas a decrease in the number and an increase in the size of GFP-Atg8 labelled structures suggests a blockage of autophagy (Sharma *et al.*, 2019; Dominguez-Martin *et al.*, 2017). Another method to study autophagy involves monitoring the amount of material degraded by this pathway over time, termed autophagic flux (Mesquita *et al.*, 2016). Autophagic flux is commonly measured by observing the autophagic cleavage of GFP from tagged cytosolic proteins such as GFP-Atg8 (Calvo-Garrido *et al.*, 2011). This technique utilises the hydrolase resistant properties of GFP such that when GFP is fused to a cytosolic protein (GFP-Atg8) and delivered to lysosomes by autophagy, free GFP accumulates while the rest of the fusion protein (Atg8) is degraded. Alternatively, when flux is blocked the fusion protein (GFP-Atg8) accumulates, since degradation is blocked, and thus free GFP disappears. Quantification of these proteins by western blot provides an effective indication of changes in autophagic flux (Welter, Thumm and Krick, 2010; Cardenal-Munoz *et al.*, 2017). One further method to study autophagy is quantitative reverse transcription polymerase chain reaction (qRT-PCR) which can be used to measure expression levels of autophagy genes (Cardenal-Munoz *et al.*, 2017). The availability of multiple well studied techniques, along with the conservation of most mammalian autophagy genes, makes *Dictyostelium* an ideal model for the study of autophagy.

In this chapter we demonstrate, using live cell fluorescent microscopy, that both decanoic acid and octanoic acid significantly increase the number of GFP-Atg8 positive structures in *Dictyostelium* in wild type and *UBXD18*$^{-}$ cells, indicating that these medium-chain fatty acids regulate autophagy independently of UBXD18. We confirm that this coincides with an alteration in autophagic flux in both wild type and *UBXD18*$^{-}$ cells treated with decanoic acid and octanoic acid, and further demonstrate that decanoic acid treatment leads to an increase in the expression of two autophagy genes in wild type cells, suggesting a role for medium-chain fatty acids in inducing autophagy in *Dictyostelium.* To assess the mechanism behind this change we show that both decanoic acid and octanoic acid modulate autophagy independently of the autophagy regulating second messenger PIP_3.

5.2 Results

5.2.1 Decanoic acid and octanoic acid induce autophagosome formation in *Dictyostelium*

During autophagy inducing conditions, Atg8 associates with emerging autophagosomes, thus employing *Dictyostelium* cells expressing GFP-Atg8 enables the quantification of autophagosome formation (Fig 5.1A). To confirm the effect of autophagy induction on autophagosome number we initially quantified the number of GFP-Atg8 positive structures in control conditions and under autophagy inducing starvation conditions. The number of GFP-Atg8 positive structures increased from an average of 2.6 autophagosomes per cell (95 % Cl: 1.7 to 3.4) to an average of 7.4 autophagosomes per cell following starvation (95 % Cl: 6.2 to 8.5, p = 0.0022, n = 6) (Fig. 5.1B and C). This increase in autophagosome number was independent of any change in autophagosome size (non-significant increase from 0.46 µm to 0.48 µm, p = 0.3939, n = 6) (Fig. 5.1D). This starvation induced increase in GFP-Atg8 structures is consistent with an induction of autophagy leading to an increase in autophagosome number (Dominguez-Martin et al., 2017).

To investigate the effects of decanoic acid and octanoic acid on autophagy in *Dictyostelium,* we quantified the average number of GFP-Atg8 structures per cell following treatment with these fatty acids. Treatment with decanoic acid (at 60 µM, a concentration that resulted in an approximately 95 % inhibition of growth) under control (non-starvation) conditions, significantly increased the number of Atg8 positive structures from an average of 2.5 autophagosomes per cell (95 % Cl: 2.0 to 3.0) to 7.3 autophagosomes per cell after 4 hours (95 % Cl: 5.3 to 9.2, p = 0.0079, n = 6) and 8.3 autophagosomes per cell following 24 hours (95 % Cl: 5.1 to 11.49, p = 0.0023, n = 6) (Fig. 5.2A and B). Treatment with octanoic acid (at 120 µM, a concentration that resulted in an approximately 95 % inhibition of growth), increased the number of Atg8 positive structures from an average of 2.5 autophagosomes per cell to 6.9 autophagosomes per cell after 4 hours (95 % Cl: 4.5 to 9.3, p = 0.0342, n = 6) and 6.7 autophagosomes per cell following 24 hours (95 % Cl: 5.1 to 8.3, p = 0.0437, n = 6) (Fig. 5.2A and B). Treatment with the autophagy inducer (AR-12, 2.5 µM) also increased the average number of Atg8 containing structures from 2.5

autophagosomes per cell to 7.5 autophagosomes per cell (95 % CI: 5.7 to 9.3, p = 0.0022, n = 6) (Fig. 5.2A and B). Protease inhibitors, employed to inhibit lysosomal activity and block autophagic flux, had no significant effects on the number of Atg8 containing structures (non-significant increase from 2.5 to 4.7 autophagosomes per cell, p > 0.9999, n = 6) (Fig. 5.2A and B). None of the treatment conditions had a significant effect on the size of Atg8 containing structures (p > 0.9999, n = 6) (Fig. 5.2A and C). Our data suggest that the increase in GFP-Atg8 structures observed following treatment with both decanoic acid and octanoic acid is consistent with an increase in autophagy.

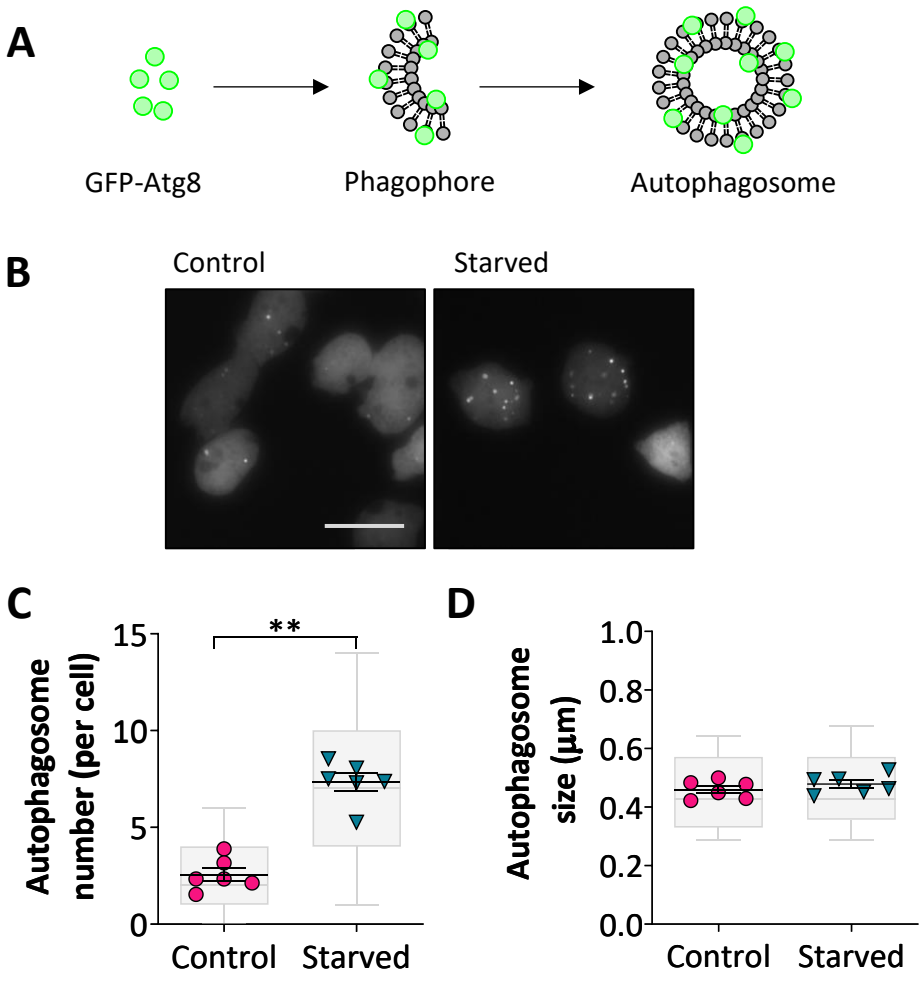

Figure 5. 1 GFP-Atg8 as an autophagy marker. A) Exogenous GFP-Atg8 is integrated into the membranes of the phagophore and autophagosome. B) Representative images of *Dictyostelium* cells expressing GFP-Atg8, untreated (control) or starved for 1 hour in nutrient free phosphate buffer. Scale bar represents 20 µm. Images were analysed for C) autophagosome number (n = 6) and D) autophagosome size (n = 6). Data represented are mean ± SEM. Significance is indicated by ** p ≤ 0.01 (Mann-Whitney test). Each data point is derived from 30 individual cells or autophagosomes, box and whisker (10-90th percentile).

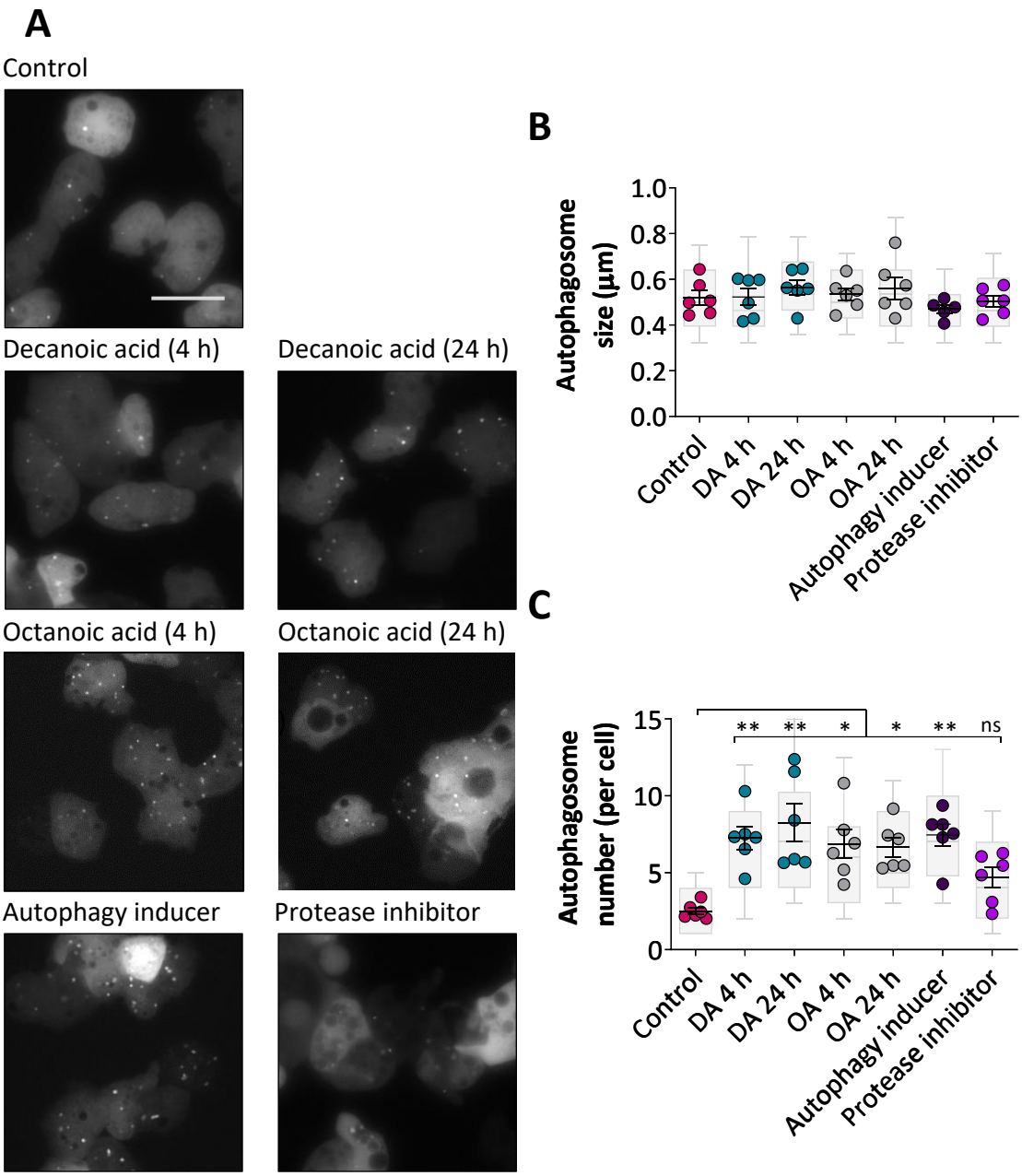

Figure 5. 4 Decanoic acid induces autophagosome formation in wild type *Dictyostelium*. A) Representative images of wild type (Ax2) *Dictyostelium* cells expressing GFP-Atg8 untreated (control) or treated with decanoic acid (60 µM) for 4 or 24 hours, octanoic acid (120 µM) for 4 or 24 hours, autophagy inducer (AR-12, 2.5 µM) or protease inhibitor (2.5x). Scale bar represents 20 µm. Images were analysed for B) autophagosome number per cell (n = 6) and C) autophagosome size (n = 6). Data represented are mean ± SEM. Significance is indicated by ns $p > 0.05$, * $p \leq 0.05$, ** $p \leq 0.01$ (Kruskal-Wallis with Dunn's multiple comparisons test). Each data point is derived from 30 individual cells or autophagosomes, box and whisker (10-90th percentile).

5.2.2 Decanoic acid and octanoic acid induce autophagosome formation independently of UBXD18

Since the cellular function of UBXD18 is poorly characterised, we initially assessed the intrinsic levels of autophagy in a cell line lacking a functional copy of this protein (*UBXD18*$^{-}$). The average number of GFP-Atg8 containing structures per *UBXD18*$^{-}$ cell was 2.4 (95% Cl: 2.2 to 2.6), compared with 2.5 in wild type cells (95% Cl: 2.0 to 3.0), suggesting that autophagosome formation is unchanged in *UBXD18*$^{-}$ ($p = 0.9719$, $n \geq 5$, Mann-Whitney test) (Fig. 5.2 and 5.3).

Since UBXD18 has been implicated in regulating the cellular response to decanoic acid in regards to growth and p97 activity, we assessed the effect of decanoic acid on autophagosome size and number in *UBXD18*$^{-}$ cells (Fig. 5.3). Decanoic acid treatment (60 µM) resulted in a significant increase in the average number of autophagosomes in *UBXD18*$^{-}$ cells, from 2.4 autophagosomes per cell in control conditions to 7.2 autophagosomes per cell following 4 hours (95% Cl: 5.8 to 8.5, $p = 0.0017$, $n \geq 4$) and 6.5 autophagosomes per cell following 24 hours (95% Cl: 4.5 to 8.5, $p = 0.0442$, $n \geq 4$) (Fig. 5.3 A and B). Treatment with octanoic acid (120 µM) also increased the number of Atg8 positive structures in *UBXD18*$^{-}$ cells, from an average of 2.4 autophagosomes per cell to 6.5 autophagosomes per cell after 4 hours (95% Cl: 4.4 to 8.6, $p = 0.0460$, $n \geq 4$) and 6.6 autophagosomes per cell following 24 hours (95% Cl: 5.0 to 8.2, $p = 0.0433$, $n \geq 4$) (Fig. 5.3 A and B). Treatment with autophagy inducer (AR-12, 2.5 µM) also increased the average number of Atg8 positive structures per cell from 2.4 to 6.7 (95% Cl: 5.1 to 8.3, $p = 0.0279$, $n \geq 4$), while treatments with protease inhibitors had no significant effect (non-significant increase from 2.4 to 4.6 autophagosomes per cell, $p > 0.9999$, $n \geq 4$) (Fig. 5.3 A and B). Consistent with our data from wild type cells, none of the treatment conditions had a significant effect on the size of Atg8 containing structures in *UBXD18*$^{-}$ cells ($p > 0.9999$, $n \geq 4$) (Fig. 5.3A and C). Our data suggest that the increase in GFP-Atg8 structures observed in *UBXD18*$^{-}$ cells following treatment with both decanoic acid and octanoic acid is consistent with an increase in autophagy.

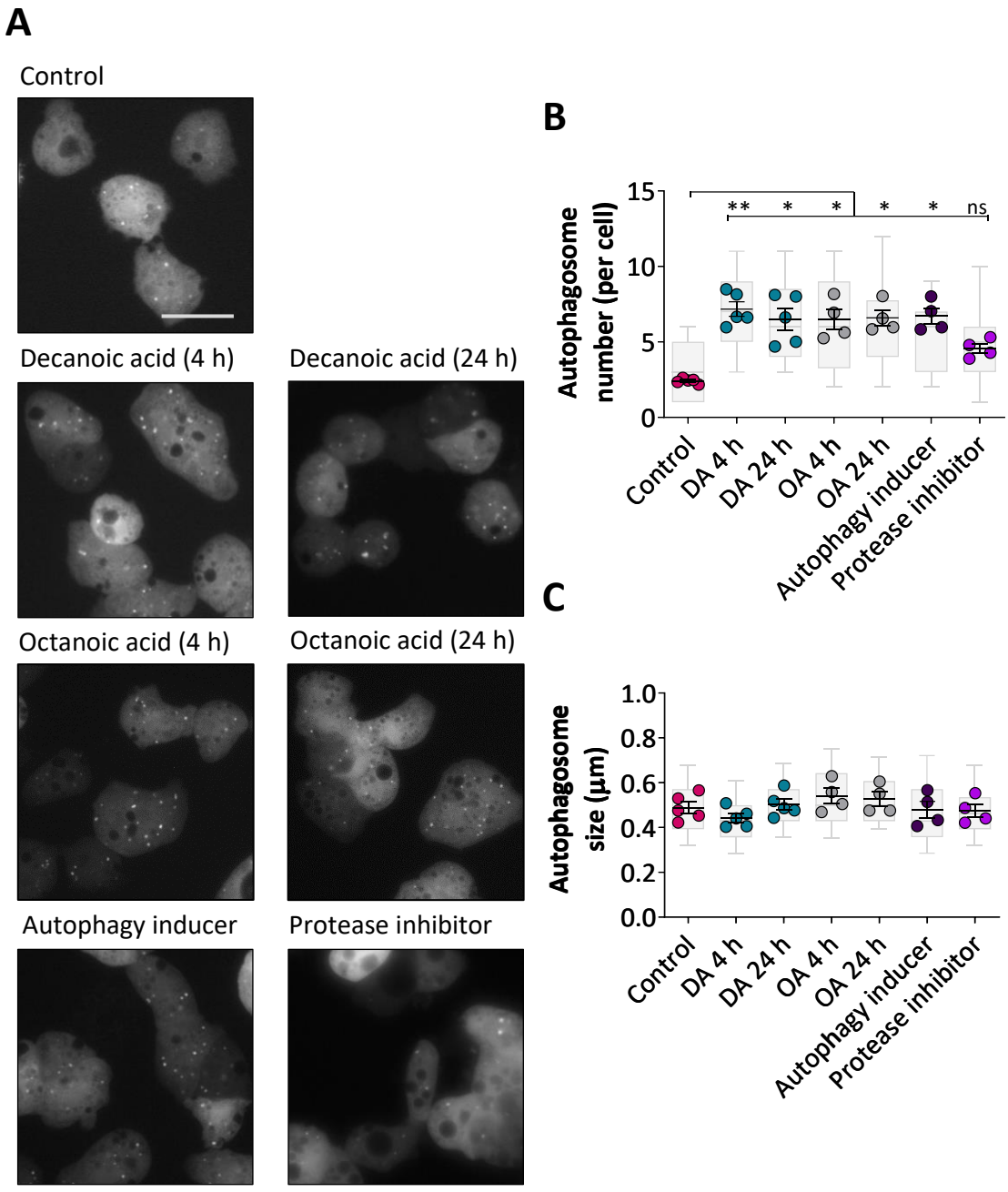

Figure 5. 7 Decanoic acid induces autophagosome formation in *UBXD18*$^{-}$.
A) Representative images of *UBXD18*$^{-}$ *Dictyostelium* cells expressing GFP-Atg8 untreated (control) or treated with 60 µM decanoic acid (DA) for 4 or 24 hours, 120 µM octanoic acid (OA) for 4 or 24 hours, autophagy inducer (AR-12 2.5 µM) or protease inhibitor (2.5x). Scale bar represents 20 µm. Images were analysed for B) autophagosome number ($n \geq 4$) and C) autophagosome size ($n \geq 4$). Data represented are mean ± SEM. Significance is indicated by ns > 0.05, * $p \leq 0.05$, ** $p \leq 0.01$. (Kruskal-Wallis with Dunn's multiple comparisons test). Each data point is derived from 30 individual cells or autophagosomes, box and whisker (10-90th percentile).

Our data representing the number of GFP-Atg8 positive structures per cell is limited by reflecting the steady-state levels of autophagosomes. Thus, it is difficult to differentiate between an increase in the number autophagosomes resulting from an increase in autophagosome induction or from a blockage in autophagy degradation. One approach to distinguish between an induction or blockage in autophagy is use of autophagic flux assays to evaluate autophagic degradation.

5.2.3 Medium-chain fatty acids alter autophagic flux in *Dictyostelium*

In order to analyse not only autophagosome formation but also the degradation of cytoplasmic constituents, we utilised an autophagic flux assay quantifying the autophagy-dependent cleavage of GFP from GFP-Atg8 by western blot analysis (Fig. 5.4). In control conditions cytoplasmic proteins along with GFP-Atg8 are known to be degraded in the autolysosome resulting in the release of free GFP (Fig. 5.4A, D and E). Following the induction of autophagy post starvation, the formation of autophagosomes is increased (Fig. 5.1) resulting in increased protein degradation, and leading to a reduction in GFP-Atg8 (71% reduction, 95% Cl: 66% to 79%, p = 0.0079, n = 5) (Fig. 5.4B, D and F) and an increase in the ratio of free GFP to GFP-Atg8 (340 % increase, 95 % Cl: 304 % to 392 %, p = 0.0079, n = 5) (Fig. 5.4G). Treatment with protease inhibitors has been demonstrated to inhibit lysosomal activity and block autophagic flux resulting in a reduction in free GFP and an accumulation of GFP-Atg8 (Cardenal-Munoz *et al.*, 2017)(Fig. 5.4C). Using this technique, changes in degradative capacity can be evaluated in the presence of medium-chain fatty acids.

To investigate the effects of decanoic acid and octanoic acid on autophagic degradation in *Dictyostelium* we employed an autophagic flux assay following treatment with these fatty acids. The levels GFP-Atg8 and free GFP were quantified in wild type untreated cells, and in cells treated with decanoic acid (60 µM) or octanoic acid (120 µM) for 4 or 24 hours (Fig. 5.5). Cells treated with autophagy inducer (AR-12, 2.5 µM), previously established to increase autophagic flux (Cardenal-Munoz *et al.*, 2017), and protease inhibitors (2.5x), previously established to block autophagic flux (Cardenal-Munoz *et al.*, 2017), were also assessed. Treatment with

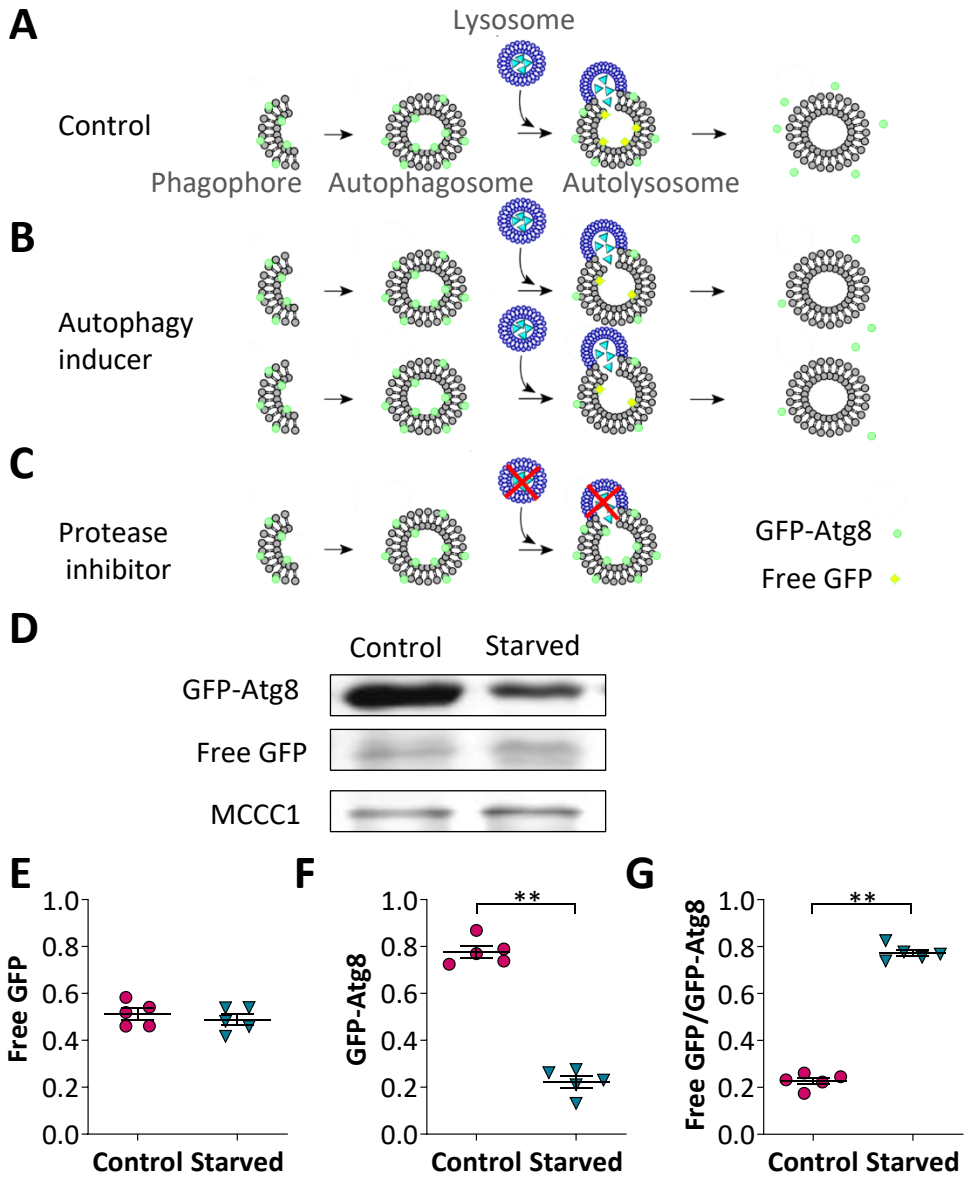

Figure 5. 10 Autophagic flux assay in *Dictyostelium* expressing GFP-Atg8.Cytosolic GFP-Atg8 is integrated into the inner and outer membranes of the phagophore and autophagosome. A) In control conditions following lysosomal fusion, engulfed cytoplasmic material is degraded inside the autolysosome by lysosomal hydrolases (blue triangles) along with GFP-Atg8 which is cleaved to form free GFP. The GFP-Atg8 located at the outer side is released to the cytosol. B) Treatment with autophagy inducer results in an increase in the formation of autophagosomes as well as an increase in degradation by autophagy, while the rate of GFP-Atg8 production in the cell remains the same. This results in an increase in autophagosomes (as observed by microscopy), while the intensity of the GFP-Atg8 band observed following western blot is reduced. C) Treatment with protease inhibitors impairs lysosomal activity leading to a reduction in free GFP. D) *Dictyostelium* cells expressing GFP-Atg8 untreated (control) or starved for 1 hour in nutrient free phosphate buffer (starved) were analysed by western blotting using an antibody against GFP, with MCCC1 as a loading control. Means and SEM of E) free GFP, F) GFP-Atg8 and G) the ratio of free GFP /GFP-Atg8 are represented ($n=5$). Significance is indicated by ** $p \leq 0.01$ (Mann-Whitney test).

decanoic acid for 4 hours resulted in a 71 % decrease in free GFP levels (95 % Cl: 67 % to 77 %, $p < 0.0001$, $n \geq 8$), with a 43 % decrease following 24 hours treatment (95 % Cl: 38 % to 50 %, $p = 0.032$, $n \geq 8$) (Fig. 5.5A and B). Treatment with octanoic acid for 4 hours also resulted in a 75 % decrease in free GFP levels (95 % Cl: 71 % to 80 %, $p < 0.0001$, $n \geq 8$), with a 47 % decrease following 24 hours (95 % Cl: 36 % to 62 %, $p = 0.024$, $n \geq 8$) (Fig. 5.5A and B). Treatment with autophagy inducer (AR- 12) caused a 40 % decrease in free GFP levels (95 % Cl: 37 % to 45 %, $p = 0.024$, $n \geq 8$) (Fig. 5.5A and B) consistent with an induction of autophagy (Cardenal-Munoz *et al.*, 2017), while no significant difference in free GFP levels were observed following treatment with protease inhibitors (39 % decrease, $p = 0.0606$, $n \geq 8$) (Fig. 5.5A and B). These results demonstrating that treatment of *Dictyostelium* with both decanoic acid and octanoic acid results in a decrease in free GFP levels, are consistent with a corresponding increase in autophagic flux (Cardenal-Munoz *et al.*, 2017).

Levels of GFP-Atg8 were also monitored following treatments with medium-chain fatty acids. A 25 % reduction in GFP-Atg8 levels was observed in cells treated with decanoic acid for 4 hours (95 % Cl: 24 % to 26 %, $p = 0.0077$, $n \geq 8$) and a 27 % decrease following 24 hours (95 % Cl: 24 % to 31 %, $p = 0.015$, $n \geq 8$) (Fig. 5.5A and C). A 38 % reduction in GFP-Atg8 levels was observed in cells treated with octanoic acid for 4 hours (95 % Cl: 37 % to 41 %, $p < 0.0001$, $n \geq 8$), and a 28 % decrease following 24 hours (95 % Cl: 20 % to 37 %, $p = 0.023$, $n \geq 8$) (Fig. 5.5A and C). Autophagy inducer also led to a 29 % decrease in GFP-Atg8 levels (95 % Cl: 28 % to 30 %, $p = 0.0011$, $n \geq 8$) indicating increased autophagic degradation of this protein (Fig. 5.5A and C). Levels of GFP-Atg8 were unchanged following treatment with protease inhibitors (0.08 % increase, $p > 0.9999$, $n \geq 8$) (Fig. 5.5A and C) consistent with a reduction of degradation caused by lysosomal inhibition (Cardenal-Munoz *et al.*, 2017).

The ratio of free GFP to GFP-Atg8 was monitored as a readout for autophagic flux. A significant reduction in this ratio was observed in cells treated with either decanoic acid or octanoic acid for 4 hours (decanoic acid caused a 68 % reduction, 95 % Cl: 63 % to 74 %, $p < 0.0001$, $n \geq 8$, and octanoic acid caused a 60 % reduction, 95 % Cl: 53 % to 70 %, $p < 0.0001$, $n \geq 8$). No significant change in the ratio of free GFP to

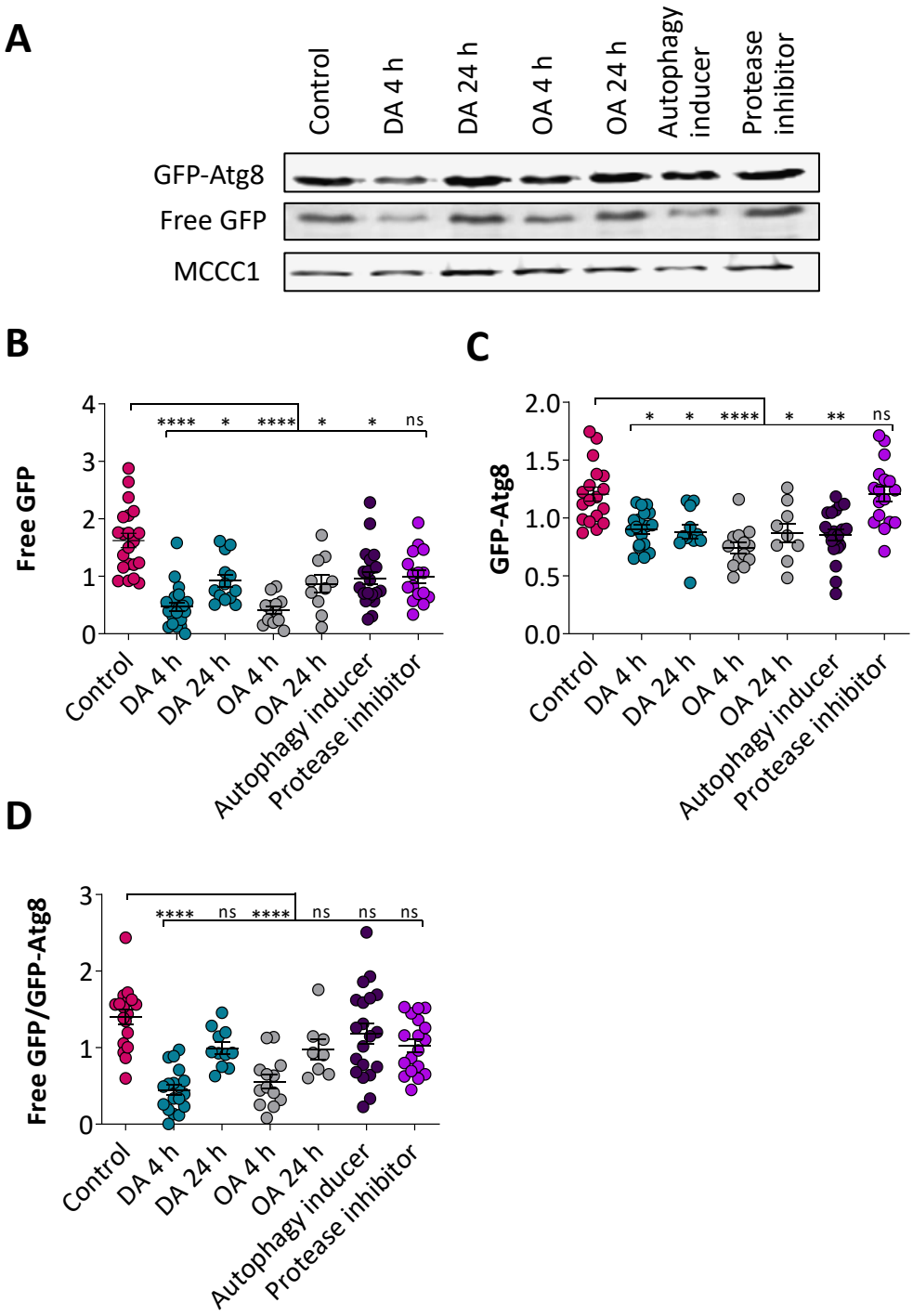

Figure 5. 13 Autophagic flux assay in wild type *Dictyostelium* expressing GFP-Atg8. A) *Dictyostelium* cells expressing GFP-Atg8 untreated (control) or treated with 60 µM decanoic acid (DA) for 4 or 24 hours (h), 120 µM octanoic acid (OA) for 4 or 24 hours, autophagy inducer (AR-12, 2.5 µM) or protease inhibitor (2.5x) were analysed by western blotting using an antibody against GFP, with MCCC1 as a loading control. Means and SEM of B) free GFP, C) GFP-Atg8 are represented normalised to loading control and D) the ratio of free GFP /GFP-Atg8 is displayed ($n \geq 8$). Significance is indicated by ns > 0.05, * $p \leq 0.05$, ** $p \leq 0.01$, **** $p \leq 0.0001$ (Kruskal-Wallis with Dunn's multiple comparisons test).

GFP-Atg8 was observed in cells treated for 24 hours with either decanoic acid (29% reduction, $p = 0.4161$, $n \geq 8$) or octanoic acid (30% reduction, $p = 0.3786$, $n \geq 8$) (Fig. 5.5D). As a result of the large decrease in free GFP observed following treatment with medium-chain fatty acids and autophagy inducer, the change in the ratio of free GFP to GFP-Atg8 is the inverse of that observed following starvation induced autophagy induction. This suggests that these fatty acids and AR-12 may promote the degradation of free GFP as well as the autophagic degradation of GFP-Atg8. Free GFP fragments may be resistant to degradation in starvation conditions, due to an increase in lysosomal pH preventing the free GFP fragments from being degraded (Korolchuk *et al.*, 2011; Mundy *et al.*, 2012), but susceptible to degradation in the absence of starvation and in the presence of autophagy inducing compounds (Fig. 5.5). Finally, a non-significant reduction in the ratio of free GFP to GFP-Atg8 was observed following treatment with protease inhibitors (27% decrease, $p = 0.23$, $n \geq 8$) (Fig. 5.5D), a trend that is consistent with an accumulation of GFP-Atg8 caused by a block in autophagic flux resulting in a reduction in released free GFP. Taken together our data suggests that both decanoic acid and octanoic acid are activating autophagic flux in *Dictyostelium.*

5.2.4 Medium-chain fatty acids alter autophagic flux independently of UBXD18

Since a role for UBXD18 in regulating the cellular response to decanoic acid has been suggested, we assessed autophagic flux in *UBXD18*$^-$ cells. As in wild type cells, 4 hour treatment with decanoic acid caused a significant, 65 %, reduction in free GFP levels in *UBXD18*$^-$ (95% Cl: 60% to 72%, $p < 0.0001$, $n \geq 9$) and 24 hour treatment with decanoic acid caused a 39% decrease (95% Cl: 35% to 43%, $p = 0.034$, $n \geq 9$) (Fig. 5.6A and B). Octanoic acid treatment for 4 hours also caused a significant, 67 %, reduction in free GFP levels in *UBXD18*$^-$ (95% Cl: 60% to 76%, $p < 0.0001$, $n \geq 9$) and 24 hour treatment caused a 40% decrease (95% Cl: 33% to 49%, $p = 0.022$, $n \geq 9$) (Fig. 5.6A and B). The autophagy inducer, AR-12, also caused a 43%, decrease in free GFP levels in *UBXD18*$^-$ cells (95 % Cl: 39 % to 49 %, $p = 0.0030$, $n \geq 9$), while protease inhibitors had no significant effects (33 % decrease, $p = 0.0739$, $n \geq 9$). These findings are consistent with medium-chain fatty acids causing an increase in autophagic flux in *UBXD18*$^-$ cells.

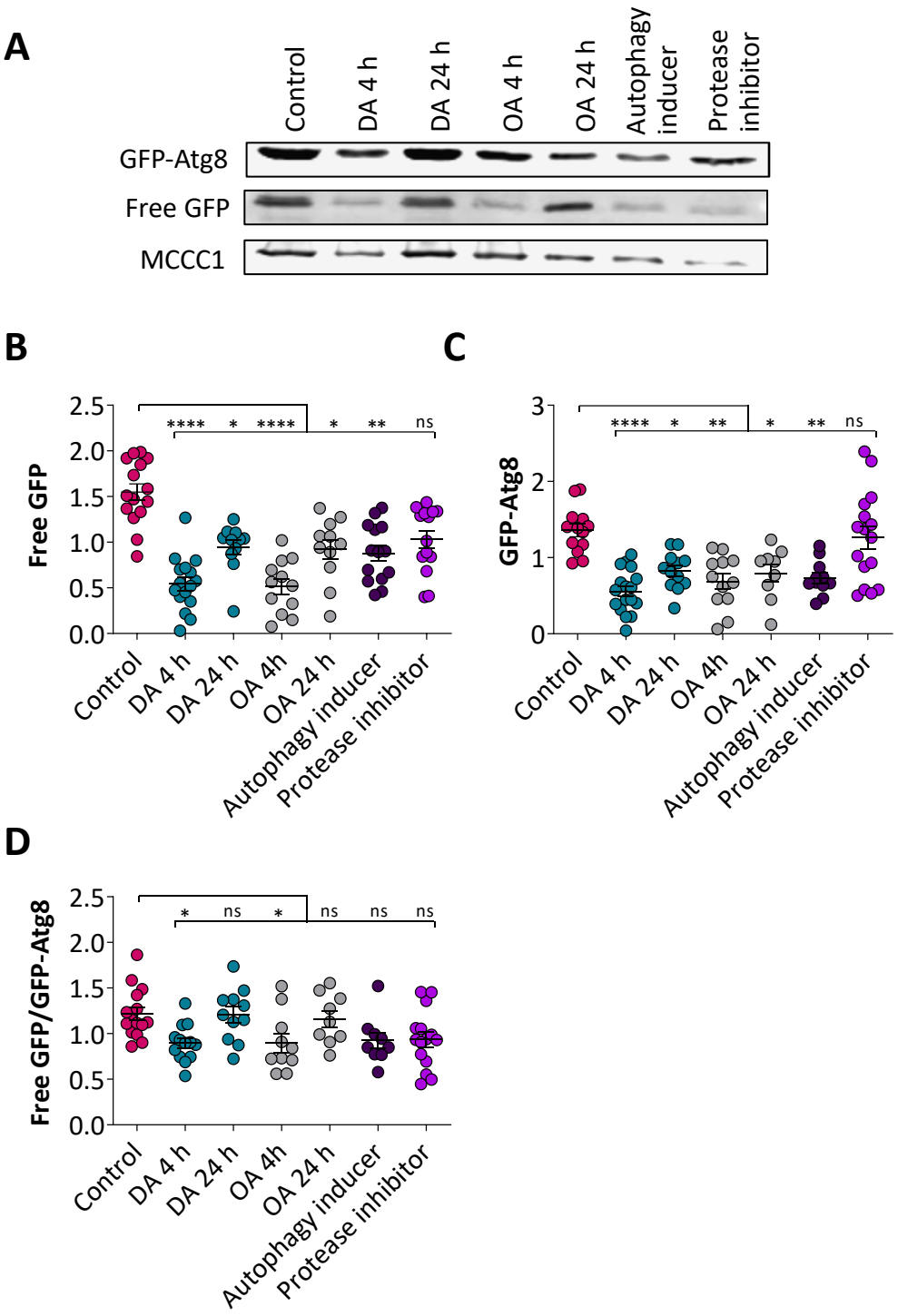

Figure 5. 16 Autophagic flux assay in *UBXD18*⁻ *Dictyostelium* expressing GFP-Atg8. A) *Dictyostelium UBXD18*⁻ cells expressing GFP-Atg8 untreated (control) or treated with 60 µM decanoic acid (DA) for 4 or 24 hours (h), 120 µM octanoic acid (OA) for 4 or 24 hours, autophagy inducer (AR-12, 2.5 µM) or protease inhibitor (2.5x) were analysed by western blotting using an antibody against GFP, with MCCC1 as a loading control. Means and SEM of B) free GFP, C) GFP-Atg8 are represented normalised to loading control and D) the ratio of free GFP /GFP-Atg8 is displayed ($n \geq 9$). Significance is indicated by ns > 0.05, * $p \leq 0.05$, ** $p \leq 0.01$, **** $p \leq 0.0001$ (Kruskal-Wallis with Dunn's multiple comparisons test).

Levels of GFP-Atg8 were also monitored in *UBXD18*$^{-}$ cells following treatments with medium-chain fatty acids. Decanoic acid treatment for 4 hours caused a 59 % reduction in GFP-Atg8 levels (95 % CI: 54 % to 65 %, $p < 0.0001$, $n \geq 9$) and 24-hour treatment led to a 39 % decrease (95 % CI: 37 % to 43 %, $p = 0.023$, $n \geq 9$) (Fig. 5.6A and C). Octanoic acid treatment for 4 hours caused a 50 % reduction in GFP-Atg8 levels (95 % CI: 41 % to 61 %, $p = 0.0014$, $n \geq 9$) and a 41 % decrease following 24 hours (95 % CI: 31 % to 55 %, $p = 0.042$, $n \geq 9$) (Fig. 5.6A and C). Treatment with autophagy inducer also led to a 48 % reduction in GFP-Atg8 levels (95 % CI: 43 % to 51 %, $p = 0.0026$, $n \geq 9$) (Fig. 5.6A and C) consistent with an increase in autophagic flux. Finally, protease inhibitors had no significant effect on GFP-Atg8 levels (7.1 % decrease, $p > 0.9999$, $n \geq 9$) consistent with a reduced autophagic degradation.

The ratio of free GFP to GFP-Atg8 was also monitored in *UBXD18*$^{-}$ cells as a readout for autophagic flux. A significant reduction in the ratio of free GFP to GFP-Atg8 was observed in cells treated for 4 hours with either decanoic acid or octanoic acid (26 % reduction following decanoic acid treatment, 95 % CI: 26 % to 28 %, $p = 0.0178$, $n \geq 9$ and a 26 % reduction following octanoic acid treatment, 95 % CI: 17 % to 38 %, $p = 0.0340$, $n \geq 9$). No significant change was observed following 24 hour treatment with decanoic acid (0.66 % reduction, $p > 0.9999$, $n \geq 9$), or octanoic acid (4.5 % reduction, $p > 0.9999$, $n \geq 9$), or following treatment with protease inhibitors (23 % decrease, $p = 0.0715$, $n \geq 9$) (Fig. 5.6D). These findings are consistent with those observed in wild type cells, suggesting that knocking out *ubxd18* has no significant effect on cellular autophagy, or the autophagic response to medium-chain fatty acids. These data indicate that that in *Dictyostelium* decanoic acid and octanoic acid are regulating autophagy independently of UBXD18.

5.2.5 Employing protease inhibitors to investigate blockage of autophagic flux

To further investigate the role of decanoic acid on autophagy in *Dictyostelium* we aimed to utilise protease inhibitors to differentiate between an induction or blockage of autophagic flux. Protease inhibitors are established to impair lysosomal function (Cardenal-Munoz *et al.*, 2017), and thus are employed to reduce autophagic flux. We have shown that treatment with protease inhibitors results in a non-significant reduction in free GFP levels together with unchanged levels of GFP-Atg8

equating to a non-significant trend towards a reduction in the ratio of free GFP to GFP-Atg8 (Fig 5.5 and 5.6). This trend is consistent with protease inhibitors causing a blockage in the degradation of GFP-Atg8.

Treating cells in the presence or absence of protease inhibitors, can provide an indication of autophagic flux, since in cells with functional autophagy, protease inhibitors block autophagic flux, while in cells with dysfunctional autophagic degradation is unaffected by further blockages in autophagy caused by protease inhibitors (Sharma *et al.*, 2019; Cardenal-Munoz *et al.*, 2017). To investigate this, we assessed free GFP and GFP-Atg8 levels in control cells alone and in combination with protease inhibitors, as well and in cells treated with decanoic acid (4 hours, 60 μM) or autophagy inducer (AR-12) alone or in combination with protease inhibitors (Fig. 5.7). Our findings revealed that protease inhibitors caused a non-significant reduction (40% decrease, $p = 0.9999$, $n \geq 7$) in the ratio of free GFP to GFP-Atg8 in control cells, a trend consistent with a blockage of autophagic flux. The ratio of free-GFP to GFP-Atg8 was not significantly reduced in cells treated with decanoic acid and protease inhibitor compared to cells treated with decanoic acid alone (24 % decrease, $p > 0.9999$, $n \geq 7$). Similarly, the ratio of free-GFP to GFP-Atg8 was not significantly reduced in cells treated with autophagy inducer in combination with protease inhibitor compared to cells treated with autophagy inducer alone (38 % decrease, $p > 0.9999$, $n \geq 7$). The absence of change in the ratio of free GFP to GFP-Atg8 following addition of protease inhibitor in these conditions may result from the initially low levels of free GFP in these treatment conditions preventing firm conclusions from this data, however, these low levels of free GFP are likely to be caused by increased autophagic degradation of GFP rather than a blockage of autophagy. Thus, these findings suggest that cells treated with decanoic acid respond comparably to cells treated with autophagy inducer in response to treatment with protease inhibitors, consistent with an induction in autophagy following treatment with decanoic acid.

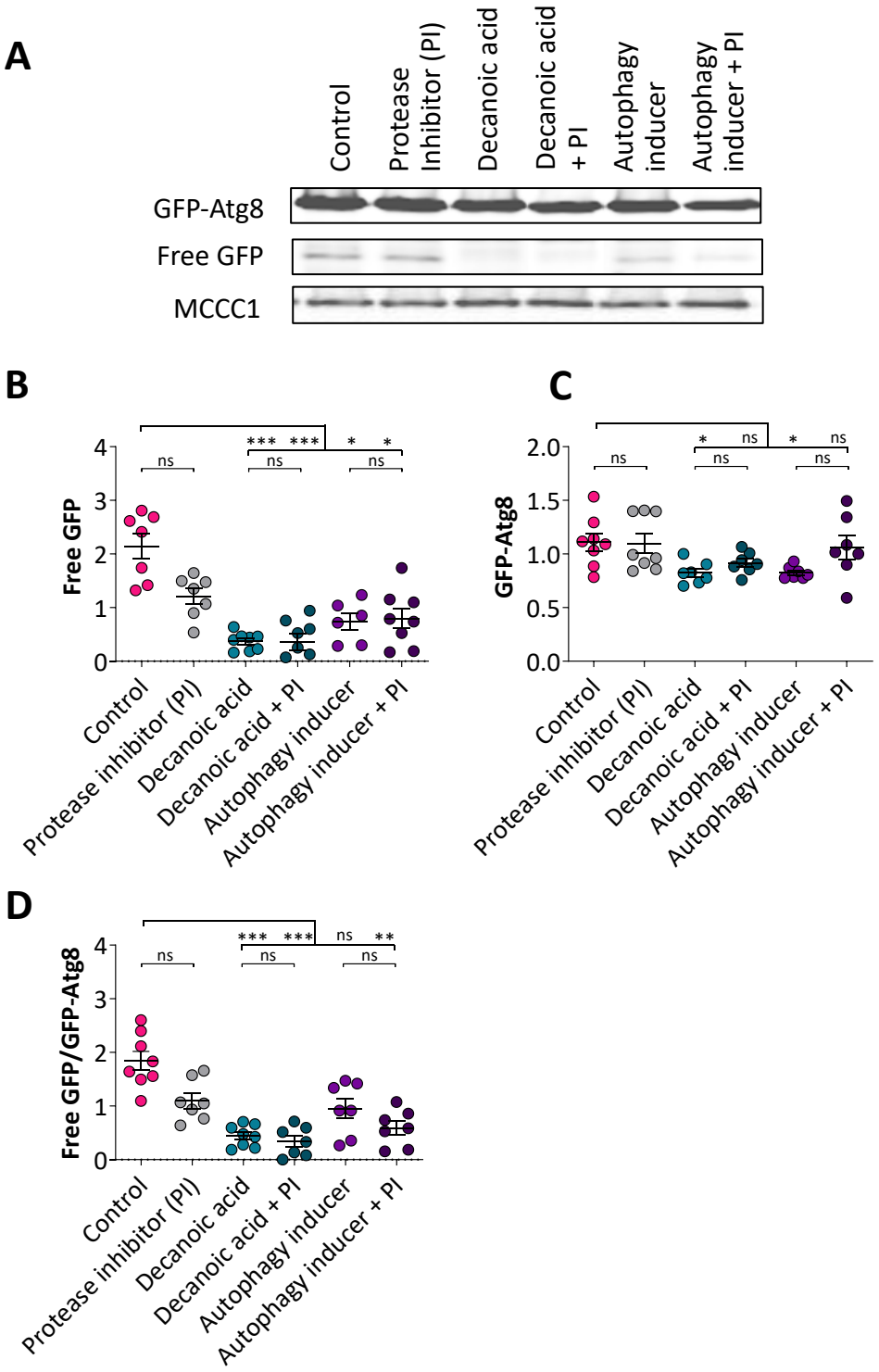

Figure 5. 19 Autophagic flux assay in the absence and presence of lysosomal protease inhibitors. A) *Dictyostelium* Ax2 cells expressing GFP-Atg8 untreated (control) or treated with protease inhibitor (PI, 2.5x) (1 hour) alone or in combination with 60 µM decanoic acid (4 hours) or autophagy inducer (AR-12, 2.5 µM) (2 hours) were analysed by western blotting using an antibody against GFP with MCCC1 as a loading control. Means and SEM of B) free GFP, C) GFP-Atg8 are represented normalised to loading control and D) the ratio of free GFP /GFP-Atg8 is displayed (n ≥ 6). Significance is indicated by ns > 0.05, * p ≤ 0.05, ** p ≤ 0.01 *** p ≤ 0.001 (Kruskal-Wallis with Dunn's multiple comparisons test).

5.2.6 Decanoic acid increases autophagy gene expression

In order to further assess the effects of decanoic acid and octanoic acid on autophagy we investigated changes in expression levels of autophagy genes following treatment with these fatty acids. mRNA levels of two autophagy genes, *atg1* and *atg8a*, were monitored following treatment with decanoic acid (60 µM) for 1, 4 or 24 hours (Fig. 5.8A and B). The expression of both *atg1* and *atg8a*, was significantly upregulated following 24-hour treatment with decanoic acid (9.2-fold increase, 95 % Cl: 4.3 to 14, p = 0.0235 and 6.2-fold increase, 95 % Cl: 3.5 to 8.9, p = 0.0315, respectively, n=3), consistent with an induction of autophagy. Conversely treatment with decanoic acid for 1 hour had no significant effect on the expression levels of *atg1* and *atg8a* (1.5-fold increase, p > 0.9999, and 0.46-fold change, p > 0.9999, respectively, n = 3) (Fig 5.8A and B), despite transcriptional upregulation of autophagy genes being possible in this time frame (Kirisako *et al.*, 1999). Treatment with decanoic acid for 4 hours caused a noticeable albeit non-significant increase in the expression levels of *atg1* and *atg8a* (6.6-fold increase, p = 0.07, and 2.7-fold increase, p = 0.3082, n = 3) (Fig 5.8A and B), despite showing comparable changes in autophagy (autophagosome number and flux) to 24-hour treatment (Fig. 5.2 and Fig. 5.5). This suggests that acute (4-hour) regulation of autophagy by decanoic acid may be mediated via changes in activation of existing autophagy proteins as well as changes in gene expression, or that induction of autophagy gene expression past a certain point does not further induce autophagy. By monitoring mRNA levels of *atg1* and *atg8a* we have demonstrated that 24-hour treatment with decanoic acid increases the expression levels of these genes consistent with an induction of autophagy.

Treatment of *Dictyostelium* with octanoic acid results in a comparable effect on autophagosome number (Fig. 5.2) and autophagic flux (Fig. 5.5) as with decanoic acid treatment. In order to further investigate the effects of octanoic acid on *Dictyostelium* autophagy we assessed the gene expression levels of the autophagy genes, *atg1* and *atg8a*, following treatment with octanoic acid (120 µM) for 1, 4 or 24 hours (Fig. 5.8C and D). None of these octanoic acid treatment conditions caused a change in relative expression levels of either *atg1* (1.1-fold increase at 1 hour, p >

0.9999, 0.99-fold change at 4 hours, p > 0.9999, 1.9-fold increase at 24 hours p > 0.9999, n = 3) or *atg8a* (1.05-fold increase at 1 hour, p > 0.9999, 0.72-fold-change at 4 hours, p > 0.9999, 1.39-fold increase at 24 hours, p > 0.9999, n = 3). This finding suggests that while octanoic acid appears to modulate autophagy in *Dictyostelium*, this effect may be independent of the gene expression levels of *atg1* and *atg8a*.

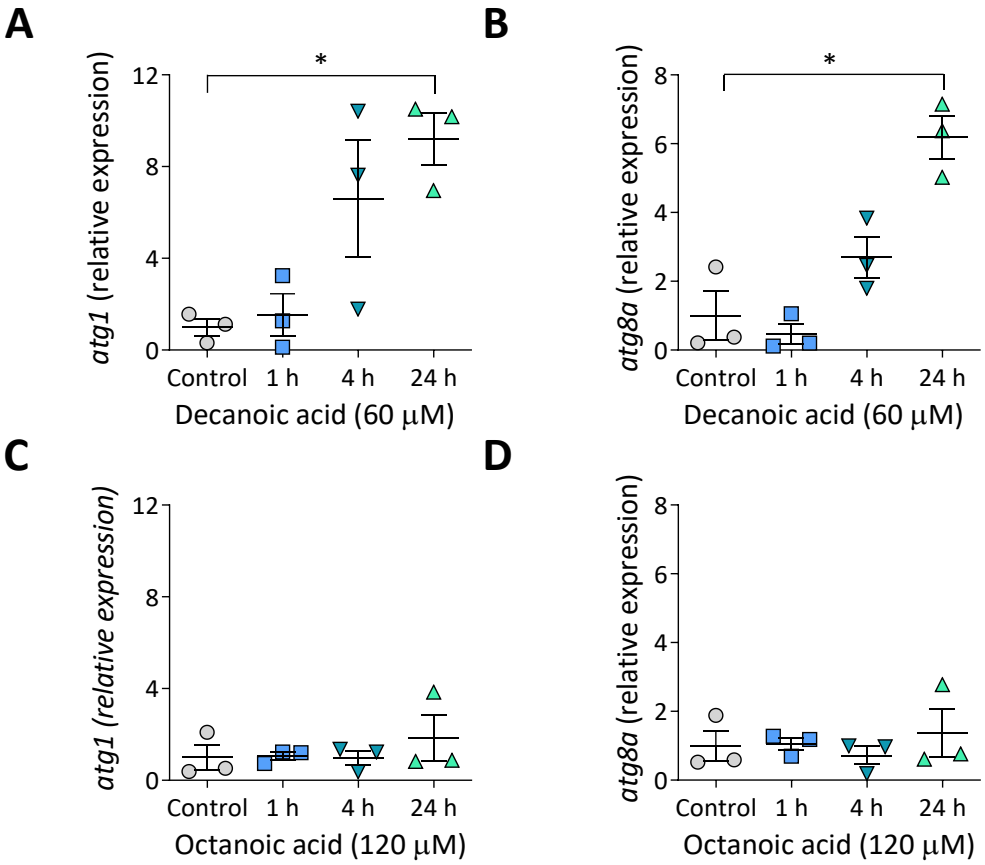

Figure 5. 22 Decanoic acid but not octanoic acid increases autophagy gene expression after 24 hours. Cells treated with decanoic acid (60 μM) (or control) were analysed by qPCR measuring the relative abundance of A) *atg1* and B) *atg8a* (n = 3). Cells treated with octanoic acid (120 μM) (or control) were also analysed by qPCR measuring the relative abundance of C) *atg1* and D) *atg8a* (n = 3). mRNA was normalised to the housekeeping gene *gapdh* in all conditions with the mRNA levels normalised so that untreated cells have a relative expression level of 1. Data represented are mean ± SEM. Significance is indicated by * p ≤ 0.05 (Kruskal-Wallis with Dunn's multiple comparisons test).

5.2.7 Medium-chain fatty acids alter autophagy independently of PIP_3

Following the identification that decanoic acid and octanoic acid activate autophagy in *Dictyostelium* independently of UBXD18, with differing effects on autophagy gene expression, we investigated a role for the autophagy regulating

second messenger PIP_3, in the cellular response to these fatty acids. PIP_3 has been identified as regulating autophagy through inhibition of the mTORC1 pathway (Jang and Lee, 2016), and since both decanoic acid and octanoic acid have been suggested to attenuate phosphoinositide phosphorylation (Chang et al., 2012), we investigated the effects of these fatty acids on PIP_3 production in *Dictyostelium* as a potential basis for the observed fatty acid induced activation of autophagy.

To monitor the effects of medium-chain fatty acids on PIP_3 production in *Dictyostelium* we observed the translocation of a PIP_3-specific PH domain fused to a fluorescent protein (PHcrac-GFP) in chemotactically competent cells. In these cells, global stimulation with the chemoattractant cAMP activates PI3K through G proteins to produce PIP_3 on the plasma membrane, leading to the transient localization of proteins containing Pleckstin Homolog (PH) domains that bind to PIP_3. Neither decanoic acid nor octanoic acid treatment significantly affected PHcrac-GFP translocation assessed by maximum membrane fluorescence (27 % decrease for decanoic acid, $p = 0.5743$, and 19 % decrease for octanoic acid, $p = 0.617$, $n = 6$) and total membrane fluorescence (21 % decrease for decanoic acid, $p > 0.9999$, and 5 % decrease for octanoic acid, $p > 0.9999$, $n = 6$) (Fig. 5.9). The PI3K inhibitor (LY294002) significantly suppressed PHcrac-GFP translocation (97 % decrease in maximum membrane fluorescence, 95 % Cl: 94 % to 103 %, $p = 0.0004$, and 85 % decrease in total membrane fluorescence, 95 % Cl: 76 % to 98 %, $p = 0.0028$, $n = 6$) (Fig. 5.9). These results demonstrate that decanoic acid and octanoic acid do not alter PIP_3 production following 4 hours of treatment, suggesting that the observed effects of these fatty acids on autophagy occur via a PIP_3 independent pathway.

We conclude that in *Dictyostelium* following treatment with decanoic acid autophagosomes accumulate, concomitantly with an increase in autophagic flux and an induction of autophagic gene expression. We further demonstrate that the effects of decanoic acid on autophagosome accumulation and autophagic flux are independent of UBXD18, and PIP_3 production. Taken together these findings provide strong evidence for decanoic acid induced activation of autophagy in *Dictyostelium* by a UBXD18 and PIP_3 independent mechanism. We further suggest that octanoic acid also causes an increase in autophagy independent of UBXD18 and PIP_3

production, however, the effects of octanoic acid on autophagy appear independent of changes in the expression levels of *atg1* or *atg8a*.

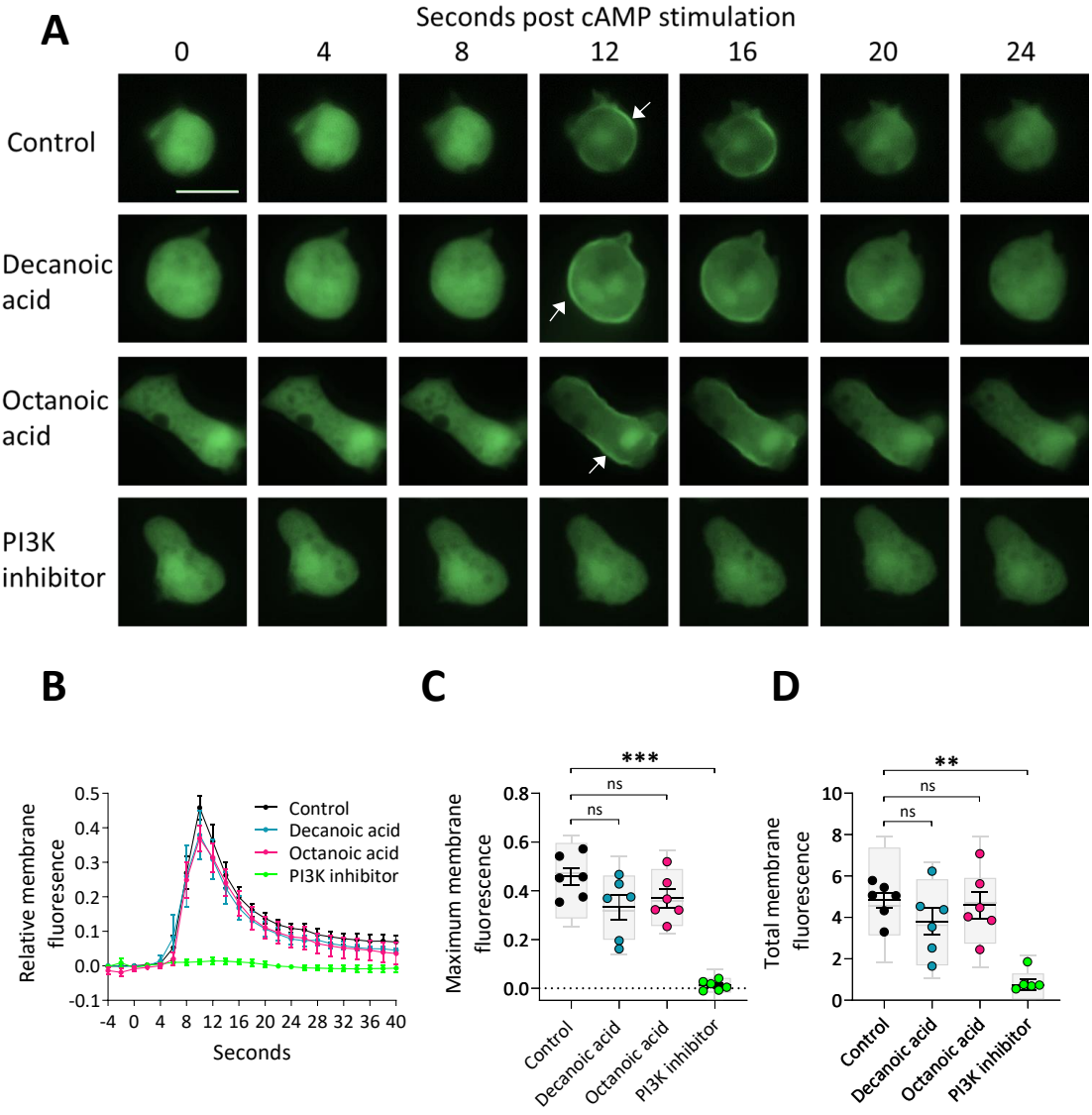

Figure 5. 9 Decanoic acid and octanoic acid act independently of PIP_3 levels in *Dictyostelium* A) Cells expressing PHcrac-GFP were treated with decanoic acid (60 µM, 4 hours), octanoic acid (60 µM, 4 hours), PI3K inhibitor (LY294002, 100 µM, 15 minutes) or solvent control (DMSO) during induction to form chemotactic competence. Cells were stimulated with cAMP (1 µM) and examined by fluorescence microscopy over time. Arrows highlight when PHcrac-GFP first becomes visually identifiable at the membrane. B) Membrane fluorescence was quantified, normalized to whole cell fluorescence, and C) maximum membrane fluorescence was compared between treatments. D) Total membrane fluorescence was calculated by analyzing the area under the curves of relative membrane fluorescence. Data represent mean and SEM from 6 independent experiments. Each data point is derived from 3 independent cells, box and whisker (10-90th percentile). Scale bar represents 10 µm. Significance is indicated by ns > 0.05, ** $p \leq 0.01$, *** $p \leq 0.001$ (Kruskal-Wallis with Dunn's multiple comparisons test).

A

	Decanoic acid	Octanoic acid
Effect on autophagosome number in Ax2	Increase	Increase
Effect on autophagosome number in *UBXD18*$^{-}$	Increase	Increase
Effect on autophagosome flux in Ax2	Increase	Increase
Effect on autophagosome flux in *UBXD18*$^{-}$	Increase	Increase
Effect on *atg1* and *atg8a* gene expression after 24 hours	Increase	No change
Effect on PIP_3 levels	No change	No change

Figure 5. 10 Summary of the *Dictyostelium* autophagic response to decanoic acid and octanoic acid A) Statistically significant increases in autophagosome number, flux (as identified by a decrease in GFP-ATG8 at 4 and 24 hours), and *atg1,* and *atg8a* gene expression, following exposure to decanoic acid or octanoic acid are highlighted in green. Neither decanoic acid or octanoic acid altered PIP_3 levels in *Dictyostelium.*

5.3 Discussion

Following the identification of UBXD18 as a target for decanoic acid, and the finding that decanoic acid acts via this protein to inhibit p97 activity, we investigated the effects of decanoic acid on autophagy, a key homeostatic pathway regulated by p97. In this chapter we demonstrate that decanoic acid activates autophagy in *Dictyostelium*, resulting in an increase in the number of autophagosomes per cell, coinciding with an increase in autophagic flux and an increase in the expression of two autophagy genes. We establish that the effect of decanoic acid on autophagy is independent of UBXD18, suggesting that decanoic acid may be acting via a mechanism distinct from UBXD18 and p97 to activate autophagy. We further demonstrate that octanoic acid also regulates autophagy independently of UBXD18 in *Dictyostelium*, as monitored by an increase in autophagosome number and autophagic flux. Finally, we show that the effects of decanoic acid and octanoic acid on autophagy are independent of the key signalling molecule PIP_3.

Since autophagy is required for the degradation of misfolded proteins and damaged organelles, dysfunction in this process can lead to a variety of diseases in humans, with mutations in autophagy related genes associated with epilepsy, neurodegenerative diseases and cancers (Jiang and Mizushima, 2014; Carvill et al., 2018; (Costa *et al.*, 2016). A link between epilepsy and autophagy was first

established following findings implicating rapamycin, an autophagy inducer, in supressing seizures in epilepsy models (Giorgi et al., 2015). Subsequently, a blockage in autophagy has been identified in patients with genetic epilepsy conditions such as tuberous sclerosis complex (TSC) (Wong, 2013; McMahon *et al.*, 2012), and Lafora disease (Knecht et al., 2010). Thus, therapies such as electroconvulsive therapy and rapamycin demonstrated to activate autophagy are under investigation as epilepsy treatments for these patients (Kim et al., 2019; Giorgi et al., 2015). Furthermore, the capacity of the classical ketogenic diet and intermittent fasting to increase starvation-induced autophagy has substantiated these dietary interventions as potential treatments for epilepsy (Yuen and Sander, 2014; (Camberos-Luna *et al.*, 2016) (Fig. 5.11). Dysfunctional autophagy is also associated with the neurodegenerative disorders, ALS, Huntington's, Parkinson's, and Alzheimer's disease, and activating autophagy has proven successful in models of all four of these disorders (Fowler and Moussa, 2018; Ravikumar et al., 2004; Caccamo et al., 2014; Castillo *et al.*, 2013). Interestingly, most current cancer drugs increase autophagy in tumour cells (Thorburn, Thamm and Gustafson, 2014), with autophagy activation suggested as an important therapeutic mechanism, however, autophagy is thought to have competing roles in cancer, with autophagy induction leading to chemoresistance, and inhibitors of autophagy also appearing promising in clinical trials (Amaravadi *et al.*, 2011). Reports of detrimental effects of autophagy activation (Cao et al., 2009) highlight the complexity of this process and the need to predict individual responses to autophagy modulators in order to allow personalised therapies. Our findings suggest that further analysis of a role for medium-chain fatty acids in autophagy regulation may identify associated therapeutic benefits in epilepsy, neurodegenerative disorders and cancers.

Fatty acids have previously been suggested to modulate autophagy with therapeutic implications, however, this process is poorly understood. Our findings connecting decanoic acid and octanoic acid to autophagy activation in *Dictyostelium* are consistent with research demonstrating that feeding mice medium-chain fatty acids restores supressed autophagy (Wang *et al.*, 2017), however, how medium-chain fatty acids regulate this process is unknown. A comprehensive understanding of the roles of fatty acids on autophagy is lacking, with most research focusing on the most

abundant dietary fatty acids, palmitic acid (long-chain saturated fatty acid, C16:0) and oleic acid (long-chain mono-unsaturated fatty acid, C18:1). Both palmitic acid and oleic acid have been reported to inhibit autophagy (Mei *et al.*, 2011; Las *et al.*, 2011; Sauvat *et al.*, 2018), as well as activate it (Martino *et al.*, 2012; Park *et al.*, 2019; Pauloin *et al.*, 2010; Mei *et al.*, 2011) (Fig 5.11). Short chain fatty acids have also been suggested to regulate autophagy (Hu *et al.*, 2010; Elamin *et al.*, 2013) (Fig. 5.11), with the length of fatty acid as well as the saturation status thought to alter the effect on autophagy (Sauvat *et al.*, 2018). There are many discrepancies regarding the roles of fatty acids on autophagy with no current consensus on how medium-chain fatty acids regulate this process. Our findings in this chapter have suggested a role for both decanoic acid and octanoic acid in regulating autophagy, but further research is required to understand the mechanisms and specificity behind these effects. In order to compare the effects of different fatty acids on autophagy, it would be preferable to assess identical concentrations rather than concentrations resulting in equivalent growth inhibition as investigated in this chapter.

Our previous data indicates that decanoic acid inhibits p97 in a UBXD18 dependent manner (Fig. 4.7), a cellular effect anticipated to cause UBXD18 dependent autophagy inhibition (Chou *et al.*, 2011; Ju *et al.*, 2009). In this chapter we suggest that both decanoic acid and octanoic acid activate autophagy in *Dictyostelium* and establish that this effect is independent of UBXD18 and p97. Consequentially the mechanism behind the effects of these fatty acids on *Dictyostelium* autophagy remains undefined. Understanding how medium-chain fatty acids regulate autophagy would provide valuable insight into potential therapeutic benefits provided by these fatty acids.

Autophagy is regulated by cellular nutrient status through multiple signalling pathways, such as adenosine monophosphate-activated protein kinase (AMPK), phosphatidylinositol 3-kinase (PI3K)/protein kinase B (AKT) and cAMP-dependent protein kinase (PKA), which regulate autophagy via the mechanistic target of rapamycin complex 1 (mTORC1) (Mavrakis *et al.*, 2006; He and Klionsky, 2009), as well as through activation of Beclin 1 (Meléndez and Neufeld, 2008) (Fig. 5.11). The classical ketogenic diet has been suggested to modulate autophagy in a similar manner to starvation (McDaniel *et al.*, 2011; Thio *et al.*, 2006; Miyamoto *et al.*, 2019;

Wang *et al.*, 2018) (Fig. 5.11). Autophagy is also known to be regulated in response to cell stress through pathways such as the RNA-dependent protein kinase-like ER kinase (PERK) pathway (Kouroku *et al.*, 2007), the inositol-requiring kinase 1 (IRE1) pathway (Bernales, McDonald and Walter, 2006), as well as through calcium release (Hoyer-Hansen *et al.*, 2007). Determining the effects of medium-chain fatty acids on these signalling pathways would provide valuable insight into the mechanisms underlying fatty acid induced autophagy activation.

Phosphoinositides have been well established to play a role in regulating autophagy, with PIP_3 playing an important role in inhibiting autophagy through the activation of AKT and mTORC1 (Jang and Lee, 2016) (Fig 5.11). While both decanoic acid and octanoic acid have been suggested to reduce production of PIP and PIP_2 in *Dictyostelium* (Chang *et al.*, 2012), effects of medium-chain fatty acids on PIP_3 have not previously been investigated. Here we demonstrate that neither decanoic acid or octanoic acid alter PIP_3 production in *Dictyostelium,* and thus suggest that these fatty acids act independently of this phosphoinositide. While PIP_3 is an important signaling molecule in the activation of mTORC1 and inhibition of autophagy, mTORC1 is regulated by multiple upstream pathways and understanding the effects of medium-chain fatty acids on mTORC1 signaling could help to explain the mechanism behind the autophagy inducing effects of these fatty acids.

The mTOR pathway is the major regulator of autophagy, maintaining the essential balance between the synthesis and degradation of cellular components. mTOR is a evolutionarily conserved serine/threonine kinase comprising two structurally and functionally different complexes, mTOR complex 1 (mTORC1) and mTOR complex 2 (mTORC2). mTORC1 senses nutrient and energy status within the cell, and when activated by high levels of energy and nutrients promotes anabolic processes such as protein and lipid synthesis and inhibits cellular catabolism through repression of autophagy by direct phosphorylation of the Atg1/ULK1 complex (Ganley *et al.*, 2009) (Fig. 5.11). Conversely, following conditions of nutrient starvation mTORC1 inhibition stimulates the formation of the Atg1/ULK1-containing pro-autophagic complex inducing the formation of autophagosomes and promoting autophagy (Sarkar, 2013). Inhibition of mTORC1 additionally regulates the subsequent steps of autophagy through altering the phosphorylation state, and thus

activity of autophagy machinery and regulators, as well as modulating the phosphorylation of transcription factors (such as transcription factor EB (TFEB)), altering their localisation and upregulating the expression of autophagy genes (Dossou and Basu, 2019) (Fig. 5.11). This activation of autophagy following starvation allows cells to break down cellular components and maintain cellular energy levels (Jung et al., 2010). Hyperactivation of mTOR is associated with reduced autophagy activity, and has been linked to the epilepsy condition TSC, as well as other disorders termed 'mTORopathies' (Taneike *et al.*, 2016; Franz and Capal, 2017). Furthermore, clinical trials with mTORC1 inhibitors have proven effective at reducing seizures in TSC patients highlighting the importance of this pathway in certain epilepsy conditions (Citraro et al., 2016; French et al., 2016). Investigating the effects of decanoic acid and octanoic acid on mTORC1 signalling could help to explain the autophagy inducing activity that we have identified and could prove valuable in elucidating the therapeutic mechanisms of these fatty acids.

In this chapter we have identified that the medium-chain fatty acids, decanoic acid and octanoic acid activate autophagy independently of UBXD18. Since activation of autophagy has been suggested as a potential treatment for epilepsy and neurodegenerative disorders, we aim to further investigate the mechanism behind fatty acid induced autophagy activation. In the following chapter we examine the effects of medium-chain fatty acids, on the major regulator of autophagy, mTORC1.

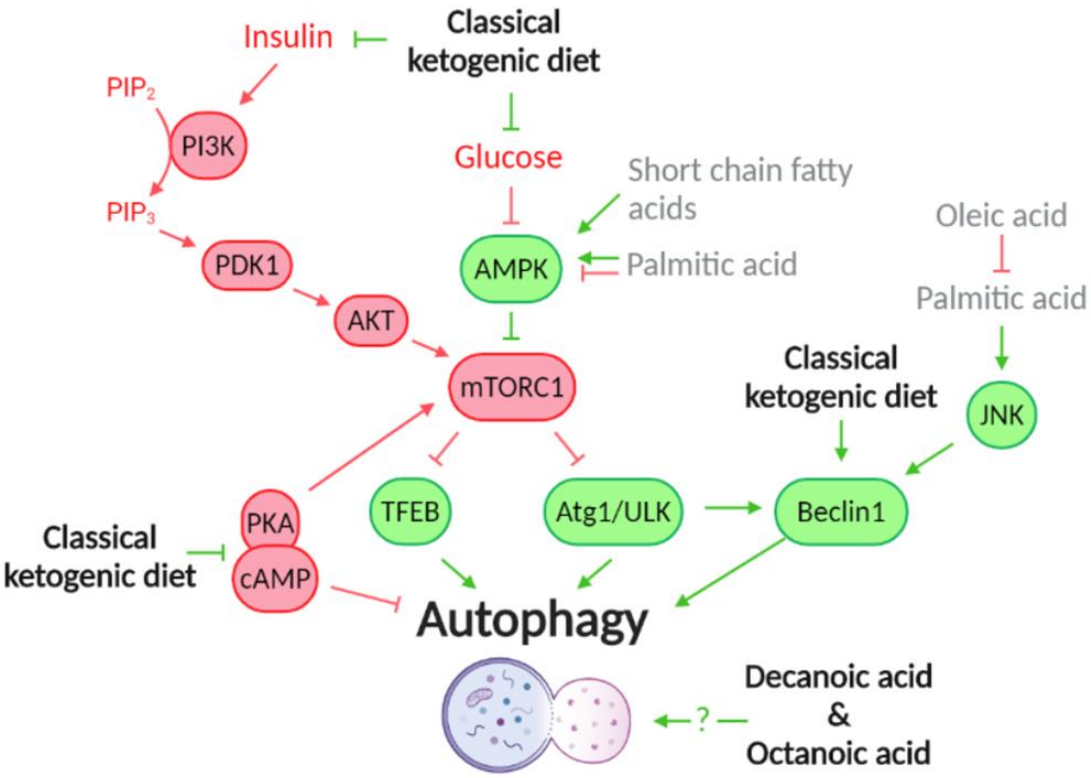

Figure 5. 11 Overview of nutrient-dependent autophagy regulation. Autophagy activating pathways are displayed in green and inhibitory pathways are shown in red. Autophagy is activated in response to starvation and the ketogenic diet through inhibition of mTORC1 (via inhibition of the PI3K/AKT pathway, or activation of AMPK), inhibition of protein kinase A (PKA) and induction of Beclin 1 dependent autophagy. The mTORC1 pathway plays a central role in nutrient-dependent autophagy response, through phosphorylation and activation of the Atg1/ULK1 complex, as well as through phosphorylation of the transcription factor TFEB leading to upregulation of autophagy gene expression. The effects of fatty acids on autophagy are unclear with short chain fatty acids thought to activate autophagy through AMPK (Hu *et al.*, 2010; Elamin *et al.*, 2013) while palmitic acid is suggested to both inhibit and activate autophagy through differential activity on AMPK (Fediuc, Gaidhu and Ceddia, 2006; Sun *et al.*, 2008). Palmitic acid has also been suggested to activate autophagy though the c-Jun N-terminal kinase (JNK) pathway (Komiya *et al.*, 2010) while oleic acid has been shown to prevent this (Sauvat *et al.*, 2018). How the medium-chain fatty acids decanoic and octanoic acid activate autophagy is currently unknown.

Chapter 6

Investigating the effect of medium-chain fatty acids on mTORC1

6.1 Introduction

In the previous chapter we identified that octanoic acid and decanoic acid regulate autophagy in *Dictyostelium* and suggested that dietary activation of this pathway could provide a useful approach to restore autophagic balance in patients with epilepsy, neurodegenerative disorders and cancers. In this chapter we investigate the effects of medium-chain fatty acids on mTORC1 the major regulator of autophagy.

The mTORC1 pathway is a highly conserved regulator of cellular nutrient and energy status which acts to maintain homeostasis by regulating cellular metabolism (Tatebe *et al.*, 2017). Following starvation, when nutrient levels are low, mTORC1 signalling is inhibited, leading to the initiation of autophagy, allowing cells to reutilise their constituents for energy (Ganley *et al.*, 2009). In addition to regulating autophagy, mTORC1 signalling also functions to activate anabolic processes such as the transcription and translation of proteins, and the synthesis of lipids. Aberrant mTORC1 signalling has been associated with a number of human diseases, from epilepsy (McMahon *et al.*, 2012), to neurodegenerative disorders (Fujikake, Shin and Shimizu, 2018), and cancers (Xie, Wang and Proud, 2016), with inhibition of this pathway providing a potential strategy for treating these conditions (Taneike *et al.*, 2016; Franz and Capal, 2017; Citraro *et al.*, 2016; Xie, Wang and Proud, 2016).

Rapamycin is a well-known inhibitor of mTORC1 which, along with its analogues (rapalogues) is under investigation for treating a range of conditions. Inhibition of mTORC1 via these compounds is thought to lead to a range of benefits, such as increased autophagy and the clearance of misfolded proteins in neurodegenerative disorders (Fujikake et al, 2018), as well as autophagy independent benefits such as the decrease of cell proliferation in cancers (Xie et al, 2016) and reduced stress response and improved mitochondrial function credited with increasing longevity (Johnson et al, 2013). Hyper-activation of mTORC1 has been observed in patients with Tuberous sclerosis complex (TSC), a neurodevelopmental disorder recently treated using the rapalogue 'Everolimus' (Svarrer *et al.*, 2019; Franz *et al.*, 2018). In patients with this condition, mutations in the genes for hamartin (*TSC1*) or tuberin (*TSC2*) result in overactivated mTORC1, leading to upregulated cell

growth and proliferation and the development of tumours. Tumours developing in the brains of these patients manifest in epilepsy and cognitive disability (Crino et al, 2006). The use of mTORC1 inhibitors to treat these patients reduces uncontrolled growth of brain cells and decreases excitability, preventing seizures (Franz & Capal, 2017; Franz et al, 2006; Li et al, 2019). While the inhibition of mTORC1 with rapamycin and rapalogues appears promising in the treatment of multiple conditions associated with hyperactivated mTORC1 signalling, off target effects of these compounds on mTORC2 cause side effects such as glucose intolerance, diabetes, and immunosuppression (Arriola Apelo and Lamming, 2016). Therefore, the Identification of alternative mTORC1 inhibitors lacking the toxicity of rapamycin would be beneficial.

The classical ketogenic diet has been suggested as an alternative means to reduce mTORC1 signalling. This effect is thought to be caused by a reduction in glucose and insulin levels in patients on the diet (McDaniel et al, 2011; Newman et al, 2017; Ostendorf & Wong, 2015; Roberts et al, 2017; Sweeney et al, 2017; Thio et al, 2006). While this dietary intervention is well established to reduce mTORC1 signalling without the toxicity associated with rapamycin, compliance of patients is low due to the restrictive nature of this diet (Ye *et al.*, 2015a). The ability of the less restrictive MCT diet to regulate this pathway has not yet been investigated. Employing *Dictyostelium* to identify the effects of medium-chain fatty acids on mTORC1 activity will help to establish whether the MCT diet could have potential in the dietary management of conditions associated with hyperactivated mTORC1 signalling.

In this chapter we use *Dictyostelium* to investigate the effects of medium-chain fatty acids on mTORC1 function. We initially demonstrate a structurally specific effect of decanoic acid in reducing mTORC1 activity. Since this effect occurs in the absence of insulin and in the presence of glucose this suggests a novel molecular mechanism for decanoic acid in mTORC1 inhibition. We demonstrate that cells lacking the UBX domain containing protein (UBXD18) are partially resistant to the effects of decanoic acid on mTORC1 signalling as well as on growth, implicating UBXD18 and its ubiquitous binding partner p97 in the mechanism of decanoic acid on mTORC1, and suggesting that the effects of decanoic acid on autophagy and mTORC1

are distinct. We further demonstrate that inhibition of p97 corresponds to a reduction in mTORC1 signalling in *Dictyostelium,* suggesting that this effect of decanoic acid on p97 activity could explain the observed mTORC1 inhibition. We then translate our findings to a rat hippocampal slice model, where acute decanoic acid treatment reduces mTORC1 signalling in the absence of insulin or reduced glucose. Finally, we employ astrocytes derived from patients with the neurodevelopmental disorder tuberous sclerosis complex (TSC), associated with deregulated mTORC1 activity, to demonstrate that decanoic acid reduces mTORC1 signalling in healthy patients and patients with *TSC1* mutations.

6.2 Results

6.2.1 Decanoic acid inhibits mTORC1 activity in *Dictyostelium*

In order to establish if the observed effects of decanoic acid and octanoic acid on autophagy are regulated via mTORC1, we investigated the effects of both fatty acids on mTORC1 signalling. In these experiments, we quantified levels of phosphorylated 4E-BP1 (p-4E-BP1), a translation repressor directly phosphorylated by mTORC1, as a read out for mTORC1 activity (Rosel *et al.*, 2012) (Fig. 6.1A). Here, *Dictyostelium* cells were treated with the fatty acids, decanoic acid (60 μM) or octanoic acid (120 μM), for 1 or 24 hours before p-4E-BP1 levels were quantified by western blot (Fig. 6.1B and C). Decanoic acid decreased p-4E-BP1 levels by 24% (95% Cl: 20% to 30%, $p = 0.0009$, $n = 10$) at 1 hour (Fig. 6.1B), and by 34% (95% Cl: 32% to 37%, $p \leq 0.0001$, $n = 10$) at 24 hours (Fig. 6.1B). Treatment with octanoic acid had no significant effect on the levels of p-4E-BP1 at either treatment duration (Fig. 6.1C) (12 % decrease, $p = 0.3830$ at 1 hour and a 15% decrease, $p = 0.2453$ at 24 hours, $n = 10$). These findings suggest that decanoic acid inhibits mTORC1 signalling in *Dictyostelium* in a structurally specific manner, and that the effects of octanoic acid on autophagy are independent of mTORC1.

Structural specificity of seizure control has previously been demonstrated in a rat hippocampal slice model, with several fatty acids and fatty acid derivatives showing potent anti-epileptiform activity (Chang *et al.*, 2015). Since we have demonstrated structural specificity of mTORC1 inhibition, with decanoic acid

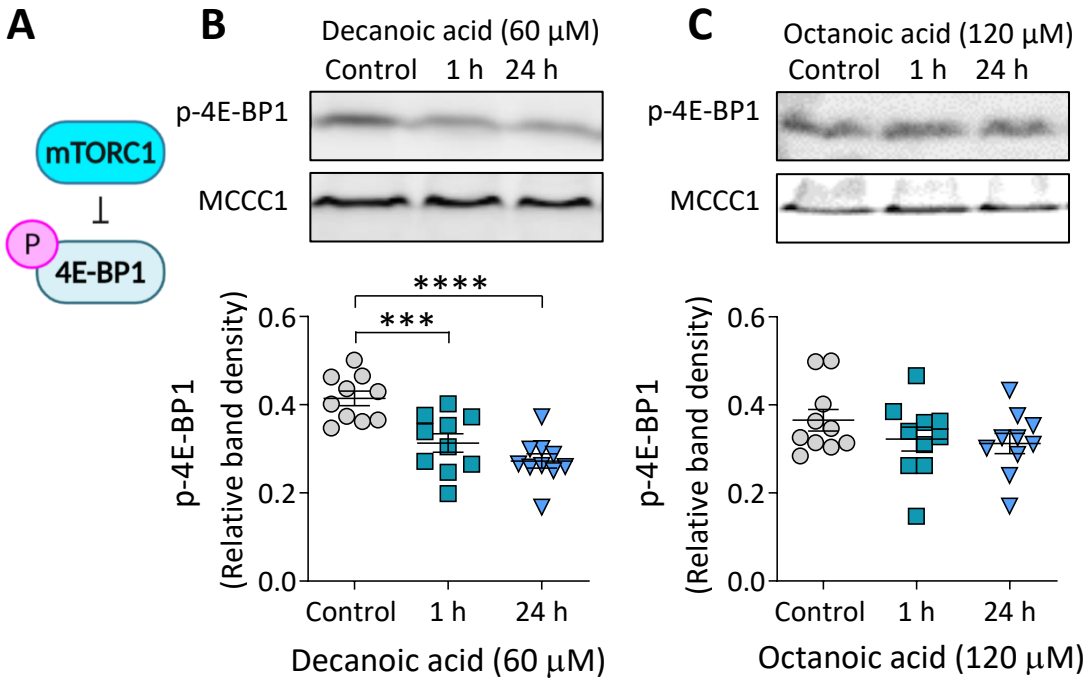

Figure 6. 1 Decanoic acid causes a reduction in p-4E-BP1 levels in *Dictyostelium*. A) Inhibition of mTORC1 prevents the phosphorylation of 4E-BP1, this phosphorylation (p-4E-BP1) is used as a read out for mTORC1 activity. p-4E-BP1 (11 kDa) levels were analysed in wild type cells treated for 1 hour or 24 hours (h) with B) decanoic acid (n = 10) or C) octanoic acid (n = 10). MCCC1 (80 kDa) was used as a loading control. Data represent the mean ± SEM. Significance is indicated by *** $p \leq 0.001$, **** $p \leq 0.0001$. 1-way ANOVA with Dunnett's post hoc test.

displaying both strong anti-epileptiform activity (Chang *et al.*, 201) and mTORC1 inhibition (Fig. 6.1B), and octanoic acid lacking both epileptiform control (Chang *et al.*, 2013) and mTORC1 inhibition (Fig. 6.1C), we investigated whether potency in reducing epileptiform activity in a rat hippocampal slice model is related to mTORC1 inhibition in *Dictyostelium*. Thus, we assessed compounds demonstrating potent anti-epileptiform activity for their effects on *Dictyostelium* cell proliferation and p-4E-BP1 levels. Compounds were chosen based on data from PTZ rat hippocampal slice models, where a decrease in the frequency of epileptiform discharge was used as a readout for anti-epileptiform activity (Chang *et al.*, 2013; Chang *et al.*, 2015) (Fig. 6.2A). 4-BCCA caused the most potent reduction in growth (100 % reduction, 95% Cl: 96% to 105 % $p \leq 0.0001$, n=7), followed by decanoic acid (84% reduction, 95 % Cl: 65 % to 112 %, $p = 0.0004$, $n = 7$), 4-EOA (54 % reduction, $p > 0.05$, $n = 7$), 5-MOA (53 %

reduction, $p > 0.05$, $n = 7$) and octanoic acid (20 % reduction, $p > 0.05$, $n = 7$) (Fig. 6.2B). This potency correlated with the previously determined anti-epileptiform activity (Fig. 6.2) (Chang *et al.*, 2013; Chang *et al.*, 2015). We further assessed these compounds for their effects on mTORC1 activity and identified that decanoic acid was the only compound to reduce p-4E-BP1 levels at 60 µM (25 % reduction, 95 % Cl: 18 % to 31 %, $p = 0.0476$, $n = 7$) (Fig 6.2C), demonstrating that the potency of these compounds in reducing epileptiform activity is not related to their mTORC1 inhibitory effect in *Dictyostelium*.

To confirm that assessing p-4E-BP1 levels is an appropriate method of monitoring mTORC1 activity we quantified *Dictyostelium* samples following starvation, a physiological process well established to reduce mTORC1 activity (Ye *et al.*, 2015b; Tan, Sim and Long, 2017). Starvation for 10 minutes in nutrient free phosphate buffer (KK2) caused a significant decrease (35 % decrease, 95 % Cl: 33 % to 41 %, $p = 0.0022$, $n = 6$) in p-4E-BP1 levels in *Dictyostelium* (Fig 6.3A). This suggests that monitoring p-4E-BP1 levels provides a suitable readout for mTORC1 activity. Furthermore, we established that the mTOR inhibitor Torin2 (10 µM) caused a significant decrease in p-4E-BP1 levels (29 % decrease, 95 % Cl: 26 % to 32 %, $p = 0.0049$, $n = 6$) (Fig 6.3B). Treatment with rapamycin did not significantly alter p-4E-BP1 levels in this model (7.3 % decrease following 1 hour, $p = 0.8763$, and a 8.9 % decrease following 24 hours, $p = 0.6025$, $n = 7$) (Fig. 6.3C), consistent with earlier studies (Dominguez-Martin *et al.*, 2017; Williams and Kay, 2018). In order to quantify p-4E-BP1 levels between samples, values were normalised to the established loading control, mitochondrial 3-methylcrotonyl-CoA carboxylase α (MCCC1) (Davidson, King and Insall, 2013). We confirmed that MCCC1 is a suitable loading control by comparing the ratio of MCCC1 levels to the levels of a second internal control (calnexin) and demonstrating that MCCC1 levels are not altered following treatment with decanoic acid (Fig. 6.3C). These controls confirm the validity of our interpretation that decanoic acid, but not octanoic acid (or the derivatives 4-BCCA, 4-EOA or 5-MOA), causes a reduction of mTORC1 signalling in *Dictyostelium*.

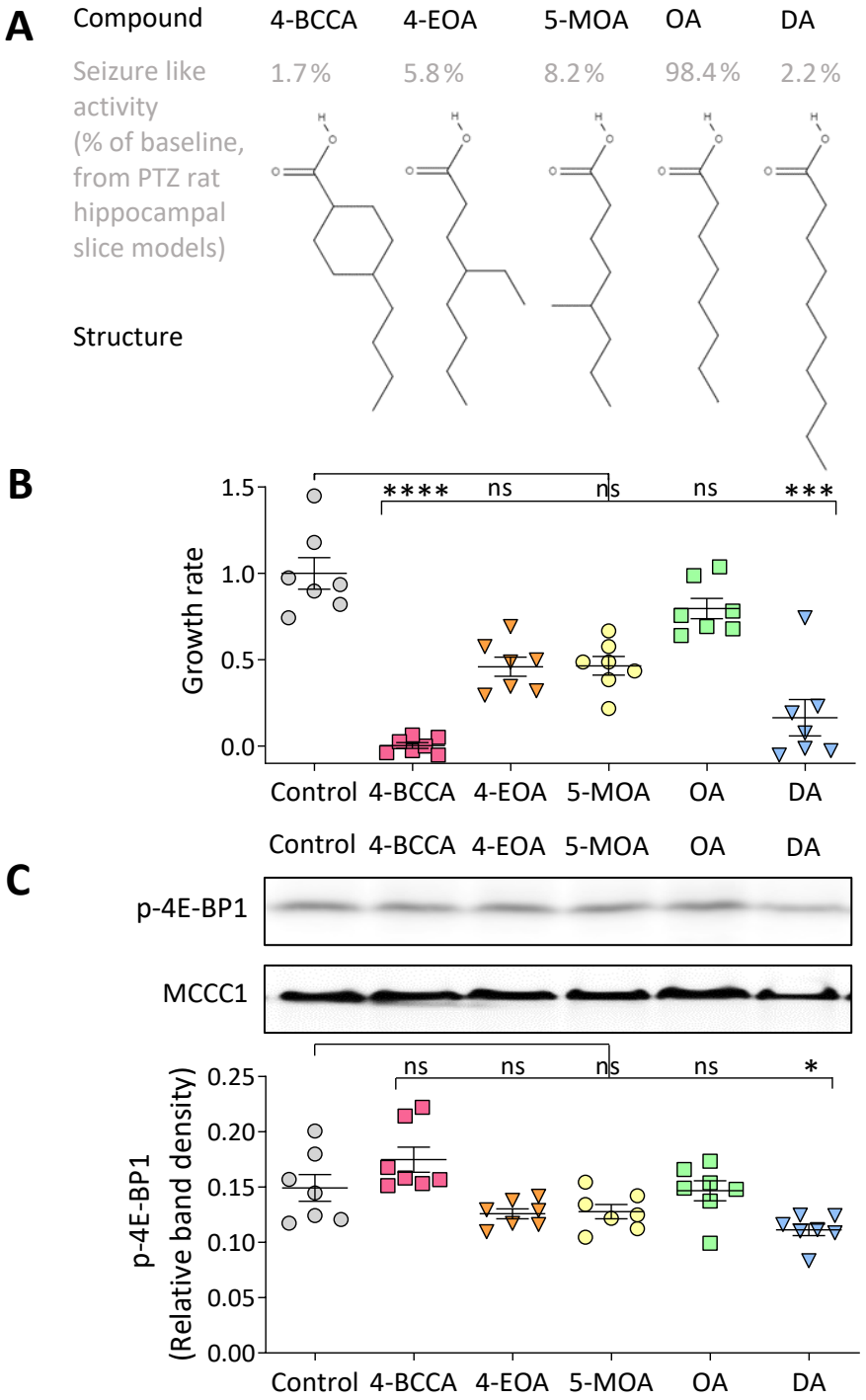

Figure 6. 2 Anti-epileptiform activity of fatty acid derivatives shows no correlation with mTORC1 inhibition. A) Chemical structures of the fatty acid derivatives, 4-butl cyclohexane carboxylic acid (4-BCCA), 4-ethyl octanoic acid (4-EOA), 5-methyl octanoic acid (5-MOA), alongside the fatty acids octanoic acid (OA) and decanoic acid (DA). Inhibition of seizure like activity by these compounds is displayed as a percentage of the baseline (Chang *et al.*, 2013; Chang *et al.*, 2015). The effects of specific modified fatty acid derivatives on B) growth (n = 7, Kruskal-Wallis test with Dunn's post hoc test) and C) phosphorylated-4E-BP1 (p-4E-BP1) levels (n = 7, Kruskal-Wallis test with Dunn's post hoc test) in wild type cells were investigated alongside octanoic acid and decanoic acid (60 µM, 24 hours). MCCC1 was used as a loading control. Data represent the mean ± SEM. Significance is indicated by ns $p > 0.05$, * $p \leq 0.05$, *** $p \leq 0.001$ and **** $p \leq 0.0001$.

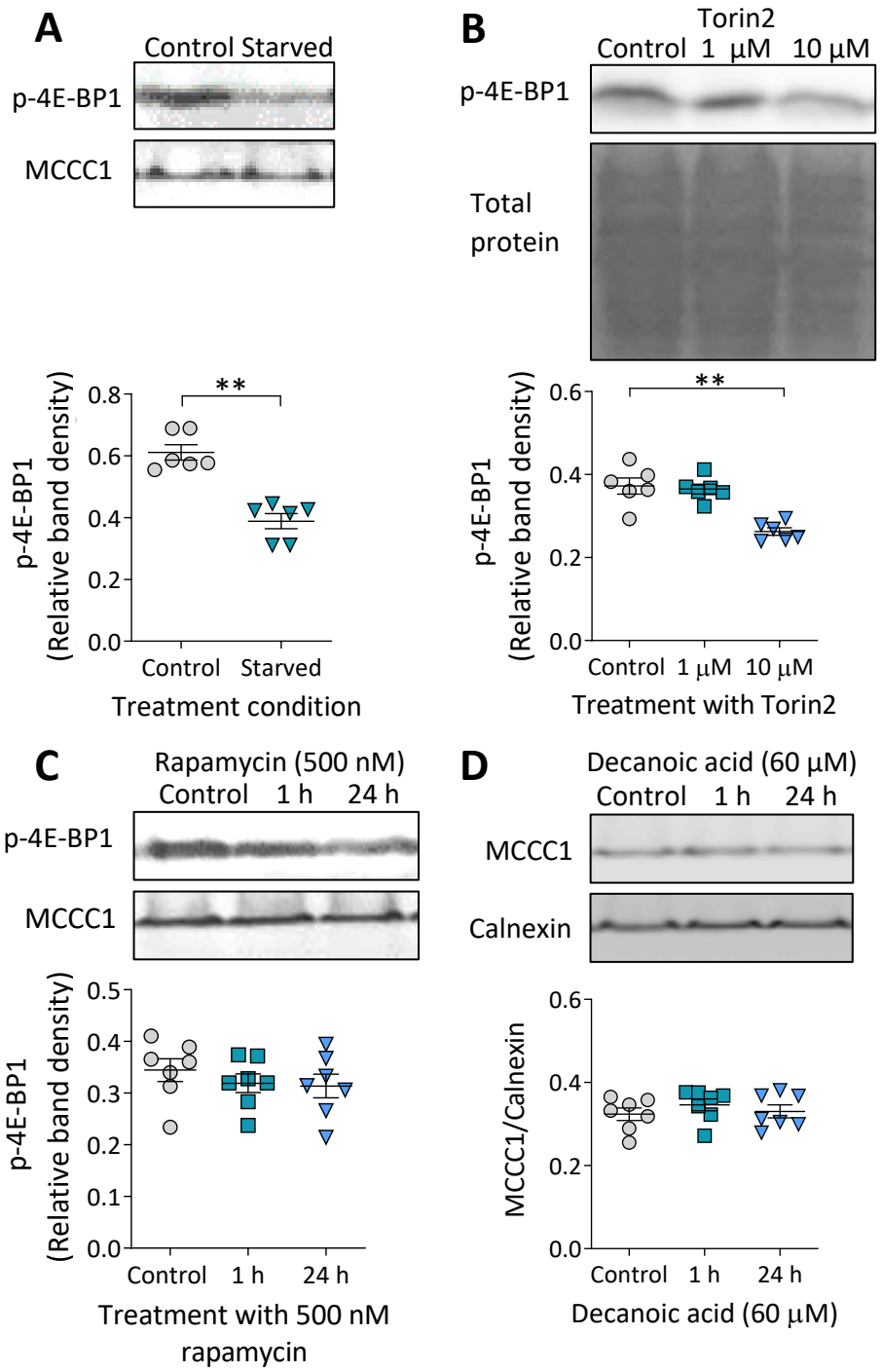

Figure 6. 3 Measuring p-4E-BP1 levels as a read out for mTORC1 in *Dictyostelium*. A) Analysis of phosphorylated-4E-BP1 (p-4E-BP1) levels in wild type cells untreated or starved for 10 minutes in nutrient free phosphate buffer. MCCC1 was used as a loading control (n = 6, Mann-Whitney test). B) Analysis of p-4E-BP1 levels in wild type cells treated with 1 or 10 µM mTOR inhibitor Torin2 for 24 hours, normalised to total protein (due to effects of Torin2 on mitochondria) (n = 6, Kruskal-Wallis test with Dunn's post hoc test). C) Analysis of p-4E-BP1 levels in wild type cells untreated or treated with 500 nM rapamycin for 1 hour (h) or 24 hours (n = 7), with MCCC1 as a loading control (Kruskal-Wallis test with Dunn's post hoc test). D) MCCC1 and Calnexin levels were analysed in wild type cells treated for 1 hour or 24 hours with decanoic acid (n = 7, Kruskal-Wallis test with Dunn's post hoc test). Data represent the mean ± SEM. Significance is indicated by ** $p \leq 0.01$.

6.2.2 Decanoic acid acts independently of AMPK or PI3K/AKT signalling in *Dictyostelium*

Since mTORC1 is activated by PI3K/AKT signalling and inhibited by AMPK signalling (Fig. 6.4A), we also investigated the effect of decanoic acid on these signalling pathways. We monitored the effects of decanoic acid on PI3K/AKT signalling using an antibody against phosphorylated AKT substrate (p-AKT-S) which detects multiple substrates phosphorylated by AKT (Williams *et al.*, 2019). No significant difference was observed in p-AKT substrate levels after treatment with decanoic acid (60 µM) for 1 hour or 24 hours (10% decrease after 1 hour, p=0.6444 and a 15% increase after 24 hours, p = 0.1219, n = 8) (Fig. 6.4B). This indicates that decanoic acid targets mTORC1 independently of PI3K/AKT signalling, consistent with our data demonstrating that decanoic acid does not alter production of PIP_3. This finding further suggests that decanoic acid inhibits mTORC1 without altering mTORC2 activation, since AKT is directly phosphorylated by mTORC2. We also evaluated the effect of decanoic acid on AMPK signalling using a phospho-AMPK-α (p-AMPK) antibody (Jaiswal and Kimmel, 2019). No significant difference was observed in p-AMPK levels following decanoic acid treatment (60 µM) for 1 hour or 24 hours (0.032 % increase following 1 hour, p > 0.9999, and a 5.9 % increase following 24 hours, p = 0.9227, n = 10) (Fig. 6.4C). Thus, our findings suggest that decanoic acid targets mTORC1 independently of both PI3K/AKT and AMPK signalling.

To verify that the use of the phosphorylated AKT substrate antibody provides an accurate readout for PI3K/AKT signalling we investigated p-AKT substrate levels following the use of a PI3K inhibitor (LY294002). We demonstrated a significant reduction in p-AKT substrate levels following 24-hour treatment with 60 µM PI3K inhibitor (15 % reduction, 95 % Cl: 13 % to 16 %, p = 0.026, n = 6) (Fig. 6.5A). Furthermore, we showed that AKT substrate phosphorylation was negligible in a $pkbA^-/pkgB^-$ double knockout (Fig. 6.5B). These findings suggest that the p-AKT substrate antibody provides a suitable readout for PI3K/AKT signalling. In addition, we confirmed that western blotting using the antibody against phospho-AMPK-α provides an appropriate method for evaluating AMPK signalling. We quantified p-AMPK levels following starvation (Fig. 6.5C), a process known to lead to phosphorylation and activation of AMPK and demonstrated that starvation for 2 hours in nutrient free phosphate buffer (development buffer) resulted in a significant

increase in p-AMPK levels (1400 % increase, 95 % CI: 710 % to 7000 %, p = 0.0022, n = 9), suggesting that this antibody provides a reliable method for the quantification of AMPK activity. Validating the suitability of these antibodies to monitor PI3K/AKT and AMPK signalling provides us with greater confidence in our results demonstrating the decanoic acid is regulating mTORC1 independently of either of these pathways.

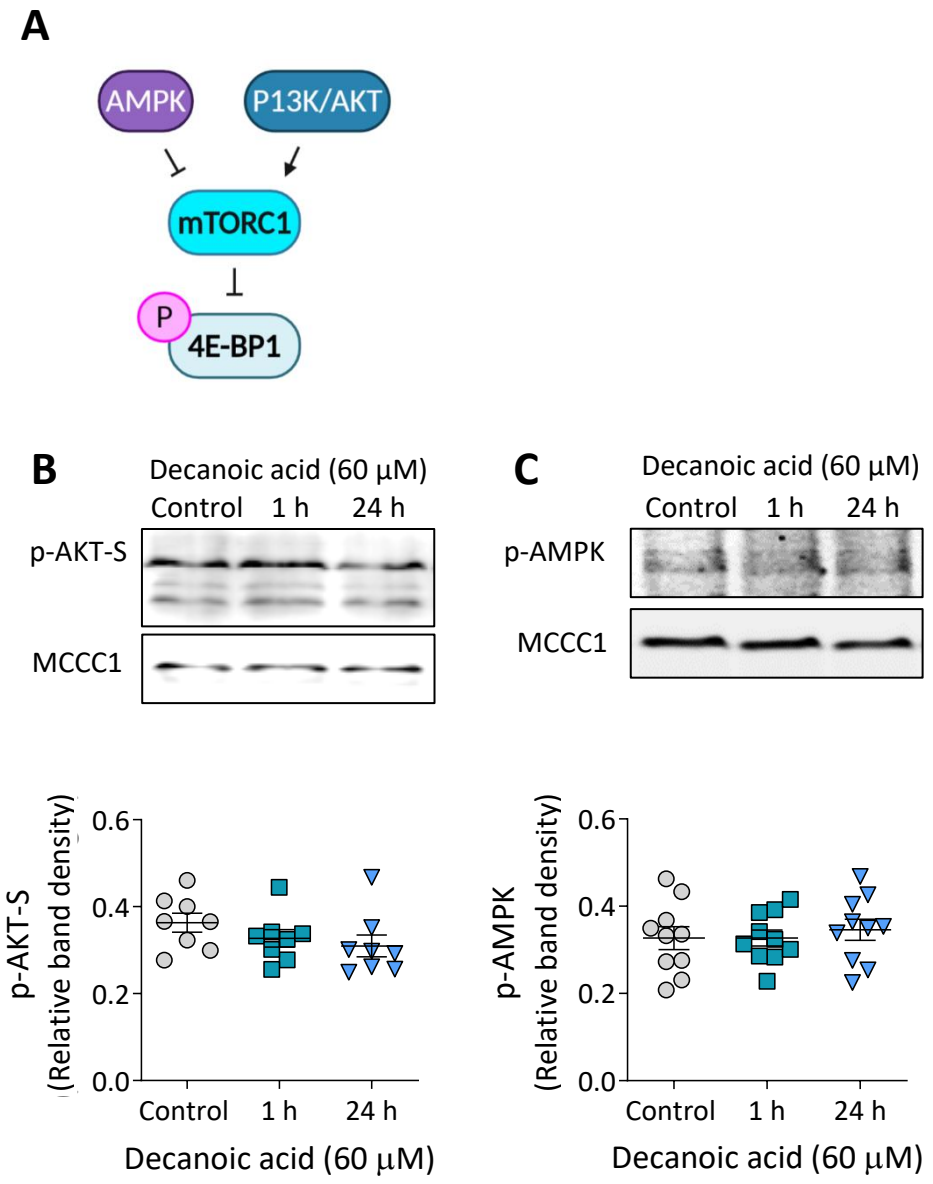

Figure 6. 4 Decanoic acid acts independently of AMPK or PI3K/AKT signalling in *Dictyostelium*. A) Simplified schematic diagram of mTORC1 pathway signalling regulated by AMPK and PI3K/AKT. B) AKT activity was evaluated in wild type cells treated for 1 hour or 24 hours with decanoic acid using an antibody against phospho-AKT substrate antibody (p-AKT-S). MCCC1 was used as a loading control (n = 8, 1-way ANOVA with Dunnett's post hoc test). C) AMPK activation was analysed using an antibody against phospho-AMPK (p-AMPK) MCCC1 was used as a loading control (n = 10, 1-way ANOVA with Dunnett's post hoc test). Data represent the mean ± SEM.

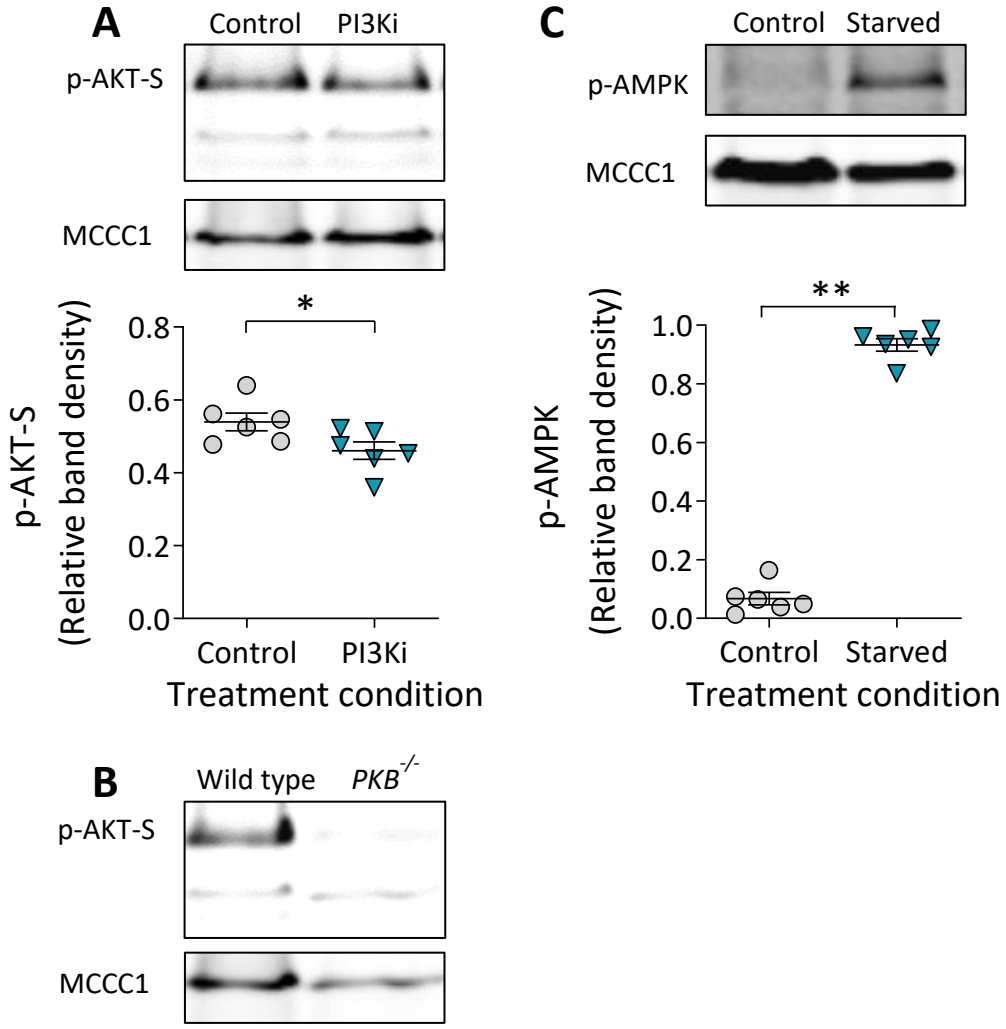

Figure 6. 5 Analysis of AKT-substrate and AMPK phosphorylation in *Dictyostelium*. A) AKT-substrate phosphorylation (p-AKT-S) was evaluated in wild type cells treated with 60 µM PI3K inhibitor for 24 hours (LY294002), with MCCC1 as a loading control (n = 6, Mann-Whitney test). B) A *pkbA*$^{-}$*/pkgB*$^{-}$ (*PKB*$^{-/-}$) double knockout shows negligible AKT-substrate phosphorylation, with MCCC1 as a loading control. C) Phosphorylated-AMPK (p-AMPK) levels were analysed in wild type cells, untreated or starved for 2 hours in nutrient free phosphate buffer. MCCC1 was used as a loading control (n = 6, unpaired t-test). Data represent the mean ± SEM. Significance is indicated by * $p \leq 0.05$, ** $p \leq 0.01$.

We have previously demonstrated that the growth response, but not the autophagic response of *Dictyostelium* to decanoic acid is partially dependent on the UBX domain containing protein UBXD18. In order to investigate a role of UBXD18 both in regulating mTORC1 activity and in the decanoic acid-dependent change in mTORC1 function, western blot analysis of 4E-BP1 phosphorylation was carried out with *UBXD18*$^{-}$ and *UBXD18*$^{-/+}$ in the absence and presence of decanoic acid. Loss of

UBXD18 caused a 37% decrease in p-4E-BP1 levels (95% CI: 29% to 47%, p = 0.0305, n = 8) compared to wild type (Fig. 6.6A). p-4E-BP1 levels were restored in the rescue cell line (*UBXD18*$^{-/+}$) (116% increase compared to *UBXD18*$^{-}$, 95% CI: 115% to 118%, p ≤ 0.0001, n = 8) (Fig. 6.6A). Analysing p-4E-BP1 levels following decanoic acid treatment (60 µM for 1 or 24 hours), showed that *UBXD18*$^{-}$ was unresponsive to treatment with this fatty acid (4.6% decrease in p-4E-BP1 following 1 hour decanoic acid treatment, p > 0.9999, n = 9, and an 8% increase following 24 hours, p = 0.1926, n = 9) (Fig 6.6B). *UBXD18*$^{-/+}$ showed restored decanoic acid sensitivity following 24-hour treatment (25% decrease in p-4E-BP1 levels, 95% CI: 23% to 29%, p = 0.0010, n = 9) (Fig. 6.6C). These findings suggest that UBXD18 is involved in regulating the sensitivity of *Dictyostelium* to decanoic acid, and thus imply that decanoic acid is acting through distinct mechanisms to regulate autophagy and mTORC1 signalling.

6.2.4 Decanoic acid induced mTORC1 inhibition in *Dictyostelium* could result from inhibition of p97 activity

Our data demonstrate that in *Dictyostelium* the inhibitory effect of decanoic acid on mTORC1 is dependent on the protein UBXD18. We proceeded to establish whether this effect is linked to our earlier finding suggesting that decanoic acid inhibits p97 activity in a UBXD18 dependent manner. To investigate this, we assessed the effect of p97 inhibition on mTORC1 activity by using the p97 inhibitor DBeQ (N2,N4-dibenzylquinazoline-2,4-diamine) (Parzych *et al.*, 2015; Ching *et al.*, 2013). p-4E-BP1 levels were monitored following DBeQ treatment (7.5 µM and 15 µM for 24 hours) (Fig. 6.7A). Treatment with DBeQ caused a significant reduction in p-4E-BP1 levels at 7.5 µM (54% reduction, 95% CI: 49% to 62% decrease, p = 0.0138, n = 9) and at 15 µM (70 % reduction, 95% CI: 66% to 77% decrease, p = 0.0001, n = 9) (Fig. 6.7A). This was consistent with a comparable inhibition of growth caused by these concentrations of DBeQ (7.5 µM DbeQ caused a 34% inhibition of growth, 95% CI: 32% to 36%, p = 0.0263, n = 9, and 15 µM DbeQ caused a 56% inhibition in growth, 95% CI: 53% to 60 %, p ≤ 0.0001, n = 9) (Fig. 6.7B). These findings indicate that the inhibitory effect of decanoic acid on p97 activity may explain the observed mTORC1 and growth inhibitory effects of decanoic acid in *Dictyostelium.* This is consistent with *UBXD18*$^{-}$ mutants displaying resistance to decanoic acid in p97 inhibition, growth inhibition

and mTORC1 inhibition. These findings suggest a potential mechanism for decanoic acid in inhibiting *Dictyostelium* growth and mTORC1 signalling via a UBXD18 dependent inhibition of p97 activation.

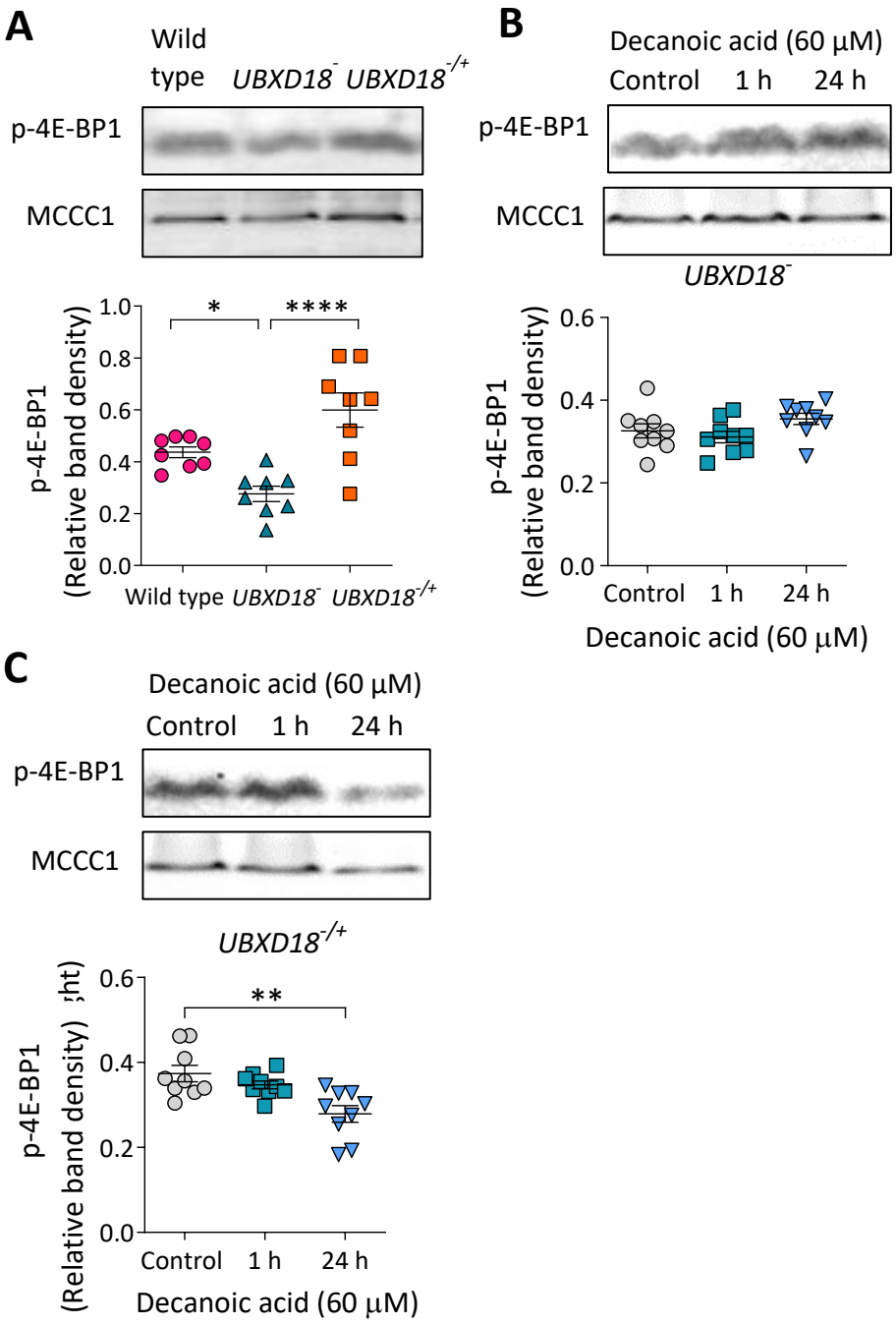

Figure 6. 6 UBXD18 regulates the sensitivity of *Dictyostelium* to decanoic acid. A) Analysis of phosphorylated-4E-BP1 (p-4E-BP1) levels in wild type, *UBXD18*$^{-}$, and *UBXD18*$^{-/+}$ cells (n = 9, 1-way ANOVA with Dunnett's post hoc test). Analysis of p-4E-BP1 levels in E) *UBXD18*$^{-}$ (n = 9, Kruskal-Wallis test with Dunn's post hoc test) or F) *UBXD18*$^{-/+}$ (n = 9, 1-way ANOVA with Dunnett's post hoc test) treated with decanoic acid (60 µM) for 1 hour or 24 hours. MCCC1 was used as a loading control. Data represent the mean ± SEM. Significance is indicated by * $p \leq 0.05$, ** $p \leq 0.01$, **** $p \leq 0.0001$.

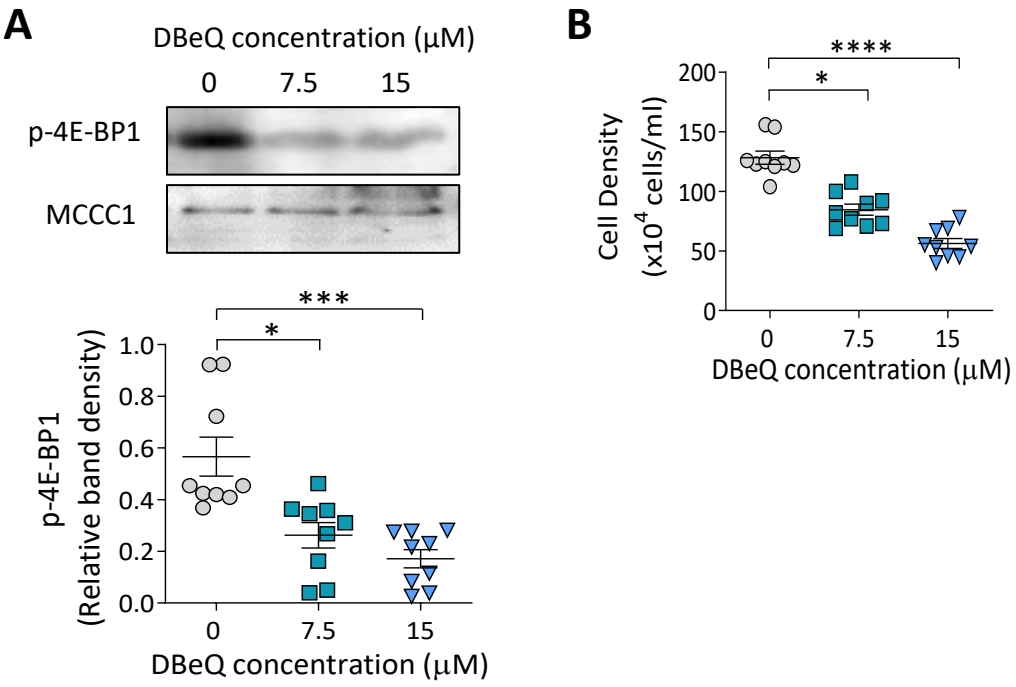

Figure 6. 7 p97 inhibitor (DBeQ) inhibits mTORC1 activity and *Dictyostelium* cell growth. A) Analysis of phosphorylated-4E-BP1 (p-4E-BP1) levels in wild type cells treated for 24 hours with p97 inhibitor (DBeQ). MCCC1 is used as a loading control (n = 9, Kruskal-Wallis test with Dunn's post hoc test). B) *Dictyostelium* cells (30 x 10^4 cells/ml) were grown for 24 hours in 0 μM, 7.5 μM, and 15 μM DbeQ, before cell growth was quantified (n = 9, Kruskal-Wallis test with Dunn's post hoc test). Data represent the mean ± SEM. Significance is indicated by * $p \leq 0.05$, *** $p \leq 0.001$, **** $p \leq 0.0001$.

6.2.5 Decanoic acid causes a reduction in mTORC1 activation in rat hippocampal brain slices

Having identified a novel effect of decanoic acid in reducing mTORC1 activity independent of altered glucose levels and insulin signaling in *Dictyostelium,* we sought to translate these findings to a mammalian system. Here, we employed rat hippocampal slice preparations maintained in artificial cerebrospinal fluid (aCSF), ensuring constant glucose levels in the absence of insulin, treated with decanoic acid (100 and 300 μM for 1 hour) (as prepared by Dr Eleonora Lugarà, UCL) prior to assessing mTORC1 activity by western blot analysis of p-4E-BP1 and total-4E-BP1 levels (Fig. 6.8). Decanoic acid at 100 μM had no significant effect on p-4E-BP1 levels (6% reduction, $p > 0.9999$, n = 6) (Fig. 6.8A and B) but, decreased p-4E-BP1 levels by 27% at 300 μM (95% CI: 22% to 34%, $p = 0.021$, n = 6) (Fig. 6.7A and B). Decanoic acid

at 100 µM or 300 µM had no significant effect on total-4E-BP1 levels (Fig. 6.8A and C), but decreased p-4E-BP1/ total-4E-BP1 levels by 28 % at 300 µM (95 % CI: 20 % to 38 %, p = 0.0165, n = 6) (Fig. 6.8A and D). These findings suggest that decanoic acid (300 µM) causes a significant decrease in mTORC1 signalling in rat hippocampal slice models.

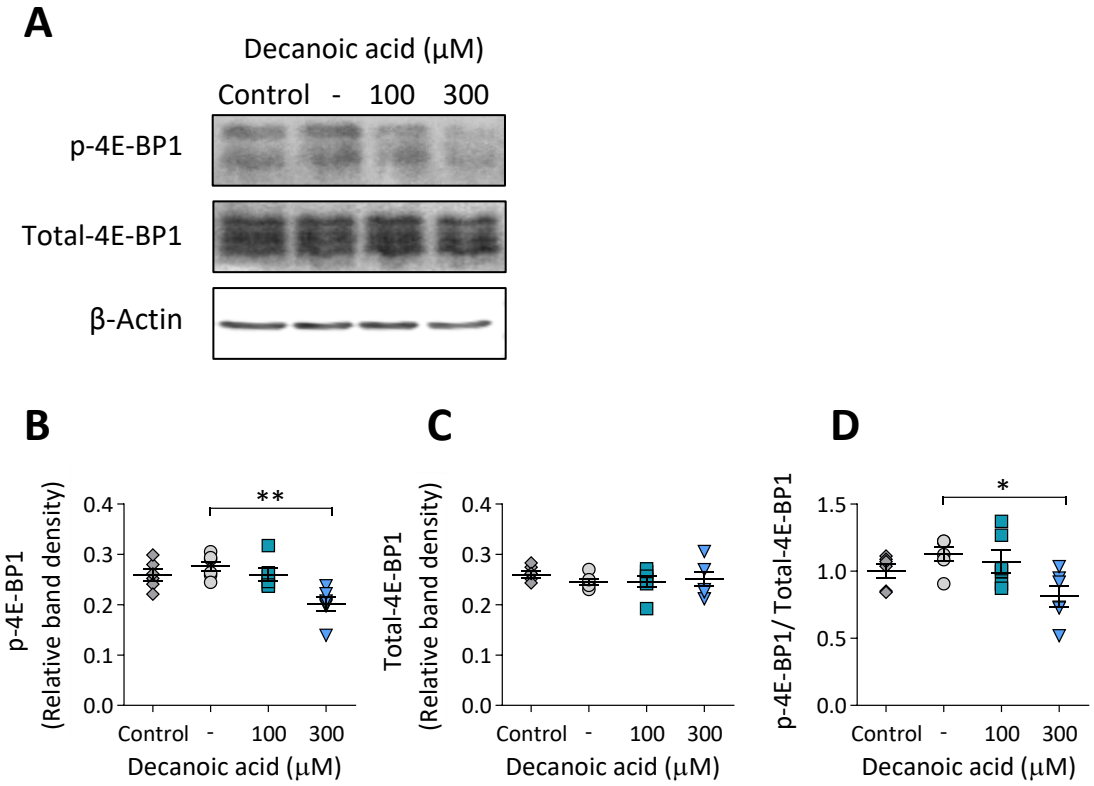

Figure 6. 8 Decanoic acid causes a reduction in p-4E-BP1 levels in rat hippocampal brain slices. A) Rat hippocampal brain slices treated for 1 hour with artificial cerebral spinal fluid (control), DMSO solvent control (-), 100 µM decanoic acid (DA) or 300 µM decanoic acid (DA) were analysed for phosphorylated-4E-BP1 (p-4E-BP1) and total-4E-BP1. β-Actin was used as a loading control. Relative band densities were plotted for B) p-4E-BP1 (n = 6) and C) total-4E-BP1 (n = 6). D) The ratio of p-4E-BP1/ total-4E-BP1 was used as a readout for mTORC1 (n = 6). Data represent the mean ± SEM. Significance is indicated by * p ≤ 0.05, ** p ≤ 0.01 (Kruskal-Wallis test with Dunn's post hoc test).

To confirm the effect of decanoic acid on mTORC1 activity in the rat hippocampal slice model, we also analysed p70 ribosomal protein S6 Kinase (S6K) phosphorylation levels. In this role, increased phosphorylation at threonine 389 (p-S6K) indicates increased mTORC1 activation (Datan *et al.*, 2014). Decanoic acid at 100 µM had no significant effect on p-S6K levels (20 % reduction, p = 0.1986, n = 6) (Fig.

6.9A and B) but significantly decreased p-S6K levels by 32% at 300 μM (95% CI: 21% to 50 %, p = 0.0165, n = 6) (Fig. 6.9A and B). No significant difference was observed in the ratio of p-S6K over total-S6K for either 100 μM or 300 μM decanoic acid (Fig. 6.9A and C), however, a non-significant reduction was observed at 300 μM decanoic acid (18% reduction, p = 0.8110, n = 6) consistent with a trend for a reduction in mTORC1 activity. Taken together these data suggest that decanoic acid (300 μM) causes a decrease in mTORC1 signalling in rat hippocampal slice models under conditions of constant glucose and in the absence of insulin, consistent with that observed in *Dictyostelium.*

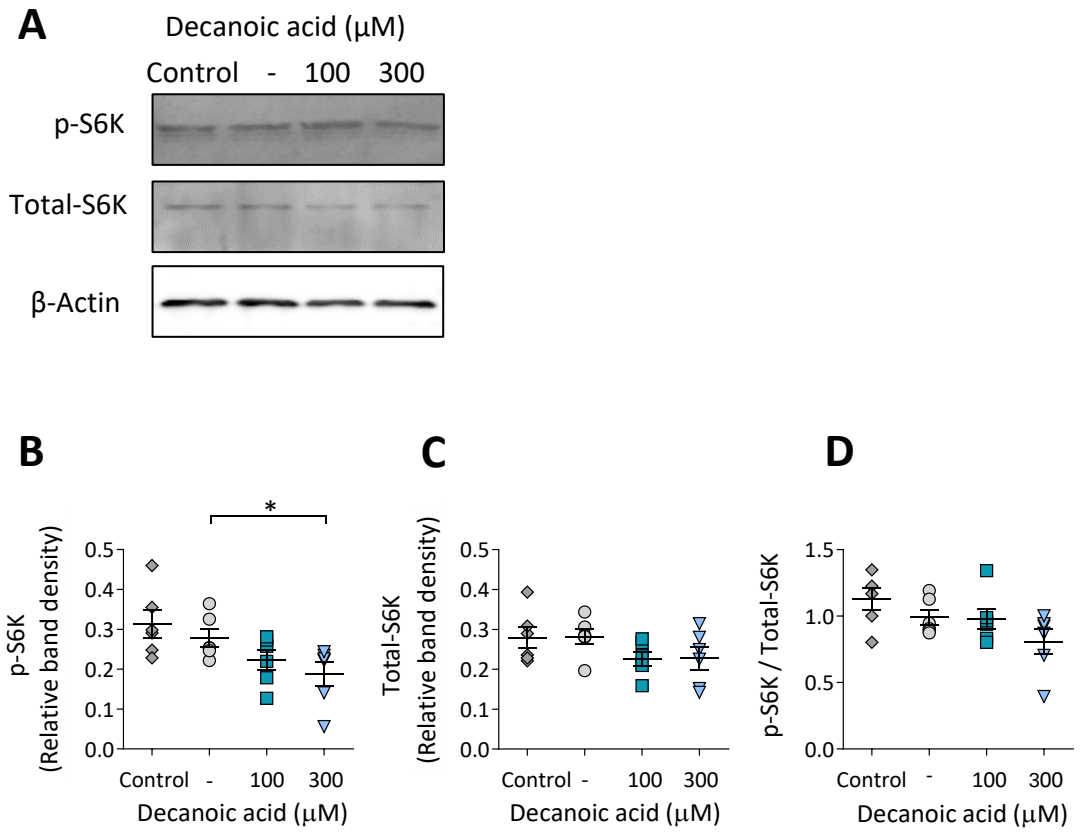

Figure 6. 9 Decanoic acid causes a reduction in p-S6K but not p-S6K/ Total-S6K levels in rat hippocampal brain slices. A) Rat hippocampal brain slices treated for 1 hour with artificial cerebral spinal fluid (control), DMSO solvent control (-), 100 μM decanoic acid (DA) or 300 μM decanoic acid (DA) were analysed for phosphorylated-S6K (p-S6K) and total-S6K. β-Actin was used as a loading control. B) Relative band densities were plotted for B) p-S6K (n = 6) and C) total-S6K (n = 6). D) The ratio of p-S6K/ total-S6K was used as a readout for mTORC1 (n = 6). Data represent the mean ± SEM. Significance is indicated by * p ≤ 0.05 (Kruskal-Wallis test with Dunn's post hoc

6.2.6 Decanoic acid acts independently of PI3K/AKT signalling in rat hippocampal slices

Our results implicate decanoic acid in inhibiting mTORC1 activity in rat hippocampal slices. In order to investigate how decanoic acid targets this pathway we assessed the effects of decanoic acid on PI3K/AKT signalling, a pathway known to activate mTORC1. We monitored the effects of decanoic acid on PI3K/AKT signalling using antibodies against phosphorylated-AKT at Thr308, p-AKT(Thr308), phosphorylation of which is controlled by the PI3K pathway, and at Ser473, p-AKT(Ser473), phosphorylation of which is required for full activation, as well as monitoring total-AKT levels (Kamimura, Tang and Devreotes, 2009; Tariqul Islam *et al.*, 2019; Alam *et al.*, 2019). No significant difference was observed in p-AKT(Thr308), p-AKT(Ser473), total-AKT or in the ratios of p-AKT(Thr308)/total-AKT or p-AKT(Ser473)/total-AKT levels after treatment with decanoic acid at 100 µM or 300 µM ($p > 0.05$, $n = 6$) (Fig. 6.10). This indicates that decanoic acid targets mTORC1 independently of PI3K/AKT signalling, and furthermore, suggests that decanoic acid inhibits mTORC1 without altering mTORC2 activation.

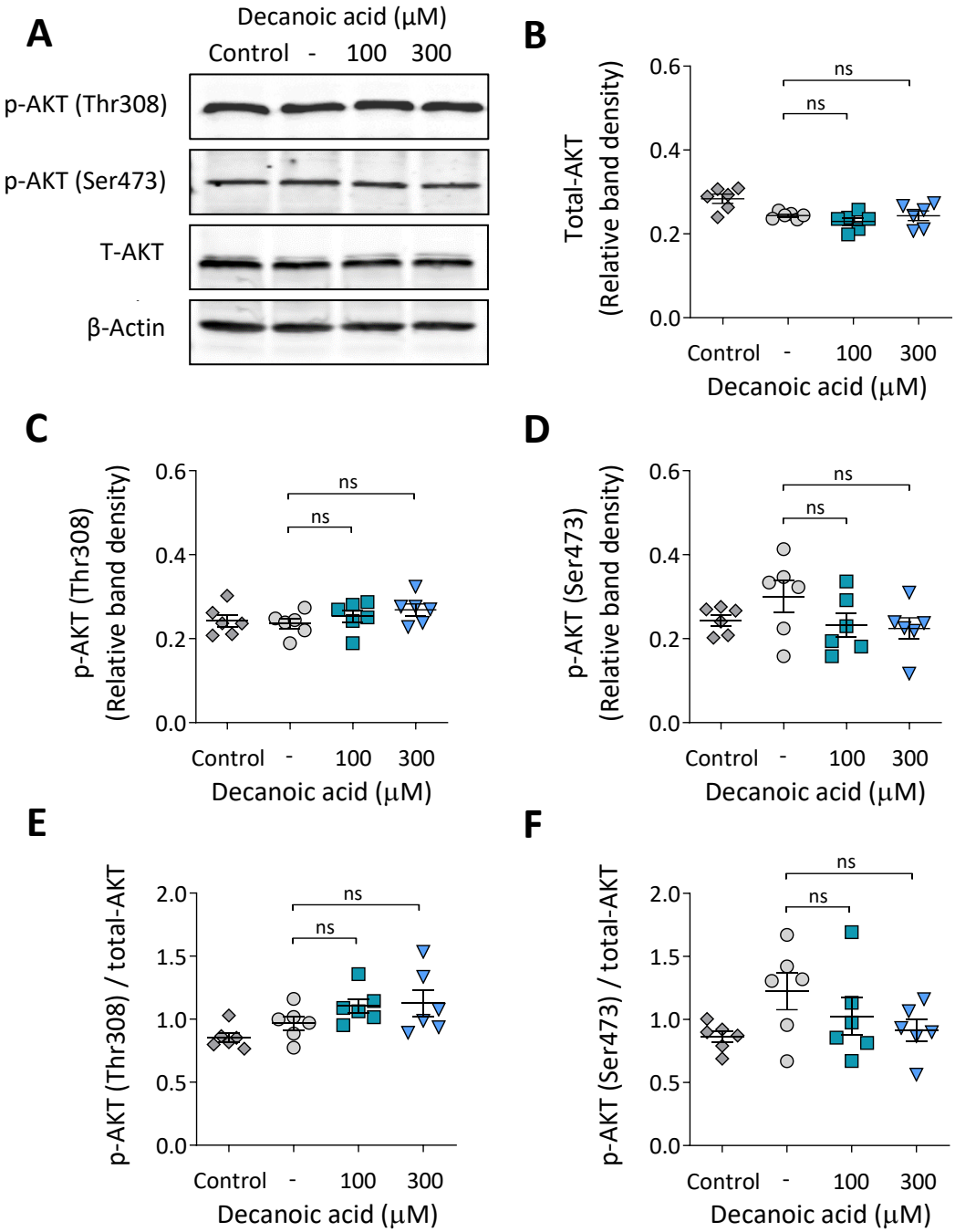

Figure 6. 10 Decanoic acid does not alter p-AKT in levels in rat hippocampal brain slices. A) Rat hippocampal brain slices treated for 1 hour with artificial cerebral spinal fluid (control), DMSO solvent control (-), 100 µM decanoic acid (DA) or 300 µM decanoic acid (DA) were analysed for phosphorylation at Thr308 (controlled by the PI3K pathway) and Ser473 (required for full activation) and for total-AKT levels, with β-Actin as a loading control. Relative band densities were plotted for B) total-AKT (n = 6) (Kruskal-Wallis test with Dunn's post hoc test) C) phospho-AKT at Thr308 (n = 6) (Kruskal-Wallis test with Dunn's post hoc test) D) phospho-AKT at Ser473 (n = 6) (Kruskal-Wallis test with Dunn's post hoc test). The ratio of E) p-AKT(Thr308)/total-AKT (n = 6) (Kruskal-Wallis test with Dunn's post hoc test) and F) p-AKT(Ser473) (n = 6) (Kruskal-Wallis test with Dunn's post hoc test) was plotted. Error bars represent the mean ± SEM. Significance is indicated by ns $p > 0.05$.

6.2.7 Decanoic acid causes a reduction in mTORC1 activation in patient derived astrocytes

To investigate the potential ability of decanoic acid to reduce mTORC1 activity in a clinically relevant setting, we monitored mTORC1 activity in astrocytes derived from patients with tuberous sclerosis complex (TSC) (as prepared by Dr Stephanie Dooves, Vrije Universiteit Amsterdam). mTORC1 signalling is reportedly activated in astrocytes during epileptogenesis (Sha *et al.*, 2012), with this cell type believed to play a significant role in the causation of seizures (Wong, 2019; Coulter and Steinhäuser, 2015; de Lanerolle, Lee and Spencer, 2010). In these experiments, patients with mutations in either *TSC1* (*TSC1*$^{-}$) or *TSC2* (*TSC2*$^{-}$) and healthy controls provided samples to produce induced pluripotent stem cells (iPSCs) that were differentiated into astrocytes (Nadadhur *et al.*, 2018; Nadadhur *et al.*, 2019) and treated with decanoic acid (300 μM for 24 hours) prior to western blot analysis of p-4E-BP1 and total-4E-BP1 levels (Fig. 6.11). Decanoic acid caused a 41% reduction in the ratio of p-4E-BP1/ total-4E-BP1 in astrocytes derived from healthy (control) patients (95 % Cl: 39 % to 42 %, $p \leq 0.0001$, $n = 30$) (Fig. 6.11B) confirming a role for decanoic acid in regulating mTORC1 activity in human cells in the absence of altered glucose or insulin signalling. Decanoic acid also caused a 46 % reduction in the ratio of p-4E-BP1/ total-4E-BP1 in astrocytes derived from patients with mutations in *TSC1* (95 % Cl: 45 % to 48 %, $p = 0.0002$, $n = 20$) (Fig. 6.11B). However, decanoic acid had no significant effect on the ratio of p-4E-BP1/ total-4E-BP1 in astrocytes derived from patients with mutations in *TSC2* (4 % reduction, $p = 0.8172$, $n = 20$) (Fig. 6.11B). Levels of p-4E-BP1 were not significantly altered following treatment with decanoic acid (control showing 1 % increase, $p = 0.9096$, $n = 30$; *TSC1*$^{-}$, 6 % decrease, $p = 0.7561$, $n = 20$; *TSC2*$^{-}$ 15 % increase, $p = 0.4775$, $n = 20$) (Fig. 6.11C). The reduction in the ratio of p-4E-BP1/ total-4E-BP1 following treatment with decanoic acid was caused by a significant increase in post treatment levels of total-4E-BP1 (Fig. 6.11D). Decanoic acid caused a 64 % increase in total-4E-BP1 levels in control patients (95 % Cl: 58 % to 73 %, $p = 0.0222$, $n = 30$), and a 74 % increase in astrocytes derived from patients with mutations in *TSC1* (95 % Cl: 69 % to 81 %, $p = 0.000139$, $n = 20$) (Fig. 6.11D). A non-significant increase (50 %) was observed in total-4E-BP1 levels in astrocytes derived from patients with *TSC2* mutations ($p = 0.4240$, $n = 20$) (Fig. 6.11D). Variation between

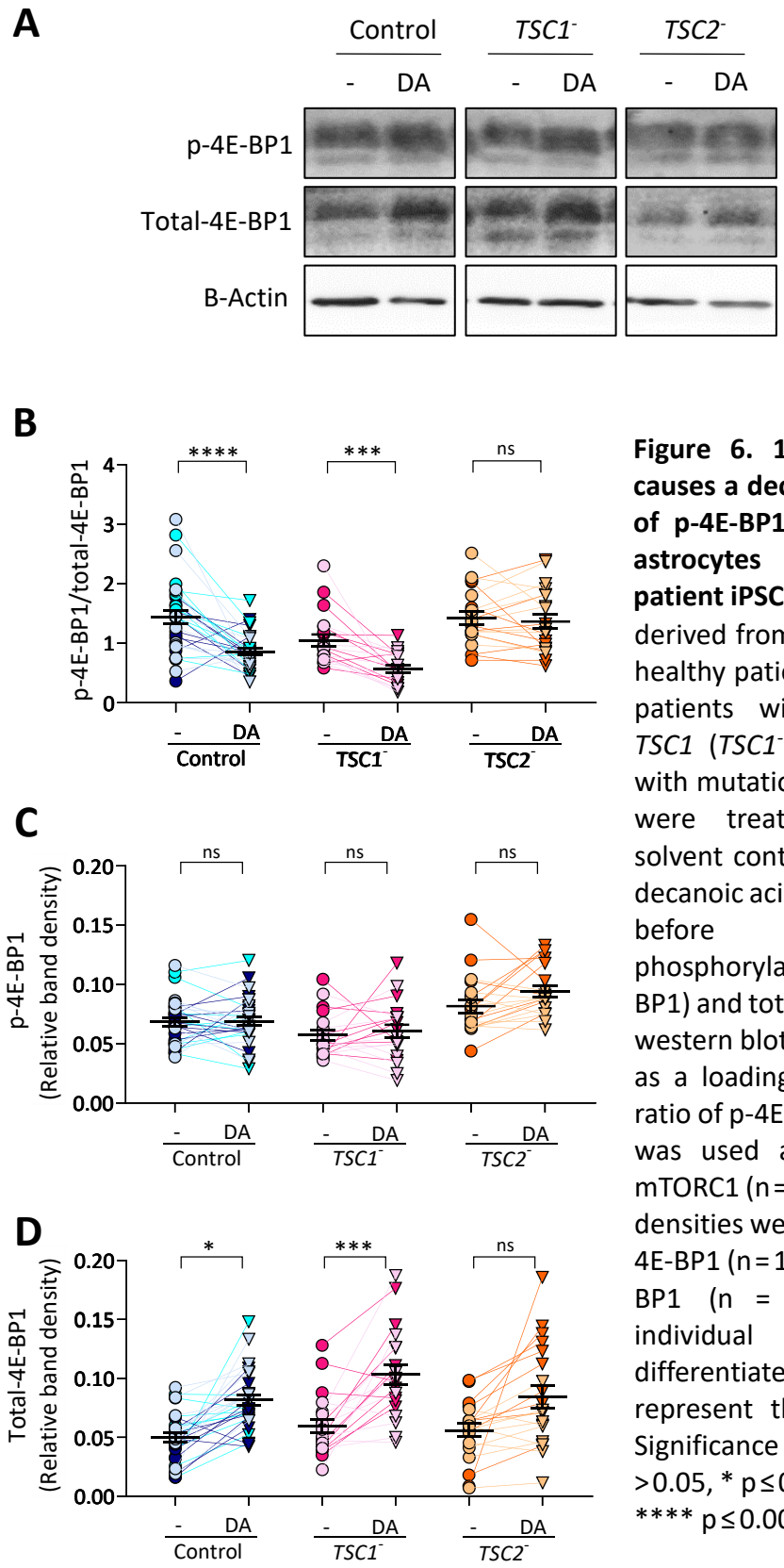

Figure 6. 11 Decanoic acid causes a decrease in the ratio of p-4E-BP1/ total-4E-BP1 in astrocytes derived from patient iPSCs. A) Astrocytes derived from iPSCs from three healthy patients (control), two patients with mutations in *TSC1* (*TSC1*$^{-}$) or two patients with mutations in *TSC2* (*TSC2*$^{-}$) were treated with DMSO solvent control (-), or 300 µM decanoic acid (DA) for 24 hours before analysis of phosphorylated-4E-BP1 (p-4E-BP1) and total-4E-BP1 levels by western blot. β-Actin was used as a loading control. B) The ratio of p-4E-BP1/ total-4E-BP1 was used as a readout for mTORC1 (n = 10). Relative band densities were plotted for C) p-4E-BP1 (n = 10) and D) total-4E-BP1 (n = 10). Data from individual patients are differentiated by colour. Data represent the mean ± SEM. Significance is indicated by ns $p > 0.05$, * $p \leq 0.05$, *** $p \leq 0.001$, **** $p \leq 0.0001$ (nested t-test).

individual patients was observed in astrocytes derived from *TSC2*$^{-}$ patients, with one patient showing no significant change in total-4E-BP1 levels following decanoic acid treatment, while one patient showed a significant increase (79 %) in total-4E-BP1 levels following decanoic acid treatment (95 % Cl: 59 % to 69 %, p = 0.0246, n = 10) (Fig. 6.11D). These data suggest that decanoic acid reduces mTORC1 signalling in astrocytes derived from healthy patients as well as from patients with *TSC1* mutations, with more data required to evaluate the effect in patients with *TSC2* mutations. To confirm the effect of decanoic acid on mTORC1 activity in patient-derived astrocytes, we also analysed p70 ribosomal protein S6 Kinase (S6K) phosphorylation levels (Fig. 6.12). Decanoic acid caused a 54% reduction in the ratio of p-S6K/ total-S6K in astrocytes derived from control patients (95 % Cl: 54 % to 55 %, p = 0.0458, n = 30) and a 69 % reduction in astrocytes derived from patients with mutations in *TSC1* (95 % Cl: 34 % to 66 %, p ≤ 0.0001, n = 20) (Fig. 6.12B). However, decanoic acid had no significant effect on the ratio of p-S6K/ total-S6K in astrocytes derived from patients with mutations in *TSC2* (3 % decrease, p = 0.9261, n = 20) (Fig. 6.12B). The reduction in the ratio of p-S6K/ total-S6K following treatment with decanoic acid was caused by a significant reduction in post treatment levels of p-S6K (Fig. 6.12C). Decanoic acid caused a 53 % decrease in p-S6K levels in astrocytes derived from control patients (95 % Cl: 51 % to 55 %, p = 0.0468, n = 30), and a 50 % decrease in p-S6K levels in astrocytes derived from patients with mutations in *TSC1* (95 % Cl: 44 % to 59 %, p ≤ 0.0001, n = 20) (Fig. 6.12C). A non-significant decrease (38 %) in p-S6K levels following decanoic acid treatment was also observed in astrocytes derived from patients with mutations in *TSC2* (p = 0.2275, n = 20) (Fig. 6.11C). Variation between individual patients was observed in astrocytes derived from patients with *TSC2* mutations, with one patient showing no significant change in p-S6K levels following decanoic acid treatment, while one patient showed a significant decrease (51 %) in p-S6K levels following decanoic acid treatment (95 % Cl: 30 % to 61 %, p = 0.0071, n = 10) (Fig. 6.12C). No significant differences were observed in total-S6K levels (Fig. 6.12D). These results suggest that decanoic acid causes a reduction in mTORC1 activity in healthy patients and in patients with *TSC1* mutations. However, due to the rarity of this condition, samples were derived from only a small number of patients (n = 3 control, n = 2 *TSC1*$^{-}$, n = 2 *TSC2*$^{-}$), highlighting the requirement for more

samples to confirm the effect of decanoic acid, especially in patients with *TSC2* mutations.

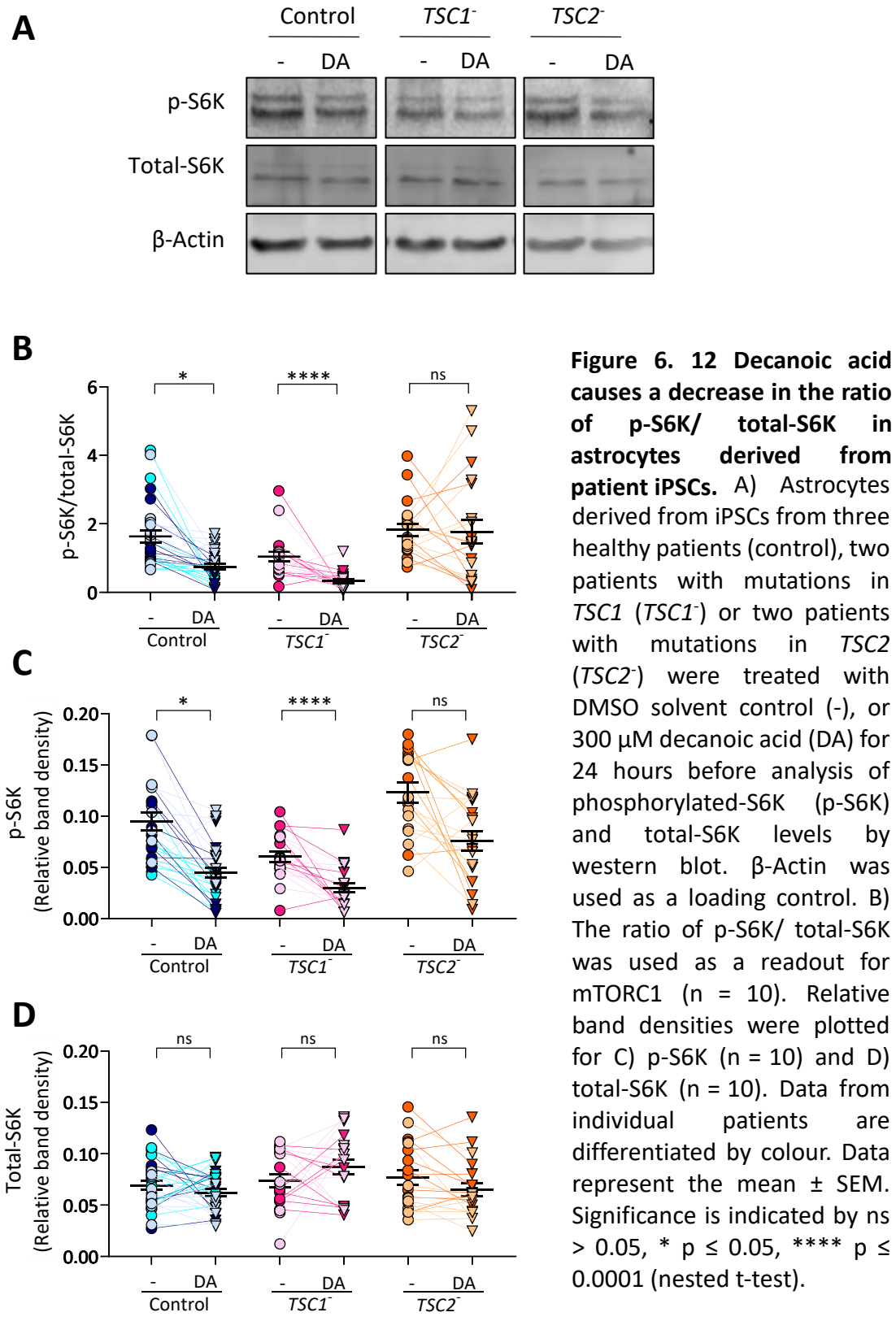

Figure 6. 12 Decanoic acid causes a decrease in the ratio of p-S6K/ total-S6K in astrocytes derived from patient iPSCs. A) Astrocytes derived from iPSCs from three healthy patients (control), two patients with mutations in *TSC1* (*TSC1*$^{-}$) or two patients with mutations in *TSC2* (*TSC2*$^{-}$) were treated with DMSO solvent control (-), or 300 µM decanoic acid (DA) for 24 hours before analysis of phosphorylated-S6K (p-S6K) and total-S6K levels by western blot. β-Actin was used as a loading control. B) The ratio of p-S6K/ total-S6K was used as a readout for mTORC1 (n = 10). Relative band densities were plotted for C) p-S6K (n = 10) and D) total-S6K (n = 10). Data from individual patients are differentiated by colour. Data represent the mean ± SEM. Significance is indicated by ns > 0.05, * p ≤ 0.05, **** p ≤ 0.0001 (nested t-test).

6.3 Discussion

Following the identification of a stimulatory effect of both decanoic acid and octanoic acid on *Dictyostelium* autophagy we investigated the major regulator of this process, mTORC1 signalling, in order to better understand the therapeutic mechanisms of these fatty acids. In this chapter, we have employed *Dictyostelium* to establish that decanoic acid displays structurally specific mTORC1 inhibition. While inhibition of mTORC1 signalling is consistent with the observed activation of autophagy, we have demonstrated that the effect of decanoic acid on mTORC1 is dependent on UBXD18, whereas we previously identified that the autophagic effects of decanoic acid are independent of this protein. We therefore conclude that the effects of decanoic acid on autophagy in *Dictyostelium* are independent from the effects on mTORC1 signalling. To describe the effects on mTORC1, we suggest that decanoic acid functions in a UBXD18 dependent manner to inhibit p97 activity and reduce mTORC1 activity. We then confirm the mTORC1 inhibitory effect of decanoic acid using a rat hippocampal slice model widely used in epilepsy research (Chang *et al.*, 2015; Chang *et al.*, 2013). We further confirm this effect in astrocytes derived from healthy patients and patients with tuberous sclerosis complex 1 (*TSC1*) mutations. Our data therefore identifies a new and evolutionarily conserved effect of decanoic acid in down regulating mTORC1 signalling, with potential relevance to a wide range of medical treatments.

Due to the importance of mTORC1 signalling in a diverse range of cellular processes, and the association of this pathway with a range of diseases, mTOR signalling has been well studied in eukaryotic organisms including in *Dictyostelium.* In both *Dictyostelium* and other eukaryotes, starvation inhibits mTORC1 signalling (Rosel *et al.*, 2012; Tan, Sim and Long, 2017; Varghese *et al.*, 2019), and our findings support this role (Fig. 6.3A). Components of the mTORC1 complex, including, TOR, Raptor and Lst8 are conserved throughout eukaryotes, as is the eukaryotic initiation factor 4E-binding protein (4E-BP1) (Morio *et al.*, 2001; Liao *et al.*, 2008). In eukaryotes including *Dictyostelium*, phosphorylation of 4E-BP1 by mTORC1 induces its dissociation from the eukaryotic translation initiation factor 4E (eIF4E), promoting initiation of protein translation (Haghighat *et al.*, 1995) and this phosphorylation is

used in this study as a read out for mTORC1 activation (Fig. 6.1A). *Dictyostelium* has also been used in a range of mTORC1-related studies regarding its role in autophagy (Mesquita *et al.*, 2016), cell migration (Liu *et al.*, 2010), and phagocytosis (Rosel *et al.*, 2012). Thus, *Dictyostelium* is a suitable model for mTORC1 research, supporting our findings of a novel mechanism of decanoic in inhibiting mTORC1 activity.

Having revealed a novel effect of decanoic acid in reducing mTORC1 activity independently of PI3K/AKT and AMPK signaling, we sought to describe a mechanism for this effect. In this chapter we have demonstrated that UBXD18 is required in *Dictyostelium* to confer sensitivity to decanoic acid in regards to mTORC1 regulation (Fig. 6.6) as well as previously described in growth (Fig. 3.16) and in the inhibition of the ubiquitous binding partner of UBXD18, p97 (Fig. 4.7). By employing a specific inhibitor (DBeQ) for p97, we confirmed that pharmacological inhibition of this protein decreased mTORC1 activity as well as cell proliferation (Ching *et al.*, 2013) (Fig. 6.7). This finding suggests that UBXD18 dependent decanoic acid induced p97 inhibition (Fig. 4.7) could explain the inhibitory effects of decanoic acid on both mTORC1 activity and cell growth in *Dictyostelium* (Fig. 6.13). We have previously demonstrated that *UBXD18*$^{-}$ displays partial resistance to the growth inhibition caused by 4-BCCA as well as decanoic acid (Fig. 4.2), suggesting that 4-BCCA may also act on *Dictyostelium* in a UBXD18 dependent manner. Here we establish that 4-BCCA has no effect on p-4E-BP1 levels in *Dictyostelium* (Fig. 6.2), indicating that these compounds target UBXD18 through independent mechanisms, with further investigation required to elucidate the mechanism and effects of 4-BCCA.

Inhibition of p97 has previously been established to reduce mTORC1 (Parzych *et al.*, 2015; Ching *et al.*, 2013), and p97 inhibitors have been proposed as a treatment for cancer and epilepsy (Tang and Xia, 2016; Han *et al.*, 2015). In cancers, expression of p97 is increased to manage excessive proteotoxic stress (Vekaria *et al.*, 2016), and p97 inhibitors are in clinical trials for the treatment of solid tumours (ClinicalTrials.gov Identifier: NCT02243917 and NCT04372641) (Stach and Freemont, 2017; Lan *et al.*, 2017). p97 also plays a role in a common form of epilepsy (autosomal dominant juvenile myoclonic epilepsy), where a mutation in a $GABA_A$ receptor (A322D mutation in the α1 subunit) results in misfolding and rapid ERAD of $GABA_A$, resulting in epilepsy (Cossette *et al.*, 2002; Han *et al.*, 2015). By inhibiting p97, α1(A322D) subunits have

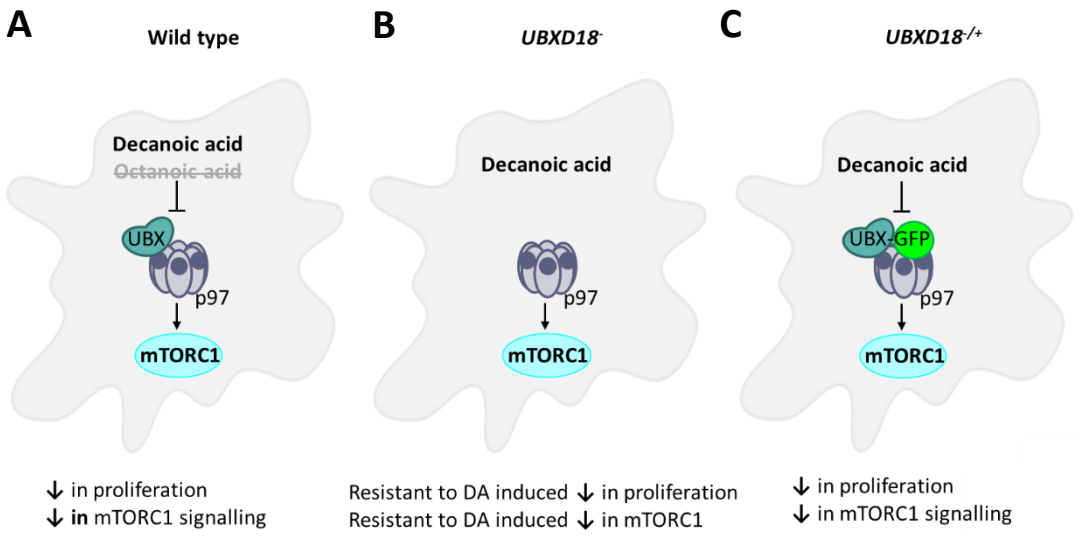

D

	Dictyostelium	Rat Hippocampus	Healthy Patient derived astrocytes	Tuberous sclerosis patient derived astrocytes
Effect of decanoic acid on 4E-BP1 activation	Decrease	Decrease	Decrease	Decrease
Effect of decanoic acid on AKT activation	No change	No change		
Effect of decanoic acid on AMPK signaling	No change			

Figure 6. 13 Summary of the effects of decanoic acid on mTORC1 signalling.
A) In wild type *Dictyostelium* cells decanoic acid but not octanoic acid leads to a reduction in both p97 activity and mTORC1 signalling consistent with a reduction in growth. B) In *UBXD18*$^{-}$ *Dictyostelium* cells decanoic acid (DA) has no effect on p97 activity or mTORC1 signalling consistent with a resistance to decanoic acid induced growth inhibition. C) In *UBXD18*$^{-/+}$ *Dictyostelium* cells decanoic acid leads to a reduction in both p97 activity and mTORC1 signalling consistent with a reduction in growth. Thus, we propose that decanoic acid (and not octanoic acid) acts to inhibit mTORC1 signalling though a UBXD18 (UBX) dependent inhibition of p97. D). Table summarising the effects of decanoic acid on mTORC1 signalling in *Dictyostelium,* a rat hippocampal model and in patient derived astrocytes.

more time to fold in the ER, allowing functional $GABA_A$ receptors to form and act as inhibitory ion channels (Han *et al.*, 2015). Our findings suggest that further analysis of a role for decanoic acid in inhibiting p97 and mTORC1 may identify associated therapeutic benefits.

Our data suggest a novel mechanism for decanoic acid in regulating mTORC1. The classical ketogenic diet is well established to reduce mTORC1 activation, with a

proposed mechanism through a reduction in glucose and insulin levels (Fig. 6.14) (McDaniel *et al.*, 2011; Ostendorf and Wong, 2015; Sweeney *et al.*, 2017; Thio *et al.*, 2006; Newman *et al.*, 2017; Roberts *et al.*, 2017). This reduction in mTORC1 signalling has been associated with the therapeutic effects of the classical ketogenic diet in treating epilepsy (McDaniel *et al.*, 2011). While several studies have suggested that decanoic acid in the MCT diet provides the therapeutic benefits in seizure control (Chang *et al.*, 2015; Wlaz *et al.*, 2015; Augustin *et al.*, 2018b; Chang *et al.*, 2016), the role of decanoic acid on mTORC1 signaling as a therapeutic mechanism for seizure

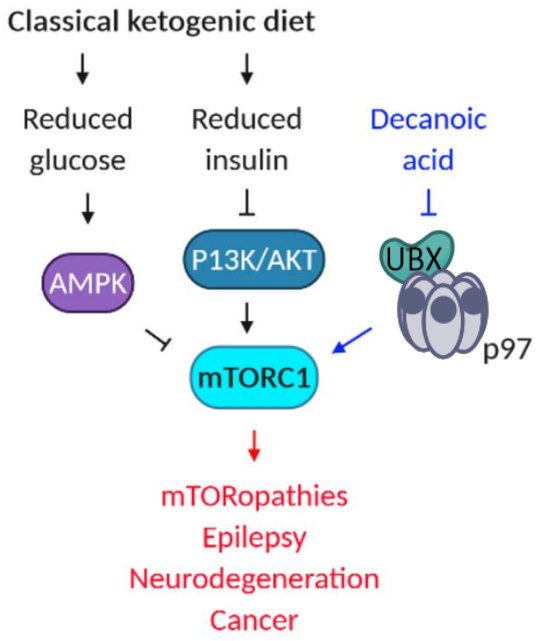

Figure 6. 14 Simplified schematic portraying the canonical effect of the classical ketogenic diet on mTORC1 and our proposed mechanism of decanoic acid through UBXD18 and p97. The classical ketogenic diet inhibits mTORC1 signalling through reduced glucose and insulin (black). We propose a novel role of decanoic acid through a UBXD18 (UBX) and p97 mediated pathway (blue). Inhibition of dysregulated mTORC1 signalling may provide a useful approach to treat a range of conditions (red).

control has not previously been reported. A small number of studies have independently investigated the effects of decanoic acid on mTORC1 activity, with inconsistent results. One study looking at the hepatic effects of medium-chain fatty acids in regards to non-alcoholic liver disease concluded that decanoic acid promoted activation of mTORC1 (Rial *et al.*, 2018), while another study investigating the effects

of decanoic acid on trophoblast development found that decanoic acid caused a significant reduction in mTORC1 signalling (Yang *et al.*, 2018). Each of these studies presented data from a single (dissimilar) cell line, with differing preparations of fatty acid (conjugated to BSA or free), and with differing treatment conditions, potentially explaining the disparity between the results. Here we demonstrate that in *Dictyostelium,* decanoic acid inhibits mTORC1 activity under conditions of constant glucose and in the absence of insulin (Fig 6.1B). Since we have translated this effect to both a rat hippocampal slice model (Fig. 6.9 and 6.10) and patient derived astrocytes (Fig. 6.11 and 6.12), again under conditions of constant glucose and in the absence of insulin signalling, our data proposes an evolutionarily conserved effect of decanoic acid, provided in the MCT diet, distinct to that proposed for the classical ketogenic diet.

The mTORC1 pathway acts as a regulator for cell growth through the phosphorylation of targets activating anabolic processes and inhibiting catabolic processes. In this role, mTORC1 inhibition has been credited with providing therapeutic effects in many areas of health, including treating epilepsy and neurodegenerative disorders, preventing the proliferation of cancer cells, improving cognitive function after traumatic brain injury, and in increasing longevity (McDaniel *et al.*, 2011; Fujikake, Shin and Shimizu, 2018; Xie, Wang and Proud, 2016; Johnson, Rabinovitch and Kaeberlein, 2013). mTORC1 inhibition is also being investigated as a therapeutic target for the neurodevelopmental disorder TSC (Tee *et al.*, 2002; Li *et al.*, 2019; Franz and Capal, 2017; Franz *et al.*, 2006; French *et al.*, 2016). Mutations in these patients result in aberrant mTORC1 signalling, leading to excessive cell proliferation and the formation of tumours, which when arising in the brain can cause epilepsy (Crino, Nathanson and Henske, 2006). mTORC1 dysregulation has been identified in astrocytes in these patients (Sosunov *et al.*, 2012), however, in cell culture, feedback loops on the TSC complex have been suggested to maintain balanced mTOR signalling (Blair, Hockemeyer and Bateup, 2018), potentially explaining why mTORC1 activation (p-4E-BP1/ total-4E-BP1 (Fig. 6.11), and p-S6K/ total-S6K (Fig. 6.12)) in astrocytes derived from patients with *TSC* mutations is unchanged from mTORC1 activation in astrocytes derived from healthy control individuals. Importantly, we demonstrate that decanoic acid reduces mTORC1

signalling in astrocytes derived from both healthy control individuals and in multiple patients with *TSC* mutations, suggesting that decanoic acid functions independently of disease state, but shows efficacy in cells derived from patients with disease-associated mutations (Fig. 6.11 and 6.12). Our data suggests that heterogeneity between patients with mutations in *TSC2* (Fig. 6.11 and 6.12), could represent differential efficacy of decanoic acid between individuals, however, additional patient derived samples would be required to confirm this. The decrease in the ratio of p-4E-BP1/ total-4E-BP1 observed following decanoic acid treatment was caused by an increase in total-4EBP1 levels rather than a decrease in p-4E-BP1 (Fig. 6.11). This increase in total-4E-BP1 levels is likely to alter functional activity of the protein (Elia *et al.*, 2017), since hypo-phosphorylated 4E-BP1 interacts strongly with eIF4E, preventing initiation of translation (Haghighat *et al.*, 1995). These findings suggest that decanoic acid downregulates mTORC1 signalling in healthy and disease associated human cells.

Inhibition of mTORC1 provides a promising strategy for the treatment of a wide range of diseases (Li, Kim and Blenis, 2014; Harrison *et al.*, 2009; Lamming and Sabatini, 2011; Franz *et al.*, 2006). The recent development of new pharmacological inhibitors for mTORC1 inhibition, based around rapamycin, have focused on identifying 'rapalogs' without the toxicity associated with rapamycin (French *et al.*, 2016). Limitations of these currently available rapalogs have led to new approaches for reducing mTORC1 such as through dietary treatment, i.e. the classical ketogenic diet (McDaniel *et al.*, 2011), however, this diet is highly restrictive for patients resulting in low compliance (Ye *et al.*, 2015a). Our data suggests that this effect may also arise through decanoic acid, provided in the MCT ketogenic diet, that is more palatable, less restrictive and aversive than the classical ketogenic diet. Thus, further investigation into dietary decanoic acid may provide a useful approach to treat a range of diseases associated with dysregulation of mTORC1.

Chapter 7

Discussion

7.1 Advances in understanding the mechanisms of action of medium-chain fatty acids

The medium-chain triglyceride (MCT) diet provides effective seizure control for patients with drug resistant epilepsy, and has recently been suggested as a potential treatment for conditions such as neurodegenerative disorders (Ota *et al.*, 2019; Taylor *et al.*, 2018), mitochondrial disorders (Kanabus *et al.*, 2016) and cancers (Jóźwiak *et al.*, 2020; Narayanan *et al.*, 2015), however, the therapeutic mechanisms underlying these effects are poorly understood. In this thesis we advance our understanding of the mechanisms of action underlying the MCT diet, providing insight into extending the application of this diet for use in a range of medical conditions.

In this project we have employed the tractable model *Dictyostelium discoideum* to identify mechanisms of action of fatty acids provided by the MCT diet. We have demonstrated that in *Dictyostelium,* the sensitivity to decanoic acid is regulated in part by a ubiquitin regulatory X (UBX) domain-containing protein (UBXD18). To investigate this mechanism, we demonstrated that UBXD18-GFP binds to the ubiquitous protein p97(-RFP) and established that decanoic inhibits p97(-RFP) activity in a UBXD18 dependent manner. Since autophagy is an important pathway regulated by p97, this process was investigated as a target for decanoic acid, and both decanoic acid and octanoic acid were shown to regulate this process independent of UBXD18 (Fig. 7.1A). Another downstream target of p97, mTORC1 was also investigated. We have demonstrated that treatment with decanoic acid but not octanoic acid leads to a decrease in mTORC1 activity, and to describe this mechanism, we suggest that decanoic acid functions through UBXD18 to inhibit p97 activity and reduce mTORC1 activity, thus, indicating that the cellular effects of decanoic acid on autophagy and mTORC1 are distinct (Fig. 7.1A). Due to the importance of mTORC1 inhibition in treating a range of conditions (Svarrer *et al.*, 2019; Citraro *et al.*, 2016; Xie, Wang and Proud, 2016), we translated this effect of decanoic acid-induced mTORC1 inhibition using a rat hippocampal slice model and patient-derived astrocytes with tuberous sclerosis complex mutations (Fig. 7.1 B and C). Our results showed that decanoic acid also decreases mTORC1 activity in these models in the

absence of insulin and under high glucose conditions. Our data therefore identifies a new and evolutionarily conserved effect of decanoic acid in down regulating mTORC1 signalling, with potential relevance to a wide range of medical treatments.

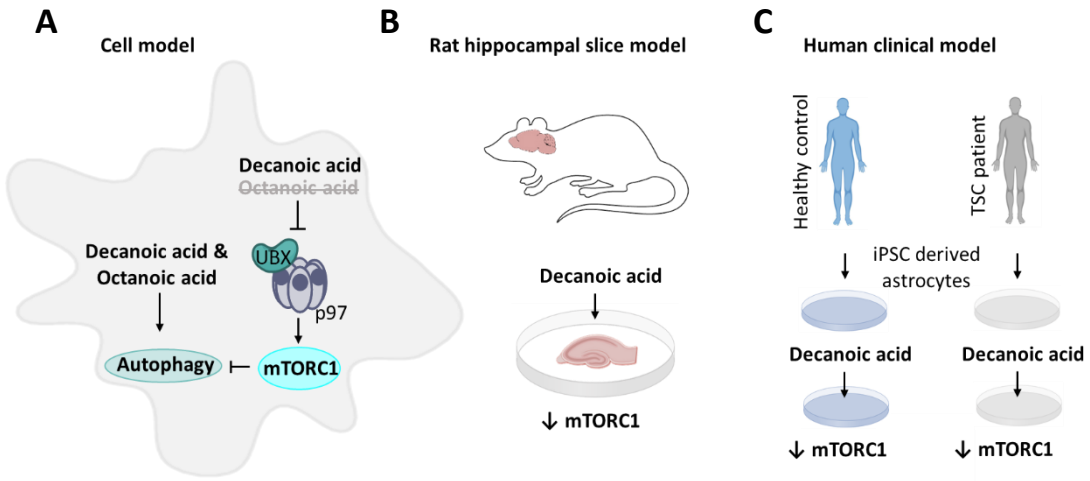

Figure 7. 1 Advances in understanding the molecular mechanism of decanoic acid in multiple model systems. A) Using *Dictyostelium discoideum* as a cell model we have identified that both decanoic acid and octanoic acid activate autophagy, independently of UBXD18. In this same model we demonstrate that decanoic acid but not octanoic acid inhibits mTORC1 and propose that this effect is resulting from a UBXD18 dependent decanoic acid induced inhibition of p97. B) We confirm that decanoic acid reduces mTORC1 signaling in a rat hippocampal slice model. C) Using patient-derived astrocytes, we demonstrate that decanoic acid reduces mTORC1 signaling in healthy patients, as well as in patients with tuberous sclerosis complex.

The classical ketogenic diet is thought to reduce mTORC1 signalling through reduced levels of glucose and insulin and this effect is believed to provide antiepileptogenic effects (McDaniel *et al.*, 2011). Our data suggests that decanoic acid provided by the MCT ketogenic diet may provide direct mTORC1 inhibition independent of glucose and insulin levels, providing an alternative means of achieving the same effect. Data indicating that the classical ketogenic diet reduces mTORC1 signalling comes from findings that phosphorylation levels of ribosomal protein S6 (p-S6) are reduced in the livers and hippocampi of rats following 2 week administration of long-chain fatty acids (KD; Bioserv F3666) (McDaniel *et al.*, 2011).

These findings, along with a corresponding reduction in p-AKT and increase in p-AMPK (McDaniel *et al.*, 2011) were correlated with a previously established reduction in glucose and insulin (Thio *et al.*, 2006) to explain the reduction in mTORC1 signalling. This proposed mechanism is supported by evidence that long-chain fatty acids and ketone bodies provided in the diet do not contribute to a reduction in mTORC1 signalling (Yasuda *et al.*, 2014; Vandoorne *et al.*, 2017). Taken together this data suggests that the inhibitory effect of decanoic acid on mTORC1 could provide an alternative means of achieving the beneficial effects of the classical ketogenic diet, without the requirement for reduced glucose and insulin.

In this thesis we have utilised *Dictyostelium* as a model to propose a mechanism for decanoic acid in regulating mTORC1 signalling though a UBXD18 dependent inhibition of p97, providing novel insight into the role of decanoic acid. While we have demonstrated that the inhibitory effect of decanoic acid on mTORC1 signalling is conserved in a rat model and in human derived astrocytes, we were limited to describing this mechanism in the simple model *Dictyostelium*. The p97 protein is highly conserved (78 % identical) between *Dictyostelium* and human, indicating that inhibitory regulation of this protein could be conserved between these species. Furthermore, interactions between fatty acids and UBX domain containing proteins have previously been implicated in blocking p97 activity in mammalian cells (Lee *et al.*, 2008). This suggests that regulation of p97 via an interaction of decanoic acid with a UBX domain containing protein represents a viable mechanism in humans, with p97 inhibition established to inhibit mTORC1 signalling (Parzych *et al.*, 2015). However, despite the high conservation between p97 proteins, the UBX domain containing protein, UBXD18, identified in *Dictyostelium* and postulated to mediate the decanoic acid induced inhibition of p97 shows a lesser degree of homology with two distinct human homologues (UBXN1 and UBXD2). Elucidating the mechanism of action of decanoic acid on mTORC1 inhibition in humans could lead to improved implementation of decanoic acid-based diets, and confirming a p97 inhibitory effect of this fatty acid could provide a rationale for use in the treatment of cancers (Vekaria *et al.*, 2016; Anderson *et al.*, 2015) and certain epilepsy conditions (Han *et al.*, 2015).

7.2 Insights into decanoic acid-based therpaies

In this thesis we provide evidence that decanoic acid inhibits mTORC1 signalling in multiple models, and thus suggest that decanoic acid-based therapies could provide benefits in conditions with hyperactivated mTOR signalling. mTORopathies represent a group of genetic disorders resulting from hyperactivated mTORC1 signalling associated with malformations of cortical development (Crino, 2015) and are characterised by refractory epilepsy, neurological alterations, overgrowth and central nervous system (CNS) manifestations (Crino, 2015). In mTORopathies, hyperactivity of mTORC1 signalling is thought to lead to alterations in cell size as well as structural alterations leading to epileptogenesis, and therapies to inhibit the activity of mTORC1 have been demonstrated to inhibit seizures and improve behavioural changes and learning deficits in patients with these conditions (Hillmann and Fabbro, 2019).

Tuberous sclerosis complex (TSC) is a mTORopathy resulting from loss of function mutations in either *TSC1* or *TSC2* (Fig. 7.2). Disruption of these genes leads to constitutive activation of mTORC1, manifesting in the development of tumours, with cortical tubers leading to seizures and behavioural changes. Therapy options for patients with TSC are limited and while the use of rapalogs, such as Everolimus, to reduce mTORC1 signalling have beneficial effects on seizures, these compounds are limited by immunosuppressive side effects (Franz *et al.*, 2018). Novel mTOR kinase domain inhibitors (TORKinibs) have been considered to overcome these issues, however, they lack the penetration of the blood brain barrier (Borsari *et al.*, 2019). Alternately, inhibition of this pathway is possible through dietary treatment with the classical ketogenic diet (McDaniel *et al.*, 2011), however, this diet is highly restrictive for patients resulting in low compliance (Ye *et al.*, 2015a). Our data demonstrates that decanoic acid reduces mTORC1 signalling in astrocytes derived from patients with *TSC1* mutations, suggesting that the MCT diet could provide a less restrictive and safer alternative therapy for these patients. Heterogeneity in treatment response for patients with *TSC2* mutations highlights the need for further research into factors influencing responsiveness to decanoic acid.

Other mTORopathies have been identified with mutations in various genes in

the mTORC1 signalling cascade (Fig. 7.2), these include focal cortical dysplasia (FCD), familial focal epilepsy with variable foci (FFEVF), hemimegalencephaly and polyhydramnios megalencephaly symptomatic epilepsy syndrome (PMSE). Currently treatment options for these patients is limited to conventional and often ineffective AEDs, highlighting the requirement for new therapies. Everolimus is in a clinical trial for use in FCD (ClinicalTrials.gov: NCT03198949) but is associated with serious negative side effects. Limited evidence suggests that the classical ketogenic diet is effective in a range of mTORopathies such as TSC (Kossoff *et al.*, 2005), focal cortical dysplasia (Pasca *et al.*, 2018) and Hemimegalencephaly (Mirzaa *et al.*, 2018). These beneficial effects are thought to arise though restoration of controlled mTORC1 signalling and our findings suggest that decanoic acid as provided in the MCT ketogenic diet could provide a safer alternative therapy for treating these mTORopathies.

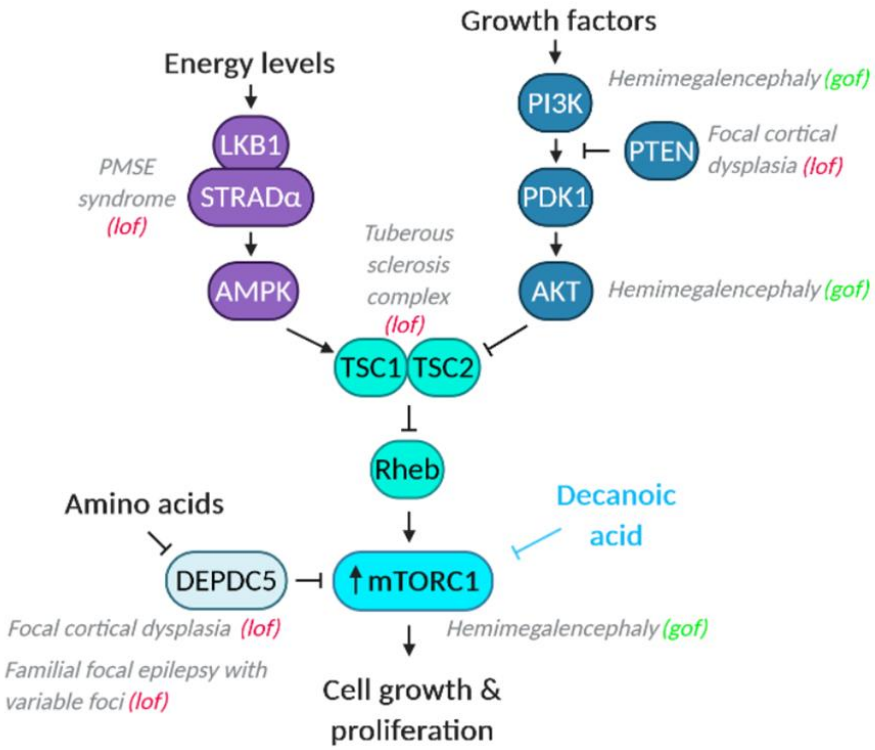

Figure 7. 2 Mutations activating mTORC1 are associated with multiple mTORopathies. mTORC1 integrates cellular energy levels via upstream kinases and modulates downstream functions such as cell growth and proliferation. Mutations in specific genes in this pathway have been implicated in several mTORopathies. Each mTORopathy is labeled in grey at the point of mutation (indicated as gain of function (gof) or loss of function (lof). Decanoic acid could provide a therapy for the management of multiple mTORopathies (Blue).

Our data demonstrating that decanoic acid but not octanoic acid inhibits mTORC1 signalling, supports previous studies describing the efficacy of this specific fatty acid (Chang *et al.*, 2013; Chang *et al.*, 2016; Hughes *et al.*, 2014). Evidence substantiating the role of decanoic acid in seizure control, has led to the development of Betashot, a high decanoic acid supplement for children and adults with epilepsy (ClinicalTrials.gov: NCT02825745). This product is advantageous over the traditional MCT diet, allowing patients to maintain a relatively normal diet while supplementing MCTs (Betashot). Formulated to contain elevated levels of decanoic acid, this product has demonstrated effectiveness in a clinical trial for seizure control, palatability, tolerability and compliance (ClinicalTrials.gov: NCT02825745). Our findings that decanoic acid but not octanoic acid provides mTORC1 inhibition suggest that a supplement high in decanoic acid, such as Betashot, could provide an enhanced therapeutic effect over traditional MCT diets in the treatment of mTORopathies.

In addition to treating mTORopathies, mTOR inhibitors are being investigated for use in other conditions such as mitochondrial disorders, Alzheimer's disease, and certain cancers. Mitochondrial disorders arise from dysfunctions in the respiratory chain, with tissues and organs highly dependent of aerobic metabolism affected in patients. The mTORC1 pathway has recently been implicated in these disorders (Wang *et al.*, 2016; Sage-Schwaede *et al.*, 2019) and has been identified as a key upstream regulator of stress responses (Khan *et al.*, 2017). The mTORC1 inhibitor rapamycin has been demonstrated to attenuate disease progression in a mouse model of the mitochondrial disorder Leigh syndrome (Johnson *et al.*, 2013), and has had beneficial effects in a child with this syndrome (Sage-Schwaede *et al.*, 2019). Although the mechanisms behind these therapeutic effects are unclear, these studies propose that mTOR inhibitors provide a potential therapeutic strategy for patients with mitochondrial disorders. The MCT ketogenic diet has previously been suggested for use in mitochondrial disorders, following the identification that decanoic acid increases mitochondrial biogenesis (Hughes *et al.*, 2014), and our findings provide further support for use of the MCT diet in mitochondrial disorders, through decanoic acid induced inhibition of mTORC1. Thus, since decanoic acid has the potential to provide multiple therapeutic benefits in patients with mitochondrial disorders, more research should be carried out into the use of MCT diets in these patients.

Aberrant mTORC1 signalling has commonly been associated with failed clearance of toxic protein aggregates, such as tau and amyloid β in Alzheimer's disease (Chang *et al.*, 2002; An *et al.*, 2003; Crino, 2016). In Alzheimer's patients activation of mTORC1 is associated with the upregulation of tau translation and phosphorylation contributing to disease pathology (Tang *et al.*, 2013; Morita and Sobue, 2009). Furthermore, inhibition of mTORC1 using rapamycin has been shown to suppress the translation of tau (Morita and Sobue, 2009) and protect against neuronal death in mice (Siman, Cocca and Dong, 2015). These findings suggest that mTORC1 inhibitors could rescue cellular neurodegeneration and indicate that decanoic acid supplementation could be beneficial in patients with this neurodegenerative disease. In addition to mTORC1 signalling, autophagy has also been suggested to play a key role in Alzheimer's, in the metabolism of Aβ and tau (Uddin *et al.*, 2018), and our data suggesting that medium-chain fatty acids activate degradation through this pathway, enhances the therapeutic relevance of the MCT diet for patients with Alzheimer's disease.

Octanoic acid has previously been investigated for use in patients with Alzheimer's disease, due to its ability to induce ketosis to bypass dysfunctional glucose metabolism in the brain (Henderson *et al.*, 2009). This fatty acid proved ineffectual at improving cognition in patients carrying the *APOE4* allele (an allele of Apolipoprotein (APOE) representing a genetic determinant of Alzheimer disease), however, octanoic acid provided cognitive benefits in patients not carrying this allele (Henderson *et al.*, 2009). Since astrocytes expressing *APOE4* have been demonstrated to exhibit lower autophagic flux under autophagy-inducing conditions than those expressing other *APOE* isoforms (Simonovitch *et al.*, 2016), our data demonstrating medium-chain fatty acid induced autophagy activation suggests that octanoic acid induced autophagy in patients lacking $APOE_4$, but not those with $APOE_4$, could explain the observed heterogeneity in response to octanoic acid. In addition, the efficacy of decanoic acid in humans with Alzheimer's disease has not yet been investigated and our findings suggest that a decanoic acid supplement could provide additional benefits to Alzheimer's patients through mTORC1 inhibition and autophagy activation as well as through bypassing glucose metabolism.

Due to the fundamental role of mTOR signalling in regulating cellular proliferation, growth, and survival, hyperactivation of this pathway is observed in various types of cancers (Tian, Li and Zhang, 2019). Activating mutations in *MTOR* that result in an increase in kinase activity are observed in a range of cancers such as breast, lung, ovarian and skin cancer (Grabiner *et al.*, 2014). Mutations in upstream genes such as *PI3K*, *AKT* and *RHEB* leading to hyperactivation of mTORC1 are also frequently detected in human cancers (Ghosh *et al.*, 2015; Hua *et al.*, 2019) (Fig. 7.3). Furthermore, loss of function mutations are also known to contribute to mTORC1 activation in cancer with *PTEN* inactivating mutations occurring in 40 % of glioblastomas (Pachow *et al.*, 2015; Akhavan, Cloughesy and Mischel, 2010; Crino, 2015), and patients with germline *PTEN* mutations at risk of thyroid and breast cancer (Sansal and Sellers, 2004) (Fig. 7.3). Due to the critical role of mTOR signalling in tumour progression, mTOR inhibitors are promising for use as cancer therapies. Several mTORC1 inhibitors have been examined in cancer models in combination with conventional therapies, and evidence for anti-tumour effects have been identified in animal and human studies (Klement, 2017). Although mTOR inhibitors show efficacy in preclinical studies, many inhibitors are associated with serious adverse effects in patients, thus safer alternatives are required. Our data suggests that dietary decanoic acid may provide a safer alternative for reducing mTORC1 signalling in a range of different cancers.

Ketogenic diets have been shown previously to enhance the effectiveness of chemotherapy and radiotherapy in various cancer types (Weber *et al.*, 2020). This efficacy is thought to arise from a reduction in glucose levels leading to the starvation of cancer cells, as well as though reduced insulin and downstream signalling of mTORC1. Medium-chain triglycerides have been demonstrated to provide more effective anti-tumour effects than long-chain triglycerides on neuroblastoma xenografts (Aminzadeh-Gohari *et al.*, 2017) and this observation is supported by our research suggesting that decanoic acid could provide direct inhibition of mTORC1. In addition to restoring balanced mTORC1 signalling in cancers, pharmacological inhibition of mTORC1 has been suggested to provide therapeutic effects though the corresponding induction in autophagy (Evans *et al.*, 2005; Paquette, El-Houjeiri and Pause, 2018; Tian, Li and Zhang, 2019). Our data implicating medium-chain fatty acids

in autophagy activation, suggest that this effect could provide an additional advantage of medium-chain triglycerides over long-chain triglycerides as a cancer treatment.

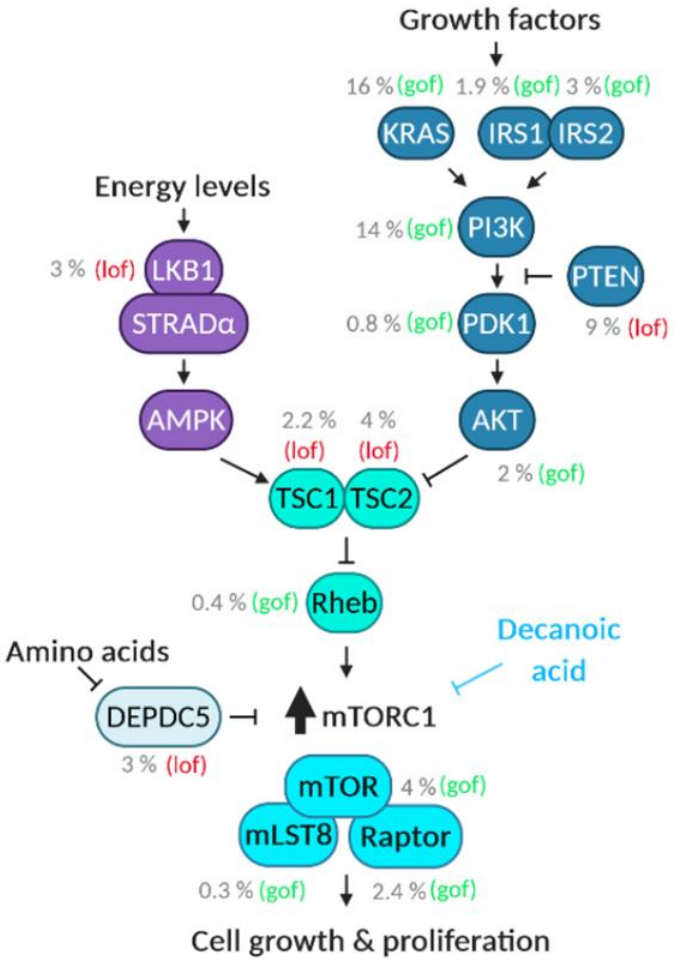

Figure 7. 3 Mutations activating mTORC1 have been implicated in several cancers. Specific genes in the mTORC1 pathway have been implicated in several cancers. The frequency of mutation in cancer patients is labeled in grey at the point of mutation (indicated as gain of function (gof) or loss of function (lof) (André F, 2017). Decanoic acid could provide a therapy for the management of multiple cancers (Blue).

7.3 Conclusion

Inhibition of mTORC1 has been suggested to provide wide-ranging clinical benefits, including as a treatment for mTORopathies, mitochondrial disorders, neurodegenerative disorders and cancer (Hillmann and Fabbro, 2019; Sage-Schwaede *et al.*, 2019; Crino, 2016; Klement, 2017). Pharmacological inhibitors based around rapamycin are under development for use in these conditions, alternatively the classical ketogenic diet is well established to inhibit mTORC1 signalling through a reduction in glucose and insulin (McDaniel *et al.*, 2011). Side effects associated with pharmacological inhibitors (French *et al.*, 2016) and the restrictive nature of the classical ketogenic diet highlight the need for safer and more tolerable methods of mTORC1 inhibition. Our data suggest that decanoic acid provided by the MCT diet could provide a safe alternative for mTORC1 inhibition, with the added benefit of autophagy activation. Thus, further investigation into dietary decanoic acid may provide a useful approach to treat a range of diseases associated with hyperactivated mTORC1 signalling.

References

Abdelwahab, M. G., Fenton, K. E., Preul, M. C., Rho, J. M., Lynch, A., Stafford, P. and Scheck, A. C. (2012) 'The Ketogenic Diet Is an Effective Adjuvant to Radiation Therapy for the Treatment of Malignant Glioma', *PLoS One,* 7(5), pp. e36197.

Akhavan, D., Cloughesy, T. F. and Mischel, P. S. (2010) 'mTOR signaling in glioblastoma: lessons learned from bench to bedside', *Neuro Oncol,* 12(8), pp. 882-889.

Alam, M. W., Borenas, M., Lind, D. E., Cervantes-Madrid, D., Umapathy, G., Palmer, R. H. and Hallberg, B. (2019) 'Alectinib, an Anaplastic Lymphoma Kinase Inhibitor, Abolishes ALK Activity and Growth in ALK-Positive Neuroblastoma Cells', *Front Oncol,* 9, pp. 579.

Allen, B. G., Bhatia, S. K., Anderson, C. M., Eichenberger-Gilmore, J. M., Sibenaller, Z. A., Mapuskar, K. A., Schoenfeld, J. D., Buatti, J. M., Spitz, D. R. and Fath, M. A. (2014) 'Ketogenic diets as an adjuvant cancer therapy: History and potential mechanism', *Redox Biol,* 2, pp. 963-970.

Altschul, S. F., Gish, W., Miller, W., Myers, E. W. and Lipman, D. J. (1990) 'Basic local alignment search tool', *J Mol Biol,* 215(3), pp. 403-410.

Amaravadi, R. K., Lippincott-Schwartz, J., Yin, X. M., Weiss, W. A., Takebe, N., Timmer, W., DiPaola, R. S., Lotze, M. T. and White, E. (2011) 'Principles and current strategies for targeting autophagy for cancer treatment', *Clin Cancer Res,* 17(4), pp. 654-666.

Aminzadeh-Gohari, S., Feichtinger, R. G., Vidali, S., Locker, F., Rutherford, T., O'Donnel, M., Stöger-Kleiber, A., Mayr, J. A., Sperl, W. and Kofler, B. (2017) 'A ketogenic diet supplemented with medium-chain triglycerides enhances the anti-tumor and anti-angiogenic efficacy of chemotherapy on neuroblastoma xenografts in a CD1-nu mouse model', *Oncotarget,* 8(39), pp. 64728-64744.

An, W. L., Cowburn, R. F., Li, L., Braak, H., Alafuzoff, I., Iqbal, K., Iqbal, I. G., Winblad, B. and Pei, J. J. (2003) 'Up-regulation of phosphorylated/activated p70 S6 kinase and its relationship to neurofibrillary pathology in Alzheimer's disease', *Am J Pathol,* 163(2), pp. 591-607.

Anderson, D. J., Le Moigne, R., Djakovic, S., Kumar, B., Rice, J., Wong, S., Wang, J., Yao, B., Valle, E., Kiss von Soly, S., Madriaga, A., Soriano, F., Menon, M. K., Wu, Z. Y., Kampmann, M., Chen, Y., Weissman, J. S., Aftab, B. T., Yakes, F. M., Shawver, L., Zhou, H. J., Wustrow, D. and Rolfe, M. (2015) 'Targeting the AAA ATPase p97 as an Approach to Treat Cancer through Disruption of Protein Homeostasis', *Cancer Cell,* 28(5), pp. 653-665.

André F, A. M., Baras AS, Baselga J, Bedard PL, Berger MF, Bierkens M, Calvo F, Cerami E, Chakravarty D, Dang KK, Davidson NE, Del Vecchio Fitz C, Dogan S, DuBois RN, Ducar MD, Futreal PA, Gao J, Garcia F, Gardos S, Gocke CD, Gross BE, Guinney J, Heins ZJ, Hintzen S, Horlings H, Hudeček J, Hyman DM, Kamel-Reid S, Kandoth C, Kinyua W, Kumari P, Kundra R, Ladanyi M, Lefebvre C, LeNoue-Newton ML, Lepisto EM, Levy MA, Lindeman NI, Lindsay J, Liu D, Lu Z, MacConaill LE, Maurer I, Maxwell DS, Meijer GA, Meric-Bernstam F, Micheel CM, Miller C, Mills G, Moore ND, Nederlof PM, Omberg L, Orechia JA, Park BH, Pugh TJ, Reardon B, Rollins BJ, Routbort MJ, Sawyers CL, Schrag D, Schultz N, Shaw KRM, Shivdasani P, Siu LL, Solit DB, Sonke GS, Soria JC, Sripakdeevong P, Stickle NH, Stricker TP, Sweeney SM, Taylor BS, Ten Hoeve JJ, Thomas SB, Van Allen EM, Van 't Veer LJ, van de Velde T, van

Tinteren H, Velculescu VE, Virtanen C, Voest EE, Wang LL, Wathoo C, Watt S, Yu C, Yu TV, Yu E, Zehir A, Zhang H. (2017) 'AACR Project GENIE: Powering Precision Medicine through an International Consortium', *Cancer Discov,* 7(8), pp. 818-831.

Arriola Apelo, S. I. and Lamming, D. W. (2016) 'Rapamycin: An InhibiTOR of Aging Emerges From the Soil of Easter Island', *J Gerontol A Biol Sci Med Sci,* 71(7), pp. 841-849.

Augustin, K., Khabbush, A., Williams, S., Eaton, S., Orford, M., Cross, J. H., Heales, S. J. R., Walker, M. C. and Williams, R. S. B. (2018a) 'Mechanisms of action for the medium-chain triglyceride ketogenic diet in neurological and metabolic disorders', *The Lancet Neurol,* 17(1), pp. 84-93.

Augustin, K., Williams, S., Cunningham, M., Devlin, A. M., Friedrich, M., Jayasekera, A., Hussain, M. A., Holliman, D., Mitchell, P., Jenkins, A., Chen, P. E., Walker, M. C. and Williams, R. S. B. (2018b) 'Perampanel and decanoic acid show synergistic action against AMPA receptors and seizures', *Epilepsia,* 59(11), pp. e172-e178.

Backman, S. A., Stambolic, V., Suzuki, A., Haight, J., Elia, A., Pretorius, J., Tsao, M. S., Shannon, P., Bolon, B., Ivy, G. O. and Mak, T. W. (2001) 'Deletion of Pten in mouse brain causes seizures, ataxia and defects in soma size resembling Lhermitte-Duclos disease', *Nat Genet,* 29(4), pp. 396-403.

Bailey, E. E., Pfeifer, H. H. and Thiele, E. A. (2005) 'The use of diet in the treatment of epilepsy', *Epilepsy Behav,* 6(1), pp. 4-8.

Bareja, A., Lee, D. E. and White, J. P. (2019) 'Maximizing Longevity and Healthspan: Multiple Approaches All Converging on Autophagy', *Front Cell Dev Biol,* 7, pp. 183.

Bazil, C. W. (2005) 'Sleep disturbances in epilepsy patients', *Curr Neurol Neurosci Rep,* 5(4), pp. 297-298.

Bell, G. S. and Sander, J. W. (2002) 'The epidemiology of epilepsy: the size of the problem', *Seizure,* 11 Suppl A, pp. 306-16.

Bernales, S., McDonald, K. L. and Walter, P. (2006) 'Autophagy counterbalances endoplasmic reticulum expansion during the unfolded protein response', *PLoS Biol,* 4(12), pp. e423.

Bialer, M. and White, H. S. (2010) 'Key factors in the discovery and development of new antiepileptic drugs', *Nat Rev Drug Discov,* 9(1), pp. 68-82.

Blair, J. D., Hockemeyer, D. and Bateup, H. S. (2018) 'Genetically engineered human cortical spheroid models of tuberous sclerosis', *Nat Med,* 24(10), pp. 1568-1578.

Bloomfield, G., Tanaka, Y., Skelton, J., Ivens, A. and Kay, R. R. (2008) 'Widespread duplications in the genomes of laboratory stocks of Dictyostelium discoideum', *Genome Biol,* 9(4), pp. R75.

Boehm, H. J., Boehringer, M., Bur, D., Gmuender, H., Huber, W., Klaus, W., Kostrewa, D., Kuehne, H., Luebbers, T., Meunier-Keller, N. and Mueller, F. (2000) 'Novel inhibitors of DNA gyrase: 3D structure based biased needle screening, hit validation by biophysical methods, and 3D guided optimization. A promising alternative to random screening', *J Med Chem,* 43(14), pp. 2664-74.

Bond, P. (2016) 'Regulation of mTORC1 by growth factors, energy status, amino acids and mechanical stimuli at a glance', *Journal of the International Society of Sports Nutrition,* 13, pp. 8.

Bonner, J. T., Clarke, W. W., Jr., Neely, C. L., Jr. and Slifkin, M. K. (1950) 'The orientation to light and the extremely sensitive orientation to temperature gradients in the slime mold Dictyostelium discoideum', *J Cell Comp Physiol,* 36(2), pp. 149-158.

Borsari, C., Rageot, D., Beaufils, F., Bohnacker, T., Keles, E., Buslov, I., Melone, A., Sele, A. M., Hebeisen, P., Fabbro, D., Hillmann, P. and Wymann, M. P. (2019) 'Preclinical Development of PQR514, a Highly Potent PI3K Inhibitor Bearing a Difluoromethyl-Pyrimidine Moiety', *ACS Med Chem Lett,* 10(10), pp. 1473-1479.

Bough, K. J., Wetherington, J., Hassel, B., Pare, J. F., Gawryluk, J. W., Greene, J. G., Shaw, R., Smith, Y., Geiger, J. D. and Dingledine, R. J. (2006) 'Mitochondrial biogenesis in the anticonvulsant mechanism of the ketogenic diet', *Ann Neurol,* 60(2), pp. 223-235.

Boyle, L., Wamelink, M. M. C., Salomons, G. S., Roos, B., Pop, A., Dauber, A., Hwa, V., Andrew, M., Douglas, J., Feingold, M., Kramer, N., Saitta, S., Retterer, K., Cho, M. T., Begtrup, A., Monaghan, K. G., Wynn, J. and Chung, W. K. (2016) 'Mutations in TKT Are the Cause of a Syndrome Including Short Stature, Developmental Delay, and Congenital Heart Defects', *Am J Hum Genet,* 98(6), pp. 1235-1242.

Branco, A. F., Ferreira, A., Simões, R. F., Magalhães-Novais, S., Zehowski, C., Cope, E., Silva, A. M., Pereira, D., Sardão, V. A. and Cunha-Oliveira, T. (2016) 'Ketogenic diets: from cancer to mitochondrial diseases and beyond', *Eur J Clin Invest,* 46(3), pp. 285-298.

Brooks, K. S., Woolf, E. C. and Scheck, A. C. (2016) 'The ketogenic diet as an adjuvant therapy for brain tumors and other cancers', *Critical dietary factors in cancer chemoprevention*: Springer, Cham, pp. 89-109.

Brown, R. S. (2005) 'Zinc finger proteins: getting a grip on RNA', *Curr Opin Struct Biol,* 15(1), pp. 94-98.

Burman, C. and Ktistakis, N. T. (2010) 'Regulation of autophagy by phosphatidylinositol 3-phosphate', *FEBS Lett,* 584(7), pp. 1302-12.

Cai, Q. Y., Zhou, Z. J., Luo, R., Gan, J., Li, S. P., Mu, D. Z. and Wan, C. M. (2017) 'Safety and tolerability of the ketogenic diet used for the treatment of refractory childhood epilepsy: a systematic review of published prospective studies', *World J Pediatr,* 13(6), pp. 528-536.

Caldero, J., Brunet, N., Tarabal, O., Piedrafita, L., Hereu, M., Ayala, V. and Esquerda, J. E. (2010) 'Lithium prevents excitotoxic cell death of motoneurons in organotypic slice cultures of spinal cord', *Neuroscience,* 165(4), pp. 1353-69.

Calvo-Garrido, J., Carilla-Latorre, S., Mesquita, A. and Escalante, R. (2011) 'A proteolytic cleavage assay to monitor autophagy in Dictyostelium discoideum', *Autophagy,* 7(9), pp. 1063-8.

Calvo-Garrido, J. and Escalante, R. (2010) 'Autophagy dysfunction and ubiquitin-positive protein aggregates in Dictyostelium cells lacking Vmp1', *Autophagy,* 6(1), pp. 100-109.

Camberos-Luna, L., Gerónimo-Olvera, C., Montiel, T., Rincon-Heredia, R. and Massieu, L. (2016) 'The Ketone Body, β-Hydroxybutyrate Stimulates the Autophagic Flux and Prevents Neuronal Death Induced by Glucose Deprivation in Cortical Cultured Neurons', *Neurochem Res,* 41(3), pp. 600-609.

Cardenal-Munoz, E., Arafah, S., Lopez-Jimenez, A. T., Kicka, S., Falaise, A., Bach, F., Schaad, O., King, J. S., Hagedorn, M. and Soldati, T. (2017) 'Mycobacterium marinum antagonistically induces an autophagic response while repressing the autophagic flux in a TORC1- and ESX-1-dependent manner', *PLoS Pathog,* 13(4), pp. e1006344.

Carrì, M. T., D'Ambrosi, N. and Cozzolino, M. (2017) 'Pathways to mitochondrial dysfunction in ALS pathogenesis', *Biochem Biophys Res Commun,* 483(4), pp. 1187-1193.

Castillo, K., Nassif, M., Valenzuela, V., Rojas, F., Matus, S., Mercado, G., Court, F. A., van Zundert, B. and Hetz, C. (2013) 'Trehalose delays the progression of amyotrophic lateral sclerosis by enhancing autophagy in motoneurons', *Autophagy,* 9(9), pp. 1308-20.

Chang, P., Augustin, K., Boddum, K., Williams, S., Sun, M., Terschak, J. A., Hardege, J. D., Chen, P. E., Walker, M. C. and Williams, R. S. (2016) 'Seizure control by decanoic acid through direct AMPA receptor inhibition', *Brain,* 139(Pt 2), pp. 431-443.

Chang, P., Orabi, B., Deranieh, R. M., Dham, M., Hoeller, O., Shimshoni, J. A., Yagen, B., Bialer, M., Greenberg, M. L., Walker, M. C. and Williams, R. S. (2012) 'The antiepileptic drug valproic acid and other medium-chain fatty acids acutely reduce phosphoinositide levels independently of inositol in Dictyostelium', *Dis Model Mech,* 5(1), pp. 115-124.

Chang, P., Terbach, N., Plant, N., Chen, P. E., Walker, M. C. and Williams, R. S. B. (2013) 'Seizure control by ketogenic diet-associated medium chain fatty acids', *Neuropharmacology,* 69, pp. 105-114.

Chang, P., Walker, M. C. and Williams, R. S. B. (2014) 'Seizure-induced reduction in PIP3 levels contributes to seizure-activity and is rescued by valproic acid', *Neurobiol Dis,* 62, pp. 296-306.

Chang, P., Zuckermann, A. M., Williams, S., Close, A. J., Cano-Jaimez, M., McEvoy, J. P., Spencer, J., Walker, M. C. and Williams, R. S. (2015) 'Seizure control by derivatives of medium chain fatty acids associated with the ketogenic diet show novel branching-point structure for enhanced potency', *J Pharmacol Exp Ther,* 352(1), pp. 43-52.

Chang, R. C., Wong, A. K., Ng, H.-K. and Hugon, J. (2002) 'Phosphorylation of eukaryotic initiation factor-2α (eIF2α) is associated with neuronal degeneration in Alzheimer's disease', *Neuroreport,* 13(18), pp. 2429-2432.

Cheng, B., Yang, X., An, L., Gao, B., Liu, X. and Liu, S. (2009) 'Ketogenic diet protects dopaminergic neurons against 6-OHDA neurotoxicity via up-regulating glutathione in a rat model of Parkinson's disease', *Brain research,* 1286, pp. 25-31.

Ching, J. K., Elizabeth, S. V., Ju, J. S., Lusk, C., Pittman, S. K. and Weihl, C. C. (2013) 'mTOR dysfunction contributes to vacuolar pathology and weakness in valosin-containing protein associated inclusion body myopathy', *Hum Mol Genet,* 22(6), pp. 1167-79.

Chou, T. F., Brown, S. J., Minond, D., Nordin, B. E., Li, K., Jones, A. C., Chase, P., Porubsky, P. R., Stoltz, B. M., Schoenen, F. J., Patricelli, M. P., Hodder, P., Rosen, H. and Deshaies, R. J.

(2011) 'Reversible inhibitor of p97, DBeQ, impairs both ubiquitin-dependent and autophagic protein clearance pathways', *Proc Natl Acad Sci U S A,* 108(12), pp. 4834-9.

Citraro, R., Leo, A., Constanti, A., Russo, E. and De Sarro, G. (2016) 'mTOR pathway inhibition as a new therapeutic strategy in epilepsy and epileptogenesis', *Pharmacol Res,* 107, pp. 333-343.

Cocorocchio, M., Baldwin, A. J., Stewart, B., Kim, L., Harwood, A. J., Thompson, C. R. L., Andrews, P. L. R. and Williams, R. S. B. (2018) 'Curcumin and derivatives function through protein phosphatase 2A and presenilin orthologues in Dictyostelium discoideum', *Dis Model Mech,* 11(1), pp. dmm032375.

Cossette, P., Liu, L., Brisebois, K., Dong, H., Lortie, A., Vanasse, M., Saint-Hilaire, J. M., Carmant, L., Verner, A., Lu, W. Y., Wang, Y. T. and Rouleau, G. A. (2002) 'Mutation of GABRA1 in an autosomal dominant form of juvenile myoclonic epilepsy', *Nat Genet,* 31(2), pp. 184-189.

Costa, J. R., Prak, K., Aldous, S., Gewinner, C. A. and Ketteler, R. (2016) 'Autophagy gene expression profiling identifies a defective microtubule-associated protein light chain 3A mutant in cancer', *Oncotarget,* 7(27), pp. 41203-41216.

Cotter, D. A., Miura-Santo, L. Y. and Hohl, H. R. (1969) 'Ultrastructural changes during germination of Dictyostelium discoideum spores', *J Bacteriol,* 100(2), pp. 1020-6.

Coulter, D. A. and Steinhäuser, C. (2015) 'Role of astrocytes in epilepsy', *Cold Spring Harb Perspect Med,* 5(3), pp. a022434.

Crino, P. B. (2015) 'mTOR signaling in epilepsy: insights from malformations of cortical development', *Cold Spring Harb Perspect Med,* 5(4) pp. a022442.

Crino, P. B. (2016) 'The mTOR signalling cascade: paving new roads to cure neurological disease', *Nat Rev Neurol,* 12(7), pp. 379-392.

Crino, P. B., Nathanson, K. L. and Henske, E. P. (2006) 'The tuberous sclerosis complex', *N Engl J Med,* 355(13), pp. 1345-56.

Dannat, K., Tillner, J., Winckler, T., Weiss, M., Eger, K. and Dingermann, T. (2003) 'Effects of medicinal compounds on the differentiation of the eukaryotic microorganism dictyostelium discoideum: can this model be used as a screening test for reproductive toxicity in humans?', *Pharmazie,* 58(3), pp. 204-210.

Datan, E., Shirazian, A., Benjamin, S., Matassov, D., Tinari, A., Malorni, W., Lockshin, R. A., Garcia-Sastre, A. and Zakeri, Z. (2014) 'mTOR/p70S6K signaling distinguishes routine, maintenance-level autophagy from autophagic cell death during influenza A infection', *Virology,* 452-453, pp. 175-190.

Davey, G. P., Peuchen, S. and Clark, J. B. (1998) 'Energy thresholds in brain mitochondria potential involvement in neurodegeneration', *J Biol Chem,* 273(21), pp. 12753-12757.

Davidson, A. J., King, J. S. and Insall, R. H. (2013) 'The use of streptavidin conjugates as immunoblot loading controls and mitochondrial markers for use with Dictyostelium discoideum', *Biotechniques,* 55(1), pp. 39-41.

de Lanerolle, N. C., Lee, T. S. and Spencer, D. D. (2010) 'Astrocytes and epilepsy', *Neurotherapeutics,* 7(4), pp. 424-438.

Dean, H. G., Bonser, J. C. and Gent, J. P. (1989) 'HPLC analysis of brain and plasma for octanoic and decanoic acids', *Clin Chem,* 35(9), pp. 1945-8.

Dingledine, R., Varvel, N. H. and Dudek, F. E. (2014) 'When and how do seizures kill neurons, and is cell death relevant to epileptogenesis?', *Adv Exp Med Biol,* 813, pp. 109-122.

Dominguez-Martin, E., Cardenal-Munoz, E., King, J. S., Soldati, T., Coria, R. and Escalante, R. (2017) 'Methods to Monitor and Quantify Autophagy in the Social Amoeba Dictyostelium discoideum', *Cells,* 6(3), pp. 18.

Dossou, A. S. and Basu, A. (2019) 'The Emerging Roles of mTORC1 in Macromanaging Autophagy', *Cancers,* 11(10), pp. 1422.

Dreveny, I., Kondo, H., Uchiyama, K., Shaw, A., Zhang, X. and Freemont, P. S. (2004) 'Structural basis of the interaction between the AAA ATPase p97/VCP and its adaptor protein p47', *EMBO J,* 23(5), pp. 1030-9.

Dubravcic, D., van Baalen, M. and Nizak, C. (2014) 'An evolutionarily significant unicellular strategy in response to starvation in Dictyostelium social amoebae', *F1000Research,* 3, pp. 133-133.

Ebert, D., Haller, R. G. and Walton, M. E. (2003) 'Energy contribution of octanoate to intact rat brain metabolism measured by 13C nuclear magnetic resonance spectroscopy', *J Neurosci,* 23(13), pp. 5928-35.

Eichinger, L., Pachebat, J. A., Glockner, G., Rajandream, M. A., Sucgang, R., Berriman, M., Song, J., Olsen, R., Szafranski, K., Xu, Q., Tunggal, B., Kummerfeld, S., Madera, M., Konfortov, B. A., Rivero, F., Bankier, A. T., Lehmann, R., Hamlin, N., Davies, R., Gaudet, P., Fey, P., Pilcher, K., Chen, G., Saunders, D., Sodergren, E., Davis, P., Kerhornou, A., Nie, X., Hall, N., Anjard, C., Hemphill, L., Bason, N., Farbrother, P., Desany, B., Just, E., Morio, T., Rost, R., Churcher, C., Cooper, J., Haydock, S., van Driessche, N., Cronin, A., Goodhead, I., Muzny, D., Mourier, T., Pain, A., Lu, M., Harper, D., Lindsay, R., Hauser, H., James, K., Quiles, M., Madan Babu, M., Saito, T., Buchrieser, C., Wardroper, A., Felder, M., Thangavelu, M., Johnson, D., Knights, A., Loulseged, H., Mungall, K., Oliver, K., Price, C., Quail, M. A., Urushihara, H., Hernandez, J., Rabbinowitsch, E., Steffen, D., Sanders, M., Ma, J., Kohara, Y., Sharp, S., Simmonds, M., Spiegler, S., Tivey, A., Sugano, S., White, B., Walker, D., Woodward, J., Winckler, T., Tanaka, Y., Shaulsky, G., Schleicher, M., Weinstock, G., Rosenthal, A., Cox, E. C., Chisholm, R. L., Gibbs, R., Loomis, W. F., Platzer, M., Kay, R. R., Williams, J., Dear, P. H., Noegel, A. A., Barrell, B. and Kuspa, A. (2005) 'The genome of the social amoeba Dictyostelium discoideum', *Nature,* 435(7038), pp. 43-57.

Elamin, E. E., Masclee, A. A., Dekker, J., Pieters, H. J. and Jonkers, D. M. (2013) 'Short-chain fatty acids activate AMP-activated protein kinase and ameliorate ethanol-induced intestinal barrier dysfunction in Caco-2 cell monolayers', *J Nutr,* 143(12), pp. 1872-81.

Elia, A., Henry-Grant, R., Adiseshiah, C., Marboeuf, C., Buckley, R. J., Clemens, M. J., Mudan, S. and Pyronnet, S. (2017) 'Implication of 4E-BP1 protein dephosphorylation and accumulation in pancreatic cancer cell death induced by combined gemcitabine and TRAIL', *Cell Death Dis,* 8(12), pp. 3204.

Evans, J. M., Donnelly, L. A., Emslie-Smith, A. M., Alessi, D. R. and Morris, A. D. (2005) 'Metformin and reduced risk of cancer in diabetic patients', *BMJ,* 330(7503), pp. 1304-5.

Faix, J., Kreppel, L., Shaulsky, G., Schleicher, M. and Kimmel, A. R. (2004) 'A rapid and efficient method to generate multiple gene disruptions in Dictyostelium discoideum using a single selectable marker and the Cre-loxP system', *Nucleic Acids Res,* 32(19), pp. e143.

Faix, J., Linkner, J., Nordholz, B., Platt, J. L., Liao, X.-H. and Kimmel, A. R. (2013) 'The application of the Cre-loxP system for generating multiple knock-out and knock-in targeted loci', *Dictyostelium discoideum Protocols*: Springer, pp. 249-267.

Fassone, E. and Rahman, S. (2012) 'Complex I deficiency: clinical features, biochemistry and molecular genetics', *J Med Genet,* 49(9), pp. 578-590.

Fauser, J. K., Matthews, G. M., Cummins, A. G. and Howarth, G. S. (2013) 'Induction of apoptosis by the medium-chain length fatty acid lauric acid in colon cancer cells due to induction of oxidative stress', *Chemotherapy,* 59(3), pp. 214-224.

Fediuc, S., Gaidhu, M. P. and Ceddia, R. B. (2006) 'Regulation of AMP-activated protein kinase and acetyl-CoA carboxylase phosphorylation by palmitate in skeletal muscle cells', *J Lipid Res,* 47(2), pp. 412-420.

Fornai, F., Longone, P., Cafaro, L., Kastsiuchenka, O., Ferrucci, M., Manca, M. L., Lazzeri, G., Spalloni, A., Bellio, N., Lenzi, P., Modugno, N., Siciliano, G., Isidoro, C., Murri, L., Ruggieri, S. and Paparelli, A. (2008) 'Lithium delays progression of amyotrophic lateral sclerosis', *Proc Natl Acad Sci U S A,* 105(6), pp. 2052-2057.

Franz, D. N. and Capal, J. K. (2017) 'mTOR inhibitors in the pharmacologic management of tuberous sclerosis complex and their potential role in other rare neurodevelopmental disorders', *Orphanet J Rare Dis,* 12(1), pp. 51.

Franz, D. N., Lawson, J. A., Yapici, Z., Ikeda, H., Polster, T., Nabbout, R., Curatolo, P., de Vries, P. J., Dlugos, D. J., Voi, M., Fan, J., Vaury, A., Pelov, D. and French, J. A. (2018) 'Everolimus for treatment-refractory seizures in TSC: Extension of a randomized controlled trial', *Neurol Clin Pract,* 8(5), pp. 412-420.

Franz, D. N., Leonard, J., Tudor, C., Chuck, G., Care, M., Sethuraman, G., Dinopoulos, A., Thomas, G. and Crone, K. R. (2006) 'Rapamycin causes regression of astrocytomas in tuberous sclerosis complex', *Ann Neurol,* 59(3), pp. 490-498.

French, J. A., Lawson, J. A., Yapici, Z., Ikeda, H., Polster, T., Nabbout, R., Curatolo, P., de Vries, P. J., Dlugos, D. J., Berkowitz, N., Voi, M., Peyrard, S., Pelov, D. and Franz, D. N. (2016) 'Adjunctive everolimus therapy for treatment-resistant focal-onset seizures associated with tuberous sclerosis (EXIST-3): a phase 3, randomised, double-blind, placebo-controlled study', *Lancet,* 388(10056), pp. 2153-2163.

Fujii, K., Kitabatake, M., Sakata, T. and Ohno, M. (2012) '40S subunit dissociation and proteasome-dependent RNA degradation in nonfunctional 25S rRNA decay', *EMBO J,* 31(11), pp. 2579-89.

Fujikake, N., Shin, M. and Shimizu, S. (2018) 'Association Between Autophagy and Neurodegenerative Diseases', *Front Neurosci,* 12, pp. 255.

Ganley, I. G., Lam du, H., Wang, J., Ding, X., Chen, S. and Jiang, X. (2009) 'ULK1.ATG13.FIP200 complex mediates mTOR signaling and is essential for autophagy', *J Biol Chem,* 284(18), pp. 12297-305.

Geng, S., Zhu, W., Xie, C., Li, X., Wu, J., Liang, Z., Xie, W., Zhu, J., Huang, C., Zhu, M., Wu, R. and Zhong, C. (2016) 'Medium-chain triglyceride ameliorates insulin resistance and inflammation in high fat diet-induced obese mice', *Eur J Nutr,* 55(3), pp. 931-940.

Ghosh, A. P., Marshall, C. B., Coric, T., Shim, E. H., Kirkman, R., Ballestas, M. E., Ikura, M., Bjornsti, M. A. and Sudarshan, S. (2015) 'Point mutations of the mTOR-RHEB pathway in renal cell carcinoma', *Oncotarget,* 6(20), pp. 17895-910.

Giorgi, F. S., Biagioni, F., Lenzi, P., Frati, A. and Fornai, F. (2015) 'The role of autophagy in epileptogenesis and in epilepsy-induced neuronal alterations', *J Neural Transm (Vienna),* 122(6), pp. 849-862.

Glick, D., Barth, S. and Macleod, K. F. (2010) 'Autophagy: cellular and molecular mechanisms', *J pathol,* 221(1), pp. 3-12.

Grabiner, B. C., Nardi, V., Birsoy, K., Possemato, R., Shen, K., Sinha, S., Jordan, A., Beck, A. H. and Sabatini, D. M. (2014) 'A diverse array of cancer-associated MTOR mutations are hyperactivating and can predict rapamycin sensitivity', *Cancer Discov,* 4(5), pp. 554-563.

Graham, D. J., Ouellet-Hellstrom, R., MaCurdy, T. E., Ali, F., Sholley, C., Worrall, C. and Kelman, J. A. (2010) 'Risk of acute myocardial infarction, stroke, heart failure, and death in elderly Medicare patients treated with rosiglitazone or pioglitazone', *JAMA,* 304(4), pp. 411-418.

Griffith, J. L. and Wong, M. (2018) 'The mTOR pathway in treatment of epilepsy: a clinical update', *Future Neurol,* 13(2), pp. 49-58.

Grosdidier, A., Zoete, V. and Michielin, O. (2011a) 'Fast docking using the CHARMM force field with EADock DSS', *J Comput Chem,* 32(10), pp. 2149-59.

Grosdidier, A., Zoete, V. and Michielin, O. (2011b) 'SwissDock, a protein-small molecule docking web service based on EADock DSS', *Nucleic Acids Res,* 39, pp. 270-277.

Gruenheit, N., Baldwin, A., Stewart, B., Jaques, S., Keller, T., Parkinson, K., Chisholm, R., Harwood, A. and Thompson, C. R. L. (2019) 'REMI-seq: Development of methods and resources for functional genomics in Dictyostelium', *bioRxiv*, pp. 582072.

Guerin, N. A. and Larochelle, D. A. (2002) 'A user's guide to restriction enzyme-mediated integration in Dictyostelium', *J Muscle Res Cell Motil,* 23(7-8), pp. 597-604.

Güveli, B. T., Rosti, R. Ö., Güzeltaş, A., Tuna, E. B., Ataklı, D., Sencer, S., Yekeler, E., Kayserili, H., Dirican, A., Bebek, N., Baykan, B., Gökyiğit, A. and Gürses, C. (2017) 'Teratogenicity of Antiepileptic Drugs', *Clin Psychopharmacol Neurosci,* 15(1), pp. 19-27.

Haghighat, A., Mader, S., Pause, A. and Sonenberg, N. (1995) 'Repression of cap-dependent translation by 4E-binding protein 1: competition with p220 for binding to eukaryotic initiation factor-4E', *EMBO J,* 14(22), pp. 5701-9.

Haidukewych, D., Forsythe, W. I. and Sills, M. (1982) 'Monitoring octanoic and decanoic acids in plasma from children with intractable epilepsy treated with medium-chain triglyceride diet', *Clin Chem,* 28(4 Pt 1), pp. 642-645.

Halawani, D. and Latterich, M. (2006) 'p97: The cell's molecular purgatory?', *Mol Cell,* 22(6), pp. 713-717.

Han, D. Y., Di, X. J., Fu, Y. L. and Mu, T. W. (2015) 'Combining valosin-containing protein (VCP) inhibition and suberanilohydroxamic acid (SAHA) treatment additively enhances the folding, trafficking, and function of epilepsy-associated gamma-aminobutyric acid, type A (GABAA) receptors', *J Biol Chem,* 290(1), pp. 325-337.

Hanada, T. (2014) 'The AMPA receptor as a therapeutic target in epilepsy: preclinical and clinical evidence', *J Receptor Ligand Channel*, 7, pp. 39-50.

Hanzelmann, P., Buchberger, A. and Schindelin, H. (2011) 'Hierarchical binding of cofactors to the AAA ATPase p97', *Structure,* 19(6), pp. 833-843.

Hardies, K., Cai, Y., Jardel, C., Jansen, A. C., Cao, M., May, P., Djémié, T., Hachon Le Camus, C., Keymolen, K., Deconinck, T., Bhambhani, V., Long, C., Sajan, S. A., Helbig, K. L., Suls, A., Balling, R., Helbig, I., De Jonghe, P., Depienne, C., De Camilli, P., Weckhuysen, S. and Consortium, A. w. g. o. t. E. R. (2016) 'Loss of SYNJ1 dual phosphatase activity leads to early onset refractory seizures and progressive neurological decline', *Brain,* 139(Pt 9), pp. 2420-30.

Hardy, J. and Allsop, D. (1991) 'Amyloid deposition as the central event in the aetiology of Alzheimer's disease', *Trends Pharmacol Sci,* 12, pp. 383-388.

Harrison, D. E., Strong, R., Sharp, Z. D., Nelson, J. F., Astle, C. M., Flurkey, K., Nadon, N. L., Wilkinson, J. E., Frenkel, K., Carter, C. S., Pahor, M., Javors, M. A., Fernandez, E. and Miller, R. A. (2009) 'Rapamycin fed late in life extends lifespan in genetically heterogeneous mice', *Nature,* 460(7253), pp. 392-395.

Hartman, A. L. (2012) 'Neuroprotection in metabolism-based therapy', *Epilepsy Res,* 100(3), pp. 286-294.

He, C. and Klionsky, D. J. (2009) 'Regulation mechanisms and signaling pathways of autophagy', *Annu Rev of genet,* 43, pp. 67-93.

Heiss, W. D., Szelies, B., Kessler, J. and Herholz, K. (1991) 'Abnormalities of energy metabolism in Alzheimer's disease studied with PET', *Ann N Y Acad Sci,* 640, pp. 65-71.

Henderson, S. T., Vogel, J. L., Barr, L. J., Garvin, F., Jones, J. J. and Costantini, L. C. (2009) 'Study of the ketogenic agent AC-1202 in mild to moderate Alzheimer's disease: a randomized, double-blind, placebo-controlled, multicenter trial', *Nutr Metab (Lond),* 6, pp. 31.

Hibi, S., Ueno, K., Nagato, S., Kawano, K., Ito, K., Norimine, Y., Takenaka, O., Hanada, T. and Yonaga, M. (2012) 'Discovery of 2-(2-oxo-1-phenyl-5-pyridin-2-yl-1,2-dihydropyridin-3-yl)benzonitrile (perampanel): a novel, noncompetitive alpha-amino-3-hydroxy-5-methyl-4-isoxazolepropanoic acid (AMPA) receptor antagonist', *J Med Chem,* 55(23), pp. 10584-600.

Hillmann, P. and Fabbro, D. (2019) 'PI3K/mTOR Pathway Inhibition: Opportunities in Oncology and Rare Genetic Diseases', *Int J Mol Sci,* 20(22), pp. 5792.

Hippocrates and Adams, F. (1985) 'The Genuine Works of Hippocrates: Translated from the Greek with a Preliminary Discourse and Annotations' *Classics of Medicine Library.*

Hoyer-Hansen, M., Bastholm, L., Szyniarowski, P., Campanella, M., Szabadkai, G., Farkas, T., Bianchi, K., Fehrenbacher, N., Elling, F., Rizzuto, R., Mathiasen, I. S. and Jaattela, M. (2007) 'Control of macroautophagy by calcium, calmodulin-dependent kinase kinase-beta, and Bcl-2', *Mol Cell,* 25(2), pp. 193-205.

Hu, G. X., Chen, G. R., Xu, H., Ge, R. S. and Lin, J. (2010) 'Activation of the AMP activated protein kinase by short-chain fatty acids is the main mechanism underlying the beneficial effect of a high fiber diet on the metabolic syndrome', *Med Hypotheses,* 74(1), pp. 123-126.

Hua, H., Kong, Q., Zhang, H., Wang, J., Luo, T. and Jiang, Y. (2019) 'Targeting mTOR for cancer therapy', *J Hematol Oncol,* 12(1), pp. 71.

Hudson, J. J., Hsu, D. W., Guo, K., Zhukovskaya, N., Liu, P. H., Williams, J. G., Pears, C. J. and Lakin, N. D. (2005) 'DNA-PKcs-dependent signaling of DNA damage in Dictyostelium discoideum', *Curr Biol,* 15(20), pp. 1880-5.

Hughes, S. D., Kanabus, M., Anderson, G., Hargreaves, I. P., Rutherford, T., O'Donnell, M., Cross, J. H., Rahman, S., Eaton, S. and Heales, S. J. (2014) 'The ketogenic diet component decanoic acid increases mitochondrial citrate synthase and complex I activity in neuronal cells', *J Neurochem,* 129(3), pp. 426-433.

Huttenlocher, P. R., Wilbourn, A. J. and Signore, J. M. (1971) 'Medium-chain triglycerides as a therapy for intractable childhood epilepsy', *Neurology,* 21(11), pp. 1097-103.

IJff, D. M., Postulart, D., Lambrechts, D. A., Majoie, M. H., de Kinderen, R. J., Hendriksen, J. G., Evers, S. M. and Aldenkamp, A. P. (2016) 'Cognitive and behavioral impact of the ketogenic diet in children and adolescents with refractory epilepsy: A randomized controlled trial', *Epilepsy Behav,* 60, pp. 153-157.

Indig, F. E., Partridge, J. J., von Kobbe, C., Aladjem, M. I., Latterich, M. and Bohr, V. A. (2004) 'Werner syndrome protein directly binds to the AAA ATPase p97/VCP in an ATP-dependent fashion', *J Struct Biol,* 146(1-2), pp. 251-259.

Insall, R. (2005) 'The Dictyostelium genome: the private life of a social model revealed?', *Genome Biol,* 6(6), pp. 222.

Iranfar, N., Fuller, D. and Loomis, W. F. (2003) 'Genome-wide expression analyses of gene regulation during early development of Dictyostelium discoideum', *Eukaryot Cell,* 2(4), pp. 664-670.

Isojarvi, J. I. and Tokola, R. A. (1998) 'Benzodiazepines in the treatment of epilepsy in people with intellectual disability', *J Intellect Disabil Res,* 42 Suppl 1, pp. 80-92.

Jaiswal, P. and Kimmel, A. R. (2019) 'mTORC1/AMPK responses define a core gene set for developmental cell fate switching', *BMC Biol,* 17(1), pp. 58.

Jang, D. J. and Lee, J. A. (2016) 'The roles of phosphoinositides in mammalian autophagy', *Arch Pharm Res,* 39(8), pp. 1129-36.

Jentink, J., Loane, M. A., Dolk, H., Barisic, I., Garne, E., Morris, J. K. and de Jong-van den Berg, L. T. (2010) 'Valproic acid monotherapy in pregnancy and major congenital malformations', *N Engl J Med,* 362(23), pp. 2185-2193.

Jiang, N., Shen, Y., Fei, X., Sheng, K., Sun, P., Qiu, Y., Larner, J., Cao, L., Kong, X. and Mi, J. (2013) 'Valosin-containing protein regulates the proteasome-mediated degradation of DNA-PKcs in glioma cells', *Cell Death Dis,* 4, pp. e647.

Jin, N., Mao, K., Jin, Y., Tevzadze, G., Kauffman, E. J., Park, S., Bridges, D., Loewith, R., Saltiel, A. R., Klionsky, D. J. and Weisman, L. S. (2014) 'Roles for PI(3,5)P2 in nutrient sensing through TORC1', *Mol Biol Cell,* 25(7), pp. 1171-85.

Johnson, S. C., Rabinovitch, P. S. and Kaeberlein, M. (2013) 'mTOR is a key modulator of ageing and age-related disease', *Nature,* 493(7432), pp. 338-45.

Johnson, S. C., Yanos, M. E., Kayser, E. B., Quintana, A., Sangesland, M., Castanza, A., Uhde, L., Hui, J., Wall, V. Z., Gagnidze, A., Oh, K., Wasko, B. M., Ramos, F. J., Palmiter, R. D., Rabinovitch, P. S., Morgan, P. G., Sedensky, M. M. and Kaeberlein, M. (2013) 'mTOR inhibition alleviates mitochondrial disease in a mouse model of Leigh syndrome', *Science,* 342(6165), pp. 1524-8.

Johri, A. and Beal, M. F. (2012) 'Mitochondrial dysfunction in neurodegenerative diseases', *J Pharmacol Exp Ther,* 342(3), pp. 619-630.

Ju, J. S., Fuentealba, R. A., Miller, S. E., Jackson, E., Piwnica-Worms, D., Baloh, R. H. and Weihl, C. C. (2009) 'Valosin-containing protein (VCP) is required for autophagy and is disrupted in VCP disease', *J Cell Biol,* 187(6), pp. 875-888.

Jóźwiak, M., Filipowska, A., Fiorino, F. and Struga, M. (2020) 'Anticancer activities of fatty acids and their heterocyclic derivatives', *Eur J Pharmacol,* 871, pp. 172937.

Kamimura, Y., Tang, M. and Devreotes, P. (2009) 'Assays for chemotaxis and chemoattractant-stimulated TorC2 activation and PKB substrate phosphorylation in Dictyostelium', *Methods Mol Biol,* 571, pp. 255-270.

Kanabus, M., Fassone, E., Hughes, S. D., Bilooei, S. F., Rutherford, T., Donnell, M. O., Heales, S. J. R. and Rahman, S. (2016) 'The pleiotropic effects of decanoic acid treatment on mitochondrial function in fibroblasts from patients with complex I deficient Leigh syndrome', *J Inherit Metab Dis,* 39(3), pp. 415-426.

Kashiwaya, Y., Takeshima, T., Mori, N., Nakashima, K., Clarke, K. and Veech, R. L. (2000) 'D-beta-hydroxybutyrate protects neurons in models of Alzheimer's and Parkinson's disease', *Proc Natl Acad Sci U S A,* 97(10), pp. 5440-4.

Keim, M., Williams, R. S. and Harwood, A. J. (2004) 'An inverse PCR technique to rapidly isolate the flanking DNA of dictyostelium insertion mutants', *Mol Biotechnol,* 26(3), pp. 221-224.

Kelley, L. A., Mezulis, S., Yates, C. M., Wass, M. N. and Sternberg, M. J. E. (2015) 'The Phyre2 web portal for protein modeling, prediction and analysis', *Nat Protoc,* 10(6), pp. 845-858.

Khabbush, A., Orford, M., Tsai, Y. C., Rutherford, T., O'Donnell, M., Eaton, S. and Heales, S. J. R. (2017) 'Neuronal decanoic acid oxidation is markedly lower than that of octanoic acid: A mechanistic insight into the medium-chain triglyceride ketogenic diet', *Epilepsia,* 58(8), pp. 1423-1429.

Khan, N. A., Nikkanen, J., Yatsuga, S., Jackson, C., Wang, L., Pradhan, S., Kivelä, R., Pessia, A., Velagapudi, V. and Suomalainen, A. (2017) 'mTORC1 Regulates Mitochondrial Integrated Stress Response and Mitochondrial Myopathy Progression', *Cell Metab,* 26(2), pp. 419-428.

Kim, D. H., Davis, R. C., Furukawa, R. and Fechheimer, M. (2009) 'Autophagy contributes to degradation of Hirano bodies', *Autophagy,* 5(1), pp. 44-51.

Kim, D. Y., Abdelwahab, M. G., Lee, S. H., O'Neill, D., Thompson, R. J., Duff, H. J., Sullivan, P. G. and Rho, J. M. (2015a) 'Ketones prevent oxidative impairment of hippocampal synaptic integrity through KATP channels', *PLoS One,* 10(4), pp. e0119316.

Kim, D. Y., Simeone, K. A., Simeone, T. A., Pandya, J. D., Wilke, J. C., Ahn, Y., Geddes, J. W., Sullivan, P. G. and Rho, J. M. (2015b) 'Ketone bodies mediate antiseizure effects through mitochondrial permeability transition', *Ann Neurol,* 78(1), pp. 77-87.

Kim, D. Y., Vallejo, J. and Rho, J. M. (2010) 'Ketones prevent synaptic dysfunction induced by mitochondrial respiratory complex inhibitors', *J Neurochem,* 114(1), pp. 130-141.

King, J. S., Veltman, D. M. and Insall, R. H. (2011) 'The induction of autophagy by mechanical stress', *Autophagy,* 7(12), pp. 1490-9.

Kirisako, T., Baba, M., Ishihara, N., Miyazawa, K., Ohsumi, M., Yoshimori, T., Noda, T. and Ohsumi, Y. (1999) 'Formation process of autophagosome is traced with Apg8/Aut7p in yeast', *J Cell Biol,* 147(2), pp. 435-446.

Klement, R. J. (2017) 'Beneficial effects of ketogenic diets for cancer patients: a realist review with focus on evidence and confirmation', *Med Oncol,* 34(8), pp. 132.

Klement, R. J., Champ, C. E., Otto, C. and Kämmerer, U. (2016) 'Anti-Tumor Effects of Ketogenic Diets in Mice: A Meta-Analysis', *PLoS One,* 11(5), pp. e0155050.

Kloppsteck, P., Ewens, C. A., Forster, A., Zhang, X. and Freemont, P. S. (2012) 'Regulation of p97 in the ubiquitin-proteasome system by the UBX protein-family', *Biochim Biophys Acta,* 1823(1), pp. 125-9.

Klug, A. (2010) 'The discovery of zinc fingers and their applications in gene regulation and genome manipulation', *Annu Rev Biochem,* 79, pp. 213-231.

Kobow, K., Kaspi, A., Harikrishnan, K. N., Kiese, K., Ziemann, M., Khurana, I., Fritzsche, I., Hauke, J., Hahnen, E., Coras, R., Muhlebner, A., El-Osta, A. and Blumcke, I. (2013) 'Deep sequencing reveals increased DNA methylation in chronic rat epilepsy', *Acta Neuropathol,* 126(5), pp. 741-756.

Komiya, K., Uchida, T., Ueno, T., Koike, M., Abe, H., Hirose, T., Kawamori, R., Uchiyama, Y., Kominami, E., Fujitani, Y. and Watada, H. (2010) 'Free fatty acids stimulate autophagy in pancreatic β-cells via JNK pathway', *Biochem Biophys Res Commun,* 401(4), pp. 561-567.

Koren, G., Nava-Ocampo, A. A., Moretti, M. E., Sussman, R. and Nulman, I. (2006) 'Major malformations with valproic acid', *Can fam physician,* 52(4), pp. 441-442.

Korolchuk, V. I., Saiki, S., Lichtenberg, M., Siddiqi, F. H., Roberts, E. A., Imarisio, S., Jahreiss, L., Sarkar, S., Futter, M., Menzies, F. M., O'Kane, C. J., Deretic, V. and Rubinsztein, D. C. (2011) 'Lysosomal positioning coordinates cellular nutrient responses', *Nat Cell Biol,* 13(4), pp. 453-460.

Kossoff, E. H., Thiele, E. A., Pfeifer, H. H., McGrogan, J. R. and Freeman, J. M. (2005) 'Tuberous sclerosis complex and the ketogenic diet', *Epilepsia,* 46(10), pp. 1684-6.

Kouroku, Y., Fujita, E., Tanida, I., Ueno, T., Isoai, A., Kumagai, H., Ogawa, S., Kaufman, R. J., Kominami, E. and Momoi, T. (2007) 'ER stress (PERK/eIF2alpha phosphorylation) mediates the polyglutamine-induced LC3 conversion, an essential step for autophagy formation', *Cell Death Differ,* 14(2), pp. 230-239.

Koves, T. R., Ussher, J. R., Noland, R. C., Slentz, D., Mosedale, M., Ilkayeva, O., Bain, J., Stevens, R., Dyck, J. R. B., Newgard, C. B., Lopaschuk, G. D. and Muoio, D. M. (2008) 'Mitochondrial Overload and Incomplete Fatty Acid Oxidation Contribute to Skeletal Muscle Insulin Resistance', *Cell Metab,* 7(1), pp. 45-56.

Kovács, Z., D'Agostino, D. P., Dobolyi, A. and Ari, C. (2017) 'Adenosine A1 Receptor Antagonism Abolished the Anti-seizure Effects of Exogenous Ketone Supplementation in Wistar Albino Glaxo Rijswijk Rats', *Front Mol Neurosci,* 10, pp. 235.

Krebs, H. A. (1966) 'The regulation of the release of ketone bodies by the liver', *Adv Enzyme Regul,* 4, pp. 339-354.

Kunz, W. S., Kudin, A. P., Vielhaber, S., Blumcke, I., Zuschratter, W., Schramm, J., Beck, H. and Elger, C. E. (2000) 'Mitochondrial complex I deficiency in the epileptic focus of patients with temporal lobe epilepsy', *Ann Neurol,* 48(5), pp. 766-773.

Kuspa, A. (2006) 'Restriction enzyme-mediated integration (REMI) mutagenesis', *Methods Mol Biol,* 346, pp. 201-209.

Kuspa, A. and Loomis, W. F. (1992) 'Tagging developmental genes in Dictyostelium by restriction enzyme-mediated integration of plasmid DNA', *Proceedings of the National Academy of Sciences,* 89(18), pp. 8803-8807.

Laffel, L. (1999) 'Ketone bodies: a review of physiology, pathophysiology and application of monitoring to diabetes', *Diabetes Metab Res Rev,* 15(6), pp. 412-426.

LaLonde, D. P. and Bretscher, A. (2011) 'The UBX protein SAKS1 negatively regulates endoplasmic reticulum-associated degradation and p97-dependent degradation', *J Biol Chem,* 286(6), pp. 4892-4901.

Lamming, D. W. and Sabatini, D. M. (2011) 'A radical role for TOR in longevity', *Cell Metab,* 13(6), pp. 617-618.

Lampert, T. J., Kamprad, N., Edwards, M., Borleis, J., Watson, A. J., Tarantola, M. and Devreotes, P. N. (2017) 'Shear force-based genetic screen reveals negative regulators of cell adhesion and protrusive activity', Proc Natl Acad Sci U S A*,* 114(37), pp. E7727-E7736.

Lan, B., Chai, S., Wang, P. and Wang, K. (2017) 'VCP/p97/Cdc48, A Linking of Protein Homeostasis and Cancer Therapy', *Curr Mol Med,* 17(9), pp. 608-618.

Lang, D. G., Wang, C. M. and Cooper, B. R. (1993) 'Lamotrigine, phenytoin and carbamazepine interactions on the sodium current present in N4TG1 mouse neuroblastoma cells', *J Pharmacol Exp Ther,* 266(2), pp. 829-835.

Larsen, T. M., Toubro, S. and Astrup, A. (2003) 'PPARgamma agonists in the treatment of type II diabetes: is increased fatness commensurate with long-term efficacy?', *Int J Obes Relat Metab Disord,* 27(2), pp. 147-161.

Las, G., Serada, S. B., Wikstrom, J. D., Twig, G. and Shirihai, O. S. (2011) 'Fatty acids suppress autophagic turnover in β-cells', *J Biol Chem,* 286(49), pp. 42534-44.

Lee, J. N., Zhang, X., Feramisco, J. D., Gong, Y. and Ye, J. (2008) 'Unsaturated fatty acids inhibit proteasomal degradation of Insig-1 at a postubiquitination step', *J Biol Chem,* 283(48), pp. 33772-83.

Levi, S., Polyakov, M. and Egelhoff, T. T. (2000) 'Green fluorescent protein and epitope tag fusion vectors for Dictyostelium discoideum', *Plasmid,* 44(3), pp. 231-238.

Li, C. L., Santhanam, B., Webb, A. N., Zupan, B. and Shaulsky, G. (2016) 'Gene discovery by chemical mutagenesis and whole-genome sequencing in Dictyostelium', *Genome Res,* 26(9), pp. 1268-76.

Li, G., Alexander, H., Schneider, N. and Alexander, S. (2000) 'Molecular basis for resistance to the anticancer drug cisplatin in Dictyostelium', *Microbiology,* 146 (Pt 9), pp. 2219-27.

Li, J., Kim, S. G. and Blenis, J. (2014) 'Rapamycin: one drug, many effects', *Cell Metab,* 19(3), pp. 373-379.

Li, J. M., Wu, H., Zhang, W., Blackburn, M. R. and Jin, J. (2014) 'The p97-UFD1L-NPL4 protein complex mediates cytokine-induced IkappaBalpha proteolysis', *Mol Cell Biol,* 34(3), pp. 335-347.

Li, M., Zhou, Y., Chen, C., Yang, T., Zhou, S., Chen, S., Wu, Y. and Cui, Y. (2019) 'Efficacy and safety of mTOR inhibitors (rapamycin and its analogues) for tuberous sclerosis complex: a meta-analysis', *Orphanet J Rare Dis,* 14(1), pp. 39.

Liang, J., Yin, C., Doong, H., Fang, S., Peterhoff, C., Nixon, R. A. and Monteiro, M. J. (2006) 'Characterization of erasin (UBXD2): a new ER protein that promotes ER-associated protein degradation', *J Cell Sci,* 119(Pt 19), pp. 4011-24.

Liao, X.-H., Majithia, A., Huang, X. and Kimmel, A. R. (2008) 'Growth control via TOR kinase signaling, an intracellular sensor of amino acid and energy availability, with crosstalk potential to proline metabolism', *Amino Acids,* 35(4), pp. 761-770.

Likhodii, S. S., Musa, K., Mendonca, A., Dell, C., Burnham, W. M. and Cunnane, S. C. (2000) 'Dietary Fat, Ketosis, and Seizure Resistance in Rats on the Ketogenic Diet', *Epilepsia,* 41(11), pp. 1400-1410.

Lim, P. J., Danner, R., Liang, J., Doong, H., Harman, C., Srinivasan, D., Rothenberg, C., Wang, H., Ye, Y., Fang, S. and Monteiro, M. J. (2009) 'Ubiquilin and p97/VCP bind erasin, forming a complex involved in ERAD', *J Cell Biol,* 187(2), pp. 201-217.

Liu, L., Das, S., Losert, W. and Parent, C. A. (2010) 'mTORC2 regulates neutrophil chemotaxis in a cAMP- and RhoA-dependent fashion', *Dev Cell,* 19(6), pp. 845-857.

Liu, Y. M. (2008) 'Medium-chain triglyceride (MCT) ketogenic therapy', *Epilepsia,* 49 Suppl 8, pp. 33-36.

Livingstone, M., Ruan, H., Weiner, J., Clauser, K. R., Strack, P., Jin, S., Williams, A., Greulich, H., Gardner, J., Venere, M., Mochan, T. A., DiTullio, R. A., Jr., Moravcevic, K., Gorgoulis, V. G., Burkhardt, A. and Halazonetis, T. D. (2005) 'Valosin-containing protein phosphorylation at Ser784 in response to DNA damage', *Cancer Res,* 65(17), pp. 7533-40.

Loomis, W. F. (2015) 'Genetic control of morphogenesis in Dictyostelium', *Dev Biol,* 402(2), pp. 146-161.

Loomis, W. F. (2016) 'A better way to discover gene function in the social amoeba Dictyostelium discoideum', *Genome Res,* 26(9), pp. 1161-4.

Lukasiuk, K. and Pitkanen, A. (2012) 'Molecular basis of acquired epileptogenesis', *Handb Clin Neurol,* 107, pp. 3-12.

Lusardi, T. A., Akula, K. K., Coffman, S. Q., Ruskin, D. N., Masino, S. A. and Boison, D. (2015) 'Ketogenic diet prevents epileptogenesis and disease progression in adult mice and rats', *Neuropharmacology,* 99, pp. 500-509.

Lynch-Day, M. A., Mao, K., Wang, K., Zhao, M. and Klionsky, D. J. (2012) 'The role of autophagy in Parkinson's disease', *Cold Spring Harb Perspect Med,* 2(4), pp. a009357.

Ma, Y., Pannicke, U., Schwarz, K. and Lieber, M. R. (2002) 'Hairpin opening and overhang processing by an Artemis/DNA-dependent protein kinase complex in nonhomologous end joining and V(D)J recombination', *Cell,* 108(6), pp. 781-794.

Maalouf, M. and Rho, J. M. (2008) 'Oxidative impairment of hippocampal long-term potentiation involves activation of protein phosphatase 2A and is prevented by ketone bodies', *J Neurosci Res,* 86(15), pp. 3322-30.

Malapaka, R. R., Khoo, S., Zhang, J., Choi, J. H., Zhou, X. E., Xu, Y., Gong, Y., Li, J., Yong, E. L., Chalmers, M. J., Chang, L., Resau, J. H., Griffin, P. R., Chen, Y. E. and Xu, H. E. (2012) 'Identification and mechanism of 10-carbon fatty acid as modulating ligand of peroxisome proliferator-activated receptors', *J Biol Chem,* 287(1), pp. 183-195.

Martino, L., Masini, M., Novelli, M., Beffy, P., Bugliani, M., Marselli, L., Masiello, P., Marchetti, P. and De Tata, V. (2012) 'Palmitate activates autophagy in INS-1E β-cells and in isolated rat and human pancreatic islets', *PLoS One,* 7(5), pp. e36188.

Maschio, M. (2012) 'Brain tumor-related epilepsy', *Curr Neuropharmacol,* 10(2), pp. 124-133.

Masino, S. A., Li, T., Theofilas, P., Sandau, U. S., Ruskin, D. N., Fredholm, B. B., Geiger, J. D., Aronica, E. and Boison, D. (2011) 'A ketogenic diet suppresses seizures in mice through adenosine A(1) receptors', *J Clin Invest,* 121(7), pp. 2679-83.

Matthews, J. M. and Sunde, M. (2002) 'Zinc fingers--folds for many occasions', *IUBMB Life,* 54(6), pp. 351-355.

Mavrakis, M., Lippincott-Schwartz, J., Stratakis, C. A. and Bossis, I. (2006) 'Depletion of type IA regulatory subunit (RIalpha) of protein kinase A (PKA) in mammalian cells and tissues activates mTOR and causes autophagic deficiency', *Hum Mol Genet,* 15(19), pp. 2962-71.

McDaniel, S. S., Rensing, N. R., Thio, L. L., Yamada, K. A. and Wong, M. (2011) 'The ketogenic diet inhibits the mammalian target of rapamycin (mTOR) pathway', *Epilepsia,* 52(3), pp. e7-e11.

McMahon, J., Huang, X., Yang, J., Komatsu, M., Yue, Z., Qian, J., Zhu, X. and Huang, Y. (2012) 'Impaired autophagy in neurons after disinhibition of mammalian target of rapamycin and its contribution to epileptogenesis', *J Neurosci,* 32(45), pp. 15704-14.

Mei, S., Ni, H.-M., Manley, S., Bockus, A., Kassel, K. M., Luyendyk, J. P., Copple, B. L. and Ding, W.-X. (2011) 'Differential roles of unsaturated and saturated fatty acids on autophagy and apoptosis in hepatocytes', *J Pharmacol Exp Ther,* 339(2), pp. 487-498.

Meima, M. and Schaap, P. (1999) 'Dictyostelium development—socializing through cAMP', *Semin Cell Dev Biol,* 10(6), pp. 567-576.

Meléndez, A. and Neufeld, T. P. (2008) 'The cell biology of autophagy in metazoans: a developing story', *Development,* 135(14), pp. 2347-60.

Mesquita, A., Calvo-Garrido, J., Carilla-Latorre, S. and Escalante, R. (2013) 'Monitoring autophagy in Dictyostelium', *Methods Mol Biol,* 983, pp. 461-470.

Mesquita, A., Cardenal-Muñoz, E., Dominguez, E., Muñoz-Braceras, S., Nuñez-Corcuera, B., Phillips, B. A., Tábara, L. C., Xiong, Q., Coria, R., Eichinger, L., Golstein, P., King, J. S., Soldati, T., Vincent, O. and Escalante, R. (2016) 'Autophagy in Dictyostelium: Mechanisms, regulation and disease in a simple biomedical model', *Autophagy,* 13(1), pp. 24-40.

Meyer, H. and Weihl, C. C. (2014) 'The VCP/p97 system at a glance: connecting cellular function to disease pathogenesis', *J Cell Sci,* 127(Pt 18), pp. 3877-83.

Meyer, H. H. (2005) 'Golgi reassembly after mitosis: the AAA family meets the ubiquitin family', *Biochim Biophys Acta,* 1744(2), pp. 108-119.

Meyer, H. H., Shorter, J. G., Seemann, J., Pappin, D. and Warren, G. (2000) 'A complex of mammalian ufd1 and npl4 links the AAA-ATPase, p97, to ubiquitin and nuclear transport pathways', *EMBO J,* 19(10), pp. 2181-92.

Mirzaa, G., Roy, A., Dobyns, W., Millen, K. and Hevner, R. (2018) 'Hemimegalencephaly and Dysplastic Megalencephaly', *In Developmental Neuropathology*.

Miyamoto, J., Ohue-Kitano, R., Mukouyama, H., Nishida, A., Watanabe, K., Igarashi, M., Irie, J., Tsujimoto, G., Satoh-Asahara, N., Itoh, H. and Kimura, I. (2019) 'Ketone body receptor

GPR43 regulates lipid metabolism under ketogenic conditions', *Proc Natl Acad Sci U S A,* 116(47), pp. 23813-23821.

Morio, T., Yasukawa, H., Urushihara, H., Saito, T., Ochiai, H., Takeuchi, I., Maeda, M. and Tanaka, Y. (2001) 'FebA: a gene for eukaryotic translation initiation factor 4E-binding protein (4E-BP) in Dictyostelium discoideum', *Biochim Biophys Acta,* 1519(1-2), pp. 65-69.

Morita, T. and Sobue, K. (2009) 'Specification of neuronal polarity regulated by local translation of CRMP2 and Tau via the mTOR-p70S6K pathway', *J Biol Chem,* 284(40), pp. 27734-45.

Mumme, K. and Stonehouse, W. (2015) 'Effects of medium-chain triglycerides on weight loss and body composition: a meta-analysis of randomized controlled trials', *J Acad Nutr Diet,* 115(2), pp. 249-263.

Mundy, D. I., Li, W. P., Luby-Phelps, K. and Anderson, R. G. (2012) 'Caveolin targeting to late endosome/lysosomal membranes is induced by perturbations of lysosomal pH and cholesterol content', *Mol Biol Cell,* 23(5), pp. 864-880.

Munoz-Braceras, S., Calvo, R. and Escalante, R. (2015) 'TipC and the chorea-acanthocytosis protein VPS13A regulate autophagy in Dictyostelium and human HeLa cells', *Autophagy,* 11(6), pp. 918-927.

Murphy, M. P. and LeVine, H., 3rd (2010) 'Alzheimer's disease and the amyloid-beta peptide', *J Alzheimers Dis,* 19(1), pp. 311-323.

Nabbout, R., Belousova, E., Benedik, M. P., Carter, T., Cottin, V., Curatolo, P., Dahlin, M., D Amato, L., d'Augères, G. B., de Vries, P. J., Ferreira, J. C., Feucht, M., Fladrowski, C., Hertzberg, C., Jozwiak, S., Lawson, J. A., Macaya, A., Marques, R., O'Callaghan, F., Qin, J., Sander, V., Sauter, M., Shah, S., Takahashi, Y., Touraine, R., Youroukos, S., Zonnenberg, B., Jansen, A., Kingswood, J. C., Consortium, T. and Investigators, T. (2018) 'Epilepsy in tuberous sclerosis complex: Findings from the TOSCA Study', *Epilepsia open,* 4(1), pp. 73-84.

Nadadhur, A. G., Alsaqati, M., Gasparotto, L., Cornelissen-Steijger, P., van Hugte, E., Dooves, S., Harwood, A. J. and Heine, V. M. (2019) 'Neuron-Glia Interactions Increase Neuronal Phenotypes in Tuberous Sclerosis Complex Patient iPSC-Derived Models', *Stem Cell Reports,* 12(1), pp. 42-56.

Nadadhur, A. G., Leferink, P. S., Holmes, D., Hinz, L., Cornelissen-Steijger, P., Gasparotto, L. and Heine, V. M. (2018) 'Patterning factors during neural progenitor induction determine regional identity and differentiation potential in vitro', *Stem Cell Res,* 32, pp. 25-34.

Nagasaki, A. and Uyeda, T. Q. (2008) 'Screening of genes involved in cell migration in Dictyostelium', *Exp Cell Res,* 314(5), pp. 1136-46.

Narayanan, A., Baskaran, S. A., Amalaradjou, M. A. and Venkitanarayanan, K. (2015) 'Anticarcinogenic properties of medium chain fatty acids on human colorectal, skin and breast cancer cells in vitro', *Int J Mol Sci,* 16(3), pp. 5014-27.

Nascimbeni, A. C., Codogno, P. and Morel, E. (2017) 'Phosphatidylinositol-3-phosphate in the regulation of autophagy membrane dynamics', *FEBS J,* 284(9), pp. 1267-1278.

Neal, E. (2016) '"Alternative" ketogenic diets', *Ketogenic Diet and Metabolic Therapies: Expanded Roles in Health and Disease*, pp. 5.

Neal, E. G., Chaffe, H., Schwartz, R. H., Lawson, M. S., Edwards, N., Fitzsimmons, G., Whitney, A. and Cross, J. H. (2008) 'The ketogenic diet for the treatment of childhood epilepsy: a randomised controlled trial', *Lancet Neurol,* 7(6), pp. 500-506.

Neal, E. G. and Cross, J. H. (2010) 'Efficacy of dietary treatments for epilepsy', *J Hum Nutr Diet,* 23(2), pp. 113-119.

Nevitt, S. J., Sudell, M., Weston, J., Tudur Smith, C. and Marson, A. G. (2017) 'Antiepileptic drug monotherapy for epilepsy: a network meta-analysis of individual participant data', *The Cochrane Database Syst Rev,* 12(12), pp. CD011412.

Newman, J. C., Covarrubias, A. J., Zhao, M., Yu, X., Gut, P., Ng, C. P., Huang, Y., Haldar, S. and Verdin, E. (2017) 'Ketogenic Diet Reduces Midlife Mortality and Improves Memory in Aging Mice', *Cell Metab,* 26(3), pp. 547-557.

Nguyen, D. K. H., Thombre, R. and Wang, J. (2019) 'Autophagy as a common pathway in amyotrophic lateral sclerosis', *Neurosci Lett,* 697, pp. 34-48.

Nichols, J. M. E., Paschke, P., Peak-Chew, S., Williams, T. D., Tweedy, L., Skehel, M., Stephens, E., Chubb, J. R. and Kay, R. R. (2019) 'The Atypical MAP Kinase ErkB Transmits Distinct Chemotactic Signals through a Core Signaling Module', *Dev Cell,* 48(4), pp. 491-505.

Ohnuma, T., Toda, A., Kimoto, A., Takebayashi, Y., Higashiyama, R., Tagata, Y., Ito, M., Ota, T., Shibata, N. and Arai, H. (2016) 'Benefits of use, and tolerance of, medium-chain triglyceride medical food in the management of Japanese patients with Alzheimer's disease: a prospective, open-label pilot study', *Clin Interv Aging,* 11, pp. 29-36.

Ostendorf, A. P. and Wong, M. (2015) 'mTOR inhibition in epilepsy: rationale and clinical perspectives', *CNS Drugs,* 29(2), pp. 91-99.

Ota, M., Matsuo, J., Ishida, I., Hattori, K., Teraishi, T., Tonouchi, H., Ashida, K., Takahashi, T. and Kunugi, H. (2016) 'Effect of a ketogenic meal on cognitive function in elderly adults: potential for cognitive enhancement', *Psychopharmacology,* 233(21), pp. 3797-3802.

Ota, M., Matsuo, J., Ishida, I., Takano, H., Yokoi, Y., Hori, H., Yoshida, S., Ashida, K., Nakamura, K., Takahashi, T. and Kunugi, H. (2019) 'Effects of a medium-chain triglyceride-based ketogenic formula on cognitive function in patients with mild-to-moderate Alzheimer's disease', *Neurosci Lett,* 690, pp. 232-236.

Otto, G. P., Wu, M. Y., Kazgan, N., Anderson, O. R. and Kessin, R. H. (2003) 'Macroautophagy is required for multicellular development of the social amoeba Dictyostelium discoideum', *J Biol Chem,* 278(20), pp. 17636-45.

Pachow, D., Wick, W., Gutmann, D. H. and Mawrin, C. (2015) 'The mTOR signaling pathway as a treatment target for intracranial neoplasms', *Neuro Oncol,* 17(2), pp. 189-199.

Paganoni, S. and Wills, A. M. (2013) 'High-fat and ketogenic diets in amyotrophic lateral sclerosis', *J Child Neurol,* 28(8), pp. 989-992.

Page, K. A., Williamson, A., Yu, N., McNay, E. C., Dzuira, J., McCrimmon, R. J. and Sherwin, R. S. (2009) 'Medium-chain fatty acids improve cognitive function in intensively treated type 1 diabetic patients and support in vitro synaptic transmission during acute hypoglycemia', *Diabetes,* 58(5), pp. 1237-44.

Palamiuc, L., Ravi, A. and Emerling, B. M. (2020) 'Phosphoinositides in autophagy: current roles and future insights', *FEBS J,* 287(2), pp. 222-238.

Pan, Y., Larson, B., Araujo, J. A., Lau, W., de Rivera, C., Santana, R., Gore, A. and Milgram, N. W. (2010) 'Dietary supplementation with medium-chain TAG has long-lasting cognition-enhancing effects in aged dogs', *Br J Nutr,* 103(12), pp. 1746-1754.

Paquette, M., El-Houjeiri, L. and Pause, A. (2018) 'mTOR Pathways in Cancer and Autophagy', *Cancers (Basel),* 10(1), pp. 18.

Park, S., Oh, T. S., Kim, S. and Kim, E. K. (2019) 'Palmitate-induced autophagy liberates monounsaturated fatty acids and increases Agrp expression in hypothalamic cells', *Anim Cells Syst (Seoul),* 23(6), pp. 384-391.

Parkhitko, A., Myachina, F., Morrison, T. A., Hindi, K. M., Auricchio, N., Karbowniczek, M., Wu, J. J., Finkel, T., Kwiatkowski, D. J., Yu, J. J. and Henske, E. P. (2011) 'Tumorigenesis in tuberous sclerosis complex is autophagy and p62/sequestosome 1 (SQSTM1)-dependent', *Proc Natl Acad Sci U S A,* 108(30), pp. 12455-60.

Parzych, K., Chinn, T. M., Chen, Z., Loaiza, S., Porsch, F., Valbuena, G. N., Kleijnen, M. F., Karadimitris, A., Gentleman, E., Keun, H. C. and Auner, H. W. (2015) 'Inadequate fine-tuning of protein synthesis and failure of amino acid homeostasis following inhibition of the ATPase VCP/p97', *Cell Death Dis,* 6, pp. e2031.

Pasca, L., Caraballo, R. H., De Giorgis, V., Reyes, J. G., Macasaet, J. A., Masnada, S., Armeno, M., Musicco, M., Tagliabue, A. and Veggiotti, P. (2018) 'Ketogenic diet use in children with intractable epilepsy secondary to malformations of cortical development: A two- centre experience', *Seizure,* 57, pp. 34-37.

Patel, S. and Latterich, M. (1998) 'The AAA team: related ATPases with diverse functions', *Trends Cell Biol,* 8(2), pp. 65-71.

Pauloin, A., Chat, S., Péchoux, C., Hue-Beauvais, C., Droineau, S., Galio, L., Devinoy, E. and Chanat, E. (2010) 'Oleate and linoleate stimulate degradation of β-casein in prolactin-treated HC11 mouse mammary epithelial cells', *Cell Tissue Res,* 340(1), pp. 91-102.

Perera, N. D. and Turner, B. J. (2016) 'AMPK signalling and defective energy metabolism in amyotrophic lateral sclerosis', *Neurochem Res,* 41(3), pp. 544-553.

Perry, C. J., Finch, P., Müller-Taubenberger, A., Leung, K.-Y., Warren, E. C., Damstra-Oddy, J., Sharma, D., Patra, P. H., Glyn, S., Boberska, J., Stewart, B., Baldwin, A., Piscitelli, F., Harvey, R. J., Harwood, A., Thompson, C., Claus, S. P., Greene, N. D. E., McNeish, A. J., Williams, C. M., Whalley, B. J. and Williams, R. S. B. (2020) 'A new mechanism for cannabidiol in regulating the one-carbon cycle and methionine levels in Dictyostelium and in mammalian epilepsy models', *Br J Pharmacol,* 177(4), pp. 912-928.

Petersen, K. F., Dufour, S., Befroy, D., Garcia, R. and Shulman, G. I. (2004) 'Impaired mitochondrial activity in the insulin-resistant offspring of patients with type 2 diabetes', *N Engl J Med,* 350(7), pp. 664-671.

Phillips, M. C. L., Murtagh, D. K. J., Gilbertson, L. J., Asztely, F. J. S. and Lynch, C. D. P. (2018) 'Low-fat versus ketogenic diet in Parkinson's disease: A pilot randomized controlled trial', *Mov Disord,* 33(8), pp. 1306-1314.

Poff, A. M., Ari, C., Seyfried, T. N. and D'Agostino, D. P. (2013) 'The Ketogenic Diet and Hyperbaric Oxygen Therapy Prolong Survival in Mice with Systemic Metastatic Cancer', *PLoS One,* 8(6), pp. e65522.

Ponting, C. P., Blake, D. J., Davies, K. E., Kendrick-Jones, J. and Winder, S. J. (1996) 'ZZ and TAZ: new putative zinc fingers in dystrophin and other proteins', *Trends Biochem Sci,* 21(1), pp. 11-13.

Raghu, P., Joseph, A., Krishnan, H., Singh, P. and Saha, S. (2019) 'Phosphoinositides: Regulators of Nervous System Function in Health and Disease', *Front Mol Neurosci,* 12, pp. 208.

Raper, K. B. (1935) 'Dictyostelium discoideum, a new species of slime mold from decaying forest leaves', *J Agric Res,* 50(2), pp. 135-147.

Reger, M. A., Henderson, S. T., Hale, C., Cholerton, B., Baker, L. D., Watson, G. S., Hyde, K., Chapman, D. and Craft, S. (2004) 'Effects of β-hydroxybutyrate on cognition in memory-impaired adults', *Neurobiol Aging,* 25(3), pp. 311-314.

Rezvani, K. (2016) 'UBXD Proteins: A Family of Proteins with Diverse Functions in Cancer', *Int J Mol Sci,* 17(10), pp. 1724.

Rial, S. A., Ravaut, G., Malaret, T. B., Bergeron, K.-F. and Mounier, C. (2018) 'Hexanoic, Octanoic and Decanoic Acids Promote Basal and Insulin-Induced Phosphorylation of the Akt-mTOR Axis and a Balanced Lipid Metabolism in the HepG2 Hepatoma Cell Line', *Molecules,* 23(9), pp. 2315.

Rijal, R., Arhzaouy, K., Strucksberg, K. H., Cross, M., Hofmann, A., Schroder, R., Clemen, C. S. and Eichinger, L. (2016) 'Mutant p97 exhibits species-specific changes of its ATPase activity and compromises the UBXD9-mediated monomerisation of p97 hexamers', *Eur J Cell Biol,* 95(6-7), pp. 195-207.

Roberts, M. N., Wallace, M. A., Tomilov, A. A., Zhou, Z., Marcotte, G. R., Tran, D., Perez, G., Gutierrez-Casado, E., Koike, S., Knotts, T. A., Imai, D. M., Griffey, S. M., Kim, K., Hagopian, K., McMackin, M. Z., Haj, F. G., Baar, K., Cortopassi, G. A., Ramsey, J. J. and Lopez-Dominguez, J. A. (2017) 'A Ketogenic Diet Extends Longevity and Healthspan in Adult Mice', *Cell Metab,* 26(3), pp. 539-546

Rogawski, M. A. and Hanada, T. (2013) 'Preclinical pharmacology of perampanel, a selective non-competitive AMPA receptor antagonist', *Acta Neurol Scand Suppl,* (197), pp. 19-24.

Roman, M. W. (2010) 'Axona (Accera, Inc): a new medical food therapy for persons with Alzheimer's disease', *Issues Ment Health Nurs,* 31(6), pp. 435-436.

Rong, Y., Liu, M., Ma, L., Du, W., Zhang, H., Tian, Y., Cao, Z., Li, Y., Ren, H., Zhang, C., Li, L., Chen, S., Xi, J. and Yu, L. (2012) 'Clathrin and phosphatidylinositol-4,5-bisphosphate regulate autophagic lysosome reformation', *Nat Cell Biol,* 14(9), pp. 924-934.

Rosel, D., Khurana, T., Majithia, A., Huang, X., Bhandari, R. and Kimmel, A. R. (2012) 'TOR complex 2 (TORC2) in Dictyostelium suppresses phagocytic nutrient capture independently of TORC1-mediated nutrient sensing', *J Cell Sci,* 125(Pt 1), pp. 37-48.

Rowland, L. P. and Shneider, N. A. (2001) 'Amyotrophic lateral sclerosis', *N Engl J Med,* 344(22), pp. 1688-700.

Rule, C. S., Patrick, M. and Sandkvist, M. (2016) 'Measuring In Vitro ATPase Activity for Enzymatic Characterization', *J Vis Exp,* 114, pp. 54305.

Sage-Schwaede, A., Engelstad, K., Salazar, R., Curcio, A., Khandji, A., Garvin, J. H., Jr. and De Vivo, D. C. (2019) 'Exploring mTOR inhibition as treatment for mitochondrial disease', *Ann Clin Transl Neurol,* 6(9), pp. 1877-1881.

Saha, S., Panigrahi, D. P., Patil, S. and Bhutia, S. K. (2018) 'Autophagy in health and disease: A comprehensive review', *Biomed Pharmacother,* 104, pp. 485-495.

Sansal, I. and Sellers, W. R. (2004) 'The biology and clinical relevance of the PTEN tumor suppressor pathway', *J Clin Oncol,* 22(14), pp. 2954-63.

Sauvat, A., Chen, G., Müller, K., Tong, M., Aprahamian, F., Durand, S., Cerrato, G., Bezu, L., Leduc, M., Franz, J., Rockenfeller, P., Sadoshima, J., Madeo, F., Kepp, O. and Kroemer, G. (2018) 'Trans-Fats Inhibit Autophagy Induced by Saturated Fatty Acids', *EBioMedicine,* 30, pp. 261-272.

Saxena, S., Roselli, F., Singh, K., Leptien, K., Julien, J.-P., Gros-Louis, F. and Caroni, P. (2013) 'Neuroprotection through excitability and mTOR required in ALS motoneurons to delay disease and extend survival', *Neuron,* 80(1), pp. 80-96.

Schaf, J., Damstra-Oddy, J. and Williams, R. S. B. (2019) 'Dictyostelium discoideum as a pharmacological model system to study the mechanisms of medicinal drugs and natural products', *Int J Dev Biol,* 63(8-9-10), pp. 541-550.

Scharfman, H. E. (2007) 'The neurobiology of epilepsy', *Curr Neurol Neurosci Rep,* 7(4), pp. 348-354.

Scheck, A. C., Abdelwahab, M. G., Fenton, K. E. and Stafford, P. (2012) 'The ketogenic diet for the treatment of glioma: Insights from genetic profiling', *Epilepsy Res,* 100(3), pp. 327-337.

Schenone, M., Dancik, V., Wagner, B. K. and Clemons, P. A. (2013) 'Target identification and mechanism of action in chemical biology and drug discovery', *Nat Chem Biol,* 9(4), pp. 232-240.

Schilde, C. and Schaap, P. (2013) 'The Amoebozoa', *Methods Mol Biol (Clifton, N.J.),* 983, pp. 1-15.

Schmauch, C., Claussner, S., Zoltzer, H. and Maniak, M. (2009) 'Targeting the actin-binding protein VASP to late endosomes induces the formation of giant actin aggregates', *Eur J Cell Biol,* 88(7), pp. 385-396.

Schuberth, C. and Buchberger, A. (2008) 'UBX domain proteins: major regulators of the AAA ATPase Cdc48/p97', *Cell Mol Life Sci,* 65(15), pp. 2360-71.

Sekine, R., Kawata, T. and Muramoto, T. (2018) 'CRISPR/Cas9 mediated targeting of multiple genes in Dictyostelium', *Sci Rep,* 8(1), pp. 8471.

Seyfried, T. N., Marsh, J., Shelton, L. M., Huysentruyt, L. C. and Mukherjee, P. (2012) 'Is the restricted ketogenic diet a viable alternative to the standard of care for managing malignant brain cancer?', *Epilepsy Res,* 100(3), pp. 310-326.

Sha, L. Z., Xing, X. L., Zhang, D., Yao, Y., Dou, W. C., Jin, L. R., Wu, L. W. and Xu, Q. (2012) 'Mapping the spatio-temporal pattern of the mammalian target of rapamycin (mTOR) activation in temporal lobe epilepsy', *PLoS One,* 7(6), pp. e39152.

Shaafi, S., Najmi, S., Aliasgharpour, H., Mahmoudi, J., Sadigh-Etemad, S., Farhoudi, M. and Baniasadi, N. (2016) 'The efficacy of the ketogenic diet on motor functions in Parkinson's disease: A rat model', *Iran J Neurol,* 15(2), pp. 63-69.

Shacka, J. J., Lu, J., Xie, Z.-L., Uchiyama, Y., Roth, K. A. and Zhang, J. (2007) 'Kainic acid induces early and transient autophagic stress in mouse hippocampus', *Neurosci Lett,* 414(1), pp. 57-60.

Sharma, D., Otto, G., Warren, E. C., Beesley, P., King, J. S. and Williams, R. S. B. (2019) 'Gamma secretase orthologs are required for lysosomal activity and autophagic degradation in Dictyostelium discoideum, independent of PSEN (presenilin) proteolytic function', *Autophagy,* 15(8), pp. 1407-1418.

Sills, M. A., Forsythe, W. I. and Haidukewych, D. (1986) 'Role of octanoic and decanoic acids in the control of seizures', *Arch Dis Child,* 61(12), pp. 1173-7.

Siman, R., Cocca, R. and Dong, Y. (2015) 'The mTOR Inhibitor Rapamycin Mitigates Perforant Pathway Neurodegeneration and Synapse Loss in a Mouse Model of Early-Stage Alzheimer-Type Tauopathy', *PLoS One,* 10(11), pp. e0142340.

Simeone, T. A., Simeone, K. A. and Rho, J. M. (2017) 'Ketone Bodies as Anti-Seizure Agents', *Neurochem Res,* 42(7), pp. 2011-2018.

Simonovitch, S., Schmukler, E., Bespalko, A., Iram, T., Frenkel, D., Holtzman, D. M., Masliah, E., Michaelson, D. M. and Pinkas-Kramarski, R. (2016) 'Impaired Autophagy in APOE4 Astrocytes', *J Alzheimers Dis,* 51(3), pp. 915-927.

Siva, N. (2006) 'Can ketogenic diet slow progression of ALS?', *Lancet Neurol,* 5(6), pp. 476.

Sosunov, A. A., Wu, X., McGovern, R. A., Coughlin, D. G., Mikell, C. B., Goodman, R. R. and McKhann, G. M., 2nd (2012) 'The mTOR pathway is activated in glial cells in mesial temporal sclerosis', *Epilepsia,* 53 Suppl 1, pp. 78-86.

Stach, L. and Freemont, P. S. (2017) 'The AAA+ ATPase p97, a cellular multitool', *Biochem J,* 474(17), pp. 2953-2976.

Stafford, P., Abdelwahab, M. G., Kim, D. Y., Preul, M. C., Rho, J. M. and Scheck, A. C. (2010) 'The ketogenic diet reverses gene expression patterns and reduces reactive oxygen species levels when used as an adjuvant therapy for glioma', *Nutr Metab (Lond),* 7, pp. 74.

Steinlein, O. K. (2008) 'Genetics and epilepsy', *Dialogues Clin Neurosci,* 10(1), pp. 29-38.

Sun, Y., Ren, M., Gao, G. Q., Gong, B., Xin, W., Guo, H., Zhang, X. J., Gao, L. and Zhao, J. J. (2008) 'Chronic palmitate exposure inhibits AMPKalpha and decreases glucose-stimulated insulin secretion from beta-cells: modulation by fenofibrate', *Acta Pharmacol Sin,* 29(4), pp. 443-50.

Svarrer, E. M. M., Fischer, C. M., Frederiksen, M. G., Born, A. P. and Hoei-Hansen, C. E. (2019) 'Everolimus as adjunctive treatment in tuberous sclerosis complex-associated epilepsy in children', *Dan Med J,* 66(12), pp. A5582.

Sveinbjornsdottir, S. (2016) 'The clinical symptoms of Parkinson's disease', *J Neurochem,* 139 Suppl 1, pp. 318-324.

Sweeney, P., Park, H., Baumann, M., Dunlop, J., Frydman, J., Kopito, R., McCampbell, A., Leblanc, G., Venkateswaran, A., Nurmi, A. and Hodgson, R. (2017) 'Protein misfolding in neurodegenerative diseases: implications and strategies', *Transl Neurodegener,* 6, pp. 6.

Takahashi, R. H., Nagao, T. and Gouras, G. K. (2017) 'Plaque formation and the intraneuronal accumulation of beta-amyloid in Alzheimer's disease', *Pathol Int,* 67(4), pp. 185-193.

Takeuchi, H., Noguchi, O., Sekine, S., Kobayashi, A. and Aoyama, T. (2006) 'Lower weight gain and higher expression and blood levels of adiponectin in rats fed medium-chain TAG compared with long-chain TAG', *Lipids,* 41(2), pp. 207-212.

Tan, H. W. S., Sim, A. Y. L. and Long, Y. C. (2017) 'Glutamine metabolism regulates autophagy-dependent mTORC1 reactivation during amino acid starvation', *Nat Commun,* 8(1), pp. 338.

Tan, K. N., Carrasco-Pozo, C., McDonald, T. S., Puchowicz, M. and Borges, K. (2017) 'Tridecanoin is anticonvulsant, antioxidant, and improves mitochondrial function', *J Cereb Blood Flow Metab,* 37(6), pp. 2035-2048.

Tan, X., Thapa, N., Liao, Y., Choi, S. and Anderson, R. A. (2016) 'PtdIns(4,5)P2 signaling regulates ATG14 and autophagy', *Proc Natl Acad Sci U S A,* 113(39), pp. 10896-901.

Tan-Shalaby, J. (2017) 'Ketogenic Diets and Cancer: Emerging Evidence', *Fed Pract,* 34(Suppl 1), pp. 37S-42S.

Taneike, M., Nishida, K., Omiya, S., Zarrinpashneh, E., Misaka, T., Kitazume-Taneike, R., Austin, R., Takaoka, M., Yamaguchi, O., Gambello, M. J., Shah, A. M. and Otsu, K. (2016) 'mTOR Hyperactivation by Ablation of Tuberous Sclerosis Complex 2 in the Mouse Heart Induces Cardiac Dysfunction with the Increased Number of Small Mitochondria Mediated through the Down-Regulation of Autophagy', *PloS one,* 11(3), pp. e0152628-e0152628.

Tang, W. K., Odzorig, T., Jin, W. and Xia, D. (2019) 'Structural Basis of p97 Inhibition by the Site-Selective Anticancer Compound CB-5083', *Mol Pharmacol,* 95(3), pp. 286-293.

Tang, W. K. and Xia, D. (2016) 'Mutations in the Human AAA(+) Chaperone p97 and Related Diseases', *Front Mol Biosci,* 3, pp. 79.

Tang, Z., Bereczki, E., Zhang, H., Wang, S., Li, C., Ji, X., Branca, R. M., Lehtiö, J., Guan, Z., Filipcik, P., Xu, S., Winblad, B. and Pei, J.-J. (2013) 'Mammalian target of rapamycin (mTor) mediates tau protein dyshomeostasis: implication for Alzheimer disease', *J Biol Chem,* 288(22), pp. 15556-15570.

Tariqul Islam, A. F. M., Scavello, M., Lotfi, P., Daniel, D., Haldeman, P. and Charest, P. G. (2019) 'Caffeine inhibits PI3K and mTORC2 in Dictyostelium and differentially affects multiple other cAMP chemoattractant signaling effectors', *Mol Cell Biochem,* 457(1), pp. 157-168.

Tatebe, H., Murayama, S., Yonekura, T., Hatano, T., Richter, D., Furuya, T., Kataoka, S., Furuita, K., Kojima, C. and Shiozaki, K. (2017) 'Substrate specificity of TOR complex 2 is determined by a ubiquitin-fold domain of the Sin1 subunit', *Elife,* 6, pp. e19594.

Taylor, M. K., Sullivan, D. K., Mahnken, J. D., Burns, J. M. and Swerdlow, R. H. (2018) 'Feasibility and efficacy data from a ketogenic diet intervention in Alzheimer's disease', *Alzheimers Dement (N Y),* 4, pp. 28-36.

Tee, A. R., Fingar, D. C., Manning, B. D., Kwiatkowski, D. J., Cantley, L. C. and Blenis, J. (2002) 'Tuberous sclerosis complex-1 and -2 gene products function together to inhibit mammalian target of rapamycin (mTOR)-mediated downstream signaling', *Proc Natl Acad Sci U S A,* 99(21), pp. 13571-6.

Thavendiranathan, P., Mendonca, A., Dell, C., Likhodii, S. S., Musa, K., Iracleous, C., Cunnane, S. C. and Burnham, W. M. (2000) 'The MCT Ketogenic Diet: Effects on Animal Seizure Models', *Exp Neurol,* 161(2), pp. 696-703.

Thio, L. L., Erbayat-Altay, E., Rensing, N. and Yamada, K. A. (2006) 'Leptin contributes to slower weight gain in juvenile rodents on a ketogenic diet', *Pediatr Res,* 60(4), pp. 413-417.

Thio, L. L., Wong, M. and Yamada, K. A. (2000) 'Ketone bodies do not directly alter excitatory or inhibitory hippocampal synaptic transmission', *Neurology,* 54(2), pp. 325-325.

Thomason, P. A., Traynor, D., Cavet, G., Chang, W. T., Harwood, A. J. and Kay, R. R. (1998) 'An intersection of the cAMP/PKA and two-component signal transduction systems in Dictyostelium', *EMBO J,* 17(10), pp. 2838-45.

Thorburn, A., Thamm, D. H. and Gustafson, D. L. (2014) 'Autophagy and cancer therapy', *Mol Pharmacol,* 85(6), pp. 830-838.

Tian, T., Li, X. and Zhang, J. (2019) 'mTOR Signaling in Cancer and mTOR Inhibitors in Solid Tumor Targeting Therapy', *Int J Mol Sci,* 20(3), pp. 755.

Tieu, K., Perier, C., Caspersen, C., Teismann, P., Wu, D. C., Yan, S. D., Naini, A., Vila, M., Jackson-Lewis, V., Ramasamy, R. and Przedborski, S. (2003) 'D-beta-hydroxybutyrate rescues mitochondrial respiration and mitigates features of Parkinson disease', *J Clin Invest,* 112(6), pp. 892-901.

Uddin, M. S., Stachowiak, A., Mamun, A. A., Tzvetkov, N. T., Takeda, S., Atanasov, A. G., Bergantin, L. B., Abdel-Daim, M. M. and Stankiewicz, A. M. (2018) 'Autophagy and

Alzheimer's Disease: From Molecular Mechanisms to Therapeutic Implications', *Front Aging Neurosci,* 10, pp. 04.

van Berkel, A. A., DM, I. J. and Verkuyl, J. M. (2018) 'Cognitive benefits of the ketogenic diet in patients with epilepsy: A systematic overview', *Epilepsy Behav,* 87, pp. 69-77.

Van der Auwera, I., Wera, S., Van Leuven, F. and Henderson, S. T. (2005) 'A ketogenic diet reduces amyloid beta 40 and 42 in a mouse model of Alzheimer's disease', *Nutr Metab (Lond),* 2, pp. 28.

Van Rooijen, L. A., Dompert, W. U., Horvath, E., Spencer, D. G., Jr. and Traber, J. (1986) 'Pharmacological aspects of the inositide response in the central nervous system: the muscarinic acetylcholine receptor', *Prog Brain Res,* 69, pp. 65-74.

Vandoorne, T., De Smet, S., Ramaekers, M., Van Thienen, R., De Bock, K., Clarke, K. and Hespel, P. (2017) 'Intake of a Ketone Ester Drink during Recovery from Exercise Promotes mTORC1 Signaling but Not Glycogen Resynthesis in Human Muscle', *Front Physiol,* 8, pp. 310.

Vanitallie, T. B., Nonas, C., Di Rocco, A., Boyar, K., Hyams, K. and Heymsfield, S. B. (2005) 'Treatment of Parkinson disease with diet-induced hyperketonemia: a feasibility study', *Neurology,* 64(4), pp. 728-730.

Varghese, S., Samuel, S., Varghese, E., Kubatka, P. and Büsselberg, D. (2019) 'High Glucose Represses the Anti-Proliferative and Pro-Apoptotic Effect of Metformin in Triple Negative Breast Cancer Cells', *Biomolecules,* 9(1), pp.16

Vaz, B., Halder, S. and Ramadan, K. (2013) 'Role of p97/VCP (Cdc48) in genome stability', *Front Genet,* 4, pp. 60.

Veech, R. L. (2004) 'The therapeutic implications of ketone bodies: the effects of ketone bodies in pathological conditions: ketosis, ketogenic diet, redox states, insulin resistance, and mitochondrial metabolism', *Prostaglandins Leukot Essent Fatty Acids,* 70(3), pp. 309-319.

Vekaria, P. H., Home, T., Weir, S., Schoenen, F. J. and Rao, R. (2016) 'Targeting p97 to Disrupt Protein Homeostasis in Cancer', *Front Oncol,* 6, pp. 181.

von Lohneysen, K., Pawolleck, N., Ruhling, H. and Maniak, M. (2003) 'A Dictyostelium long chain fatty acyl coenzyme A-synthetase mediates fatty acid retrieval from endosomes', *Eur J Cell Biol,* 82(10), pp. 505-514.

Waheed, A., Ludtmann, M. H., Pakes, N., Robery, S., Kuspa, A., Dinh, C., Baines, D., Williams, R. S. and Carew, M. A. (2014) 'Naringenin inhibits the growth of Dictyostelium and MDCK-derived cysts in a TRPP2 (polycystin-2)-dependent manner', *Br J Pharmacol,* 171(10), pp. 2659-70.

Wang, A., Mouser, J., Pitt, J., Promislow, D. and Kaeberlein, M. (2016) 'Rapamycin enhances survival in a Drosophila model of mitochondrial disease', *Oncotarget,* 7(49), pp. 80131-80139.

Wang, B. H., Hou, Q., Lu, Y. Q., Jia, M. M., Qiu, T., Wang, X. H., Zhang, Z. X. and Jiang, Y. (2018) 'Ketogenic diet attenuates neuronal injury via autophagy and mitochondrial pathways in pentylenetetrazol-kindled seizures', *Brain Res,* 1678, pp. 106-115.

Wang, D. and Mitchell, E. S. (2016) 'Cognition and Synaptic-Plasticity Related Changes in Aged Rats Supplemented with 8- and 10-Carbon Medium Chain Triglycerides', *PLoS One,* 11(8), pp. e0160159.

Wang, M. E., Singh, B. K., Hsu, M. C., Huang, C., Yen, P. M., Wu, L. S., Jong, D. S. and Chiu, C. H. (2017) 'Increasing Dietary Medium-Chain Fatty Acid Ratio Mitigates High-fat Diet-Induced Non-Alcoholic Steatohepatitis by Regulating Autophagy', *Sci Rep,* 7(1), pp. 13999.

Wang, P., Yang, L., Cheng, G., Yang, G., Xu, Z., You, F., Sun, Q., Lin, R., Fikrig, E. and Sutton, R. E. (2013) 'UBXN1 interferes with Rig-I-like receptor-mediated antiviral immune response by targeting MAVS', *Cell Rep,* 3(4), pp. 1057-70.

Warburg, O., Wind, F. and Negelein, E. (1927) 'The metabolism of tumors in the body', *J Gen Physiol,* 8(6), pp. 519-530.

Watts, G. D., Wymer, J., Kovach, M. J., Mehta, S. G., Mumm, S., Darvish, D., Pestronk, A., Whyte, M. P. and Kimonis, V. E. (2004) 'Inclusion body myopathy associated with Paget disease of bone and frontotemporal dementia is caused by mutant valosin-containing protein', *Nat Genet,* 36(4), pp. 377-381.

Weber, D. D., Aminzadeh-Gohari, S., Tulipan, J., Catalano, L., Feichtinger, R. G. and Kofler, B. (2020) 'Ketogenic diet in the treatment of cancer - Where do we stand?', *Mol Metab,* 33, pp. 102-121.

Welter, E., Thumm, M. and Krick, R. (2010) 'Quantification of nonselective bulk autophagy in S. cerevisiae using Pgk1-GFP', *Autophagy,* 6(6), pp. 794-797.

Wheless, J. W. (2008) 'History of the ketogenic diet', *Epilepsia,* 49 Suppl 8, pp. 3-5.

Wilder, R. M. 'The effects of ketonemia on the course of epilepsy'. *Mayo Clin Proc*, 307-308.

Williams, R. S., Boeckeler, K., Graf, R., Muller-Taubenberger, A., Li, Z., Isberg, R. R., Wessels, D., Soll, D. R., Alexander, H. and Alexander, S. (2006) 'Towards a molecular understanding of human diseases using Dictyostelium discoideum', *Trends Mol Med,* 12(9), pp. 415-24.

Williams, T. D. and Kay, R. R. (2018) 'The physiological regulation of macropinocytosis during Dictyostelium growth and development', *J Cell Sci,* 131(6).

Williams, T. D., Peak-Chew, S. Y., Paschke, P. and Kay, R. R. (2019) 'Akt and SGK protein kinases are required for efficient feeding by macropinocytosis', *J Cell Sci,* 132(2), pp. jcs213736.

Winklhofer, K. F. and Haass, C. (2010) 'Mitochondrial dysfunction in Parkinson's disease', *Biochim Biophys Acta,* 1802(1), pp. 29-44.

Wlaz, P., Socala, K., Nieoczym, D., Zarnowski, T., Zarnowska, I., Czuczwar, S. J. and Gasior, M. (2015) 'Acute anticonvulsant effects of capric acid in seizure tests in mice', *Prog Neuropsychopharmacol Biol Psychiatry,* 57, pp. 110-116.

Wong, M. (2013) 'Cleaning up epilepsy and neurodegeneration: the role of autophagy in epileptogenesis', *Epilepsy Curr,* 13(4), pp. 177-178.

Wong, M. (2019) 'The role of glia in epilepsy, intellectual disability, and other neurodevelopmental disorders in tuberous sclerosis complex', *J Neurodev Disord,* 11(1), pp. 30.

Xie, J., Wang, X. and Proud, C. G. (2016) 'mTOR inhibitors in cancer therapy', *F1000Res,* 5, pp. F1000 Faculty Rev-2078.

Xu, I. M., Lai, R. K., Lin, S. H., Tse, A. P., Chiu, D. K., Koh, H. Y., Law, C. T., Wong, C. M., Cai, Z., Wong, C. C. and Ng, I. O. (2016) 'Transketolase counteracts oxidative stress to drive cancer development', *Proc Natl Acad Sci U S A,* 113(6), pp. E725-734.

Xu, X., Muller-Taubenberger, A., Adley, K. E., Pawolleck, N., Lee, V. W., Wiedemann, C., Sihra, T. S., Maniak, M., Jin, T. and Williams, R. S. (2007) 'Attenuation of phospholipid signaling provides a novel mechanism for the action of valproic acid', *Eukaryot Cell,* 6(6), pp. 899-906.

Yamanaka, K., Sasagawa, Y. and Ogura, T. (2012) 'Recent advances in p97/VCP/Cdc48 cellular functions', *Biochim Biophys Acta,* 1823(1), pp. 130-137.

Yang, C., Lim, W., Bazer, F. W. and Song, G. (2018) 'Decanoic acid suppresses proliferation and invasiveness of human trophoblast cells by disrupting mitochondrial function', *Toxicol Appl Pharmacol,* 339, pp. 121-132.

Yang, X. and Cheng, B. (2010) 'Neuroprotective and anti-inflammatory activities of ketogenic diet on MPTP-induced neurotoxicity', *J Mol Neurosci,* 42(2), pp. 145-153.

Yasuda, M., Tanaka, Y., Kume, S., Morita, Y., Chin-Kanasaki, M., Araki, H., Isshiki, K., Araki, S., Koya, D., Haneda, M., Kashiwagi, A., Maegawa, H. and Uzu, T. (2014) 'Fatty acids are novel nutrient factors to regulate mTORC1 lysosomal localization and apoptosis in podocytes', *Biochim Biophys Acta,* 1842(7), pp. 1097-108.

Ye, F., Li, X.-J., Jiang, W.-L., Sun, H.-B. and Liu, J. (2015a) 'Efficacy of and patient compliance with a ketogenic diet in adults with intractable epilepsy: a meta-analysis', *J Clin Neurol,* 11(1), pp. 26-31.

Ye, J., Palm, W., Peng, M., King, B., Lindsten, T., Li, M. O., Koumenis, C. and Thompson, C. B. (2015b) 'GCN2 sustains mTORC1 suppression upon amino acid deprivation by inducing Sestrin2', *Genes Dev,* 29(22), pp. 2331-6.

Ye, Y., Meyer, H. H. and Rapoport, T. A. (2001) 'The AAA ATPase Cdc48/p97 and its partners transport proteins from the ER into the cytosol', *Nature,* 414(6864), pp. 652-656.

Yuen, A. W. and Sander, J. W. (2014) 'Rationale for using intermittent calorie restriction as a dietary treatment for drug resistant epilepsy', *Epilepsy Behav,* 33, pp. 110-114.

Zhao, W., Varghese, M., Vempati, P., Dzhun, A., Cheng, A., Wang, J., Lange, D., Bilski, A., Faravelli, I. and Pasinetti, G. M. (2012) 'Caprylic triglyceride as a novel therapeutic approach to effectively improve the performance and attenuate the symptoms due to the motor neuron loss in ALS disease', *PLoS One,* 7(11), pp. e49191.

Zhao, Z., Lange, D. J., Voustianiouk, A., MacGrogan, D., Ho, L., Suh, J., Humala, N., Thiyagarajan, M., Wang, J. and Pasinetti, G. M. (2006) 'A ketogenic diet as a potential novel therapeutic intervention in amyotrophic lateral sclerosis', *BMC Neurosci,* 7(1), pp. 29.

Zuccoli, G., Marcello, N., Pisanello, A., Servadei, F., Vaccaro, S., Mukherjee, P. and Seyfried, T. N. (2010) 'Metabolic management of glioblastoma multiforme using standard therapy together with a restricted ketogenic diet: Case Report', *Nutr Metab (Lond),* 7, pp. 33.

Appendix

Publications

1) **Warren EC**, Walker MC, and Williams RSB. (2018) 'All You Need Is Fats—for Seizure Control: Using Amoeba to Advance Epilepsy Research', *Fron Cell Neurosci,* 12, pp. 199.

2) Sharma D, Otto G, **Warren EC**, Beesley P, King JS, and Williams RSB. (2019) 'Gamma secretase orthologs are required for lysosomal activity and autophagic degradation in Dictyostelium discoideum, independent of PSEN (presenilin) proteolytic function', *Autophagy,* 15(8), pp. 1407-1418.

3) Perry CJ, Finch P, Muller-Taubenberger A, Leung KY, **Warren EC**, Damstra-Oddy J, Sharma D, Patra PH, Glyn S, Boberska J, et al. (2020) 'A new mechanism for cannabidiol in regulating the one-carbon cycle and methionine levels in Dictyostelium and in mammalian epilepsy models', *Br J Pharmacol,* 177(4), pp.912-928.

4) Perry CJ, **Warren EC**, Damstra-Oddy J, Storey C, Francione LM, Annesley SJ, Fisher PR, Müller-Taubenberger A, Williams RBS. (2020) 'A *Dictyostelium discoideum* mitochondrial fluorescent tagging vector that does not affect respiratory function', *Biochem Biophys Rep*, 22, pp. 100751**.**

5) **Warren EC**, Dooves S, Lugarà E, Damstra-Oddy J, Schaf J, Heine VM, Walker MC, Williams RSB (2020). 'Decanoic acid inhibits mTORC1 activity independent of glucose and insulin signaling'. *Proc Natl Acad Sci U S A,* 117(38), pp.23617.

frontiers in Cellular Neuroscience

MINI REVIEW
published: 11 July 2018
doi: 10.3389/fncel.2018.00199

All You Need Is Fats—for Seizure Control: Using Amoeba to Advance Epilepsy Research

Eleanor C. Warren[1], *Matthew C. Walker*[2] *and Robin S. B. Williams*[1]*

[1]Centre for Biomedical Sciences, School of Biological Sciences, Royal Holloway, University of London, Egham, United Kingdom, [2]Department of Clinical and Experimental Epilepsy, Institute of Neurology, University College London, London, United Kingdom

Since the original report of seizure control through starvation in the 1920s, the ketogenic diet has been considered an energy-related therapy. The diet was assumed to be functioning through the effect of reduced carbohydrate intake regulating cellular energy state, thus giving rise to seizure control. From this assumption, the generation of ketones during starvation provided an attractive mechanism for this altered energy state; however, many years of research has sought and largely failed to correlate seizure control and ketone levels. Due to this focus on ketones, few studies have examined a role for free fatty acids, as metabolic intermediates between the triglycerides provided in the diet and ketones, in seizure control. Recent discoveries have now suggested that the medium-chain fats, delivered through the medium-chain triglyceride (MCT) ketogenic diet, may provide a key therapeutic mechanism of the diet in seizure control. Here we describe an unusual pathway leading to this discovery, beginning with the use of a tractable non-animal model—*Dictyostelium*, through to the demonstration that medium-chain fats play a direct role in seizure control, and finally the identification of a mechanism of action of these fats and related congeners leading to reduced neural excitability and seizure control.

Keywords: decanoic acid, *Dictyostelium*, epilepsy, ketogenic diet, ketones, non-animal models

OPEN ACCESS

Edited by:
Carl E. Stafstrom, Johns Hopkins Medicine, United States

Reviewed by:
Hongyu Sun, Carleton University, Canada
Christina Gross, Cincinnati Children's Hospital Medical Center, United States
David Ruskin, Trinity College, United States

***Correspondence:**
Robin S. B. Williams
robin.williams@rhul.ac.uk

Received: *05 April 2018*
Accepted: *18 June 2018*
Published: *11 July 2018*

Citation:
Warren EC, Walker MC and Williams RSB (2018) All You Need Is Fats—for Seizure Control: Using Amoeba to Advance Epilepsy Research. Front. Cell. Neurosci. 12:199. doi: 10.3389/fncel.2018.00199

INTRODUCTION

Identifying the key therapeutic target of drugs is of great importance for biomedical science, since this enables rapid screening to develop improved compounds (Chang et al., 2012), and strengthens our understanding of the basic physiology underlying disease phenotypes. To confirm a mechanism of a compound it is essential to remove or silence the target gene, in order to demonstrate a subsequent loss of response to the compound. However, ablation of potential protein targets in mammalian models is problematic, due to the diploid nature of cells (making gene ablation difficult) and the complex array of related proteins often with overlapping catalytic function (e.g., in various isoforms or protein families). To address these issues, simple tractable models can be used, where gene ablation is rapid and efficient and a low complexity genome provides less redundancy in cellular function (Williams et al., 2002), to provide innovative proposals relating to drug targets that can then be validated in mammalian models. Using this approach, cells lacking the proposed target, having lost response to the compound, would confirm a direct activity for the compound against the target.

AN INNOVATIVE TRACTABLE MODEL SYSTEM PROVIDES THE GREAT LEAP FORWARD

The social amoeba, *Dictyostelium discoideum*, provides an unconventional system for molecular neuroscience research. This organism grows naturally in the leaf litter of temperate forests, existing in both single and multicellular stages (**Figure 1**; Williams et al., 2006). *Dictyostelium* belongs to the Phylum Amoebozoa, where phylogenetic analysis suggests that it diverged from the animal linage after plants, but before yeast and fungi. Despite the earlier divergence, many *Dictyostelium* proteins maintain more homology with human proteins than those of unicellular fungi (Eichinger et al., 2005). The haploid nature of *Dictyostelium* enables rapid gene ablation by insertional mutagenesis (Faix et al., 2013), and the production of mutant libraries (Kuspa, 2006). The model can then be used to investigate acute cellular effects, chronic growth effects and developmental effects of compounds to demonstrate cellular function (Robery et al., 2013; Waheed et al., 2014; Cocorocchio et al., 2016, 2018). It is important to verify that targets identified from mutant library screens are specific to the compound of interest and are not conferring broad resistance to a range of compounds. Furthermore, while *Dictyostelium* contains many proteins highly conserved with humans, some proteins are absent or have non-conserved functions. It is therefore not possible to make translatable findings about non-conserved proteins in *Dictyostelium*, and due to potential differences in cellular function of *Dictyostelium* and human proteins, it is imperative to validate findings in mammalian models.

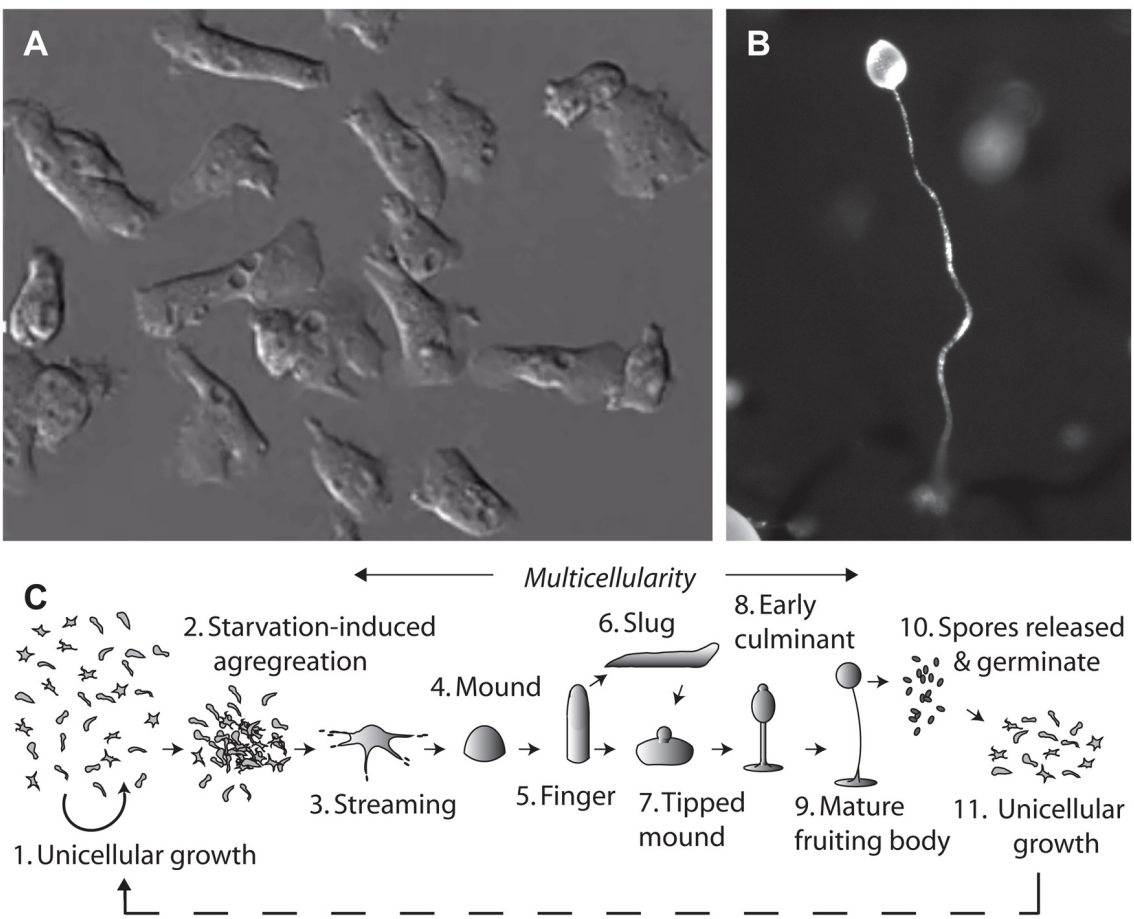

FIGURE 1 | The tractable model organism, *Dictyostelium discoideum* has been used to investigate cellular mechanisms of epilepsy treatments and medium-chain triglyceride (MCT) ketogenic diet associated fatty acids. The organism can exist in **(A)** a single cell stage, with cells around 10 μm in diameter. Due to their haploid nature, genes can be easily ablated and isogenic mutants analyzed in drug target studies. Under starvation conditions *Dictyostelium* cells form **(B)** multicellular fruiting bodies, of around 1–2 mm in height, comprising a spore head held above the substratum by dead vacuolated stalk cells, where the process of aggregation and development has been widely studied. **(C)** The life cycle of *Dictyostelium* begins with unicellular growth, where cells consume bacteria and divide by binary fission. Following the onset of starvation, cells enter a development cycle where cells aggregate and enter a multicellular stage through streaming to form a mound and then finger structure. Motile slugs are able to migrate towards favorable locations and develop, or development may progress straight into a tipped mound, early culminant and then mature fruiting body. Spores within the head of the fruiting body, which are able to survive unfavorable conditions, can then be released, and germinate to re-enable unicellular growth.

Dictyostelium has been used in a range of projects to investigate the cellular and molecular mechanisms of the widely used epilepsy treatment valproic acid (VPA). It has been used to demonstrate a common mechanism of action of bipolar disorder treatments through inositol depletion (Williams et al., 2002; Eickholt et al., 2005), and in a conserved mechanism to regulate the MAP Kinase pathway in neuroprotection (Boeckeler et al., 2006). *Dictyostelium* has been valuable in identifying an uptake mechanism for VPA via an orthologe of the mammalian solute carrier family 4 (SLC4) bicarbonate transporter (Terbach et al., 2011). Importantly, it was also the first system to suggest a mechanism of VPA in regulating phosphoinositide turnover in relation to seizure control (Xu et al., 2007; Chang et al., 2012), which was subsequently validated using *in vivo* mammalian models (Chang et al., 2014). *Dictyostelium* was also employed in the identification of a range of compounds related to VPA that showed efficacy in neuroprotection and seizure control in mammalian models (Chang et al., 2013, 2015, 2016). One of the compounds identified through this pathway, decanoic acid, provides a major constituent administered in the medium-chain triglyceride (MCT) ketogenic diet.

METABOLISM OF THE KETOGENIC DIET

Ketogenic diets have been used to treat seizures since the 1920s (Wheless, 2008). A modified form of the diet, the MCT ketogenic diet introduced in 1971 (Neal, 2017), provides a restricted carbohydrate diet, with around 45% of dietary energy delivered as fatty acids, an improvement on the classic ketogenic diet which makes up 60%–80% of dietary energy. This advancement of the diet allows more carbohydrate and protein to be consumed which improves tolerability and reduces gastrointestinal side effects. While the classic ketogenic diet relies on long-chain fatty acids, the MCT ketogenic diet provides energy in the form of medium-chain fatty acids within triglycerides, consisting of the eight-carbon octanoic acid and the ten-carbon decanoic acid in a 40–60 ratio (Sills et al., 1986; Liu, 2008). Cleavage of triglycerides in the gut leads to the release of free fatty acids, which are absorbed through the gut wall and are metabolized in the liver, where β-oxidation leads to the production of ketone bodies (β-hydroxybutyrate, acetoacetate and acetone) which are only seen in patients on a carbohydrate restricted (or starvation) diet (Haidukewych et al., 1982; Augustin et al., 2018). Although most fatty acids are degraded at this stage (Sills et al., 1986), some medium-chain fatty acids along with ketone bodies are distributed via the vascular system throughout the body and to the brain (Wlaź et al., 2012, 2015).

SEIZURE CONTROL ACTIVITIES OF KETONES AND FREE FATTY ACIDS

As the most investigated mechanism for ketogenic-diet dependent seizure control, many studies have focused on a role of ketones, with variable outcomes. In the absence of dietary carbohydrates, ketones are generated and distributed at concentrations of around 5 mM (Veech, 2004), where they are thought to provide an alternate energy source to glucose. In clinical studies, ketone levels poorly correlate with anticonvulsant efficacy, and this ketone-based mechanism has not been widely supported in animal model studies (Likhodii et al., 2000; Thavendiranathan et al., 2000). Ketones have been demonstrated to regulate GABA and glutamate levels (Lutas and Yellen, 2013), but do not directly act at GABA or glutamate receptors at physiological concentrations (Donevan et al., 2003), nor do they directly alter hippocampal synaptic transmission (Thio et al., 2000). Ketones do not directly block seizure activity in hippocampal slice models, induced to generate seizure-like activity with either pentelentetrazol (PTZ) or low magnesium conditions (Chang et al., 2016; **Figure 2**) or in 4-aminopyridine induced *ex vivo* seizure models (Thio et al., 2000). Although the role of ketones in the ketogenic diet is controversial there is evidence in support of their efficacy. Ketones have been demonstrated to regulate mitochondrial function (Kim et al., 2015b) implicating cellular energy regulation. The ketogenic diet has also been suggested to function in seizure control through increasing activation of adenosine A1 receptors in a mouse model, however it remains to be determined if this effect is through ketone-dependent or fat-dependent mechanisms (Masino et al., 2011). Ketones have also been demonstrated to regulate synaptic KATP channels, providing a further potential mechanism in seizure control (Kim et al., 2015a; Li et al., 2017). Finally, ketones may function through epigenetic effects, regulating gene expression in relation to seizure susceptibility (Kobow et al., 2013; Lusardi et al., 2015). A comprehensive evaluation of the current experimental understanding of the efficacy of ketone bodies is reviewed elsewhere (Simeone et al., 2018).

The first investigation of medium-chain fatty acids relating to seizure control arose through several papers identifying elevated levels of both octanoic acid and decanoic acid in the plasma of patients on the MCT ketogenic diet (Haidukewych et al., 1982; Sills et al., 1986; Dean et al., 1989). Here, decanoic acid was shown at an average level of 157 μM (87–552 μM) and octanoic acid at 310 μM (104–859 μM). The relatively low number of patients assessed in these studies (up to 12 individuals) prevented a correlation between fatty acid levels and seizure control. Subsequently, an *in vivo* study of straight-chain fatty acids identified strong effects of long-chain fatty acids (e.g., palmitic acid containing 16 carbons) in a picrotoxin-induced seizure model in mice, with small but significant effects of decanoic acid in delaying the onset of clonic convulsions without an effect on survival time. The opposite effect was found for decanoic acid with subcutaneous PTZ induced seizures, where survival time was increased but clonic convulsions were not delayed (Nakamura et al., 1990). The small magnitude of the effect and the large variability of response did not provide clear support for a mechanism of decanoic acid in seizure control. More compelling evidence was provided by later studies.

It has been identified in *Dictyostelium* that medium-chain fatty acids regulate phosphoinositide signaling, in a

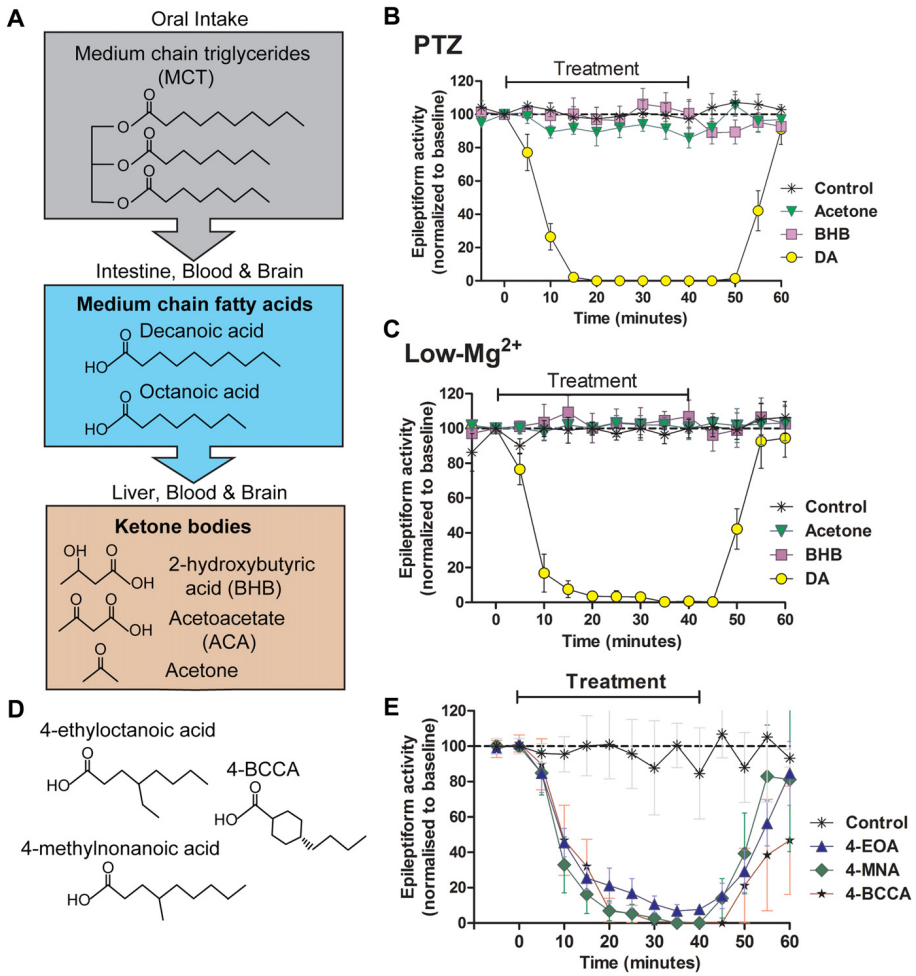

FIGURE 2 | Seizure-like activity in an *in vivo* model is acutely blocked by decanoic acid (DA) and related compounds but not by ketones. The MCT ketogenic diet involves the oral intake of **(A)** medium-chain triglycerides, which are converted into the fatty acids decanoic acid and octanoic acid in the intestine. These medium-chain fatty acids are then transferred to the liver, where they are further metabolized to form ketone bodies. Fatty acids and ketones are transported in the blood to the brain where they are able to cross the blood brain barrier. Following the identification of decanoic acid as a potential therapeutic effector of the MCT ketogenic diet in *Dictyostelium*, its seizure control activity was compared to that of the ketones acetone and β-hydroxybutyrate (BHB), with seizure-like activity induced in a rat hippocampal slice model following **(B)** pentelentetrazol (PTZ) or **(C)** low magnesium treatment. In both models, epileptiform activity was not blocked by either ketones (BHB or acetone) at high concentrations (10 mM). In contrast, the medium-chain fatty acid, DA rapidly blocked activity at 1 mM. Data is derived from Chang et al. (2016). **(D,E)** A range of novel compounds and related structures implicated through the use of *Dictyostelium* have also been demonstrated to show seizure control activity, where seizure-like activity is induced in a rat hippocampal slice model following PTZ treatment. Data derived from Chang et al. (2014).

similar but more potent mechanism to valproic acid (Chang et al., 2012). This study further demonstrated that some of these fatty acids blocked PTZ-induced epileptiform activity in an *in vitro* rat hippocampal model (**Figure 2**), again with a more potent effect than VPA. This anti-seizure effect occurred within 10 min of treatment, continually perfused with artificial CSF with high glucose content suggesting that the mechanism of seizure control was not dependent upon the build-up of ketones through the metabolism of fatty acids. Further studies identified that decanoic acid, and derivatives of octanoic acid show strong seizure control in a PTZ induced rat hippocampal model for seizure activity, again under perfusing CSF conditions unlikely to allow ketone generation (Chang et al., 2013). Medium-chain fatty acids were effective in a (perforant path stimulation-induced) status epilepticus *in vivo* model within 20 min of administration. A further study confirmed that branched-chain octanoic acid compounds showed strong structure-specific seizure control activity in a PTZ-induced hippocampal seizure model (Chang et al., 2015), in addition to blocking excitotoxic cell death induced by low magnesium levels in primary hippocampal neurons. Some related structures in this study showed potent control of epileptiform activity (**Figure 2**), without the negative side effect of VPA on histone deacetylase activity, widely associated with teratogenicity (Phiel et al., 2001; Gurvich et al., 2004).

Medium-chain fatty acids have also been demonstrated to function in seizure control in *in vivo* models. In one study in

mice, seizure thresholds were increased in the *in vivo* 6 Hz model using a single bolus oral gavage dose of decanoic acid at 10 mmol/kg and 30 mmol/kg, and a similar increase was observed in the MES threshold model at 50 mmol/kg p.o., although no effect was observed at decanoic acid doses up to 50 mmol/kg p.o following seizure induction with i.v. PTZ (Wlaź et al., 2015). This group also showed that octanoic acid provided as a single bolus oral gavage dose at 20 mmol/kg and 30 mmol/kg significantly increased the dose of i.v. PTZ required to induce myoclonic twitch, and at 30 mmol/kg increased the dose of i.v. PTZ required to induce clonus, and that octanoic acid increased the seizure threshold above 10 mmol/kg in the 6-Hz model (Wlaź et al., 2012). The comparative importance of octanoic acid and decanoic acid was also examined in a mouse study. In this study, dietary treatment of mice with medium-chain triglycerides comprising either only octanoic acid or only decanoic acid was followed by induction of seizure like activity using both the 6 Hz model and the latency to first generalized seizure in the flurothyl model (Tan et al., 2016). This study showed that decanoic acid (only) triglycerides increased seizure thresholds whereas octanoic acid (only) triglycerides did not, supporting a role for decanoic acid in seizure control. It is also worthwhile to note that, since this study showed both decanoic acid and octanoic acid triglycerides provided a common level of ketosis, but only the decanoic acid triglyceride diet provided seizure control, this decanoic acid-dependent seizure control activity is likely to be unrelated to the generation of ketones. These studies therefore support a mechanism of seizure control through decanoic acid.

In many of these *in vivo* studies, a therapeutic role of fatty acids has been overlooked due to the perceived role of ketones as the mechanism of the diet. Therefore, it remains to be determined if free fatty acids may provide the therapeutic effects underlying the diet. For example, in one study (Mantis et al., 2014), augmentation of the ketogenic diet with glucose increased seizure susceptibility in a genetic mouse model, however, this study did not describe ketone levels or free fatty acid levels following glucose administration, thus it remains unclear if the role of glucose in these experiments was due to effects on ketosis or free fatty acid levels.

The MCT ketogenic diet leads to elevated levels of both octanoic acid and decanoic acid in the plasma of patients (Haidukewych et al., 1982), however, most studies suggest that decanoic acid and not octanoic acid is responsible for the therapeutic benefits of the diet (Chang et al., 2013, 2016; Hughes et al., 2014; Tan et al., 2016). So is there a benefit of including octanoic acid in the diet? Interestingly, recent studies have shown that octanoic acid, rather than decanoic acid, is preferentially metabolized in neurones by β-oxidation (Khabbush et al., 2017). This finding suggests that the presence of octanoic acid in the MCT ketogenic diet may allow decanoic acid to escape catabolism, thus accumulating, to enhance a therapeutic mechanism in preventing seizures. This finding supports an earlier *in vivo* study in mice using the 6 Hz seizure test that demonstrates an increased anticonvulsant activity of combined octanoic acid and decanoic acid in comparison to decanoic acid alone (Wlaź et al., 2015).

CELLULAR TARGETS FOR FREE FATTY ACIDS IN RELATION TO NEURONAL EXCITABILITY AND SEIZURE CONTROL

Two molecular mechanisms for decanoic acid have recently been proposed. As an acute mechanism for seizure control, decanoic acid has been shown to reduce excitatory postsynaptic currents (EPSCs) using whole cell patch clamp recordings from CA1 pyramidal neurons, likely through inhibition of excitatory AMPA receptors (Chang et al., 2016). By expressing distinct AMPA receptor subunits (GluA1, GluA2 and GluA3) in a *Xenopus* oocyte model, a direct inhibitory effect of decanoic acid against AMPA receptors was then confirmed, enabling detailed electrophysiological characterization (Chang et al., 2016). These studies showed that decanoic acid directly inhibits the two most abundant AMPA receptors subunit combinations found in the brain, with greatest potency against GluA2/3 (IC_{50} = 0.52 mM) and GluA1/2 (IC_{50} = 1.16 mM). This inhibitory effect was voltage-dependent, where potency against GluA2/3 receptors at −80 mV (IC_{50} of 1.11 mM) was elevated following depolarization to −40 mV (to IC_{50} of 0.43 mM), suggesting stronger inhibitory activity during prolonged seizure activity.

As a chronic mechanism of action, decanoic acid has also recently been demonstrated to activate the nuclear receptor, PPARγ, leading to increased mitochondrial proliferation (Hughes et al., 2014). Using cultured neuronal cells, decanoic acid but not octanoic acid was shown to trigger mitochondrial biogenesis and elevate the activity of the mitochondrial complex I. Since seizure activity is commonly found arising from a wide array of mitochondrial mutations (Zsurka and Kunz, 2015), this mechanism of decanoic acid is thought to increase ATP availability and improve brain energy metabolism, leading to an increase in seizure threshold and to a reduction in seizure activity following long term treatment.

CONCLUSION

Understanding the mechanism of action of the MCT ketogenic diet in regulating neuronal excitability is critical for improving the treatment of patients with drug resistant epilepsy. Although the diet has clearly shown therapeutic relevance (Liu, 2008; Neal et al., 2008), evidence for a ketone-dependent mechanism in this function remains limited. The recent proposal for the efficacy of the diet is that fats provided through triglycerides in MCT supplements, in particular decanoic acid (Chang et al., 2013, 2015, 2016), may provide a direct function in blocking seizure activity independent of ketosis. Furthermore, novel compounds related to these medium-chain fatty acids may offer new approaches for seizure control without dietary restrictions (Chang et al., 2013). The studies outlined here provide a range of corollaries that should be considered in future experimentation. These include closely monitoring both

fatty acid and ketone levels at a cellular and *in vivo* level, in both research and clinical settings to clarify the distinct contributions of fatty acids and ketones in epilepsy treatment. Furthermore, further studies may investigate improvements in the diet by modifying the fatty acid content of the diet, in addition to exploring other secondary targets of these fatty acids, and in the development of related chemicals that may function through the same therapeutic mechanism but lack the rapid metabolic degradation shown for medium-chain fatty acids.

AUTHOR CONTRIBUTIONS

EW (RHUL), MW (UCL) and RW (RHUL) contributed equally to the manuscript.

FUNDING

This article was supported by an iCASE studentship (Biotechnology and Biological Sciences Research Council, BBSRC) to RW and MW.

REFERENCES

Augustin, K., Khabbush, A., Williams, S., Eaton, S., Orford, M., Cross, J. H., et al. (2018). Mechanisms of action for the medium-chain triglyceride ketogenic diet in neurological and metabolic disorders. *Lancet Neurol.* 17, 84–93. doi: 10.1016/S1474-4422(17)30408-8

Boeckeler, K., Adley, K., Xu, X., Jenkins, A., Jin, T., and Williams, R. S. (2006). The neuroprotective agent, valproic acid, regulates the mitogen-activated protein kinase pathway through modulation of protein kinase A signalling in *Dictyostelium discoideum*. *Eur. J. Cell Biol.* 85, 1047–1057. doi: 10.1016/j.ejcb.2006.04.013

Chang, P., Augustin, K., Boddum, K., Williams, S., Sun, M., Terschak, J. A., et al. (2016). Seizure control by decanoic acid through direct AMPA receptor inhibition. *Brain* 139, 431–443. doi: 10.1093/brain/awv325

Chang, P., Orabi, B., Deranieh, R. M., Dham, M., Hoeller, O., Shimshoni, J. A., et al. (2012). The antiepileptic drug valproic acid and other medium-chain fatty acids acutely reduce phosphoinositide levels independently of inositol in Dictyostelium. *Dis. Model. Mech.* 5, 115–124. doi: 10.1242/dmm.008029

Chang, P., Terbach, N., Plant, N., Chen, P. E., Walker, M. C., and Williams, R. S. (2013). Seizure control by ketogenic diet-associated medium chain fatty acids. *Neuropharmacology* 69, 105–114. doi: 10.1016/j.neuropharm.2012.11.004

Chang, P., Walker, M. C., and Williams, R. S. (2014). Seizure-induced reduction in PIP3 levels contributes to seizure-activity and is rescued by valproic acid. *Neurobiol. Dis.* 62, 296–306. doi: 10.1016/j.nbd.2013.10.017

Chang, P., Zuckermann, A. M., Williams, S., Close, A. J., Cano-Jaimez, M., McEvoy, J. P., et al. (2015). Seizure control by derivatives of medium chain fatty acids associated with the ketogenic diet show novel branching-point structure for enhanced potency. *J. Pharmacol. Exp. Ther* 352, 43–52. doi: 10.1124/jpet.114.218768

Cocorocchio, M., Baldwin, A. J., Stewart, B., Kim, L., Harwood, A. J., Thompson, C. R. L., et al. (2018). Curcumin and derivatives function through protein phosphatase 2A and presenilin orthologues in *Dictyostelium discoideum*. *Dis. Model. Mech.* 11:dmm032375. doi: 10.1242/dmm.032375

Cocorocchio, M., Ives, R., Clapham, D., Andrews, P. L., and Williams, R. S. (2016). Bitter tastant responses in the amoeba Dictyostelium correlate with rat and human taste assays. *ALTEX* 33, 225–236. doi: 10.14573/altex.1509011

Dean, H. G., Bonser, J. C., and Gent, J. P. (1989). HPLC analysis of brain and plasma for octanoic and decanoic acids. *Clin. Chem.* 35, 1945–1948.

Donevan, S. D., White, H. S., Anderson, G. D., and Rho, J. M. (2003). Voltage-dependent block of N-methyl-D-aspartate receptors by the novel anticonvulsant dibenzylamine, a bioactive constituent of L-(+)-β-hydroxybutyrate. *Epilepsia* 44, 1274–1279. doi: 10.1046/j.1528-1157.2003.07203.x

Eichinger, L., Pachebat, J. A., Glöckner, G., Rajandream, M. A., Sucgang, R., Berriman, M., et al. (2005). The genome of the social amoeba *Dictyostelium discoideum*. *Nature* 435, 43–57. doi: 10.1038/nature03481

Eickholt, B. J., Towers, G., Ryves, W. J., Eikel, D., Adley, K., Ylinen, L., et al. (2005). Effects of valproic acid derivatives on inositol trisphosphate depletion, teratogenicity, GSK-3β inhibition, and viral replication—screening approach for new bipolar disorder drugs based on the valproic acid core structure. *Mol. Pharmacol* 67, 1423–1433. doi: 10.1124/mol.104.009308

Faix, J., Linkner, J., Nordholz, B., Platt, J. L., Liao, X. H., and Kimmel, A. R. (2013). The application of the Cre-loxP system for generating multiple knock-out and knock-in targeted loci. *Methods Mol. Biol.* 983, 249–267. doi: 10.1007/978-1-62703-302-2_13

Gurvich, N., Tsygankova, O. M., Meinkoth, J. L., and Klein, P. S. (2004). Histone deacetylase is a target of valproic acid-mediated cellular differentiation. *Cancer Res.* 64, 1079–1086. doi: 10.1158/0008-5472.can-03-0799

Haidukewych, D., Forsythe, W. I., and Sills, M. (1982). Monitoring octanoic and decanoic acids in plasma from children with intractable epilepsy treated with medium-chain triglyceride diet. *Clin. Chem.* 28, 642–645.

Hughes, S. D., Kanabus, M., Anderson, G., Hargreaves, I. P., Rutherford, T., O'Donnell, M., et al. (2014). The ketogenic diet component decanoic acid increases mitochondrial citrate synthase and complex I activity in neuronal cells. *J. Neurochem.* 129, 426–433. doi: 10.1111/jnc.12646

Khabbush, A., Orford, M., Tsai, Y. C., Rutherford, T., O'Donnell, M., Eaton, S., et al. (2017). Neuronal decanoic acid oxidation is markedly lower than that of octanoic acid: a mechanistic insight into the medium-chain triglyceride ketogenic diet. *Epilepsia* 58, 1423–1429. doi: 10.1111/epi.13833

Kim, D. Y., Abdelwahab, M. G., Lee, S. H., O'Neill, D., Thompson, R. J., Duff, H. J., et al. (2015a). Ketones prevent oxidative impairment of hippocampal synaptic integrity through KATP channels. *PLoS One* 10:e0119316. doi: 10.1371/journal.pone.0119316

Kim, D. Y., Simeone, K. A., Simeone, T. A., Pandya, J. D., Wilke, J. C., Ahn, Y., et al. (2015b). Ketone bodies mediate antiseizure effects through mitochondrial permeability transition. *Ann. Neurol.* 78, 77–87. doi: 10.1002/ana.24424

Kobow, K., Kaspi, A., Harikrishnan, K. N., Kiese, K., Ziemann, M., Khurana, I., et al. (2013). Deep sequencing reveals increased DNA methylation in chronic rat epilepsy. *Acta Neuropathol.* 126, 741–756. doi: 10.1007/s00401-013-1168-8

Kuspa, A. (2006). Restriction enzyme-mediated integration (REMI) mutagenesis. *Methods Mol. Biol.* 346, 201–209. doi: 10.1385/1-59745-144-4:201

Li, J., O'Leary, E. I., and Tanner, G. R. (2017). The ketogenic diet metabolite β-hydroxybutyrate (β-HB) reduces incidence of seizure-like activity (SLA) in a K_{atp}- and $GABA_b$-dependent manner in a whole-animal *Drosophila melanogaster* model. *Epilepsy Res.* 133, 6–9. doi: 10.1016/j.eplepsyres.2017.04.003

Likhodii, S. S., Musa, K., Mendonca, A., Dell, C., Burnham, W. M., and Cunnane, S. C.. (2000). Dietary fat, ketosis, and seizure resistance in rats on the ketogenic diet. *Epilepsia* 41, 1400–1410. doi: 10.1111/j.1528-1157.2000.tb00115.x

Liu, Y. M. (2008). Medium-chain triglyceride (MCT) ketogenic therapy. *Epilepsia* 49, 33–36. doi: 10.1111/j.1528-1167.2008.01830.x

Lusardi, T. A., Akula, K. K., Coffman, S. Q., Ruskin, D. N., Masino, S. A., and Boison, D. (2015). Ketogenic diet prevents epileptogenesis and disease progression in adult mice and rats. *Neuropharmacology* 99, 500–509. doi: 10.1016/j.neuropharm.2015.08.007

Lutas, A., and Yellen, G. (2013). The ketogenic diet: metabolic influences on brain excitability and epilepsy. *Trends Neurosci.* 36, 32–40. doi: 10.1016/j.tins.2012.11.005

Mantis, J. G., Meidenbauer, J. J., Zimick, N. C., Centeno, N. A., and Seyfried, T. N. (2014). Glucose reduces the anticonvulsant effects of the ketogenic diet in EL mice. *Epilepsy Res.* 108, 1137–1144. doi: 10.1016/j.eplepsyres.2014.05.010

Masino, S. A., Li, T., Theofilas, P., Sandau, U. S., Ruskin, D. N., Fredholm, B. B., et al. (2011). A ketogenic diet suppresses seizures in mice through adenosine A_1 receptors. *J. Clin. Invest.* 121, 2679–2683. doi: 10.1172/JCI57813

Nakamura, J., Miwa, T., Sasaki, H., Shibasaki, J., and Kaneto, H. (1990). Effect of straight chain fatty acids on seizures induced by picrotoxin and pentylenetetrazole in mice. *J. Pharmacobiodyn.* 13, 76–81. doi: 10.1248/bpb1978.13.76

Neal, E. (2017). ""Alternative" ketogenic diets," in *Ketogenic Diet and Metabolic Therapies*, ed. S. A. Masino (New York, NY: Oxford University Press), 40–49.

Neal, E. G., Chaffe, H., Schwartz, R. H., Lawson, M. S., Edwards, N., Fitzsimmons, G., et al. (2008). The ketogenic diet for the treatment of childhood epilepsy: a randomised controlled trial. *Lancet Neurol.* 7, 500–506. doi: 10.1016/s1474-4422(08)70092-9

Phiel, C. J., Zhang, F., Huang, E. Y., Guenther, M. G., Lazar, M. A., and Klein, P. S. (2001). Histone deacetylase is a direct target of valproic acid, a potent anticonvulsant, mood stabilizer, and teratogen. *J. Biol. Chem.* 276, 36734–36741. doi: 10.1074/jbc.M101287200

Robery, S., Tyson, R., Dinh, C., Kuspa, A., Noegel, A. A., Bretschneider, T., et al. (2013). A novel human receptor involved in bitter tastant detection identified using *Dictyostelium discoideum*. *J. Cell Sci.* 126, 5465–5476. doi: 10.1242/jcs.136440

Sills, M. A., Forsythe, W. I., and Haidukewych, D. (1986). Role of octanoic and decanoic acids in the control of seizures. *Arch. Dis. Child.* 61, 1173–1177. doi: 10.1136/adc.61.12.1173

Simeone, T. A., Simeone, K. A., Stafstrom, C. E., and Rho, J. M. (2018). Do ketone bodies mediate the anti-seizure effects of the ketogenic diet? *Neuropharmacology* 133, 233–241. doi: 10.1016/j.neuropharm.2018.01.011

Tan, K. N., Carrasco-Pozo, C., McDonald, T. S., Puchowicz, M., and Borges, K. (2016). Tridecanoin is anticonvulsant, antioxidant, and improves mitochondrial function. *J. Cereb. Blood Flow Metab.* 37, 2035–2048. doi: 10.1177/0271678x16659498

Terbach, N., Shah, R., Kelemen, R., Klein, P. S., Gordienko, D., Brown, N. A., et al. (2011). Identifying an uptake mechanism for the antiepileptic and bipolar disorder treatment valproic acid using the simple biomedical model Dictyostelium. *J. Cell Sci.* 124, 2267–2276. doi: 10.1242/jcs.084285

Thavendiranathan, P., Mendonca, A., Dell, C., Likhodii, S. S., Musa, K., Iracleous, C., et al. (2000). The MCT ketogenic diet: effects on animal seizure models. *Exp. Neurol.* 161, 696–703. doi: 10.1006/exnr.1999.7298

Thio, L. L., Wong, M., and Yamada, K. A. (2000). Ketone bodies do not directly alter excitatory or inhibitory hippocampal synaptic transmission. *Neurology* 54, 325–331. doi: 10.1212/WNL.54.2.325

Veech, R. L. (2004). The therapeutic implications of ketone bodies: the effects of ketone bodies in pathological conditions: ketosis, ketogenic diet, redox states, insulin resistance, and mitochondrial metabolism. *Prostaglandins Leukot. Essent Fatty Acids* 70, 309–319. doi: 10.1016/j.plefa.2003.09.007

Waheed, A., Ludtmann, M. H., Pakes, N., Robery, S., Kuspa, A., Dinh, C., et al. (2014). Naringenin inhibits the growth of Dictyostelium and MDCK-derived cysts in a TRPP2 (polycystin-2)-dependent manner. *Br. J. Pharmacol.* 171, 2659–2670. doi: 10.1111/bph.12443

Wheless, J. W. (2008). History of the ketogenic diet. *Epilepsia* 49, 3–5. doi: 10.1111/j.1528-1167.2008.01821.x

Williams, R. S. B., Boeckeler, K., Gräf, R., Müller-Taubenberger, A., Li, Z., Isberg, R. R., et al. (2006). Towards a molecular understanding of human diseases using *Dictyostelium discoideum*. *Trends Mol. Med.* 12, 415–424. doi: 10.1016/j.molmed.2006.07.003

Williams, R. S. B., Cheng, L., Mudge, A. W., and Harwood, A. J. (2002). A common mechanism of action for three mood-stabilizing drugs. *Nature* 417, 292–295. doi: 10.1038/417292a

Wlaź, P., Socała, K., Nieoczym, D., Łuszczki, J. J., Żarnowska, I., Żarnowski, T., et al. (2012). Anticonvulsant profile of caprylic acid, a main constituent of the medium-chain triglyceride (MCT) ketogenic diet, in mice. *Neuropharmacology* 62, 1882–1889. doi: 10.1016/j.neuropharm.2011.12.015

Wlaź, P., Socała, K., Nieoczym, D., Żarnowski, T., Żarnowska, I., Czuczwar, S. J., et al. (2015). Acute anticonvulsant effects of capric acid in seizure tests in mice. *Prog. Neuropsychopharmacol. Biol. Psychiatry* 57, 110–116. doi: 10.1016/j.pnpbp.2014.10.013

Xu, X., Müller-Taubenberger, A., Adley, K. E., Pawolleck, N., Lee, V. W., Wiedemann, C., et al. (2007). Attenuation of phospholipid signaling provides a novel mechanism for the action of valproic acid. *Eukaryot. Cell* 6, 899–906. doi: 10.1128/ec.00104-06

Zsurka, G., and Kunz, W. S. (2015). Mitochondrial dysfunction and seizures: the neuronal energy crisis. *Lancet Neurol.* 14, 956–966. doi: 10.1016/s1474-4422(15)00148-9

Conflict of Interest Statement: The authors declare that the research was conducted in the absence of any commercial or financial relationships that could be construed as a potential conflict of interest.

AUTOPHAGY
2019, VOL. 15, NO. 8, 1407–1418
https://doi.org/10.1080/15548627.2019.1586245

Taylor & Francis
Taylor & Francis Group

RESEARCH PAPER

OPEN ACCESS Check for updates

Gamma secretase orthologs are required for lysosomal activity and autophagic degradation in *Dictyostelium discoideum*, independent of PSEN (presenilin) proteolytic function

Devdutt Sharma[a], Grant Otto [a], Eleanor C. Warren[a], Philip Beesley[a], Jason S. King [b], and Robin S. B. Williams [a]

[a]School of Biological Sciences, Royal Holloway, University of London, Egham, UK; [b]Department of Biomedical Sciences, University of Sheffield, Sheffield, UK

ABSTRACT

Mutations in the γ-secretase complex are strongly associated with familial Alzheimer disease. Both proteolytic and non-proteolytic functions for the γ-secretase complex have been previously described in mammalian model organisms, but their relative contributions to disease pathology remain unclear. Here, we dissect the roles of orthologs of the γ-secretase components in the model system *Dictyostelium*, focusing on endocytosis, lysosomal activity and autophagy. In this model, we show that the orthologs of PSEN (psenA and psenB), Ncstn (nicastrin) and Aph-1 (gamma-secretase subunit Aph-1), are necessary for optimal fluid-phase uptake by macropinocytosis and in multicellular development under basic pH conditions. Disruption of either psenA/B or Aph-1 proteins also leads to disrupted phagosomal proteolysis as well as decreased autophagosomal acidification and autophagic flux. This indicates a general defect in lysosomal trafficking and degradation, which we show leads to the accumulation of ubiquitinated protein aggregates in cells lacking psenA/B and Aph-1 proteins. Importantly, we find that all the endocytic defects observed in *Dictyostelium* PSEN ortholog mutants can be fully rescued by proteolytically inactive *Dictyostelium* psenB and human PSEN1 proteins. Our data therefore demonstrates an evolutionarily conserved non-proteolytic role for presenilin, and γ-secretase component orthologs, in maintaining *Dictyostelium* lysosomal trafficking and autophagy.

Abbreviations: Atg8: autophagy protein 8a; Aph-1: gamma-secretase subunit Aph-1; crtA: calreticulin; ER: endoplasmic reticulum; GFP: green fluorescent protein; GSK3B: glycogen synthase kinase 3 beta; Ncstn: nicastrin; PSEN1: presenilin 1; psenA and psenB: *Dictyostelium* presenilin A and B; TRITC; tetramethylrhodamine isothiocyanate.

ARTICLE HISTORY
Received 2 November 2017
Revised 1 February 2019
Accepted 19 February 2019

KEYWORDS
Alzheimer disease; autophagy; development; *Dictyostelium*; γ-secretase; lysosomal trafficking; presenilin

Introduction

Many studies have sought to explore a role for the γ-secretase complex (and PSEN [presenilin] proteins) in the pathology of Alzheimer disease [1–4]. One function of the mammalian complex (consisting of PSEN1 [presenilin 1], APH1 [aph-1 homolog, gamma-secretase subunit], NCSTN [nicastrin] and PSENEN/PEN2 [presenilin enhancer, gamma-secretase subunit]) or PSEN1 proteins alone is to regulate endocytosis, lysosomal acidification, and autophagy [5–7]. This role has been implicated in disease pathology, since mutations in PSEN1 proteins associated with familial Alzheimer disease result in elevated lysosomal pH, and aberrant autophagy in mouse models [7–9]. Dysfunctional endosomal-lysosomal and autophagic pathways have also been implicated in the pathogenesis of several other neurodegenerative disorders, including amyotrophic lateral sclerosis (ALS) and Parkinson disease [10–13]. These studies have given rise to a theory of neurodegenerative disease pathology relating to reduced protein clearance [13–15].

The role of the γ-secretase complex is primarily thought to be through its proteolytic activity and cleavage of target proteins [2–4,16]. Here, PSEN proteins contain two key aspartic acid residues necessary for the proteolytic activity of the complex in cleaving a range of substrates including the amyloid-β and NOTCH proteins [17]. However, the γ-secretase complex has also been proposed to act through non-proteolytic scaffolding functions in a variety of model organisms [18–24]. In mammalian models, these functions include stabilizing the binding of CTNNB1 and GSK3β, where Alzheimer disease causing mutations result in reduced stability of CTNNB1 [18,19,25,26], and in endoplasmic reticulum (ER) calcium regulation [27,28]. In *D. melanogaster*, presenilin proteins have been found to modulate the levels of CREBBP (cyclic-AMP Response Element Binding protein) independently of proteolytic activity [29]. A similar non-proteolytic function for presenilin proteins or the γ-secretase complex has also been proposed in both *C. elegans* [30] and the moss *P. patens* [20]. However, although protease-independent functions of the γ-secretase complex have been observed in evolutionarily diverse species, our understanding of the mechanistic significance of these functions and relevance to Alzheimer pathology remains limited.

CONTACT Robin S. B. Williams robin.williams@rhul.ac.uk Centre for Biomedical Sciences, School of Biological Sciences, Royal Holloway University of London, Egham, TW20 0EX, UK

Supplemental data for this article can be accessed here.

To better understand the role of the γ-secretase complex, several studies have employed the social amoeba *Dictyostelium discoideum* [22,31]. *Dictyostelium* contains orthologs of the core components of the complex including two PSEN (presenilin) proteins (psenA and B), Aph-1 and Ncstn [22,23,31]. In *Dictyostelium*, the complex components play roles in multicellular development, in cyclic AMP signalling and in intracellular calcium release [22] as well as in phagocytosis [31]. Although proteolytic targets(s) for the complex in *Dictyostelium* have not been defined, *Dictyostelium* psenA and psenB proteins show proteolytic activity in a Notch reporter assay [22]. In multicellular development, psenB plays a non-proteolytic (scaffold) function, since removal of the two key catalytic aspartic acids (348 and 394) does not block the formation of mature fruiting bodies. Furthermore, the roles of psenA and psenB proteins in *Dictyostelium* development are also complemented using the proteolytically inactive human PSEN1 protein, lacking the key catalytic aspartic acids 257 and 385 [22]. These studies have demonstrated the relevance of using *Dictyostelium* to examine the cellular and developmental roles of presenilin proteins and orthologs of other γ-secretase components.

Dictyostelium has been widely used as a model organism in a range of cell and molecular studies, often enabling translation to mammalian models [32,33]. It has been used in the study of endosomal- and autophagy-lysosomal systems and related pathways where WASH is required for lysosomal recycling and both autophagic and phagocytic digestion [34]; mucolipin is required for lysosomal exocytosis [35]; myosin I is involved in membrane recycling from early endosomes [36] as well as many other discoveries [37–41]. Here we advance our understanding of the role of the *Dictyostelium* orthologs of γ-secretase complex components in endocytosis and autophagy by demonstrating that these components are required for the efficient activity of these processes. We further show that regulation of endocytosis and autophagy activities occurs through a proteolysis-independent mechanism, where these activities are conserved in the human PSEN1 protein. We also show that loss of these proteolysis-independent functions leads to an increase in large poly-ubiquitinated autophagosome-like vesicles, demonstrating an ancient and conserved non-proteolytic role of presenilin and orthologs of other components of the γ-secretase complex in proteostasis.

Results

Dictyostelium *mutants lacking γ-secretase component orthologs are unable to endocytose efficiently*

Since the γ-secretase complex has been implicated in endocytosis in mammalian model organisms [5,6,42], we initially set out to investigate if orthologous components of this complex also play roles in *Dictyostelium* macropinocytosis – the dominant form of endocytosis and fluid-phase uptake in this organism. In wild-type cells, uptake of TRITC-Dextran was linear for 60 minutes and was therefore used to determine the rate of macropinocytosis (Figure 1(a,b), Figure S1). Macropinocytosis in the absence of the γ-secretase complex orthologs was analysed through the use of stable isogenic cells lacking Ncstn [22], Aph-1 or both presenilin proteins (psenA/B [22]). We observed that loss of all three γ-secretase component orthologs caused a 40–50% decrease in fluid-phase uptake (Figure 1(c)), and this effect was not due to altered exocytosis (Figure S2). These data suggest a role for the three γ-secretase component orthologs in regulating endocytosis in *Dictyostelium*.

A previous study has suggested that the *Dictyostelium* γ-secretase complex shows both proteolytic and non-proteolytic functions of psenB [22], thus we sought to distinguish these roles in macropinocytosis. In these experiments, the *Dictyostelium* psenB-GFP protein was expressed in PsenA$^-$/B$^-$ cells, in addition to a mutated version of the protein lacking the two key aspartic acid residues necessary for proteolytic activity (psenBDD-GFP) [22]. In both cases, wild type macropinocytosis levels were restored (Figure 1(b,c)), suggesting that this role of psenB is through a non-proteolytic function. Furthermore, expression of the wild type (PSEN1-GFP) and proteolytically inactive (PSEN1DD-GFP) human PSEN1 protein also rescued the macropinocytosis defect in PsenA$^-$/B$^-$ cells (Figure 1(b,c), Figure S1) demonstrating the evolutionary conservation of this function, although expression of proteolytically active PSEN1-GFP did not restore the macropinocytosis defect in cells lacking Ncstn (Figure S3). These data suggest that, in *Dictyostelium*, macropinocytosis was dependent upon Aph-1, Ncstn and a non-proteolytic function of psenB.

Dictyostelium *mutants lacking γ-secretase component orthologs show pH-dependent development*

Since nutrients ingested in macropinosomes are degraded by fusion with lysosomes [43], and deficiencies in acidification decrease endocytic rate [44] we next investigated a role for orthologs of γ-secretase complex components in lysosomal acidification. For these experiments, we initially employed a qualitative development assay, where *Dictyostelium* mutants with severe acidification defects are unable to form mature fruiting bodies in neutral pH conditions [45]. We therefore tested the ability of mutants lacking orthologs of γ-secretase complex components to develop over 24 hours under neutral (pH 7) and basic conditions (pH 9). In both conditions, wild type cells were able to develop into mature fruiting bodies consisting of a basal disk, a stalk, and a spore head. However, while Ncstn$^-$ and Aph-1$^-$ cells were able to form fruiting bodies under neutral conditions, both failed to develop at pH 9 (Figure 2(b), Figure S4), consistent with defective lysosomal acidification. As reported previously [22], PsenA$^-$/B$^-$ cells were unable to develop under neutral conditions showing more severe developmental defects than Ncstn$^-$ or Aph-1$^-$ cells, halting at the mound stage, but development was reduced further under basic conditions at pH 9 (Figure 2(a)).

We then speculated that if the block in development of PsenA$^-$/B$^-$ cells at neutral pH was related to defects in lysosomal acidification, development may be restored by simply reducing the extracellular pH. We therefore examined development of PsenA$^-$/B$^-$ cells at pH 5 [22,45]. While acidic conditions had no observable effects on the development of wild type cells the development of PsenA$^-$/B$^-$ cells was partially rescued, forming morphologically normal but smaller sized fruiting bodies (Figure 2(c)). This rescue suggested that

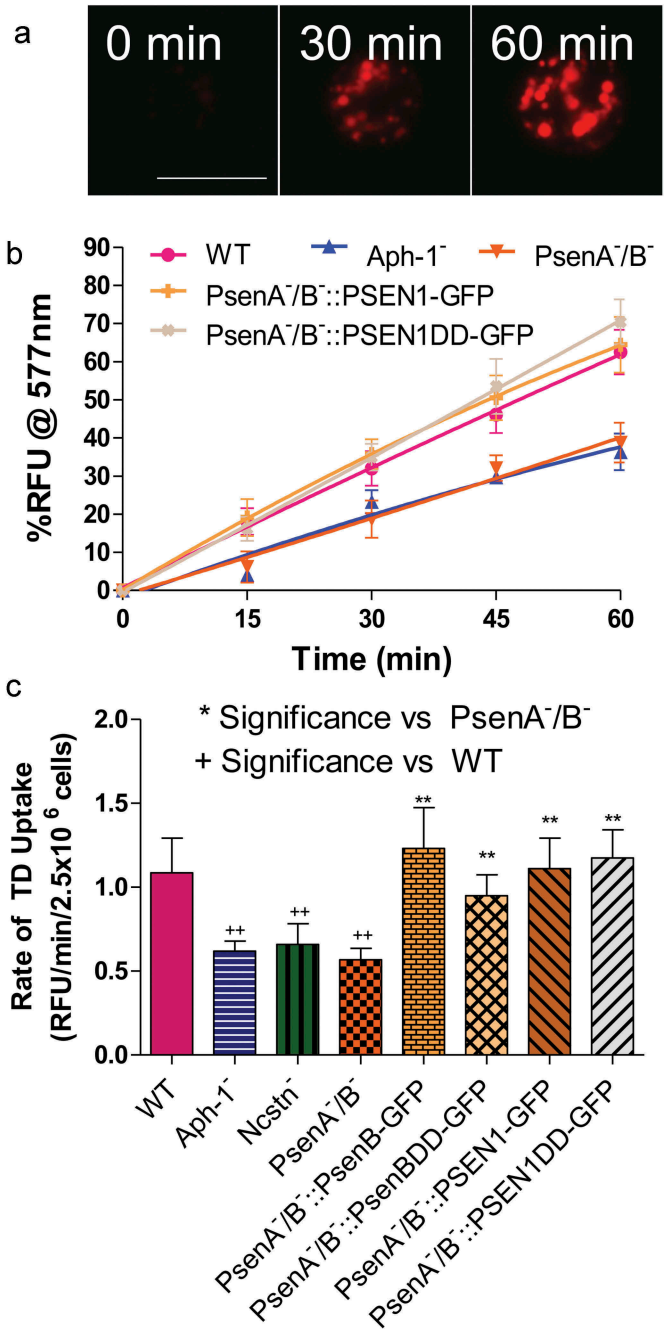

Figure 1. *Dictyostelium* mutants lacking γ-secretase component orthologs are unable to endocytose at wild type levels. *Dictyostelium* cells were shaken in media containing fluorescent TRITC-Dextran, and fluorescence uptake was used to monitor macropinocytosis over time, in wild-type cells, PsenA^{-}/B^{-}, Aph-1^{-} and Ncstn^{-} cells, and PsenA^{-}/B^{-} following rescue by the proteolytic and non-proteolytic human PSEN1 proteins (PsenA^{-}/B^{-}::PSEN1-GFP and PsenA^{-}/B^{-}::PSEN1DD). (**a**) Representative images showing uptake of TRITC-Dextran by wild-type cells over a 60-min period. Scale bar: 10μ m. (**b**) Quantification of macropinocytosis over 60 min (±SEM). (**c**) Rate of macropinocytosis over 60 min (±SD). Data are provided from at least three independent experiments with technical duplicates. $^{++}$p > 0.01 to wild type, **p > 0.01 to PsenA^{-}/B^{-}.

the developmental defects observed are at least partly due to defects in pH homeostasis, consistent with a role for the *Dictyostelium* orthologs of γ-secretase complex components in lysosomal acidification. However, the differences in the developmental phenotype between PsenA^{-}/B^{-} cells and Ncstn^{-} or Aph-1^{-} mutants indicate that psenA and psenB proteins may also function through other independent roles in *Dictyostelium* development.

Importantly, the development of PsenA^{-}/B^{-} cells was fully rescued by expression of either proteolytically active or inactive *Dictyostelium* psenB or human PSEN1 proteins (Figure S5) [22] indicating a non-proteolytic role for these proteins in pH regulation.

Dictyostelium *mutants lacking orthologs of γ-secretase components show defective lysosomal degradation*

In order to directly test whether disruption of orthologs of the γ-secretase complex components leads to defects in lysosomal activity, we measured the ability of mutant cells lacking these components to degrade phagosomes. As a professional phagocyte, *Dictyostelium* cells readily engulf extracellular particles into endocytic vesicles which immediately fuse with lysosomes to be degraded. We therefore utilised a simple assay measuring the phagosomal proteolysis of beads coated with the self-quenching dye DQ-BSA, which becomes fluorescent upon proteolysis (Figure 3(a)) [46]. In this assay, we observed a significant decrease in proteolysis upon loss of multiple *Dictyostelium* orthologs of γ-secretase complex components. Ablation of Aph-1 or PsenA/B caused a reduction in proteolysis activity to 41.4%±4.1% (p = 0.05) and 42.1%+12.8% (p = 0.03) respectively relative to wild type cells (Figure 3(b)). Upon expression of proteolytically active, or inactive *Dictyostelium* psenB, relative proteolysis was restored to 78.9%±9.9% (p = 0.10) and 128.5%±25.1% (p = 0.36) and expression of active or inactive human PSEN1 resulted in a degradation rate of 98.8%±12.6% (p = 1.00) and 120.8%±7.9% (p = 0.35). The reduction in phagosomal proteolysis following loss of Aph-1 was not restored by expression of human PSEN1 (Figure S6). Although this assay does not distinguish between defective phagosome-lysosome fusion and decreased lysosomal activity, these data demonstrate that full degradative activity is dependent upon the presence of Aph-1, and psenB functioning through a non-proteolytic mechanism, and this activity is conserved in the human PSEN1 protein.

Loss of γ-secretase components orthologs causes defective autophagy

The degradation of intracellular components by autophagy is also dependent on lysosomal activity. As autophagy is required for normal development of *Dictyostelium* [37] and has been heavily implicated in supressing the accumulation of mis-folded proteins characteristic of Alzheimer and several other neurodegenerative diseases [11,13,15,47,48], we next investigated the effects of loss of orthologs of γ-secretase components on autophagy.

We first measured autophagosome acidification and degradation in mutant lacking Aph-1 and psenA/B activity. In these experiments, we employed a fluorescent marker, GFP-Atg8, which becomes lipidated and incorporated into the membrane of nascent autophagosomes as they expand. Following completion, autophagosomes rapidly fuse with lysosomes and acidify – quenching the luminal GFP fluorescence, while the exterior GFP-Atg8 is removed [38,41]. In *Dictyostelium* cells this can be clearly observed by microscopy and by quantifying the time required for GFP quenching after autophagosome formation, where a rate of

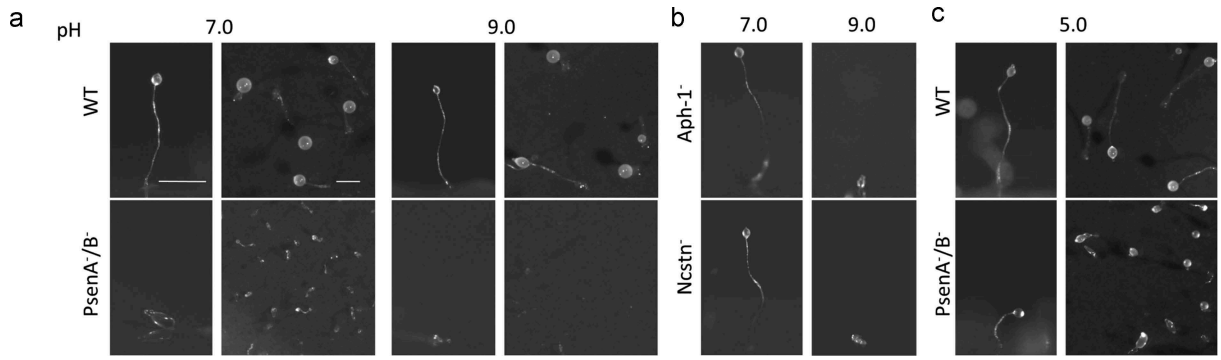

Figure 2. *Dictyostelium* mutants lacking γ-secretase component orthologs are unable to development under varying pH conditions. The development of *Dictyostelium*, through starvation over a 24-h period on nitrocellulose filters, leads to the formation of fruiting bodies consisting of round spore heads held aloft by a stalk, and provides a qualitative approach to monitor development in mutants. (**a**) At pH 7 and pH 9, wild type cells are capable of normal multi-cellular development forming fruiting bodies. In contrast, PsenA$^-$/B$^-$ cells are unable to develop at pH 7, forming short variable structures, and development is further inhibited at pH 9 where cells are unable to aggregate. (**b**) Aph-1$^-$ and Ncstn$^-$ cells form wild-type fruiting bodies at pH 7 but development is blocked at pH 9 (see also **Figure S4**). (**c**) Under acidic conditions, pH 5, wild-type cells form morphologically normal fruiting bodies, and PsenA$^-$/B$^-$ development is partially rescued, showing the formation of small fruiting bodies with round spore heads and stalks, similar to that shown for wild-type cells. Images are representative of triplicate experiments. Scale bar: 1 mm.

acidification can be defined for individual vesicles (Figure 3(c); MovieS1) [38,41]. In wild type cells, GFP-Atg8 quenched in 35.3 ± 6.8 seconds (Figure 3(d)). In contrast, Aph-1$^-$ cells showed significantly increased acidification time to 49.8 ± 6.8 seconds ($p < 0.001$), and PsenA$^-$/B$^-$ cells also significantly increased quenching time to 46.4 ± 9.7 seconds ($p < 0.001$). The acidification defect in PsenA$^-$/B$^-$ cells was rescued upon expression of proteolytically active versions of *Dictyostelium* psenB (32.2 ± 4.7 seconds) as well as a proteolytically inactive version of the protein (31.5 ± 6.5 seconds) suggesting this effect was mediated by non-proteolytic functions of these proteins. The acidification defect in PsenA$^-$/B$^-$ cells was also rescued by both proteolytically active and inactive versions of human PSEN1 protein (32.8 ± 6.4 and 28.8 ± 5.6 seconds respectively). Therefore, the defects in lysosomal activity we observed upon disruption of Aph-1 and psenA/B proteins also impact on autophagosome maturation, suggesting an explanation for both the observed defects in *Dictyostelium* development as well as cell pathology in the absence of these proteins.

Alterations in the process of vesicle acidification have been shown to regulate autophagy [15], in which cells recycle material for energy. In *Dictyostelium*, interruption in the autophagic pathway results in a decrease in the number and an increase in the size of GFP-Atg8 labelled structures [34,38,49]. As a result, we monitored their size and frequency in Aph-1$^-$ and PsenA$^-$/B$^-$ cells for signs of autophagic dysfunction. Wild type cells expressing GFP-Atg8 show a majority of small (below 0.4μ m) diameter structures (79%), with very few structures above 0.8 μm (1.4%) representing normal functioning autophagosomes (Figure 4(a,b). In Aph-1$^-$ cells, a significant reduction was seen in the occurrence of small structures to 26% ($p < 0.01$) and a significant increase in the formation of large GFP-Atg8-positive structures, to 17% ($p < 0.05$) typical of cells with reduced autophagy [37,39]. Similarly, PsenA$^-$/B$^-$ cells also showed single large GFP-Atg8 structures. These data suggest that loss of Aph-1 and psenA/B proteins caused autophagic dysfunction.

To test for the relevance of proteolytic activity in regulating autophagic function, we again expressed both active and inactive forms of both *Dictyostelium* psenB and human PSEN1 in PsenA$^-$/B$^-$ cells expressing GFP-Atg8. In these live-cell experiments, fluorescence was primarily derived from GFP-Atg8 (Figure S7), rather than fluorescently labelled psenB, Aph-1 and Ncstn proteins that localize to the ER (Figure S8). Expression of each form of presenilin rescued the ability of cells to form numerous small GFP-Atg8 structures, confirming this effect was related to loss of presenilin, again independent of proteolytic activity, and with conserved function shown in the human protein (Figure 4(a,b)).

Finally, we investigated a role for the *Dictyostelium* γ-secretase component orthologs in autophagic degradation, by employing a western blot approach to examine autophagic flux as indicated by the cleavage of free GFP from GFP-Atg8 [50]. Comparing wild-type cells with PsenA$^-$/B$^-$ and Aph-1$^-$ cells expressing GFP-Atg8, we measured the ratio of free GFP to total GFP-Atg8 in the absence and presence of lysosomal protease inhibitors as a measure of autophagic degradation. We showed that treatment of wild-type cells with protease inhibitor significantly inhibited the release of free GFP from GFP-Atg8 ($p < 0.05$) consistent with reduced autophagic degradation (Figure 5(a,b)). Ablation of psenA/B or Aph-1 resulted in a 39% and 49% decrease in the ratio of free GFP:GFP-Atg8, which was not significantly changed upon protease inhibitor treatment, suggesting a severe reduction in autophagic flux in PsenA$^-$/B$^-$ and Aph-1$^-$ cells. Expression of the human PSEN1 in the PsenA$^-$/B$^-$ cells restored wild-type autophagic levels. These experiments confirm a role for psenA/B and Aph-1 proteins in autophagic regulation and demonstrate that this cellular function is conserved with the human PSEN1 protein.

Loss of γ-secretase components orthologs results in large ubiquitin-positive structures

In *Dictyostelium*, large GFP-Atg8-positive structures typically consist of high molecular weight ubiquitinated protein that cannot be cleared when autophagy is impaired [39]. We therefore examined the colocalization of GFP-Atg8 with ubiquitin-positive structures in the mutants lacking psenA/B and Aph-1 proteins. In wild type cells, the multiple small GFP-Atg8 puncta

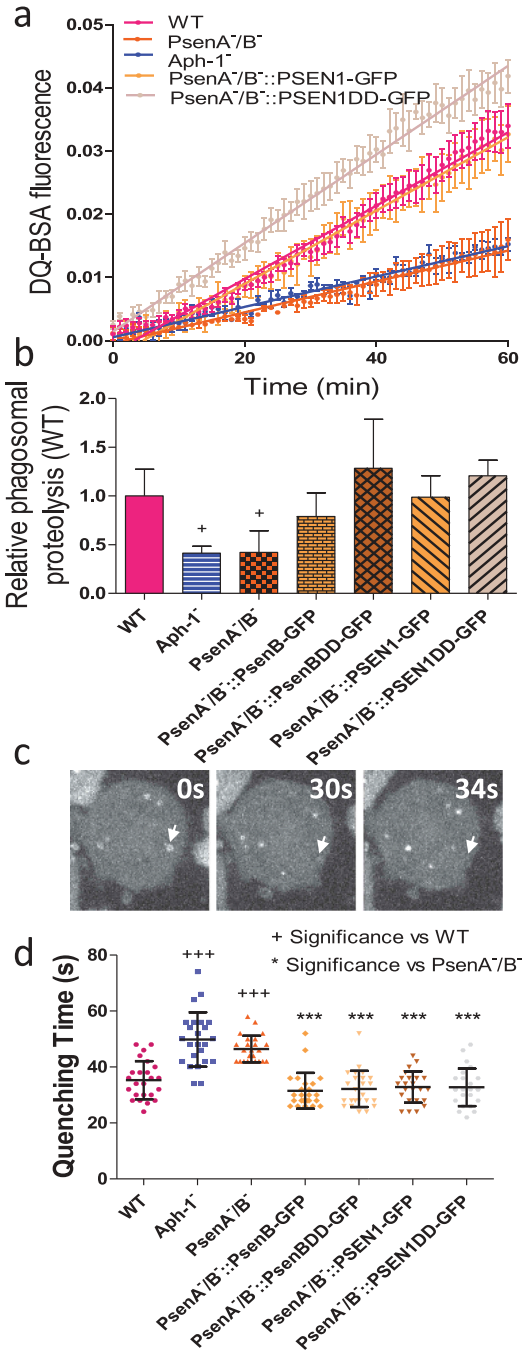

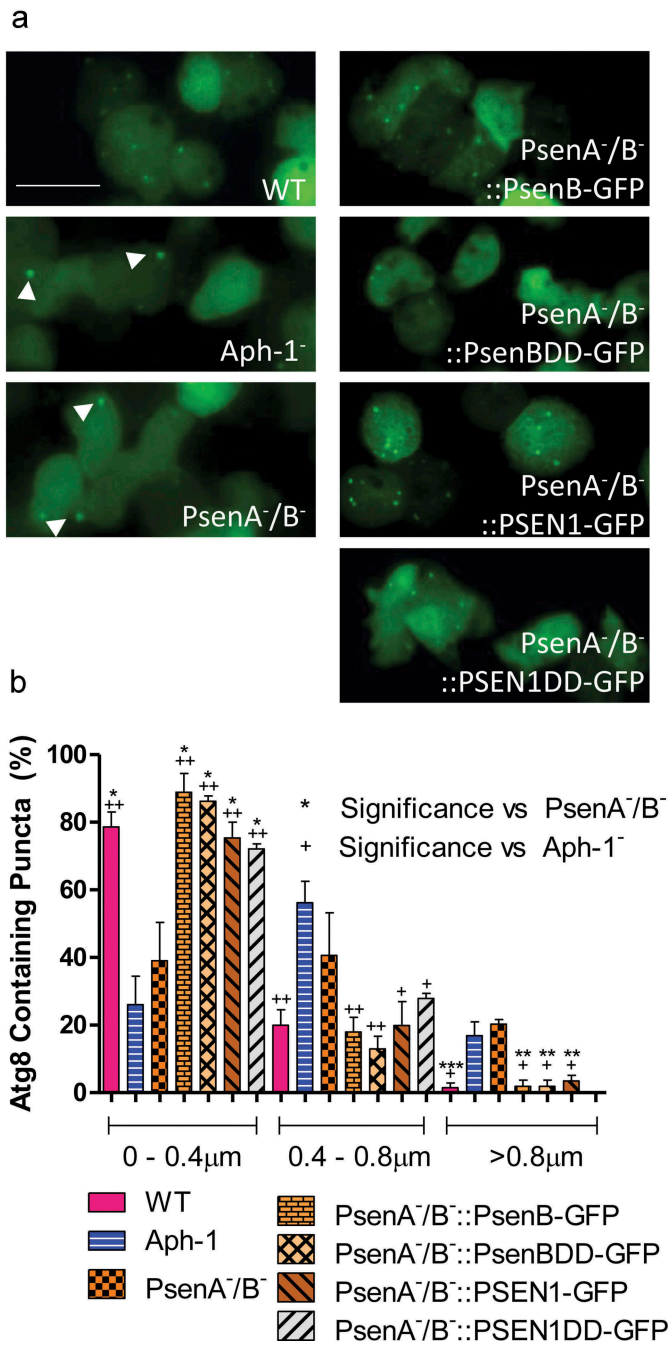

Figure 3. *Dictyostelium* mutants lacking γ-secretase component orthologs show abnormal lysosomal activity. Phagosome degradation is quantified by monitoring the increase in fluorescence of DQ-BSA-coated beads, taken up by phagocytosis, which becomes unquenched upon hydrolysis. This approach was used to assess in wild type cells, PsenA⁻/B⁻, and Aph-1⁻ cells, and PsenA⁻/B⁻ cells following rescue by the proteolytic and non-proteolytic *Dictyostelium* psenB or the equivalent human PSEN1 proteins (PsenB-GFP and PsenBDD-GFP or PSEN1-GFP and or PSEN1DD-GFP) respectively. (**a**) Quantification of proteolysis shows loss of a functional γ-secretase complex reduces phagolysosomal degradation, and this is restored by proteolytically active or inactive human PSEN1, from quadruplicate independent experiments (±SEM), which is reflected in (**b**) the rate of lysosomal acidification in (±SD). +P < 0.05. (**c**) *Dictyostelium* cells exhibit puncta of GFP-Atg 8 that may be tracked (arrow) over time to determine the quenching time of GFP due to acidification. (**d**) Quantification of GFP-Atg8 quenching time shows an increase in the absence of a functional γ-secretase complex, and this is restored by both *Dictyostelium* and human presenilin proteins (both proteolytically active and inactive) (n = 25). +++p > 0.001 to wild type, ***p > 0.001 to PsenA⁻/B.

Figure 4. *Dictyostelium* mutants lacking γ-secretase component orthologs show aberrant size and localisation of GFP-Atg8. Visualization of GFP-Atg8 localisation in wild type cells, PsenA⁻/B⁻ and Aph-1⁻ and PsenA⁻/B⁻ cells following rescue by the proteolytic and non-proteolytic *Dictyostelium* psenB or the equivalent human PSEN1 proteins (PsenB-GFP and PsenBDD-GFP or PSEN1-GFP and or PSEN1DD-GFP) respectively. (**a**) Wild-type cells show multiple small and distributed GFP-Atg8-containing autophagosomes, whereas a single large punctum is seen in a proportion of PsenA⁻/B⁻ and Aph-1⁻ cells, that is no longer observed when cells are rescued following expression of *Dictyostelium* psenB orhuman PSEN1 (proteolytically active or inactive). Scale bar: 10µ m. (**b**) Quantification of the size of GFP-Atg8 -containing autophagosomes shows an increase in the absence of a functional γ-secretase complex, and this is restored by both *Dictyostelium* and human presenilin proteins (both proteolytically active and inactive). Data are derived from triplicate experiments measuring approximately 50 cells per experiment. '+' compares to Aph-1⁻, '*'compares to PsenA⁻/B⁻, where * or + is P < 0.05, ** or ++ is P < 0.01, *** or +++ is P < 0.05.

that were observed did not contain ubiquitinated proteins (Figure 6(a)). In contrast, the large GFP-Atg8-positive structures observed following loss of the γ-secretase complex, in both Aph-1⁻ and PsenA⁻/B⁻ cells, colocalized with ubiquitinated protein.

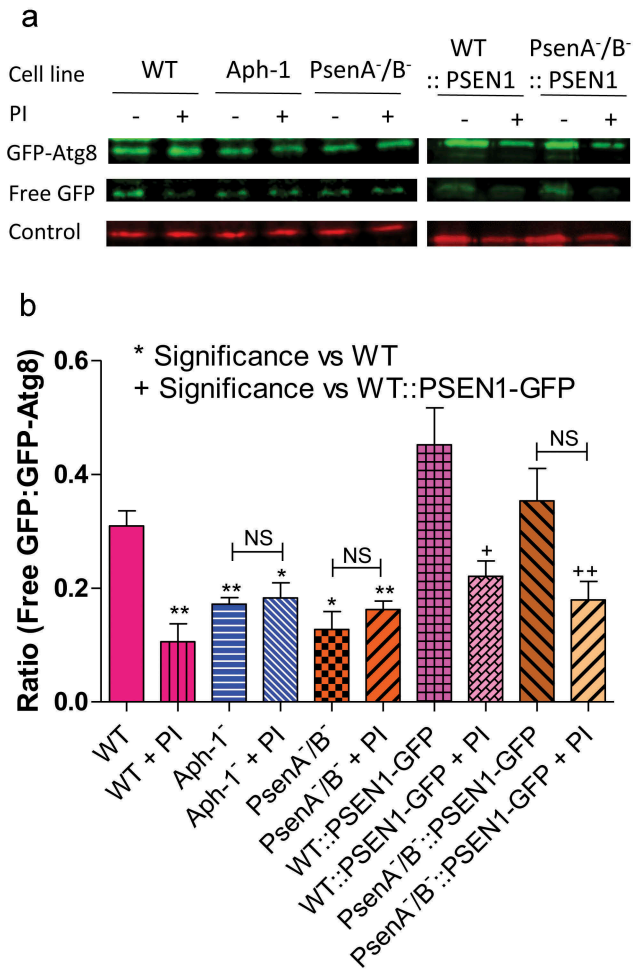

Figure 5. *Dictyostelium* mutants lacking γ-secretase component orthologs show decreased autophagic flux. Representative western blot analysis using an anti-GFP antibody enables comparison of levels of free GFP to GFP-Atg8 in the presence or absence of protease inhibitor (PI) treatment, allowing the comparison of wild type, Aph-1$^-$, and PsenA$^-$/B$^-$ cell autophagic flux, and following rescue by the proteolytically active human PSEN1 protein (PSEN1-GFP). (**a**) Levels of free GFP are reduced in wild-type cells following PI treatment. In both Aph-1$^-$ and PsenA$^-$/B$^-$ cells, free GFP levels are reduced in the absence of PI, and remain low following PI treatment. Expression of PSEN1-GFP in the PsenA$^-$/B$^-$ cells restores free GFP levels in untreated cells, and PI sensitivity. Endogenously biotinylated mitochondrial protein MCCC1 was used as a loading control. (**b**) Quantitation of free GFP to GFP-Atg8 ratios shows the absence of a functional γ-secretase complex reduces autophagic flux, and this is restored by the human PSEN1 protein. Data are derived from triplicate independent experiments (±SEM). '*' compares to wild type, '+' compares to PsenA$^-$/B$^-$, where * or + is $P < 0.05$, ** or ++ is $P < 0.01$; NS, not significant.

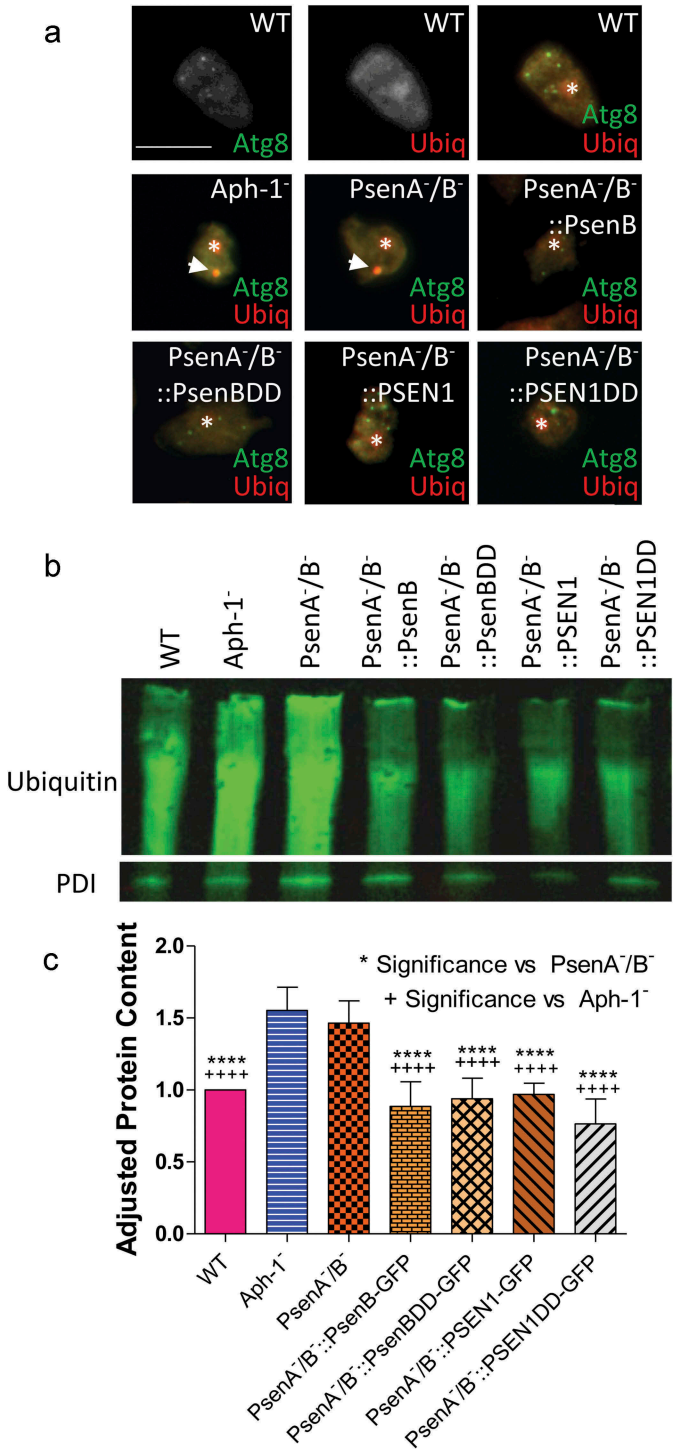

Figure 6. *Dictyostelium* mutants lacking γ-secretase component orthologs show ubiquitination defects. Analysis of ubiquitination levels in wild-type cells, PsenA$^-$/B$^-$ and Aph-1$^-$ and PsenA$^-$/B$^-$ cells following rescue by the proteolytic and non-proteolytic *Dictyostelium* PsenB or the equivalent human PSEN1 proteins (PsenB-GFP and PsenBDD-GFP or PSEN1-GFP and PSEN1DD-GFP) respectively. (**a**) In cells expressing GFP-Atg8, immunofluorescence analysis shows co-localization of GFP and ubiquitin in single large puncta in Aph-1$^-$ and PsenA$^-$/B$^-$ cells that are absent in wild-type cells, and are absent following rescue with the presenilin proteins. Scale bar: 10μ m. (**b**) Representative western blot analysis using anti-ubiquitin in the wild type, mutants and following rescue as indicated. Anti-PDI was used as a loading control for normalisation. (**c**) Quantification of anti-ubiquitin western blot shows a ~ 50% increase in large molecular weight ubiquitinated protein in cells lacking a functional γ-secretase complex when compared to normalized wild type levels. This increase is restored to wild type levels in PsenA$^-$/B$^-$ cells expressing *Dictyostelium* PsenB or human PSEN1 proteins regardless of proteolytic activity. Data are derived from 5 independent experiments.

Rescue of this phenotype in the PsenA$^-$/B$^-$ cells with both the proteolytically active and inactive version of the *Dictyostelium* PsenB and human PSEN1 proteins led to clearance of these ubiquitinated structures.

We then confirmed the effect of the loss of psenA/B and Aph-1 proteins on the accumulation of high molecular weight ubiquitinated proteins by western blotting (Figure 6(b,c)). Consistent with our results above, both the Aph-1$^-$ and PsenA$^-$/B$^-$ cells showed a significant increase in high molecular weight ubiquitinated proteins (by 55% and 46% respectively; $p = 0.0002$ and $p = 0.0001$ respectively) again suggesting impaired protein degradation in these mutants. Accumulation of high molecular weight ubiquitinated protein

was reversed by restoration of presenilin activity for both the *Dictyostelium* psenB (wild type and proteolytically inactive) and human PSEN1 (wild type and proteolytically inactive) rescue strains (Figure 6(b)). Importantly, accumulation of high molecular weight ubiquitinated protein indicated that these presenilin proteins and Aph-1 are physiologically important in maintaining basal autophagy levels and clearing misfolded proteins in *Dictyostelium*. Furthermore the function of these presenilin proteins are non-proteolytic and are conserved between *Dictyostelium* and humans.

Discussion

In this study, we have shown that in *Dictyostelium*, orthologous components of the γ-secretase complex have roles in macropinocytosis, phagocytosis and autophagy, most likely through mediating lysosomal acidification. Recent studies in mammalian models of Alzheimer disease have investigated the role of these components in vesicular trafficking [7,11,13,15,48,51–53], and suggest that dysfunction of these processes may contribute to the progression and pathology of Alzheimer disease. These studies typically describe aberrant intracellular degradation as a result of dysfunction of presenilin proteins, rather than the entirety of the complex [5,42,51,52]. Here, we used *Dictyostelium discoideum* as a model to investigate orthologous components of the γ-secretase complex, taking advantage of the ability to delete individual genes in stable isogenic cultures to monitor changes in cell and developmental function, and to restore protein activity using wild type and proteolytically inactive presenilin proteins to rescue mutant phenotypes [22,31]. Using these approaches we show that in *Dictyostelium*, ablation of Ncstn, Aph-1 or both psenA/B genes results in deficient endocytosis and pH-dependent development, and loss of Aph-1 and psenA/B proteins gives rise to defects in lysosomal acidification and autophagy. We further show that these functions are dependent on the non-proteolytic activity of the psenA/B proteins that are conserved in the human PSEN1 protein.

We show that loss of Ncstn, Aph-1 or both psenA/B proteins inhibits macropinocytosis, a process by which cells take up large quantities of extracellular fluid. However, the exact mechanism that drives and controls the process is not yet fully understood [54]. *Dictyostelium* has proven to be an important model organism in macropinocytosis research and has led to a number of related discoveries, including the role of RasS in maintaining normal actin function in this process [55], the roles of phosphatidylinositol 3-kinases in macropinocytosis control [56], and the role of WASH in macropinosome recycling [49,54]. Further, both axeB/neurofibromin [57] and ndkC/nucleoside diphosphate kinase C [58] function to negatively regulate macropinocytosis. In mammalian cells, a number of these key regulatory pathways are conserved across evolution, including the function of RAS proteins, phosphatidylinositol 3-kinases, F-actin and WASH [49,59–61]. Our data now adds to this list, suggesting that orthologous components of the γ-secretase complex are necessary for optimal fluid uptake in *Dictyostelium* [55,57,62], involving a non-proteolytic activity of psenB protein, and these defects can be rescued by expression of a human PSEN1 protein. These results are consistent with but extend those shown in mammalian Alzheimer disease models, where loss of γ-secretase function results in aberrant macropinocytosis [5,6], and dysfunctional protein aggregate clearance for affected neuronal cells [5,6,42,52].

After extracellular material has been internalized, vesicles move through the intracellular endocytic pathway before finally fusing with lysosomes for degradation of vesicular material [63–65]. We show here, that *Dictyostelium* cells lacking Ncstn, Aph-1 or both psenA/B proteins fail to develop under basic pH conditions, consistent with that seen in other mutants that are unable to appropriately acidify their vesicles [45]. We then confirmed this role directly, by measuring autophagosome acidification, phagosome proteolysis [34,41] and autophagic flux in cells lacking Aph-1 or both psenA/B proteins. In mammalian models, dysfunctional lysosomal pH regulation has been linked to Alzheimer disease [66], in addition to other disease such as Pompe [67] and Niemann-Pick disease [68], as well as cholesterol uptake, and atherosclerosis – all resulting in inefficient degradation of intra-endosome material. In regard to Alzheimer disease, presenilin proteins have been implicated in a non-proteolytic, complex-independent role in maintaining lysosomal pH [15,51,52]. These studies suggest that presenilin regulates lysosomal pH through vacuolar-ATPase-mediated lysosomal acidification, resulting in altered calcium levels [51]. In *Dictyostelium*, we have shown that Ncstn, Aph-1 and psenA/B proteins are localized in the endoplasmic reticulum and this localization is unaltered in the absence of other complex components (Figure S8), consistent with that shown for Vmp1 involved with lysosomal function and autophagy [39] and a role of the complex in interacting with v-ATPase proteins for vesicle acidification and lysosomal activity. It is important to note here that our data do not explicitly link macropinocytosis and acidification defects, and further studies will need to investigate this in detail.

Previous research in *Dictyostelium* suggested that the γ-secretase complex is important for phagocytosis, and that this process is dependent upon proteolytic activity [31]. Our study confirms the role of Aph-1 and psenA/B proteins in phagocytosis, but demonstrates that it is not reliant upon proteolytic activity [22]. These data quantify the loss of (phago-)lysosomal proteolysis in cells lacking the orthologs of multiple γ-secretase complex components, and together with data on macropinocytosis, suggest that material ingested through both processes are unlikely to be efficiently degraded, and these effects are commonly observed in cellular models for Alzheimer disease [5,6,66].

Another cellular process dependent upon lysosomal degradation is autophagy [69]. *Dictyostelium* has been widely used to investigate autophagy and the importance of autophagy, and its role in multicellular development [40]. Here we show that cells lacking psenA/B or Aph-1 proteins share a number of phenotypes with autophagy dysfunctional mutants, including defective GFP-Atg8 localization [37,39], co-localisation between GFP-Atg8 and ubiquitin aggregates [39], and an abundance of high molecular weight ubiquitinated protein [39,70], reduced

autophagic flux, and aberrant development. These data demonstrate that orthologs of multiple γ-secretase complex components play a key role in the autophagic process in *Dictyostelium*. Consistent with this, neurons of patients diagnosed with Alzheimer disease also accumulate neurotoxic peptides due to inefficient lysosomal acidification and a resultant build-up of autophagosomes rich in amyloid precursor protein [7,8,52]. We further show that, in *Dictyostelium*, this deficiency in autophagy and accumulation of ubiquitinated proteins is not caused by loss of psenB proteolytic activity, and this activity can be fulfilled by the human PSEN1 protein [7,51].

In this study, we demonstrate that the *Dictyostelium* orthologs of γ-secretase complex components play a key role in regulating macropinocytosis, phagocytosis, acidification of lysosomal vesicles, and autophagy. The reduction of these activities following the loss of two (psenA/B and Aph-1) or three (psenA/B, Aph-1 and Ncstn) orthologs of γ-secretase complex components suggest that these phenotypes may be regulated by a *Dictyostelium* γ-secretase complex, but we cannot explicitly demonstrate that these roles are not independent. Similarly, the interrelatedness of these cellular function is also consistent with a common role for a *Dictyostelium* γ-secretase complex in this process, and that this function is not dependent on the proteolytic activity of the putative γ-secretase complex. Finally, we demonstrate that these roles of the psenA/B proteins can be rescued in *Dictyostelium* through expression of human PSEN1. Thus we propose that, in *Dictyostelium*, an orthologous γ-secretase complex plays a key role in maintaining endocytosis, lysosomal trafficking and autophagy through a non-proteolytic function, conserved between *Dictyostelium* and humans across the vast evolutionary gap that separates these two organisms.

Materials and methods

Cell culture and maintenance

Dictyostelium wild type strain Ax2 were grown in HL5 medium (Formedium, HLB0103) supplemented with 10% glucose (Sigma-Aldrich, G8270). PsenA$^-$/B$^-$ cells and rescue strains, and Ncstn$^-$ cells have been previously described [22], and are maintained in HL5 medium supplemented with/without 10 μg/ml hygromycin (Formedium, HYG1000).

Plasmid construction and transformation

Aph-1$^-$ mutant cells were generated by homologous integration using the Cre-Lox system [71].

Briefly, a knockout vector was designed consisting of a 5′ and 3′ arm of homology (primers:

GTG GAT CCT ATA AGT ATT TTA AAG ATT/AAC TGC AGA GAT ATT TAA AAA TGT TTC TTA CC and TTA TTC CAT GGA GTT TAT AAC GTT TT/AAT GGT ACC TTG ATA ATG TTA AAA TGA) in order to ablate a central 762 base pair region of the gene. The linearized vector was electroporated into wild-type *Dictyostelium* cells, and transformants were screened by PCR in order to identify homologous recombinants [72].

Macropinocytosis and exocytosis assay

Rate of TRITC-Dextran uptake was measured as described previously [62]. Briefly, 2.5 × 10^7 cells were resuspended in 5 ml of HL5 medium supplemented with 100 μl or 100 mg/ml TRITC-Dextran (Sigma-Aldirch, T1162). At time points 0, 15, 30, 45, 60, 90, and 120 min, 500 μl of this suspension was removed, washed in phosphate buffer and measured on a Perkin Elmer LS50B spectrophotometer. Relative change in fluorescence was calculated and normalised against total protein content of each respective cell line. The rate of uptake was measured using the linear function in GraphPad Prism.

To determine whether efflux was also affected by γ-secretase ablation a simple assay was utilised [73]. Briefly, 2.5 × 10^7 cells were incubated in HL-5 with 100 mg/ml TRITC-Dextran for a period of 3 h. Following incubation, cells were washed and resuspended in 5 ml of phosphate buffer before shaking incubation. At time points 0, 15, 30, 45, 60, 90 and 120 min 500 μl of the suspension was removed and the fluorescence measured. Change in fluorescence was calculated relative to the measurement at time point 0 min of each respective cell line. The rate of efflux was calculated using GraphPad Prism.

Dictyostelium development at varying pH

In these assays, 1 × 10^7 cells were plated and allowed to develop on 47mm nitrocellulose filters (Millipore, HAWP04700) over 24 h [74]. Each filter was placed on an absorbent 3M paper pad (Millipore, AP1004700) soaked in phosphate buffer of varying pH. Phosphate buffer was prepared using varying amounts of KH_2PO_4 and K_2HPO_4 to modulate pH without altering ionic strength. Subsequent developmental phenotypes were imaged using a dissection microscope (Leica) and a QICAM FAST 1394 camera (QImaging).

Fluorescence microscopy and quantification

Cells were imaged on an Olympus IX71 wide-field fluorescence microscope. Images were captured using a QICAM FAST 1394 camera. For measurement of Atg8-positive structure size cells were analysed using ImageJ [75] and cell size was measured across the largest diameter. More than 100 GFP-Atg8 positive structures were measured, using around 50 cells per experiment including at least three independent experimental repeats. For live-cell imaging, cells were imaged under a layer of ~1.5-mm thick 1% phosphate buffered agarose [49].

Analysis of autophagosome maturation

The autophagy reporter GFP-Atg8 was expressed in cells using the extrachromosomal expression plasmid pDM430 [38]. To both reduce the movement of vesicles in the Z-plane and stimulate autophagosome formation cells were compressed under a thin layer of 1% agarose in HL-5 medium as previously described [38]. Cells were seeded in glass-bottomed microscopy dishes before removal of most of the medium, application of a ~ 2-mm thick agarose slab and

compression by blotting with paper and capillary action. After 10 min, images were captured using a Perkin-Elmer Ultraview VoX inverted spinning disc microscope, using a 100 × 1.4NA objective and Hammamatsu C9100-50 EM-CCD camera. 4 Z planes at 1μM spacing were captured every 2 s. The point of autophagosome completion was determined by the characteristic enlargement and diming of GFP fluorescence [41]. The time until GFP-fluorescence was undetectable was subsequently measured from randomised, blinded movies captured from at least three independent experiments.

Phagosomal proteolysis assays

Phagosomal proteolytic activity was measured by feeding cells DQgreen/Alexa Fluor 594 (DQ-BSA; Invitrogen, D12050) co-labelled 3-μm silica beads (Kisker Biotech, PSI-3.0COOH) as previously described [76]. Briefly 3×10^5 cells/well were seeded in a 96-well plate before addition of beads, and fluorescence measured on a plate reader each minute in triplicate. Proteolysis was normalised to Alexa Fluor 594 fluorescence, over time to account for potential differences in bead uptake and rates normalized to wild-type cells to calculate relative activity.

Western blotting and immunofluorescence

Analysis of high molecular weight ubiquitinated protein was carried out by western blot as previously described [70]. Briefly, the proteins of 2×10^5 cells were separated by SDS gel electrophoresis and the membrane was probed with α-PDI [77] (an ER marker protein, disulfide isomerase a kind gift from Annette Muller-Taübenberger) as a loading control and α-ubiquitin (Cell Signalling Technology, P4D1) at 1:50, and 1:1000 dilutions, respectively. Relative amounts of high molecular weight ubiquitinated protein were calculated using Image Studio Lite (LI-COR Biosciences) and these were normalized against wild-type levels of ubiquitinated protein.

For colocalization of ubiquitin and GFP-Atg8, cells were fixed in −80°C methanol as previously described [78]. After fixation cells were probed with α-GFP (Chromotek, 3H9) and anti-ubiquitin (New England Biolabs, 3936S) antibodies at 1:500 and 1:200 dilution concentrations, secondary antibodies used were anti-rat Alexa Fluor 488 and anti-mouse Alexa Fluor 350 (Life Technologies, A-21,210 and A-31,552 respectively) at 1:1000 concentration dilutions. Cells were then imaged to visualise colocalization between ubiquitin and GFP-Atg8-positive structures.

To analyze autophagic flux a western blot based approach was utilised [50]. Briefly, 1.3×10^6 cells were seeded in a 6 well plate before treatment with protease inhibitors (Roche Life Science, 05892791001) for 1 h, when cells were harvested and proteins extracted. Western blots were probed with an anti-GFP antibody (1:1000 dilution) and levels of the endogenously biotinyated mitochondrial protein MCCC1 detected with a streptavidin-conjugated antibody used as a loading control [79] (Thermo Fisher Scientific, S21378). The fluorescent ratio of free GFP to GFP-Atg8 was calculated to determine a measure of autophagic flux.

To visualize *Dictyostelium* γ-secretase components localization, cells were fixed using 80°C methanol [78] and probed with antibodies. Briefly, cells overexpressing GFP-tagged components were seeded onto coverslips and fixed by submerging in −80°C methanol for 30 min. Following fixation, cells were washed in room temperature phosphate-buffered saline, stained with anti-GFP and anti-crtA (calreticulin) antibodies (a kind gift from Annette Muller-Taübenberger), subsequently stained with appropriate secondary antibodies to allow for ER visualization, and nuclei were stained with DAPI.

Statistical analysis

Statistical analysis depended upon the data analyzed. For normally distributed data a two-way ANOVA was utilised when comparing multiple data groups to each other. For data that is not normally distributed the Mann-Whitney test was used, and for data that was compared to a single normalised mean value a one sample T-test was used. Statistical analysis was carried out using GraphPad Prism Software.

Author contributions

DS, PB, JSK and RSBW designed the study. DS, GO, EW and JSK performed the research, data analysis and modelling. The paper was written by DS, PB, JSK and RSBW.

Data availability

All data related to this study are available in the paper or via supplementary material.

Disclosure statement

No potential conflict of interest was reported by the authors.

Funding

This work was supported by NC3Rs; Royal Society University Research Fellowship under Grant UF140624; MRC under Grant (G0700091); Wellcome Trust under Grant GR077544AIA, and a BBSRC studentship award.

ORCID

Grant Otto http://orcid.org/0000-0001-8709-3366
Jason S. King http://orcid.org/0000-0003-0596-4506
Robin S. B. Williams http://orcid.org/0000-0002-9826-6020

References

[1] Scheuner D, Eckman C, Jensen M, et al. Secreted amyloid beta-protein similar to that in the senile plaques of Alzheimers disease is increased in vivo by the presenilin 1 and 2 and APP mutations linked to familial Alzheimers disease. Nat Med. 1996 Aug;2(8):864–870. PubMed PMID: 8705854.
[2] De Strooper B, Annaert W, Cupers P, et al. A presenilin-1-dependent gamma-secretase-like protease mediates

release of Notch intracellular domain. Nature. 1999 Apr 8;398 (6727):518–522. PubMed PMID: 10206645.

[3] De Strooper B, Iwatsubo T, Wolfe MS. Presenilins and gamma-secretase: structure, function, and role in Alzheimer Disease. Cold Spring Harb Perspect Med. 2012 Jan;2(1):a006304. PubMed PMID: 22315713; PubMed Central PMCID: PMC3253024.

[4] De Strooper B, Saftig P, Craessaerts K, et al. Deficiency of presenilin-1 inhibits the normal cleavage of amyloid precursor protein. Nature. 1998 Jan 22;391(6665):387–390. PubMed PMID: 9450754.

[5] Zhang M, Haapasalo A, Kim DY, et al. Presenilin/gamma-secretase activity regulates protein clearance from the endocytic recycling compartment. FASEB J. 2006 Jun;20(8):1176–1178. PubMed PMID: 16645046.

[6] Tamboli IY, Prager K, Thal DR, et al. Loss of gamma-secretase function impairs endocytosis of lipoprotein particles and membrane cholesterol homeostasis. J Neurosci. 2008 Nov 12;28 (46):12097–12106. PubMed PMID: 19005074.

[7] Lee JH, Yu WH, Kumar A, et al. Lysosomal proteolysis and autophagy require presenilin 1 and are disrupted by Alzheimer-related PS1 mutations. Cell. 2010 Jun 25;141 (7):1146–1158. PubMed PMID: 20541250; PubMed Central PMCID: PMCPMC3647462.

[8] Pasternak SH, Bagshaw RD, Guiral M, et al. Presenilin-1, nicastrin, amyloid precursor protein, and gamma-secretase activity are co-localized in the lysosomal membrane. J Biol Chem. 2003 Jul 18;278(29):26687–26694. PubMed PMID: 12736250.

[9] Wolfe MS. Toward the structure of presenilin/gamma-secretase and presenilin homologs. Biochim Biophys Acta. 2013 Dec;1828 (12):2886–2897. PubMed PMID: 24099007; PubMed Central PMCID: PMCPMC3801419.

[10] Frakes AE, Ferraiuolo L, Haidet-Phillips AM, et al. Microglia induce motor neuron death via the classical NF-kappaB pathway in amyotrophic lateral sclerosis. Neuron. 2014 Mar 05;81 (5):1009–1023. PubMed PMID: 24607225; PubMed Central PMCID: PMCPMC3978641.

[11] Ghavami S, Shojaei S, Yeganeh B, et al. Autophagy and apoptosis dysfunction in neurodegenerative disorders. Prog Neurobiol. 2014 Jan;112:24–49. PubMed PMID: 24211851.

[12] Menzies FM, Fleming A, Rubinsztein DC. Compromised autophagy and neurodegenerative diseases. Nat Rev Neurosci. 2015 Jun;16(6):345–357. PubMed PMID: 25991442.

[13] Nixon RA. The role of autophagy in neurodegenerative disease. Nat Med. 2013 Aug;19(8):983–997. PubMed PMID: 23921753.

[14] Ulamek-Koziol M, Furmaga-Jablonska W, Januszewski S, et al. Neuronal autophagy: self-eating or self-cannibalism in Alzheimers disease. Neurochem Res. 2013 Sep;38(9):1769–1773. PubMed PMID: 23737325; PubMed Central PMCID: PMCPMC3732752.

[15] Wolfe DM, Lee JH, Kumar A, et al. Autophagy failure in Alzheimers disease and the role of defective lysosomal acidification. Eur J Neurosci. 2013 Jun;37(12):1949–1961. PubMed PMID: 23773064; PubMed Central PMCID: PMCPMC3694736.

[16] Capell A, Grunberg J, Pesold B, et al. The proteolytic fragments of the Alzheimers disease-associated presenilin-1 form heterodimers and occur as a 100-150-kDa molecular mass complex. J Biol Chem. 1998 Feb 6;273(6):3205–3211. PubMed PMID: 9452432.

[17] Parks AL, Curtis D. Presenilin diversifies its portfolio. Trends Genet. 2007 Mar;23(3):140–150. PubMed PMID: 17280736.

[18] Kang DE, Soriano S, Frosch MP, et al. Presenilin 1 facilitates the constitutive turnover of beta-catenin: differential activity of Alzheimers disease-linked PS1 mutants in the beta-catenin-signaling pathway. J Neurosci. 1999 Jun 1;19(11):4229–4237. PubMed PMID: 10341227.

[19] Kang DE, Soriano S, Xia X, et al. Presenilin couples the paired phosphorylation of beta-catenin independent of axin: implications for beta-catenin activation in tumorigenesis. Cell. 2002 Sep 20;110 (6):751–762. PubMed PMID: 12297048.

[20] Khandelwal A, Chandu D, Roe CM, et al. Moonlighting activity of presenilin in plants is independent of gamma-secretase and evolutionarily conserved. Proc Natl Acad Sci U S A. 2007 Aug 14;104 (33):13337–13342. PubMed PMID: 17684101; PubMed Central PMCID: PMCPMC1948938.

[21] Li D, Parks SB, Kushner JD, et al. Mutations of presenilin genes in dilated cardiomyopathy and heart failure. Am J Hum Genet. 2006 Dec;79(6):1030–1039. PubMed PMID: 17186461; PubMed Central PMCID: PMCPMC1698711.

[22] Ludtmann MH, Otto GP, Schilde C, et al. An ancestral non-proteolytic role for presenilin proteins in multicellular development of the social amoeba Dictyostelium discoideum. J Cell Sci. 2014;127:1576–1584.

[23] Otto GP, Sharma D, Williams RS. Non-catalytic roles of presenilin throughout evolution. J Alzheimers Dis. 2016 Apr 12;52 (4):1177–1187. PubMed PMID: 27079701; PubMed Central PMCID: PMCPMC4927835.

[24] Murayama M, Tanaka S, Palacino J, et al. Direct association of presenilin-1 with beta-catenin. FEBS Lett. 1998 Aug 14;433 (1–2):73–77. PubMed PMID: 9738936.

[25] Zhang Z, Hartmann H, Do VM, et al. Destabilization of beta-catenin by mutations in presenilin-1 potentiates neuronal apoptosis. Nature. 1998 Oct 15;395(6703):698–702. PubMed PMID: 9790190.

[26] Xia X, Qian S, Soriano S, et al. Loss of presenilin 1 is associated with enhanced beta-catenin signaling and skin tumorigenesis. Proc Natl Acad Sci U S A. 2001 Sep 11;98(19):10863–10868. PubMed PMID: 11517342; PubMed Central PMCID: PMCPMC58565.

[27] Shilling D, Muller M, Takano H, et al. Suppression of InsP3 receptor-mediated Ca2+ signaling alleviates mutant presenilin-linked familial Alzheimers disease pathogenesis. J Neurosci. 2014 May 14;34(20):6910–6923. PubMed PMID: 24828645; PubMed Central PMCID: PMCPMC4019804.

[28] Tu H, Nelson O, Bezprozvanny A, et al. Presenilins form ER Ca2+ leak channels, a function disrupted by familial Alzheimers disease-linked mutations. Cell. 2006 Sep 8;126(5):981–993. PubMed PMID: 16959576; PubMed Central PMCID: PMCPMC3241869.

[29] Boyles RS, Lantz KM, Poertner S, et al. Presenilin controls CBP levels in the adult Drosophila central nervous system. PLoS One. 2010 Dec 14;5(12):e14332. PubMed PMID: 21179466; PubMed Central PMCID: PMCPMC3001863.

[30] Sarasija S, Norman KR. A gamma-secretase independent role for presenilin in calcium homeostasis impacts mitochondrial function and morphology in caenorhabditis elegans. Genetics. 2015 Dec;201(4):1453–1466. PubMed PMID: 26500256; PubMed Central PMCID: PMCPMC4676538.

[31] McMains VC, Myre M, Kreppel L, et al. Dictyostelium possesses highly diverged presenilin/gamma-secretase that regulates growth and cell-fate specification and can accurately process human APP: a system for functional studies of the presenilin/gamma-secretase complex. Dis Model Mech. 2010 Sep-Oct;3(9–10):581–594. PubMed PMID: 20699477; PubMed Central PMCID: PMC2931536.

[32] Chang P, Orabi B, Deranieh RM, et al. The antiepileptic drug valproic acid and other medium-chain fatty acids acutely reduce phosphoinositide levels independently of inositol in Dictyostelium. Dis Model Mech. 2012 Jan;5(1):115–124. PubMed PMID: 21876211; PubMed Central PMCID: PMCPMC3255550.

[33] Waheed A, Ludtmann MH, Pakes N, et al. Naringenin inhibits the growth of Dictyostelium and MDCK-derived cysts in a TRPP2 (polycystin-2)-dependent manner. Br J Pharmacol. 2014 May;171 (10):2659–2670. PubMed PMID: 24116661; PubMed Central PMCID: PMCPMC4009007.

[34] King JS, Gueho A, Hagedorn M, et al. WASH is required for lysosomal recycling and efficient autophagic and phagocytic digestion. Mol Biol Cell. 2013 Sep;24(17):2714–2726. PubMed PMID: 23885127; PubMed Central PMCID: PMCPMC3756923.

[35] Lima WC, Leuba F, Soldati T, et al. Mucolipin controls lysosome exocytosis in Dictyostelium. J Cell Sci. 2012 May 01;125(Pt 9):2315–2322. PubMed PMID: 22357942.
[36] Neuhaus EM, Soldati T. A myosin I is involved in membrane recycling from early endosomes. J Cell Biol. 2000 Sep 04;150 (5):1013–1026. PubMed PMID: 10973992; PubMed Central PMCID: PMCPMC2175260.
[37] Otto GP, Wu MY, Kazgan N, et al. Dictyostelium macroautophagy mutants vary in the severity of their developmental defects. J Biol Chem. 2004 Apr 09;279(15):15621–15629. PubMed PMID: 14736886.
[38] King JS, Veltman DM, Insall RH. The induction of autophagy by mechanical stress. Autophagy. 2011 Dec;7(12):1490–1499. PubMed PMID: 22024750; PubMed Central PMCID: PMCPMC3327616.
[39] Calvo-Garrido J, Escalante R. Autophagy dysfunction and ubiquitin-positive protein aggregates in Dictyostelium cells lacking Vmp1. Autophagy. 2010 Jan;6(1):100–109. PubMed PMID: 20009561.
[40] Otto GP, Wu MY, Kazgan N, et al. Macroautophagy is required for multicellular development of the social amoeba Dictyostelium discoideum. J Biol Chem. 2003 May 16;278(20):17636–17645. PubMed PMID: 12626495.
[41] Dominguez-Martin E, Cardenal-Munoz E, King JS, et al. Methods to monitor and quantify autophagy in the social amoeba dictyostelium discoideum. Cells. 2017 Jul 03;6(3). PubMed PMID: 28671610. doi:10.3390/cells6030018
[42] Fukumori A, Okochi M, Tagami S, et al. Presenilin-dependent gamma-secretase on plasma membrane and endosomes is functionally distinct. Biochemistry. 2006 Apr 18;45(15):4907–4914. PubMed PMID: 16605258.
[43] Klionsky DJ, Emr SD. Autophagy as a regulated pathway of cellular degradation. Science. 2000 Dec 1;290(5497):1717–1721. PubMed PMID: 11099404; PubMed Central PMCID: PMCPMC2732363.
[44] Gekle M, Mildenberger S, Freudinger R, et al. Endosomal alkalinization reduces Jmax and Km of albumin receptor-mediated endocytosis in OK cells. Am J Physiol. 1995 May;268(5 Pt 2): F899–906. PubMed PMID: 7539587.
[45] Davies L, Farrar NA, Satre M, et al. Vacuolar H(+)-ATPase and weak base action in Dictyostelium. Mol Microbiol. 1996 Oct;22 (1):119–126. PubMed PMID: 8899714.
[46] Gopaldass N, Patel D, Kratzke R, et al. Dynamin A, Myosin IB and Abp1 couple phagosome maturation to F-actin binding. Traffic. 2012 Jan;13(1):120–130. PubMed PMID: 22008230.
[47] Feng T, Tammineni P, Agrawal C, et al. Autophagy-mediated regulation of BACE1 protein trafficking and degradation. J Biol Chem. 2017 Feb 03;292(5):1679–1690. PubMed PMID: 28028177; PubMed Central PMCID: PMCPMC5290944.
[48] Li Q, Liu Y, Sun M. Autophagy and Alzheimers disease. Cell Mol Neurobiol. 2017 Apr;37(3):377–388. PubMed PMID: 27260250.
[49] Buckley CM, Gopaldass N, Bosmani C, et al. WASH drives early recycling from macropinosomes and phagosomes to maintain surface phagocytic receptors. Proc Natl Acad Sci U S A. 2016 Oct 04;113(40):E5906–E5915. PubMed PMID: 27647881; PubMed Central PMCID: PMCPMC5056073.
[50] Cardenal-Munoz E, Arafah S, Lopez-Jimenez AT, et al. Mycobacterium marinum antagonistically induces an autophagic response while repressing the autophagic flux in a TORC1- and ESX-1-dependent manner. PLoS Pathog. 2017 Apr;13(4): e1006344. PubMed PMID: 28414774; PubMed Central PMCID: PMCPMC5407849.
[51] Lee JH, McBrayer MK, Wolfe DM, et al. Presenilin 1 maintains lysosomal Ca(2+) homeostasis via TRPML1 by regulating vATPase-mediated lysosome acidification. Cell Rep. 2015 Sep 01;12(9):1430–1444. PubMed PMID: 26299959; PubMed Central PMCID: PMCPMC4558203.
[52] Neely KM, Green KN, LaFerla FM. Presenilin is necessary for efficient proteolysis through the autophagy-lysosome system in a gamma-secretase-independent manner. J Neurosci. 2011 Feb 23;31(8):2781–2791. PubMed PMID: 21414900; PubMed Central PMCID: PMCPMC3064964.
[53] Steele JW, Fan E, Kelahmetoglu Y, et al. Modulation of autophagy as a therapeutic target for Alzheimers disease. Postdoc J. 2013 Feb;1(2):21–34. PubMed PMID: 28286801; PubMed Central PMCID: PMCPMC5342246.
[54] Buckley CM, King JS. Drinking problems: mechanisms of macropinosome formation and maturation. FEBS J. 2017 Nov;284 (22):3778–3790. PubMed PMID: 28544479.
[55] Chubb JR, Wilkins A, Thomas GM, et al. The Dictyostelium RasS protein is required for macropinocytosis, phagocytosis and the control of cell movement. J Cell Sci. 2000 Feb;113(Pt 4):709–719. PubMed PMID: 10652263.
[56] Hoeller O, Bolourani P, Clark J, et al. Two distinct functions for PI3-kinases in macropinocytosis. J Cell Sci. 2013 Sep 15;126(Pt 18):4296–4307. PubMed PMID: 23843627; PubMed Central PMCID: PMCPMC3772393.
[57] Bloomfield G, Traynor D, Sander SP, et al. Neurofibromin controls macropinocytosis and phagocytosis in Dictyostelium. Elife. 2015 Mar 27;4. PubMed PMID: 25815683; PubMed Central PMCID: PMCPMC4374526. doi:10.7554/eLife.04940
[58] Annesley SJ, Bago R, Bosnar MH, et al. Dictyostelium discoideum nucleoside diphosphate kinase C plays a negative regulatory role in phagocytosis, macropinocytosis and exocytosis. PLoS One. 2011;6(10):e26024. PubMed PMID: 21991393; PubMed Central PMCID: PMCPMC3186806.
[59] Commisso C, Davidson SM, Soydaner-Azeloglu RG, et al. Macropinocytosis of protein is an amino acid supply route in Ras-transformed cells. Nature. 2013 May 30;497(7451):633–637. PubMed PMID: 23665962; PubMed Central PMCID: PMCPMC3810415.
[60] Kozma R, Ahmed S, Best A, et al. The Ras-related protein Cdc42Hs and bradykinin promote formation of peripheral actin microspikes and filopodia in Swiss 3T3 fibroblasts. Mol Cell Biol. 1995 Apr;15(4):1942–1952. PubMed PMID: 7891688; PubMed Central PMCID: PMCPMC230420.
[61] Sasaki AT, Janetopoulos C, Lee S, et al. G protein-independent Ras/PI3K/F-actin circuit regulates basic cell motility. J Cell Biol. 2007 Jul 16;178(2):185–191. PubMed PMID: 17635933; PubMed Central PMCID: PMCPMC2064438.
[62] Hacker U, Albrecht R, Maniak M. Fluid-phase uptake by macropinocytosis in Dictyostelium. J Cell Sci. 1997 Jan;110(Pt 2):105–112. PubMed PMID: 9044041.
[63] Gruenberg J, Maxfield FR. Membrane transport in the endocytic pathway. Curr Opin Cell Biol. 1995 Aug;7(4):552–563. PubMed PMID: 7495576.
[64] Luzio JP, Rous BA, Bright NA, et al. Lysosome-endosome fusion and lysosome biogenesis. J Cell Sci. 2000 May;113(Pt 9):1515–1524. PubMed PMID: 10751143.
[65] Hu YB, Dammer EB, Ren RJ, et al. The endosomal-lysosomal system: from acidification and cargo sorting to neurodegeneration. Transl Neurodegener. 2015;4:18. PubMed PMID: 26448863; PubMed Central PMCID: PMCPMC4596472.
[66] Maxfield FR. Role of endosomes and lysosomes in human disease. Cold Spring Harb Perspect Biol. 2014 May 01;6(5):a016931. PubMed PMID: 24789821; PubMed Central PMCID: PMCPMC3996470.
[67] Fukuda T, Roberts A, Ahearn M, et al. Autophagy and lysosomes in Pompe disease. Autophagy. 2006 Oct-Dec;2(4):318–320. PubMed PMID: 16874053.
[68] Kirkegaard T, Roth AG, Petersen NH, et al. Hsp70 stabilizes lysosomes and reverts Niemann-Pick disease-associated lysosomal pathology. Nature. 2010 Jan 28;463(7280):549–553. PubMed PMID: 20111001.
[69] Mizushima N, Ohsumi Y, Yoshimori T. Autophagosome formation in mammalian cells. Cell Struct Funct. 2002 Dec;27 (6):421–429. PubMed PMID: 12576635.
[70] Xiong Q, Unal C, Matthias J, et al. The phenotypes of ATG9, ATG16 and ATG9/16 knock-out mutants imply autophagy-dependent and -independent functions. Open Biol.

2015 Apr;5(4):150008. PubMed PMID: 25878144; PubMed Central PMCID: PMCPMC4422124.

[71] Faix J, Kreppel L, Shaulsky G, et al. A rapid and efficient method to generate multiple gene disruptions in Dictyostelium discoideum using a single selectable marker and the Cre-loxP system. Nucleic Acids Res. 2004 Oct 26;32(19):e143. PubMed PMID: 15507682; PubMed Central PMCID: PMCPMC528815.

[72] Gaudet P, Pilcher KE, Fey P, et al. Transformation of Dictyostelium discoideum with plasmid DNA. Nat Protoc. 2007;2(6):1317–1324. PubMed PMID: 17545968.

[73] Rivero F, Maniak M. Quantitative and microscopic methods for studying the endocytic pathway. Methods Mol Biol. 2006;346:423–438. PubMed PMID: 16957305.

[74] Williams RS, Eames M, Ryves WJ, et al. Loss of a prolyl oligopeptidase confers resistance to lithium by elevation of inositol (1,4,5) trisphosphate. EMBO J. 1999 May 17;18(10):2734–2745. PubMed PMID: 10329620; PubMed Central PMCID: PMCPMC1171355.

[75] Schneider CA, Rasband WS, Eliceiri KW. NIH Image to ImageJ: 25 years of image analysis. Nat Methods. 2012 Jul;9(7):671–675. PubMed PMID: 22930834; PubMed Central PMCID: PMCPMC5554542.

[76] Sattler N, Monroy R, Soldati T. Quantitative analysis of phagocytosis and phagosome maturation. Methods Mol Biol. 2013;983:383–402. PubMed PMID: 23494319.

[77] Muller-Taubenberger A, Lupas AN, Li H, et al. Calreticulin and calnexin in the endoplasmic reticulum are important for phagocytosis. Embo J. 2001 Dec 03;20(23):6772–6782. PubMed PMID: 11726513; PubMed Central PMCID: PMCPMC125758.

[78] Hagedorn M, Neuhaus EM, Soldati T. Optimized fixation and immunofluorescence staining methods for Dictyostelium cells. Methods Mol Biol. 2006;346:327–338. PubMed PMID: 16957300.

[79] Davidson AJ, King JS, Insall RH. The use of streptavidin conjugates as immunoblot loading controls and mitochondrial markers for use with Dictyostelium discoideum. Biotechniques. 2013 Jul;55(1):39–41. PubMed PMID: 23834384.

Received: 24 April 2019 | Revised: 6 September 2019 | Accepted: 17 September 2019

DOI: 10.1111/bph.14892

RESEARCH PAPER

A new mechanism for cannabidiol in regulating the one-carbon cycle and methionine levels in *Dictyostelium* and in mammalian epilepsy models

Christopher J. Perry[1] | Paul Finch[1] | Annette Müller-Taubenberger[2] | Kit-Yi Leung[3] | Eleanor C. Warren[1] | Joseph Damstra-Oddy[1] | Devdutt Sharma[1] | Pabitra H. Patra[4] | Sarah Glyn[4] | Joanna Boberska[4] | Balint Stewart[5] | Amy Baldwin[6] | Fabiana Piscitelli[7] | Robert J. Harvey[8,9] | Adrian Harwood[6] | Christopher Thompson[5] | Sandrine P. Claus[4] | Nicholas D.E. Greene[4] | Alister J. McNeish[4] | Claire M. Williams[4] | Benjamin J. Whalley[4] | Robin S.B. Williams[1]

[1]Centre for Biomedical Sciences, Department of Biological Sciences, Royal Holloway University of London, Egham, UK

[2]Department of Cell Biology, Biomedical Center, LMU Munich, Planegg, Germany

[3]Development Biology and Cancer Program, UCL Great Ormond Street Institute of Child Health, London, UK

[4]The School of Chemistry, Food Biosciences and Pharmacy, University of Reading, Reading, UK

[5]Faculty of Life Sciences, Manchester University, Manchester, UK

[6]Neuroscience and Mental Health Research Institute, Cardiff University, Cardiff, UK

[7]Institute of Biomolecular Chemistry, Consiglio Nazionale delle Ricerche, Rome, Italy

[8]School of Health and Sport Sciences, University of the Sunshine Coast, Sippy Downs, QLD, Australia

[9]Sunshine Coast Health Institute, University of the Sunshine Coast, Birtinya, QLD, Australia

Correspondence
Robin S. B. Williams, Centre for Biomedical Sciences, Department of Biological Sciences, Royal Holloway University of London, Egham, Surrey TW20 0EX, UK.
Email: robin.williams@rhul.ac.uk

Background and Purpose: Epidiolex™, a form of highly purified cannabidiol (CBD) derived from *Cannabis* plants, has demonstrated seizure control activity in patients with Dravet syndrome, without a fully elucidated mechanism of action. We have employed an unbiased approach to investigate this mechanism at a cellular level.

Experimental Approach: We use a tractable biomedical model organism, *Dictyostelium*, to identify a protein controlling the effect of CBD and characterize this mechanism. We then translate these results to a Dravet syndrome mouse model and an acute in vitro seizure model.

Key Results: CBD activity is partially dependent upon the mitochondrial glycine cleavage system component, GcvH1 in *Dictyostelium*, orthologous to the human glycine cleavage system component H protein, which is functionally linked to folate one-carbon metabolism (FOCM). Analysis of FOCM components identified a mechanism for CBD in directly inhibiting methionine synthesis. Analysis of brain tissue from a Dravet syndrome mouse model also showed drastically altered levels of one-carbon components including methionine, and an in vitro rat seizure model showed an elevated level of methionine that is attenuated following CBD treatment.

Conclusions and Implications: Our results suggest a novel mechanism for CBD in the regulating methionine levels and identify altered one-carbon metabolism in Dravet syndrome and seizure activity.

Abbreviations: 5mTHF, 5′methyl THF; bsR, blasticidin S deaminase; CBD, cannabidiol; FOCM, folate one-carbon metabolism; GCS, glycine cleavage system; GCSH, human glycine cleavage system component H; GCVH1, *Dictyostelium* glycine cleavage system component H1; THF, tetrahydrofolate.

Funding information
Action Medical Research, Grant/Award Number: GN2403; Medical Research Council, Grant/Award Number: N003713; GW Research Ltd; University of Reading; BBSRC DTP, Grant/Award Number: N/A; GW Pharmaceuticals Ltd; National Institute for Health Research Biomedical Research Centre at Great Ormond Street Hospital for Children NHS Foundation Trust and University College London; Great Ormond Street Hospital Children's Charity; Bioimaging core facility

1 | INTRODUCTION

The use of *Cannabis* extracts as a medicinal treatment has been recorded for nearly 2,000 years (BRAND & ZHAO, 2017), covering a range of disorders including pain management, multiple sclerosis, and epilepsy (Devinsky et al., 2014). Of the ~100 cannabinoids found within, or derived from, *Cannabis* species, cannabidiol (CBD) is among the most abundant of the non-psychoactive cannabinoids and has received considerable interest as a therapeutic treatment (Jones et al., 2010; Jones et al., 2012). CBD has been shown to provide antiepileptiform and anti-seizure properties within numerous in vitro and in vivo mammalian epilepsy models (Jones et al., 2012; Klein et al., 2017). CBD is also used as a lead cannabinoid-based treatment for severe epilepsies such as Dravet syndrome (Devinsky et al., 2017) and Lennox–Gastaut syndrome (Devinsky et al., 2018; Thiele et al., 2018). A range of targets for CBD in seizure control have also been identified, including glycine receptors (Xiong et al., 2012), GPR55 (Kaplan, Stella, Catterall, & Westenbroek, 2017), NMDA receptors (Rodriguez-munoz, Onetti, Cortes-Montero, Garzon, & Sanchez-Blazquez, 2018), transient receptor potential of vanilloid type-1 channels (Vilela et al., 2017) and voltage-dependent anion selective channels (Rimmerman et al., 2013).

The cell and molecular basis of epilepsy and seizures is well-accepted to be related to electrical signalling and ion channel activity; however, a range of models have suggested that deregulation of several key amino acids is also involved in, or associated with, seizures and epilepsy (Bejarano & Rodriguez-navarro, 2015; Gupta et al., 2004). For example, numerous studies have proposed altered mitochondrial function in epilepsy pathology (Doccini et al., 2015; Kumar et al., 2016; Panneman, Smeitink, & Rodenburg, 2018; Pearson-smith, Liang, Rowley, Day, & Patel, 2017). Mitochondria contain the glycine cleavage system (GCS) that is responsible for regulation of glycine levels (Kikuchi & Hiraga, 1982) subsequently controlling numerous functions including protein synthesis and neurotransmission (Kolker, 2018). The GCS also plays a role in providing glycine-derived one-carbon units into the folate one-carbon metabolism (FOCM), leading through folate-containing intermediates, to production of methionine from homocysteine (Ducker & Rabinowitz, 2017). Isotope labelling has directly demonstrated 1C donation from glycine to FOCM in humans and mice in vivo (Lamers et al., 2009; Leung et al., 2017). Methionine fulfils a fundamentally important role in protein synthesis and as a precursor to S-adenosyl methionine (SAM) that is responsible for the transfer of a methyl group to a number of acceptor molecules including neurotransmitters and DNA methyltransferases (Moore, Le, & Fan, 2013). SAM is further hydrolysed to form adenosine and homocysteine which can again be converted into methionine or instead into cysteine. These various metabolites and amino acids have been described as "primordial" metabolites (Boison, 2016), suggested to provide the original components for the beginning of life, and are thus highly conserved across many species. In addition, many of these components are regulated by mitochondrial function and relate to energy production, where both have been proposed as mechanistic targets for cannabinoids (Bénard et al., 2012).

Understanding the molecular mechanisms of newly developed medicines provides an important aspect of validation, where simple biomedical model systems such as the social amoeba *Dictyostelium discoideum* have proved effective (Cunliffe et al., 2015; Warren,

What is already known

- CBD, a key constituent of Epidiolex™, is effective in the treatment of specific drug-resistant epilepsies.
- A full understanding of mechanisms for CBD-dependent s eizure control remains to be established.

What does this study add

- We identified a molecular mechanisms of CBD in regulating the one-carbon cycle components including methionine.
- We show one-carbon cycle components are deregulated in a Dravet model and during seizure-like activity.

What is the clinical significance

- Our data will increase clinical focus on one-carbon metabolism in epilepsy and other CBD-treatable disorders.
- Clinical studies relating to Dravet syndrome, in particular, will benefit from monitoring one-carbon signalling.

Walker, & Williams, 2018). *D. discoideum* is a eukaryote more evolutionarily related to animals than to plants and bacteria that possesses a range of highly conserved signalling pathways and proteins that have been linked to human diseases (Müller-taubenberger, Kortholt, & Eichinger, 2013). It exists in both a single cell stage, where cells divide by binary division, and a multicellular stage induced by starvation leading to the formation of small (~1 mm tall) fruiting bodies. Using *D. discoideum*, insertional mutant libraries have been employed to identify genes controlling the effect of a natural product or medicinal treatment (Cocorocchio et al., 2018; Waheed et al., 2014), including treatments for epilepsy (Chang et al., 2012; Warren et al., 2018) and bipolar disorder (Kelly, Sharma, Wilkinson, & Williams, 2018; Williams, Cheng, Mudge, & Harwood, 2002). In many of these studies, discoveries based in *D. discoideum* have been subsequently validated in mammalian models (Chang et al., 2013; Chang et al., 2015; Chang, Walker, & Williams, 2014; Waheed et al., 2014). Thus, employing *D. discoideum* to investigate the cellular mechanisms of CBD may provide a suitable, innovative approach to identify therapeutic mechanisms of this important cannabinoid.

In the initial phase of this study, we used *D. discoideum* to better understand the molecular mechanism of CBD. We show that CBD affects *D. discoideum* cell proliferation and by performing an unbiased genome wide screen, we identify a role for the mitochondrial GCS component, GCVH1, homologous to the human protein GSCH in this effect. Analysis of glycine, one-carbon cycle intermediates (methionine and cysteine), and folates confirmed a role for GCVH1 in regulating these components through attenuating activity of the GCS and suggested a novel molecular mechanism of CBD through inhibition of methionine synthase activity. We then examined the regulation of one-carbon-related amino acids in the brain of a mouse model of Dravet syndrome (*Scn1A*$^{+/-}$), a CBD responsive condition in humans (Thiele et al., 2018), and identified altered levels of glycine, methionine, and cysteine, implicating dysregulation of one-carbon metabolism in this disease. Moreover, methionine levels were altered in this model following chronic CBD treatment. We finally investigated this effect using an in vitro mammalian model of seizure activity, where methionine levels were shown to rapidly increase during seizure activity and this increase was corrected by CBD treatment.

2 | METHODS

2.1 | *D. discoideum* growth assay

D. discoideum cell lines grown in HL5 medium on a 10-cm dish were plated onto a 24-well plate at 5 × 10^3 cells per well in 495 μl of media (HL5, Formedia, UK). For each well, 5 μl of CBD from 100-mM stock in DMSO was added to achieve final concentrations ranging from 0- to 20-μM CBD (DMSO made up 1% of final volume). Cells were maintained at 22°C, counted after 72 hr (lag phase), and then every 24 hr. These data are presented as normalized (fold change from control [untreated, Day 7]) to correct for variation between independent experiments. Each concentration was analysed using at least six independent experiments, where rate of exponential cell growth (Days 4 to 6) at each concentration was used to create secondary plots (concentration–response curves), providing IC_{50} values for each cell type (wild type, mutants, and rescue lines), determined using non-linear regression analysis.

2.2 | *D. discoideum* development assay

Wild-type *D. discoideum* cells in the exponential phase of growth were washed in KK2 buffer (16.2-mM KH_2PO_4, 4-mM K_2HPO_4) and 1 × 10^7 cells placed onto a nitrocellulose filter (Millipore, Cork). Absorbent pads (Millipore, Cork) were placed in 2-ml culture dishes and soaked with 0.5-ml KK2 buffer containing CBD from 100-mM stock in DMSO to achieve a final concentration of 20 μM (DMSO made up 1% of final volume). Nitrocellulose filters and cells were placed upon absorbent pads and maintained in a humid environment at 22°C for 24 hr. Fruiting body morphology was recorded using a dissection microscope and camera.

2.3 | Restriction enzyme-mediated integration screen

A mutant library containing approximately 5,000 insertional mutants was created by restriction enzyme-mediated integration. Library cells taken from the exponential growth phase were screened for resistance to 9.47-μM CBD (80% inhibitory concentration) taken from 100-mM stock in DMSO. Cells were maintained at 22°C and screened over a 3-week period, with the media replaced every 2 days. Resistant mutants were isolated, and isogenic strains created. Location of the blasticidin S deaminase (bsR) insertion was identified using whole-genome next-generation sequencing (NGS).

2.4 | NGS analysis

Five hundred-nanogram DNA was fragmented on the Covaris S2 to a target size of 300 bp (intensity: 4, duty cycle: 10%, cycles-per-burst: 200, time: 80 s). A library was then prepared using the NEB DNA Ultra II kit (New England Biolabs, E7645), with bead selection for 300- to 400-bp fragments and five cycles of PCR. Sequencing was performed by UCL Genomics on an Illumina NextSeq 500, using a 150-bp paired-end protocol. NGS assemblies were performed using Sequencher software (RRID:SCR_001528), using Velvet (Zerbino & Birney, 2008) for de novo assembly, or GSNAP (RRID:SCR_005483) for bsR-cassette-guided assembly, to reveal the sites of bsR-cassette insertions in the *D. discoideum* genome using BLAST searches (RRID:SCR_001653).

2.5 | Creation of *gcvH1*$^-$ cell line and overexpression cell lines

In order to recapitulate the resistance seen in the insertional *gcvH1*$^-$ mutant, a *gcvH1*$^-$ cell line was created via homologous recombination. Primers to both the 5′ and 3′ region of *gcvH1* were used to amplify PCR products for both regions (Figure S1). A 281-bp fragment was amplified from the 5′ region, while a 343-bp fragment was amplified of the 3′ region (Figure S1). Both fragments were ligated into the pLPBLP plasmid flanking the bsR gene with their reading frames in opposite orientation to bsR. A knockout cassette consisting of bsR and the flanking *gcvH1* fragments was created by a *Spe*I/*Kpn*I restriction digest. Wild-type cells were transformed with the digested plasmid by electroporation. Transformants were selected by growing in liquid medium containing 10 μg·ml^{-1} blasticidin and screened for homologous recombinants. Primers were designed that would produce diagnostic knockout fragments unique to the homologously integrated transformants, as well as the necessary controls (Figure S1).

To create a gcvH1 overexpression plasmid (Figure S1), the gcvH1 cDNA was cloned into an extra-chromosomal vector (Fischer et al., 2004), enabling expression of the 42-kDa fluorescently labelled protein (Figure S2). The PCR product was digested with *Eco*RI and *Bam*HI and then ligated into the extra-chromosomal plasmid pDXA-389-2 and sequenced to confirm that no mutations were introduced. The resulting plasmid was transformed into *gcvH1*$^-$ cells and selected using geneticin (10 mg·ml^{-1}) to create an overexpression cell line. A cDNA encoding the *Homo sapiens* orthologue human glycine cleavage system component H (GCSH) was codon optimized for *D. discoideum* and amplified using primers 11 + 12. This was also inserted into pDXA-389-2 and a further overexpression cell line was created that overexpresses the human GCSH cDNA. In both cases, the recombinant proteins were tagged with RFP at the C-terminus.

2.6 | Analysis of *D. discoideum gcvH1* and *H. sapiens GCSH* expression by RT-PCR

Total RNA was extracted from cell lines using an RNeasy mini-kit (Qiagen). cDNA was synthesized from total RNA treated with DNase (Life Technologies) using a first-strand cDNA synthesis kit (Thermo Scientific). Gene expression was confirmed via RT-PCR using the primers 13 + 14 for the *D. discoideum* gene and primers 15 + 16 for the *H. sapiens* gene. A control was used based upon the constitutive expression of the *lg7* housekeeping gene using primers 17 + 18.

2.7 | Western blot analysis to confirm the presence of RFP fusion proteins in the overexpression cell lines

Cell lysates from cell lines were separated by gel electrophoresis, transferred to nitrocellulose membranes (Merck Millipore, IPFL00010), and analysed by Western blotting. A mouse anti-RFP primary antibody (Chromotek, 6G6 anti-RFP, 1:1,000) and a goat anti-mouse secondary antibody (Li-Cor goat anti-mouse IRDye®, 1:1,000) were used to confirm the presence of RFP. A conjugated anti-streptavidin antibody (Invitrogen, Streptavidin Alexa Fluor 680 conjugate) was used as a loading control. Blots were analysed using Odyssey software.

2.8 | Fluorescence and live-cell microscopy

The immuno-related procedures used comply with the recommendations made by the *British Journal of Pharmacology* (Alexander et al., 2018). For immunolabelling, *gcvH1*$^-$ cells, expressing either *D. discoideum* gcvH1-RFP or *H. sapiens* GCSH-RFP, were plated on round 12-mm glass coverslips and after 20 min were fixed with 15% picric acid/2% paraformaldehyde in 10-mM PIPES, pH 6.0, for 20 min and postfixed with 70% ethanol for 10 min. Cells were then washed three times in PBS, once with 10-mM PIPES and twice with PBS/1% glycine, and incubated in blocking buffer (PBS plus 2% BSA) for 1 hr at room temperature (RT). After blocking, the cells were washed three times with PBS and incubated with primary antibodies for 2 hr at RT, followed by the incubation with secondary antibodies and DAPI, to stain DNA, for 1 hr at RT. After immunostaining, samples were washed three times in PBS and embedded using Dako mounting medium (Agilent Technologies). For visualization of filamentous actin, cells were stained with Atto 488-phalloidin (Sigma Aldrich). In order to visualize mitochondrial porin, cells were stained with mouse monoclonal anti-porin antibodies (70-100-1; Troll et al., 1993), and Alexa 488-conjugated goat anti-mouse IgG. DNA was visualized by staining with DAPI. For live-cell microscopy, cells were seeded in μ-dishes (Ibidi, Germany) or open chambers as described previously (Fischer, Haase, Simmeth, Gerisch, & Muller-Taubenberger, 2004).

Confocal microscopy was performed at the Bioimaging core facility of the Biomedical Center (LMU Munich) using an inverted Leica TCS SP8 equipped with lasers for 405-, 488-, 552-, and 638-nm excitation. Images were acquired with an HC PL APO 63×/1.40 oil PH3 objective. Recording was sequentially to avoid bleed through. Atto-488 and Alexa-488 and RFP were recorded with the hybrid photo detectors and DAPI with the conventional photomultiplier tube.

2.9 | Amino acid analysis by GC–MS

GC–MS analysis of amino acid levels within either cell lysate or brain tissue was adapted from an earlier study (Svagera, Hanzlikova, Simek, & Husek, 2012), where 40 μl of sample (cell lysate or plasma) was spiked with 10 μl of DL-4-chlorophenylalanine (internal standard) followed by 10 μl of the reducing agent Tris(3-hydroxypropyl)phosphine (0.5% w/v in water). Samples were gently mixed and left to stand for 1 min before adding 40-μl trichloroacetic acid (0.6 M in water), vortexed twice, and samples centrifuged at 3,000 *g* for 10 min. Using 80 μl of supernatant, in a clean glass culture tube, 40 μl of a 3:1

1-propanol:pyridine mixture was added, followed by 130 μl of a reactive mixture containing a 10:3:1 mix of 2,2,4-trimethylpentane, butyl acetate, and propyl chloroformate. Samples were vortexed for 30 s and centrifuged at 3,000 *g* for 10 s, and the upper organic phase removed and used in GC–MS analysis. GC–MS was carried out on an HP5890 Series II chromatograph interfaced to an HP5972 MSD mass spectrometer; 2-μl samples were injected in splitless mode (injector temp 240°C, purge delay 1.0 min) on a J&W DB5 column or Abel AB-5MS (30 m × 0.25 mm dia × 0.25 μ film) using helium as the carrier gas at constant flow of 30 $cm \cdot s^{-1}$. The column oven was programmed from 90°C (2 min) to 300°C at 7.5°C·min^{-1}, the GC–MS interface temperature was 300°C. Retention times and mass spectra of derivatives of amino acids were determined in TIC mode and confirmed to be in agreement with library and literature data. Quantitative analysis was carried out in SIM mode using 4-chlorophenylalanine as internal standard. Chromatograms were integrated using MZmine (RRID:SCR_012040) or manually using Agilent MSD Chemstation to yield peak areas of amino acid derivatives relative to that from the internal standard, and peak areas were processed using Prism software (RRID: SCR_005375). To ensure unbiased analysis, samples were blinded and randomized prior to quantification. Samples size was estimated using data from a similar technique, where calculations with an observed effect of ≥20% suggested group size should be up to nine to observe an effect.

2.10 | Treatment of *D. discoideum* with CBD for folate and amino acid (GC–MS and NMR) analysis

Cells (5×10^6 cells) in the exponential phase of growth were plated onto a 10-cm tissue culture dish in 10 ml of HL5 medium. Cells were allowed to adhere for 30 min, and then the medium was replaced containing 1.89-μM CBD from 100-mM stock in DMSO. Plates were maintained at 22°C for 12 hr. Following the 12-hr incubation, cells were washed three times with KK2 buffer (16.2-mM KH_2PO_4, 4-mM K_2HPO_4), pelleted, and stored at −80°C. Prior to GC–MS analysis, 200 μl of sterile KK2 buffer with protease inhibitors was added to samples, which were briefly vortexed and subjected to five freeze thaw cycles from −80°C to 30°C. Samples were centrifuged at 5,000 *g* for 5 min and the cell lysate collected. The cell lysate was further centrifuged at 21,000 *g* for 10 min and the lysate collected for GC–MS analysis. To ensure unbiased analysis, samples were blinded and randomized prior to quantification.

2.11 | Quantification of folate-mediated one-carbon metabolism intermediates by MS

Analysis of multiple folates was performed by UPLC–MS/MS as described previously (Leung et al., 2017; Pai et al., 2015). Buffer containing 20-mM ammonia acetate, 0.1% ascorbic acid, 0.1% citric acid, and 100-mM DTT at pH 7 was added to cell pellets. Cell suspensions were sonicated for 10 s using a hand-held sonicator at 40% amplitude on ice. Protein was removed by precipitation with addition of two volumes of acetonitrile, mixing for 2 min and centrifugation for 15 min at 12,000 *g* and 4°C. Supernatants were transferred to fresh tubes, lyophilized, and stored at −80°C prior to analysis.

Lyophilized blinded samples were resuspended in 30-μl water (Milli-Q) and centrifuged for 5 min at 12,000 *g* at 4°C. Supernatants were transferred to glass sample vials for UPLC–MS/MS analysis. Metabolites were resolved by reversed-phase chromatography using Acquity UPLC BEH C18 column (50 mm × 2.1 mm; 1.7-μm bead size, Waters Corporation, UK). Solvents for UPLC were buffer A, 5% methanol, 95% Milli-Q water, and 5-mM dimethylhexylamine at pH 8.0; buffer B, 100% methanol. The column was equilibrated with 95% buffer A: 5% buffer B. The sample injection volume was 25 μl. The UPLC protocol consisted of 95% buffer A: 5% buffer B for 1 min, followed by a gradient of 5–60% buffer B over 9 min and then 100% buffer B for 6 min before re-equilibration for 4 min. The metabolites were eluted at a flow rate of 500 nl·min^{-1}. The UPLC was coupled to a XEVO-TQS mass spectrometer (Waters Corporation, UK) operating in negative-ion mode using the following settings: capillary 2.5 kV, source temperature 150°C, desolvation temperature 600°C, cone gas flow rate 150 L·hr^{-1}, and desolvation gas flow rate 1,200 L·hr^{-1}. Folates were measured by multiple reaction monitoring with optimized cone voltage and collision energy for precursor and product ions (as described in Leung et al., 2013).

2.12 | LC–MS-IT-TOF analysis of cellular CBD levels in *D. discoideum*

Cell pellets, blinded and randomized prior to quantification, were homogenized in acetone and sonicated in an ultrasonic bath for 8 min. An internal standard for CBD quantification by isotope dilution (d4-CBD 10 pmol) was added to the homogenate and extracted four times with acetone. The lipid-containing solution was dried down, weighed, and pre-purified by open bed chromatography on silica gel. Fractions were obtained by eluting the column with 99:1, 90:10, and 50:50 (v/v) chloroform/methanol. The 99:1 fraction was used for CBD quantification by LC–MS-IT-TOF analysis as described previously (Piscitelli, Pagano, Lauritano, Izzo, & Di Marzo, 2017).

2.13 | Amino acid analysis by NMR

Intracellular metabolites were extracted as previously described (Viant, 2007). Briefly, a two-phase extract was generated using a mixture of methanol, chloroform, and water in the volume ratio of 4:4:2.85. The aqueous phase containing water-soluble low molecular weight endogenous metabolites was transferred to microtubes, and solvents were removed using a vacuum concentrator Eppendorf AG (Eppendorf, Hamburg, Germany), 8 hr at 60°C. Samples were then reconstituted in 70 μl of NMR phosphate buffer (pH 7.4) 0.2 M (80% of D_2O, 20% of H_2O, 3-(trimethylsilyl)propionic-2,2,3,3-d4 acid;

Sigma-Aldrich) 1 mM, serving as NMR reference, vortexed for 10 s, and centrifuged at 12 000 g at 4°C for 10 min; 60 μl of resulting supernatant was pipetted into a 1.7-mm capillary tube (Bruker, UK) for NMR analysis.

NMR analysis was carried out using a Bruker AV700 NMR instrument equipped with a 5-mm inverse cryoprobe. A standard one-dimensional nuclear Overhauser effect spectroscopy experiment was performed on each sample, using a standard preset pulse sequence (noesypr1d, 90° pulse length at 9.25 μs, total acquisition time of 2 s, and water pre-saturation during relaxation delay of 5 s). All samples were analysed at 297 K and free induction decay was acquired on 19,607 data points (spectral width 9,803.9 Hz) using 512 scans (eight dummy scans). Free induction decay was then zero filled to 64 k points, and line broadening of 0.6 Hz was applied prior to fast Fourier transform. Phase and baseline corrections were performed manually using MestreNova software (version 10.0 m MestreLab Research). NMR spectra were referenced to 3-(trimethylsilyl) propionic-2,2,3,3-d4 acid peak at 0 ppm. All samples were blinded prior to analysis.

2.14 | Amino acid analysis of brain samples of a heterozygous *Scn1a* mouse model treated with CBD

129S-*Scn1a*$^{tm1Kea/Mmjax}$ heterozygote ($^{+/-}$) male mice (Jackson Laboratory, USA), maintained in the Bioresource Unit, University of Reading, were crossed with female C57BL/6 mice (Charles River, UK) to obtain hybrid *Scn1a* heterozygote ($^{+/-}$) and wild-type animals used in this study. This strain of *Scn1a*$^{+/-}$ mice show the characteristics of Dravet syndrome, a severe form of childhood epilepsy (Miller, Hawkins, McCollom, & Kearney, 2014). *Scn1a*$^{+/-}$ (epileptic) animals were randomly assigned to either vehicle (ethanol: kolliphor®: 0.9% saline = 2:1:17; n = 10) or CBD (100 mg·kg^{-1} twice daily subcutaneous injection, n = 10; GW Pharmaceuticals batch number 070214) for 6 weeks from postnatal Day 8 onwards. Likewise, a wild-type group was taken as healthy control (n = 9) and treated with vehicle for 6 weeks. All the animals were group housed and maintained in a 12 hr:12 hr dark:light cycle at an RT of 21°C and humidity of 50 ± 10%, with ad libitum access to food and water. This experiment was conducted in the dark cycle (dim red light 8:00–20:00), and injections were made at circa 8 a.m. and circa 8 p.m. by both male and female experimenters. The dose of CBD used here was selected to compare with the effective clinical dose used in humans to treat Dravet syndrome and epilepsy in other rodent models (Patra et al., 2019) estimated using a method as described earlier (Nair & Jacob, 2016). At the end of the treatment period, all animals were humanely killed by cervical dislocation for collection of blood (heparinized tube; Fisher Scientific, UK) and brain (flash frozen in liquid nitrogen). Tissue was stored at −80°C until used in amino acid analyses. The experiments were conducted following UK Home Office regulations (Animals [Scientific Procedures] Act, 1986) under licence 70/8397 "Mouse Model of Dravet Syndrome" and was approved by the Animal Welfare and Ethics Review Board at the University of Reading. We used previous data from a similar technique and standard sample size calculations to estimate group size to observe an effect ≥20%, suggesting a group size should be up to nine animals to observe an effect. To ensure unbiased analysis, samples were blinded and randomized prior to quantification. Unfortunately, we could not determine the effect of CBD on one-carbon cycle amino acids in healthy animals as our previous preliminary data did not warrant inclusion of this group in a chronic dosing study as CBD is well tolerated in healthy rodents. Animal studies are reported in compliance with the ARRIVE guidelines (Kilkenny, Browne, Cuthill, Emerson, & Altman, 2010) and with the recommendations made by the *British Journal of Pharmacology*.

2.15 | Acute seizure model of rat primary hippocampal neurons treated with pentylenetetrazol and CBD

Pregnant female Sprague-Drawley rats (4–5 months old) at 18 days of gestation were culled by concussion. The embryos were removed and 5×10^5 cells were extracted from the embryo hippocampi, seeded onto a six-well plate and matured for 21 days in modified neurobasal medium (Thermo Fisher Scientific, UK) with B27 supplement (1 ml/50 ml). Intervention groups were treated with CBD from 100-mM stock in DMSO to a final concentration of 1.89 μM and incubated at 37°C and 5% CO_2 with sample provided for analysis randomized and blinded. After 1 hr of incubation, both intervention and untreated cells were treated with pentylenetetrazol (PTZ) from 1-M stock to a final concentration of 5 mM and placed at 37°C and 5% CO_2 for 20-min cells. Media was aspirated and the cells were washed three times with ice cold PBS. Cells were lysed for 10 min using 200-μl RIPA buffer containing protease inhibitors and then collected using a cell scraper. Samples were immediately frozen at −80°C and used in subsequent GC–MS and protein analyses.

2.16 | Data and analysis

The data and statistical analysis comply with the recommendations of the *British Journal of Pharmacology* on experimental design and analysis in pharmacology (Curtis et al., 2018). The distribution of all experimental data was tested for using the Anderson–Darling test for normality. All data that showed a Gaussian distribution were analysed using parametric tests. No outliers were excluded from analysis. Normally distributed data from two groups were statistically analysed using a Student's t-test. The one-way ANOVA statistical test was used to test for significance between the means of three or more independent groups of normally distributed data. In conjunction with the one-way ANOVA, Tukey multiple comparison tests were performed to test for significance between all possible pairs of means. All experimental data involving two independent variables were analysed using a two-way ANOVA. The two-way ANOVA was used to test for an interaction between these independent variables and

the dependent variable. In conjunction with the two-way ANOVA, a Bonferroni multiple comparison test was performed to test for significance between all possible pairs of means. Post hoc analysis in ANOVA tests was only performed if the F-test value of the ANOVA reached significance ($P < .05$). N values are defined as a sample derived from an individual animal or experiment, that is, technical replicates were not considered as an n value. Only data with $n \geq 5$ were statistically analysed. Data were considered statistically significant if $P < .05$. Data provided in the results are not paired, and thus the number in each group does not need to be identical (providing each set of data was sufficiently powered). We have thus always performed a minimum of six experiments and that each group was statistically powered to see the effect size observed.

2.17 | Materials

CBD was provided by GW Research Ltd.

2.18 | Nomenclature of targets and ligands

Key protein targets and ligands in this article are hyperlinked to corresponding entries in http://www.guidetopharmacology.org, the common portal for data from the IUPHAR/BPS Guide to PHARMACOLOGY (Harding et al., 2018), and are permanently archived in the Concise Guide to PHARMACOLOGY 2017/18 (Alexander et al., 2017).

3 | RESULTS

3.1 | Investigating cellular mechanisms of CBD in the model system *D. discoideum*

To investigate a molecular mechanism of CBD, independent of previously described targets and effects, we initially employed the tractable model *D. discoideum*. Treatment with CBD at concentrations from 0 to 20 μM caused a concentration-dependent inhibition of unicellular growth, providing a readout for mechanistic studies (Figure 1a). Growth inhibition had an IC_{50} of 1.9 μM (95% CI [1.6–2.2 μM]; Figure 1b), where growth was significantly reduced at 0.5 μM ($P < .05$) and blocked at 20 μM CBD. This concentration is close to steady-state plasma levels shown in clinical studies (Devinsky et al., 2017; Devinsky et al., 2018), rather than high concentrations reported in some investigations (Bih et al., 2015). These data suggest the presence of CBD-sensitive processes in *D. discoideum*, with regulation of a potential target at similar concentrations shown to block seizure activity in mammalian models (Jones et al., 2012; Kaplan et al., 2017; Klein et al., 2017).

We continued by analysing the effect of CBD on *D. discoideum* development, a process where starvation initiates aggregation and the formation of multicellular fruiting bodies over a 24-hr period (Kelly et al., 2018). In this model, development and cellular growth can be mutually exclusive cell functions, controlled by groups of both independent and common proteins, providing the opportunity to assess the effect of CBD on both functions. Cell aggregation and development led to the formation of mature fruiting bodies in the absence and presence of CBD (20 μM; Figure 1c), demonstrating that CBD had no effect on development. Hence, the CBD target is necessary for cellular growth but is not involved in multicellular development, suggesting a specific molecular effect in this model rather than a general toxic effect.

3.2 | Identification of *D. discoideum* GCVH1 and *H. sapiens* GCSH as regulators of CBD cellular function

In order to understand the effect of CBD on *D. discoideum* growth, we sought to identify molecular requirements for CBD action by isolating mutants with reduced CBD sensitivity in a genetic screen of an insertional mutant library (Figure 2a). A library of mutants was treated with CBD at a concentration that inhibits cell growth by 80% (9.5 μM). After 2-week incubation, four CBD-resistant mutants were isolated and the insertionally inactivated gene potentially controlling CBD sensitivity was identified using inverse PCR (Keim, Williams, & Harwood, 2004) or whole-genome sequencing (Figure S1). This approach identified a CBD-resistant *gcvH1*$^{-}$ mutant, with an insertion in exon 1 of *gcvH1* (DDB_G0287773) encoding the glycine cleavage system H protein (GCVH1; Figure 2b). The *gcvH1*$^{-}$ mutant was recapitulated in wild-type cells by removal of a central part of the encoding gene by homologous recombination and the mutant was confirmed to have lost *gcvH1* expression (Figures S2 and S3).

We further assessed if *D. discoideum* GCVH1 is a likely homologue of GCSH (UniProt P23434). GCSH and GCVH1 are of similar size and domain structure and contain a mitochondrial-targeting peptide sequence at the N-terminus (Figure 2b). Similarly, both proteins possess a lipoyl-binding domain containing a highly conserved motif (Figure 2c), including a key lysine residue that binds the lipoic acid co-factor to facilitate shuttling of the glycine intermediates within the GCS. This motif is highly conserved throughout the kingdom of life (Figure 2d; Kikuchi & Hiraga, 1982). This analysis suggests that the *D. discoideum* GCVH1 protein is likely to represent a homologue of the mammalian GSCH, with similar catalytic activity and function. Since changes in glycine (Boison, 2016; Lynch, 2004; Xiong et al., 2012) and components of glycine in the one-carbon cycle such as adenosine have been associated with epilepsy (Boison, 2016; Kobow et al., 2013), we continued our analysis of this mutant rather than the other identified mutants (Figure S1).

We then investigated whether the *D. discoideum* GCVH1 protein localizes to mitochondria, consistent with the localization of GCSH in mammalian systems using fluorescently tagged gcvH1 (GCVH-RFP) expressed in *gcvH1*$^{-}$ cells (Figures 3 and S3). Visualization of the resulting GCVH1-RFP expressing cells showed localization in small intracellular dots corresponding to mitochondria seen by phase-contrast microscopy (Figures 3a, S4, S5, and S6). A

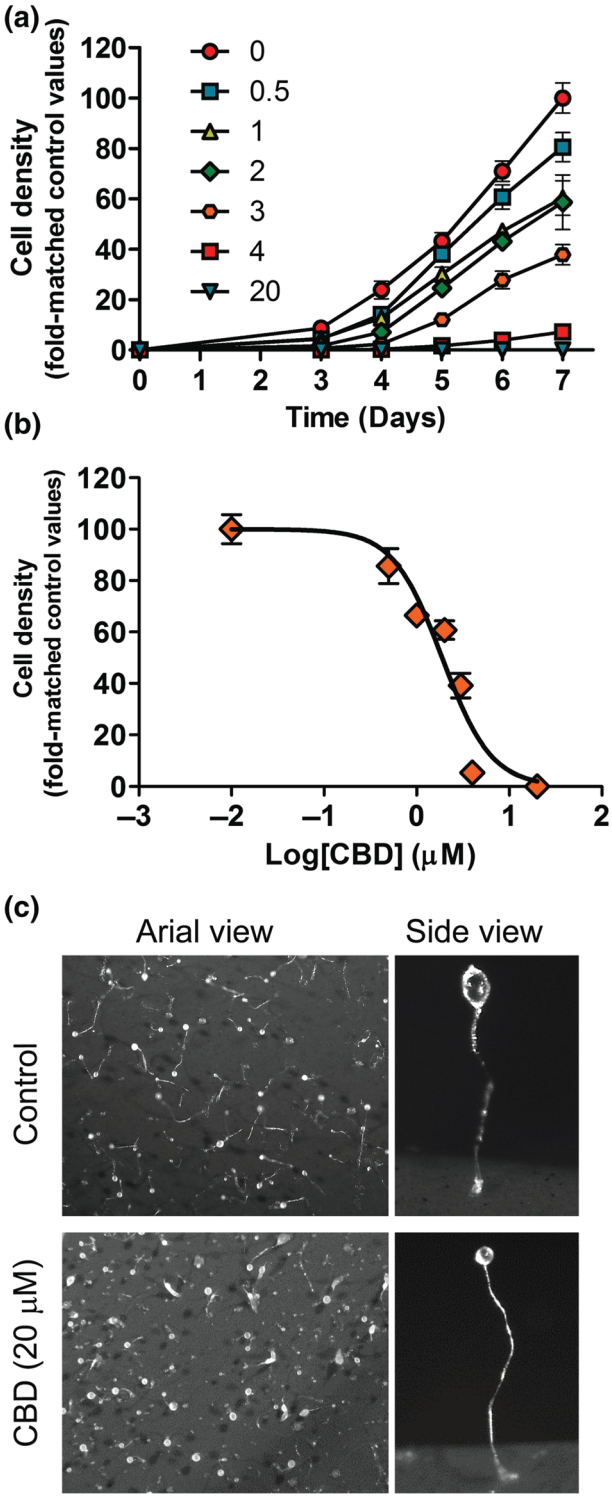

FIGURE 1 Cannabidiol (CBD) is likely to have molecular targets in *D. discoideum* cell affecting proliferation but not development. (a) The effect of CBD on *D. discoideum* cell growth was treated over a 7-day period under a range of indicated concentrations (μM), with CBD blocking growth at 4 μM (data derived from 6 to 9 independent experiments) and presented as normalized to fold change from control values (untreated, Day 7). (b) A concentration–response curve of normalized cell density against the Log (concentration) of CBD was used to calculate the IC_{50} value with a 95% confidence interval. (c) The effect of CBD on *D. discoideum* development was analysed using cells plated upon nitrocellulose filters under starvation conditions where fruiting bodies were formed, shown for a field of fruiting bodies (aerial view) and for a single fruiting body. Treatment of cells with either 20 μM CBD or vehicle alone did not block development (n = 9)

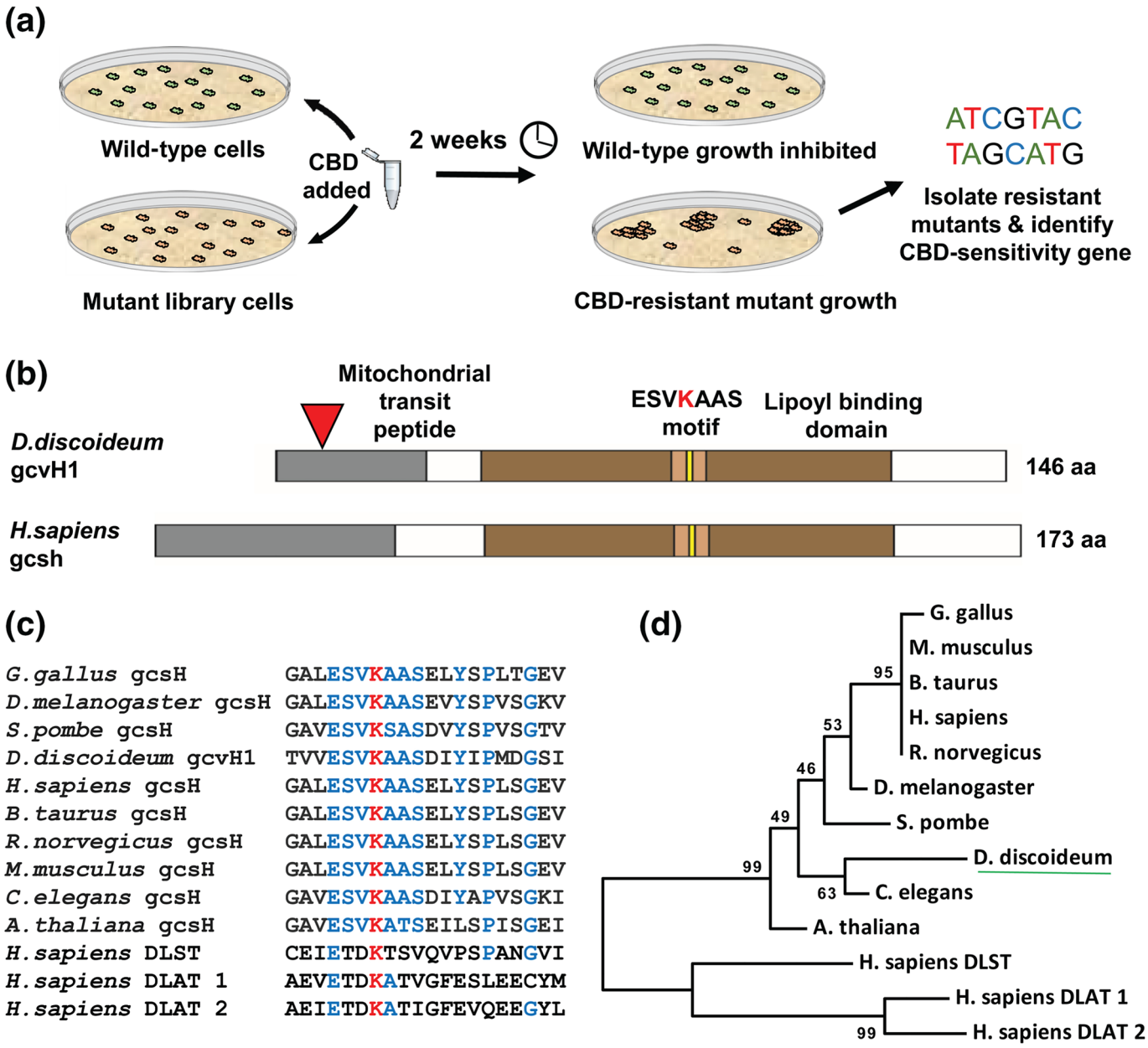

FIGURE 2 Identifying a role for the glycine cleavage system component, GCVH1, in regulating the cellular effect of CBD in *D. discoideum*. (a) A genetic screen of an insertional mutant library was carried out to identify mutants unaffected by the inhibitory effects of CBD on growth. (b) This screen identified GCVH1 as a potential molecular target for CBD, with an insertion in the first of three exons (red triangle), interrupting the coding region. Both the *D. discoideum* and the *H. sapiens* GCVH1 proteins are of similar size and contain highly conserved functional domains, include a mitochondrial localization sequence/transit peptide and a lipoyl binding domain, containing the ESVKAAS motif for lipoic acid binding. (c) The lipoic acid binding motif is highly conserved across a broad range of species but absent in the related dihydrolipoyllysine-residue succinyltransferase (DLST/DLAT) proteins. (d) Such conservation highlights the evolutionary similarity of *D. discoideum* GCVH1 to orthologues found in higher organisms

similar localization was seen on overexpression of *H. sapiens* GCSH-RFP (Figures 3b and S4). To validate this localization, cells were fixed and probed with antibodies to both RFP and porin, a mitochondrial protein (Troll et al., 1992). Porin labelling encapsulated both GCVH1-RFP and GCSH-RFP proteins (Figure 3a,b), consistent with a mitochondrial matrix localization of both GCS proteins and the mitochondrial membrane localization of porin. These data, together with three-dimensional reconstruction of labelling (Figures 3c, S4, S5, and S6), confirm a localization of the GCVH1 and the *H. sapiens* orthologue GCSH in mitochondria in *D. discoideum*, consistent with a role for these proteins in the GCS.

To confirm a role for gcvH1 in the regulation of CBD sensitivity, growth resistance to CBD was assessed in the *gcvH1*$^{-}$ mutant and following rescue with GCVH1-RFP and GCSH-RFP proteins. The *gcvH1*$^{-}$ cell line showed partial resistance to CBD (Figures 4a and S7) with a growth inhibitory constant (IC_{50}) of

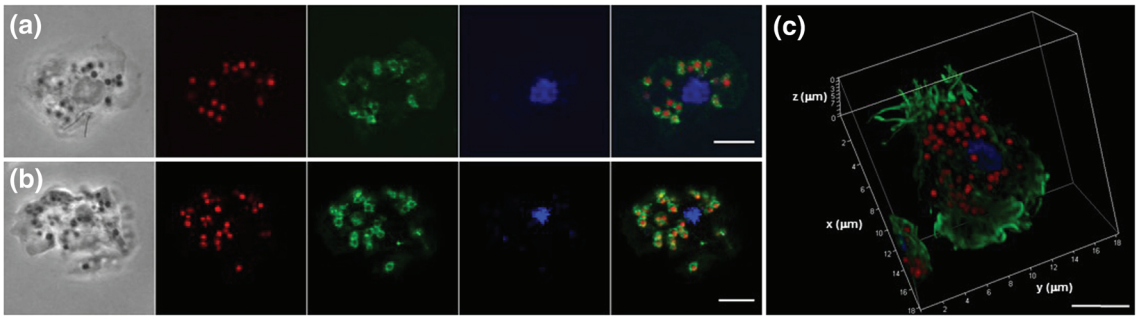

FIGURE 3 The *D. discoideum* GCVH1 and *H. sapiens* GCSH proteins localize to mitochondria in *D. discoideum*. (a) Confocal imaging of *D. discoideum* gcvH1$^-$ cells expressing *D. discoideum* GCVH1-RFP, imaged using phase contrast, with RFP fluorescence (red), a porin antibody (green), and DAPI to visualize DNA (blue), and with a merged fluorescence image on the right. (b) Shows *D. discoideum* gcvH1$^-$ cells expressing *H. sapiens* GCSH-RFP, imaged using phase contrast, with RFP fluorescence (red), a porin antibody (green), and DAPI to visualize DNA (blue), and with a merged fluorescence image on the right. (c) Three-dimensional reconstruction of *D. discoideum* gcvH1$^-$ cells expressing *D. discoideum* GCVH1-RFP, using RFP fluorescence (red), filamentous actin imaged using Atto488-phalloidin (green), and DAPI to visualize DNA (blue). Scale bars correspond to 5 μm

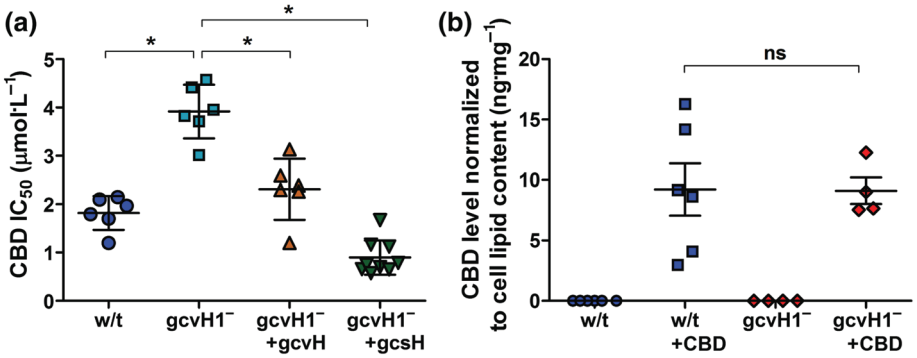

FIGURE 4 The CBD-resistant phenotype through loss of GCVH1 is rescued by both *D. discoideum* GCVH1 and *H. sapiens* GCSH proteins and is not caused by reduced CBD uptake or increased removal/degradation. (a) Concentration–response assays of wild-type, gcvH1$^-$, and rescue cell lines with either the *D. discoideum* or *H. sapiens* genes replaced was carried out. Data are mean +/− SEM (*, $P < .05$ one-way ANOVA, Tukey post hoc test). (b) Cellular CBD levels were quantified within wild-type *D. discoideum* and gcvH1$^-$ cell lines using LC–MS-IT-TOF following a prolonged CBD treatment regime ($n = 4$ or 6 as indicated). Data are mean +/− SEM ($P > .05$, Student's *t*-test)

4.2 μM (95% CI [3.2–5.3 μM]). Expressing either *D. discoideum* GCVH1-RFP or *H. sapiens* GCSH-RFP protein in *gcvH1*$^-$ restored sensitivity to growth inhibition, with IC_{50} of 2.2 μM (95% CI [1.6–2.9 μM]) and 0.82 μM (95% CI [0.67–1.0 μM]) respectively (Figures 4a, S3, and S7). These data support a role for both GCVH1 and GCSH in regulating CBD sensitivity, in addition to confirming a common function of the *D. discoideum* and the *H. sapiens* proteins.

To ensure the resistance observed in the *gcvH1*$^-$ mutant was not from increased xenobiotic degradation or a decreased uptake and increased removal of CBD, we quantified cellular CBD levels in mutant and wild-type cells. Here, cells were treated with CBD (1.89 μM) for 12 hr, and cellular CBD levels were quantified by LC–MS. No significant difference in CBD levels was found between wild-type and the *gcvH1*$^-$ cell lines (Figure 4b). This supports the hypothesis that the effect of CBD is dependent upon a pathway controlled by the mitochondrial GCS (GCVH1 or GCSH) but not by CBD metabolic degradation or transport.

3.3 | Monitoring one-carbon cycle amino acids and folates in *D. discoideum* following CBD treatment

We then sought to examine the molecular mechanism underlying the role of GCVH1 in CBD sensitivity, focusing on the function of the GCS and the interacting FOCM components (Figure 5a). In these experiments, we first examined the role of GCVH1 in regulating glycine, methionine, and cysteine levels using GC–MS. We found that glycine levels were significantly increased in *gcvH1*$^-$ cells compared to wild-type cells ($P < .05$), with a moderate decrease in methionine levels ($P < .05$) and no change in cysteine levels, supporting a role for the encoded protein in the GCS (Figure 5b). We then examined the effect of CBD treatment in both wild-type *gcvH1*$^-$ cells (using 1.89 μM for 12 hr), where CBD gave no change in glycine levels. In contrast, methionine levels were significantly reduced in wild-type cells following CBD treatment ($P < .05$), and this effect was lost in *gcvH1*$^-$ cells, consistent with a CBD-dependent inhibitory effect on methionine synthesis that is suppressed in *gcvH1*$^-$ cells (Figure 5b).

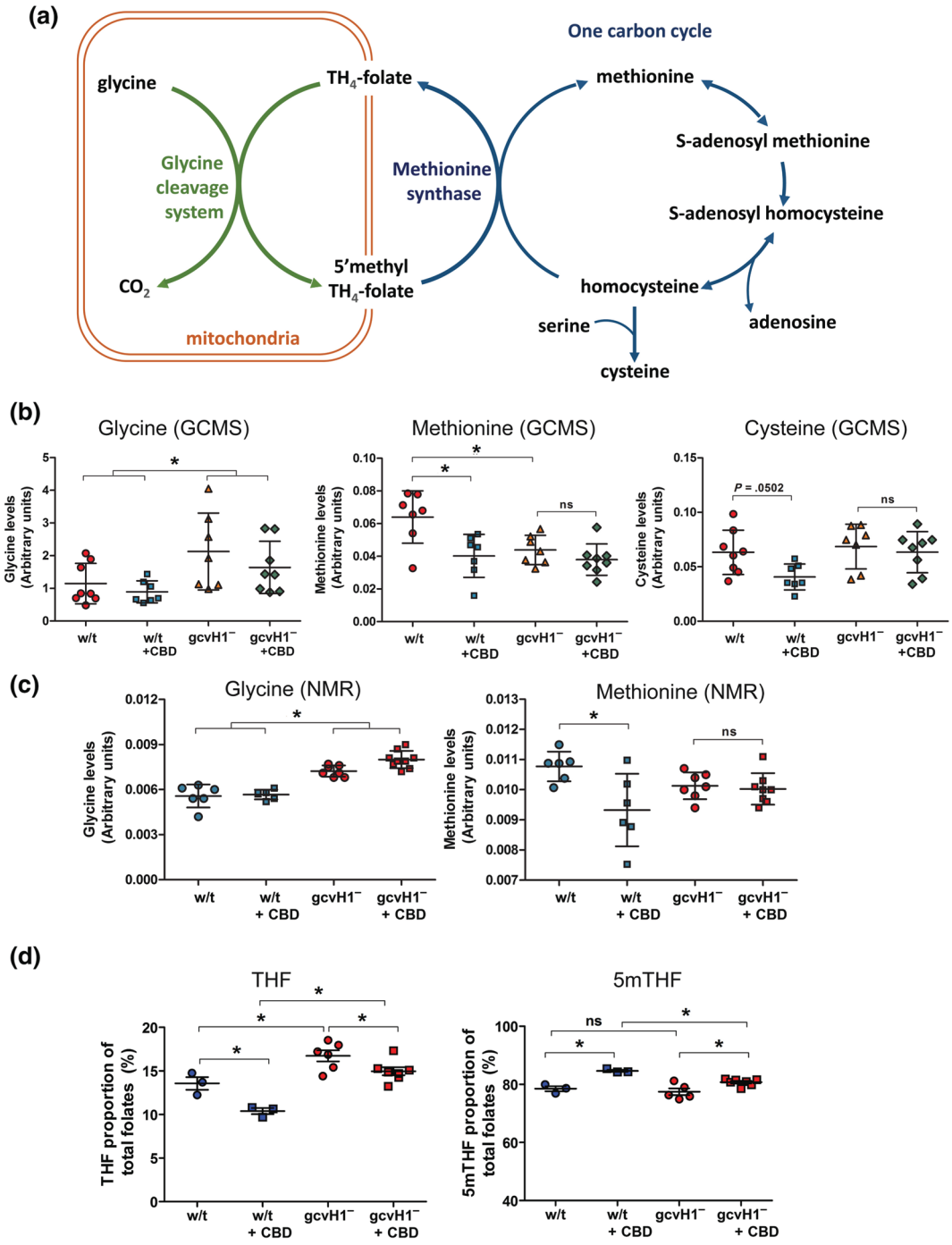

FIGURE 5 CBD treatment regulates the one-carbon cycle and folate signalling dependent upon the glycine cleavage system in *D. discoideum*. (a) A schematic diagram showing how the glycine cleavage system (GCS—green) found within the mitochondria (orange) is linked to the one-carbon cycle (blue), involving key amino acids—glycine, methionine, and cysteine, with methionine synthase providing the key point of interaction between the two systems. (b) To analyse changes in these systems, both wild-type and gcvH1⁻ cell lines were treated with CBD (1.89 μM, 24 hr) or vehicle alone, and their amino acid composition was analysed by GC–MS (n = 6–9). Analysis shows that gcvH1 ablation and CBD treatment alters the levels of methionine and glycine. (c) Amino acid level changes were supported using NMR analysis (n = 6–9). All data are mean +/− SEM (*, P < .05, two-way ANOVA, Bonferroni post hoc test). (d) Folate-containing compounds tetrahydrofolate (THF) and 5-methyltetrahydrofolate (5mTHF) were also assessed following equivalent treatment conditions (n = 3–7) consistent with a reduction in the glycine cleavage system by loss of GCVH1, and a CBD dependent increase in 5′mTHF consistent with a mechanism of CBD through inhibition of methionine production. All data are mean +/− SEM (*, P < .05, two-way ANOVA, Bonferroni post hoc test)

Similar notable trend towards reduced cysteine levels ($P = .0502$) were observed in wild-type cells following CBD treatment that was again absent in the *gcvH1*$^{-}$ mutant (Figure 5b). These data support a role for CBD in reducing methionine synthase activity, dependent upon GCS activity. We independently confirmed these changes using an NMR-based approach with an identical treatment regimen used in the GC–MS analysis. Again, glycine levels were elevated in the *gcvH1*$^{-}$ mutant compared to wild-type cells ($P < .05$; Figure 5c) but did not change following CBD treatment. Here, CBD treatment again caused a significant reduction in wild-type methionine levels ($P < .05$) with this effect lost in the *gcvH1*$^{-}$ mutant (Figure 5c), again consistent with GC–MS results. Thus, these two distinct approaches highlight a common effect of CBD in reducing methionine levels and show that the effects of CBD on these components are reliant upon activity of the GCS.

We continued by analysing the potential effect of CBD treatment on the relative abundance of folate mediators of one-carbon metabolism, with exploratory analysis of wild-type and *gcvH1*$^{-}$ cells, using LC–MS/MS. Comparison of folate profile in wild-type and untreated *gcvH1*$^{-}$ cells identified a significant ($P < .05$) increase in tetrahydrofolate (THF) levels in mutant, consistent with impaired activity of the GCS (Leung et al., 2017; Figure 5d). Following CBD treatment, wild-type cells showed a significant 23% reduction in THF levels ($P < .05$), with a concomitant 8% increase in 5-methylTHF (5mTHF; $P < .05$; Figure 5d). As with lower methionine abundance, this effect is consistent with a CBD-dependent block in methionine synthase activity. In comparison, *gcvH1*$^{-}$ cells showed a reduced sensitivity to the effect of CBD, with only a 7% increase in THF and a 3% decrease in 5mTHF following treatment (both $P < .05$). Hence, difference in THF levels between *gcvH1*$^{-}$ cells and wild-type cells ($P < .05$) was of greater magnitude following CBD treatment (Figure 5d). These data implicate a role for CBD in reducing methionine synthase activity in this model as a potential mechanism underlying diminished THF production, with ablation of *gcvH1*$^{-}$ attenuating this effect.

3.4 | Monitoring amino acid regulation in a Dravet syndrome epilepsy model following CBD treatment

We then investigated potential changes in amino acid signalling in epilepsy models. First, we employed a heterozygous *Scn1a*$^{+/-}$ mouse model lacking one copy of the $Na_V1.1$ protein (Thiele et al., 2018) that is used as a model for a variety of seizure types from simple febrile seizures to severe genetic disorders such as Dravet (Nakayama et al., 2018) and Lennox–Gastaut syndromes (Zhou et al., 2018). We initially analysed brain amino acid levels in healthy (wild-type) and *Scn1a*$^{+/-}$ mice, where a significant increase in glycine ($P < .05$) and methionine ($P < .05$) levels and a decrease in cysteine ($P < .05$) levels were found in these epileptic model mice compared to wild-type controls (Figure 6a). We also examined potential changes in these amino acids following 6-week CBD treatment (twice daily subcutaneous injection at 100 mg·kg^{-1}). In CBD-treated *Scn1a*$^{+/-}$ animals, glycine, methionine, and cysteine remained deregulated compared to untreated animals (Figure 6a), consistent with a role of these elevated amino acid levels providing a trait marker for Dravet syndrome, although methionine levels significantly increased ($P < .05$) following CBD treatment above that of untreated animals. This CBD-dependent increase was unexpected, as brain levels of methionine are normally tightly regulated in healthy animals (Gupta et al., 2004; Selmer, Lund, Brandal, Undlien, & Brodtkorb, 2009). These insights suggest that

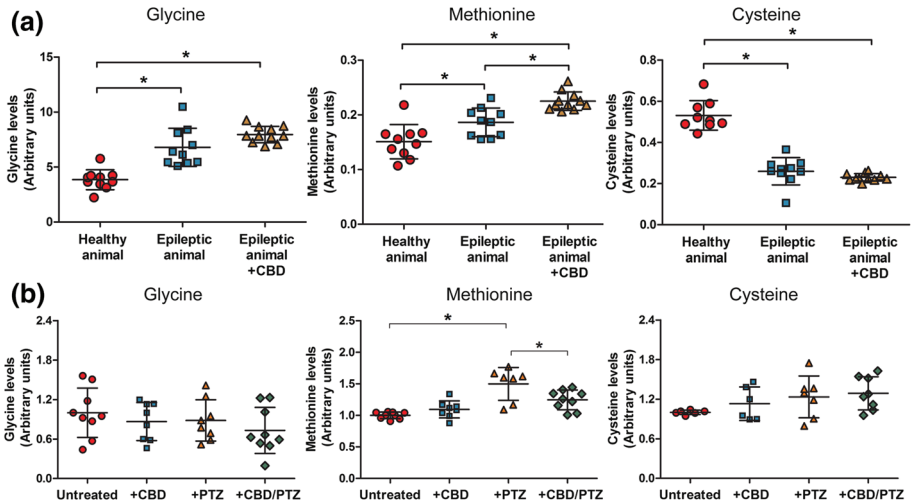

FIGURE 6 A Dravet syndrome model and an in vitro seizure model implicate the one-carbon (amino acid) cycle as a potential mechanistic target of cannabidiol (CBD) treatment in epilepsy. (a) Analysis of one-carbon cycle amino acids (glycine, methionine, and cysteine) in a mouse *Scn1a*$^{+/-}$ Dravet model suggests significant dysregulation of these amino acids in brain tissue, with chronic CBD-treatment further modifying methionine levels. (b) Analysis of rat primary hippocampal neurons, pretreated with CBD (60 min 1.89 μM), or following induction of seizure-like activity induced with PTZ (with or without CBD treatment), shows no alteration in glycine or cysteine levels but demonstrates elevates methionine levels upon seizure induction, with this increase attenuated by CBD treatment. Data are shown as mean ± SEM (*, $P < .05$, one-way ANOVA, Tukey post hoc test, $n \geq 7$)

in the Dravet model, extended treatment with CBD modulates levels of methionine, a key component of one-carbon metabolism.

3.5 | Monitoring one-carbon metabolism amino acids in an in vitro seizure model following CBD treatment

Since the Dravet model mice showed altered levels of methionine following long-term CBD treatment, we also employed an in vitro seizure model to investigate potential changes in this amino acid (and glycine and cysteine) at a cellular level following acute CBD treatment. Here, primary hippocampal neurons from wild-type rats were matured for 21 days to develop synaptic connections and pretreated with CBD (1.89 μM for 60 min) followed by the induction of seizure-like activity by treatment with 5-mM PTZ for 20 min (Chang et al., 2014). PTZ is known to be a $GABA_A$ receptor antagonist and has been used extensively in epilepsy research to induce seizure activity by preventing the inhibitory response of GABA (Armand, Louvel, Pumain, & Heinemann, 1998). In this acute model, neurons showed a significant increase in methionine levels following seizure induction ($P < .05$), consistent with that observed in the Dravet model brain, while this increase was significantly reduced by pretreatment with CBD ($P < .05$; Figure 6b). No significant changes in cysteine or glycine levels were found following seizure-like activity or with CBD treatment in this model (Figure 6b). These data suggest that induction of seizure-like activity elevates neuronal methionine levels, and acute CBD treatment attenuates this effect. Thus, both chronic and acute CBD treatment regulate methionine levels, suggesting a novel effect not previously reported and potentially related to the therapeutic mechanism of CBD.

4 | DISCUSSION

Understanding the therapeutic mechanism(s) of *Cannabis*-derived compounds has been a recent priority in research, particularly in the treatment of epilepsy. Here, we investigated potential mechanisms underlying the molecular function of CBD using *D. discoideum* as a tractable 3Rs (replacement, refinement, or reduction) model organism that has been used in a range of other pharmacogenetic studies including those focused on epilepsy (Chang et al., 2012; Kelly et al., 2018; Warren et al., 2018). Using this model enabled the identification of a mechanism for CBD dependent upon the mitochondrial GCS protein, GCVH1, a component of FOCM, where this role that is conserved with the human orthologue (GCSH). We demonstrated that GCVH1 localized to mitochondria, consistent with studies of GCSH in other models (Lamers et al., 2009; Leung et al., 2017). Loss of GCVH1 significantly elevated glycine levels, increased THF levels, and reduced 5mTHF levels, all confirming impaired activity of the GCS in this mutant (Figure 5). Loss of GCVH1 also led to lower methionine levels (using GC/MS analysis), consistent with impaired GCS activity leading to decreased conversion of homocysteine to methionine via methionine synthase (MTR). Thus, loss of GCVH1 gives rise to metabolic outcomes that resembles those in mouse and human studies (Lamers et al., 2009; Leung et al., 2017) and highlights an evolutionarily conserved function of this important metabolic pathway.

We then demonstrated that CBD functions to modulate methionine levels and folate intermediates in the one-carbon cycle, dependent upon GCVH1 activity, revealing a novel role for CBD in inhibition of methionine production. The increased resistance of *gcvH1*$^-$ mutants to CBD is modest, with a twofold decrease in sensitivity, suggesting that this mechanism may represent one of multiple cellular mechanisms commonly found in therapeutic natural products and drugs (Kobayashi, Endoh, Ohmori, & Akiyama, 2019; Zhang, Huai, Miao, Qian, & Wang, 2019) but still demonstrates a role for the GCS in regulating CBD cellular effects. However, in our studies, CBD treatment did not increase glycine levels, arguing against a direct inhibitory effect of CBD on the GCS. Excitingly, treatment of wild-type cells with CBD lowered methionine levels, and this effect was lost in the *gcvH1*$^-$ mutant, suggesting a mechanism of CBD action through inhibition of methionine production. Although we were unable to detect homocysteine in cells, cysteine levels showed a trend for a CBD-dependent reduction in wild-type cells that was absent in the *gcvH1*$^-$ mutant, also consistent with a role for CBD in regulating GCS-dependent one-carbon metabolism. CBD treatment also caused a decrease in relative abundance of THF and an increase in 5mTHF, supporting the hypothesis of a role for CBD in suppressing methionine synthase activity, with this affect attenuated by loss of GCVH1. These data therefore provide evidence for CBD-dependent regulation of one-carbon metabolism in *D. discoideum*, in which methionine levels are lowered in a GCS-dependent manner, revealing a new molecular pathway modulated by CBD.

We then sought to translate this research to a relevant epilepsy model. Employing a mouse *Scn1a*$^{+/-}$ mutant to investigate a potential mechanism of CBD provided a logical approach, as this model reproduces seizure types found in patients with Dravet syndrome (Marini et al., 2011) and Lennox–Gastaut syndrome (Selmer et al., 2009). Surprisingly, we demonstrated that brain levels of glycine, methionine, and cysteine were all significantly altered in the model, suggesting that neuronal levels of these amino acids may provide trait markers for epilepsy. Interestingly, epilepsy is a key feature of non-ketotic hyperglycinemia (also known as glycine encephalopathy), an autosomal recessive neurometabolic disorder characterized by elevated levels of glycine in blood and CSF (Swanson et al., 2015) caused by mutation of components of the GCS (Kure et al., 2006). These observations provide a potential link between Dravet syndrome, mitochondrial function and glycine levels, and non-ketotic hyperglycinemia. Since mitochondrial dysfunction in Dravet syndrome has been suggested from studies of patient skin fibroblasts (Doccini et al., 2015), in patients (Panneman et al., 2018), in a zebrafish model (Kumar et al., 2016), and in epilepsy-related oxidative stress (Pearson-Smith et al., 2017), our data support and extend these findings. Thus, this mechanism may now be added to those already proposed for CBD in epilepsy treatment (Xiong et al., 2012; Kaplan et al., 2017, Rodriguez-Munoz et al., 2018, Vilela et al., 2017, Rimmerman et al., 2013).

In vivo studies can be complicated by chronic treatment causing long-term cellular and physiological changes in the brain and the presence of a variety of cell types. To overcome these considerations, we analysed a role for CBD in regulating glycine, methionine, and cysteine levels using an acute neuronal seizure model (Chang et al., 2014). This approach defines acute changes found during seizures, and in response to drug treatment, where changes in level of these components would identify a role in seizures. We showed that seizure-like activity did not alter glycine or cysteine levels in neurons themselves, however methionine levels were significantly increased, and this increase was attenuated by CBD treatment. These data are consistent with an acute role for CBD in reducing methionine production in seizure activity but do not prove this—since CBD may simply block seizure activity, and hence a seizure-dependent increase in methionine. This could be examined in further experiments, with other anticonvulsants used to block seizure activity and methionine levels examined, and this represents a limitation in the present study. However, our results clearly indicate that seizure activity elevates methionine levels, revealing a new and unexpected effect of seizure activity. Differing effects of CBD treatment in the Dravet in vivo model and in primary neurons in vitro may be due to a range of factors including long-term cellular and physiological changes in brain following treatment. Whole-brain material also comprises a variety of cell types, where the GCS is mainly in glia cells not neurons, and these aspects will need further investigation.

One-carbon metabolism includes a wide range of components implicated in neuronal excitability, seizure activity, and epilepsy. Glycine acts as a co-agonist at excitatory NMDA receptors to provide a key neuronal glutamatergic (excitability) mechanism and through specific excitatory and inhibitory receptors (Lynch, 2004). The production of SAM provides a central function in the cycle, acting as the primary donor of methyl groups within cells for both DNA and neurotransmitter methylation (Moore et al., 2013). Adenosine has also been shown to regulate seizure activity (Boison, 2016) and is involved in DNA methylation to regulate epileptogenesis (Kobow et al., 2013), although CBD treatment attenuates the reduction in DNA methylation induced by cell differentiation (Pucci et al., 2013). Finally, homocysteine is a pro-convulsant and is elevated in patients with recurrent seizure activity during treatment with antiepileptic drugs (Baldelli et al., 2010). Thus, one-carbon metabolism provides a wide variety of potential impacts on seizure activity and epilepsy control, further emphasized by the current study.

In summary, our data provide new insights to altered metabolism in epilepsy as a disease state, and potential therapeutically relevant mechanisms of CBD action. Future research should thus investigate changes in one-carbon metabolism in epilepsy, including Dravet syndrome, and other CBD-treatable disorders, particularly where potential mitochondrial dysfunction may underlie some pathological symptoms. We further suggest that pharmacological regulation of methionine levels during seizure activity may provide a novel therapeutic approach for seizure control and one-carbon cycle components may provide diagnostic markers within a clinical setting.

ACKNOWLEDGEMENTS

We are grateful for support by the Bioimaging core facility at the Biomedical Center of the LMU Munich. N.G. is supported by Great Ormond Street Hospital Children's Charity and the National Institute for Health Research Biomedical Research Centre at Great Ormond Street Hospital for Children NHS Foundation Trust and University College London. Chris Perry was supported by a PhD studentship funded by GW Pharmaceuticals Ltd. Eleanor Warren was supported by a BBSRC DTP studentship. Pabitra Patra was supported by a PhD part-funded by the University of Reading and GW Research Ltd. N.G. and K.L. were funded by the Medical Research Council (Grant N003713) and Action Medical Research (Grant GN2403). B.J.W. is a current employee of GW Pharmaceuticals. The work was supported by GW Research Ltd. The authors have no additional financial interests.

CONFLICT OF INTEREST

B.J.W. is a current employee of GW Pharmaceuticals. The work was supported by GW Research Ltd.

AUTHOR CONTRIBUTIONS

C.J.P., B.J.W., and R.S.B.W. designed the research. C.J.P., P.F., A.M.T., K.Y.L., E.W., J.O., D.S., P.H.P., S.G., J.B., F.P., R.J.H.,S.P.C., J.B., A.M., and C.M.W. performed the research. B.S., A.B., A.H., C.T., and N.D.E.G. contributed new reagents or analytic tools. C.J.P., S.C., K.Y.L., R.S.B.W. analysed the data. C.J.P., R.J.H., N.D.E.G., and R.S.B.W. wrote the manuscript.

DECLARATION OF TRANSPARENCY AND SCIENTIFIC RIGOUR

This Declaration acknowledges that this paper adheres to the principles for transparent reporting and scientific rigour of preclinical research as stated in the *BJP* guidelines for **Design & Analysis**, **Immunoblotting and Immunochemistry**, and **Animal Experimentation**, and as recommended by funding agencies, publishers and other organisations engaged with supporting research.

ORCID

Annette Müller-Taubenberger https://orcid.org/0000-0003-1163-9232
Amy Baldwin https://orcid.org/0000-0002-2162-3771
Robert J. Harvey https://orcid.org/0000-0001-5956-6664
Sandrine P. Claus https://orcid.org/0000-0002-3789-9780
Nicholas D.E. Greene https://orcid.org/0000-0002-4170-5248
Alister J. McNeish https://orcid.org/0000-0002-3466-8442
Robin S.B. Williams https://orcid.org/0000-0002-9826-6020

REFERENCES

Alexander, S. P., Kelly, E., Marrion, N. V., Peters, J. A., Faccenda, E., Harding, S. D., … Collaborators, C. (2017). The concise guide to PHARMACOLOGY 2017/18: Overview. *British Journal of Pharmacology*, *174*(Suppl 1), S1–S16.

Alexander, S. P., Roberts, R. E., Broughton, B. R., Sobey, C. G., George, C. H., Stanford, S. C., … Insel, P. A. (2018). Goals and practicalities of immunoblotting and immunohistochemistry: A guide for submission to

the British Journal of Pharmacology. *British Journal of Pharmacology*, *175*, 407–411. https://doi.org/10.1111/bph.14112

Armand, V., Louvel, J., Pumain, R., & Heinemann, U. (1998). Effects of new valproate derivatives on epileptiform discharges induced by pentylenetetrazole or low Mg^{2+} in rat entorhinal cortex-hippocampus slices. *Epilepsy Research*, *32*, 345–355. https://doi.org/10.1016/s0920-1211(98)00030-8

Baldelli, E., Leo, G., Andreoli, N., Fuxe, K., Biagini, G., & Agnati, L. F. (2010). Homocysteine potentiates seizures and cell loss induced by pilocarpine treatment. *Neuromolecular Medicine*, *12*, 248–259. https://doi.org/10.1007/s12017-009-8110-1

Bejarano, E., & Rodriguez-navarro, J. A. (2015). Autophagy and amino acid metabolism in the brain: Implications for epilepsy. *Amino Acids*, *47*, 2113–2126. https://doi.org/10.1007/s00726-014-1822-z

Bénard, G., Massa, F., Puente, N., Lourenço, J., Bellocchio, L., Soria-Gómez, E., … Hebert-Chatelain, E. (2012). Mitochondrial CB(1) receptors regulate neuronal energy metabolism. *Nature Neuroscience*, *15*, 558–564. https://doi.org/10.1038/nn.3053

Bih, C. I., Chen, T., Nunn, A. V., Bazelot, M., Dallas, M., & Whalley, B. J. (2015). Molecular targets of cannabidiol in neurological disorders. *Neurotherapeutics*, *12*, 699–730.

Boison, D. (2016). The biochemistry and epigenetics of epilepsy: Focus on adenosine and glycine. *Frontiers in Molecular Neuroscience*, *9*, 26.

Brand, E. J., & Zhao, Z. (2017). Cannabis in Chinese medicine: Are some traditional indications referenced in ancient literature related to cannabinoids? *Frontiers in Pharmacology*, *8*, 108.

Chang, P., Orabi, B., Deranieh, R. M., Dham, M., Hoeller, O., Shimshoni, J. A., … Williams, R. S. (2012). The antiepileptic drug valproic acid and other medium-chain fatty acids acutely reduce phosphoinositide levels independently of inositol in *Dictyostelium*. *Disease Models & Mechanisms*, *5*, 115–124. https://doi.org/10.1242/dmm.008029

Chang, P., Terbach, N., Plant, N., Chen, P. E., Walker, M. C., & Williams, R. S. (2013). Seizure control by ketogenic diet-associated medium chain fatty acids. *Neuropharmacology*, *69*, 105–114. https://doi.org/10.1016/j.neuropharm.2012.11.004

Chang, P., Walker, M. C., & Williams, R. S. (2014). Seizure-induced reduction in PIP3 levels contributes to seizure-activity and is rescued by valproic acid. *Neurobiology of Disease*, *62*, 296–306. https://doi.org/10.1016/j.nbd.2013.10.017

Chang, P., Zuckermann, A. M., Williams, S., Close, A. J., Cano-Jaimez, M., Jp, M. E., … Williams, R. S. (2015). Seizure control by derivatives of medium chain fatty acids associated with the ketogenic diet show novel branching-point structure for enhanced potency. *The Journal of Pharmacology and Experimental Therapeutics*, *352*, 43–52. https://doi.org/10.1124/jpet.114.218768

Cocorocchio, M., Baldwin, A. J., Stewart, B., Kim, L., Harwood, A. J., Thompson, C. R. L., … Williams, R. S. B. (2018). Curcumin and derivatives function through protein phosphatase 2A and presenilin orthologues in *Dictyostelium discoideum*. *Disease Models & Mechanisms*, *11*, 10.

Cunliffe, V. T., Baines, R. A., Giachello, C. N., Lin, W. H., Morgan, A., Reuber, M., … Williams, R. S. (2015). Epilepsy research methods update: Understanding the causes of epileptic seizures and identifying new treatments using non-mammalian model organisms. *Seizure*, *24*, 44–51. https://doi.org/10.1016/j.seizure.2014.09.018

Curtis, M. J., Alexander, S., Cirino, G., Docherty, J. R., George, C. H., Giembycz, M. A., … MacEwan, D. J. (2018). Experimental design and analysis and their reporting II: Updated and simplified guidance for authors and peer reviewers. *British Journal of Pharmacology*, *175*, 987–993. https://doi.org/10.1111/bph.14153

Devinsky, O., Cilio, M. R., Cross, H., Fernandez-Ruiz, J., French, J., Hill, C., … Martinez-Orgado, J. (2014). Cannabidiol: Pharmacology and potential therapeutic role in epilepsy and other neuropsychiatric disorders. *Epilepsia*, *55*, 791–802. https://doi.org/10.1111/epi.12631

Devinsky, O., Cross, J. H., Laux, L., Marsh, E., Miller, I., Nabbout, R., … & CANNABIDIOL IN DRAVET SYNDROME STUDY, G (2017). Trial of cannabidiol for drug-resistant seizures in the Dravet syndrome. *The New England Journal of Medicine*, *376*, 2011–2020.

Devinsky, O., Patel, A. D., Cross, J. H., Villanueva, V., Wirrell, E. C., Privitera, M., … & GROUP, G. S (2018). Effect of cannabidiol on drop seizures in the Lennox-Gastaut syndrome. *The New England Journal of Medicine*, *378*, 1888–1897.

Doccini, S., Meschini, M. C., Mei, D., Guerrini, R., Sicca, F., & Santorelli, F. M. (2015). Mitochondrial respiratory chain defects in skin fibroblasts from patients with Dravet syndrome. *Neurological Sciences*, *36*, 2151–2155.

Ducker, G. S., & Rabinowitz, J. D. (2017). One-carbon metabolism in health and disease. *Cell Metabolism*, *25*, 27–42.

Fischer, M., Haase, I., Simmeth, E., Gerisch, G., & Muller-Taubenberger, A. (2004). A brilliant monomeric red fluorescent protein to visualize cytoskeleton dynamics in *Dictyostelium*. *FEBS Letters*, *577*, 227–232. https://doi.org/10.1016/j.febslet.2004.09.084

Gupta, M., Polinsky, M., Senephansiri, H., Snead, O. C., Jansen, E. E., Jakobs, C., & Gibson, K. M. (2004). Seizure evolution and amino acid imbalances in murine succinate semialdehyde dehydrogenase (SSADH) deficiency. *Neurobiology of Disease*, *16*, 556–562. https://doi.org/10.1016/j.nbd.2004.04.008

Harding, S. D., Sharman, J. L., Faccenda, E., Southan, C., Pawson, A. J., Ireland, S., … Nc, I. (2018). The IUPHAR/BPS guide to PHARMACOLOGY in 2018: Updates and expansion to encompass the new guide to IMMUNOPHARMACOLOGY. *Nucleic Acids Research*, *46*, D1091–D1106. https://doi.org/10.1093/nar/gkx1121

Jones, N. A., Glyn, S. E., Akiyama, S., Hill, T. D., Hill, A. J., Weston, S. E., … Williams, C. M. (2012). Cannabidiol exerts anti-convulsant effects in animal models of temporal lobe and partial seizures. *Seizure*, *21*, 344–352. https://doi.org/10.1016/j.seizure.2012.03.001

Jones, N. A., Hill, A. J., Smith, I., Bevan, S. A., Williams, C. M., Whalley, B. J., & Stephens, G. J. (2010). Cannabidiol displays antiepileptiform and antiseizure properties in vitro and in vivo. *The Journal of Pharmacology and Experimental Therapeutics*, *332*, 569–577. https://doi.org/10.1124/jpet.109.159145

Kaplan, J. S., Stella, N., Catterall, W. A., & Westenbroek, R. E. (2017). Cannabidiol attenuates seizures and social deficits in a mouse model of Dravet syndrome. *Proceedings of the National Academy of Sciences of the United States of America*, *114*, 11229–11234. https://doi.org/10.1073/pnas.1711351114

Keim, M., Williams, R. S., & Harwood, A. J. (2004). An inverse PCR technique to rapidly isolate the flanking DNA of *Dictyostelium* insertion mutants. *Molecular Biotechnology*, *26*, 221–224. https://doi.org/10.1385/MB:26:3:221

Kelly, E., Sharma, D., Wilkinson, C. J., & Williams, R. S. B. (2018). Diacylglycerol kinase (DGKA) regulates the effect of the epilepsy and bipolar disorder treatment valproic acid in *Dictyostelium discoideum*. *Disease Models & Mechanisms*, *11*.

Kikuchi, G., & Hiraga, K. (1982). The mitochondrial glycine cleavage system. Unique features of the glycine decarboxylation. *Molecular and Cellular Biochemistry*, *45*, 137–149. https://doi.org/10.1007/bf00230082

Kilkenny, C., Browne, W., Cuthill, I. C., Emerson, M., & Altman, D. G. (2010). Animal research: Reporting *in vivo* experiments: The ARRIVE guidelines. *British Journal of Pharmacology*, *160*, 1577–1579.

Klein, B. D., Jacobson, C. A., Metcalf, C. S., Smith, M. D., Wilcox, K. S., Hampson, A. J., & Kehne, J. H. (2017). Evaluation of cannabidiol in animal seizure models by the epilepsy therapy screening program (ETSP). *Neurochemical Research*, *42*, 1939–1948. https://doi.org/10.1007/s11064-017-2287-8

Kobayashi, K., Endoh, F., Ohmori, I., & Akiyama, T. (2019). Action of antiepileptic drugs on neurons. *Brain & Development*. pii: S0387-7604(19)30186-X

Kobow, K., Kaspi, A., Harikrishnan, K. N., Kiese, K., Ziemann, M., Khurana, I., … El-Osta, A. & Blumcke, I. (2013). Deep sequencing reveals increased DNA methylation in chronic rat epilepsy. *Acta Neuropathologica*, *126*, 741–756.

Kolker, S. (2018). Metabolism of amino acid neurotransmitters: The synaptic disorder underlying inherited metabolic diseases. *Journal of Inherited Metabolic Disease*. In Press

Kumar, M. G., Rowley, S., Fulton, R., Dinday, M. T., Baraban, S. C., & Patel, M. (2016). Altered glycolysis and mitochondrial respiration in a zebrafish model of Dravet syndrome. *eNeuro*, 3.

Kure, S., Kato, K., Dinopoulos, A., Gail, C., Degrauw, T. J., Christodoulou, J., … Matsubara, Y. (2006). Comprehensive mutation analysis of GLDC, AMT, and GCSH in nonketotic hyperglycinemia. *Human Mutation*, *27*, 343–352. https://doi.org/10.1002/humu.20293

Lamers, Y., Williamson, J., Theriaque, D. W., Shuster, J. J., Gilbert, L. R., Keeling, C., … 3RD (2009). Production of 1-carbon units from glycine is extensive in healthy men and women. *The Journal of Nutrition*, *139*, 666–671.

Leung, K. Y., De Castro, S. C., Cabreiro, F., Gustavsson, P., Copp, A. J., & Greene, N. D. (2013). Folate metabolite profiling of different cell types and embryos suggests variation in folate one-carbon metabolism, including developmental changes in human embryonic brain. *Molecular and Cellular Biochemistry*, *378*, 229–236. https://doi.org/10.1007/s11010-013-1613-y

Leung, K. Y., Pai, Y. J., Chen, Q., Santos, C., Calvani, E., Sudiwala, S., … Greene, N. D. E. (2017). Partitioning of one-carbon units in folate and methionine metabolism is essential for neural tube closure. *Cell Reports*, *21*, 1795–1808. https://doi.org/10.1016/j.celrep.2017.10.072

Lynch, J. W. (2004). Molecular structure and function of the glycine receptor chloride channel. *Physiological Reviews*, *84*, 1051–1095. https://doi.org/10.1152/physrev.00042.2003

Marini, C., Scheffer, I. E., Nabbout, R., Suls, A., De Jonghe, P., Zara, F., & Guerrini, R. (2011). The genetics of Dravet syndrome. *Epilepsia*, *52* (Suppl 2), 24–29.

Miller, A. R., Hawkins, N. A., McCollom, C. E., & Kearney, J. A. (2014). Mapping genetic modifiers of survival in a mouse model of Dravet syndrome. *Genes, Brain, and Behavior*, *13*, 163–172.

Moore, L. D., Le, T., & Fan, G. (2013). DNA methylation and its basic function. *Neuropsychopharmacology*, *38*, 23–38. https://doi.org/10.1038/npp.2012.112

Müller-taubenberger, A., Kortholt, A., & Eichinger, L. (2013). Simple system-substantial share: The use of *Dictyostelium* in cell biology and molecular medicine. *European Journal of Cell Biology*, *92*, 45–53. https://doi.org/10.1016/j.ejcb.2012.10.003

Nair, A. B., & Jacob, S. (2016). A simple practice guide for dose conversion between animals and human. *J Basic Clin Pharm*, *7*, 27–31. https://doi.org/10.4103/0976-0105.177703

Nakayama, T., Ishii, A., Yoshida, T., Nasu, H., Shimojima, K., Yamamoto, T., … Hirose, S. (2018). Somatic mosaic deletions involving *SCN1A* cause Dravet syndrome. *American Journal of Medical Genetics. Part A*, *176*, 657–662.

Pai, Y. J., Leung, K. Y., Savery, D., Hutchin, T., Prunty, H., Heales, S., … Greene, N. D. (2015). Glycine decarboxylase deficiency causes neural tube defects and features of non-ketotic hyperglycinemia in mice. *Nature Communications*, *6*, 6388.

Panneman, D. M., Smeitink, J. A., & Rodenburg, R. J. (2018). Mining for mitochondrial mechanisms: Linking known syndromes to mitochondrial function. *Clinical Genetics*, *93*, 943–951. https://doi.org/10.1111/cge.13094

Patra, P. H., Barker-Haliski, M., White, H. S., Whalley, B. J., Glyn, S., Sandhu, H., … McNeish, A. J. (2019). Cannabidiol reduces seizures and associated behavioral comorbidities in a range of animal seizure and epilepsy models. *Epilepsia*, *60*, 303–314. https://doi.org/10.1111/epi.14629

Pearson-smith, J. N., Liang, L. P., Rowley, S. D., Day, B. J., & Patel, M. (2017). Oxidative stress contributes to status epilepticus associated mortality. *Neurochemical Research*, *42*, 2024–2032.

Piscitelli, F., Pagano, E., Lauritano, A., Izzo, A. A., & Di Marzo, V. (2017). Development of a rapid LC-MS/MS method for the quantification of cannabidiol, cannabidivarin, δ(9)-tetrahydrocannabivarin, and cannabigerol in mouse peripheral tissues. *Analytical Chemistry*, *89*, 4749–4755. https://doi.org/10.1021/acs.analchem.7b01094

Pucci, M., Rapino, C., Di Francesco, A., Dainese, E., D'Addario, C., & Maccarrone, M. (2013). Epigenetic control of skin differentiation genes by phytocannabinoids. *British Journal of Pharmacology*, *170*, 581–591. https://doi.org/10.1111/bph.12309

Rimmerman, N., Ben-Hail, D., Porat, Z., Juknat, A., Kozela, E., Daniels, M. P., … Vogel, Z. (2013). Direct modulation of the outer mitochondrial membrane channel, voltage-dependent anion channel 1 (VDAC1) by cannabidiol: A novel mechanism for cannabinoid-induced cell death. *Cell Death & Disease*, *4*, e949.

Rodriguez-Munoz, M., Onetti, Y., Cortes-Montero, E., Garzon, J., & Sanchez-Blazquez, P. (2018). Cannabidiol enhances morphine antinociception, diminishes NMDA-mediated seizures and reduces stroke damage via the sigma 1 receptor. *Molecular Brain*, *11*, 51.

Selmer, K. K., Lund, C., Brandal, K., Undlien, D. E., & Brodtkorb, E. (2009). *SCN1A* mutation screening in adult patients with Lennox-Gastaut syndrome features. *Epilepsy & Behavior*, *16*, 555–557. https://doi.org/10.1016/j.yebeh.2009.08.021

Svagera, Z., Hanzlikova, D., Simek, P., & Husek, P. (2012). Study of disulfide reduction and alkyl chloroformate derivatization of plasma sulfur amino acids using gas chromatography-mass spectrometry. *Analytical and Bioanalytical Chemistry*, *402*, 2953–2963.

Swanson, M. A., Coughlin, C. R. Jr., Scharer, G. H., Szerlong, H. J., Bjoraker, K. J., Spector, E. B., … Applegarth, D. A. (2015). Biochemical and molecular predictors for prognosis in nonketotic hyperglycinemia. *Annals of Neurology*, *78*, 606–618. https://doi.org/10.1002/ana.24485

Thiele, E. A., Marsh, E. D., French, J. A., Mazurkiewicz-Beldzinska, M., Benbadis, S. R., Joshi, C., … Gunning, B. (2018). Cannabidiol in patients with seizures associated with Lennox-Gastaut syndrome (GWPCARE4): A randomised, double-blind, placebo-controlled phase 3 trial. *Lancet*, *391*, 1085–1096.

Troll, H., Malchow, D., Muller-Taubenberger, A., Humbel, B., Lottspeich, F., Ecke, M., … Benz, R. (1992). Purification, functional characterization, and cDNA sequencing of mitochondrial porin from *Dictyostelium discoideum*. *The Journal of Biological Chemistry*, *267*, 21072–21079.

Troll, H., Winckler, T., Lascu, I., Muller, N., Saurin, W., Veron, M., & Mutzel, R. (1993). Separate nuclear genes encode cytosolic and mitochondrial nucleoside diphosphate kinase in *Dictyostelium discoideum*. *The Journal of Biological Chemistry*, *268*, 25469–25475.

Viant, M. R. (2007). Revealing the metabolome of animal tissues using 1H nuclear magnetic resonance spectroscopy. *Methods in Molecular Biology*, *358*, 229–246.

Vilela, L. R., Lima, I. V., Kunsch, E. B., Pinto, H. P. P., De Miranda, A. S., Vieira, E. L. M., … Moreira, F. A. (2017). Anticonvulsant effect of cannabidiol in the pentylenetetrazole model: Pharmacological mechanisms, electroencephalographic profile, and brain cytokine levels. *Epilepsy & Behavior*, *75*, 29–35. https://doi.org/10.1016/j.yebeh.2017.07.014

Waheed, A., Ludtmann, M. H., Pakes, N., Robery, S., Kuspa, A., Dinh, C., … Carew, M. A. (2014). Naringenin inhibits the growth of *Dictyostelium* and MDCK-derived cysts in a TRPP2 (polycystin-2)-dependent manner. *British Journal of Pharmacology*, *171*, 2659–2670.

Warren, E. C., Walker, M. C., & Williams, R. S. B. (2018). All you need is fats—For seizure control: Using amoeba to advance epilepsy research. *Frontiers in Cellular Neuroscience*, 12.

Williams, R. S. B., Cheng, L., Mudge, A. W., & Harwood, A. J. (2002). A common mechanism of action for three mood-stabilizing drugs. *Nature*, *417*, 292–295. https://doi.org/10.1038/417292a

Xiong, W., Cui, T., Cheng, K., Yang, F., Chen, S. R., Willenbring, D., … Xu, Y. & Zhang, L. (2012). Cannabinoids suppress inflammatory and neuropathic pain by targeting α3 glycine receptors. *The Journal of Experimental Medicine*, *209*, 1121–1134. https://doi.org/10.1084/jem.20120242

Zerbino, D. R., & Birney, E. (2008). Velvet: Algorithms for de novo short read assembly using de Bruijn graphs. *Genome Research*, *18*, 821–829. https://doi.org/10.1101/gr.074492.107

Zhang, W., Huai, Y., Miao, Z., Qian, A., & Wang, Y. (2019). Systems pharmacology for investigation of the mechanisms of action of traditional Chinese medicine in drug discovery. *Frontiers in Pharmacology*, *10*, 743.

Zhou, P., He, N., Zhang, J. W., Lin, Z. J., Wang, J., Yan, L. M., … Shi, Y. W. (2018Nov). Novel mutations and phenotypes of epilepsy-associated genes in epileptic encephalopathies. *Genes, Brain, and Behavior*, *17*(8), e12456.

SUPPORTING INFORMATION

Additional supporting information may be found online in the Supporting Information section at the end of this article.

How to cite this article: Perry CJ, Finch P, Müller-Taubenberger A, et al. A new mechanism for cannabidiol in regulating the one-carbon cycle and methionine levels in *Dictyostelium* and in mammalian epilepsy models. *Br J Pharmacol*. 2020;177:912–928. https://doi.org/10.1111/bph.14892

Biochemistry and Biophysics Reports 22 (2020) 100751

Contents lists available at ScienceDirect

Biochemistry and Biophysics Reports

journal homepage: www.elsevier.com/locate/bbrep

A *Dictyostelium discoideum* mitochondrial fluorescent tagging vector that does not affect respiratory function

Christopher J. Perry[a], Eleanor C. Warren[a], Joseph L. Damstra-Oddy[a], Claire Storey[b], Lisa M. Francione[b], Sarah J. Annesley[b], Paul R. Fisher[b], Annette Müller-Taubenberger[c], Robin S.B. Williams[a,*]

[a] Centre for Biomedical Sciences, School of Biological Sciences, Royal Holloway University of London, Egham, Surrey, TW20 0EX, UK
[b] Department of Physiology, Anatomy and Microbiology, La Trobe University, Melbourne, Victoria, 3086, Australia
[c] Department of Cell Biology, Biomedical Center, LMU Munich, 82152, Planegg-Martinsried, Germany

ARTICLE INFO

Keywords:
Dictyostelium discoideum
Mitochondria
Fluorescent tagging
Live cell imaging

ABSTRACT

Visualizing mitochondria in living *Dictyostelium discoideum* cells using fluorescent dyes is often problematic due to variability in staining, metabolism of the dyes, and unknown potential effects of the dyes on mitochondrial function. We show that fluorescent labelling of mitochondria, using an N-terminal mitochondrial localization sequence derived from the *D. discoideum* protein GcvH1 (glycine cleavage system H1) attached to a red fluorescent protein enables clear mitochondrial imaging. We also show that this labelling has no effect upon mitochondria load or respiratory function.

1. Introduction

Mitochondria play important roles, most notably cellular energy production by oxidative phosphorylation [1], hence the aptly coined phrase “the powerhouse of the cell” [2]. Mitochondria are also involved in Ca^{2+} management [3], production of ROS [4], redox signalling [5,6] and apoptosis [7]. Many studies investigating mitochondrial function observe mitochondrial morphology and their dynamics within the cell [8]. Such observations can be achieved by the use of various fluorescent dyes such as Rhodamine 123 (R123) [9], tetramethylrhodamine-methyl-ester (TMRM) [10] and JC-1 (tetraethylbenzimi-dazolylcarbocyanine iodide) [11]. However, these dyes rely upon a mitochondrial membrane potential and can be washed out if the mitochondria experience depolarisation [12]. Furthermore, these dyes are unsuitable for use with aldehyde fixation due to resulting changes in mitochondrial metabolic state [12]. Other fluorescent dyes developed for visualizing mitochondria include the Mitotracker Red and Green dyes. Mitotracker Red binding depends on both the presence of a mitochondrial membrane potential while Mitotracker Green binding does not. These dyes can be used in combination with a number of cell fixation methods, however, they may cause cytotoxic effects following prolonged use. Other methods of real time mitochondrial imaging include the use of fluorescently tagged mitochondrial localised proteins, where the tagged protein is recognised by the mitochondrial ‘Translocase of the outer/inner membrane’ (TOM/TIM) protein complexes and transported into the mitochondria [13]. The transport of mitochondrial proteins into the mitochondrial matrix is facilitated by an N-terminal pre-sequence [14]. This pre-sequence can consist of 10–80 amino acid residues and is usually cleaved off by the matrix processing peptidase following localization [15]. However, these fluorescent proteins can interfere with the function of the native protein and impede mitochondrial function. As such, non-cytotoxic mitochondrial markers are required.

Dictyostelium discoideum is a tractable model system widely used for research in a range of fields including cell and developmental biology, evolutionary biology, as well as in immunology and molecular pharmacology studies. In cell and developmental biology, *D. discoideum* is often used to improve our understanding of cell motility [16,17]. In molecular pharmacology research, *D. discoideum* has been used to investigate mechanisms of action of pharmaceutical drugs including treatments for epilepsy [18–20] and neurodegenerative disorders [21,22]. Other studies investigate mechanisms of action of bioactive natural products such as curcumin, naringenin and a range of bitter tastants [23–25]. One recent study, identifying a mitochondrial protein,

Abbreviations: MLS, mitochondrial localization sequence; REMIT, red mitochondrial-tagging plasmid; RFP, red fluorescent protein; ROS, reactive oxygen species; TOM/TIM, Translocase of the outer/inner membrane

* Corresponding author.
E-mail address: Robin.williams@rhul.ac.uk (R.S.B. Williams).

https://doi.org/10.1016/j.bbrep.2020.100751
Received 30 January 2020; Received in revised form 5 March 2020; Accepted 10 March 2020
Available online 25 March 2020

GcvH1, involved in the cellular function of cannabinoids on the glycine cleavage system [26], highlights the presence of an N-terminal mitochondrial localization sequence and thus raises the possibility of using this sequence for mitochondrial tagging in *D. discoideum*. To further these studies, a non-cytotoxic mitochondrial marker is required that can be used in *D. discoideum* without affecting cellular respiratory function.

In this study we created a novel expression plasmid (REMIT; red mitochondria) for real time visualization of mitochondria in *D. discoideum*. The REMIT plasmid allows the expression of an enhanced RFP protein (mRFPmars) [27] with a mitochondrial localization sequence situated at its N-terminus. We show that transfection of REMIT into *D. discoideum* cells facilitates the localization of mRFPmars to the mitochondrial matrix. We also show that the presence of mRFPmars within the mitochondria has no effect on mitophagy or cellular respiratory function. We therefore present a method that allows the real time visualization of mitochondria within *D. discoideum* cells with no deleterious effects.

2. Methods

2.1. Creation of the REMIT plasmid and over-expression D. discoideum cell lines

Primers (fwd: ATAGAATTCATGTTAAAAACCTTAAGATTTG and rev: TATGGATCCCCATTCATGATCG) complementary to the 5' region of *gcvH1* were used to amplify the 99-bp mitochondrial localization sequence (Fig. 1). The PCR product was digested with *Eco*RI and *Bam*HI and cloned into the extra chromosomal plasmid pDXA-389-2 [27,28].

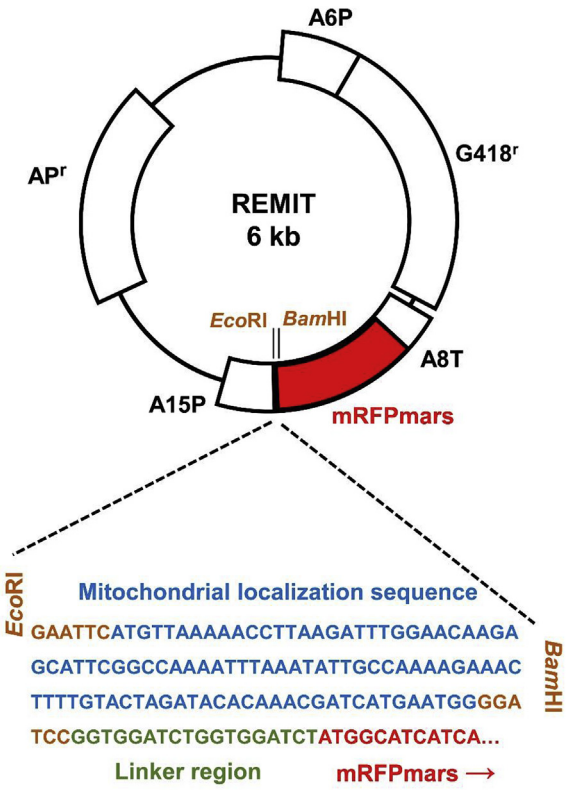

Fig. 1. REMIT plasmid construction. The mitochondrial localization sequence was ligated into the pDXA-389-2 plasmid 5' of the mRFPmars gene using *Eco*RI and *Bam*HI restriction sites. Actin 6 promoter, A6P; actin promoter 15, AP15; Ampicillin resistance cassette, AP^r; monomeric red fluorescence protein, mRFPmars; actin terminator 8, A8T; Geneticin resistance cassette, $G418^r$. (For interpretation of the references to colour in this figure legend, the reader is referred to the Web version of this article.)

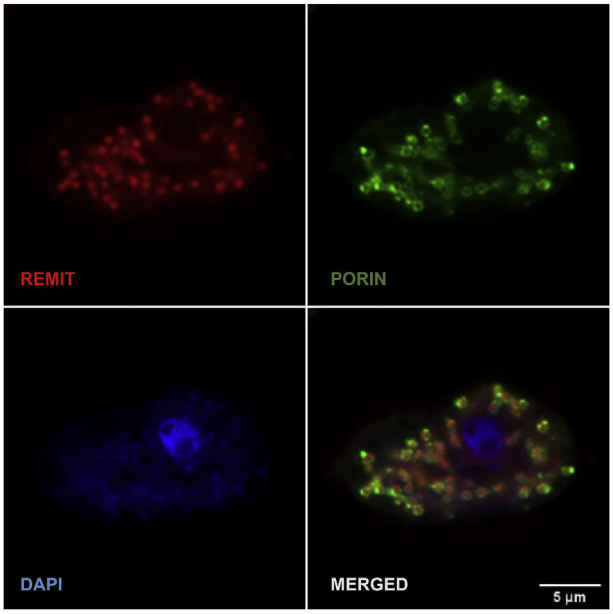

Fig. 2. Fixed-cell imaging of REMIT localizing to the mitochondria. (A) *D. discoideum* cells expressing REMIT-mRFPmars (red), were fixed and immunolabelled using an anti-porin antibody (green), and stained with DAPI to visualize DNA (blue). Confocal single plane imaging showed red fluorescent protein localizing to mitochondria in *D. discoideum*. Scale bar correspond to 5 µm. (For interpretation of the references to colour in this figure legend, the reader is referred to the Web version of this article.)

The PCR product was inserted into the multiple cloning site located immediately 5' of the mRFPmars gene, and sequenced to confirm that no mutations were introduced. Insertion of the PCR product at this location enabled expression of a 27 kDa mRFPmars with a 33 amino acid residue localization sequence linked to its N-terminus via a 6 amino acid residue linker region (Fig. 1). The resulting plasmid was transfected into wildtype (AX3) cells and selected using geneticin (10 µg/ml) to create a REMIT over-expression cell line [29]. The GREMIT plasmid was based upon the same targeting region inserted into the GFP vector pDM1209 [30].

2.2. Fluorescence and live-cell microscopy

For immunolabeling, cells expressing REMIT were plated on round 12-mm glass coverslips, and after 20 min were fixed with 15% picric acid/2% paraformaldehyde in 10 mM PIPES, pH 6.0, for 20 min and post-fixed with 70% ethanol for 10 min [31]. Cells were then washed three times in PBS, once with 10 mM PIPES, and twice with PBS/1% glycine, and incubated in blocking buffer (PBS plus 2% bovine serum albumin) for 1 h at room temperature (RT). After blocking, the cells were washed three times with PBS and incubated with primary antibodies (2 µg/ml mouse monoclonal anti-porin antibody (Developmental studies hybridoma bank (DSHB); 70-100-1) [32], and 1:1000 rat anti-RFP (6G6 anti-red rat mAb, Chromatek) for 2 h, followed by the incubation with secondary antibodies (1:1000 Alexa 488-conjugated goat anti-mouse IgG (Invitrogen; A28175) and 1:1000 rabbit anti-rat (Alexa fluor® 488 rabbit anti-rat IgG, Life technologies), for 1 h. After immunostaining, samples were washed three times in PBS and embedded using Fluoromount-G™, with DAPI (1:1000 of 1 mg/ml DAPI dissolved in methanol; Invitrogen, 00-4959) to stain DNA. For live-cell microscopy, cells were seeded in µ-dishes (Ibidi, 80606), or open chambers as described previously [28].

Confocal microscopy was performed at the Bioimaging core facility of the Biomedical Center (LMU Munich) using an inverted Leica TCS SP8 equipped with lasers for 405, 488, 552, and 638 nm excitation.

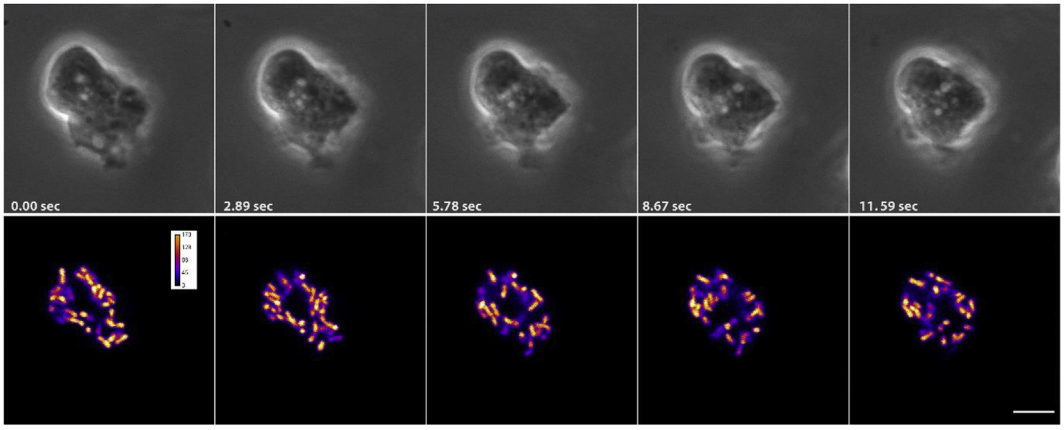

Fig. 3. Live-cell imaging of REMIT localizing to the mitochondria. (A) Time lapse single plane imaging on a confocal microscope showing *D. discoideum* cells transfected with REMIT-mRFPmars. The upper panel shows phase contrast images, the lower panels the intensity of the mRFPmars signal according to grey levels depicted in colour-mode fire [38], scale bar 5 μm. Images correspond to Supplementary movie 1. Similar live cell imaging using red fluorescence are provided in Supplementary movie 2, using under agar inverted fluorescence in Supplementary movie 3, Z stack imaging in Supplementary movie 4, and 3D reconstruction of live-cell imaging in Supplementary movie 5. (For interpretation of the references to colour in this figure legend, the reader is referred to the Web version of this article.)

Images were acquired with a HC PL APO 63x/1.40 oil PH3 objective. Recording was sequential to avoid bleed-through. Alexa-488, and RFP were recorded with the hybrid photo detectors, DAPI with the conventional photomultiplier tube.

High resolution live-cell imaging was performed using an inverted Zeiss LSM 900 Airyscan 2 microscope [33]. Images were acquired with a Plan-Apochromat 63x/1.40 oil DIC objective with a GaASP-PMT detector (450–700 nm) in the MPCX SR-4y modus at an excitation of 558 nm. Z-stacks (25 corresponding to 4.32 μm) were recorded over time (2.55 s per z-stack). 3D reconstructions of single z-stacks were performed using the Imaris software package (Bitplane, Zurich, Switzerland).

2.3. Western blot analysis to monitor mitochondrial loading

Cell lysates (30 μg) were separated by gel electrophoresis, transferred to nitrocellulose membranes (Merck Millipore, IPFL00010), and analysed by Western blotting. A mouse anti-porin primary antibody (0.2 μg/ml, DSHB, 70-100-1) and a goat anti-mouse secondary antibody (1:10000, Li-Cor, 926–32210) were used to confirm the presence of porin. A streptavidin conjugate (1:5000, Invitrogen, S21378) which binds to the mitochondrial protein MCCC1 (mitochondrial 3-methylcrotonyl-CoA carboxylase α [34]) was used to measure the levels of this mitochondrial protein. Blots were analysed using Odyssey software. Total protein loaded was stained with Revert 700 Total Protein Stain (Li-Cor, 926–11010) and imaged and quantified on the Odyssey CLx.

2.4. Mitochondrial respirometry function

The effects that REMIT expression may have on mitochondrial stress were investigated in real time [35]. In these experiments, a Seahorse XF^{e24} Extracellular Flux Analyzer was used to measure mitochondrial respirometry within REMIT expressing cells, wildtype cells and cells expressing mRFPmars lacking the mitochondrial localization sequence. Mitochondrial respirometry was measured in terms of the basal O_2 consumption rate, the O_2 consumption rate devoted to the synthesis of ATP, the maximum O_2 consumption rate, the contribution of Complex I to the maximum O_2 consumption rate, the contribution of Complex II to the maximum O_2 consumption rate, and the O_2 consumption rate devoted to mitochondrial function other than ATP synthesis, i.e. “proton leak”.

2.5. Statistical analysis

The distribution of all experimental data was tested using the Anderson-Darling test for normality. All data that showed a Gaussian distribution were analysed using parametric tests. Data from two groups not showing a Gaussian distribution were analysed using a Mann-Whitney T-test. The one-way analysis of variance (ANOVA) statistical test was used to test for significance between the means of three or more independent groups of normally distributed data.

3. Results and discussion

The *D. discoideum* mitochondrial localization sequence (MLS) (Fig. 1) was derived from the GcvH1 protein, a member of the mitochondrial glycine cleavage system enzyme complex [26]. The glycine cleavage system is located within the mitochondrial matrix and has a loose affiliation with the inner mitochondrial membrane. We cloned the GcvH1 MLS onto the N-terminus of mRFPmars [27] to form the REMIT vector that was then transfected into wildtype *D. discoideum* cells. To validate the mitochondrial localization of mRFPmars in these cells, mRFPmars fluorescence was examined in fixed cells [36] (Fig. 2), showing highly localised distribution in mitochondrial-like structures. Since porin is localised in the outer mitochondrial membrane, we examined this localization, indicating REMIT mRFPmars in the mitochondrial matrix with porin surrounding this labelling (Fig. 2). We then assessed the use of REMIT mRFPmars for labelling mitochondria in live cell imaging experiments. By using live-cell confocal microscopy, REMIT-expressing cells revealed a highly discrete labelling of mitochondria in real time (Fig. 3, and Supplementary movies 1,2), also visible using under-agar inverted fluorescence microscopy (Supplementary movie 3). A similar localization was found using a GFP-encoding vector, GREMIT (Supplementary Fig. 1). We also employed high resolution live-cell imaging to monitor mitochondrial dynamics (Supplementary movie 4), and this enabled 3-dimensional reconstruction of mitochondrial distribution in live cells (Supplementary movie 5).

Supplementary video related to this article can be found at https://doi.org/10.1016/j.bbrep.2020.100751

In order to maintain a healthy population of mitochondria within the cells, all mitochondria experiencing damage or dysfunction will undergo mitophagy. This process results in defective mitochondria being targeted to the lysosome for autophagic degradation, thereby maintaining cell health [37]. Because transfection with REMIT leads to the localization of mRFPmars to the mitochondria we investigated whether this resulted in mitochondrial damage or dysfunction,

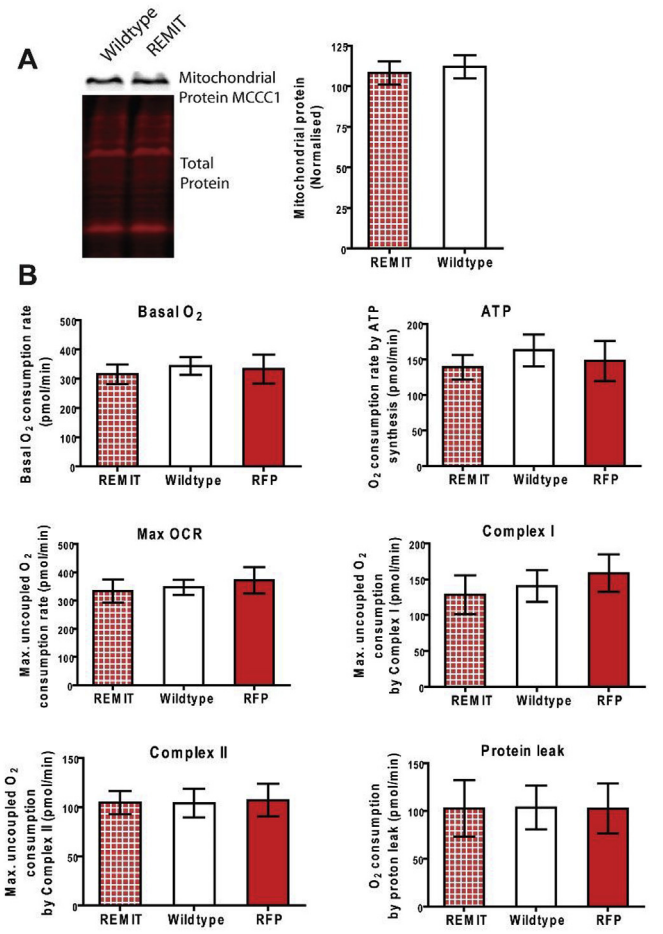

Fig. 4. Expression of REMIT within *D. discoideum* has no effect on mitochondrial load or respiratory function. Mitochondrial load and respiratory function was evaluated in *D. discoideum* cells transfected with the REMIT plasmid. (A) Western blot analysis was used to assess levels of a mitochondrial-specific marker protein (MCCC1) and total protein levels. Data represent the mean and SEM ($P > 0.05$), $n = 6$ (Mann-WhitneyU test). (B) Mitochondrial respiratory function was evaluated in cells transfected with REMIT, with wildtype cells, and with the REMIT plasmid lacking the localization sequence (RFP). Respiratory function was quantified in terms of basal O_2 consumption rate, O_2 consumption rate devoted to the synthesis of ATP, maximum O_2 consumption rate, contribution of complex I to the maximum O_2 consumption rate, contribution of complex II to the maximum O_2 consumption rate, O_2 consumption rate devoted to mitochondrial function other than ATP synthesis, i.e. "proton leak". Data represent the mean and SEM ($P > 0.05$), $n = 6$ (One way ANOVA).

resulting in mitophagy, or alternatively increased mitochondrial load (the mitochondrial protein content). To assess mitochondrial loading, we compared levels of a mitochondrial protein, mitochondrial 3-methylcrotonyl-CoA carboxylase α [34], in wildtype cells and cells transfected with REMIT using Western blot analysis (Fig. 4A). From this analysis, no change in mitochondrial load was identified following REMIT transfection.

The requirement of mitochondria to carry out normal respiratory function is fundamental to maintaining a healthy cell. Any deleterious effect on respiratory function as a result of REMIT transfection would result in downstream processes being disrupted. Thus, it is necessary to confirm that mitochondrial respiratory function is not disrupted. Mitochondrial respirometry function was therefore measured in terms of the basal O_2 consumption rate, the O_2 consumption rate devoted to the synthesis of ATP, the maximum O_2 consumption rate, the contribution of complex I to the maximum O_2 consumption rate, the contribution of complex II to the maximum O_2 consumption rate, and the O_2 consumption rate devoted to mitochondrial function other than ATP synthesis, i.e. "proton leak" (Fig. 4B). These data were obtained from cells transfected with REMIT, cells transfected with REMIT lacking the MLS, and untransfected wildtype cells. For all six conditions no significant difference ($P > 0.05$) was found between the three cell lines. This shows that mitochondrial function is not affected despite the presence of mRFPmars localised within the mitochondrial matrix.

These experiments thus show that transfection of *D. discoideum* cells with REMIT provides a quick, cheap and convenient method to visualize mitochondria in real time. The use of REMIT would be advantageous in studies involving the need for both visualization and normal respiratory function. These studies can include investigation into mitochondrial fission and fusion events, mitochondrial dynamics and mitochondrial morphology.

Author statement

CJP and RSBW conceived the research and wrote the paper. ECW and JD-O contributed to imaging and measuring mitochondria load. CS, LMF, SJA, PRF analysed mitochondrial function. AM-T provided confocal microscopy and 3D modelling. All authors contributed to editing the paper.

Declaration of competing interest

The authors declare that they have no known competing financial interests or personal relationships that could have appeared to influence the work reported in this paper.

Acknowledgement

Christopher Perry and Joseph Damstra-Oddy were supported by PhD studentships funded by GW Research Ltd. Eleanor Warren was supported by a BBSRC DTP studentship. We thank Dr Hellen Ishikawa-Ankerhold (LMU Munich) for help with 3D-reconstructions.

Appendix A. Supplementary data

Supplementary data to this article can be found online at https://doi.org/10.1016/j.bbrep.2020.100751.

References

[1] S.A. Detmer, D.C. Chan, Functions and dysfunctions of mitochondrial dynamics, Nat. Rev. Mol. Cell Biol. 8 (2007) 870–879, https://doi.org/10.1038/nrm2275.
[2] P. Siekevitz, Powerhouse of the cell, Sci. Am. 197 (1957) 9.
[3] G. Szabadkai, A.M. Simoni, K. Bianchi, D. De Stefani, S. Leo, M.R. Wieckowski, R. Rizzuto, Mitochondrial dynamics and Ca2+ signaling, Biochim. Biophys. Acta 1763 (2006) 442–449, https://doi.org/10.1016/j.bbamcr.2006.04.002.
[4] M.P. Murphy, How mitochondria produce reactive oxygen species, Biochem. J. 417 (2009) 1–13, https://doi.org/10.1042/BJ20081386.
[5] D.C. Joshi, J.C. Bakowska, Determination of mitochondrial membrane potential and reactive oxygen species in live rat cortical neurons, J Vis Exp (2011), https://doi.org/10.3791/2704.
[6] Y. Collins, E.T. Chouchani, A.M. James, K.E. Menger, H.M. Cocheme, M.P. Murphy, Mitochondrial redox signalling at a glance, J. Cell Sci. 125 (2012) 801–806, https://doi.org/10.1242/jcs.098475.
[7] S.Y. Jeong, D.W. Seol, The role of mitochondria in apoptosis, BMB Rep. 41 (2008) 11–22, https://doi.org/10.5483/bmbrep.2008.41.1.011.
[8] K. Mitra, J. Lippincott-Schwartz, Analysis of mitochondrial dynamics and functions using imaging approaches, Curr. Protoc. Cell Biol. Chapter 4 (2010), https://doi.org/10.1002/0471143030.cb0425s46 Unit 4 25 21-21.
[9] L.B. Chen, Fluorescent labeling of mitochondria, Methods Cell Biol. 29 (1989) 103–123, https://doi.org/10.1016/s0091-679x(08)60190-9.
[10] K.M. Heiskanen, M.B. Bhat, H.W. Wang, J. Ma, A.L. Nieminen, Mitochondrial depolarization accompanies cytochrome c release during apoptosis in PC6 cells, J. Biol. Chem. 274 (1999) 5654–5658, https://doi.org/10.1074/jbc.274.9.5654.
[11] M. Poot, Y.Z. Zhang, J.A. Kramer, K.S. Wells, L.J. Jones, D.K. Hanzel, A.G. Lugade, V.L. Singer, R.P. Haugland, Analysis of mitochondrial morphology and function with novel fixable fluorescent stains, J. Histochem. Cytochem. 44 (1996) 1363–1372, https://doi.org/10.1177/44.12.8985128.
[12] X. Liu, L. Yang, Q. Long, D. Weaver, G. Hajnoczky, Choosing proper fluorescent

dyes, proteins, and imaging techniques to study mitochondrial dynamics in mammalian cells, Biophys. Rep. 3 (2017) 64–72, https://doi.org/10.1007/s41048-017-0037-8.
[13] S. Kutik, B. Guiard, H.E. Meyer, N. Wiedemann, N. Pfanner, Cooperation of translocase complexes in mitochondrial protein import, J. Cell Biol. 179 (2007) 585–591, https://doi.org/10.1083/jcb.200708199.
[14] T. Saitoh, M. Igura, T. Obita, T. Ose, R. Kojima, K. Maenaka, T. Endo, D. Kohda, Tom20 recognizes mitochondrial presequences through dynamic equilibrium among multiple bound states, EMBO J. 26 (2007) 4777–4787, https://doi.org/10.1038/sj.emboj.7601888.
[15] J.C. Young, N.J. Hoogenraad, F.U. Hartl, Molecular chaperones Hsp90 and Hsp70 deliver preproteins to the mitochondrial import receptor Tom70, Cell 112 (2003) 41–50, https://doi.org/10.1016/s0092-8674(02)01250-3.
[16] H. Senoo, Y. Kamimura, R. Kimura, A. Nakajima, S. Sawai, H. Sesaki, M. Iijima, Phosphorylated Rho-GDP directly activates mTORC2 kinase towards AKT through dimerization with Ras-GTP to regulate cell migration, Nat. Cell Biol. 21 (2019) 867–878, https://doi.org/10.1038/s41556-019-0348-8.
[17] J.M.E. Nichols, P. Paschke, S. Peak-Chew, T.D. Williams, L. Tweedy, M. Skehel, E. Stephens, J.R. Chubb, R.R. Kay, The atypical MAP kinase ErkB transmits distinct chemotactic signals through a core signaling module, Dev. Cell 48 (2019) 491–505, https://doi.org/10.1016/j.devcel.2018.12.001 e499.
[18] E. Kelly, D. Sharma, C.J. Wilkinson, R.S.B. Williams, Diacylglycerol kinase (DGKA) regulates the effect of the epilepsy and bipolar disorder treatment valproic acid in Dictyostelium discoideum, Dis. Model. Mech. 11 (2018), https://doi.org/10.1242/dmm.035600.
[19] P. Chang, B. Orabi, R.M. Deranieh, M. Dham, O. Hoeller, J.A. Shimshoni, B. Yagen, M. Bialer, M.L. Greenberg, M.C. Walker, R.S. Williams, The antiepileptic drug valproic acid and other medium-chain fatty acids acutely reduce phosphoinositide levels independently of inositol in Dictyostelium, Dis. Model. Mech. 5 (2012) 115–124, https://doi.org/10.1242/dmm.008029 dmm.008029 [pii].
[20] X. Xu, A. Muller-Taubenberger, K.E. Adley, N. Pawolleck, V.W. Lee, C. Wiedemann, T.S. Sihra, M. Maniak, T. Jin, R.S. Williams, Attenuation of phospholipid signaling provides a novel mechanism for the action of valproic acid, Eukaryot. Cell 6 (2007) 899–906, https://doi.org/10.1128/EC.00104-06.
[21] D. Sharma, G. Otto, E. Warren, P. Beesley, J.S. King, R.S.B. Williams, Gamma secretase orthologs are required for lysosomal activity and autophagic degradation in Dictyostelium discoideum, independent of PSEN (presenilin) proteolytic function, Autophagy 15 (2019) 11, https://doi.org/10.1080/15548627.2019.1586245.
[22] M.H. Ludtmann, G.P. Otto, C. Schilde, Z.H. Chen, C.Y. Allan, S. Brace, P.W. Beesley, A.R. Kimmel, P. Fisher, R. Killick, R.S. Williams, An ancestral non-proteolytic role for presenilin proteins in multicellular development of the social amoeba Dictyostelium discoideum, J. Cell Sci. 127 (2014) 1576–1584, https://doi.org/10.1242/jcs.140939.
[23] A. Waheed, M.H. Ludtmann, N. Pakes, S. Robery, A. Kuspa, C. Dinh, D. Baines, R.S. Williams, M.A. Carew, Naringenin inhibits the growth of Dictyostelium and MDCK-derived cysts in a TRPP2 (polycystin-2)-dependent manner, Br. J. Pharmacol. 171 (2014) 2659–2670, https://doi.org/10.1111/bph.12443.
[24] M. Cocorocchio, A.J. Baldwin, B. Stewart, L. Kim, A.J. Harwood, C.R.L. Thompson, P.L.R. Andrews, R.S.B. Williams, Curcumin and derivatives function through protein phosphatase 2A and presenilin orthologues in Dictyostelium discoideum, Dis. Model. Mech. 11 (2018) 10, https://doi.org/10.1242/dmm.032375.
[25] M. Cocorocchio, R. Ives, D. Clapham, P.L. Andrews, R.S. Williams, Bitter tastant responses in the amoeba Dictyostelium correlate with rat and human taste assays, ALTEX 33 (2016) 11, https://doi.org/10.14573/altex.1509011.
[26] C.J. Perry, P. Finch, A. Muller-Taubenberger, K.Y. Leung, E.C. Warren, J. Damstra-Oddy, D. Sharma, P.H. Patra, S. Glyn, J. Boberska, B. Stewart, A. Baldwin, F. Piscitelli, R.J. Harvey, A. Harwood, C. Thompson, S. Claus, N.D.E. Greene, A. McNeish, C.M. Williams, B.J. Whalley, R.S.B. Williams, A new mechanism for Cannabidiol in regulating the one-carbon cycle and methionine levels in Dictyostelium and in mammalian epilepsy models, Br. J. Pharmacol. (2019), https://doi.org/10.1111/bph.14892.
[27] M. Fischer, I. Haase, E. Simmeth, G. Gerisch, A. Muller-Taubenberger, A brilliant monomeric red fluorescent protein to visualize cytoskeleton dynamics in *Dictyostelium*, FEBS Lett. 577 (2004) 227–232.
[28] A. Muller-Taubenberger, Application of fluorescent protein tags as reporters in live-cell imaging studies, Methods Mol. Biol. 346 (2006) 229–246, https://doi.org/10.1385/1-59745-144-4:229.
[29] P. Gaudet, P. Fey, R. Chisholm, Transformation of dictyostelium with plasmid DNA by electroporation, CSH Protoc. 2008 (2008), https://doi.org/10.1101/pdb.prot5103 pdb prot5103.
[30] P. Paschke, D.A. Knecht, A. Silale, D. Traynor, T.D. Williams, P.A. Thomason, R.H. Insall, J.R. Chubb, R.R. Kay, D.M. Veltman, Rapid and efficient genetic engineering of both wild type and axenic strains of Dictyostelium discoideum, PloS One 13 (2018) e0196809, , https://doi.org/10.1371/journal.pone.0196809.
[31] M. Hagedorn, E.M. Neuhaus, T. Soldati, Optimized fixation and immunofluorescence staining methods for Dictyostelium cells, Methods Mol. Biol. 346 (2006) 327–338, https://doi.org/10.1385/1-59745-144-4:327.
[32] H. Troll, T. Winckler, I. Lascu, N. Muller, W. Saurin, M. Veron, R. Mutzel, Separate nuclear genes encode cytosolic and mitochondrial nucleoside diphosphate kinase in Dictyostelium discoideum, J. Biol. Chem. 268 (1993) 25469–25475.
[33] J. Huff, A. Bergter, B. Leubbers, Application Note: multiplex mode for the LSM 9 series with Airyscan 2: fast and gentle confocal super-resolution in large volumes, Nat. Methods (2019), https://doi.org/10.1038/d42473-019-00173-w.
[34] A.J. Davidson, J.S. King, R.H. Insall, The use of streptavidin conjugates as immunoblot loading controls and mitochondrial markers for use with Dictyostelium discoideum, Biotechniques 55 (2013) 39–41, https://doi.org/10.2144/000114054.
[35] S. Lay, O. Sanislav, S.J. Annesley, P.R. Fisher, Mitochondrial stress tests using Seahorse respirometry on intact Dictyostelium discoideum cells, Methods Mol. Biol. 1407 (2016) 41–61, https://doi.org/10.1007/978-1-4939-3480-5_4.
[36] H. Troll, D. Malchow, A. Muller-Taubenberger, B. Humbel, F. Lottspeich, M. Ecke, G. Gerisch, A. Schmid, R. Benz, Purification, functional characterization, and cDNA sequencing of mitochondrial porin from Dictyostelium discoideum, J. Biol. Chem. 267 (1992) 21072–21079.
[37] I. Kim, S. Rodriguez-Enriquez, J.J. Lemasters, Selective degradation of mitochondria by mitophagy, Arch. Biochem. Biophys. 462 (2007) 245–253, https://doi.org/10.1016/j.abb.2007.03.034.
[38] J. Schindelin, I. Arganda-Carreras, E. Frise, V. Kaynig, M. Longair, T. Pietzsch, S. Preibisch, C. Rueden, S. Saalfeld, B. Schmid, J.Y. Tinevez, D.J. White, V. Hartenstein, K. Eliceiri, P. Tomancak, A. Cardona, Fiji: an open-source platform for biological-image analysis, Nat. Methods 9 (2012) 676–682, https://doi.org/10.1038/nmeth.2019.

Decanoic acid inhibits mTORC1 activity independent of glucose and insulin signaling

Eleanor C. Warren[a], Stephanie Dooves[b], Eleonora Lugarà[c], Joseph Damstra-Oddy[a], Judith Schaf[a], Vivi M. Heine[b,d], Mathew C. Walker[c], and Robin S. B. Williams[a,1]

[a]Centre for Biomedical Sciences, Department of Biological Sciences, Royal Holloway University of London, Egham TW20 0EX, United Kingdom; [b]Department of Child and Youth Psychiatry, Amsterdam Universitair Medische Centra, Amsterdam Neuroscience, Vrije Universiteit Amsterdam, 1081 HV Amsterdam, The Netherlands; [c]Clinical and Experimental Epilepsy UCL, Queen Square Institute of Neurology, University College London, London WC1N 3BG, United Kingdom; and [d]Department of Complex Trait Genetics, Centre for Neurogenomics and Cognitive Research, Amsterdam Neuroscience, Vrije Universiteit Amsterdam, 1081 HV Amsterdam, The Netherlands

Edited by Peter N. Devreotes, Johns Hopkins University School of Medicine, Baltimore, MD, and approved August 10, 2020 (received for review May 7, 2020)

Low-glucose and -insulin conditions, associated with ketogenic diets, can reduce the activity of the mechanistic target of rapamycin complex 1 (mTORC1) signaling pathway, potentially leading to a range of positive medical and health-related effects. Here, we determined whether mTORC1 signaling is also a target for decanoic acid, a key component of the medium-chain triglyceride (MCT) ketogenic diet. Using a tractable model system, *Dictyostelium*, we show that decanoic acid can decrease mTORC1 activity, under conditions of constant glucose and in the absence of insulin, measured by phosphorylation of eukaryotic translation initiation factor 4E-binding protein 1 (4E-BP1). We determine that this effect of decanoic acid is dependent on a ubiquitin regulatory X domain-containing protein, mediating inhibition of a conserved *Dictyostelium* AAA ATPase, p97, a homolog of the human transitional endoplasmic reticulum ATPase (VCP/p97) protein. We then demonstrate that decanoic acid decreases mTORC1 activity in the absence of insulin and under high-glucose conditions in ex vivo rat hippocampus and in tuberous sclerosis complex (TSC) patient-derived astrocytes. Our data therefore indicate that dietary decanoic acid may provide a new therapeutic approach to down-regulate mTORC1 signaling.

Dictyostelium discoideum | epilepsy | mTOR | decanoic acid | tuberous sclerosis complex

Inhibition of mechanistic target of rapamycin complex 1 (mTORC1) has been suggested as a common mechanism contributing to the therapeutic benefits of ketogenic diets through a reduction in glucose and insulin (1–4). This inhibitory activity may provide a component of the therapeutic efficacy of these diets in the treatment of patients with drug-resistant epilepsies (5), cancers (6), and neurodegenerative disorders (7), and in providing lifespan extension (4). Inhibition of mTORC1 has been proposed to lead to increased autophagy and the clearance of misfolded proteins in neurodegenerative disorders (8), the decrease of cell proliferation in cancers (9), and reduced stress response and improved mitochondrial function credited with increasing longevity (10). Hyperactivation of mTORC1 activity is also found in the neurodevelopmental disorder tuberous sclerosis complex (TSC) (11), resulting from mutations in either the gene for hamartin (TSC1) or tuberin (TSC2), causing the development of tumors and manifesting in epilepsy, cognitive disability, and neurobehavioral abnormalities (12). The use of mTORC1 inhibitors to treat patients with TSC appears clinically promising (13, 14). mTORC1 signaling is also disrupted by mutations in p97 (also called VCP or cdcD, referred to as human p97; hp97), an evolutionarily conserved AAA ATPase (15), contributing to the pathogenesis of degenerative diseases (16). This critical ATPase functions in processes such as endoplasmic reticulum-associated degradation (ERAD) (17), autophagy (18), and DNA damage repair (19), with UBX domain-containing proteins making up the largest group of cofactors required for p97 function (20).

Ketogenic diets were initially developed to mimic starvation, with the low-carbohydrate and high-fat intake leading to the generation of ketone bodies (21). The initial form of the diet, termed the "classical" ketogenic diet, requires 90% of dietary energy to be delivered through fats and, despite its efficacy, is difficult to maintain due to stringent dietary restrictions (22). To reduce these restrictions, a modified form of the diet, called the medium-chain triglyceride (MCT) ketogenic diet, was introduced in 1971 (23), requiring around 30% less dietary energy delivered as fats, with improved tolerability (24, 25). Metabolic breakdown of these dietary triglycerides in the intestine leads to the release of the fatty acids octanoic acid (C8) and decanoic acid (C10), which are absorbed and transported in the blood to the brain, where they cross the blood–brain barrier (26). Recently, it has been suggested that ketosis may not be necessary for an antiseizure effect of the MCT diet and that decanoic acid alone can mediate an antiseizure effect (21). Several mechanisms of action have been suggested for decanoic acid, including the direct inhibition of excitatory α-amino-3-hydroxy-5-methyl-4-isoxazolepropionic acid (AMPA) receptors (5, 27), the activation of the nuclear peroxisome proliferator-activated receptor gamma receptor leading to increased mitochondrial proliferation (28), as well as the inhibition of phosphoinositide turnover and the inhibition of diacylglycerol kinase (29, 30). However, a potential disadvantage of nonketogenic MCT diets is a lack of effect on glucose

Significance

The mTORC1 complex provides a critical role in cell function, regulating a variety of processes including growth and autophagy. mTORC1 signaling is hyperactivated in a range of common diseases including cancer, epilepsy, and neurodegenerative disorders. Hence, mTORC1 signaling provides an important target for regulation in many contexts. Here, we show that decanoic acid, a key component of a widely used medicinal diet, reduces mTORC1 activity. We identify this in a tractable model system, and validate it in ex vivo rat brain tissue and in human iPSC-derived astrocytes from patients with a clinically relevant disease. Thus, we provide insight into an easily accessible therapeutic approach for a range of diseases.

Author contributions: E.C.W. and R.S.B.W. designed research; E.C.W., S.D., E.L., J.D.-O., J.S., V.M.H., and M.C.W. performed research; E.C.W. analyzed data; and E.C.W. and R.S.B.W. wrote the paper.

Competing interest statement: M.C.W. and R.S.B.W. are named inventors on related patents WO2019002435A1, WO2012069790A1, WO2016038379A1, and WO2018189113.

This article is a PNAS Direct Submission.

[1]To whom correspondence may be addressed. Email: robin.williams@rhul.ac.uk.

This article contains supporting information online at https://www.pnas.org/lookup/suppl/doi:10.1073/pnas.2008980117/-/DCSupplemental.

First published September 2, 2020.

and insulin and therefore mTORC1 signaling, but this has not been previously investigated. We therefore wished to test this hypothesis that decanoic acid has no effect on mTORC1 activity.

The eukaryotic social amoeba *Dictyostelium discoideum* is a simple model organism which provides a valuable system for biomedical research. *Dictyostelium* has a well-described life cycle where it exists in both single and multicellular stages (31). Many *Dictyostelium* proteins are more homologous to human proteins than to those of unicellular fungi, making it a valuable organism for studying processes relevant to humans (32). The generation of libraries of *Dictyostelium* mutants has enabled pharmacogenetic studies leading to the identification of targets for compounds (33, 34). This approach allows rapid identification of proteins that control sensitivity to a compound, thus implicating the proteins or the wider pathways in the action of the compound. In epilepsy research, *Dictyostelium* has been employed to identify a mechanism of the commonly used antiepileptic drug valproate to reduce phosphoinositide signaling (30), with more potent compounds showing improved efficacy in seizure models (30, 35, 36). Through this research originating in *Dictyostelium*, decanoic acid has been identified as an effective seizure control agent (30, 37), contributing to the development and progression to clinical trials of an MCT diet with an altered decanoic acid content (NCT02825745; https://clinicaltrials.gov/ct2/show/NCT02825745).

In this study, we investigate a role for decanoic acid in mTORC1 function. We initially show that decanoic acid causes a reduction of mTORC1 activity in a structurally specific manner in *Dictyostelium*, in the absence of insulin and in the presence of glucose, suggesting a specific molecular mechanism for decanoic acid in regulating this pathway. To identify this mechanism, we screened a mutant library to identify a decanoic acid-resistant mutant lacking a UBX domain-containing protein (UBXD18) that is partially resistant to the effects of decanoic acid on growth and mTORC1 signaling. We establish that UBXD18 binds the *Dictyostelium* p97 protein, decanoic acid reduces the activity of *Dictyostelium* p97 in a UBXD18-dependent manner, and p97 inhibition is sufficient to cause a reduction in mTORC1 signaling in this model. We then translate our findings to a rat hippocampal slice model and astrocytes derived from patients with the neurodevelopmental disorder TSC, to demonstrate that decanoic acid also reduces normal and dysregulated mTORC1 signaling in mammalian systems.

Results

Decanoic Acid Reduces mTORC1 Signaling in *Dictyostelium*. As wide-ranging therapeutic benefits of the classical ketogenic diet have been associated with inhibition of mTORC1 signaling (1, 4, 8, 9) (Fig. 1*A*), we employed *Dictyostelium* to investigate the effects of the MCT diet constituents decanoic acid and octanoic acid on this activity. We initially assessed the effects of these medium-chain fatty acids on *Dictyostelium* unicellular growth and multicellular development to establish relevant concentrations of decanoic acid and octanoic acid to investigate in this model. *Dictyostelium* cell growth was quantified in the presence of a range of concentrations of both fatty acids, with cell counts being recorded once every 24 h from 3 to 7 d posttreatment (Fig. 1 *B* and *C*). Treatment with both fatty acids caused a dose-dependent inhibition of growth. The rate of the exponential growth phase was then used to plot nonlinear regression curves, and half-maximal inhibitory concentrations (IC_{50} values) were calculated. Decanoic acid provided an IC_{50} of 18 μM (Fig. 1 *B* and *D*), while octanoic acid was less potent with an IC_{50} of 86 μM (Fig. 1 *C* and *D*). Since *Dictyostelium* also show a multicellular development cycle, we also investigated these fatty acids in regulating this process, where starving cells form fruiting bodies comprising dead vacuolated stalks holding spore heads aloft under control condition cells (*SI Appendix*, Fig. S1). This developmental process was unaffected by decanoic acid and octanoic acid at concentrations of fatty acids (200 μM) far greater than that shown to inhibit cell growth, suggesting that these compounds regulate molecular targets required for cell proliferation but not development (Fig. 1 *B–D* and *SI Appendix*, Fig. S1). These data also suggest that the medium-chain fatty acids have a specific molecular effect on *Dictyostelium* rather than a general toxic effect.

In order to monitor the effects of decanoic acid and octanoic acid on mTORC1 signaling in *Dictyostelium*, we quantified levels of phosphorylated 4E-BP1 (p-4E-BP1), a translation repressor directly phosphorylated by mTORC1 (Fig. 1*A*) (38, 39). Concentrations of decanoic acid and octanoic acid corresponding to an ∼95% reduction in growth rate (60 and 120 μM, respectively) (Fig. 1*D*) were employed, providing concentrations relevant to those observed in plasma of patients on the MCT diet (decanoic acid, 157 μM; octanoic acid, 310 μM) (24, 40). *Dictyostelium* cells were treated with fatty acids for 1 or 24 h before p-4E-BP1 levels were quantified by Western blot (Fig. 1 *E* and *F*). Decanoic acid decreased p-4E-BP1 levels at 1 and 24 h (Fig. 1*E*), while treatment with octanoic acid had no significant effect on the levels of p-4E-BP1 at either treatment duration (Fig. 1*F*). Starvation, a physiological process well-established to reduce mTORC1 activity (41, 42), also caused a significant decrease in p-4E-BP1 levels in *Dictyostelium* (*SI Appendix*, Fig. S2*A*), as did two established mTOR inhibitors (38, 43) (*SI Appendix*, Fig. S2 *B* and *C*). Rapamycin did not significantly alter p-4E-BP1 levels under our conditions (*SI Appendix*, Fig. S2*D*), consistent with findings showing a lack of autophagic response to rapamycin in *Dictyostelium* (44).

Since mTORC1 is activated by phosphatidylinositol 3-kinase (PI3K)/AKT signaling and inhibited by AMP-activated protein kinase (AMPK) signaling (Fig. 1*A*), we also investigated a role for decanoic acid in these signaling pathways. We monitored the effects of decanoic acid on PI3K/AKT signaling by measuring levels of a phosphorylated AKT substrate (p-AKT-S) (45, 46) (*SI Appendix*, Fig. S2 *E* and *F*). No significant difference was observed in p-AKT-S levels after treatment with decanoic acid (60 μM) for 1 or 24 h (Fig. 1*G*). This indicated that decanoic acid targets mTORC1 independent of PI3K/AKT signaling under these conditions, and further suggests that decanoic acid inhibits mTORC1 without altering mTORC2 activation. In these growing cells, it was not possible to assay PI3K signaling through monitoring phosphorylation of the activation loops of the AKT homologs PKBR1 (T309) and PKBA (T278), since this signaling is undetectable during growth (45, 47) (*SI Appendix*, Fig. S2*G*). We also evaluated the effect of decanoic acid on AMPK signaling by assessing phospho-AMPKα (p-AMPK) levels (39, 48) (*SI Appendix*, Fig. S2 *H–K*), where no significant difference was observed (Fig. 1*H*).

Identification of UBXD18 as a Potential Molecular Target for Decanoic Acid. We sought to identify potential molecular targets for decanoic acid by isolating decanoic acid-resistant mutants using an unbiased genetic screen of a library of *Dictyostelium* insertional mutants (Fig. 2*A* and *SI Appendix*, Fig. S3*A*). The library of mutants was screened with a concentration of decanoic acid that inhibits wild-type cell growth (120 μM; 7 d). Using this approach, mutants resistant to decanoic acid were isolated, and the location of the insertion site within the genome of these mutants was determined to identify genes controlling decanoic acid sensitivity. From this, a decanoic acid-resistant mutant, *UBXD18*$^{-}$, was identified (Fig. 2*B*), with the mutagenic insertion in the region coding for the ubiquitin-associated domain of the *ubxd18* gene (DDB_G0276057).

Proteomic analysis enabled the initial characterization of the *Dictyostelium* UBXD18 protein. The UBXD18 protein sequence shared homology with two human UBX domain-containing proteins (UBXN1, UniProt Q04323; UBXD2, UniProt Q92575) (Fig. 2*B*), with highly conserved UBX domains (*SI Appendix*, Fig. S3*B*). The *Dictyostelium* UBX domain shared 28% identical and 51% similar amino acids with the UBX domain of UBXN1, and

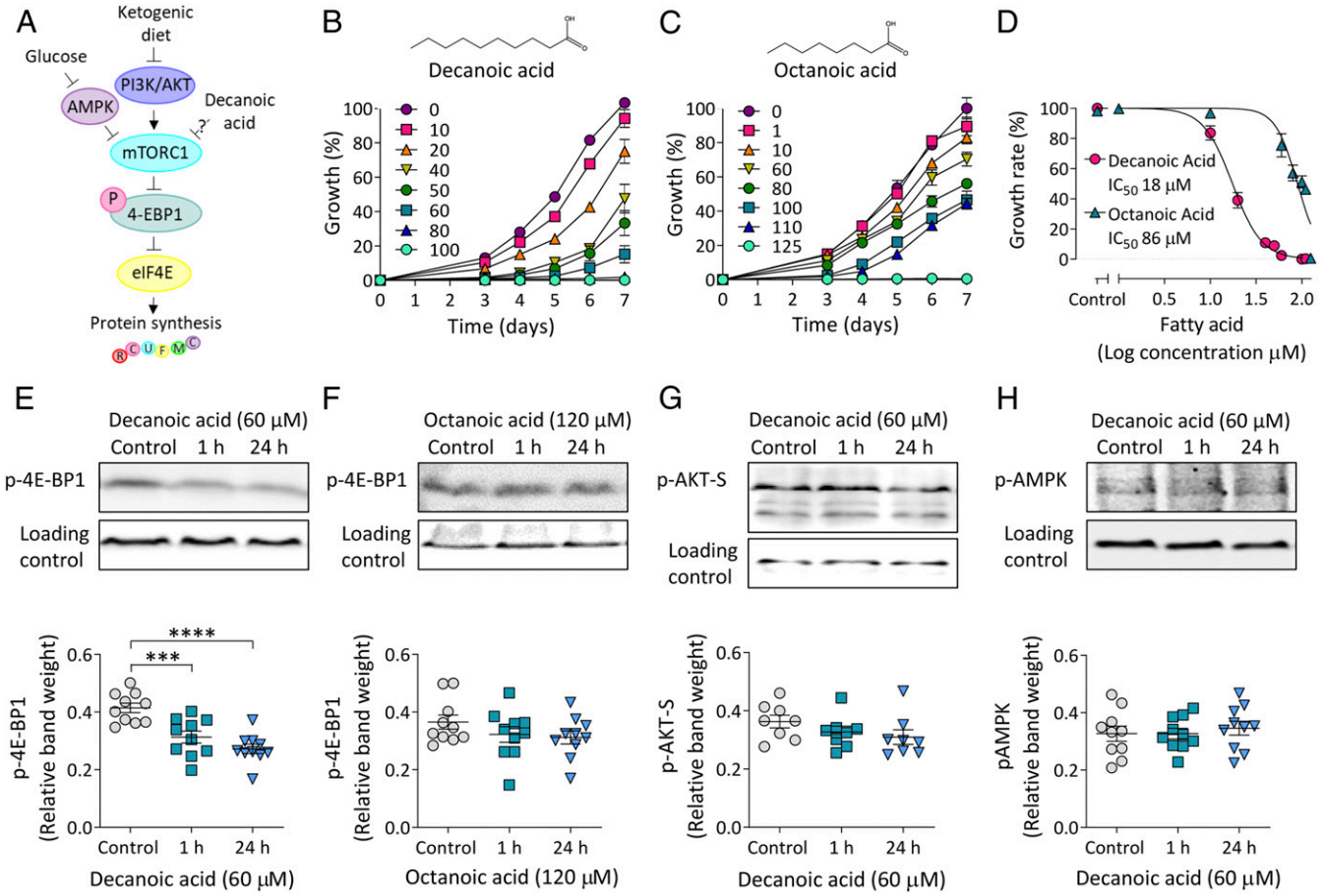

Fig. 1. Decanoic acid causes a reduction in p-4E-BP1 levels in *Dictyostelium*. (*A*) Simplified schematic diagram of mTORC1 pathway signaling. Glucose activates mTORC1 through inhibition of AMPK. Conversely, the ketogenic diet inhibits mTORC1 through inhibition of PI3K/AKT signaling. Phosphorylation of 4E-BP1 by mTORC1 induces 4E-BP1 to dissociate from eukaryotic translation initiation factor 4E (eIF4E), promoting the initiation of translation, and this phosphorylation is used in this study as a readout for mTORC1 activation. (*B* and *C*) *Dictyostelium* cells were treated with (*B*) decanoic acid ($n = 12$) or (*C*) octanoic acid ($n = 6$) for 7 d at a range of concentrations (μM). Percentage growth was plotted normalized to the solvent control (0 μM, 0.2% DMSO) at 7 d. (*D*) Dose–response curves of normalized growth rate plotted against log concentration of compound were used to calculate IC_{50} values. (*E* and *F*) p-4E-BP1 levels were analyzed in wild-type cells treated for 1 or 24 h with (*E*) decanoic acid ($n = 10$) (one-way ANOVA with Dunnett's post hoc test) or (*F*) octanoic acid ($n = 10$) (one-way ANOVA with Dunnett's post hoc test) at concentrations corresponding to an ∼95% reduction in growth rate. Methylcrotonyl-CoA carboxylase (MCCC1) served as a loading control. (*G*) AKT activity was evaluated in wild-type cells treated for 1 or 24 h with decanoic acid using an anti–phospho-AKT substrate antibody, with MCCC1 as a loading control ($n = 10$) (one-way ANOVA with Dunnett's post hoc test). (*H*) AMPK activation was analyzed using an antibody against phospho-AMPK, with MCCC1 as a loading control ($n = 10$) (one-way ANOVA with Dunnett's post hoc test). Data represent the mean ± SEM. Significance is indicated by $^{***}P \leq 0.001$, $^{****}P \leq 0.0001$.

27% identical and 51% similar amino acids with the UBX domain of UBXD2 (*SI Appendix*, Fig. S3*B*). A binding loop (s3/s4) known to interact with the AAA ATPase p97 was partially conserved between these proteins (*SI Appendix*, Fig. S3*B*) (49), suggesting that these proteins are p97-binding partners. Cladistic analysis of all *Dictyostelium* and human UBX proteins (*SI Appendix*, Fig. S3*C*) confirmed that the UBXN1 and UBXD2 proteins are the most likely homologs of the *Dictyostelium* UBXD18 protein.

The Effects of Decanoic Acid on *Dictyostelium* Growth and mTORC1 Signaling Are Dependent on UBXD18. We next generated an independent *UBXD18*$^{-}$ mutant to confirm that the UBXD18 protein regulates sensitivity to decanoic acid (Fig. 3*A* and *SI Appendix*, Fig. S4*A*). This recapitulated mutant was produced by insertion of a 1,592-bp blasticidin resistance sequence into the central region of the *ubxd18* gene, and was confirmed by loss of gene expression (*SI Appendix*, Fig. S4 *A* and *C*). UBXD18 activity was also reintroduced to *UBXD18*$^{-}$ by expression of *ubxd18* complementary DNA (cDNA) in the mutant (*SI Appendix*, Fig. S4*B*), where the presence of green fluorescent protein (GFP)-UBXD18 was confirmed by Western blot analysis (*SI Appendix*, Fig. S4*D*). Wild-type, knockout (*UBXD18*$^{-}$), and rescue (*UBXD18*$^{-/+}$) cells were then assessed for the effect of decanoic acid on growth to quantify resistance (Fig. 3*B*), with IC_{50} values indicating comparative sensitivity (Fig. 3*C*). This analysis demonstrated that *UBXD18*$^{-}$ was partially resistant to the effect of decanoic acid, with an IC_{50} value twofold higher than that of the parental cell line (*UBXD18*$^{-}$ IC_{50} 37 μM, compared with wild-type IC_{50} 18 μM) (Fig. 3*C*). Reintroducing *ubxd18* gene expression restored a decanoic acid-sensitive phenotype (*UBXD18*$^{-/+}$, IC_{50} 13 μM) (Fig. 3*C*). To establish if UBXD18 confers partial resistance to the other medium-chain fatty acids provided in the MCT diet, *UBXD18*$^{-}$ was also assessed for the effect of octanoic acid on growth (*SI Appendix*, Fig. S5), where no significant change in sensitivity was observed (wild-type, IC_{50} 79 μM; *UBXD18*$^{-}$, IC_{50} 87 μM), suggesting structural specificity in the targeting of UBXD18 by decanoic acid.

The role of UBXD18 in both regulating mTORC1 activity and controlling the effect of decanoic acid in reducing mTORC1 activity was investigated by Western blot analysis. Here, 4E-BP1 phosphorylation was monitored in wild-type, *UBXD18*$^{-}$, and *UBXD18*$^{-/+}$ in

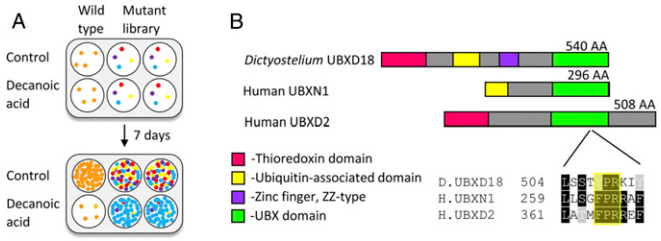

Fig. 2. *Dictyostelium* UBXD18 protein, identified from a mutant library screen to regulate decanoic acid sensitivity, contains the evolutionarily conserved UBX domain. (*A*) A genetic screen of an insertional mutant library was carried out to identify mutants partially resistant to the growth-inhibitory effects of medium-chain fatty acids. (*B*) The genetic screen identified a gene encoding UBX domain-containing protein 18 (DDB_G0276057) as being a potential target for decanoic acid. The two most highly conserved human proteins, UBXN1 and UBXD2, are shown alongside a schematic of the *Dictyostelium* UBXD18 protein. These proteins share a common UBX domain with a highly conserved s3/s4 loop involved in binding p97 (highlighted).

the presence of decanoic acid. Loss of UBXD18 caused a decrease in p-4E-BP1 levels compared with wild type, and p-4E-BP1 levels were restored by reintroduction of the protein ($UBXD18^{-/+}$) (Fig. 3*D*). Analyzing p-4E-BP1 levels following decanoic acid treatment (60 μM for 1 or 24 h) showed that $UBXD18^{-}$ was unresponsive to treatment (Fig. 3*E*), and $UBXD18^{-/+}$ showed restored decanoic acid sensitivity following 24-h treatment (Fig. 3*F*).

Characterization of UBXD18 as a Binding Partner for Ddp97. Our results demonstrate that UBXD18 controls sensitivity to decanoic acid in both growth and mTORC1 regulation in *Dictyostelium*. Since UBXD18 contains a p97 interaction motif (20, 49) (Fig. 2*B*) and the *Dictyostelium* p97 (Ddp97) and human p97 (hp97) proteins show conserved domain structure and a high sequence identity (78%) (Fig. 4*A*), we used immunoprecipitation analysis to investigate an interaction between UBXD18 and Ddp97. In these experiments, cell lines were generated coexpressing *Dictyostelium* GFP-UBXD18 (or free GFP as a control) and Ddp97-RFP (red fluorescent protein) (*SI Appendix*, Fig. S4). To monitor binding, cell lysates were mixed with agarose beads coated with anti-GFP antibody, and the interacting proteins were isolated and analyzed using Western blot with anti-GFP and anti-RFP antibodies. Ddp97-RFP was found to bind to GFP-UBXD18 but not to free GFP (Fig. 4*B*), suggesting that UBXD18 interacts with Ddp97. In support of this, GFP-UBXD18 and Ddp97-RFP were found to colocalize throughout the cytoplasm and nucleus (Fig. 4*C*), consistent with that suggested for the mammalian homologs (50, 51).

Investigating the Effect of Decanoic Acid on Ddp97 Activity. An interaction between UBXD18 and Ddp97 suggests a role for UBXD18 in regulating Ddp97 function, and thus implicates Ddp97 in the cellular changes caused by decanoic acid in *Dictyostelium*. To analyze this, we assessed the effect of decanoic acid on Ddp97 activity by treating wild-type cells expressing Ddp97-RFP with decanoic acid, octanoic acid, or the established selective p97 inhibitor DBeQ (*N*2,*N*4-dibenzylquinazoline-2,4-diamine) (16, 52) for 24 h before immunoprecipitation of Ddp97-RFP and direct assessment of ATPase activity (53) (Fig. 5). Treatment with decanoic acid (60 μM) decreased Ddp97-RFP ATPase activity (Fig. 5 *A* and *D*), while octanoic acid (120 μM) had no significant effect, and the p97 inhibitor DBeQ (7.5 μM) also significantly reduced activity. Having demonstrated that decanoic acid but not octanoic acid acts to reduce Ddp97-RFP activity, we assessed the effect of decanoic acid on this activity in cells lacking UBXD18 ($UBXD18^{-}$) (Fig. 5 *B* and *E*), where decanoic acid did not affect

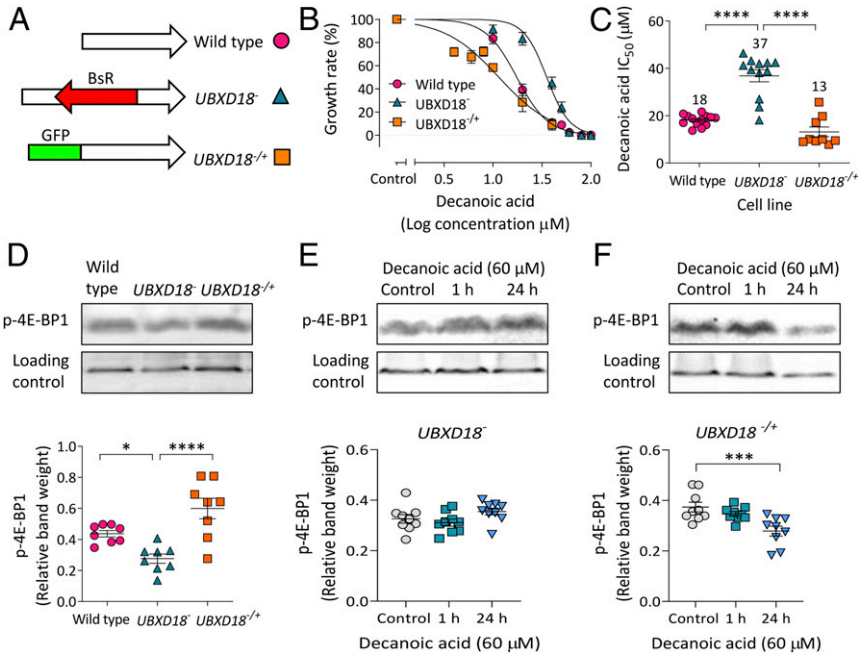

Fig. 3. UBXD18 regulates the sensitivity of *Dictyostelium* to decanoic acid. (*A*) A UBXD18 knockout ($UBXD18^{-}$) was generated by inserting a blasticidin resistance sequence (BsR) into the *ubxd18* gene, and a rescue ($UBXD18^{-/+}$) was generated by expressing the *ubxd18* gene attached to GFP. (*B*) Growth analysis of wild-type ($n = 12$), $UBXD18^{-}$ ($n = 12$), and $UBXD18^{-/+}$ ($n = 9$) *Dictyostelium* cells in decanoic acid, displayed as dose–response curves of normalized cell density plotted against log concentration. (*C*) IC_{50} values were compared between wild type ($n = 12$), $UBXD18^{-}$ ($n = 12$), and $UBXD18^{-/+}$ ($n = 9$) (one-way ANOVA with Dunnett's post hoc test). (*D*) Analysis of p-4E-BP1 levels in wild type, $UBXD18^{-}$, and $UBXD18^{-/+}$, with MCCC1 as a loading control ($n = 8$) (one-way ANOVA with Dunnett's post hoc test). (*E* and *F*) Analysis of p-4E-BP1 levels in (*E*) $UBXD18^{-}$ ($n = 9$) (Kruskal–Wallis test with Dunn's post hoc test) or (*F*) $UBXD18^{-/+}$ ($n = 9$) (one-way ANOVA with Dunnett's post hoc test) treated with decanoic acid (60 μM) for 1 or 24 h, with MCCC1 as a loading control. Data represent the mean ± SEM. Significance is indicated by $*P \leq 0.05$, $***P \leq 0.001$, $****P \leq 0.0001$.

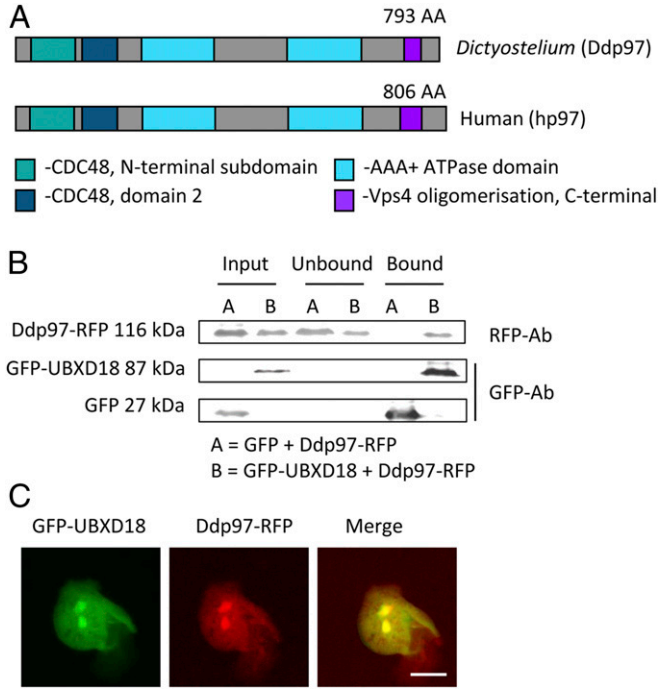

Fig. 4. *Dictyostelium* UBXD18 interacts with Ddp97. (*A*) Schematic of the *Dictyostelium* (Ddp97) and human (hp97) p97 proteins, showing 78% sequence identity. (*B*) Cell lysates of *Dictyostelium* cells coexpressing GFP-UBXD18 (or free-GFP as a control) and Ddp97-RFP were subjected to immunoprecipitation with GFP trap beads and the interaction was analyzed by Western blot using anti-GFP and anti-RFP antibodies (representative of three independent experiments). Ddp97-RFP was pulled down by GFP-UBXD18 and not by the GFP-only control. (*C*) Colocalization of GFP-UBXD18 and Ddp97-RFP by visualizing fluorescence in live cells (representative of three independent experiments). (Scale bar, 10 μm.)

Ddp97-RFP activity. Reintroduction of UBXD18 into *UBXD18*$^{-/+}$ also restored the decanoic acid-dependent reduction of Ddp97-RFP activity (Fig. 5 *C* and *F*). These findings suggest that decanoic acid functions through a mechanism involving UBXD18 to reduce Ddp97 activity in *Dictyostelium*.

Having established an effect of decanoic acid in inhibiting *Dictyostelium* p97 activity, we assessed the effect of inhibiting p97 on mTORC1 activity by using DBeQ. In these experiments, cells were treated with DBeQ (7.5 and 15 μM for 24 h), and cell lysates were analyzed for 4E-BP1 phosphorylation by Western blot (Fig. 5*G*). Treatment with DBeQ caused a significant reduction in p-4E-BP levels at both 7.5 and 15 μM (Fig. 5*G*). This was consistent with a comparable inhibition of growth caused by these concentrations of DBeQ (*SI Appendix*, Fig. S6). These findings suggest that the inhibitory effect of decanoic acid on *Dictyostelium* p97 activity may be sufficient to explain the observed mTORC1 and growth inhibition effects (Fig. 5*H*).

Decanoic Acid Reduces mTORC1 Activity in Rat Hippocampal Slices. Having identified an effect of decanoic acid in reducing mTORC1 activity independent of altered glucose levels and insulin signaling in *Dictyostelium*, we sought to translate these findings to a mammalian system. Here, we employed rat hippocampal slice preparations maintained in artificial cerebrospinal fluid, ensuring constant glucose levels in the absence of insulin, treated with decanoic acid (100 and 300 μM for 1 h) prior to assessing mTORC1 activity by Western blot analysis of p-4E-BP1 and total-4E-BP1 levels (Fig. 6). Decanoic acid at 100 μM had no significant effect on p-4E-BP1 levels (Fig. 6 *A* and *B*) but significantly decreased p-4E-BP1 levels at 300 μM (Fig. 6 *A* and *B*) and neither concentration altered total-4E-BP1 levels (Fig. 6*A* and *SI Appendix*, Fig. S7). These combined data showed a decrease in p-4E-BP1/total-4E-BP1 levels following treatment with 300 μM decanoic acid (Fig. 6*C*). Consistent with that observed in *Dictyostelium*, no change in p-AKT(Thr308)/total-AKT or p-AKT(Ser473)/total-AKT was observed in rat hippocampal slices following decanoic acid treatment (*SI Appendix*, Fig. S8).

Decanoic Acid Reduces mTORC1 Activity in Patient-Derived Astrocytes. To investigate a potential role for decanoic acid in reducing mTORC1 activity in a clinically relevant setting, we monitored this activity in astrocytes derived from patients with tuberous sclerosis complex. mTORC1 signaling is reportedly activated in astrocytes during epileptogenesis (54), with this cell type believed to play a significant role in seizure induction (55–57). In these experiments, induced pluripotent stem cells (iPSCs) derived from patients with mutations in genes encoding either TSC1 or TSC2, or healthy controls, were differentiated into astrocytes (58) and treated with decanoic acid (300 μM for 24 h) prior to Western blot analysis of p-4E-BP1 and total-4E-BP1 levels. Decanoic acid treatment caused a reduction in the ratio of p-4E-BP1/total-4E-BP1 in astrocytes derived from healthy (control) patients (Fig. 7 *A*–*C*), confirming a role for decanoic acid in regulating mTORC1 activity in human cells in the absence of altered glucose or insulin signaling. Decanoic acid also caused a reduction in the ratio of p-4E-BP1/total-4E-BP1 in astrocytes derived from patients with mutations in TSC1 (Fig. 7 *A*–*C*). However, decanoic acid had no significant effect on this ratio in astrocytes derived from patients with mutations in TSC2 (Fig. 7 *A*–*C*). In these assays, levels of p-4E-BP1 were not significantly altered following treatment (*SI Appendix*, Fig. S9 *A* and *B*), but the reduction in the ratio of p-4E-BP1/total-4E-BP1 was caused by a significant increase in levels of total-4E-BP1 (*SI Appendix*, Fig. S9 *C* and *D*). Interestingly, variability was observed between cells from different TSC2 patients, with cells from one patient showing no significant change in total-4E-BP1 levels following decanoic acid treatment, while cells from another patient showed a significant increase (*SI Appendix*, Fig. S10 *A* and *B*).

To confirm the effect of decanoic acid in reducing mTORC1 activity in patient-derived astrocytes, we also analyzed p70 S6 kinase (S6K) phosphorylation levels. For this activity, decreased phosphorylation at threonine 389 (p-S6K) indicated decreased mTORC1 activation (59) (Fig. 7*D*). Analysis of the same protein extracts showed that decanoic acid treatment also caused a reduction in the ratio of p-S6K/total-S6K in astrocytes derived from control patients and patients with mutations in TSC1 (Fig. 7 *D*–*F*) but showed no effect in astrocytes derived from patients with mutations in TSC2 (Fig. 7 *D*–*F*). The reduction in this ratio was caused by a significant reduction in levels of p-S6K (*SI Appendix*, Fig. S9 *E* and *F*) without changes in total-S6K levels (*SI Appendix*, Fig. S9 *G* and *H*). Variability was also observed between cells from individual TSC2 patients, with cells from one patient showing no significant change in p-S6K levels following decanoic acid treatment, while cells from the other showed a significant decrease (*SI Appendix*, Fig. S10 *C* and *D*).

Discussion

Ketogenic diets are well-established treatments for epilepsies (21) and cancers (6) with exciting potential for use in other areas of health such as treating neurodegenerative disorders (7); however, the therapeutic mechanisms underlying these effects are poorly understood. In this study, we have used *Dictyostelium* as a tractable model to establish that decanoic acid, one of the major constituents of the MCT ketogenic diet, inhibits mTORC1 signaling. In order to identify the mechanism behind this effect, we showed that the effects of decanoic acid on mTORC1 are dependent on a UBX domain-containing protein (UBXD18). We demonstrated that decanoic acid inhibits the activity of the

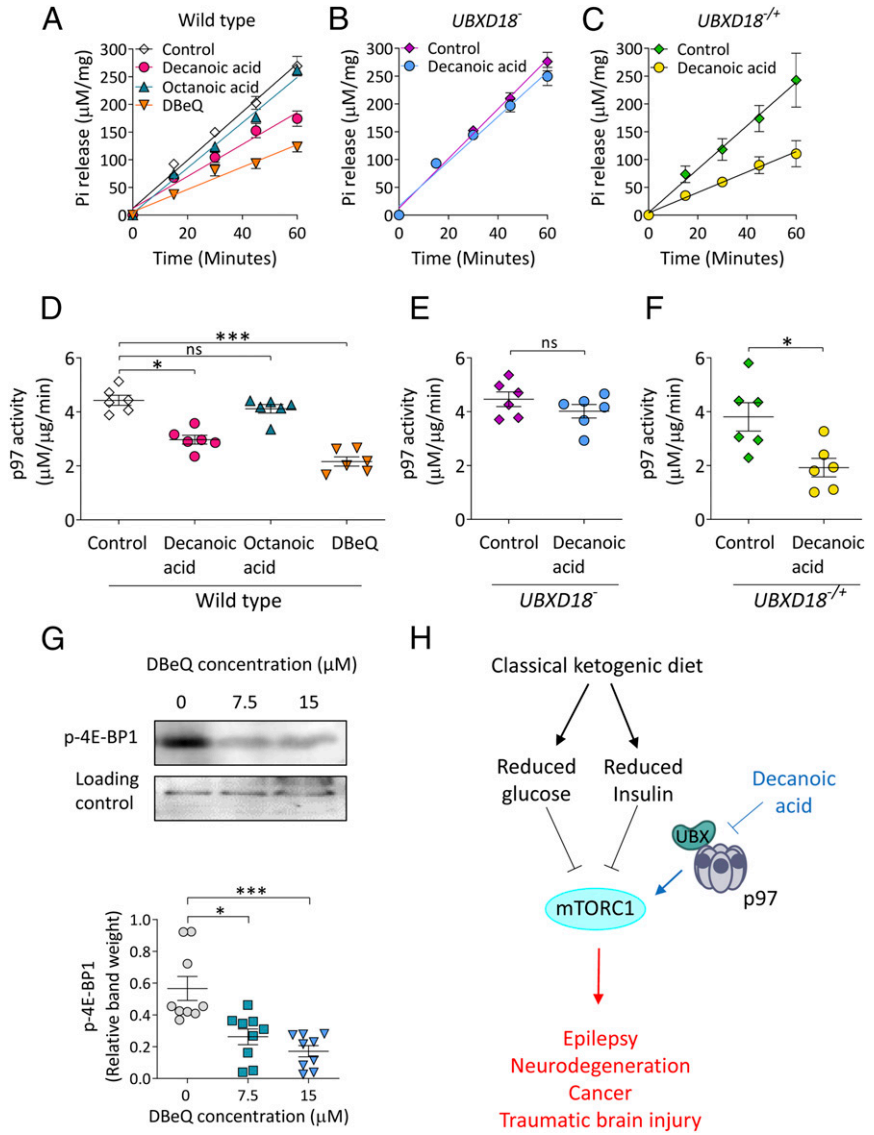

Fig. 5. Decanoic acid inhibits Ddp97 activity in a UBXD18-dependent manner. (*A*) Analysis of phosphate (Pi) release from an ATP hydrolysis reaction with Ddp97-RFP isolated from wild-type *Dictyostelium* cells treated with decanoic acid (60 μM), octanoic acid (120 μM), or DBeQ (7.7 μM) for 24 h ($n = 6$). (*B* and *C*) Phosphate release was analyzed from ATP hydrolysis reactions with Ddp97-RFP isolated from (*B*) *UBXD18*$^{-}$ and (*C*) *UBXD18*$^{-/+}$ treated with decanoic acid (60 μM) for 24 h ($n = 6$). (*D–F*) Specific enzyme activity (phosphate [μM] released relative to protein concentration [μg]) was plotted versus time (min) and subjected to linear regression analysis. The gradient was plotted, representing the rate of ATP hydrolysis (Ddp97 activity μM phosphate·μg protein^{-1}·min^{-1}) for (*D*) wild type (Kruskal–Wallis test with Dunn's post hoc test), (*E*) *UBXD18*$^{-}$ (Mann–Whitney *t* test), and (*F*) *UBXD18*$^{-/+}$ (Mann–Whitney *t* test) ($n = 6$). (*G*) Analysis of p-4E-BP1 levels in wild-type cells treated for 24 h with DMSO control (0 μM) or p97 inhibitor (DBeQ) at 7.5 or 15 μM ($n = 9$) (Kruskal–Wallis test with Dunn's post hoc test). MCCC1 served as a loading control. (*H*) Simplified schematic portraying the canonical effect of the classical ketogenic diet on mTORC1 through reduced glucose and insulin (black), downstream diseases displaying elevated mTORC1 (red), and a role of decanoic acid through a UBXD18- and p97-mediated pathway (blue). Data represent the mean ± SEM. Significance is indicated by $*P \leq 0.05$, $**P \leq 0.01$, $***P \leq 0.001$; ns, not significant, $P > 0.05$.

ubiquitous binding partner of UBXD18, p97, in a UBXD18-dependent manner, and further showed that direct p97 inhibition is sufficient to reduce mTORC1 signaling in *Dictyostelium*. We translated this effect of decanoic acid into a rat hippocampal slice model, demonstrating decanoic acid-dependent inhibition of mTORC1 signaling in the absence of glucose deprivation or insulin signaling. Finally, we employed astrocytes derived from patients with mutations in TSC1 or TSC2 associated with dysregulated mTORC1 activity (11, 58) to demonstrate that treatment with decanoic acid results in decreased mTORC1 activation in healthy patients and patients with TSC1 mutations.

We provide mechanistic insight for the role of decanoic acid in regulating mTORC1 activity in *Dictyostelium*, through a UBX domain-containing protein and *Dictyostelium* p97. UBX proteins have previously been shown to directly regulate the activity of p97 in human cells (20). By employing a specific inhibitor for p97 (DBeQ), we also confirmed that pharmacological inhibition of *Dictyostelium* p97 decreased mTORC1 activity and cell proliferation (16) (Fig. 5*G* and *SI Appendix*, Fig. S6), suggesting that decanoic acid-induced p97 inhibition could explain the inhibitory effects on mTORC1 activity and growth in the model system (Fig. 5*H*). Although the role of human p97 in regulating mTORC1 has yet to be established, there is evidence that inhibition of p97 results in the disruption of amino acid homeostasis, potentially leading to the observed reduction in mTORC1 (16, 52). Our data provide an indication that decanoic acid may prevent the interaction of *Dictyostelium* p97 with its regulatory cofactor UBXD18, thus reducing *Dictyostelium* p97 activity and leading to a reduction

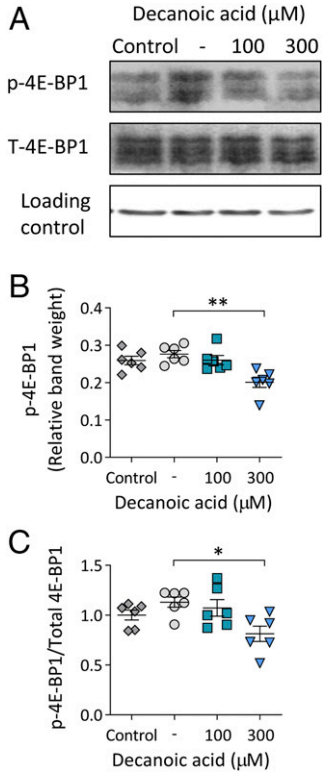

Fig. 6. Decanoic acid causes a reduction in p-4E-BP1 levels in rat hippocampal brain slices. (*A*) Rat hippocampal brain slices in artificial cerebrospinal fluid (control), treated for 1 h with DMSO solvent control (-), 100 μM decanoic acid, or 300 μM decanoic acid were analyzed for p-4E-BP1 and total-4E-BP1 (T-4E-BP1), with beta-actin as a loading control. Multiple bands correspond to the three isoforms of 4E-BP1. (*B*) Relative band weights were plotted for p-4E-BP1 ($n = 6$) (Kruskal–Wallis test with Dunn's post hoc test). (*C*) The ratio of p-4E-BP1/T-4E-BP1 was used as a readout for mTORC1 ($n = 6$) (Kruskal–Wallis test with Dunn's post hoc test). Data represent the mean ± SEM. Significance is indicated by $*P \leq 0.05$, $**P \leq 0.01$.

in mTORC1. Interactions between long-chain fatty acids and UBX domain-containing proteins have previously been implicated in blocking p97 activity in mammalian cells (60), suggesting that regulation of p97 via an interaction of decanoic acid with a UBX domain-containing protein represents a viable potential mechanism in humans.

Inhibition of p97 has been proposed as a treatment for cancer and epilepsy (61, 62). In cancers, expression of p97 is increased to manage excessive proteotoxic stress (63), and thus p97 inhibitors are in clinical trials as cancer treatments (64, 65). p97 also plays a role in a common form of epilepsy (autosomal dominant juvenile myoclonic epilepsy), where a mutation in a $GABA_A$ receptor subunit (A322D mutation in the α1-subunit) results in misfolding and rapid ERAD of the α1-subunit, resulting in epilepsy (62, 66). By inhibiting p97, α1(A322D) subunits have more time to fold in the endoplasmic reticulum, allowing functional $GABA_A$ receptors to form and act as inhibitory ion channels (62). Our findings suggest that further analysis of a role for decanoic acid in inhibiting p97 and mTORC1 may identify associated therapeutic benefits.

Our data suggest a mechanism for decanoic acid in regulating mTORC1 independent of glucose and insulin. The classical ketogenic diet is known to reduce mTORC1 activation, with a proposed mechanism through lowering glucose and insulin levels (1–4) associated with the therapeutic effects of the classical ketogenic diet in treating epilepsy. However, the role of the MCT ketogenic diet fatty acids in this function has not previously been reported. Several studies have suggested that decanoic acid in the MCT diet provides therapeutic benefits in seizure control (5, 26, 27, 67), and here we have identified that in *Dictyostelium*, decanoic acid inhibits mTORC1 activity under conditions of constant glucose and in the absence of insulin (Fig. 1*E*). Since we have translated this effect to both a rat hippocampal slice model (Fig. 6) and patient-derived astrocytes (Fig. 7), again under conditions of constant glucose and in the absence of insulin signaling, our data support an evolutionarily conserved effect of decanoic acid, provided in the MCT diet, distinct from that proposed for the classical ketogenic diet.

The mTORC1 pathway acts as a regulator for cell growth through the phosphorylation of targets activating anabolic processes and inhibiting catabolic processes. In this role, mTORC1 inhibition has been credited with providing therapeutic effects in many areas of health, including treating epilepsy and neurodegenerative disorders, preventing the proliferation of cancer cells, improving cognitive function after traumatic brain injury, and increasing longevity (8–10). mTORC1 inhibition has also been investigated as a therapeutic target for the neurodevelopmental disorder TSC associated with deregulated mTORC1 activity (11, 13, 14, 68). The cause of epilepsy in TSC patients is often related to the formation of cortical tubers, characterized by cortical dyslamination, dysplastic neurons, and astrogliosis (69). Although astrogliosis may be secondary to neuronal pathology, studies in animals and humans suggest that TSC involves a primary defect in astrocytes (55), supported by mTOR dysregulation (70). In cell culture, however, patient-derived cells have been suggested to employ a feedback loop to regulate the TSC and maintain balanced mTOR signaling (71). Importantly, we show that decanoic acid reduces mTORC1 signaling in cells derived from both healthy individuals and patients with TSC mutations, suggesting that decanoic acid functions independent of disease state and shows efficacy in cells derived from patients with disease-associated mutations (Fig. 7). However, heterogeneity between astrocytes derived from patients with mutations in TSC2 were observed (*SI Appendix*, Fig. S10), which suggests that decanoic acid might provide differential efficacy between individuals.

Inhibition of mTORC1 has been suggested to provide wide-ranging clinical benefits, including as a treatment for cancer, epilepsy, neurodegenerative diseases, and aging (14, 72–76). The recent development of new pharmacological inhibitors for mTORC1 inhibition, based around rapamycin, have focused on identifying "rapalogues" without the toxicity associated with rapamycin (68). Alternately, inhibition of this pathway is possible through dietary treatment, namely the classical ketogenic diet (1–4); however, this diet is highly restrictive for patients, resulting in low compliance. Our data suggest that a nonketogenic decanoic acid-rich diet that is less restrictive and avoids the potential adverse effects of ketosis could also provide therapeutic effects through inhibiting this pathway. Thus, further investigation into dietary decanoic acid may provide a useful approach to treat mTORopathies in addition to providing a range of associated health effects.

Materials and Methods

Detailed methods are available in *SI Appendix*.

***Dictyostelium* Growth Assay.** *Dictyostelium* cells in the presence of compound or a dimethyl sulfoxide (DMSO) control were grown at 22 °C in HL5, and the cell number was quantified.

Cell Development Assays. Exponentially growing cells were developed on nitrocellulose filters on absorbent pads soaked in phosphate buffer containing compound or DMSO control. Developmental phenotypes were imaged after 24 h.

***Dictyostelium* Mutant Library Screen.** A *Dictyostelium* mutant library was grown alongside wild-type cells in decanoic acid or DMSO control and screened for the appearance of resistant colonies. Resistant mutants were isolated and selected isogenically and mutation sites were identified using inverse PCR.

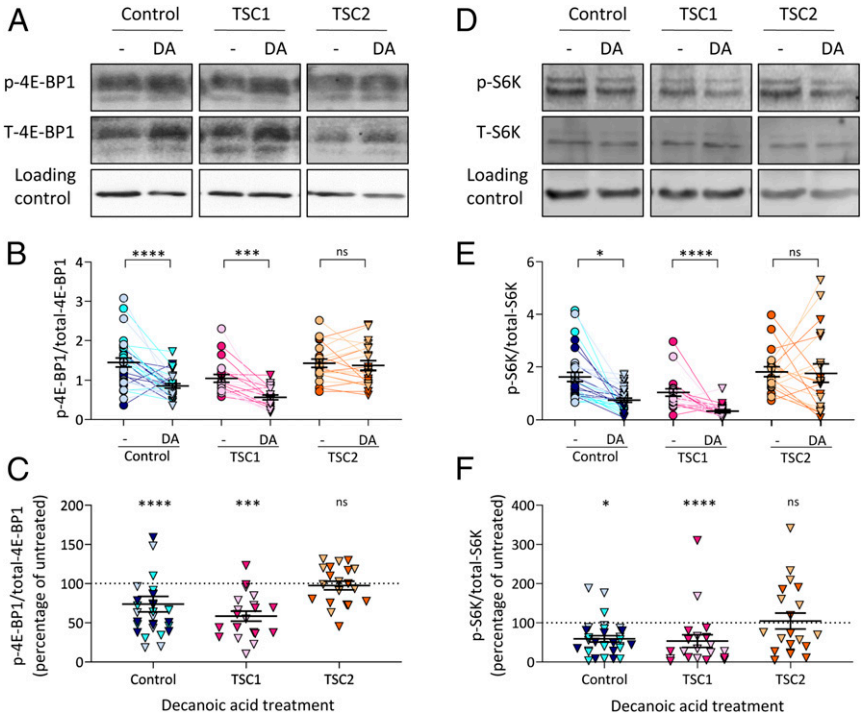

Fig. 7. Decanoic acid decreases the ratio of p-4E-BP1/total-4E-BP1 and p-S6K/total-S6K in iPSC-derived astrocytes from healthy individuals and patients with TSC1 mutations. (*A*) Astrocytes derived from iPSCs from three healthy individuals (control), two patients with mutations in TSC1, or two patients with mutations in TSC2 were treated with DMSO solvent control (-) or 300 μM decanoic acid (DA) for 24 h before analysis of p-4E-BP1 and T-4E-BP1 levels, using beta-actin as a loading control. (*B*) The ratio of p-4E-BP1/total-4E-BP1 was used as a readout for mTORC1 ($n = 10$ per patient) (nested *t* test). (*C*) The percentage change in p-4E-BP1/total-4E-BP1 levels following decanoic acid treatment is plotted normalized to the untreated samples (DMSO solvent control) ($n = 10$ per patient) (nested *t* test). (*D*) The same samples were analyzed for levels of p-S6K and total-S6K, using beta-actin as a loading control. (*E*) The ratio of p-S6K/total-S6K was used as a readout for mTORC1 ($n = 10$ per patient) (nested *t* test). (*F*) The percentage change in p-S6K/total-S6K levels following decanoic acid treatment is plotted normalized to the untreated samples (DMSO solvent control) ($n = 10$ per patient) (nested *t* test). Data from individual patients are differentiated by color. Data represent the mean ± SEM. Significance is indicated by $*P \leq 0.05$, $***P \leq 0.001$, $****P \leq 0.0001$; ns, $P > 0.05$.

Knockout Generation. *UBXD18*$^{-}$ cells were generated by homologous integration. A knockout cassette was generated by PCR amplification over the REMI insertion site using genomic DNA extracted from the mutant. The PCR product was electroporated into *Dictyostelium* wild-type cells.

Creation of GFP-UBXD18 and Ddp97-RFP Constructs. *ubxd18* or *Dictyostelium p97* cDNA was cloned into extrachromosomal vectors before electroporation into *Dictyostelium* cells.

Western Blotting. Samples were prepared in Laemmli buffer, separated by sodium dodecyl sulfate polyacrylamide gel electrophoresis, transferred to membranes, and probed with antibodies as described. Blots were visualized using the Odyssey CLx Imager (LI-COR), quantified using LI-COR Image Studio, and normalized to the loading control or total (unphosphorylated) protein (as specified).

Immunoprecipitation. GFP-TrapA beads were used for immunoprecipitation of GFP-fusion proteins before analysis by Western blot.

ATPase Assay. *Dictyostelium* cells, expressing Ddp97-RFP, were treated for 24 h with compound. RFP-TrapA beads were used for the immunoprecipitation of RFP-tagged proteins and ATPase activity was monitored as described (53).

Rat Hippocampal Slice Preparation for Western Blot. Adult Sprague–Dawley rats were used to prepare hippocampal slices as detailed (30). Animal experiments were conducted in accordance with Animals (Scientific Procedures) Act 1986 and approved by the local University College London ethics committee.

Patient-Derived Astrocyte Differentiation and Preparation for Western Blot. iPSCs from three individual control patients, two patients with TSC1 mutations, and two patients with TSC2 mutations were differentiated into astrocytes as described (58). The following cell lines were obtained from the National Institute of General Medical Sciences Human Genetic Cell Repository at the Coriell Institute for Medical Research: GM23964, GM23973, GM06149, GM02332, GM03958, and GM06102. An additional control line was kindly provided by Eleonora Aronica, Amsterdam Universitair Medisched Centra. All experiments were exempt from approval of the Medical Ethical Toetsingscommissie, the institutional review board of the Vrije Universiteit Medical Center.

Data Availability. All data are available in the text and *SI Appendix*.

ACKNOWLEDGMENTS. We thank Adrian Harwood and Chris Thompson and their laboratories for providing us with the *Dictyostelium* mutant library. E.C.W. was supported by a Biotechnology and Biological Sciences Research Council Doctoral Training Partnership studentship sponsored by Vitaflo. J.D.-O. was supported by a PhD studentship funded by GW Pharmaceuticals, Ltd. J.S. was supported by a Royal Holloway Department of Biological Sciences PhD studentship award.

1. A. P. Ostendorf, M. Wong, mTOR inhibition in epilepsy: Rationale and clinical perspectives. *CNS Drugs* **29**, 91–99 (2015).
2. P. Sweeney *et al*., Protein misfolding in neurodegenerative diseases: Implications and strategies. *Transl. Neurodegener.* **6**, 6 (2017).
3. L. L. Thio, E. Erbayat-Altay, N. Rensing, K. A. Yamada, Leptin contributes to slower weight gain in juvenile rodents on a ketogenic diet. *Pediatr. Res.* **60**, 413–417 (2006).
4. M. N. Roberts *et al*., A ketogenic diet extends longevity and healthspan in adult mice. *Cell Metab.* **26**, 539–546.e5 (2017).

5. K. Augustin *et al*., Perampanel and decanoic acid show synergistic action against AMPA receptors and seizures. *Epilepsia* **59**, e172–e178 (2018).
6. T. N. Seyfried, J. Marsh, L. M. Shelton, L. C. Huysentruyt, P. Mukherjee, Is the restricted ketogenic diet a viable alternative to the standard of care for managing malignant brain cancer? *Epilepsy Res.* **100**, 310–326 (2012).
7. I. Van der Auwera, S. Wera, F. Van Leuven, S. T. Henderson, A ketogenic diet reduces amyloid beta 40 and 42 in a mouse model of Alzheimer's disease. *Nutr. Metab. (Lond.)* **2**, 28 (2005).
8. N. Fujikake, M. Shin, S. Shimizu, Association between autophagy and neurodegenerative diseases. *Front. Neurosci.* **12**, 255 (2018).
9. J. Xie, X. Wang, C. G. Proud, mTOR inhibitors in cancer therapy. *F1000 Res.* **5**, 2078 (2016).
10. S. C. Johnson, P. S. Rabinovitch, M. Kaeberlein, mTOR is a key modulator of ageing and age-related disease. *Nature* **493**, 338–345 (2013).
11. A. R. Tee *et al*., Tuberous sclerosis complex-1 and -2 gene products function together to inhibit mammalian target of rapamycin (mTOR)-mediated downstream signaling. *Proc. Natl. Acad. Sci. U.S.A.* **99**, 13571–13576 (2002).
12. P. B. Crino, K. L. Nathanson, E. P. Henske, The tuberous sclerosis complex. *N. Engl. J. Med.* **355**, 1345–1356 (2006).
13. M. Li *et al*., Efficacy and safety of mTOR inhibitors (rapamycin and its analogues) for tuberous sclerosis complex: A meta-analysis. *Orphanet J. Rare Dis.* **14**, 39 (2019).
14. D. N. Franz *et al*., Rapamycin causes regression of astrocytomas in tuberous sclerosis complex. *Ann. Neurol.* **59**, 490–498 (2006).
15. D. Barthelme, R. T. Sauer, Origin and functional evolution of the Cdc48/p97/VCP AAA+ protein unfolding and remodeling machine. *J. Mol. Biol.* **428**, 1861–1869 (2016).
16. J. K. Ching *et al*., mTOR dysfunction contributes to vacuolar pathology and weakness in valosin-containing protein associated inclusion body myopathy. *Hum. Mol. Genet.* **22**, 1167–1179 (2013).
17. Y. Ye, H. H. Meyer, T. A. Rapoport, The AAA ATPase Cdc48/p97 and its partners transport proteins from the ER into the cytosol. *Nature* **414**, 652–656 (2001).
18. J. S. Ju *et al*., Valosin-containing protein (VCP) is required for autophagy and is disrupted in VCP disease. *J. Cell Biol.* **187**, 875–888 (2009).
19. F. E. Indig *et al*., Werner syndrome protein directly binds to the AAA ATPase p97/VCP in an ATP-dependent fashion. *J. Struct. Biol.* **146**, 251–259 (2004).
20. C. Schuberth, A. Buchberger, UBX domain proteins: Major regulators of the AAA ATPase Cdc48/p97. *Cell. Mol. Life Sci.* **65**, 2360–2371 (2008).
21. K. Augustin *et al*., Mechanisms of action for the medium-chain triglyceride ketogenic diet in neurological and metabolic disorders. *Lancet Neurol.* **17**, 84–93 (2018).
22. H. C. Kang, D. E. Chung, D. W. Kim, H. D. Kim, Early- and late-onset complications of the ketogenic diet for intractable epilepsy. *Epilepsia* **45**, 1116–1123 (2004).
23. E. Neal, ' "Alternative" ketogenic diets' in *Ketogenic Diet and Metabolic Therapies*, S. A. Masino, Ed. (Oxford University Press, New York, 2017), chap. 2, pp. 5–15.
24. M. A. Sills, W. I. Forsythe, D. Haidukewych, Role of octanoic and decanoic acids in the control of seizures. *Arch. Dis. Child.* **61**, 1173–1177 (1986).
25. Y. M. Liu, Medium-chain triglyceride (MCT) ketogenic therapy. *Epilepsia* **49** (suppl. 8), 33–36 (2008).
26. P. Wlaź *et al*., Acute anticonvulsant effects of capric acid in seizure tests in mice. *Prog. Neuropsychopharmacol. Biol. Psychiatry* **57**, 110–116 (2015).
27. P. Chang *et al*., Seizure control by decanoic acid through direct AMPA receptor inhibition. *Brain* **139**, 431–443 (2016).
28. S. D. Hughes *et al*., The ketogenic diet component decanoic acid increases mitochondrial citrate synthase and complex I activity in neuronal cells. *J. Neurochem.* **129**, 426–433 (2014).
29. E. Kelly, D. Sharma, C. J. Wilkinson, R. S. B. Williams, Diacylglycerol kinase (DGKA) regulates the effect of the epilepsy and bipolar disorder treatment valproic acid in *Dictyostelium discoideum*. *Dis. Model. Mech.* **11**, dmm035600 (2018).
30. P. Chang *et al*., The antiepileptic drug valproic acid and other medium-chain fatty acids acutely reduce phosphoinositide levels independently of inositol in *Dictyostelium*. *Dis. Model. Mech.* **5**, 115–124 (2012).
31. W. F. Loomis, Genetic control of morphogenesis in *Dictyostelium*. *Dev. Biol.* **402**, 146–161 (2015).
32. L. Eichinger *et al*., The genome of the social amoeba *Dictyostelium discoideum*. *Nature* **435**, 43–57 (2005).
33. M. Cocorocchio *et al*., Curcumin and derivatives function through protein phosphatase 2A and presenilin orthologues in *Dictyostelium discoideum*. *Dis. Model. Mech.* **11**, dmm032375 (2018).
34. C. J. Perry *et al*., A new mechanism for cannabidiol in regulating the one-carbon cycle and methionine levels in *Dictyostelium* and in mammalian epilepsy models. *Br. J. Pharmacol.* **177**, 912–928 (2020).
35. X. Xu *et al*., Attenuation of phospholipid signaling provides a novel mechanism for the action of valproic acid. *Eukaryot. Cell* **6**, 899–906 (2007).
36. P. Chang, M. C. Walker, R. S. Williams, Seizure-induced reduction in PIP_3 levels contributes to seizure-activity and is rescued by valproic acid. *Neurobiol. Dis.* **62**, 296–306 (2014).
37. P. Chang *et al*., Seizure control by ketogenic diet-associated medium chain fatty acids. *Neuropharmacology* **69**, 105–114 (2013).
38. F. S. Chang *et al*., A two-pore channel protein required for regulating mTORC1 activity on starvation. *BMC Biol.* **18**, 8 (2020).
39. J. M. Nichols *et al*., Cell and molecular transitions during efficient dedifferentiation. *eLife* **9**, e55435 (2020).
40. H. G. Dean, J. C. Bonser, J. P. Gent, HPLC analysis of brain and plasma for octanoic and decanoic acids. *Clin. Chem.* **35**, 1945–1948 (1989).
41. J. Ye *et al*., GCN2 sustains mTORC1 suppression upon amino acid deprivation by inducing Sestrin2. *Genes Dev.* **29**, 2331–2336 (2015).
42. H. W. S. Tan, A. Y. L. Sim, Y. C. Long, Glutamine metabolism regulates autophagy-dependent mTORC1 reactivation during amino acid starvation. *Nat. Commun.* **8**, 338 (2017).
43. A. F. M. Tariqul Islam *et al*., Caffeine inhibits PI3K and mTORC2 in *Dictyostelium* and differentially affects multiple other cAMP chemoattractant signaling effectors. *Mol. Cell. Biochem.* **457**, 157–168 (2019).
44. E. Domínguez-Martín *et al*., Methods to monitor and quantify autophagy in the social amoeba *Dictyostelium discoideum*. *Cells* **6**, 18 (2017).
45. Y. Kamimura, M. Tang, P. Devreotes, Assays for chemotaxis and chemoattractant-stimulated TorC2 activation and PKB substrate phosphorylation in *Dictyostelium*. *Methods Mol. Biol.* **571**, 255–270 (2009).
46. T. D. Williams, S. Y. Peak-Chew, P. Paschke, R. R. Kay, Akt and SGK protein kinases are required for efficient feeding by macropinocytosis. *J. Cell Sci.* **132**, jcs224998 (2019).
47. Y. Kamimura *et al*., PIP_3-independent activation of TorC2 and PKB at the cell's leading edge mediates chemotaxis. *Curr. Biol.* **18**, 1034–1043 (2008).
48. P. Jaiswal, A. R. Kimmel, mTORC1/AMPK responses define a core gene set for developmental cell fate switching. *BMC Biol.* **17**, 58 (2019).
49. I. Dreveny *et al*., Structural basis of the interaction between the AAA ATPase p97/VCP and its adaptor protein p47. *EMBO J.* **23**, 1030–1039 (2004).
50. P. Wang *et al*., UBXN1 interferes with Rig-I-like receptor-mediated antiviral immune response by targeting MAVS. *Cell Rep.* **3**, 1057–1070 (2013).
51. J. Liang *et al*., Characterization of erasin (UBXD2): A new ER protein that promotes ER-associated protein degradation. *J. Cell Sci.* **119**, 4011–4024 (2006).
52. K. Parzych *et al*., Inadequate fine-tuning of protein synthesis and failure of amino acid homeostasis following inhibition of the ATPase VCP/p97. *Cell Death Dis.* **6**, e2031 (2015).
53. C. S. Rule, M. Patrick, M. Sandkvist, Measuring in vitro ATPase activity for enzymatic characterization. *J. Vis. Exp.* ((114), 54305 (2016).
54. L. Z. Sha *et al*., Mapping the spatio-temporal pattern of the mammalian target of rapamycin (mTOR) activation in temporal lobe epilepsy. *PLoS One* **7**, e39152 (2012).
55. M. Wong, The role of glia in epilepsy, intellectual disability, and other neurodevelopmental disorders in tuberous sclerosis complex. *J. Neurodev. Disord.* **11**, 30 (2019).
56. D. A. Coulter, C. Steinhäuser, Role of astrocytes in epilepsy. *Cold Spring Harb. Perspect. Med.* **5**, a022434 (2015).
57. N. C. de Lanerolle, T. S. Lee, D. D. Spencer, Astrocytes and epilepsy. *Neurotherapeutics* **7**, 424–438 (2010).
58. A. G. Nadadhur *et al*., Patterning factors during neural progenitor induction determine regional identity and differentiation potential in vitro. *Stem Cell Res. (Amst.)* **32**, 25–34 (2018).
59. E. Datan *et al*., mTOR/p70S6K signaling distinguishes routine, maintenance-level autophagy from autophagic cell death during influenza A infection. *Virology* **452–453**, 175–190 (2014).
60. J. N. Lee, X. Zhang, J. D. Feramisco, Y. Gong, J. Ye, Unsaturated fatty acids inhibit proteasomal degradation of Insig-1 at a postubiquitination step. *J. Biol. Chem.* **283**, 33772–33783 (2008).
61. W. K. Tang, D. Xia, Mutations in the human AAA^+ chaperone p97 and related diseases. *Front. Mol. Biosci.* **3**, 79 (2016).
62. D. Y. Han, X. J. Di, Y. L. Fu, T. W. Mu, Combining valosin-containing protein (VCP) inhibition and suberanilohydroxamic acid (SAHA) treatment additively enhances the folding, trafficking, and function of epilepsy-associated γ-aminobutyric acid, type A ($GABA_A$) receptors. *J. Biol. Chem.* **290**, 325–337 (2015).
63. P. H. Vekaria, T. Home, S. Weir, F. J. Schoenen, R. Rao, Targeting p97 to disrupt protein homeostasis in cancer. *Front. Oncol.* **6**, 181 (2016).
64. L. Stach, P. S. Freemont, The AAA+ ATPase p97, a cellular multitool. *Biochem. J.* **474**, 2953–2976 (2017).
65. B. Lan, S. Chai, P. Wang, K. Wang, VCP/p97/Cdc48, a linking of protein homeostasis and cancer therapy. *Curr. Mol. Med.* **17**, 608–618 (2017).
66. P. Cossette *et al*., Mutation of GABRA1 in an autosomal dominant form of juvenile myoclonic epilepsy. *Nat. Genet.* **31**, 184–189 (2002).
67. P. Chang *et al*., Seizure control by derivatives of medium chain fatty acids associated with the ketogenic diet show novel branching-point structure for enhanced potency. *J. Pharmacol. Exp. Ther.* **352**, 43–52 (2015).
68. J. A. French *et al*., Adjunctive everolimus therapy for treatment-resistant focal-onset seizures associated with tuberous sclerosis (EXIST-3): A phase 3, randomised, double-blind, placebo-controlled study. *Lancet* **388**, 2153–2163 (2016).
69. R. J. Leventer, R. Guerrini, W. B. Dobyns, Malformations of cortical development and epilepsy. *Dialogues Clin. Neurosci.* **10**, 47–62 (2008).
70. A. A. Sosunov *et al*., The mTOR pathway is activated in glial cells in mesial temporal sclerosis. *Epilepsia* **53** (suppl. 1), 78–86 (2012).
71. J. D. Blair, D. Hockemeyer, H. S. Bateup, Genetically engineered human cortical spheroid models of tuberous sclerosis. *Nat. Med.* **24**, 1568–1578 (2018).
72. A. Elia *et al*., Implication of 4E-BP1 protein dephosphorylation and accumulation in pancreatic cancer cell death induced by combined gemcitabine and TRAIL. *Cell Death Dis.* **8**, 3204 (2017).
73. A. Haghighat, S. Mader, A. Pause, N. Sonenberg, Repression of cap-dependent translation by 4E-binding protein 1: Competition with p220 for binding to eukaryotic initiation factor-4E. *EMBO J.* **14**, 5701–5709 (1995).
74. J. Li, S. G. Kim, J. Blenis, Rapamycin: One drug, many effects. *Cell Metab.* **19**, 373–379 (2014).
75. D. E. Harrison *et al*., Rapamycin fed late in life extends lifespan in genetically heterogeneous mice. *Nature* **460**, 392–395 (2009).
76. D. W. Lamming, D. M. Sabatini, A radical role for TOR in longevity. *Cell Metab.* **13**, 617–618 (2011).